CARE Conf 04-010-HHH

WAMS 2004

Workshop on
Accelerator Magnet Superconductors

22-24 March, Archamps, France

Proceedings

Acknowledgement

We acknowledge the support of the European Community-Research Infrastructure Activity under the
FP6 “Structuring the European Research Area” programme (CARE, contract number RII3-CT-2003-506395)

WAMS-2004
Workshop on Accelerator Magnet Superconductors

1st workshop of the HEHIHB-AMT network – CARE Program Hosted by the
Accelerator Technology Department -CERN Archamps (F), 22-24 March 2004

FOREWORD FROM THE CHAIRMAN

After the massive effort for the LHC, whose commissioning will take place in 2007, the accelerator magnet community in Europe is organizing the post-LHC phase. In the frame of the recently funded EU program CARE (see the web site [1]) the network **HEHIHB** (High Energy High Intensity Hadron Beams, also nicknamed **HHH**) foresees a working package dedicated to the collaboration for advancement on Accelerator Magnet Technology (**AMT**), (see the web site [2]). The network is synergic to the JRA (Joint Research activity) called NED (Next European Dipole, (see the web site [3]) aiming at the development of superconductor and winding technology for the construction of a Nb_3Sn model dipole magnet in the 13-15 T range.

One of the scopes of the network HHH-AMT is to help and orient the eventual development of superconductors for accelerators by European industry according to the needs envisaged for the programs for the period 2005-2015.

In the above mentioned frame, the coordinators of the HHH-AMT working package (Lucio Rossi, and Luca Bottura, deputy) have organized this Workshop on Accelerator Magnet Superconductors – WAMS to deal with the status of the world R&D on superconducting materials and cables for high field magnets (B > 10T), with particular focus on the needs for NED (lead by A. Devred, A. den Ouden, deputy). The workshop has also reviewed the status of HTS and transmission line cables for potential use in low field superconducting magnets for injectors and beam transfer lines, as well as cables for pulsed magnets that might be used in future hadron colliders or injectors. One further objective has been to review the capabilities of European laboratories in support of superconductor R&D.

WAMS has been held from 22 March to 24 March, three intense days of work at the International Business Park of Archamps (France, near the border with Geneva and 10 km far from CERN).

Attendance to the workshop has been by invitation only with more than 100 participants (against an initial plan of 50 participants) included speakers. The success of the workshop has been assured by the high level of talks, discussions and collateral events, the main being the launching of a high field dipole program of the European fusion community, with obvious synergy with the HEP program.

Lucio Rossi CERN AT (Accelerator Technology) Department

[1] http://esgard.lal.in2p3.fr/Project/Activities/Current/
[2] http://cern.ch/amt
[3] http://lt.tnw.utwente.nl/project.php?projectid=9

Organising Committee

Chairman : Lucio ROSSI, CERN, AT Department (Accelerator Technology)

Tel +41 22 767 1117 (Lucio.Rossi@cern.ch)

Co-chairman: Luca BOTTURA, CERN, AT Department (Accelerator Technology)

Tel +4122 767 3729 (Luca.Bottura@cern.ch)

Editors : Luca BOTTURA, CERN, AT Department (Accelerator Technology)

Tel +4122 767 3729 (Luca.Bottura@cern.ch)

Marco BUZIO, CERN, AT Department (Accelerator Technology)

Tel +4122 767 73724 (Marco.Buzio@cern.ch)

Thomas TAYLOR, (former) CERN, AT Department (Accelerator Technology)

Tel +4122 767 3732 (Thomas.Taylor@cern.ch)

Secretary and co-editor : Claudine BOSTEELS, CERN, AT Department (Accelerator Technology)

Tel +4122 767 5764 (Claudine.Bosteels@cern.ch)

WAMS2004
Workshop on Accelerator Magnet Superconductors

CARE EU program
N3 network (Hadron Colliders)-Advance in Accelerator Magnet Technology
Archamps (near CERN)

22 March 2004

h.9.00	h.9.15	**L. Rossi**	**Welcome and Scope of the workshop**
SESSION I : Review of needs for accelerators magnets programs and needs for Sc ***Chair Ph. Lebrun***			
h.9.15	h.10.00	L. Bottura	Need of high field and/or pulsed field Sc magnets for HEP Colliders
h.10.00	h.10.45	D. Leroy	Requirements on Sc materials, strands and cables for the future needs
h.10.45	***h.11.00***	***Coffee break***	
h.11.00	h.11.30	E. Salpietro	The ITER Sc magnets program
h.11.30	h.12.00	A. Yamamoto	Status and plan for superconducting magnet development at KEK
h.12.00	h.12.30	J. Strait	The USA LARP high field magnet program
h.12.30	***h.14.00***	***LUNCH***	
SESSION II : Review of Sc programs for high field ***Chair E. Salpietro***			
h.14.00	h.14.45	R. Scanlan	The USA experience on Nb3Sn and Bi-based superconductors and future plans
h.14.45	h.15.30	D. Larbalestier	Thoughts on the competitive merits of Nb3Sn, Nb-Ti-Ta and MgB2
h.15.30	h.16.00	V. Pantsyrnyi	Nb3Sn and HF material development at the Bochvar Institute
h.16.00	***h.16.15***	***Coffee break***	
h.16.15	h.17.00	T. Takeuchi	Status and perspective of the Nb3Al development in Japan
h.17.00	h.17.30	D. Uglietti	Strain dependence of jc in Nb3Sn, MgB2 and Bi,Pb(2223)
h.17.30	h.18.00	J.L. Duchateau	The Nb3Sn for ITER and CEA activities
h.18.00	h.18.30	A. Della Corte	The activities of ENEA on Sc developments

23 March 2004

SESSION III: Review of HTs and MgB2 programs ***Chair A. Devred***			
h.9.00	h.9.45	H.C. Freyhardt	Panorama of the coated conductor developments in EU
h.9.45	h.10.15	G. Grasso	Bi-2223 developments at INFM-Genova
h.10.15	h.10.45	S. Schlachter	Status and perspectives of MgB2
h.10.45	***h.11.00***	***Coffee break***	
h.11.00	h.11.30	R. Musenich	The INFN research program on MgB2
h.11.30	h.12.00	R. Fluekiger	Nb3Sn and MgB2 developments in Geneva
h.12.00	***h.13.30***	***LUNCH***	
SESSION IV: Review of European Industry ***Chair D. Leroy***			
h.13.30	h.14.00	Ch. Verwaerde	Alstom plan and activities on LTS and Nb3Sn materials
h.14.00	h.14.30	J.H.Lindenhovius	SMI activities and plans on PIT Nb3Sn
h.14.30	h.15.00	H. Krauth	EAS activities and plans on LTS and HTS materials
h.15.00	h.15.30	R. Liikamaa	OK-EM activities and plans on LTS and HTS materials
h15.30	***h.15.45***	***Coffee break***	
h.15.45	h.16.15	J. Bock	Nexans activites and plans on HTS materials
h.16.15	h.16.45	G. Grasso	Columbus activities and plans on MgB2
h.16.45	h.17.15	S. Zannella	The activities and plans of Edison on HTS and MgB2
h.17.15	h.17.45	J. Rieger	Siemens activities in superconductivity
h.17.45	h.18.45	**Panel discussion *Ph. Lebrun*** **how to collaborate in a frame of Industrial competition?** **The US-DOE model (R. Scanlan)** **The ITER model (P. Bruzzone)**	
h.19.30		***Social dinner***	

24 March 2004

SESSION V : Cables and testing facilities Chair D. Larbalestier			
h.9.00	h.9.30	R. Scanlan	Rutherford cables for High Field in the US
h.9.30	h.10.00	P. Bruzzone	High Field cables development for ITER
h.10.00	h.10.30	D. Leroy	Cable design and R&D for NED
h.10.30	***h.10.45***	***Coffee break***	
h.10.45	h.11.15	A. Ghosh	Cable design for pulsed Sc magnets (cos-theta design)
h.11.15	h.11.45	A. Kovalenko	Cable Design and Related Issues in a Fast-Cycling Superconducting Magnets
h.11.45	h.12.15	F. Schmidt	Review of transmission line cables
h.12.15	h.13.00	A. den Ouden	Review of capabilities and measuring facilities in EU laboratories
h.13.00	***h.14.15***	***LUNCH***	
SESSION VI : winding technology Chair *A. Yamamoto*			
h.14.15	h.14.45	E. Baynham	Nb3Sn Accelerator magnets - Insulation technology review
h.14.45	h.15.15	S. Gourlay	The point of view of the winding technique wrt Sc and cable properties
h.15.15	h.16.15	**Panel discussion *W. Scandale* Key points - open questions Materials & Conductors (R. Scanlan) Magnets (T. Taylor) System integrations (E. Salpietro)**	
h.16.15	**h.16.30**	**L. Rossi**	**Summary and conclusions**

CONTENTS

REQUIREMENTS AND GENERAL R&D

MAGNETS FOR FUTURE HIGH ENERGY AND HIGH INTENSITY HADRON BEAMS

L. Bottura
CERN, Geneva, Switzerland

Abstract
This paper gives a summary of the general needs and trends in superconducting magnet development for future high energy, high intensity hadron beam accelerators. Although a large part of the discussion is based on LHC upgrades, and the associated need for large aperture and increased peak field in the coils, some space is also given to the development of different technologies such as those required for pulsed magnets in the low to medium field range, superconducting undulators, or combined function magnets. I finally review the motivation for the development and sketch a plan for medium term R&D.

1. INTRODUCTION

The technology of superconducting bending (dipoles) and focussing (quadrupoles) magnets has gone since the beginning hand-in-hand with the developments in accelerator technology, so much that the two are considered since a quarter of a century good companions [1]. This is particularly true for circular colliders, the technology of choice today for high energy and high intensity hadron beams, where the field strength in the bending dipoles is proportional to the energy of the beam E, and the strength and aperture of the final focussing quadrupoles are a major driver for the luminosity L at the interaction points.

As the quest for new discoveries and for more measurements of basic particle properties at increased precision continues, there is a steady push to increase the energy and the luminosity in existing and future accelerators. This qualitative statement is best quantified by the *physics discovery potential* (PDP), which is a relative measure of the probability of a new discovery, observing in particular its dependence on energy and luminosity. Taking as an example the case of the LHC, the estimated scaling of the PDP for the discovery of a Higgs boson at an energy of 120 GeV scales as follows [2]:

$$PDP = (E - 1)\sqrt{L} \tag{1}$$

in the range 4 TeV to 7 TeV. The physics reach of a given machine can hence be extended by increasing energy, luminosity or both. Magnet technology will have to follow accordingly, producing magnets with yet higher field and wider bore.

The aim of this paper is to give a view of the magnet developments that will be demanded in the medium term to follow the evolution of large scale accelerator programs. The requirements on magnets will be discussed in terms of peak field B, aperture D, specific geometry and configuration, as useful to identify key technologies that need R&D to achieve the objectives set by accelerator physics.

2. MAGNET SCALING LAWS

To be more specific on the requirements, we recall below the simple analytical dependencies of the main parameters for accelerator magnet design, peak field B and bore aperture D, on energy and luminosity. In the following discussion we neglect the peaking factor on the field, so that in a dipole

the peak field can be taken as equal to the bore field and in a quadrupole we have that the peak field is proportional to the product of field gradient G and bore radius D/2:

$$B = G\frac{D}{2} \tag{2}$$

Once the collider geometry is fixed, and in particular if the curvature radius of the central beam trajectory ρ is given, the scaling between the bending field B and the particle momentum p is the simple proportionality [3]:

$$B[\mathrm{T}] = \frac{1}{0.2998}\frac{p[\mathrm{GeV/c}]}{\rho[\mathrm{m}]} \tag{3}$$

which implies that an increase of the beam momentum (and associated energy) can only be achieved increasing proportionally the dipole field in the bending magnets.

The relation between luminosity L and the characteristics of the magnets in the Interaction Region (IR), i.e. located in front of the Interaction Point (IP), is more involved. The definition of the luminosity L is the following:

$$L = \frac{N_b^2 f_{rep}}{4\pi\sigma^{*2}} F(\theta_c) \tag{4}$$

where N_b is the number of particles per bunch, σ^* is the transverse beam size, $F(\theta_c)$ is a geometric factor that depends on the crossing angle θ, and f_{rep} is the average bunch repetition frequency given by the product of the number of bunches n_b and of the bunch revolution frequency f_0:

$$f_{rep} = n_b f_0 \tag{5}.$$

Once the machine and its injector chain are optimised for maximum beam intensity, the most effective way to increase the luminosity at the interaction points is by reducing the transverse beam size σ^*. The value of σ^* depends on the beam emittance ε and on the value of the betatron function at the IP:

$$\sigma^* = \sqrt{\varepsilon\beta^*} \tag{6}$$

The beam emittance, in turn, is broadly conserved from injection through acceleration to collision, but the value of the betatron function can be changed by modifying the characteristics of the final focussing quadrupoles, in front of the IP. In the drift space bewteen the IP and the final focussing quadrupole, separated by a distance L^*, the betatron function grows parabolically from the value at the interaction point, β^*, to the maximum value β^{max}:

$$\beta^{\max} = \beta^* + \frac{L^{*2}}{\beta^*} \approx \frac{L^{*2}}{\beta^*} \tag{7}.$$

The corresponding beam size in the quadrupole σ^{max}, using Eq. (6) at the quadrupole location and substituting (7), is given by:

$$\sigma^{\max} = \sqrt{\varepsilon\beta^{\max}} \approx \sqrt{\frac{\varepsilon}{\beta^*}} L^* \tag{8}$$

that shows that the beam diverges from the IP towards the IR magnets. The magnet aperture D required to clear enough space for the beam passage can be expressed in terms of the beam size as follows:

$$D \approx K_\beta N \sigma^{\max} + \delta_x + \delta_{al} \tag{9}$$

where N is a multiplying constant, K_β is a factor that accounts for β-beating, δ_x is the maximum orbit error and δ_{al} is the maximum of the sum of the geometric tolerances on the bore position and alignment errors. We see from Eq. (9) that, as expected, the magnet aperture must scale as the maximum beam size. Using Eqs. (8) and (9), and neglecting for this discussion the geometric quantities δ_x and δ_{al}, we have hence that:

$$D \propto \sqrt{\frac{\varepsilon}{\beta^*}} L^* \tag{10}$$

from which we observe that if the layout of the interaction region is left unchanged (i.e. at constant L^*) a decrease of the beta function at the IP implies an increase of the bore diameter of the final focussing quadrupole. An alternative to limit the magnet bore diameter, and still achieve a decrease of the beta function, is to put the final focussing quadrupole closer to the IP. This option is limited by the space requirements from the detectors that enclose the IP and by the need of heavy shielding, especially when considering luminosity in the range of 10^{34} to 10^{35} cm^{-2} s^{-1} as we do here.

A common feature of the configuration of the IR magnets of modern colliders is that the IP is close to the focal point of the final focussing quadrupole. This relation is only approximate, as in reality the value of the betatron function depends on the whole optics in the matching section as well as the final focus. Nonetheless we make use of it to gain further insight in the scaling. Using the normalised quadrupole gradient, defined by:

$$k\left[\frac{1}{\mathrm{m}^2}\right] = 0.2998 \frac{G[\mathrm{T/m}]}{p[\mathrm{GeV/c}]} \tag{11}$$

we can express the relation between the distance L^* and focal point location as follows:

$$kL^{quad}L^* \approx 1 \tag{12}$$

where we have introduced the magnetic length of the quadrupole L^{quad}. From Eq. (12) we observe that a change in the distance between the final focussing quadrupole and the interaction point implies an increase of the integrated gradient of the quadrupole. Combining Eqs. (12) and (10), we finally obtain the following scaling for the product of the quadrupole gradient and bore diameter, which is proportional to the peak field in the coil:

$$B \approx GD \propto \sqrt{\frac{\varepsilon}{\beta^*}} \tag{13}$$

which shows in summary that to decrease the betatron function at the interaction point we would need a final focussing quadrupole with larger aperture, or larger gradient, and in any case higher peak field on the coil.

Many additional factors have an influence on the required magnet aperture. One of the main unknowns for high luminosity colliders is the effect of parasitic interactions that take place among the particle bunches as they approach the IP [4]. This effect may eventually limit the luminosity. This *beam-beam* interaction can be reduced increasing the crossing angle of the two colliding beams, separating them faster as the beam bunches fly out of the IP. A larger crossing angle, however, also requires more space, i.e. a larger free bore, for the separated beams in the magnet facing the IP.

A second factor that is of large importance for the IR magnets is the radiation dose and heat loads from the collisions at the IP [5]. Radiation and collision debris are intercepted by the magnets and cause material damage, limiting the lifetime of the magnet, as well as nuclear heating that must be removed at cryogenic temperatures. In order to limit both effects, heavy shielding is required in front of the IR magnets, thus setting a lower limit to the minimum distance L^* of the magnet to the IP, and hence on the magnet aperture (see Eq. (10)). In addition it is generally beneficial to leave a wide aperture to let radiation and collision debris traverse the magnet, and intercept them at the downstream side.

3. MAGNET REQUIREMENTS FOR AN LHC UPGRADE

As discussed by Brüning [5] and Ruggiero [4] there is a good case for increasing the luminosity and the energy of the LHC above its nominal and, eventually, ultimate performance, aiming naturally at extending the physics reach of such an exceedingly large and complex instrument. The present commissioning and running-in plan [6] foresees an initial year of operation in the 6 TeV range (corresponding to a dipole field of approximately 7 T) and a luminosity of 10^{33} cm^{-2} s^{-1}.

The energy and luminosity will then be increased over the first 3 years of operation to their nominal values of 7 TeV (corresponding to a dipole field of 8.33 T) and 10^{34} cm^{-2} s^{-1} respectively. It is conceivable that using the engineering margin built in the accelerator design, the performance could be increased above the nominal values. Ultimate energy is expected to be in the 7.5 TeV range (corresponding to a dipole field of 9 T), while ultimate luminosity is estimated at 2.3×10^{34} cm^{-2} s^{-1}. The actual values that will be achieved depend, nonetheless, on many beam and operation parameters, discussed in [5] and [4], that go beyond the scope of magnet technology.

The lifetime of the magnets facing the experiments in the radiation environment is estimated at 6 years at nominal conditions, and 2 years at ultimate conditions [5]. By then the number of events accumulated for a particular channel of interest will be such that further operation at the same level of luminosity is not expected to significantly improve the statistics. Provided that the accelerator performance evolves as sketched above, a replacement of the magnets in the interaction region should hence be planned for the years 2013 to 2017.

An LHC upgrade scenario has been elaborated on this basis, and is presented in the various references cited in the bibliography. The backbone of the scenario is to stage the upgrade in two phases after reaching ultimate luminosity, by which we intend the maximum luminosity that will be possible in the LHC configuration as achieved around 2010. The two phases are the following:

- Phase 1 – luminosity increase to 10^{35} cm^{-2} s^{-1} with modest hardware changes, and in particular leaving the LHC arcs unchanged. This phase concentrates on improving the layout of the

interaction region, including mainly the final focussing quadrupoles and the separation/recombination dipoles;

- Phase 2 – energy increase to 14 TeV, achieved by a major hardware change in the LHC arc as well as the injector chain.

3.1 Phase 1

Various alternatives have been considered in Phase 1, going from a straightforward update of the magnet performance to a major change in the magnet layout and optics. A summary of the various options considered in these studies, from [7] and [8], is reported in Fig. 1. The corresponding magnet parameters for the quadrupoles and dipoles are given in Tab. 1.

As discussed in the previous section an increase in luminosity requires an increase in the aperture of the final focus quadrupole, as well as an increase of the peak field in the coil (see Eq. (13)). The quadrupole gradient in these studies is kept at values close to the present level, pending a verification of the limits of the present technology. Indeed, as discussed in [5], to profit from high-Jc superconducting strands it may be better to design large aperture quadrupoles with moderate gradient than quadrupoles with smaller aperture but higher gradient.

Among the options considered in Fig. 1, some of the variants include a change of the topology of the magnets in front of the interation region. The variant with a separation doublet in front of the IP reduce the length where parasitic beam-beam interactions take place, but increase the distance between the IP and the focussing quadrupoles. Hybrid solutions, with interleaved dipoles and quadrupoles, or large crosing angles, have been considered to reduce the distance between the final focus quadrupoles and the interaction point, hence reducing the aperture requirements in accordance with Eq. (10).

		baseline	quadrupole first	dipole first	duadrupole beteen dipoles	dipole first large crossing angle	quadrupole first large crossing angle
L^*	(m)	23	23	52.8	42.5	34	23
β^*	(m)	0.5	0.16	0.26	0.19	0.15	0.10
$D^{quadrupole}$	(mm)	70	110	100	100	100	100
G	(T/m)	200	200	200	200	200	200
D^{dipole}	(mm)	80	110	135	165	75	105
B^{dipole}	(T)	2.75	15.3	15	14.6	14.5	14.3

Table 1. Summary of main magnet parameters (aperture, gradient, peak field) for the configurations considered for an upgrade of the LHC interaction region as reported in Fig. 1.

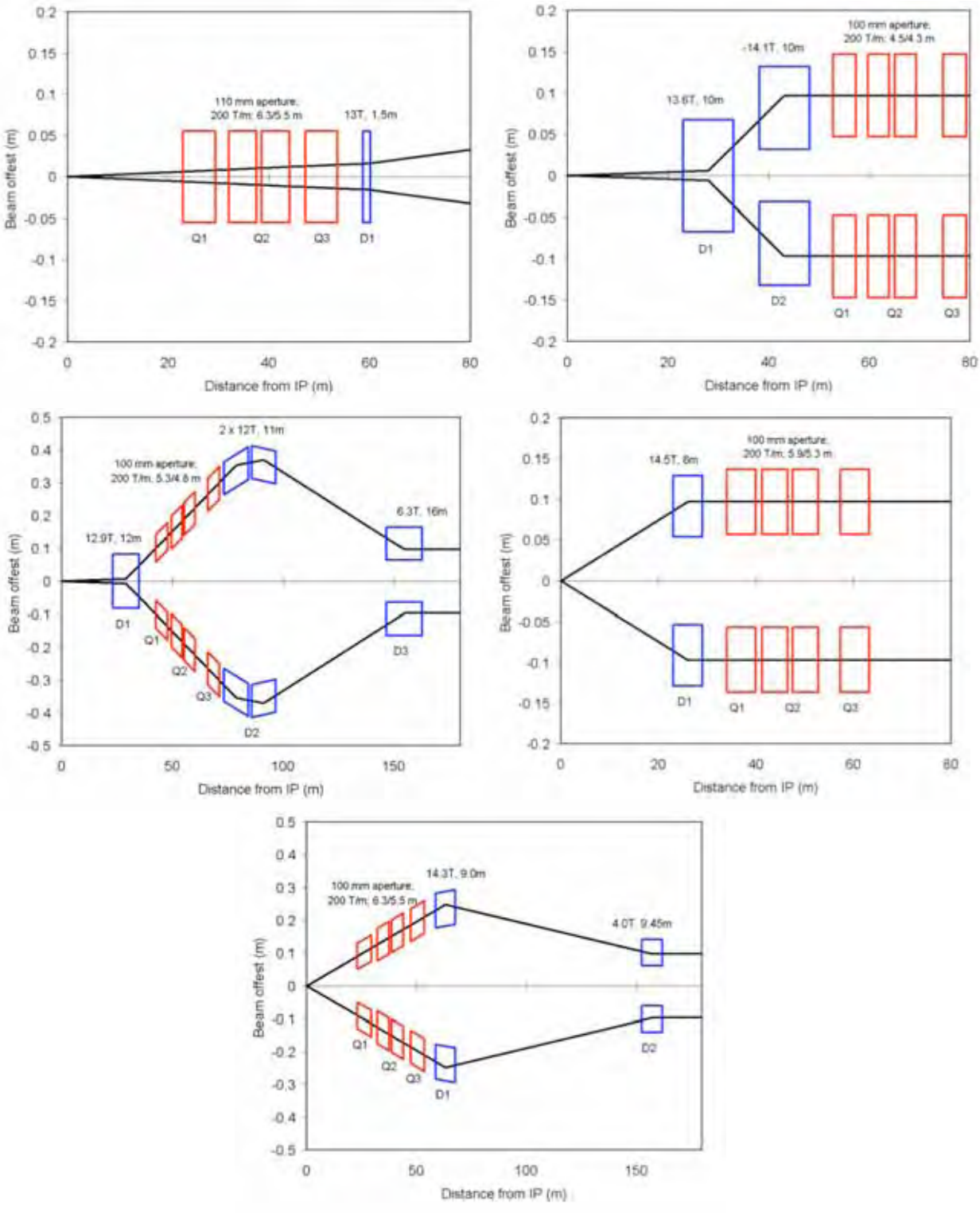

Figure 1. Various alternatives for a Phase 1 upgrade of the LHC interaction region. The present scheme has the focussing quadrupoles first (top-left). Alternatives considered have separation dipoles first (top-right), interleaved separation dipoles and focussing quadrupoles (middle-left), dipoles first with large crossing angle (middle-right) or quadrupoles first with large crossing angle (bottom).

Scanning the envelope of the set of parameters found in this study we see that Phase 1 of the LHC upgrade will require the development of dipoles and quadrupoles with aperture of the order of 100 mm, peak field in the dipoles of 15 T and field gradient in the quadrupole of 200 T/m. Taking appropriate enginnering margins this implies magnets design with peak field in the range of 16 to 17 T for dipoles and 12 to 13 T for quadrupoles.

Finally, the IR magnets for the Phase 1 of the LHC upgrade will have to sustain exceptional radiation dose and heat loads. The radiation dose and the power from the IP scales linearly with the luninosity. at the target luminosity of 10^{35} cm^{-2} s^{-1} the power from the IP amounts to 9 kW per beam. Innovative heat removal solutions shall be found to avoid large cryogenic overheads. As far as the radiation dose is concerned, at the target luminosity, magnets with the same insulation technology as used presently would have a lifetime of 6 months, which is clearly not acceptable. Again, innovative materials and shielding shall be prepared for the Phase 1 upgrade.

3.2 Phase 2

An energy increase in the existing tunnel, as planned for the Phase 2 of the LHC upgrade, will need an increase of the dipole field, as results from Eq. (3). Energy doubling from 7 TeV per proton to 14 TeV per proton will mean an increase of the dipole field from 8.33 T to above 16 T. This can be conceived maintaining the magnet aperture constant, around 50 mm.

An implication of an energy increase that is not directly spelled out in [5] and [4] is that also the lattice quadrupoles will have to feature doubled integrated strength, as results from Eq. (11). For a constant lattice geometry, i.e. keeping the magnetic lengths of the FODO lattice cell, this implies doubling the field gradient in the focussing and defocussing quadrupoles, aiming at $G \approx 450$ T/m and peak field in the quadrupole coils in the 14 T range. Although it is clear that a complete optimization of the cell layout is needed to set precisely the requirements for the lattice magnets, we see already that doubling the LHC energy will be possible only when the technology for 15 T dipoles and quadrupoles will be at hand and sufficiently established to allow large scale manufacturing at acceptable cost. For this reason it is important that during Phase 1 the R&D program on magnet technology addresses the design and fabrication of both high field quadrupoles as well as dipoles, whose results will give key input for the energy upgrade.

As for the IR magnets in Phase 1 of the upgrade, heat loads will be one of the problems that will require innovative solutions. Taking as a reference the cooling scheme of the LHC, the heat loads at superfluid helium temperature (1.9 K) are expected to scale up by a factor of 2, from the present 0.4 W/m to 0.8 W/m. At the intermediate temperature level of the LHC beam screen, 4.6 K to 20 K, the increase of the heat load can be as much as one order of magnitude, from the present value of 1.7 W/m to 17 W/m at doubled energy and ten-fold luminosity. This large rise results mainly from the increased synchrotron radiation that scales with the fourth power of the beam energy.

A second important consideration when planning for an energy upgrade is on the injector chain. The present dynamic range of acceleration in the LHC, around 15, is already very large, and cannot be expanded easily to cover the desired energy span. A much better situation would be obtained injecting in the last ring at 1 TeV, i.e. at twice the present value (450 GeV), or higher. To achieve this increase there are two possible alternatives:

- Upgrade the injector chain, and in particular the SPS, adding an additional, superconducting booster ring (a Super-SPS) that would accelerate and eject beam at 1 TeV or higher. The dipole magnets for this ring would require a bore field in the range of 2 to 4 T, aperture in the range of 80 to 100 mm, and high field ramp-rate in the range of 1 to 5 T/s. A superconducting option for the SPS was already considered more than 30 years ago, at the time of its conceptual design [9], and discarded because the technology was not judged available for construction. Note that an upgrade of the injector chain also requires novel, superconducting

transfer lines for the increased energy. These represent several km of magnets with complex powering schemes, for which a cost optimization is surely worthwhile;

- Add a booster ring in the LHC tunnel that would receive beam from the existing SPS (at 450 GeV), accelerate over a limited dynamic range, up to 1 TeV or higher, and eject into the upgraded LHC. This booster would require dipoles with bore field in the range of 2 T at most, 50 mm aperture and moderate field ramp-rate, typically 0.1 T/s or smaller depending on the operating constraints.

As discussed in [5] and [4] an increase of the injection energy is expected to produce an increase in the beam performance, and less difficulties in the acceleration, even in the present LHC configuration. It is hence logic to plan for an upgrade of the LHC injectors sufficiently in advance before an energy upgrade.

In summary, based on the considerations above, a feasible plan for the LHC upgrade would be the following

- develop and install large aperture, high field dipoles and quadrupoles for an upgrade of the LHC interaction region aiming at a ten-fold increase in luminosity. The dipoles have a bore field of B ≈ 15 T, and aperture D ≈ 100 mm, the quadrupoles have a field gradient of G ≈ 200 T/m, and aperture D ≈ 100 mm. These magnets need to be compliant with the large radiation and heat load coming from the interactions at the IP. Technology development, rather than unit cost, is a major driver for the R&D, and these magnets can be regarded as prototypes for the large scale production that would be needed for an energy upgrade. Magnets for the upgrade would be needed by 2014, and the cost estimate for this program is 300 MEUR (≈ 450 MCHF).
- develop and install magnets for an increase of the injection energy into the LHC. Pursue initially both alternatives, i.e. B ≈ 2 to 4 T, D ≈ 100 mm, dB/dt ≈ 1 to 5 T/s pulsed dipoles (and quadrupoles) for a Super-SPS, and low field B ≈ 2 T, D ≈ 50 mm DC dipoles (and quadrupoles) for an LHC booster ring. This activities could profit largely from parallel and independently driven R&D on compact, high intensity hadron collider such as the GSI-IAF, discussed later on. Cost reduction is a major driver in this R&D. The acceptable cost range for these magnets (per unit bending power produced) is 20 to 25 kEUR/Tm, which is comparable to the present LHC magnets. An upgrade of the injector chain can be planned at the earliest by 2015, once the LHC will have produced sufficient results in the present configuration. The associated cost is estimated at 250 MEUR (≈ 375 MCHF)
- finally, develop and install dipoles and quadrupoles for an energy upgrade to reach 14 TeV per proton in the existing tunnel. The dipoles have a bore field of B ≈ 16 T, and aperture D ≈ 50 mm, the quadrupoles have a field gradient of G ≈ 450 T/m, and aperture D ≈ 50 mm. As is the case for the upgrade of the injection chain, the cost of these magnets will be a major driver in the R&D and industrialization of the production. An acceptable magnet cost (per unit bending power produced) would be at a level of 10 to 15 kEUR/Tm, i.e. below the cost of the present LHC magnets. Given the R&D required, and the operation constraints, an LHC energy upgrade is credible only by year 2020, and the total cost associated is estimated at 3000 MEUR (≈ 4500 MCHF).

This scenario, and in particular the first item, is consistent with the present, worldwide R&D programs on high field superconducting accelerator magnets. Work on the upgrade of the LHC high-luminosity interaction regions is taking place under the auspices of the US-LHC Accelerator Research Program (US-LARP) [10] as well as with the Nb3Sn cable development that forms the core of the recently launched Next European Dipole (NED) Joint Research Activity (JRA) within the Coordinated Accelerator Research in Europe program (CARE) of the European Steering Group for Accelerator R&D (ESGARD) [11], [12]. Indeed, the targets outlined above appear to be possible today mostly

thanks to the work performed within the US National Program for the development of high-performance Nb3Sn wires, which has led to a spectacular increase in J_c in the past 4 years, and a series of record-breaking dipole magnet models opening the 15 T range. This series started with the 50 mm bore, cos θ, MSUT model, built at Twente University and cold tested at CERN in 1995, which reached 11 T on its first quench at 4.4 K [13], and continued with the 50-mm-aperture, cos θ, D20 model, built and cold tested at LBNL, which, after some training, reached 13.5 T at 1.8 K in 1997 [14]. Lately, the 25-mm-gap, racetrack dipole, RD-3 model, also built and cold tested at LBNL, reached after some training 14.7 T at 4.2 K in 2001 [15]. Finally, the HD1 racetrack dipole, an evolution of the RD-3, has reached in 2003 the record field of 16 T after just more than ten training quenches [16].

4. PULSED MAGNETS FOR THE GSI-IAF

The Gesellschaft fuer Schwerionenfosrschung (GSI) in Darmstadt has proposed to build a new, International Accelerator Facility (IAF) for radioactive ions and antiprotons [17]. The central part of this complex are the two rings SIS100 and SIS300 that will be built in the same tunnel and will have magnetic rigidity Bρ = 100 Tm and Bρ = 300 Tm respectively. To achieve this magnetic rigidity the dipoles of SIS100 will have a bore field of 2 T in a rectangular bore of 130 mm x 65 mm. The dipoles of SIS300 will require a peak field of 6 T in a round bore with a diameter of 100 mm. The magnets for these two rings are especially challenging because the operation mode of the complex foresees fast ramping of the energy. SIS100 should undergo a full cycle in 1 s, corresponding to a ramp-rate of 4 T/s. The ramp-rate requirements for SIS300, which will operate as a storage ring, are more soft, but still the aim is to ramp the ring at 0.5 to 1 T/s.

The main challenge for the magnets of SIS-100 and SIS-300 is to achieve the field and ramp-rate specified without showing ramp-rate limitated behaviour as observed in superconducting magnets for accelerators [18] and thermonuclear fusion [19]. An additional requirement, and especially for SIS100 which will be the work-horse of the complex, is that the magnets will have to withstand long-term operation that will cumulate to several hundreds of millions of cycles.

An artist view of the dipole designs being considered for The SIS100 ring is reported in Fig. 2. The SIS100 dipole is based on a superferric design, derived from the Nuclotron dipole magnets and optimised for low stored energy as well as low AC loss in pulsed operation. With the present configuration a 2.6 m long dipole magnet stores 45 kJ, i.e. nearly 3 times less energy than a conventional design as presently used in the SPS or at the existing SIS18 ring at GSI. The reduction of the stored energy is clearly a must to limit pulsed electric power requirements at the high ramp-rates demanded. The AC loss achieved at liquid helium temperature is around 20 W/m, and there is a potential for further reduction by a factor 2 by adopting a taylored magnet design with the iron at an intermediate temperature (80 K). The R&D program on the SIS100 magnets is actively pursued and is planned to produce prototypes for the final design by end 2004.

The SIS300 dipole, whose schematic cross section is reported in Fig. 3, will be a conductor dominated design, where the Rutherford cables in the cos(θ) coils with 100 mm aperture are either coated or have a central core to reduce AC loss. This cable design is the result of a demonstration program that has been pursued jointly at GSI and BNL, aiming at testing a dipole for a ring option with 200 T m rigidity (rather as 300 T m as in the present baseline). A prototype magnet, GSI001 with a single layer coil and similar in construction to the RHIC dipole, was built and tested successfully at BNL, demonstrating operation up to 4 T bore field in pulsed conditions up to 4 T/s. The magnet sustained short pulse sequences between 2 T/s (500 repeated cycles) and 4 T/s (3 repeated cycle) without quenching [20], [21]. Most probably a two-layer coil design will be necessary to achieve the 6 T peak field requested for the 300 T m rigidity, as shown in Fig. 3. The R&D program for SIS300 is presently addressing issues of temperature margin and should produce a model magnet to verify quench performances and heat loads, both in steady state and pulsed operating conditions.

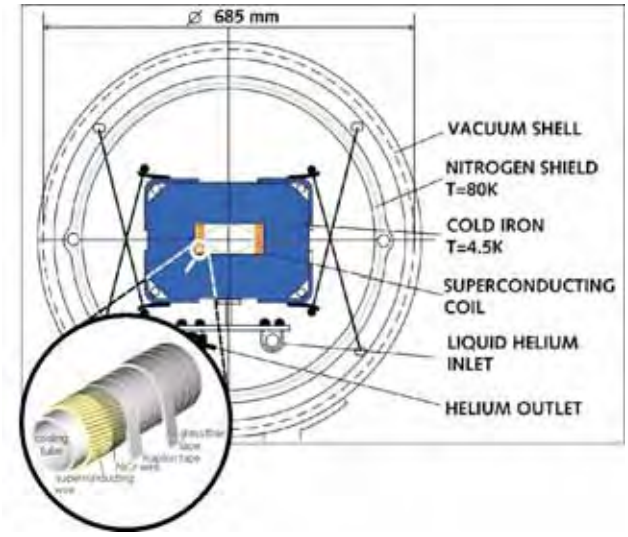

Figure 2. Cross section of the dipole design that is presently considered for the SIS100 ring at the GSI-IAF. The inset shows an exploded view of the NbTi superconductor. This design has been obtained taking as a reference the superferric Nuclotron dipole.

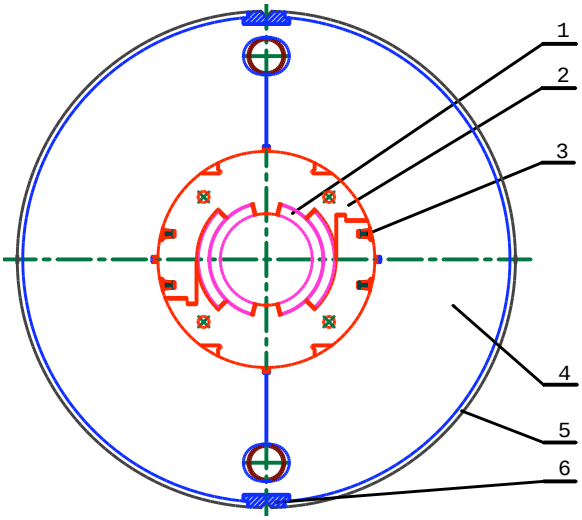

Figure 3. Schematic cross section of the one of the options presently considered for the dipoles of the SIS300 ring at the GSI-IAF, from [22]. This design has been obtained as an evolution of the UNK dipole prototype magnets. The numbering refers to (1) coil, (2) collars, (3) keys, (4) iron yoke, (5) outer skin, (6) staples.

Further important matters to be adressed for both SIS100 and SIS300 are the dynamic field quality at the large ramp-rate specified, as well as the ability to withstand the exceptional number of cycles planned for the accelerator complex without failure, nor decrease in performance. Specifically to this last point a joint INTAS activity between GSI, VNIIKP, SINTEZ and CERN has been launched to investigate the possibility to use alternative cable designs, sketched in Fig. 4, that have better cooling and could provide additional engineering margin for long term operation.

The set of parameters that are presently considered for the GSI-IAF main ring magnets are very close to those that would be needed for an upgrade of the LHC injector chain, i.e. the Super-SPS variant described earlier. This folds in nicely with the planning for an LHC upgrade, both in terms of objectives and timing. Therefore, we can expect that the upgrade of the LHC injector chain can take direct advantage of the on-going R&D at the GSI, and possibly use manufacturing and testing facilities that would be put in place for the procurement of the SIS100 and SIS300 cables and magnets.

Figure 4. Cable design options for increased cooling and energy margin that are being considered for the SIS100 dipole magnet. A short cable test is planned to compare the performances of selected designs

5. SPECIAL DEVELOPMENTS

The developments detailed in the two preceding sections represent at the date of writing what we expect to be the mainstream of the R&D on accelerator magnets for the coming next year. Nonetheless, they do not represent the full picture, which needs to be completed with on-going activities and plans for magnets with special features, or for special applications. Below are few specific examples that are either in the conception, design or demonstration phase.

5.1 Quadrupoles for Compact Interaction Region Designs

We have been considering so far the magnet technology requirements stemming from the development of circular colliders. In linear colliders magnet technology is nonetheless important in the high gradient and compact final focussing quadrupoles.

One such example is the Tera Electron volts Superconducting Linear Accelerator (TESLA). The layout proposed in the Technical Design Report (TDR) has a final focussing quadrupole with a 250 T/m and a 56 mm aperture, i.e. close to the parameters as presently produced for the LHC [23]. The special feature of this magnet is the fact that it operates in the 4 T background field produced by the detector solenoid, as shown in Fig. 5.

A specific development has been launched for this demanding operating condition. To achieve the field gradient specified, the quadrupole design described in [24] has a peak field on the coil of 8.6 T at an operating current of 14 kA, with the design point at 80 % of the quench current along the magnet loadline (at 10.4 T). Nb3Sn has been selected as the superconductor to have sufficient operating margin. The second issue is the large and complex force distribution due to the presence of a background field. The force generated by the field of the detector adds up to 120 tonnes/m on a coil octant. The IR magnets are expected to be available by the mid 2010's for the first IP of TESLA.

BNL is pursuing a development of comparable scope [25] aiming at the design of a 20 mm bore, 144 T/m quadrupole with a nested 1300 T/m^2 sextupole magnet for the final focus (QD0) of the NLC detector. This magnet is located in the background field of the detector solenoid and must be extremely compact. The outer magnet diameter in the design produced, including the cryostat, is as small as 114 mm.

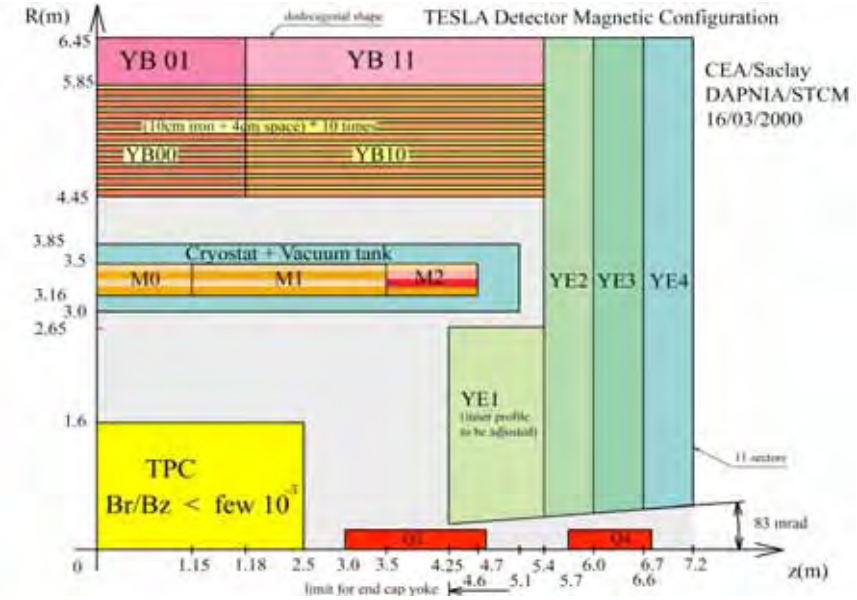

Figure 5. Layout of the first TESLA IR, with the final focussing quadrupole Q1 inside the detector, from [24].

5.2 Undulators and Wigglers

Superconducting undulators and wigglers are of interest because of the large bending power that can be achieved on the pole tips of a superconducting winding. For a given bending ratio the magnet is hence more compact, if compared to a classical electromagnet or to a permanent magnet design, and can fit in tightly constrained space. Alternatively, the high field feature can be used to increase the bending strength and induce larger synchrotron light emission to extract beam energy over a predefined spectrum, monitor the beam or damp transverse particle motion.

Machine	Manufacturer	Coil gap (mm)	Number of poles	Period length (mm)	Peak field on axis (T)	Peak field on coil (T)	Year	Ref.
Daresbury	RAL	62	3	500	5		1981	[26]
LURE	CEA/Saclay	67	5	260	5	7	1988	[27]
Daresbury	Oxford Instruments		3		6		1991	[28]
TERAS	ETL/Sumitomo	48	3		10		1995	[29]
MAX II	Tampere Univ.	36	3	244	6	6.4	1996	[30]
AURORA-2D	Sumitomo	40	3	342	7		1999	[31]
MAX II	MAX-Lab	12	47	61	3.5	4.1		[32]
BESSY II	BINP	19	17	148	7	8.1		[33]
CESR	LNS	76.2	7	400	2.1	4.1		[34]

Table 2. Main features of selected superconducting undulators and wigglers as produced around the world.

Among the many superconducting wigglers and undulators existing in the world, see Tab. 2 that has been extracted from [34], one such application is being pursued at LHC in the synchrotron light monitor that shall be used for the measurement of the beam profile at the Interaction Point 4 [35]. The magnet design, shown schematically in Fig. 6, is based on a NbTi strand and reaches a peak field of 5 T [36]. A prototype of a half period of the undulator has reached a bore field of 4 T without quench and a maximum field of 5.25 T after training.

Extrapolation to the operating conditions of a Super-LHC with doubled energy would require a field in the gap of at least 7 T, or larger, for the synchrotron light monitor to produce useful diagnostics [5]. Although a magnet design has not been produced, we can expect that higher Jc material (e.g. Nb3Sn) would be needed.

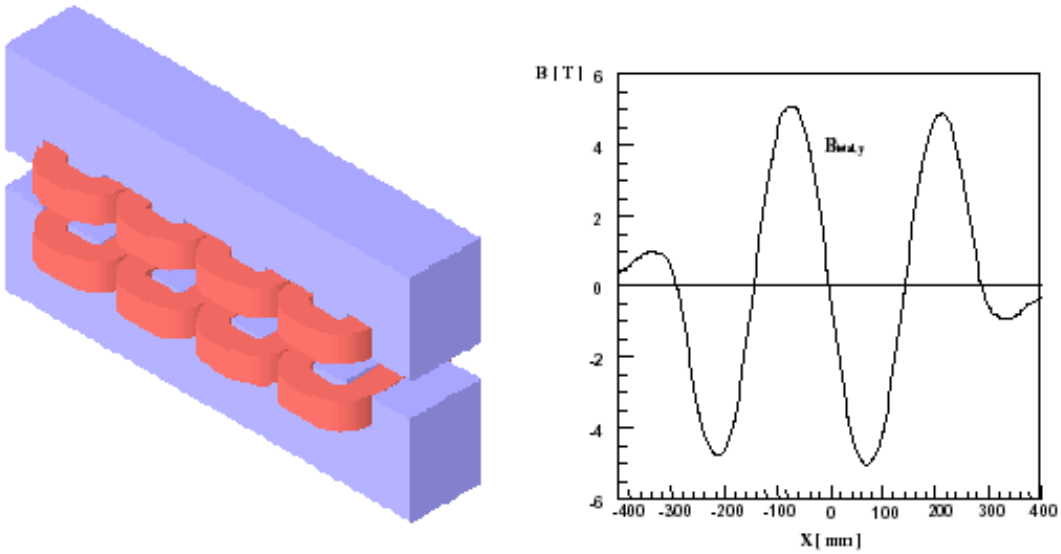

Figure 6. Undulator for the LHC Synchrotron Radiation monitor for the measurement of the beam profile, from [36].

5.3 Combined Functions Magnets

Combined function magnets have been commonly used in accelerators since the first realisation of the weak-focussing principle. The desired field profile is realised in classical magnets by shaping appropriately the iron poles. In case of superconducting combined function magnets the contribution of the iron to the field is small, and to obtain the field profile the coil geometry has a non-conventional shape.

One such example is the combined function dipole and quadrupole magnets that are being built at KEK for the arc section of the 50 GeV proton beam line of the J-PARC neutrino oscillation experiment between Tokai-mura and Kamioka [37], [38], [39]. At the nominal operating point the magnet has a 2.8 T dipole field component superposed to a 18.7 T/m field gradient. The beam line is expected to come in operation in 2006. The combined function magnet has the advantage of a very efficient use of the beam line length, with no unused space between magnetic elements. The KEK design, shown in Fig. 7, has a single layer of conductors which are located in the cross section so as to generate the required field profile to within few units. Special techniques such as the use of low-cost plastic spacers and high precision winding on a computer-assisted machine have been used to reduce the cost of the magnets.

The interesting feature of this magnet is the fact that it has no conductors over a large portion of one side, where the fied is lower, and can hence provide a natural opening for access to the bore. This feature could be used, for instance, to evacuate synchrotron radiation in high field bending and focussing magnets. End design is however not trivial, as well as mechanical support in case of extrapolation to higher fields.

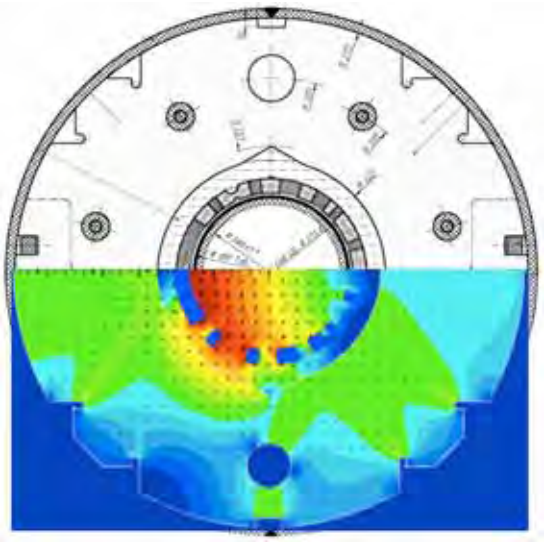

Figure 7. Combined function magnet (dipole and quadrupole) as presently developed for the J-PARC neutrino oscillation experiment [39]

5.4 Magnets for High Radiation Loads

The magnet design can be made tolerant to radiation loads, as generated by particle showers or synchrotron radiation, by changing the design of the cross section. One possibility, as described by Mokhov [40] is to remove cold material from the midplane, where particle showers and synchrotron radiation are mostly concentrated, and intercept the particles and heat loads at higher temperature. A dipole design that goes in this direction is shown schematically in Fig. 8.

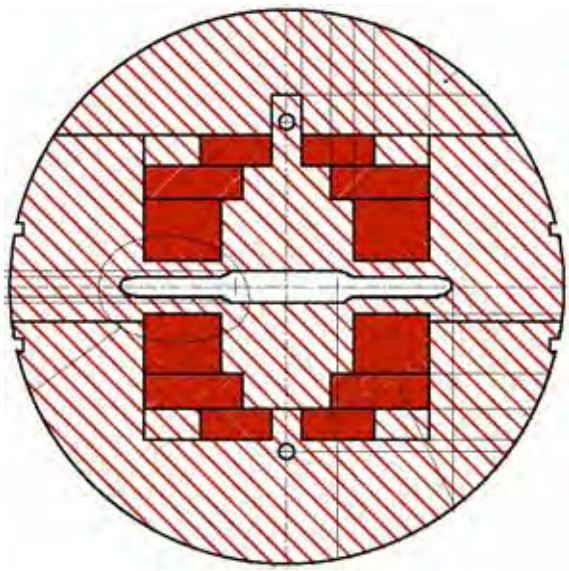

Figure 8. Dipole magnet design with central slit to decrease radiation heat load and dose in the superconducting coil, as described in [40]

The coil is open on the midplane, and the iron is shaped so that the first solid material, where heat load is deposited, is outside the coil perimeter. The midplane slit can be equipped with a dedicated cooling circuit that intercepts heat loads before they diffuse to the superconducting cable. A design of this type is not as efficient as a cos(θ) cable arrangement in terms of A turns required to generate a given bore field. Nonetheless, given the lower cryogenic power to be removed from the coil

and the improved life time, it may still prove optimal for the few magnets needed in a high luminosity IR. Indeed, this could be the separation dipole in front of the IP in one of the variants with the dipole first for the LHC IR upgrade sketched in Fig. 1.

6. SUMMARY

In summary, we can expect the accelerator magnet R&D of the coming 10 years to concentrate on:

- high field, large aperture, radiation resistant dipoles and quadrupoles. Peak field in the dipole is in the range of 16 to 17 T, coil diameter of 100 mm. For the quadrupoles the peak field is in the range of 12 to 13 T and coil diameter of 100 mm. Main challenges are mostly related to the high field, and specifically the development of a suitable high-Jc superconductor in the relevant range of operating field and temperature. the mechanical design, quench protection, heat removal and radiation hardness of the coil insulation;
- pulsed dipoles and quadrupoles in the low to intermediate field range, 2 to 6 T, with coil diameter in the range of 50 to 100 mm, and ramp-rate of few (up to 4) T/s. In this case the main challenges are to achieve the specified ramp-rate with no ramp-rate limitation (premature quenches), low AC loss and low stored energy, as well as field quality suitable for accelerator operation (typical field homogeneity over the good field region within few 10^{-4}). Because these magnets will be used in moderate size series, cost reduction is a major issue in this development
- magnets for specific applications that require either complex magnetic configurations (e.g. wigglers), or combined functions (e.g. dipole + gradient) or additional constraints on the operating conditions (e.g. focussing magnets in background field or magnets for extreme heat load conditions). These special developments will provide verification of alternative design concepts and will likely be test-beds for new techniques.

The spectrum of R&D outlined above is vast, and the challenges will require innovation in materials science (superconducting strands, structures, insulation techniques) as well as new design principles. Most of the work along the lines above has started, either at the stage of conceptual design or with specific R&D and prototyping. Indeed, it is the main aim of these proceedings to describe the material aspects that are most relevant to the development of magnets of future high energy and high intensity hadron colliders.

7. ACKNOWLEDGEMENTS

I am indebted to F. Ruggiero and O. Brüning for the documentation and clarifications on the LHC upgrade scenario. The brief but illuminating discussions with T. Taylor have dissipated uncertainties and doubts. Similarly, I owe to S. Fartoukh some insight in the complicacies of beam physics close to the IP. Finally, I wish to thank A. Devred, D. Tommasini, P. Schnizer, P. Wanderer and A. Yamamoto for the material provided and reported in this note.

8. REFERENCES

[1] M.N. Wilson, Superconducting Magnets for Accelerators: a Review, IEEE Trans. Appl. Sup., 7 (2), 727-732, 1997.

[2] Prof. A. Verdier, Operating LHC at Lower Energies, Proc. of LHC Performance Workshop – Chamonix XII, CERN-AB-2003-008 ADM, 274-278, 2003

[3] J. Rossbach, P. Schmüser, Basic Course on Accelerator Optics, Proceedings of CAS, Fifth General Accelerator Physics Course, CERN 94-01, 17-79, 1994.

[4] F. Ruggiero, LHC Accelerator R&D and Upgrade Scenarios, LHC PR 666, 2003.

[5] O. Brüning, et al. LHC Luminosity and Energy Upgrade: A Feasibility Study, LHC PR 626, 2002.

[6] R. Bailey, What LHC Operation will look like, Proc. of LHC Project Workshop – Chamonix XIII, CERN-AB-2004-014 ADM, 219-221, 2004.

[7] T.M. Taylor, Superconducting Magnets for a Super LHC, Proc. of EPAC 2002, 129-133.

[8] J. Strait, et al., Towards a New LHC Interaction Region Design for a Luminosity Upgrade, Proc. of PAC 2003, 42-44.

[9] The 300 GeV Programme, CERN /1050, 1972.

[10] US LHC Accelerator Research Program High-Field Magnet R&D, Proc. of WAMS Workshop, Archamps, March 22-24, 2004.

[11] A. Devred, High Field Accelerator Magnets Beyond LHC, Proc. of PAC 2003, 146-150.

[12] A. Devred, et al., High Field Accelerator Magnet R&D in Europe, IEEE Trans. Appl. Sup., 14 (2), 339-344, 2004.

[13] A. den Ouden, H. ten Kate, et al., "Quench characteristics of the 11 T Nb3Sn model dipole magnet MSUT," Proc. of 15th Int. Conf. on Magnet Technology, Beijing, China, Science Press, pp. 339–342, 1998.

[14] A.D. McInturff, R. Benjegerdes, et al., "Test Results for a High Field (13T) Nb3Sn Dipole," Proc. of 1997 Part. Accel. Conf., pp. 3212–3214, 1998.

[15] R. Benjegerdes, P.Bish, et al., "Fabrication and Test Results of a High Field, Nb3Sn Superconducting Racetrack Dipole Magnet," Proc. of 2001 Part. Accel. Conf., pp. 208–210, 2001.

[16] A.F. Lietzke, et al., Test results for HD1, a 16 Tesla Nb3Sn Dipole Magnet, IEEE Trans. Appl. Sup., 14 (2), 345-348, 2004.

[17] An International Accelerator Facility for Beams of Ions and Antiprotons, Conceptual Design Report, W.F. Henning, H.H. Gutbrod, K-D. Groß, V. Metag Editors, GSI, Darmstadt, November 2001

[18] A. Devred, T. Ogitsu, Ramp-rate Sensitivity of SSC Dipole Magnet Prototypes, Frontiers of Accelerator Technology, World Scientific, 184-308, 1996.

[19] M.M. Steeves, et al., Test Results from the Nb3Sn US-Demonstration Poloidal Coil, Adv. Cryo. Eng., 37 A, 345-354, 1991.

[20] P. Wanderer, et al., Initial Test of a Fast-Ramped Superconducting Model Dipole for GSI's Proposed SIS200 Accelerator, Proc. of PAC 2003, 2162-2164.

[21] P. Wanderer, BNL Upton, Private Communication, September 2003.

[22] L. Tkachenko, IHEP Protvino, Private Communication, September 2003.

[23] TESLA - Technical Design Report, F. Richard, et al. Editors, DESY 2001-011, 2001.

[24] A. Devred, C. Gourdin, et al., Conceptual Design for the Final Focus Quadrupole Magnets for TESLA, DESY TESLA-2001-17, CEA/DSM DAPNIA-STCM-01-03, 2001.

[25] B. Parker, Superconducting Final Focus Magnet Issues, Presented at Nanobeam 2002, 26th Advanced ICFA Beam Dynamics Workshop on Nanometre Size Colliding Beams, September 2-6, 2002, Lausanne, Switzerland.

[26] D.E. Baynam, B.E. Wyborn, A 5 T superconducting wiggler magnet, IEEE Trans. Mag., 17 (5), 1595-1598, 1981.

[27] J.P. Jacquemin, J. Perot, Design and test of a 5T superconducting wiggler, IEEE Trans. Mag., 24 (2), 1226-1229, 1988.

[28] J.S.H. Ross, K.D. Smith, The development of a superconducting 6T wiggler magnet for the Daresbury SRS, IEEE Trans. Appl. Sup., 3 (1), 813-816, 1993.

[29] S. Sugiyama, H. Ohgaki, et al., Design and manufacture of a 10-T superconducting wiggler magnet at TERAS, Rev. Sci. Instrum., 66 (2), 1960-1963, 1995.

[30] R. Mikkonen and L. Soderlund, A 6 T superconducting wiggler for synchrotron radiation, IEEE Trans. Mag., 32 (4), 2617-2620, 1996.

[31] Y. Mikami, S. Yamada, et al., Development of a 7 Tesla superconducting wiggler, IEEE Trans. Appl. Sup., 9 (2), 483-486, 1999.

[32] G. LeBlanc, E. Wallen, M. Eriksson, The MAX wiggler, Proc. of EPAC 2000, 2334-2336.

[33] D. Berger, M. Fedurin, et al., A superconducting 7T multipole wiggler for the BESSY II synchrotron radiation source, Proc. of PAC 2001, 2450-2452.

[34] A. Devred, Selected Issues Related to the Design and Manufacturing of CESR Wigglers, Private Communication, 2004.

[35] R.Jung, P.Komorowski, L.Ponce, D.Tommasini, The LHC 450 GeV to 7 TeV Synchrotron Radiation Profile Monitor using a Superconducting Undulator, 10th Beam Instrumentation Workshop, Brookhaven National Laboratory, New York, May 2002.

[36] Preliminary Conceptual Design of the 5 T Superconducting Undulators for the LHC 450 GeV to 7 TeV Synchrotron Radiation Profile Monitor, LHC Project Note 299, CERN, 2002

[37] T. Ogitsu, et al., Superconducting Magnet System at th 50 GeV Proton Beam Line for the J-PARC Neutrino Experiment, IEEE Trans. Appl. Sup., 14 (2), 604-607, 2004.

[38] T. Nakamoto, et al., Design of Superconducting Combined Function Magnets for the 50 GeV Proton Beam Line for the J-PARC Neutrino Experiment, IEEE Trans. Appl. Sup., 14 (2), 616-619, 2004.

[39] A. Yamamoto, Status and Plan for Superconducting Accelerator Magnet Development at KEK, Proc. of WAMS Workshop, Archamps, March 22-24, 2004.

[40] N.V. Mokhov, et al., Energy Deposition Limits in a Nb3Sn Separation Dipole in Front of the LHC High-Luminosity Inner Triplet, Proc. of PAC 2003, 1748-1750.

REQUIREMENTS ON SC MATERIALS, STRAND AND CABLE FOR THE FUTURE

D. Leroy
CERN, Accelerator Technology Department, Geneva - Switzerland

Abstract
This paper discusses a few aspects on magnet design, superconducting materials, filament dimension, strand current density, and topology of cable requested to face the high magnetic field for the future needs of CERN

1. INTRODUCTION

For its future needs, CERN will have to build magnets of various types depending on the domain of applications [1].

1. The most demanding are dipoles and quadrupoles having high field between 10 T and 15 T on the conductor and large aperture bores between 90 mm to 160 mm in lengths of circa 10 m. These magnets have a very high stored energy and are submitted to high energy particle losses inducing possible quenches. The heat deposition linked to beam losses are difficult to calculate but it implies that the operating field could be at 80 % of the maximum field. The temperature margin is a crucial value to be taken into consideration. This paper will consider only the maximum field allowable at the present time.

2. Another domain of application are superconducting accelerator magnets at field of 2 to 6 T but operated in a pulsed mode of 0.5 T/s to 5 T/s. The aperture bores and the lengths are respectively of the order of 100 mm and 10 m.

3. The accelerator application can use very long superconducting magnets at low field of 2 T. These magnets have a low cost but have many corrector winding to compensate the iron saturation. The past experience has shown that the lower cost per Tm can be obtained by using the superconducting material at the max field that the sc material can afford. This paper will not deal with the low field superconducting magnets.

The report will review some aspects of the magnet design and the requirements on the materials, strands and cables.

2. MAGNET DESIGN FOR HIGH FIELD AND LARGE APERTURES

2.1 Generalities on critical current densities.

The maximum bore fields in dipoles is proportional to the cable width and to the overall critical density in the coils. Taking into account the insulation thickness of the cables, it appears that to reach dipolar fields as high as 15 T, critical current densities in the non copper part of the order of 1500 A/mm^2, at 15 T, 4.2 K have to be accessible [2].

2.2 Limits of the layer cos θ magnet design

All the magnet structures, built for accelerators are based on the same general layout, called layer design (Fig. 1). They have been built with success for fields up to 10.5 T with NbTi [3] and up to 11 T and 13 T with Nb_3Sn [4, 5]. A design for a 88 mm aperture has been calculated and is presented below [2].

The coil aperture is 44 mm; there is 3 mm space between the two layers. The iron yoke is separated from the coils by an intermediate spacer (collars) of 25 mm thickness and is surrounded by a

28 mm thick stainless steel shrinking cylinder. The inner layer consists of 4 blocks of conductors while the outer is made of 3, adjacent blocks being distant from at least 2 mm. The iron yoke is 350 mm thick.

The critical current density in the non-copper area of the Nb_3Sn strand is assumed to be 1500 A/mm^2 at 15 T, 4.2 K. The copper to non-copper ratio is 1.25. The bore field as calculated is 14.4 T at 4.2 K for a maximum quenching field on the conductor of 15 T taking into account a cable degradation of 10 %. To reach 15 T in the aperture, the magnet has to be operated at 1.9 K.

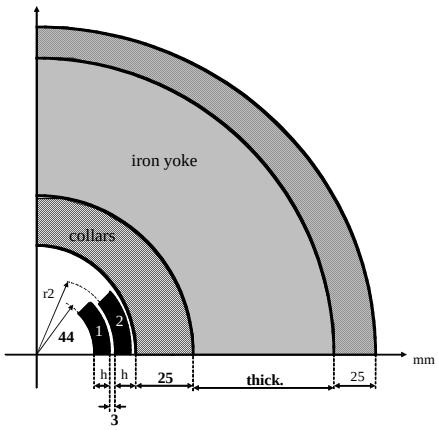

Fig.1 Magnet cross section (layer design)

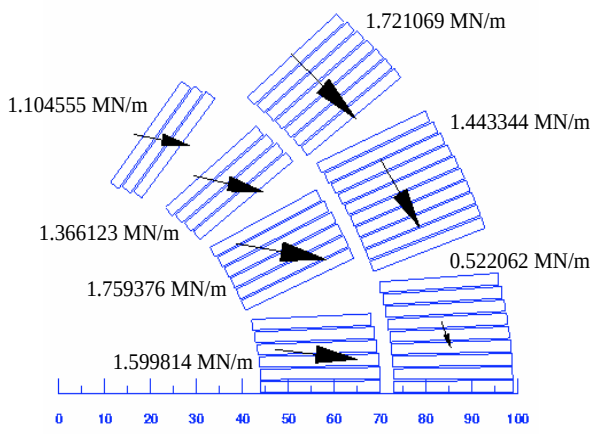

Fig.2 Magnetic force distribution

Fig 2 shows the distribution of the magnetic forces. The axial forces are as high as 1.8 MN for a stored energy of 1.8 MJ/m.

We do not know the limits of the layer cosθ magnet design. They offer a good field quality in large apertures but can be limited by compressive stresses that are maximum at the mid-plane of the layer. At 15 T, j=1500 A/mm^2, the magnetic compressive stresses are 150 MPa on the inner layer and 160 MPa on the outer layer in a 88 mm bore dipole. To the magnetic stresses, it has to be added the stresses due to the mechanical structure deflection under the main horizontal forces that vary from 7 MN/m to 15 MN/m when the field goes from 12 to 15 T. To keep the contact between the conductor and the mechanical support structure at the upper angle of the coil layer, a coil pre-stress of the order of 50 MPa has to be added during the magnet assembly and stays on the mid-plane conductor. It is known that the critical current density in the Nb_3Sn material is sensitive to stresses and degrades for stresses higher than 200 MPa. For the layer design, when the aperture goes from 88 mm to 130 mm and 160 mm, the maximum compression stress due to magnetic forces goes from 150 MPa to 215 MPa and 255 MPa. It seems that, with the high critical current densities in Nb_3Sn superconducting cables, the cos θ layer design could be limited to apertures of circa 90 mm if the degradation process is well understood and perhaps overcome.

2.3 Motor type design

In this design, the rectangular conductors are located in notches machined in a metallic structure (Fig. 3). The winding is performed by inserting the cables in the metallic structure, positioned horizontally with the notches open vertically.

The ends are rather difficult since the cable sees a hard bending. Passing from one notch to the other will take place in the ends where the conductor from the top of a notch goes to the bottom of the other notch.

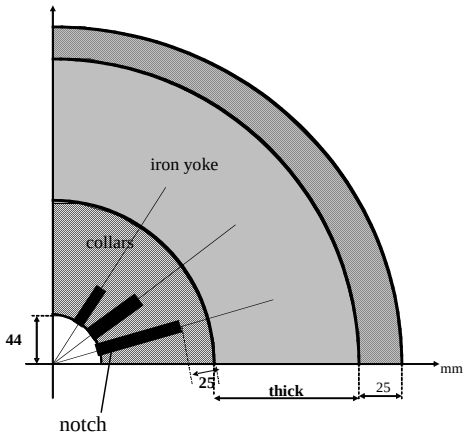

Fig. 3 Magnet cross section (motor type design)

This kind of winding in an open structure and not on a mandrel has already been made at LBNL (Isabelle) for a single layer design. A magnet using the slot design type has already been built at CEA Saclay [6] using a NbTi cable. Figure 4 shows a model magnet investigated at CEA Saclay. It needs a good and clever tooling. This type of approach could be made with the Nb_3Sn cables, which seems to be less "nervous" than the NbTi cables. After winding, the reaction and the impregnation could be performed in the same metallic structure, which becomes a mechanical support for the electro-magnetic forces. Due to the expansion of the Nb_3Sn at reaction, the conductor, located in the closed volume of the notch could need less pre-stress at assembly. Bladders could be incorporated in the notches to put a pre-stress if needed.

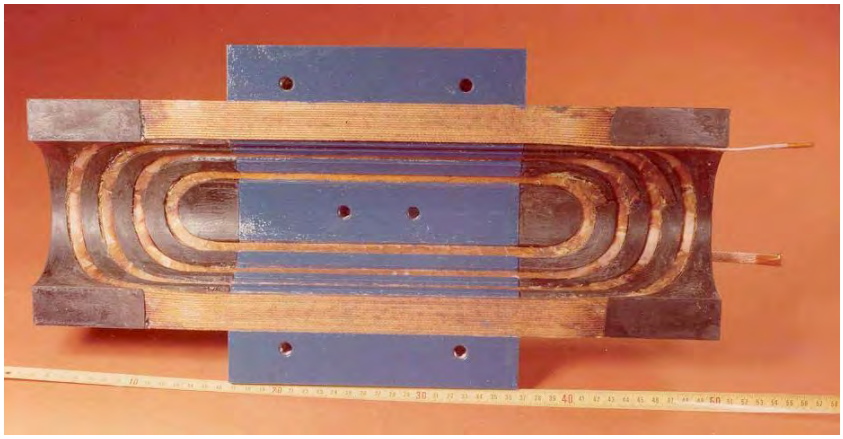

Fig.4 Model magnet built at CEA Saclay

The external mechanical structure would be the same as for the layer design. The two poles are associated by a lateral welding. The yoke is split horizontally and contained in a shrinking cylinder. Cooling of the deepest conductors could be made with copper drains.

In this design, the magnetic forces (Fig. 5) in each slot are radial and are better distributed on the external mechanical structure. The cable is submitted however to an hard bend in the ends of the winding, which is can be conceivable for large aperture dipole magnets. The maximum compressive stress due to magnetic forces stays in the vicinity of 140 MPa for apertures varying from 88 to 160 mm. This magnetic design is less efficient than the layer design. It leads to 13.8 T in the bore for a maximum quenching field of 15 T on the conductor.

A difficulty could be the quench protection for long magnets, which would require quench heaters incorporated in the notches. In this design, the inter-strand losses are reduced since the field is ~ parallel to the broad face of the cables. The quench back effect is then reduced except if the adjacent resistance between the strands of the cables is small.

The advantages of the motor-type design compared to layer design are: more free space on the mid-plane, and about twice more margin on the block closest to the mid-plane with respect to the upper block as in layer magnets, which could be interesting for beam losses.

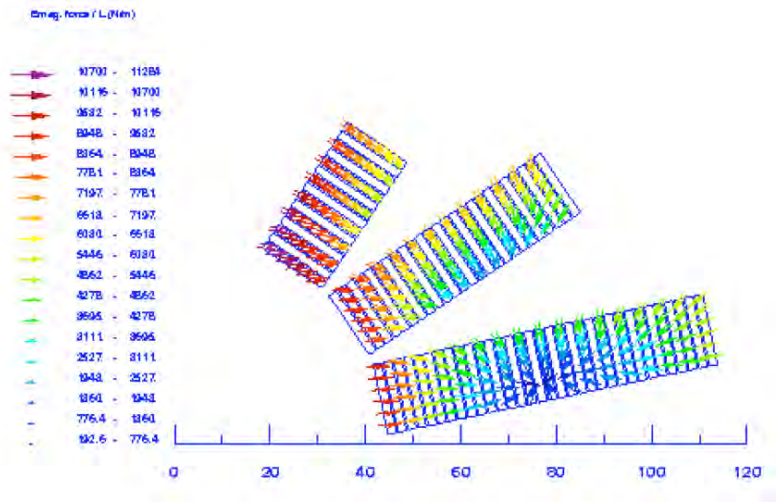

Fig 5 Magnetic forces in a motor-type dipole of 88 mm

2.4 Compensation of the field harmonics due to the filament size

The Nb3Sn filaments have an effective diameter larger than 50 μm leading to high magnetization effects at low field. The field components inside the winding are expressed by:

$$Br=[B_1+B_0(r_2-R/r_2-r_1)+B_0(R^3-r_1^3/3R^2(r_2-r_1)]\sin\theta$$

$$B_\theta=[B_1+B_0(r_2-R/r_2-r_1)-B_0(R^3-r_1^3/3R^2(r_2-r_1)]\cos\theta$$

where $B_1$and B_0 are respectively the iron contribution and the coil contribution to the main field, R is the radial coordinate. It can be seen how the field varies inside the winding. By inserting a paramagnetic material inside the coil winding, currents will be generated inside the material according to:

$$j'z=dM_\theta/dr - dMr/d\theta$$

These currents will create field components in opposition to the field components created by the sc diamagnetic currents. At 5 T, an iron wedge in the inner layer of the 15 T magnet will still generate a sextupole of 25 units [2] (Fig. 6).

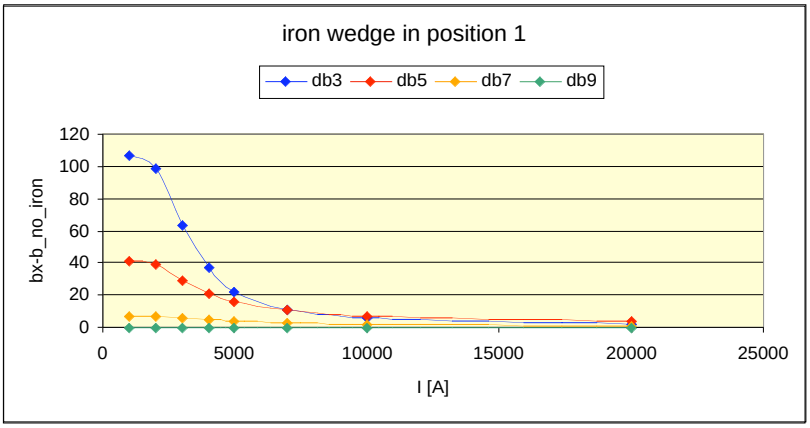

Fig. 6 Multipoles due to iron wedge to compensate the diamagnetic effects

3. SUPERCONDUCTING MATERIALS,STRANDS AND CABLES

A kind of axiom is that it is feasible to build a good magnet at a field X when a current density between 1000-2000 A/mm^2 is obtainable at the field X.

3.1 Superconducting materials

The values of critical current densities in the non copper part can be seen in a plot from S.Gourlay [7] (figure 7).

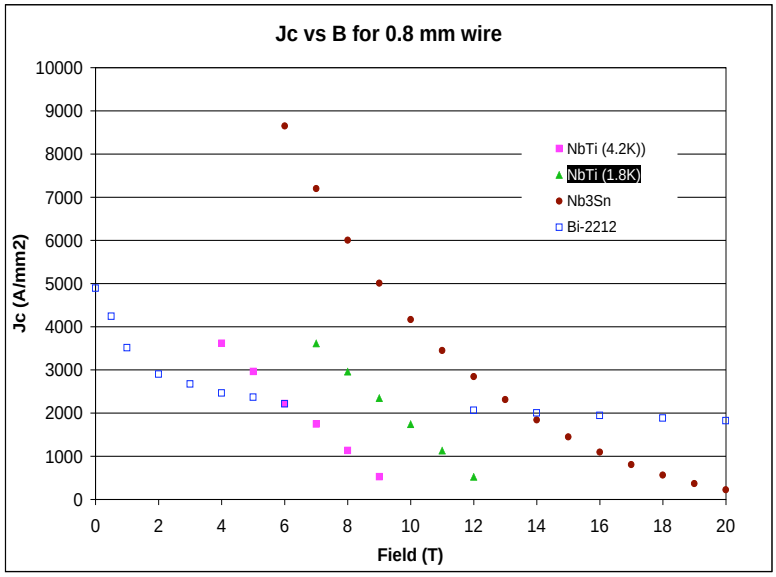

Fig.7 Critical current densities in non copper

From this graph, the following values can be kept in mind:

NbTi 1200 A/mm^2 at 11 T, 1.9 K (obtained)
NbTiTa 1200 A/mm^2 at 12 T, 1.9 K (to be proven)
Nb_3Sn 1500 A/ mm^2 at 15T, 3000 A/mm^2 at 12T and 4.2 K (under development).
Bi-2212 2000 A/mm^2 at 20 T, 4.2 K

Working at 1.9 K with Nb3 Sn could bring a field increase of 0.7 T for the same critical current density.

With the Bi-2212, no accelerator magnet has been built and tested yet.

To build accelerator magnets in the range of 15 T, the Nb_3Sn is the usable superconducting material that is today in an advanced phase of development. For magnets in the vicinity of 10 T, NbTi material at 1.9 K stays the preferable material.

3.2 Filament size, matrix material, strand diameter

The requirements on the filament size are governed by the flux jump stability, the diamagnetic losses and the effect on the field harmonics at low field.

For the NbTi, filament diameter of 6-7 μm are obtained industrially in a copper matrix on a large scale, like for LHC, thanks to the introduction of a Nb barrier around the NbTi bars. The strand diameter is around 1 mm for a current of 500 A at 10 T. Filament size of the order of 3.5 μm can even been obtained in a copper matrix. Below 3 μm, a matrix of CuNi or CuMn has to be used. If the filament size has still to be reduced, the strand diameter will be smaller than 0.5 mm. In this case, the cabling with a high number of strands to fabricate a high current cable needed for the accelerator magnets can be challenging.

With the Nb_3Sn present technology used to reach high critical current density, the filament size is today close to 100 μm but should be reduced to less than 50 μm in the future.

3.3 Strands

Long length accelerator magnets are operated at high current, close to 20 kA, to have a small self-inductance and a reliable quench protection. The usual strand diameter is in the range of 1mm to have cables made of ~40 strands. The copper amount requested for the magnet protection in case of quench has to be calculated for each magnet design. A copper to non-copper ranging between 1.1 and 1.3 can be used for Nb3Sn magnets whereas a ratio of 1.5 to 1.8 is recommended for NbTi magnets. The total amount of copper in Nb3Sn conductor can be reduced in compression with NbTi, since the enthalpy of the bronze helps to reduce the temperature in case of a quench.

4. INTER-STRAND RESISTANCE

There is an electrical resistance (Rc) between the strands of the 2 layers of the cable and a distributed conductivity along the length of the 2 adjacent strands. The inter-strand resistance Rc has a major impact on the ac losses. The cable losses vary with the square of the cable aspect ratio and are very significant for wide flat cables (e.g 26 mm for a 15T magnet designed with 2 layer coils). The values of Rc are governed by the coating material, the strand deformation, the coating rugosity and the local pressure at cabling.

4.1 Coating Materials and Rc values

Table 1 indicates some values of Rc obtained in Rutherford type cables. SnAg is used for LHC. Without coating, the Nb3Sn strands have a tendency of sintering at the reaction temperature of 700 °C. Cr is used for ITER but is difficult in cabling Rutherford type cables requested for accelerator magnets of the layer design.

Table 1 Some values of the inter-strand resistance

Material	Rc(μΩ)	Comments
SnAg	10-50	after a cable heat treatment at 200 °C, not usable at 700 °C
Sn Ni	100-500	not usable at 700° C(?)
Ni	500	-diffuses in Cu at 700 °C(?) -suffers from environmental constrains
Cr	700-1000	-usable at 700 °C -depends strongly on the deposition process

4.2 Cored Cables with a Stainless Steel or Ta core

Another possibility to cut the inter- strand currents is to introduce in the cable between the 2 layers of strand a foil made of stainless steel or Ta as proposed by L.Krempasky and M.Wilson (Fig. 8). The thickness of the foil is in the range of 25-50 μm. The values of Rc are around 1 Ω for cored cables. During the LHC cable R&D phase, M.Wilson has proposed to improve the cable electrical stability, by soldering the adjacent strands.

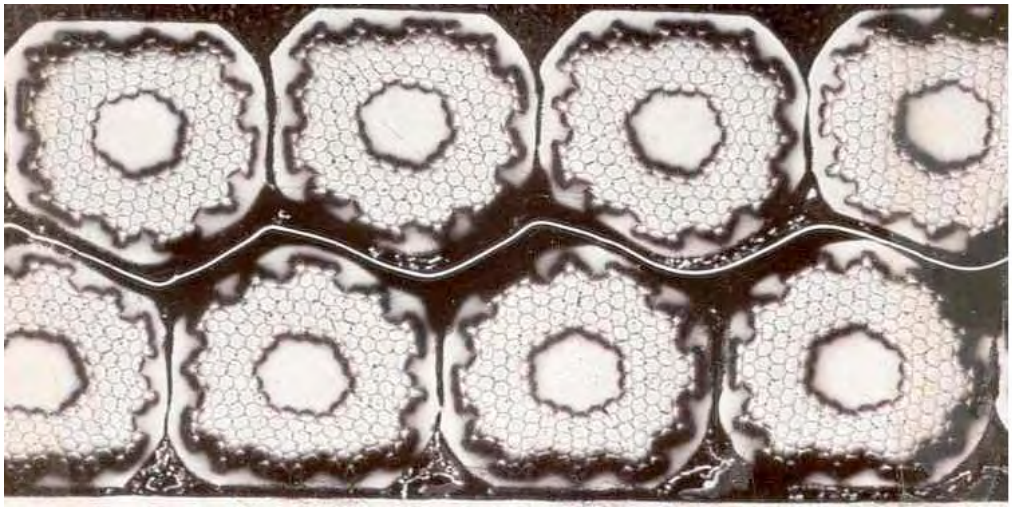

Fig. 8 A cored cable

4.3 Materials for strand coating

In the frame of the LHC programme, many materials have been looked and measured. The values reported in Table 2 are normalised in $\mu\Omega mm^2$, product of the resistance times the contact area.

Table 2 Materials for coating

$\mu\Omega mm^2$	material	Comments
10	SnAg	soft coating, creeps
100	SnNi	
500	Ni, ZnNi	hard coating, cracks occurred Ni oxidized preferentially to Zn
1000	Ni+NiP Zn	thick oxide layer
10^4	passived Zn	Oxide layer
10^6	Oxidized Cu	

4.4 Strand deformation and coating surface topology

The coating roughness and the local pressure at cabling play a role since the inter-strand currents are passing through small local contacts squeezed at cabling. Figures 9 and 10 show the deformed contact surface after cabling and the surface local irregularities through which the inter-strand currents are passing. These figures have been obtained by measurements on the LHC strands and cables made by J M Depond at CERN.

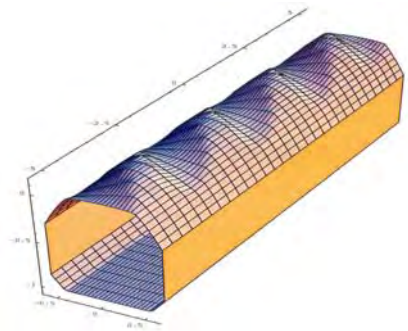

Fig. 9. Strand deformation at cabling

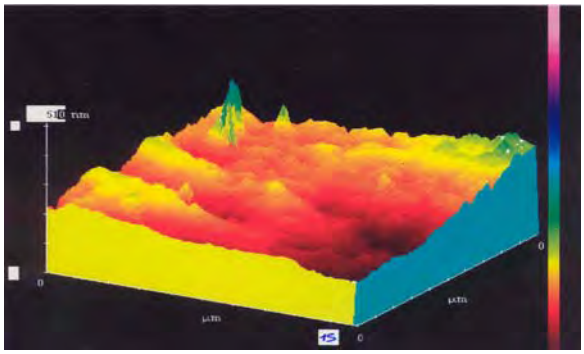

Fig. 10 Rugosity of the coated strand

5. CABLES

Cabling requires special machines and dedicated tools (mandrels and rollers) of high mechanical precision. The geometrical dimensions of cables are obtained after trials. They have to insure a good mechanical stability for winding. In case on the Nb_3Sn cables, degradation due to cabling has to be measured. The relations given here are based on the work made at LNBL [8] for Nb_3Sn and at CERN for NbTi. The expressions that are for strands of diameter around 1mm give the relations for the thin edge ($width\_inner$), the thick edge ($width\_outer$) versus the strand diameter and the number of strands.

for keystoned cable:

$$height = 1.04\frac{nbr\_str}{2}\phi_{str}\ ;\ width\_inner = 2*0.87\phi_{str}\ ;\ width\_outer = 2*0.95\phi_{str}$$

where ϕ_{str} is the strand diameter and nbr_str the number of strands in the cable;

for rectangular cable:

$$height = 1.04\frac{nbr\_str}{2}\phi_{str};\ width = 2*0.87\phi_{str}$$

The geometrical dimensions of NbTi cables are as following for keystoned cables:

$$height = 1.015\frac{nbr\_str}{2}\phi_{str}\ ;\ width\_inner = 2*0.82\phi_{str}\ ;\ width\_outer = 2*0.95\phi_{str}$$

The edges of the cables must not be sharp and be free of burrs to avoid problems of electrical insulation.

6. MAGNETS

The following paragraphs comment the feasibility of magnets for the various applications.

6.1 AC magnets in the range of 5 T and 0.2T/s

The superconducting material is NbTi operated at 4.2 K in a circulating sub-cooled helium. These magnets can be like the TEVATRON magnets. At FNAL, the cables were of the Zebra type (one copper strand adjacent to an oxidised strand). At CERN a magnet using a Rutherford cable impregnated with SnIn alloy to reduce the cable losses has been built and can produce 5 T in 25 sec. The magnet technology is well known.

6.2 AC magnet in the range of 5 T and 5 T/sec.

An example of this type of magnet is the GSI project. The superconducting material is NbTi at 4.2 K. The strand diameter is ~0.8mm. The filament size is 3 μm in a copper or a CuMn matrix. The diamagnetic losses in the NbTi filaments are dominating at field ramp since the cables have a stainless steel core. The filament twist pitch is in the range of 6-10 mm.

The conductor cooling is realized by making holes in the insulation. During the GESS collaboration (CEA-Saclay, Karlsruhe, Rutherford Lab) magnets of these field ramp characteristics have been built in 1974. Some magnets had Cu drains for cooling.

For a long chain of magnets in series, high current (10-20 kA) are preferable to reduce the self-inductance and then the impact on the electrical mains at the machine ramp. The magnet technology is known.

6.3 DC high field magnets- up to 10.5 T

The superconducting material is NbTi working at 1.9 K. The critical current density Jc reaches 1100 A/mm2 at 11 T. The strands are made of 10'000 filament having a diameter of 5-7 μm embedded in a copper matrix with a Cu to Superconductor ratio of 1.6-1.8.
The cable compaction ranges between 88 to 90 % allowing a content of 3 % of helium II that participates to the enthalpy. At superfluid helium, beam losses in the coils up to the equivalent of $10mW/cm^3$ should not induce a quench in the magnet where the cables are insulated by a double wrap and polyimide ribbon.
The magnet construction uses a known technology applied on an industrial scale for LHC (1248 dipoles, 15 m long). A bore field of 10.5T has been reached in magnets of this type like MFISC [3] and MFRESCA [9] that is in operation at 10.3 T for many years at CERN.

6.4 DC High field magnet up to 11 - 11.5 T

The superconducting material candidate is NbTiTa at 1.9 K that has to be developed. The raw material must have, more particularly, a high homogeneity, a small grain size. Unfortunately, even if Bc_2 is increased by 1 T at 1.9 K, high critical current densities have not been reached. No real systematic attempt has been conclusive to obtain high Jc (after the work made by Mc Inturff & Larbalestier for the construction of quadrupoles) The development of the NbTiTa alloy would permit an increase of the magnet field by 1 T. The technology for the magnet construction is known and is similar to the NbTi technology working at 1.9 K.

6.5 DC high field magnet at 4.2 K in the range of 15-16 T

The superconducting material is Nb_3Sn made by the processes called Internal Tin Diffusion (ITD), and Powder In Tube (PIT). Another technology called Bronze Route has allowed building magnets up to 9.4 T in the aperture, but is not able to reach the critical current densities required for magnets of 15 T. With the ITD and the PIT process, critical current densities of 1500 A/mm^2 at 15 T and 3000 A/mm^2 at 12 T are close to be reached on an industrial scale thanks to the development made in USA.

Development is starting as well in Europe via the NED project [10]. Up to now, the equivalent filament size, defined by magnetisation measurements, is in the range of 80 – 100 μm, still too thick for accelerator type magnets and to avoid flux jumps. The R&D work is concentrated now on the aim of high critical current densities with filaments in the range of 30 to 50 μm. For a magnet designed to quench at 15 T, the temperature margin would be 1.4 K at 13 T and 2.6 K at 12 T. To reach higher dipole fields, the magnet must be operated at 1.9 K.

The technology of construction for accelerator magnets consists in making the reaction at ~650 °C after the winding of the coils. The creation of the Nb_3Sn phase creates a volumic expansion in the strand of ~30 % that could lead to a change in strand dimensions of ~3 % transversally and ~3% longitudinally. However, at Fermi Lab, it has been reported that the strand diameter expansion in the range of 2 to 3 % depends on the process of fabrication and the cable length contracts during reaction. There is an experience of construction of short models but the construction of long magnets is still challenging.

7. CONCLUSIONS

The conclusions refer to the quenching magnet field. The operation field has to take into consideration other factors like beam losses and the temperature margin. The calculation tools and the expertise exist for the design of magnets for the future needs. The calculation tools and the expertise exist for the calculations of the strand and cable characteristic effects on the magnets.

The superconducting NbTi material is well known and is usable for long magnets up to 10.5 T, in DC mode or 6 T in AC mode up to at least 5 T/s.

The superconducting NbTiTa material needs development to gain 1 T in the bore field. The technology of construction is known but the development effort has to be balanced with the small gain of 1 T.

The Nb_3Sn has made enormous progress thanks to the efforts in USA. A field up to 16 T has been reached in a small gap dipole by the group of LBNL. The development of the Nb_3Sn conductor has to be pursued. We must be able to build large bore magnets with Nb_3Sn in the range of 12-16 T following the wind and react route. The construction of long magnets is still challenging.

ACKNOWLEDGEMENTS

The construction of superconducting magnets for accelerators has an history of more than 35 years. During all this years, many contributors and many laboratories have developed the strand, cable, and magnet technology so that many of their ideas seem to be in the public domain. It is impossible to mention here, in the references, all the authors. They are well known in the superconducting community for accelerators magnets. The author wish to thank all the persons at CERN and in the other laboratories for their contribution in the topics mentioned inside this paper and present his excuses for those, very numerous, who are not named in the references.

REFERENCES

[1] L. Bottura, Need of high field and / or pulsed Sc magnets for HEP Colliders, WAMS (Workshop on Accelerator Magnet Superconductors), 22-24 March 2004, Archamps, France.

[2] D. Leroy and O. Vincent-Viry, Preliminary Magnetic Designs for Large Bore and High Field Dipole Magnets, to be published (2004)

[3] D. Leroy, L. Oberli, D. Perini, A. Siemko, G. Spigo, Design Features and Performances of a 10 T Twin Aperture Model Dipole for LHC, 15 th International Conference on Magnet Technology, Beijing, China (1997)

[4] A. den Ouden, H.H.J. ten Kate et al., Quench characteristics of the 11 T Nb3Sn model dipole magnet MSUT. In L. Liangzhen, S. Guolia and Y. Luguang (eds.), Proceedings of 15th International Conference on Magnet Technology (MT 15), Beijing, China: Science Press, pp. 339-342,(1998)

[5] A.D. McInturff, R. Benjegerdes et al., Test results for a high field (13 T) Nb3Sn dipole, Proc. of 1997 Particle Accelerator Conference (PAC'97), IEEE Catalogue 97CH36167, pp. 3212–3214, (1998).

[6] A. Patoux, J. Perot First Results of Slot Dipole at Saclay, III International ICFA Workshop, Protvino, USSR (1981)

[7] S.A. Gourlay, U S L H C Accelerator R&D Program,WAAM,17-18 March 2003, Archamps, France.

[8] R. Scanlan, The USA experience on Nb3Sn and Bi-based superconductors and future plans, WAMS (Workshop on Accelerator Magnet Superconductors), 22-24 March 2004, Archamps, France.

[9] D. Leroy, G. Spigo, A. Verweij, H. Boschmann, R. Dubbeldam, J. Gonzalez-Pelayo, Design and Manufacture of a Large Bore 10 T Superconducting Dipole for the CERN Cable Test FacilityProceedings of the 16th International Conference on Magnet Technology (1999), Ponte Vedra Beach, USA

[10] A. Devred, D.E. Baynham, L. Bottura, M. Chorowski, P. Fabbricatore, D. Leroy, A. den Ouden, J.M. Rifflet, L. Rossi, O. Vincent-Viry and G. Volpini. High Field Accelerator Magnet R&D in Europe" Proceedings of the MT18 Conference, 20-24 October 2003, Morioka, Japan

US LHC ACCELERATOR RESEARCH PROGRAM HIGH-FIELD MAGNET R&D

James Strait
Fermi National Accelerator Laboratory, Batavia, IL 60510, USA
For the BNL-FNAL-LBNL-SLAC US LHC Accelerator Collaboration

Abstract
The US LHC Accelerator Research Program is a collaboration of four US National Laboratories (Fermilab, BNL, LBNL and SLAC) which has been formed to work with CERN on the commissioning, accelerator physics, and upgrades of the LHC. The largest single part of this program is planned to be the development of the next generation of high field superconducting magnets, made with Nb3Sn, for a new interaction region that would be part of an LHC luminosity upgrade.

1. INTRODUCTION

The US LHC Accelerator Research Program (US LARP) is a collaboration of four US National Laboratories (Fermilab, BNL, LBNL and SLAC), which has been formed to work with CERN to advance the performance of the LHC by helping commission the machine, conducting accelerator physics research, and doing R&D towards upgrades of the LHC. The goals of this program are:

To advance high energy physics:
- Help bring the LHC on and up to design performance quickly.
- Improve LHC performance by advances in understanding and instrumentation.
- Use LHC as a tool to gain deeper knowledge of accelerator science and technology.
- Extend LHC as a frontier high energy physics instrument with a timely luminosity upgrade.

To advance U.S. accelerator science and technology:
- Keep skills sharp by helping commission the LHC.
- Conduct forefront accelerator physics research and development.
- Advance U.S. capabilities to improve the performance of our own machines.
- Prepare U.S. scientists to design the next generation hadron collider.
- Develop technologies necessary for the next generation of hadron colliders.

To advance international cooperation in high energy accelerators, which is crucial for the future of high energy physics.

The major elements of the US LARP are 1) to help commission the LHC, both hardware commissioning, principally of the equipment that the US National Laboratories are providing for the LHC, and commissioning of the full LHC complex with beams; 2) development of beam instrumentation and second generation collimators to help commission the LHC and bring it to design performance; 3) to use the LHC as a vehicle for fundamental accelerator physics research, and 4) to perform accelerator physics studies and advanced magnet R&D directed towards a timely luminosity upgrade. The US LARP high-field magnet R&D program is the main subject of this paper.

2. NEW INTERACTION REGIONS FOR A LUMINOSITY UPGRADE

The final focus system in the interaction regions (IR) is expected to be among the systems that will eventually limit the performance of the LHC, and replacing them with new higher performance magnets, possibly with a new layout or optical configuration, is expected to be one of the main routes

to higher luminosity. A survey of possible new IR's has been presented in [1], and a detailed study of all of the options for increasing the LHC luminosity beyond its nominal value is reported in [2].

Three major factors drive the designs of new IRs: minimizing β^*, minimizing the effects of long-range parasitic beam-beam interactions, and the large radiation power due to the pp collisions (9 kW/beam at 10^{35} cm^{-2} s^{-1}) directed towards the IRs. The first two factors point towards maximizing the magnet apertures and minimizing their distances to the IP, and the solutions to the third must be considered in designing the new configuration. The two main types of final focus systems under consideration – quadrupoles first or dipoles first - determine the principle magnet requirements which in turn drive the magnet R&D program.

The first type, shown in Fig. 1, essentially duplicates the existing IR design, in which the quadrupole triplet is the closest set of magnet to the interaction point (IP), and the two beams, which collide with a small crossing angle on the order of 0.5 mrad, pass through the same single aperture quadrupoles. Use of Nb_3Sn superconductor allows a considerably higher pole-tip field than in the baseline NbTi quadrupoles. This permits a larger aperture (up to 110 mm[3] versus 70 mm in the baseline design) for the same 200 T/m operating gradient, which finally allows a smaller β^* to be achieved. About a factor of 3 reduction in β^* appears possible by this route[1]. A pair of dipoles deflect the beams into the twin-aperture magnets that make up the rest of the machine. The first, single aperture dipole of this pair is shown in Fig. 1. Use of Nb_3Sn here allows this magnet to be very strong (up to 15 T), which separates the beams more quickly than in the baseline design and modestly reduces the number of parasitic beam-beam interactions. Since this magnet can be very short, much of the collision debris exits the magnet rather than being absorbed in it.

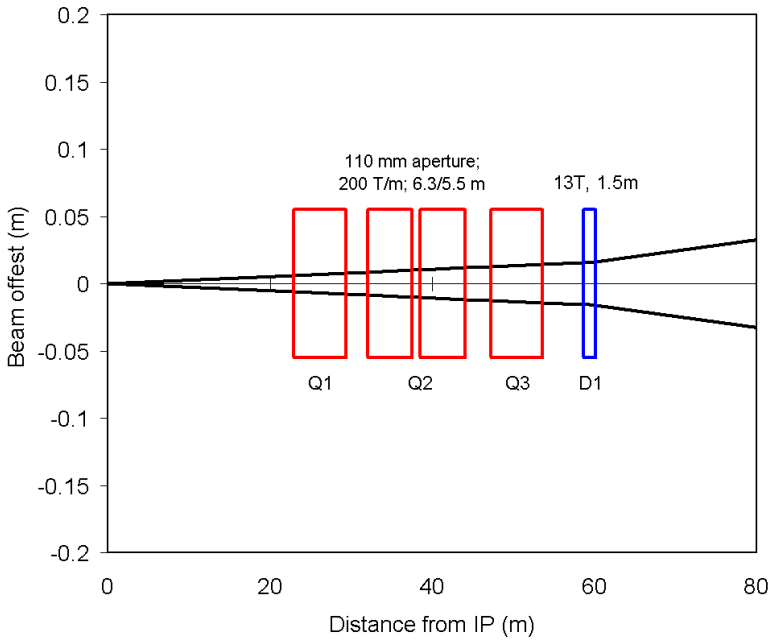

Fig. 1 Quadrupoles-first interaction region.

In the second type of IR, show in Fig. 2, the beam separation dipoles and quadrupole triplet are exchanged. The early separation of the beams reduces the number of parasitic collisions by more than a factor of three. Also, correction of quadrupole field errors is more robust, since the beams pass through the quadrupoles on axis and independent correction elements can be used for each beam. However, the quadrupoles are considerably farther from the IP, increasing β_{max} for a given β^*. The D1 also suffers very large energy deposition from collision debris, since the majority of the forward

charged particles will be swept into it by the large magnetic field [4]. An added challenge is to maintain good field quality in the D2 with strong coupling between the two close, high-field apertures.

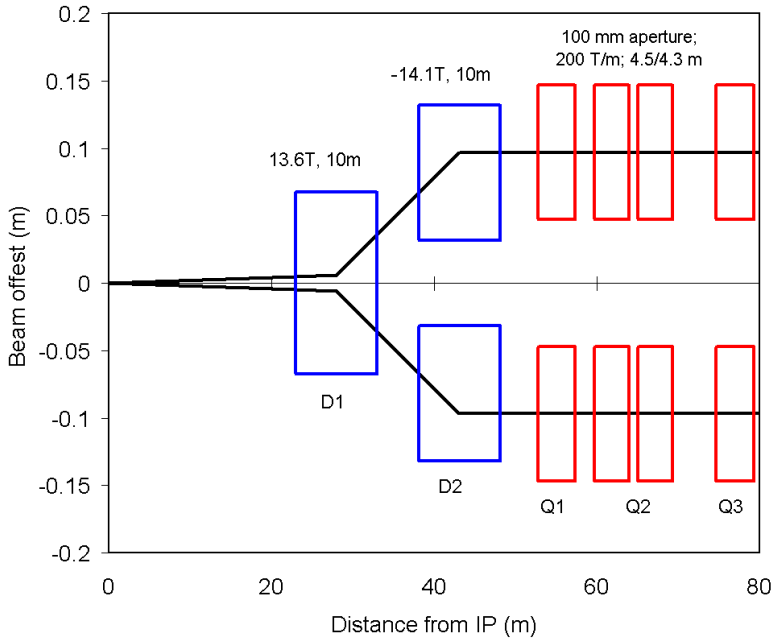

Fig. 2 Dipoles-first interaction region.

Energy deposition and radiation are major issues for the new IRs, which will determine the designs of the magnets and place significant restrictions on the usable materials. Figure 3 shows the peak density and total power deposited in a quadrupole-first IR as a function of position along the beam at L = 2.5 x 10^{34} cm^{-2} s^{-1}[5]. Scaling this result to the goal of 10^{35} cm^{-2} s^{-1}, the peak power density is more than 4 mW/g. At this radiation level, the lifetime of G11-CR is less than six months. The peak linear power density of at least 120 W/m and the total power deposition in the inner triple of at least 1.6 kW will be major challenges for the magnet design and for the cryogenic system.

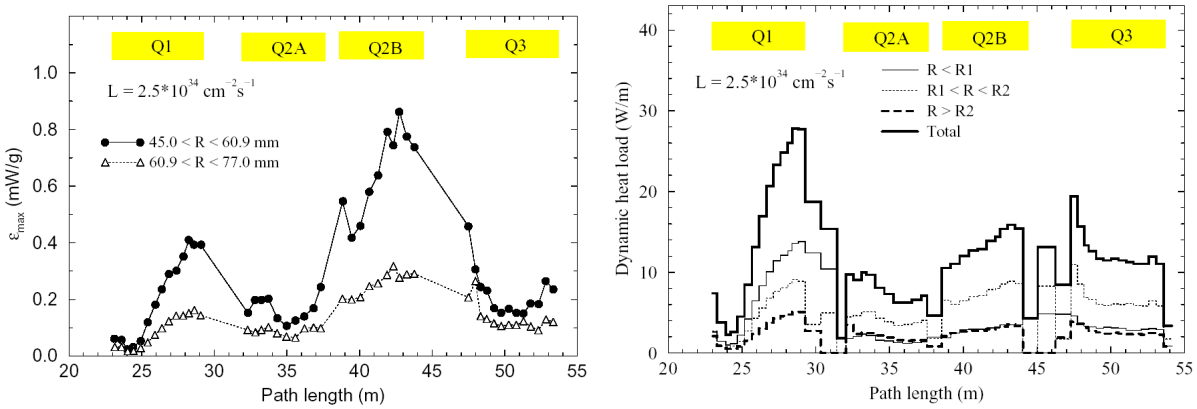

Fig. 3 Peak local power deposition (left) and linear power density (right) in a quadrupole-first IR at L = 2.5 x 10^{34} cm^{-2} s^{-1}.

The problem is even more severe in a dipole first IR. Figure 4 shows the power density in a cross-section at the non-IP end of the D1 dipole for two different dipole design concepts[4]. The peak deposition occurs on the mid-plane, as most forward charged particles from the p-p collisions are swept out of the beam by the high magnetic field. The peak power density at L = 10^{35} cm^{-2} s^{-1} is on the order of 50 mW/g, more than an order of magnitude above the quadrupole first case at the same luminosity, and more than two orders of magnitude above the peak levels expected to be encountered in the baseline IR magnets. The total power deposited in this one 10-m long magnet is calculated to be 3.5 kW. Clearly only the most radiation-hard materials can be used, and "exotic" designs, such as the one shown on the right of Fig. 4 which has no material on the mid-plane in the coil region, may be required.

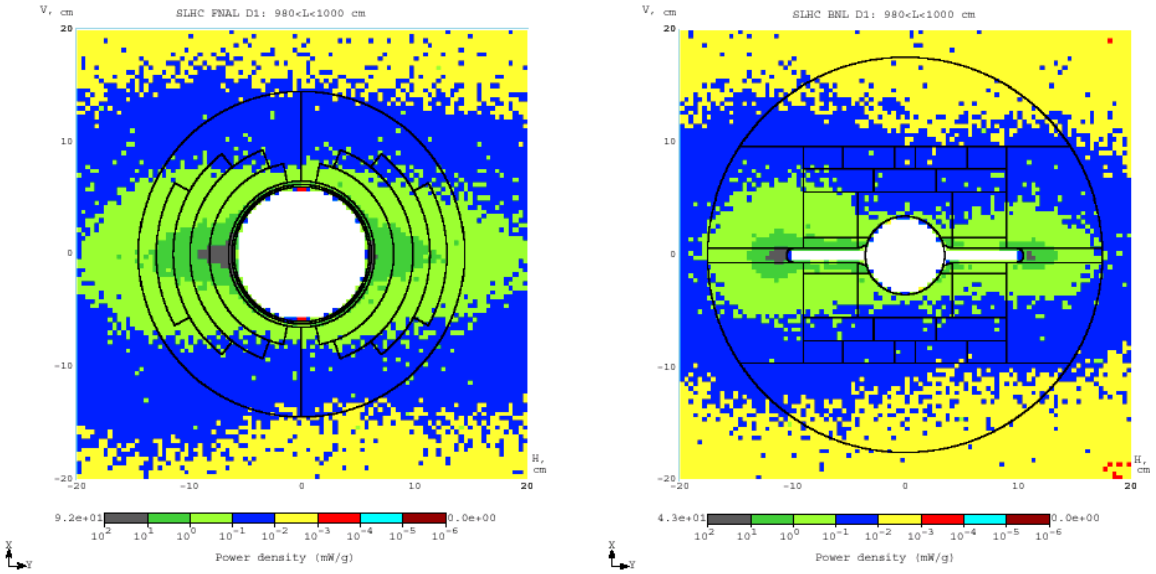

Fig. 4 Power density isocontours (mW/g) at the non-IP end of two different design concepts for a D1 in a dipole-first IR at L = 2.5 x 10^{34} cm^{-2} s^{-1}.

2. MAGNET R&D FOR A LUMINOSITY UPGRADE OF LHC

The actual form of the upgraded interaction regions will not be decided until there is a reasonable amount of running experience with the LHC, which will indicate which factors are most important in limiting the machine performance, and therefore which design will offer the best route to higher luminosity. In order to explore the range of magnet designs that may be required, the US LARP, working in close collaboration with CERN, will initially pursue R&D on both quadrupoles and dipoles. In particular, the aim is to develop quadrupoles with the largest possible aperture with operating gradient >200 T/m, as required for any new IR, and large-aperture dipoles of the highest possible field that can operate in the extreme radiation environment of a dipole-first IR. The goal of this program is to complete R&D leading to one or more accelerator-ready designs, ready for production in the early part of the next decade, which we anticipate as being the time scale required for a luminosity upgrade. Certainly a vigorous program to develop Nb_3Sn technology will be required to support this goal.

The main phases of this program are the following:

2004-05:
- Accelerator physics studies of IR issues and designs.
- Magnet design studies to identify feasible designs and critical R&D issues.
- Begin technology R&D focused on the critical topics.

2006-09:

- Model magnet R&D to develop quadrupole and dipole technologies and learn what are feasible goals for IR upgrade designs.
- Continue focused technology development.
- Continue accelerator physics studies, including beam studies once the LHC is operational.
- Choose upgrade IR design in 2009 or 2010.

2010-2012:

- Develop final designs to a production ready state, including assembly of one or more prototypes.
- Prepare for magnet production for the new IR.

Initial conceptual design studies have begun on both dipoles and quadrupoles. For example, Fig. 5 shows magnetic field calculations comparing race-track coil and cos2θ quadrupole designs[6]. The more conventional shell-type magnet has a coil aperture of 110 mm, which is the largest that can achieve an operating gradient of 200 T/m with a 20% operational margin assuming a Nb_3Sn critical current density of 3000 A/mm^2 at 12 T and 4.2 K[3]. The race-track coil has an aperture across the poles of 92 mm, which yields approximately the same physical aperture for two beams with a horizontal or vertical crossing plane as the 110 mm circular aperture quadrupole. Results of this very preliminary study indicate that the gradient that can be achieved with the race-track design, for the same peak field in the coil, is only a few percent less than with the cos2θ design. However, the superconductor volume is almost 60% larger in the race-track design, the stored energy per unit length is almost twice as large, and the field quality appears to be more sensitive to random conductor placement errors. The race-track coil is attractive for use with the difficult and brittle Nb_3Sn superconductor, and this could may outweigh the disadvantages of superconductor volume and stored energy, but it certainly cannot be used in a twin-aperture design, due to the much greater width of the coils on the mid-plane.

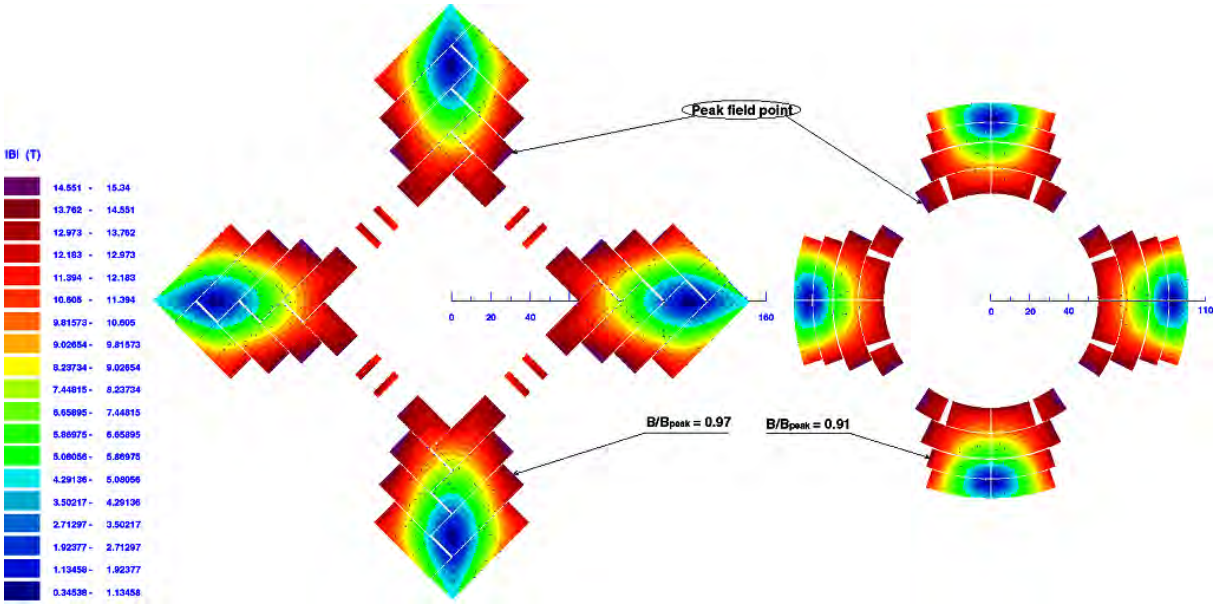

Fig. 5 Coil cross-sections of 92 mm race-track and 100 mm cos2θ quadrupole conceptual designs.

Design studies for a 15 T dipole with an open coil mid-plane, as required for the extreme radiation environment of a dipole-first IR, are at a very early conceptual stage. For example, Fig. 6 shows a concept for a block-type coil, built into a steel support structure which holds the upper and lower coils apart[7]. The closest material along the mid-plane is well outside the coil region, and, in

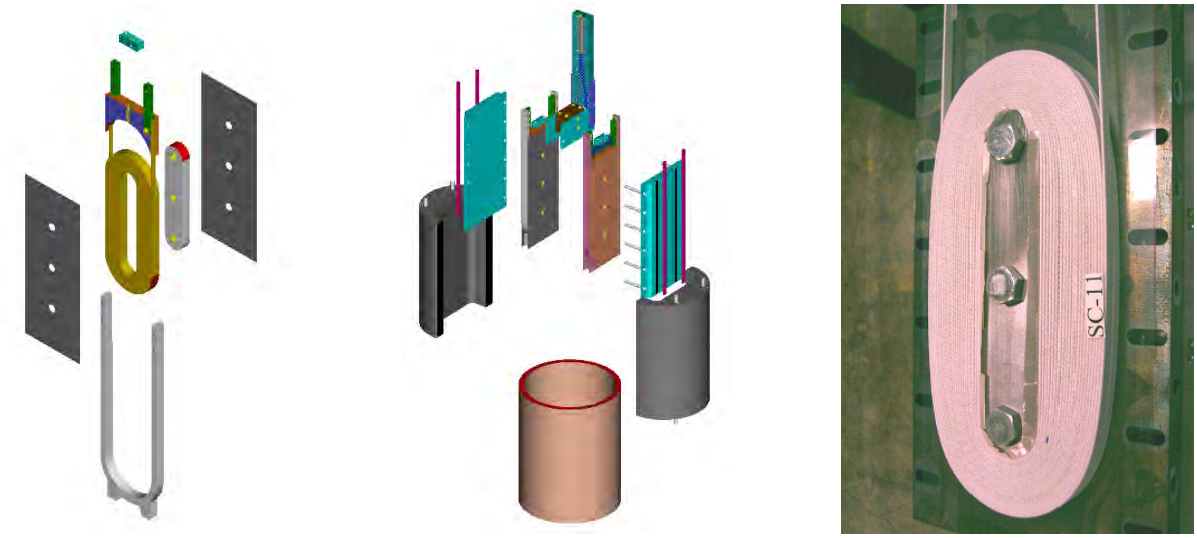

Fig. 7 Sub-scale models. Left: 3D CAD model of an individual race track coil. Center: 3D CAD model of a 2-coil subscale model assembly. Right: Photograph of an actual subscale coil.

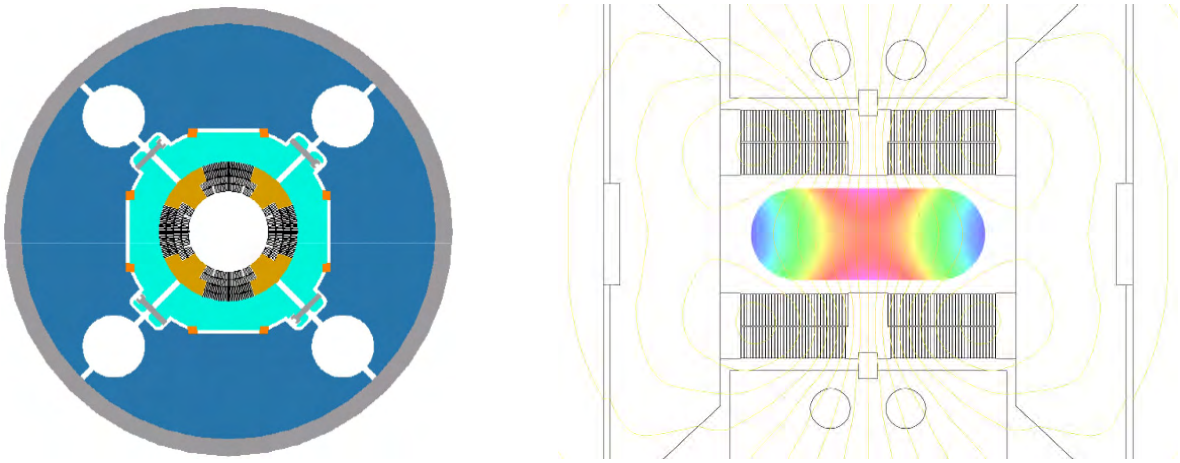

Fig. 8 Design concepts for simplified quadrupole (left) and dipole (right) models.

The programs at the three US Laboratories, while not explicitly coordinated, nonetheless complement each other. The emphasis of the LBNL program is the development of new technologies with the goal of achieving the highest possible field, without, however, initially being concerned about the practicality of the configuration for use in an accelerator. The Fermilab program focuses on development of practical designs for accelerator applications that would operate at moderately high fields in the range of 10-12 T. BNL is directed towards development of react-and-wind technology for both Nb_3Sn and high temperature superconductors (HTS).

The LBNL magnet group has built a sequence of magnets in different geometries which have each, in turn, reached a world-record field for accelerator-like magnets. D20 was a $\cos\theta$ coil, which reached 13.5 T[11]. This was followed by RD-3b, which achieved 14.5 T in a common coil configuration[12]. The current record field of 16 T is held by HD-1, a block-coil magnet (see Fig. 9)[13]. This magnet illustrates the LBNL approach, in that it makes very efficient use of the superconductor and support structure to demonstrate the high-field capability of Nb_3Sn. But with only a 10 mm aperture and little attention paid yet to field quality, it is relatively far from what would be required for use in an accelerator. The next step in LBNL's plan is to reconfigure the mechanical

support of the HD-1 coils to allow it to go to higher field by operating it at 1.8 K. They are currently planning a larger bore block-type dipole capable of reaching similar field strength to HD-1, but with a larger coil bore and spacers to address field quality. A cross-section of such a coil is shown in Fig. 9[14]. Note the very large volume of superconductor required to achieve this very high field with a practical bore size for an accelerator beam.

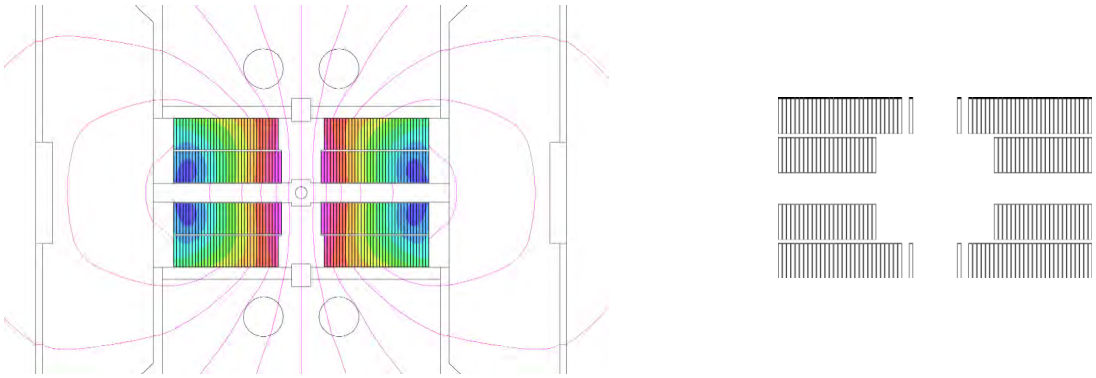

Fig. 9 Cross-section of the HD-1 coil (left), which reached 16 T and of a proposed HD-2 (right), which would achieve a similar field with larger bore.

Fermilab is pursuing two basic dipole coil designs (see Fig. 10), considering practical apertures, field quality, and manufacturability as key goals. Based in large part on the judgment that magnets of the highest possible field are unlikely to be economical for large-volume applications, such as the arcs of a future hadron collider, Fermilab is focusing on a more "modest" operating field of 10-12 T (12-14 T at the conductor limit). The first design is a conventional shell type coil, which due to the small bending radii at the coil ends, requires a wind-and-react approach. The second is a block-type design in a common coil configuration. Here the bending radii at the ends are set by the (vertical) aperture spacing and hence this design is amenable to the react-and-wind approach. The first models of both types failed to reach their design field. It is now understood that this resulted from superconductor instability due to the large effective filament size of the 1 mm modified jelly roll wire used. A program to understand the instability issue has been launched, involving both short-sample wire and cable tests and sub-scale models. A recent sub-scale coil made from 1 mm diameter powder-in-tube conductor with an effective filament size around 50 μm has achieved its short-sample limit, as expected by the instability threshold calculations[15]. With this issue at least partially understood, Fermilab will now return to testing full-featured model magnets, while continuing to quantify the understanding of the instability question.

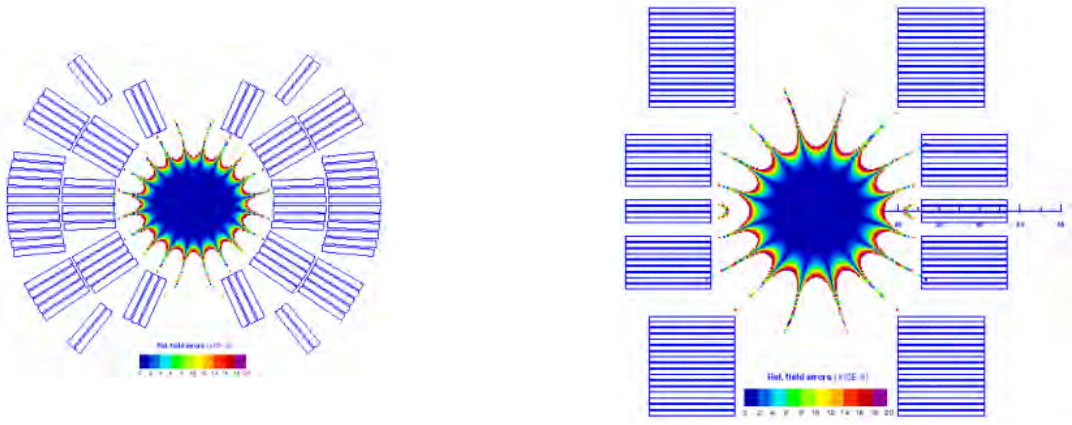

Fig. 10 Shell-type (left) and common-coil block type (right) Nb_3Sn dipoles.

BNL bases much of its development of conductors and methods for react-and-wind assembly on small 10-turn racetrack coils, similar to the sub-scale models described above. Figure 11 is a recent 10-turn coil made from BSCCO 2212 HTS cable. They use a set of Nb_3Sn racetrack coils in a common-coil configuration to provide a background field in which they insert strand or cable samples, or 10-turn test coils, as shown in Fig. 11[16]. Although HTS is still rather far from being suitable for use in a more application oriented program such as the US LARP, its continued progress suggest that it may eventually be useful at least in specialized applications, for example, in regions of high heat load such as in a dipole-first interaction region.

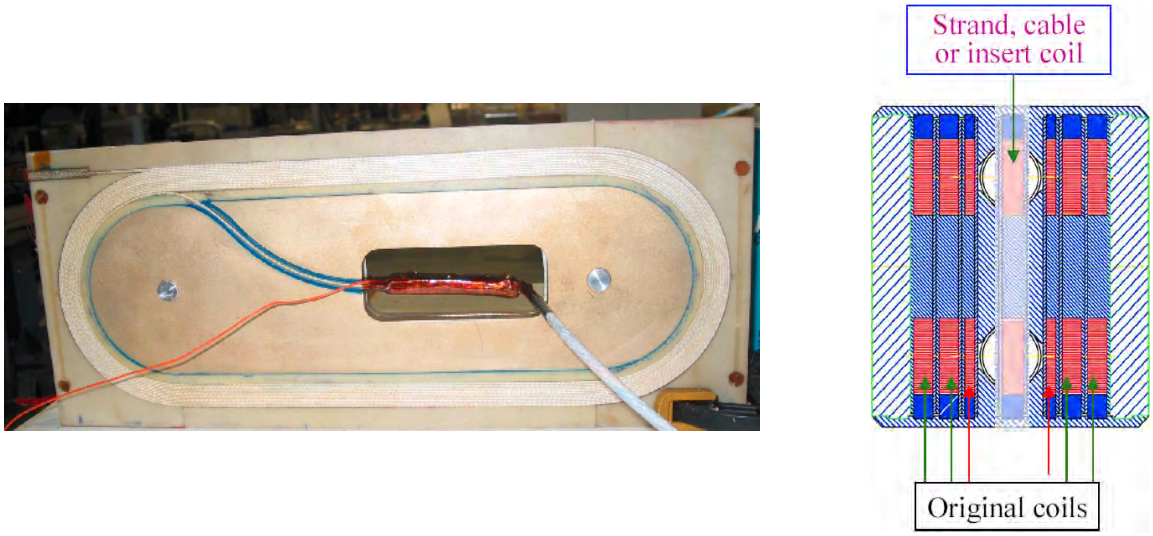

Fig. 11 Ten-turn HTS coil (left), and common-coil magnet (right) used to provide background field for conductor tests.

3. SUMMARY

The US LHC Accelerator Research Program will be an important part of the world effort to advance both high energy physics and accelerator physics and technology which underpin particle physics. The US LARP collaboration is working with CERN to advance the LHC by helping to commission the machine, developing advanced beam instruments and second generation collimators, performing fundamental accelerator physics calculations and experiments, and conducting accelerator physics studies and magnet R&D aimed at a timely luminosity upgrade. The magnet R&D program focuses on the development of a large aperture (≥100 mm) quadrupole with operating gradient ≥ 200 T/m, and a large aperture, high field (~15 T operating field) dipole suitable for the extreme radiation environment of a dipole-first IR. The goal is to develop at least one of these to a production ready state by about 2012, to permit a luminosity upgrade to be implemented in the middle of the next decade. The LARP magnet R&D program builds on a vigorous base program at LBNL, Fermilab and BNL, which is developing high-field magnets for the next generation of accelerators. The current world record field in an accelerator-type magnet is held by HD-1 at LBNL. The Fermilab program aims at developing practical designs, and is currently addressing conductor stability issues. BNL is focusing on react-and-wind technology development for both Nb_3Sn and HTS coils.

4. ACKNOWLEGEMENTS

The work I report here is mostly that of others in the US LHC Accelerator collaboration. The credit goes to the collaboration, and any errors in this paper are mine. I would like to thank those from

whom I took the information I presented in this paper and those who helped proofread it, specifically M. Anerella, S. Gourlay, R. Gupta, M. Harrison, V.V. Kashikhin, G. Sabbi, A.V. Zlobin.

5. REFERENCES

[1] J. Strait, et al., Towards a New LHC Interaction Region Design for a Luminosity Upgrade, PAC 2003, Portland, OR.

[2] O. Brüning, et al., LHC Luminosity and Energy Upgrade: A Feasibility Study, LHC Project Report 626, December 2002.

[3] A.V. Zlobin, et al., Aperture Limitations for 2nd Generation Nb_3Sn LHC IR Quadrupoles, PAC 2003, Portland, OR.

[4] N.V. Mokhov, et al., Energy Deposition Limits in a Nb3Sn Separation Dipole in Front of the LHC High-Luminosity Inner Triplet, PAC 2003, Portland, OR.

[5] T. Sen, et al., Beam Physics Issues for a Possible 2nd Generation LHC IR, EPAC 2002, Paris, France, p. 371.

[6] V.V. Kashikhin, et al., 2nd Generation LHC IR Quadrupoles Based on Nb3Sn Racetrack Coils, to be presented at EPAC 2004, Lucerne, Switzerland, July 2004.

[7] R. Gupta, et al., Open Midplane Dipole Design for LHC IR Upgrade, presented at the 18th International Conference on Magnet Technology (MT-18), Morioka City, Japan, October 20-24, 2003.

[8] R. R. Hafalia, et al., An Approach for Faster High Field Magnet Technology Development, presented at the 2002 Applied Superconductivity Conference, Houston, TX, 4-9 August 2002.

[9] S. Caspi et al., IEEE Trans. Appl. Superconduct., vol. 11, no.1, March 2001, p. 2272.

[10] G. Sabbi, private communication.

[11] A.D. McInturff, et al., Test Results for a High Field (13 T) Nb_3Sn Dipole, Particle Accelerator Conference, Vancouver, Canada, May, 1997.

[12] R. Benjegerdes, et al., Fabrication and Test Results of a High Field Nb_3Sn Superconducting Racetrack Dipole Magnet, Proceedings of the 2001 Particle Accelerator Conference, p. 208.

[13] S.E. Bartlett, et al., Test Results for HD1, a 16T Nb_3Sn Dipole Magnet, presented at the 18th International Conference on Magnet Technology (MT-18), Morioka City, Japan, 20-24 October 2003.

[14] S. Gourlay, private communication.

[15] S. Feher et al., Cable Testing for Fermilab's High Field Magnets Using Small Racetrack Coils, to be presented at ASC 2004, Jacksonville, FL, October 2004.

[16] R. Gupta, React and Wind Magnets with Nb_3Sn and Bi-2212, presented at the Low Temperature Superconductor Workshop, Monterey, CA, Nov. 10-12, 2003.

STATUS AND PLAN FOR SUPERCONDUCTING ACCELERATOR MAGNET DEVELOPMENT AT KEK

Akira Yamamoto
KEK, High Energy Accelerator Research Organization
1-1 Oho, Tsukuba, Ibaraki, 305-0801, Japan

Abstract
Progress of the superconducting accelerator dipole and quadrupole magnet development at KEK is discussed. A new superconducting beam line project at J-PARC project is introduced, as well as a Nb_3Sn magnet for the focusing of a neutron beam, a Nb_3Sn solenoid for pion capture, and basic development of Nb_3Sn and Nb_3Al conductors.

1. INTRODUCTION

Superconducting accelerator/beam-line magnet technology at KEK has progressed steadily since a superconducting beam line, π1, was constructed as the first superconducting magnet application at the KEK 12 GeV proton synchrotron. Two large-bore dipoles and a septum magnet were developed and successfully operated [1-3]. This application provided an opportunity to gain practical experience in parallel with in-house R&D on dipoles for a possible superconducting synchrotron at KEK [2, 4, 5]. Although it was later decided to build the synchrotron as an electron machine (TRISTAN), using normal conducting magnets, the work provided a strong basis for further progress on superconducting magnets at KEK, such as the low-beta insertion quadrupole magnet system for TRISTAN [6, 7]. This effort continued with R&D work on the SSC dipole [8] and the design and fabrication of the low-beta insertion quadrupole and corrector system for KEK-B [9]. It is interesting to recall that a unique block-coil dipole, designed to reach 10 T using NbTi conductor at 1.9 K, was also developed at KEK in the early 1980s [2, 10].

Cooperative work for the CERN/LHC magnets was started in 1989, and dipole models with 15 mm wide superconducting cable and using stainless-steel collars were successfully developed to reach 10.3 T [11-13]. Development of quadrupole magnets for the low-beta insertions has been carried out since 1995 [14-17]. The 6.3 m long, 70 mm bore magnet is designed to operate at up to 215 T/m in superfluid helium at 1.9 K. Following detailed prototype work at KEK the production of the magnets was entrusted to Toshiba, which recently completed the series of 19 units. This whole series of magnets was tested in a purpose-built 7 m long vertical cryostat at KEK [18]. KEK has undertaken to provide 16 of the 32 magnets required for the four interaction regions at the LHC [19]. They are being integrated into cryostats at Fermilab, which is providing the other 16 quadrupole units and the cryostat systems. In addition to the technical challenge, this project has provided the KEK team with the opportunity to gain experience in multi-national collaboration in state-of-the-art superconducting magnet technology.

Table 1 summarizes the progress of the superconducting magnet development at KEK, and Fig. 1 shows cross-sections of some of the dipoles and quadrupoles that were built. The Tristan-QCS and the KEK-B magnets were built to run within the field of the detector solenoid, and were therefore not equipped with iron yokes. It can be seen that KEK has acquired particular expertise in the development of magnets with relatively large aperture, and in Figs. 2 and 3 achieved field as a function of aperture is compared with that of magnets produced elsewhere.

Table 1
History of Accelerator Magnet Development at KEK

	SC	Temp (K)	Coil config.	Aperture (mm)	Design	Tested	Year
Dipoles:					(T)		
π1 Dipole	NbTi	4.2	Cos θ	270	4.0	3.8	1980
π1-Septum	NbTi	4.2	Current Sheet	16x134	1.6	1.8	1981
Tristan	NbTi	4.2	cos θ		5	5	1980
		1.8				6.8	1980
SSC	NbTi	4.2	cos θ	40	6.6	6.8	1985
10T-Dipole	NbTi	1.9	Block	63	10	9.3	1984
LHC (50mm)	NbTi	1.9	cos θ	50	10	10.3	1991
LHC (56 mm)	NbTi	1.9	cos θ	56	8.4	9.6	1993
Quadrupoles:					(T/m)		
Panofsky	NbTi	42	Current Sheet	430x125	15	13.9	1981
Tristan-QCS	NbTi	4.2	cos 2θ	140	70	87	1988
Tristan-QCS-I	NbTi	1.9	cos 2θ	140	114	114	1996
KEK-B	NbTi	4.2	cos 2θ	260	21.7	24	1997
LHC-MQXA-1m	NbTI	1.9	cos 2θ	70	215	250	1997
LHC-MQXA	NbTi	1.9	cos 2θ	70	215	230	2001

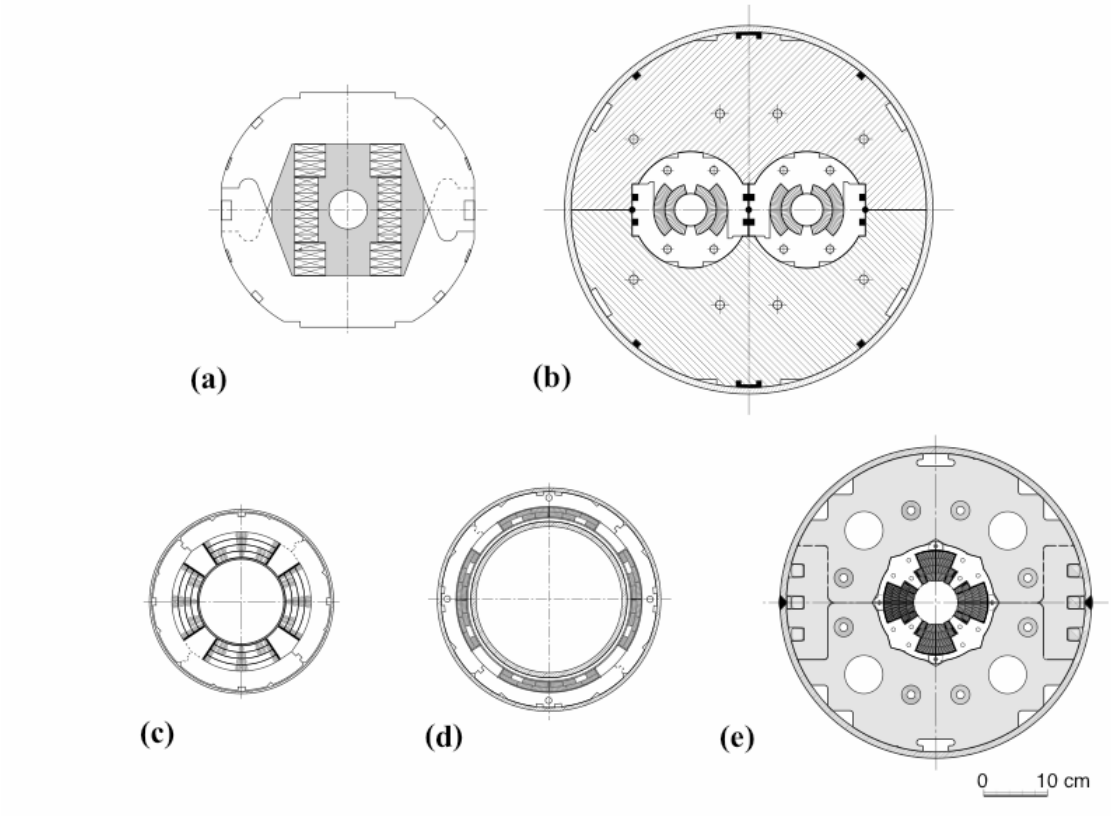

Fig. 1 Dipoles and low-beta insertion quadrupole magnets developed at KEK: (a) Block dipole, (b) LHC dipole model, (c) Tristan-QCS, (d) KEK0B IRQ, and (f) LHC IRQ (MQXA).

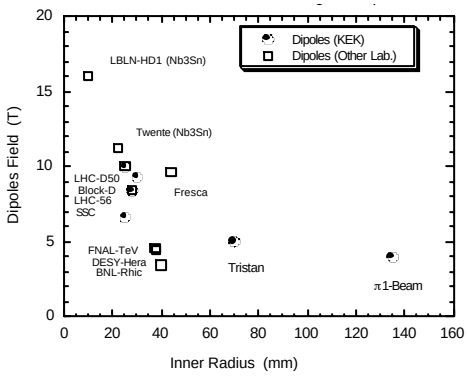

Fig. 2 Dipole field as a function of aperture.

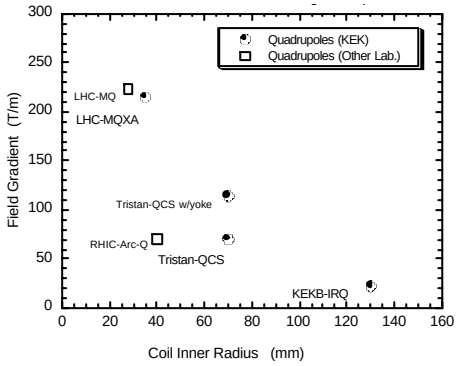

Fig. 3 Quadrupole field as a function of aperture.

2. SUPERCONDUCTING MAGNETS FOR THE J-PARC PROJECT

A superconducting proton beam line is to be built for the Tokai-to-Kamioka (T2K) neutrino experiment at the J-PARC facility presently under construction [20, 21]. The primary proton beam extracted from the 50 GeV synchrotron needs to be bent by 87 degrees to direct the neutrino beam to Kamioka, 290 km west of the J-PARC site in Tokai. The beam optics and magnet design were optimized for maximum cost effectiveness, as a result of which a combined function magnet system is proposed [22, 23]. This uses 28 magnet units of a single type, providing dipole and quadrupole fields in the same bore by use of a left/right asymmetric, one-layer coil. Table 2 gives the design parameters of this magnet and its cross-section is shown in Fig. 4. The design features a coil aperture large enough to accommodate the beam halos, in order to avoid eventual associated quenching. The single layer asymmetric coil is wound with NbTi/Cu superconducting cable, as shown in Fig. 5. Pre-stress is applied by a collaring yoke via a phenolic spacer. A full-scale prototype magnet is being developed and will be tested this year.

Table 2
Main parameters of the dipole-quadrupole combined function magnet for J-PARC

Beam Energy	50 GeV
Dipole field	2.586 T
Quadrupole field	18.62 T/m
Magnetic length	3.3 m
Operation current	7,345 A
Operating temperature	< 5 K
Load line ratio	72 %
Inductance	14 mH
Stored energy	386 kJ

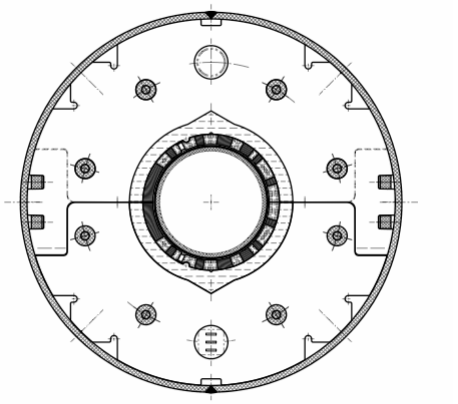

Fig. 4 Cross-section of the J-PARC combined function magnet.

Fig. 5 Test winding at KEK of the left/right asymmetric coil for the combined function magnet for the J-PARC neutrino experiment.

3. BASIC R&D FOR FUTURE PROGRAMS

3.1 Advanced superconductor development

The next generation of high-energy proton accelerators will require magnets in which the field in the winding is more than 10 T. Moreover, the nature of these magnets is such that it will be necessary to use conductors having a current density of over 2 000 A/mm^2 at 12 T in the superconductor. The stability of strands and the ability to produce them reliably in production runs are also very important, as is the necessity of reasonable production cost. We have been developing a new approach to the realization of high quality Nb_3Sn superconductor, in order to render it more homogeneous, yet with similar reaction conditions. Reduction of the bronze area in the conductor is effective to increase the overall current density. A new configuration of niobium and tin, the so-called distributed tin (DT) method [24], has been developed in cooperation with Mitsubishi Electric, Japan, to achieve the above requirement. The tin areas are uniformly distributed among bundles of thin niobium filaments. This configuration provides a high superconductor occupation ratio by using sophisticated processing. Tin diffuses more easily into every niobium filaments than with the conventional internal tin or pipe method, because the niobium filaments are thin and the diffusion path is always kept open. Figure 6 shows the cross section of such a DT conductor. A test fabrication of the DT conductor has been successfully performed and a current density of 2100 A/mm^2 at 12 T has been achieved [24]. We expect even higher current densities when the heat treatment procedure will have been fully optimized.

Nb_3Al superconductor has better strain tolerance and higher J_c potential than Nb_3Sn conductor, and has been investigated for future accelerator magnets in collaboration with National Institute for Materials Science, NIMS and Hitachi Cables and Wires. Several test wires of around 0.8 mm diameter, which have relatively small filament diameter (~50 micron) and low matrix ratio (~1.0), have been fabricated, and the heat treatment and area reduction conditions after a rapid quenching process have been studied [25]. Figure 7 shows the cross section of the Nb_3Al conductor. The highest non-copper J_c achieved during this study was about 1740 A/mm^2 at 10 T and 4.2 K, as shown in Fig. 8. This is ongoing work, and further improvements can be expected through the optimization of (i) Nb to Nb_3Al ratio, (ii) filament diameter, (iii) filament numbers, (iv) heat treatment (to be adapted to the maximum field in the range of 12 – 20 T at which the conductor is to be used), and (v) grain size.

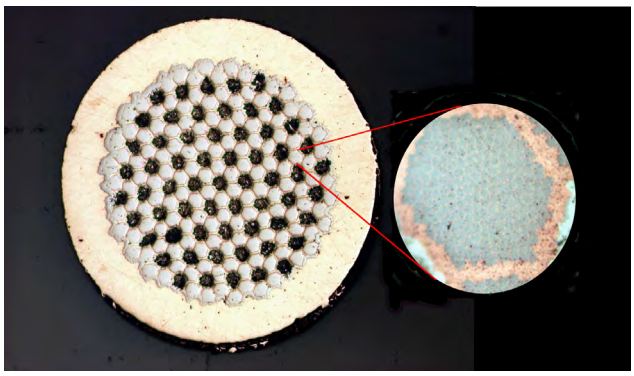

Fig. 6 Cross-section of the DT superconductor.

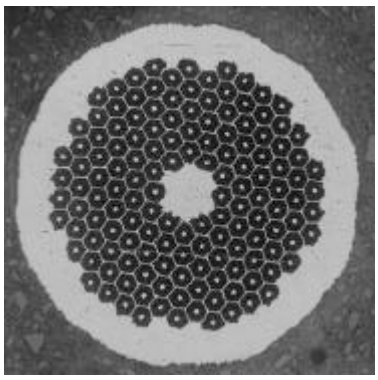

Fig. 7 X-section of Nb_3Al superconductor.

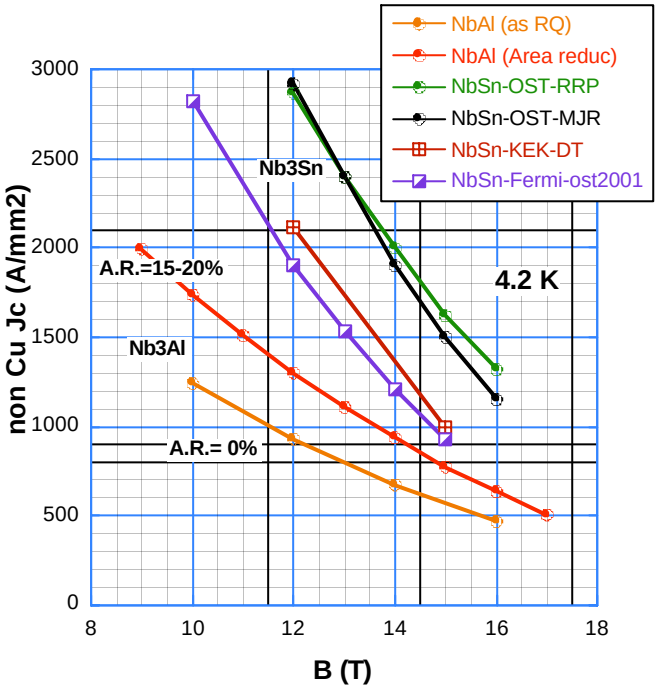

Fig. 8 Current density of Nb3Al and Nb3Sn conductor as a function of magnetic field.

3.2 Nb_3Sn superconducting sextupole magnet development

As a basic R&D program associated with the intense cold-neutron beam to be realized at the J-PARC facility, a Nb_3Sn superconducting sextupole magnet is being developed. The magnet is needed to focus the cold-neutron beam, this function being provided via the interaction between the neutron magnetic dipole moment and the external inhomogeneous magnetic field [26]. The main parameters of the superconducting coil and conductor are given in Table 3, and a cross-section of the coil is shown in Fig. 9. The requirement for a non-linear field gradient in a large aperture leads to a very high magnetic field in the coil. For this reason the magnet, which is foreseen to be bath-cooled in liquid helium, must be based on the use of Nb_3Sn or Nb_3Al superconductor.

Table 3
Main parameters of the Nb_3Sn sextupole magnet

Coil inner radius	23 mm
Length	500 mm
Sextupole field	12,7890 T/m^2
Max. field in winding	8.75 T
Current	1,000 A
J_c in winding	580 A/mm^2
Superconductor:	
Material (company)	Nb_3Sn (SMI)
Diameter	1.0 mm
Copper ratio	0.45
No. filaments	192
Filament pitch	25 mm
Insulation	T-glass (0.075 mm x 2)

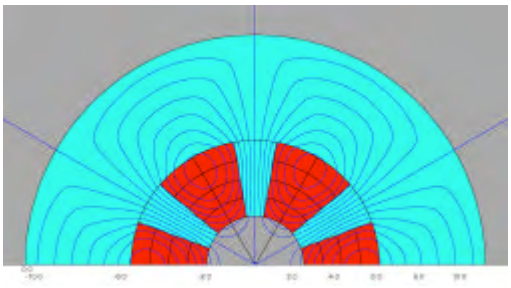

Fig. 9 Cross-section of the Nb_3Sn sextupole, with flux lines.

3.3 Superconducting solenoid for pion capture

A high intensity secondary beam with Phase Rotation, PRISM [27,28], is proposed as a unique facility to be built at the J-PARC facility. Figure 10 shows a tentative general layout of the PRISM facility. The major goal is to provide an intense low energy muon flux of 10^{11-12} per second, which will be several orders of magnitude higher than that ever achieved previously. This will open up new possibilities for particle physics, in particular the study of Lepton-Flavor Violation (LFV) through the process of rare muon decay, with a sensitivity of 10^{-18} in the branching ratio[27]. The high-field superconducting magnet is required to capture the pions in the secondary beam with maximum efficiency.

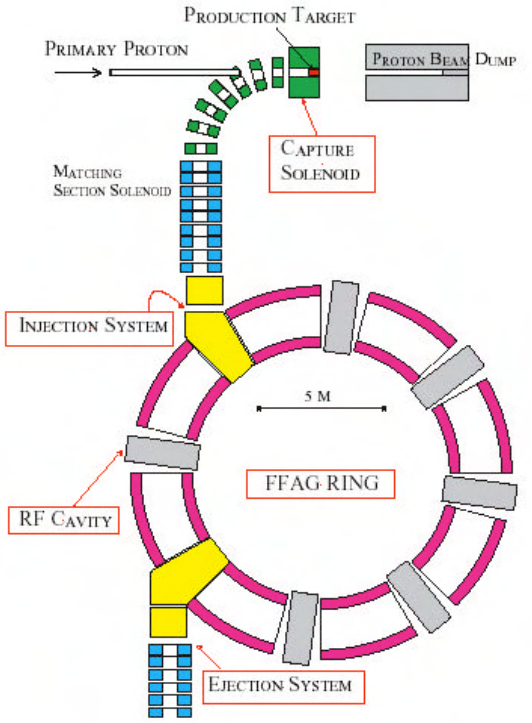

Fig. 10 Concept of PRISM.

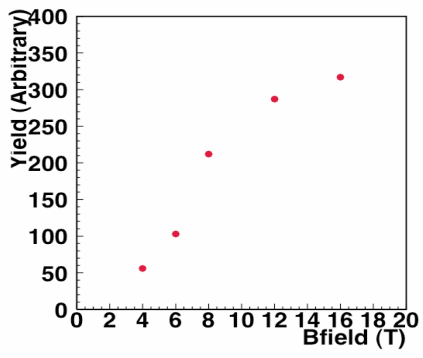

Fig. 11. Pion yield as a function of field.

It is well known that a solenoidal field is very efficient to capture secondary particles generated at a production target in a primary proton beam [29]. The maximum transverse momentum of the captured secondary particle (P_t) is given by P_t (GeV/c) = 0.3 x B(T) x R/2 (m), where B is the solenoidal magnetic field, and R is the effective aperture radius of the solenoidal field. For a critical transverse momentum of 0.09 GeV/c in the present configuration, the necessary multiple of bending power and radius, B x R, is 0.6 T.m. The useful aperture is 5 cm, so a field of 12 T is desirable [30]. Figure 11 shows pion yield as a function of the solenoidal field. Nb_3Sn or Nb_3Al superconductor will be a prime candidate for the coil of such a magnet, required ideally to operate well beyond 10 T and subjected to intense radiation emanating from the interaction of the 1 MW primary proton beam with the production target. The target will be located in the bore of the pion capture solenoid.

4. SUMMARY AND CONCLUSION

Progress in the development of superconducting accelerator dipole and quadrupole magnets at KEK is presented. A field of 10 T at 1.9 K has been achieved in the NbTi based superconducting magnets, and these are now reaching the ultimate performance which can be envisaged using this material. A new superconducting beam line project for J-PARC is presently a major development activity. After careful study to minimize the cost of the project, it has been decided to use superconducting combined function magnets with the maximum field of 4.7 T in the large diameter, asymmetric coil. Development of high field magnets requiring A15 superconductors is being carried out in two other projects: a pion capture solenoid, for PRISM, and a sextupole magnet for neutron focusing. In parallel we also continue basic R&D on Nb_3Sn and Nb_3Al, the target performance being 3000 A/mm^2 at 12 T.

In addition to its expertise, KEK has accumulated significant hardware infrastructure for the development and testing of superconducting magnets of the type used in accelerators. The 7 m long vertical test cryostat cited earlier is unique in the world, and this is housed in a dedicated building in which 6.5 m long magnets can be conveniently manipulated. In addition to a well-equipped machine shop, the laboratory also possesses winding tables, presses and ovens for the efficient fabrication of test coils and prototypes. KEK has often worked in partnership with industry in Japan and is fully familiar with how to deal with the specification and contractual details of this aspect of the work. Our laboratory should therefore be well-placed to make a significant contribution to the high field magnet program that is the subject of this workshop.

REFERENCES

[1] H. Hirabayashi, "Development of superconducting magnets for beam lines and accelerator at KEK", IEEE Trans. Magnetics, 17, No. 1 (1981) p. 728.

[2] H. Hirabayashi, "Dipole magnet development in Japan", IEEE Trans. Magnetics, 19, No. 3 (1983) p. 198.

[3] A. Yamamoto et al., "A superconducting secondary beam line in the 12 GeV proton synchrotoron at KEK", Nucl. Instr. & Methods, A257 (1987) p. 105.

[4] S. Mitsunobu et al., "Test dipole magnets for the Tristan superconducting proton ring", IEEE Trans. Nuclear Science, 28, No. 3 (1981) p. 3266.

[5] K. Hosoyama et al., "A NbTi superconducting dipole magnet installed in a pressurized helium II cooling bath", Japn. J. Appl. Phys., Vol. 21, No. 12 (1982) p. 1711.

[6] K. Tsuchiya et al., "Performance of the eight superconducting quadrupole magnets for the TRISTAN low-beta insertion", IEEE Trans. Magnetics, 27 (1991) p. 1940.

[7] K. Tsuchiya et al., "Test results of spare TRISTAN insertion quadrupole magnet with yoke added in superfluid helium", IEEE Trans. Appl. Supercon. Vol. 7, No. 2 (1997) p. 570.

[8] K. Hosoyama, et al., "A status report on the development of 5-cm aperture 1-m long SSC dipole magnet at KEK", Supercollider 5, ed. P. Hale, Plenum Press, New York, (1994) 229.

[9] K. Tsuchiya et al., "Superconducting final focusing system for KEKB", Proc. of the 2001 Particle Accelerator Conf. (2001) p. 181.

[10] T. Shintomi, et al., "The construction and test results of a 10 T dipole magnet", IEEE Trans. Nuclear Science, 32 (1985) p. 3719.

[11] A. Yamamoto et al., "Development of twin aperture dipole magnets for the Large Hadron Collider", IEEE Trans. Appl. Supercond. Vol. 5, No. 2, (1995) p. 1016,

[12] A. Yamamoto et al., "Test results of a single aperture 10 T dipole model magnet for the Large Hadron Collider", IEEE Trans. Magnetics, Vol. 32, No. 4, (1995) p. 2116.

[13] C. Giloux et al., "Test results of a variant-design LHC twin-aperture dipole magnet2, IEEE Trans. Appl. Supercond. Vol. 13, No. 2, (2003), p. 1313.

[14] A. Yamamoto et al., "Design study of a superconducting insertion quadrupole magnet for the Large Hadron Collider", IEEE Trans. Appl. Supercond. Vol. 7, No. 2 (1997) p. 747.

[15] K. Tsuchiya et al., "Magnetic design of a low-beta quadrupole magnet for the LHC interaction regions", IEEE Trans. Appl. Supercond. Vol. 10, No. 1 (2000) p. 135.

[16] T. Nakamoto et al., "Production and performance of the LHC interaction region quadrupoles at KEK", IEEE Trans. Appl. Supercond. Vol. 13, No. 2 (2003) p. 1321.

[17] N. Ohuchi et al., "Status of LHC low-beta quadrupole magnets, MQXA, at KEK", Proc. of 2003 Particle Accelerator Conf. IEEE 0-7803-7739-9, (2003) p. 1978.

[18] N. Kimura et al., "A pressurized He-II cryogenic system for the superconducting magnet test facility at KEK", Adv. Cryo. Eng., Vol. 47 (2002) p. 123.

[19] R. Ostojic, "The LHC insertion magnets," IEEE Trans. Appl. Supercond. Vol. 12, No. 1 (2002) p. 196.

[20] http://www-nu.kek.jp/jhfnu/

[21] http://www-ps.kek.jp/nbi2003/

[22] T. Ogitsu et al., "Superconducting magnet system at the 50 GeV proton beam line for the J-PARC neutrino beam line", to be published in IEEE Trans. Appl. Supercond. Vol. 14, (2004).

[23] T. Nakamoto et al., "Design of superconducting combined function magnets at the 50 GeV proton beam line for the J-PARC neutrino experiment", to be published in IEEE Trans. Appl. Supercond. Vol. 14, (2004).

[24] M. Wake et al., "Development of high current density Nb_3Sn conductor with distributed tin configuration", to be published in Proc. of ICMC-2003.

[25] T. Kobayashi, et al., "Development of Nb_3Al superconducting wire for accelerator magnets", to be published in IEEE Trans. Appl. Supercond. (2004), (MT-18 proceedings).

[26] R.Q. Apsey, D.E. Baynham, C.A. Scott, "Filamentary Niobium-Tin hexapole magnet", Proc. of the 6^{th} Int. Conf. On Magnet Tech. (MT-6), (1977) p. 546.

[27] Y. Kuno, "PRISM; Experimental possibilities", High Intensity Muon Sources, edited by Y. Kuno, and T. Yokoi (World Scientific, 1999), p. 247.

[28] Y. Mori, "PRISM: A phase rotator to obtain an intense monochromatic muon beam", High Intensity Muon Sources, edited by Y. Kuno, and T. Yokoi (World Scientific, 1999), p. 213.

[29] A. P. Banford, "The transport of charge particle beams", E & F.N. Spon Ltd. (1966).

[30] A. Yamamoto "Design study of a superconducting magnet for pion capturing", High Intensity Muon Sources, edited by Y. Kuno, and T. Yokoi (World Scientific, 1999), p. 228.

THE ITER SUPERCONDUCTING MAGNET PROGRAMME

E. Salpietro
European Fusion Development Agreement, Boltzmannst. 2, D-85748, Garching, Germany

Abstract
This note summarises the main objectives, development lines, evolution and results of the European Fusion programme during the last twenty years, from the Next European Torus (NET) till the present effort in the scope of the International Thermonuclear Experimental Reactor (ITER).

1. INTRODUCTION

The European fusion programme has evolved in the past twenty years, adapting to the changes in scope and boundary conditions. In 1983 the Next European Torus (NET) Team was created to design the fusion device to follow the Joint European Torus (JET). [1]

The NET magnet system was all superconducting, designed with Nb3Sn and NbTi superconducting strands, supercritical helium forced flow cooled and high current in the cables, in excess of 40 kA.

Following the agreement between United States and Russian Federation in 1987 the International Thermonuclear Fusion Reactor (ITER) Conceptual Design Activity started (CDA), it lasted three years, and in 1990, it was completed. [2]

The second phase of ITER started in 1992, named Engineering Design Activity (EDA). It lasted six years from 1992 to 1998. The partners for these two fases were Russia, United States, Europe and Japan. [3]

After completion of the the EDA, the United States abandoned the project, ITER-FEAT started in 1999 and is going on to now. In table I are reported the major parameters of the ITER machines as designed in the different phases. [4]

Table 1. ITER parameters

ITER CDA 1988-1990	
Plasma Major Radius	6.0 m
D.N. Vertical Elongation 95%	2
Plasma Current	22 MA
Magnetic Filed at 5.8m / max.	4.9T/10.4T
ITER EDA 1992-1998	
Plasma Major Radius	8.1m
S.N. Vertical Elongation 95%	1.6
Plasma Current	21 MA
Magnetic Field at 8.1m/max	5.7T/12.5T
ITER FEAT 1999-today	
Plasma Major Radius	6.2m
S.N. Vertical Elongation 95 %	1.7
Plasma Current	15/17 MA
Toroidal Field at 6.2m/max	5.3T/11.8T

2. THE BASIC CONSTRAINTS FOR THE LAYOUT OF THE ITER CONDUCTOR

The ITER device (Fig. 1) mainly consists of the cryostat, the magnet system, the vacuum vessel, the blanket and the divertor. The ITER-FEAT magnet system (Fig. 2) consists of 18 toroidal field (TF) coils, a central solenoid (CS), six poloidal field (PF) coils and correction coils (CCs).

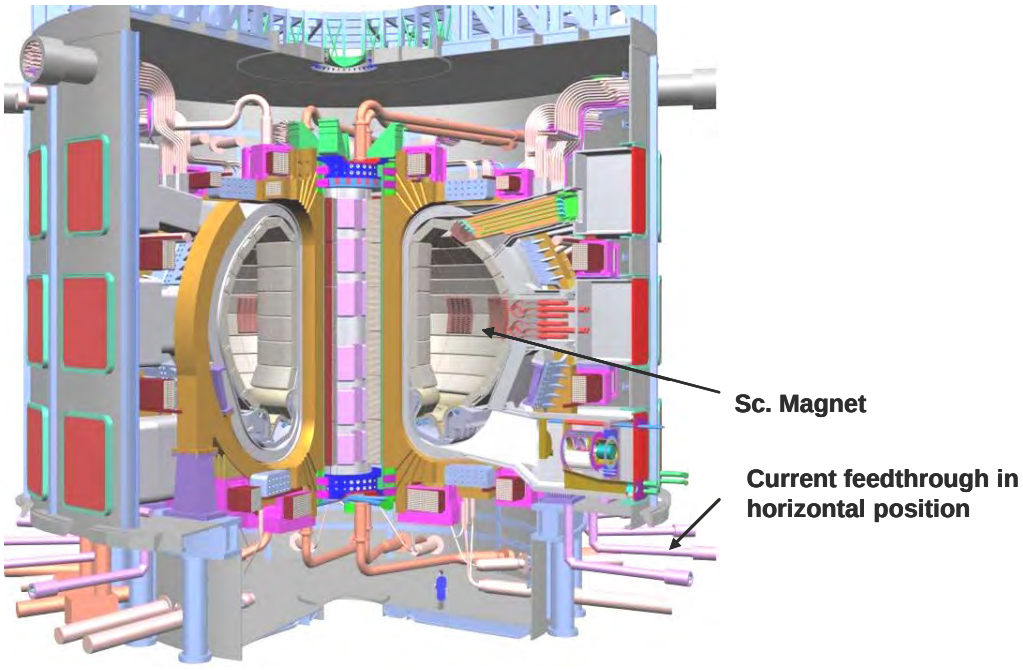

Figure 1. ITER device.

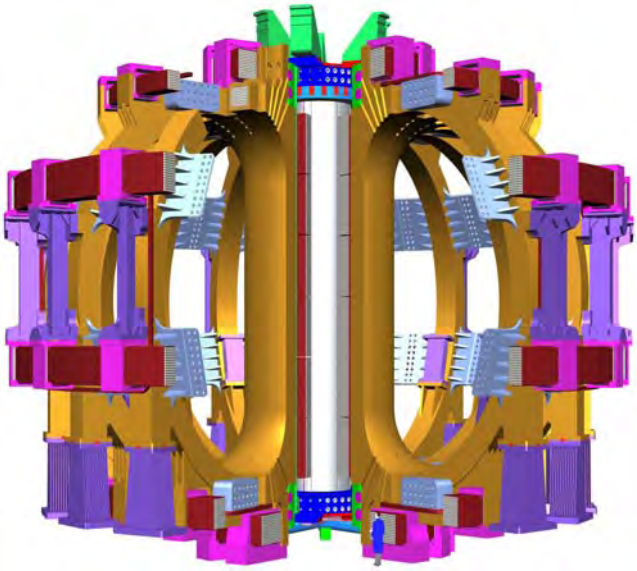

	Field (T)	***Current (kA)***
CS coil	13.5	42
TF coil	11.8	68
PF coil	4 Š 6	45
Correction coil	< 6	10
Cryostat feedthrough	< 4	≤ 68
Current lead	< 30 mT	≤ 68
External current feeder	~ mT	≤ 68

Figuer 2. Magnet System Components.

The TF coil case, which encloses the winding pack, is the main structural component of the magnet system. The TF coil inboard legs are wedged all along their side walls. In the inner regions, the coils are connected by inner intercoil structures (IIS). At the outboard leg, the out-of-plane support

is provided by outer intercoil structures (OIS) integrated with the TF coil cases. These are welded structures acting as shear panels, which are connected to each other to form four toroidal belts. There is electrical insulation between TF coils at the inboard leg wedged region and at the IIS and OIS.

The CS assembly consists of a stack of six independent modules and is hung from the top of the TF coils through its pre-load structure. This structure, which consists of a set of tie-plates located outside and inside the coil stack, provides axial pressure on the stack. The number of CS modules is chosen to suit the plasma equilibrium requirements.

The six PF coils (PF1 to PF6) are attached to the cases through flexible plates to allow radial expansion. The position and size of these coils are chosen to suit the plasma equilibrium and control requirements.

Both CS and TF coils operate at high field and use Nb3Sn-type superconductor. The PF and CC coils use NbTi superconductor. All coils are cooled at 4.5K. The whole magnet system is supported by flexible columns and pedestals, one under each TF coil. Each TF coil is electrically insulated from its support. The TF coil case also supports the vacuum vessel weight and operational loads.

Table 2 gives the ITER-FEAT main magnet parameters and Fig. 3 shows the ITER conductors layout.

Table 2. ITER-FEAT main magnet parameters.

Number of TF coils	18
Magnetic energy in TF coils (GJ)	~ 41
TF coil current (kA)	68
Maximum field in TF coils (T)	11.8
CS current, initial magnetization, [end-of-burn] (kA)	41.5, [45.2]
CS peak field, initial magnetization, [end-of-burn] (T)	13.5, [12.8]
PF coil current, normal operation, [backup mode] (kA)	45, [52]
Correction coil current (kA)	10
Weight of TF coils including structures (t)	5,621
Weight of CS including structures (t)	926
Weight of PF coils including clamps (t)	2,835
Weight of CCs including clamps (t)	80
Total weight of magnet system (t)	~ 10,135

Figure 3. Conductors of the two ITER model coils: CSMC conductor, left, exploded TFMC conductor, right.

3. ITER MAGNETS R&D

In order to demonstrate the feasibility of the magnetic system, a comprehensive research and development programme has been launched in 1992. The main elements of the programme are the Central Solenoid Model Coil (CSMC) and the Toroidal Field Model Coil (TFMC). A third, complementary element is the Poloidal Field Coil Insert (PFCI).

The Central Solenoid Model Coil (CSMC) [5] has been built with the contribution of United States, Japan and Europe, and has been assembled and tested in the Naka site of JAERI, in Japan. The main CSMC parameters and test results are reported in Fig. 4 and Fig. 5.

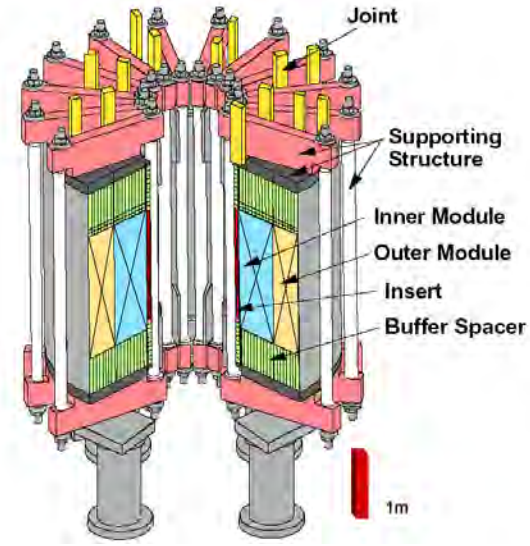

Coil Design Parameters

	CSI	CSMC IM	CSMC OM
Maximum Field	13 T	13 T	7.3 T
Operating Current	40 kA	46 kA	46 kA
Outer Diameter	1.57 m	2.71 m	3.62 m
Height	2.80 m	2.80 m	2.80 m
Weight	7.7 t	49.3 t	52 t
Stored Energy	11 MJ	640 MJ	

Figure 4. CS Model Coil.

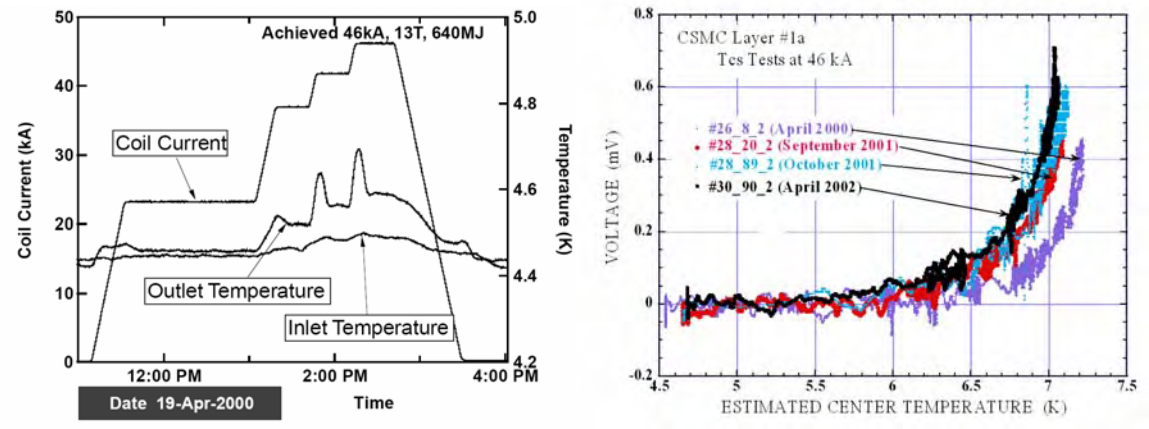

Figure 5. CS Model Coil test results. Left: CSMC successfully achieved design values, right: small degradation (0.1 to 0.2 K) saturated after few cycles.

It can be seen from the currentt waveform of Fig. 5 that the design parameters were achieved at first attempt (no training), some changes in the electric characteristic of the coil was detected in the following testing. This is probably due to a settlement of the cable inside the jacket. A lower coil

performance (Jc,n) compared to strand was measured: it is probably due to current redistribution inside the cable and bending strain effects, which at present are not simulated in the interpretation codes.

The second element of the R&D programme is the Toroidal Field Model Coil (TFMC) [6] (Fig.6), which has been built entirely in the European Union and has been tested in 2001 alone at FZK Karlsruhe (Germany).

In 2002,the TFMC together with the LCT coil was tested to simulate the effect of the transversal forces. The TFMC showed reduction of n and AC losses, as the CSMC, but it did not change performances with cycles, neither reduction of temperature current sharing from strand, after a proper strand data set was used. (Figs. 7-8).

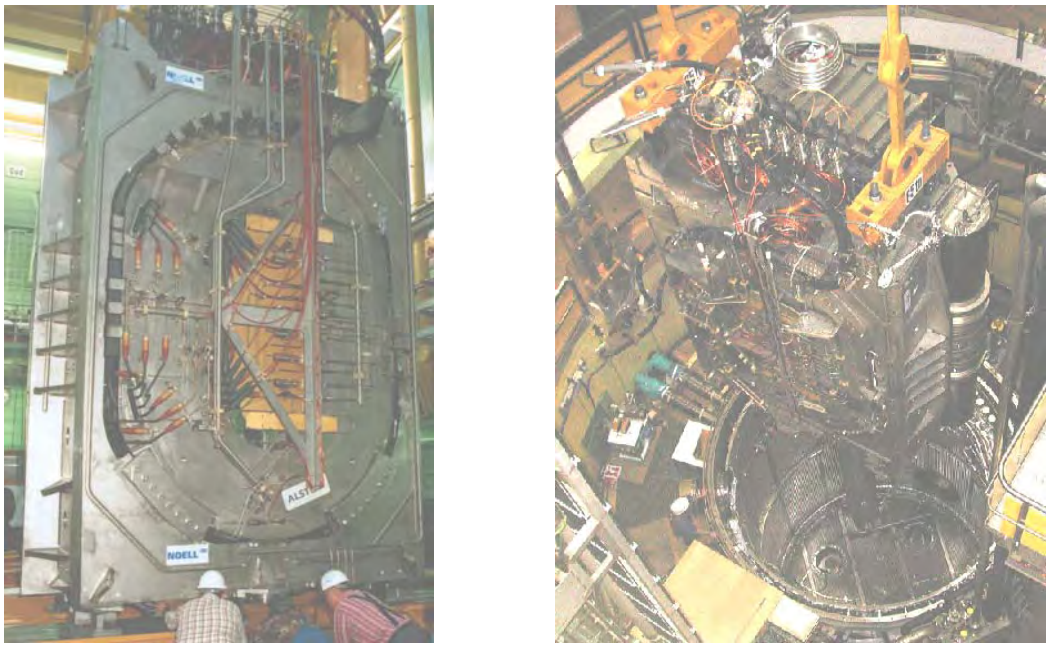

Figure 6. TF Model Coil.

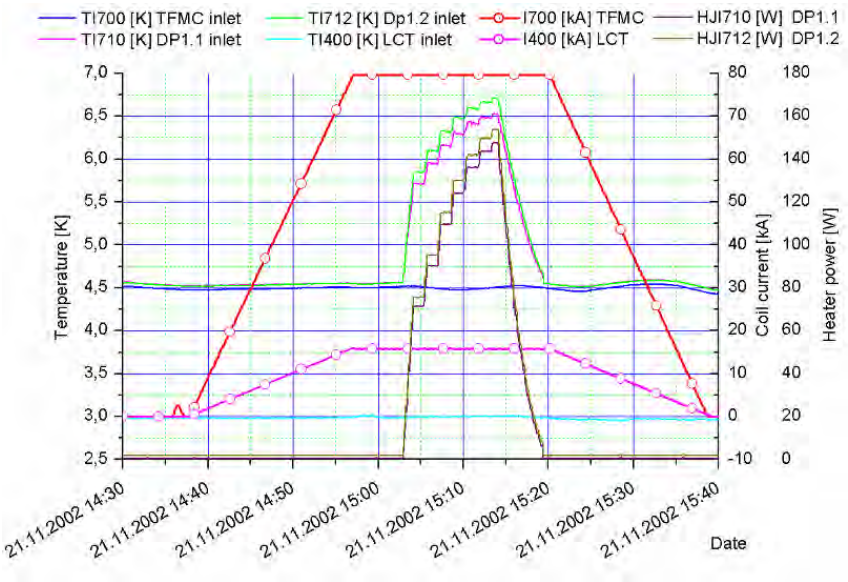

Figure 7. TF Model Coil performance.

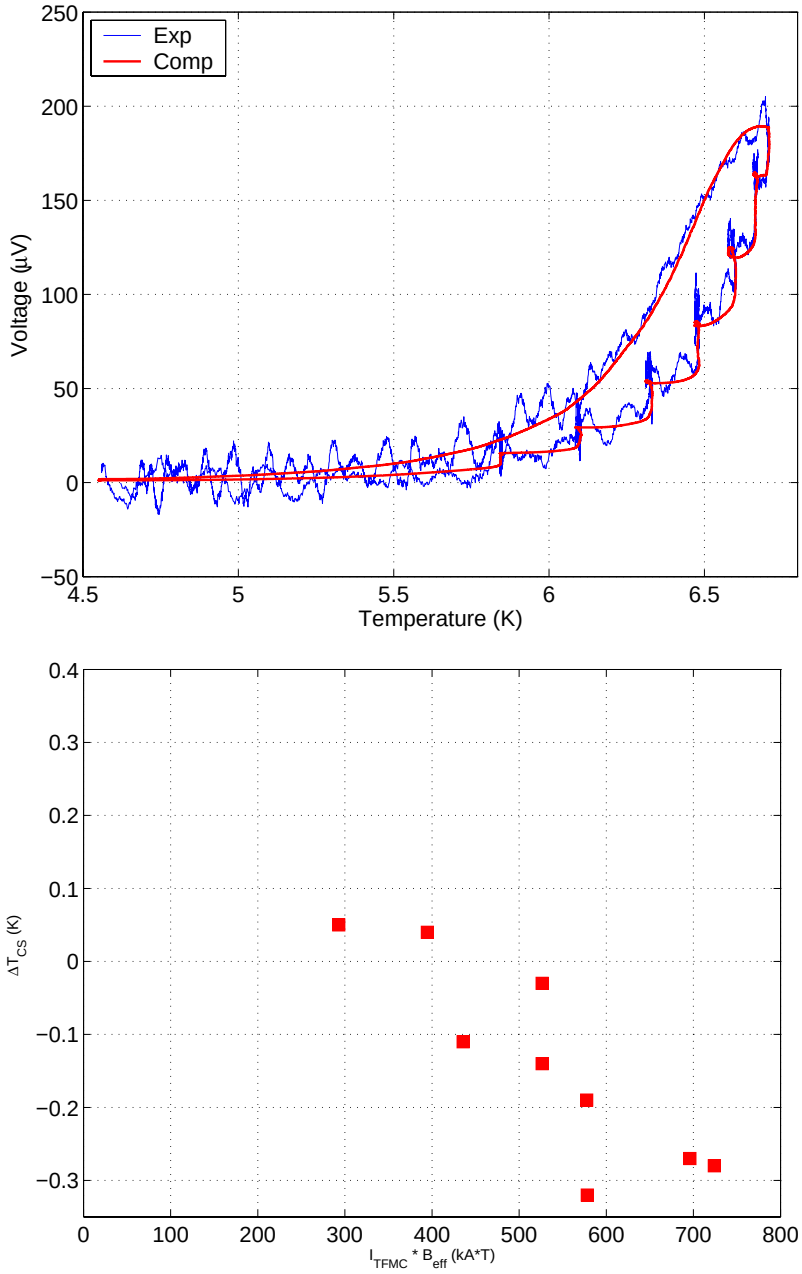

Figure 8. Simulation of the voltage–temperature characteristics in a run of the TFMC (top) and difference between the current sharing temperature Tcs as obtained from strand data and as measured in different runs (bottom) corresponding to a wide range of transverse Lorentz force.

It can be noted (Fig. 9) that the standard Summer's low is not accurate enough when high compressive strain is present. The performance dependence on applied Lorentz forces, can be explained by the fact that the interpretation code doesn't take into account the bending strain effect.

The bending strain effect [7] was already investigated by Ekin in 1980 (Fig. 10) and this can explain the more pronounced degradation of performance (with bending strain) experienced by the CSMC (lower compressive strain due to Incoloy Jacket) than the TFMC (SS Jacket) as it is experimentally confirmed by the test results reported in Fig. 11.

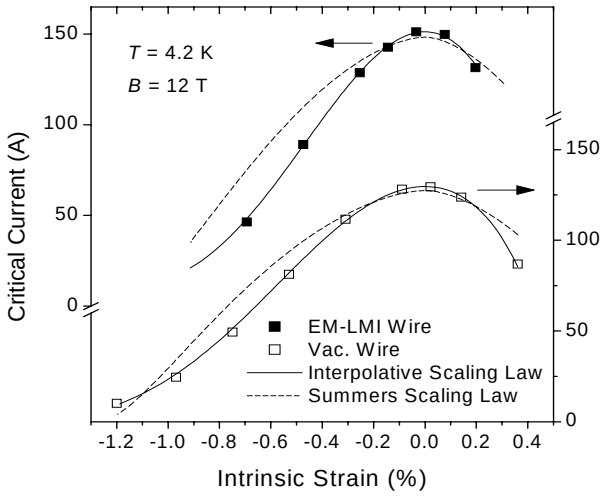

Figure 9. Standard Summer´s Law is not accurate

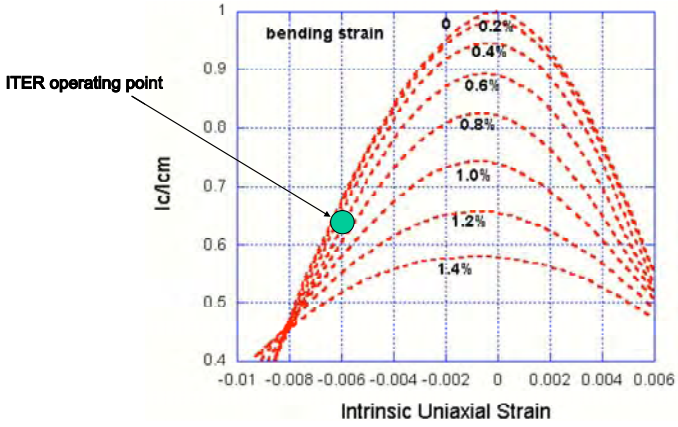

Figure 10. Bending strain tests - Influence at high compression

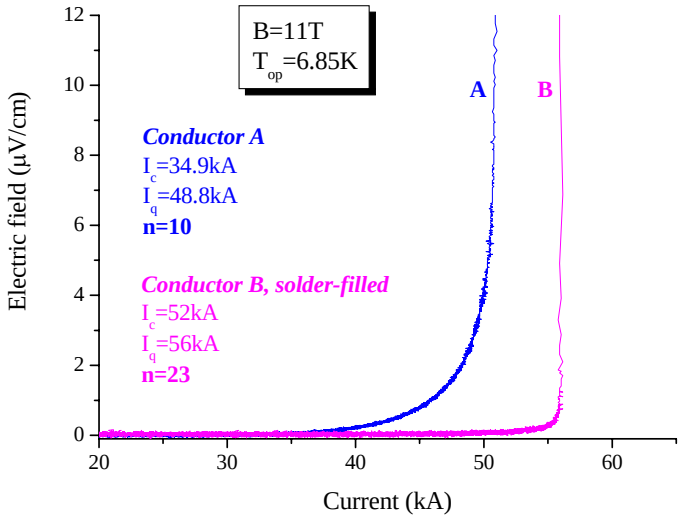

Fig. 11, DC test results on voltage-current characteristics on two Nb3Sn cables.

The third element of the R&D is the Poloidal Field Conductor Insert (PFCI) [8], which is being built in Europe (Fig. 12) with a cable supplied by the Russian Federation, and will be tested in 2005 at Naka (J). All conductors used in the model coil have been tested in the SULTAN facility; Hall probes array has been used in order to determine the current distribution inside the cable and therefore improve the interpretation of the test results.

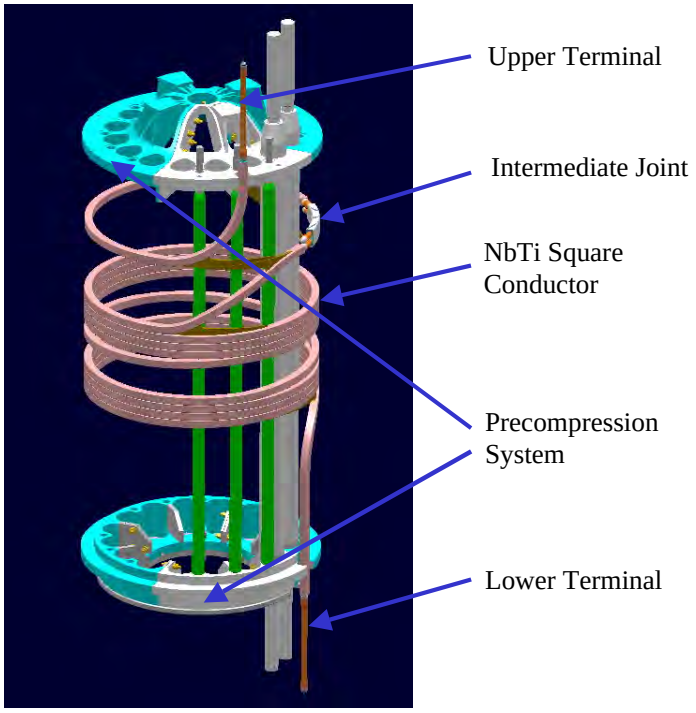

Coil Design Parameters

		PFI
Maximum Field		6.3 T
Maximum Operating Current		50 kA
Maximum Field Change		2 T/s
Conductor length		49.50 m
Main Winding Envelope	Outer Diameter	1.57 m
	Inner Diameter	1.39 m
	Height	1.40 m
Height		1.40 m
Weight		6 t

Figure 12. PF Insert Coil

4. ITER CONDUCTOR OPTIMIZATION

Following the test results of the model coil and inserts, as well as the progress in the strand fabrication, a conductor development programme has been launched in Europe to optimize the ITER conductor. [9] Six companies are presently producing strand in accordance to the specifications reported in Table 3.

The development programme outlined in Fig. 13 is designed to qualify the strand and cables at every stage of fabrication, and under applied tensile load up to the last but one stage.

The longitudinal strain dependence of the strand critical current is measured in the “small” FBI facility on a strand jacketed in a SS tube; the same test is curried out in the “big” FBI facility in subcables jacketed in SS tubes. The principle and details of the FBI facilities are shown in Figs. 14 and 15.

Table 3. Advanced Nb3Sn Strand specification, tender.

Outer diameter of the strand	**0.81 mm** ±3 μm
Effective filament diameter	< 50 μm (typical)
Strand pitch	< **20 mm**
Hard Cr -coating	2 μm +0.5 μm / Š0 μm
Non -Cu critical current density (at 12 T, 4.2 K, 0.1 μV/cm)	Min. guaranteed: **800 A/mm** ^{2} Target value: 1100 A/mm ^{2}
Non -Cu hysteresis losses on a ±3T field cycle (Flux jumping not acceptable)	< **1000 kJ/m** ^{3}
n-value at 12 T and 4.2 K	> 20
n^{τ} time constant	< 5 ms
RRR after reaction heat treatment	> 100
Cu:non -Cu ratio	1.0 ± 0.05
Minimum acceptable lengt h of strand	1.5 km or multiples (target value > 3 km)
Heat treatment cycle	Unified cycle, as proposed by ITER IT

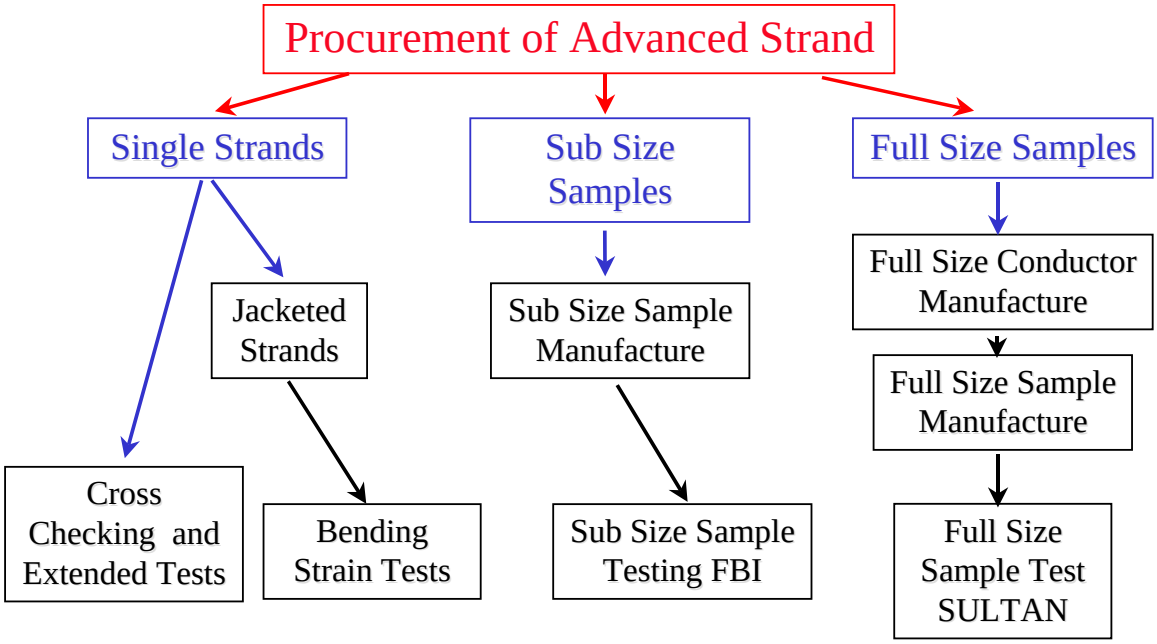

Figure 13. Conductor development programme – main stages

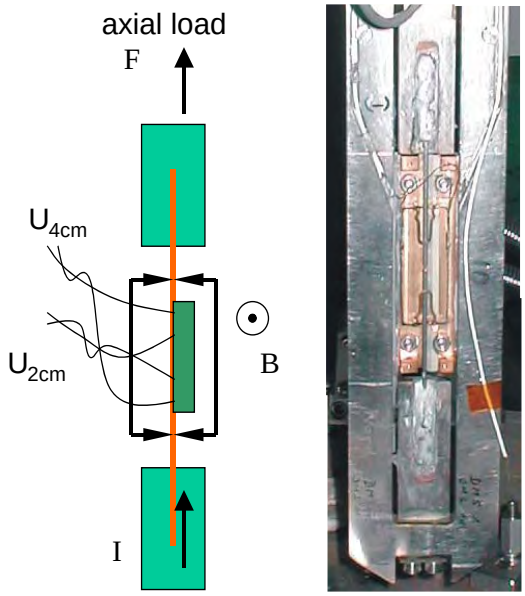

„Small“ FBI

SC-strands : 20 cm, Ø 2 mm

split-coil magnet : 13.5 T

maximum force : 1 kN

maximum current : < 400 A

(with active cooling of current leads)

strain measured by Extensometers

all tests done in LHe

Figure 14. FBI Facility – Status and preliminary results

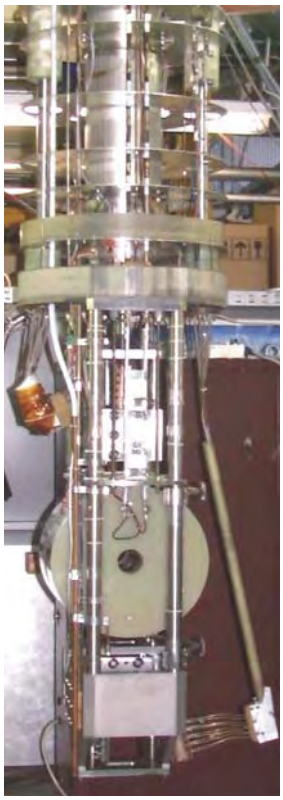

- subsize cable : 110 cm, Ø 2 cm
- split-coil magnet : 14 T
- maximum force : 100 kN
- maximum current : 10 kA

‘ Facility should be ready for first measurements in April 2004.

Figure 15. “Big” FBI Facility

To assess the effect of bending strain on critical current the SS jacketed strand is reacted in the standard ITER sample older and tested, then transferred to other cylinder radius and measured again. The FBI, now, has been improved and it is possible to measure the critical current with the 10 microVolt/m criteria.

Mechanical modeling (Fig. 16) of the superconducting cables is being developed: the aim is to compute the strain in the filaments after heat treatment and during operation. [10] The algorithm scheme being developed for cables homogenisation is the following:

1. Compute effective coefficients at micro level
2. Compute effective coefficients at macro level
3. Apply increment of forces and/or temperature at the macro level, solve global homogeneous problem
4. Compute global strain [E11, E,22, E12]
5. Apply [E11, E22, E12] to meso level cell by equivalent kinematical loading (displacement on the boarder)
6. Solve the kinematical problem, compute stress (unsmearing for meso level) and strain
7. Apply [E11, E22, E12] from meso to micro level cell by equivalent kinematical loading (displacement on the border)
8. Solve the kinematical problem, compute stress (unsmearing for micro level) and strain
9. Verify yielding of the material at the physically true situation at the micro level. If yes change mechanical parameter of the material and repeat the procedure.

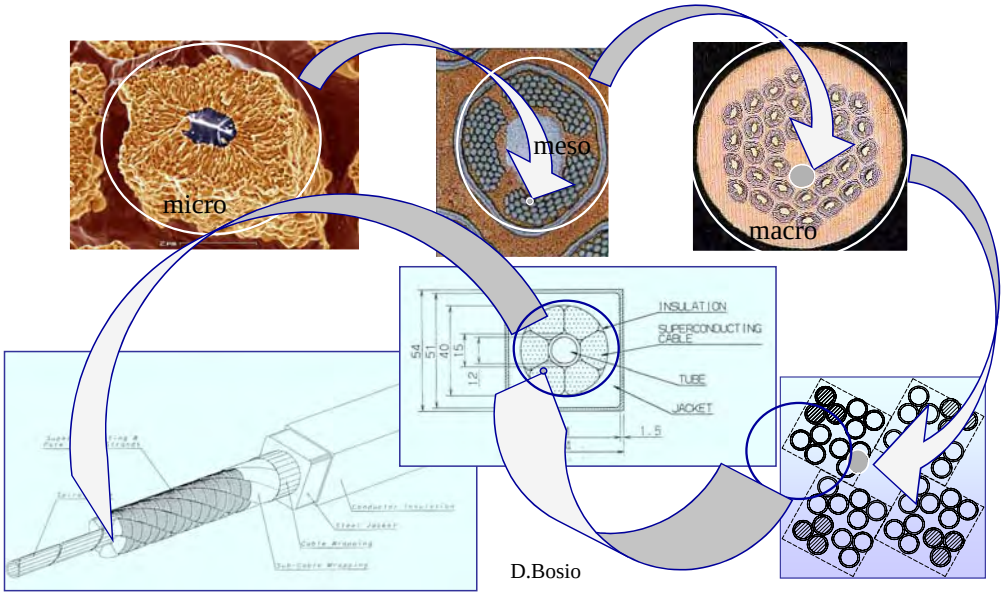

Figure 16. Mechanical Modeling of ITER Superconducting Cables

The final intention is to perform an analysis of the mechanical state of a complete cable. This analysis will start from the model of a last-but-one stage, or a *petal* as it is called in the present jargon, through homogeneisation, finally to a model of the complete cable.

The analysis model for the 3x3x4 petal is composed of two types of Finite Elements: rod elements schematising the strands and specially formulated contact elements along the sub-cable to schematise strand-to-strand interactions. The rod type elements are characterized by the mechanical and thermal properties derived numerically from the first level of this analysis.

The identification of mechanical parameters for the homogenised petal model will be based on three kinds of theoretical analyses:

- Homogenisation based on the results of previous investigations and taking into account the specific spatial organisation of the sub-elements of the petal;
- Identification of the homogeneous model of the petal using various techniques of parametric identification;
- Non symbolic constitutive model using Artificial Neural Networks

The final level of this complex study consists of a Finite Element analysis of the six petals cable, each petal considered as homogeneous with the characteristics derived from the tree previous parameter identification methods.

The effects of the compaction due to the jacket as well as the effects due to the thermal treatment from 923°K to 4°K can be analysed. Once the global behaviour of the cable is studied the "unsmearing" analyses will provide the strain state of the individual stand.

At present the model has reached the following objectives

- A homogenized constitutive macro model for the complex geometry and non-linear, temperature dependent material properties is developed;
- Identification of the micro cell (averaged geometrical characteristics) and micro level homogenisation (Nb3Sn – bronze cell);
- Identification of the meso cell (averaged geometrical characteristics) and meso level homogenisation (homomicro – bronze cell);
- Mechanical and thermal characteristics for the micro and meso homogenised model: orthotropic material.

An application of the code has been made to compute the residual strain in a Nb3Sn strand produced by VAC, going from reaction heat treatment to 4 K. The results of 0.271% residual strain that has been computed is very close to the experimental value.

Other on-going modelling efforts are:

- A predictive code (Thermo-Hydraulic Electro-Magnetic Analysis – THELMA) has been developed in 2001-2002 by University of Bologna, University of Udine and Polytecnic of Turin under the co-ordination of ENEA and EFDA for the analysis of superconductive magnets in transient conditions [11]
- A reconstruction tool (CUrrent Numerical DETermination – CUNDET) is under development since 2001 by C.R.E.A.T.E. for the current distribution estimation from experimental measurements. [12]

It is now necessary to test extensively the predictive code against a set of experimental data and apply it to the prediction of results of new campaigns, and to validate the reconstruction code against experimentaql results and the predictive code.

5. RADIATION EFFECTS

The insulation system of the toroidal field model coil has been tested under radiation. The test results are such that the insulation system is at the limit. Therefore a new insulation system is being developed. Figure 17 shows the resin composition and fig. 18 the results on the various insulation systems.

	TFMC 1	TFMC 2	Test 1	Test 2 (blended)		Test 3	Test 4	Test 5	Test 6	Test 7
Type	DGEBA	DGEBA	Cyanate Ester	DGEBA about 60%	Cyanate Ester about 40%	DGEBA purified	DGEBA	DGEBA compatible	DGEBA	DGEBA purified
Resin	Araldite F	MY745	AroCy-L10	PY306	AroCy-L10	MY790-1	CW229	MY790	LY1025/CH *****)	MY790-1
Hardener	HY905	HY905	----	--	--	HY1102	HW229	HY5200	HY906	HY1102
Additives	DY040	DY072 DY073	Mn Acetyl-acetonat in Nonyl-phenol		Mn Acetyl-acetonat in Nonyl-phenol	***)	(filled)**)	***)	Orlitherm 44	
Impregn. Temp.	75 +/- 5 °C	80 – 85 °C	40°C	70°C		50°C	70°C	70°C	80°C	75°C
Impregn. Viscosity	< 80 mPa s	< 80 mPa s	100 mPa s @25°C	350 mPa s	@25°C	350 mPa s @25°C	2000 mPa s @60°C	~500 mPa s @40°C	70 mPa s @80°C	350 mPa s @25°C
Curing Temp.	100 - > 135°C	90 - > 105°C	80°C gel/ 140°C	80°C 100-160°C	gel 5 hours	80°C gel/ 120-140°C	80°C gel/ 110-140°C	100°C gel 120-160°C/ +180°C Nh	100°C gel/ 130°C	70°C gel/ 120°C ****)
Supplier	Huntsman	Huntsman	Huntsman	Huntsman	Huntsman	Huntsman	Huntsman	Huntsman	ABB	Huntsman
Filler Material	R-Glass + Kapton H	R-Glass + Kapton H	R-Glass + Kapton H	R-Glass +	Kapton H	R-Glass + Kapton H	Ca-Glass fibres	R-Glass + Kapton H	R-Glass + Kapton H	R-Glass + Kapton H
	Currently used	Currently used	Proposed by Huntsman *) high price	Proposed 60% low price	by Huntsman + 40% high	Proposed by Huntsman low price	Proposed by Huntsman	If available without filler (Huntsman)	Currently used	Proposed by Huntsman low price

*) Huntsman is a follow-up company of Vantico which was a follow-up company of former CIBA-Geigy
**) contains less than 0.1% of boron (100% is the full volume of impregnated material)
***) highly purified, no metal compounds in resin and hardener.
****)same resin system as Test 3, but reduced curing temperature
*****) highly chlorine purified resin

Figure 17. Search for systems with higher radiation resistance

A resin system made of epoxy and Cyanide has been chosen for qualification. Also, the effect of the radiation on superconducting strand is being assessed. [13]

It seems that the radiation effect on superconductors characteristic is negligible at the fluence level expected for operation of ITER.

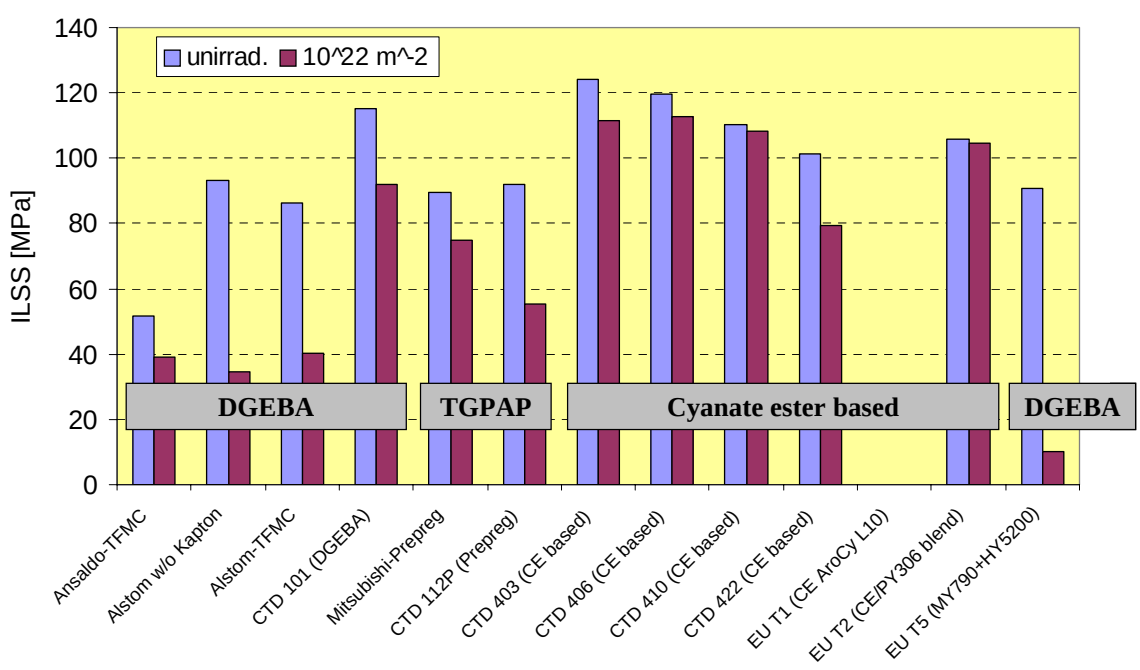

Figure 18. Results of SBS screening tests on various insulation materials

6. CONCLUSIONS

The feasibility of the ITER coils with Nb3Sn strand is demonstrated by the extensive research and development programme carried out worldwide.

The feasibility demonstration of the niobium titanium coils awaits the testing of the poloidal field conductor insert to be curried out in 2005.

An extensive development programme has been launched in Europe, to qualify the advanced performance strand to improve the ITER conductors.

Design codes are being developed to compute the current distribution and strain distribution in the cables in order to better assess the performance of the coils.

An advanced insulation system is being qualified also after irradiation.

REFERENCES

[1] "NET, Fusion Technology"; special issue; July 1988, volume 14

[2] "ITER Conceptual Design"; International Atomic Energy Agency, Vienna 1990

[3] "ITER-EDA Final Design Report"; International Atomic Energy Agency, Vienna 1998

[4] "Technical Basis for ITER-FEAT Outline Design"; International Atomic Energy Agency, Vienna 2000

[5] H. Tsuji et al., "ITER R&D: Magnets: Central Solenoid Model Coil"; Fusion Engineering and Design 55 (2001), 153-170

[6] N. Mitchell, E. Salpietro; "ITER R&D: Magnets: Toroidal Field Model Coil"; Fusion Engineering and Design 55 (2001), 171-190

[7] J.W. Ekin; "Strain scaling law and the prediction of uniaxial and bending strain effects in multifilamentary superconductors"; Filamentary A15 Superconductors, Plenum Press, New York, USA, 1980, 187-203

[8] C. Sborchia et al.; PFCI design and fabrication

[9] A. Vostner, E. Salpietro; "The European Nb3Sn Advanced Strand Development Programme"; SOFT Venice, Italy, 20-24 September 2004

[10] D. Boso et al.; "A Multilevel Homogenised Model for Superconducting Strands Thermomechanics"; submitted to Cryogenics on 2 February 2004

[11] T. Bonicelli et al.; "Superconductive cables current distribution analysis"; Proceedings of the 22nd Symposium on Fusion Technology, Helsinki, Finland, Sep. 2002

[12] A. Formisano and R. Martone, "Optimization of magnetic sensors for current reconstruction", Compel, 22 (2003), 535-548.

[13] K. Bittner-Rohrhofer et al.; "Low temperature fatigue properties of advanced cyanate-ester blends after reactor irradiation"; Adv. Cryog. Eng.; 50/ICMC Conference 2003, 22-26 Sept

NB_3SN ACCELERATOR MAGNETS - INSULATION REVIEW

D. E. Baynham, S. J. Canfer
CCLRC Rutherford Appleton Laboratory, UK

Abstract
In this paper we present a brief review of insulation techniques and consider the critical issues and limitations in relation to the technical challenge presented by future high field dipoles for accelerator application. We present the key issues and use these to define a preliminary insulation specification for a 15T magnet to be studied within the framework of the NED programme [1]. From the basic specification we outline a series of studies to be undertaken under the auspices of NED and look forward to see how we might improve insulation and magnet performance by improving our knowledge of materials.

1. INTRODUCTION

Electrical insulation is one of the most challenging issues governing the engineering exploitation of Nb_3Sn conductors. This is especially true for accelerator magnet applications where the requirement for high current operation and small bending radii dictate the wind and react manufacturing route. The status of insulation development for accelerator magnets has been reviewed by Devred [2].

2. INSULATION TECHNIQUES FOR ACCELERATOR MAGNETS

In this section we review the status of insulation technology and look at new or innovative developments which are underway. For convenience we refer to these as conventional and innovative.

2.1 Conventional

The conventional approach, established over some 10-20 years has been to use a glass or quartz tape wrap or a braid to insulate the basic cable. In some cases the glass insulation has been supplemented by mica film inserted between the turns e.g.: the University of Twente 11 T dipole [3]. In the earliest applications the tape or braid was applied to the cable with its commercial sizing intact. However, it was found that removal of this sizing at the Nb_3Sn heat treatment stage was difficult and could lead to poor electrical resistance levels between turns. Removal of the sizing is now usually done before applying the insulation to the cable. This does make the insulation stage more difficult and does make the insulation more fragile for winding.

Tape insulation is applied as a double layer wrap to give adequate overlap. Braid insulation can be applied using a specialised machine or for short lengths ~100 m the braid can be applied as a sleeve to the cable [4].

After insulation the cable is wound using a conventional machine but great care is required in handling of the cable, clamping and forming around the tight bends at the magnet ends. After winding the coil is clamped in a mould and undergoes the heat treatment process of ~1 week at 650 - 700 C. This heat treatment is carried out in a vacuum or inert (Argon) atmosphere. During heat

treatment there is a risk of damage due to expansion movements. This risk will be increased for the long coils required for future accelerators.

After heat treatment the glass is extremely fragile and great care is required if the coil is to be transferred from a heat treatment mould to an impregnation mould. The final stage in coil manufacture is vacuum impregnation with epoxy. This is a relatively complex process with some risk of failure. It also represents a significant cost for large scale magnet production. Impregnation with epoxy means that helium is excluded from the winding and can play no part in coil stability or heat removal (except at the coil surfaces).

2.2 Novel/Innovative

While many variants/improvements on the conventional insulation route have been developed, the basic process remains similar to the one developed for some of the earliest Nb_3Sn filamentary magnets [5].

2.2.1 Sizing

Significant advances have been achieved by improvements in 'sizing' or in fact by 're-sizing'. Sizing is applied to the glass filaments by the manufacturer to allow commercial handling processes to be used to fabricate tapes.

The commercial sizing is organic and it is not easy to find the precise composition due to commercial secrecy. One approach has therefore been to remove the commercial sizing as a first step and to replace this with a known sizing material to aid conductor wrapping and coil winding. Such an approach has been successfully used by the Berkeley Group using palmitic acid to re-size insulation braid [4].

Apart from this improvement the other steps in magnet manufacture closely follow the procedure given in Section 2.1.

2.2.2 Inorganic/Ceramic route

A more radical approach is to replace the organic sizing with an inorganic or ceramic precursor. This approach is being developed at CEA Saclay and LBNL. In this approach the glass tape is impregnated with a ceramic precursor which fully penetrates the tape fibres. The tape is used to wrap the cable in the conventional way for coil winding.

The standard heat treatment to form the Nb_3Sn also achieves the heat treatment of the ceramic to give a robust insulation and a structurally complete coil. The coil will still have some porosity and the aim is to remove the impregnation stage. For this to be possible the insulation bonded with ceramic must have sufficient mechanical and electrical integrity for magnet assembly and operation. If some porosity can be maintained then helium will penetrate the winding to aid stability.

This route can also be finished by a vacuum impregnation. Significant advances have been made in tape preparation (see Fig. 1).

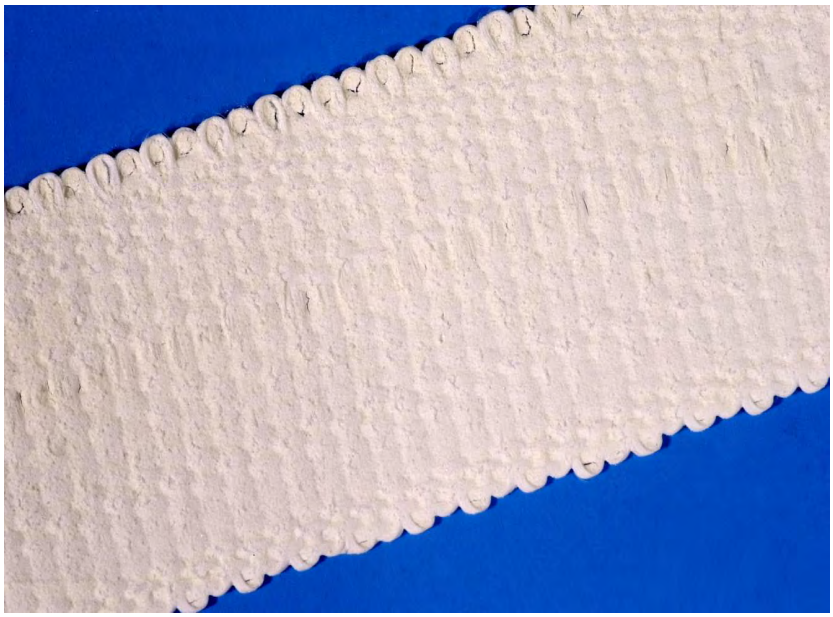

Fig. 1. Ceramic precursor on glass fibre tape produced by Saclay (Courtesy of Francoise Rondeaux)

3. INSULATION – KEY ISSUES, SPECIFICATION

In this section we address some of the key insulation issues and limitations and develop a target specification for a high field magnet.

3.1 Electrical Insulation Strength

The conductor insulation must have sufficient electrical integrity to withstand turn-to-turn voltages generated during a quench. Ground insulation i.e. to the coil support structure, will require a higher specification in terms of breakdown voltage but this can be achieved by additional insulation layers. In this context we consider only the insulation on the cable.

We estimate that the maximum turn-to-turn voltage generated in a quench of a 15 m accelerator dipole will be ~ 250 V which equates to an intrinsic voltage of ~ 600 V/mm for a typical insulation thickness of 0.4 mm turn to turn. Allowing for a safety factor of 4 these values translate into 1 kV turn to turn or 2-3 kV/mm in the insulation laminate. The dielectric strength requirements are therefore not especially demanding when compared with standard laminate (G10) materials which exhibit 20-30 kV/mm. However, these properties do have to be achieved through a complete winding, heat treatment, impregnation, coil assembly and thermal cycle process.

While dielectric properties are not so demanding the need for integrity is very high. Insulation failure will have serious consequences because of the high stored energy density in a 15 T dipole.

3.2 Thickness

Insulation thickness is important for 3 reasons:

3.2.1 Current density

Typically, the insulation will occupy ~20% of the winding space and will impact on current density overall. Current density improvement is therefore a driver to reduce insulation thickness

3.2.2 Thermal contraction

In a dipole winding the insulation will affect the azimuthal thermal contraction of the winding block. If the insulation is essentially a glass/epoxy laminate the transverse thermal contraction will be strongly dependent on glass content e.g. 50 % glass by volume will give an integrated thermal contraction 6-7x10^{-3} while 60 % glass by volume will give ~4x10^{-3} which is much closer to the conductor properties.

Low glass content will affect the pre-compression required at room temperature. However, the desire to compress the winding heavily at the impregnation stage to achieve high glass content must be tempered with the risk of crushing insulation and creating a fault. Over-compression at this stage may also prevent resin penetration which can also lead to reduced mechanical and electrical properties.

3.2.3 Winding modulus

Insulation thickness will affect the winding modulus and will influence movement under magnetic loads. Again the desire is to compress to reduce insulation thickness, increase glass content and hence modulus.

The above arguments are drivers for reducing insulation thickness. However, as discussed in Section 3.1 insulation integrity is paramount for production magnets. A very thin insulation, if it could be realised, would have little tolerance for cable imperfections and may be prone to damage at high loads. So the simple geometric spacing provided by the insulation is in itself an important factor which should not be discarded. In our view a robust insulation which facilitates coil manufacture with high integrity is more important than 10% improvement in current density.

Typically, for S glass, the minimum commercial tape thickness is ~0.1mm giving an insulation thickness on the cable of ~0.2mm with double overlap. The thickness can be reduced by using a single tape wrap with mica insulation inserted between turns [3]. Tape thickness is not so much a fundamental property of the materials but more one of commercial availability. In principle, tapes of 0.06-0.08mm could be made and used for winding.

Braid offers potential reductions in thickness because it is nominally a single layer.

3.3 Mechanical Properties

The mechanical properties of the insulation must be compatible with all phases from cable taping, through winding, heat treatment, impregnation, assembly (collaring ~ 200 MPa), cool down (thermal stresses) and magnet operation. We have already commented on the winding requirements. In this section we will address the operational requirements. In a cos-theta or block type design the principal loading in the straight section will be compressive, applied through the cable and insulation laminate thickness see Fig. 2. Typically, magnetic loading will be 150-200 MPa (average) with high local stresses due to the cable structure.

For a standard, G10 type, laminate a compressive strength of 600-800 MPa through the thickness is readily achievable. For an insulation laminate made in-situ with heat treatment, i.e. magnet fabrication conditions, ultimate compressive strengths are not known.

The design of a high field dipole will aim to eliminate tensile stresses and minimise shear stress in the straight sections. However, it is clear that localised shear and tensile stresses will be present in the straight sections and it is difficult to eliminate more global shear stresses in the coil ends. The insulation should therefore have capacity to resist shear and tension loads. The scale of these stresses should form part of the NED magnet design study.

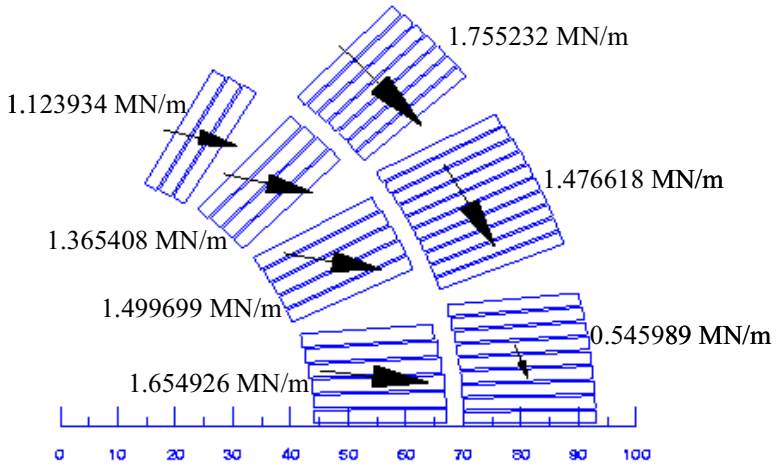

Fig. 2. Mechanical forces on a 15 T, 88 mm aperture dipole [6].

3.4 Radiation Hardness

For an LHC upgrade or future high energy accelerator applications increased radiation hardness of the coil insulation is important. Currently radiation resistance of this insulation is a limiting factor.

Conventional epoxy-glass materials are limited to doses of 10^8 Gy. Dipoles used in interaction region applications may receive doses in excess of this, although the dose can be reduced by an order of magnitude by design - for example block coil as opposed to cos-theta. The block coil design moves the sensitive winding away from the damaging particles [9]. Cyanate-ester resins, although expensive, have received attention by the fusion community and may offer increased radiation resistance compared to epoxies. However they are also organic materials and will be susceptible to radiation induced damage, particularly by high-energy neutrons. An inorganic material should offer the ultimate solution to radiation stability, hence the interest of CTD and Saclay in this area.

Testing of radiation hardness should be a part of the NED programme as it will be a critical factor in the design and determination of useful lifetime of the dipole.

3.5 Thermal Conductivity

Thermal conductivity of the insulation is a parameter which can be important for magnet operation. Between cables it will have some influence on stability (MPZ) but is unlikely to be high enough for the effect to be significant for magnet performance. Thermal conductivity will also influence the peak temperature due to steady state or transient beam losses. For a laminate of glass/epoxy conductivity is dependent largely on the epoxy content. Typically, a laminate will have transverse thermal conductivity ~ 0.05 W/m/K. There is not much scope to improve this in a Nb_3Sn dipole [10].

3.6 Helium Porosity

An insulation system that allows penetration of helium to the internal part of the cable is an objective of the innovative, ceramic-bonded insulation. With ‘conventional’ epoxy-impregnated, helium porosity is not feasible. Overall, the benefits of porosity with its potential for improved conductor

stability will need to be balanced against the mechanical properties required at 15 T. Porosity will reduce the mechanical properties of the insulation/winding and could lead to movements or stress cracking under high stress conditions.

3.7 Outline Specification

The target specification for insulation is given in Table 2.

4. NED INSULATION DEVELOPMENT PROGRAMME

An R&D programme for insulation development has been set up under the overall Next European Dipole Programme (NED). Two R&D strands are planned:

(i) Conventional insulation development by CCLRC, Rutherford Appleton Laboratory

(ii) Innovative insulation development by CEA Saclay. This programme will build on the existing CEA developments with the aim of meeting NED specification level.

4.1 R&D Programme Overview

The programme will include all facets of insulation development from magnet design and analysis to define mechanical requirements and specification through to testing of large scale samples.

Generic tests will be developed to characterise materials and process routes. These tests will include; electrical insulation, thermal contraction, and a range of mechanical tests including tensile, compressive, shear and work of fracture.

In addition special test samples will be developed to give better simulation of real winding behaviour e.g. compression stacks and short beam shear. These samples will be characterised in standard testing machines with capability to operate at 300 K, 77 K and 4.2 K.

For characterisation of epoxy systems specialised equipment such as a Dynamic Mechanical Analyser and a Differential Scanning Calorimeter will be used. A DMA can be used to evaluate temperature dependence of mechanical properties. A DSC can evaluate parameters such as reaction kinetics and T_g (glass transition temperature).

4.2 Materials Improvement

The aim of the programme will also be to develop new processes and tests with the objective of improved performance.

Work of fracture is a materials property that is not well understood in resin and composite materials at low temperatures. Fracture properties are significant for magnet performance because crack propagation can induce quenches and crack propagation is determined by fracture toughness. A better understanding of fracture properties in insulation materials could lead to enhanced magnet performance. Reducing or eliminating cracking at relatively low stresses has more relevance to magnet stability than improving the ultimate strength.

Historically epoxy resins have been formulated for use at low temperature by either using high levels of filler to reduce thermal contraction, or by making the epoxy inherently tough. High filler loadings are not compatible with vacuum impregnation processing routes. There are opportunities to improve fracture properties of the basic resin systems using recently developed materials such as:

Table 2. Tentative target specification.

1	GENERAL	Design
1.1	Insulation thickness per cable	0.2 mm
1.2.1	Winding compatibility: capable of being applied to the cable and formed into a dipole winding by a semi-automatic winding system	Minimal fraying or abrasion at winding
1.2.2	Conductor bend radius minimum	20 mm
1.3	Compatibility with Nb_3Sn heat treatment cycle	Minimal degradation of basic components
1.4	Thermal cycles to low temperature:	10
1.5	Running cycles:	100
1.6	For conventional organic insulation scheme and innovative scheme if applicable: ability to be impregnated with liquid of viscosity up to	200 mPa.s
2	MECHANICAL (design stresses are before irradiation)	Design
2.1.1	Applied conductor winding load	50 kgf
2.1.2	Compression during heat treatment	20 MPa
2.1.3	Coil re-shaping after heat treatment before impregnation	10 MPa
2.1.4	Compressive stress after coil fabrication – at 300 K and 4 K	200 MPa
2.2	Shear: Short-beam shear strength at 4K	50 MPa
2.3	Tension: Transverse tensile strength of insulation laminate at 4K	25 MPa
2.4	Fracture specification: need to know properties at 300K and 4K	TBD
2.5	Thermal contraction (to match conductor contraction). Integrated thermal contraction [300K to 4K]	0.003 to 0.004
2.6	Thermal conductivity at 4.2K	>20mW/mK
3	ELECTRICAL	Design
3.1	Breakdown voltage inter-turn	1000 V (2500 V/mm)
3.2	Breakdown voltage inter-turn tested in helium at 300K	500 V
4	RADIATION	Design
4.1	Lifetime	10 years
4.2	LHC Interaction region, maximum 10% reduction in mechanical and electrical properties after the following exposure:	
	Cos-theta design dose	650 MGy
	Fluence >0.1 MeV	$30x10^{16}$ cm^{-2}
	Block coil design Dose	55 Mgy
	Fluence >0.1 MeV	$2.5x10^{16}$ cm^{-2}
	Neutron dose at high energy (>10 MeV)	

(i) Dendritic hyperbranched polymers, which have been shown to be able to double the interlaminar fracture resistance of epoxy based composites and to reduce the internal stress level by as much as 80 % with only 10 phr of modifier. These property improvements were obtained without affecting the viscosity, and thus the processibility, nor the glass transition temperature of the epoxy resin [7].

(ii) Nanofillers (clay). Layered clays were used as nanoparticle fillers in fibre reinforced polymeric materials (epoxy composites). Transverse cracking in response to cryogenic cycling was significantly reduced when nanoparticle fillers were used at concentrations much lower than those used for traditional fillers e.g. 5 phr. Nanoclays have been shown to modify traditional fibre reinforced composite materials and enhance their resistance to thermal cycling induced stresses [8].

5. SUMMARY

Insulation for Nb_3Sn magnets remains one of the most challenging issues for the engineering exploitation of Nb_3Sn conductors in future accelerators. The design, processing route, materials properties and end product are totally interdependent. The aim through NED is to achieve a better specification for insulation in a 15 Tesla dipole magnet – this will be an interaction between magnet design, fabrication route and materials.

The aim is also to explore and develop new materials with appropriate characteristics for this critical application.

REFERENCES

[1] http://lt.tnw.utwente.nl/project.php?projectid=9

[2] A. Devred, "High-field accelerator magnets beyond LHC," Proc. 2003 Particle Accelerator Conference, pp. 146-150

[3] A. den Ouden, S. Wesel, E. Krooshop, R. Dubbeldam and H.H.J. ten Kate, "An experimental 11.5 T Nb_3Sn LHC type of dipole magnet," Applied Supercond. Centre, Univ. of Twente, The Netherlands. IEEE Trans. on Magnetics, vol. 30, No. 4, July 1994, pp. 2320-2323

[4] Arkan et al, "Studies on S-2 fiber glass insulation for Nb_3Sn cable", FNAL TD98-063 (1998)

[5] R.Q. Apsey, D.E. Baynham, C.A. Scott, "Filamentary niobium-tin hexapole magnet," MT-6 (1977), p. 546

[6] O. Vincent-Viry, "Preliminary design of a 88 mm aperture, 15 T dipole," NED steering committee meeting, January 2004

[7] R. Mezzenga et al., "A review of dendritic hyperbranched polymers as modifiers in epoxy composites," Comp. Si. Tech. 61 (2001), pp. 787-795

[8] J.F.Timmerman, "Nanoclay reinforcement effects on the cryogenic microcracking of carbon fiber/epoxy composites," Comp. Si. Tech. 62 (2002), pp. 1249-1258

[9] Mohkov et al, "SC magnets in high radiation environment at supercolliders," presented at 43rd workshop: Super Magnets for Supercolliders, Erice, October 2003

http://supercon.lbl.gov/erice/

[10] A. den Ouden and H.H.J. ten Kate, "Thermal conductivity of mica/glass insulation for impregnated Nb_3Sn windings in accelerator magnets," Cryogenics, vol. 34, p. 385

ACCELERATOR MAGNET FABRICATION AS RELATED TO STRAND AND CABLE PROPERTIES

Stephen A. Gourlay
Lawrence Berkeley National Laboratory, Berkeley, CA

Abstract
The requirements for new accelerator applications are increasing the demand for high performance magnets. Progress in the development of superconducting materials, particularly Nb_3Sn, has encouraged increased activity in several R&D programs world-wide. New techniques for design, analysis and fabrication of magnets using these materials are being developed. This report highlights some of the advantages and challenges of Nb_3Sn for accelerator magnet design and fabrication.

1. INTRODUCTION

Achieving fields above 10 T requires the use of conductor with performance parameters that exceed the limits of NbTi. Possibilities include High Temperature Superconductors (HTS) or the A15 compounds. High Temperature Superconductors have been under intensive study and development for some time. The properties of these materials make them interesting for applications requiring high fields and/or high heat loads, such as interaction region quadrupoles. However, their mechanical properties and cost are still major drawbacks. Until significant progress is made, these materials will probably only be considered for use in cases where performance is essential to meet operational requirements. And even then, mechanical issues such as non-recoverable strain degradation have not been thoroughly studied. One possibility that has some near-term potential is the recently discovered MgB_2 superconductor. It could be considered for low-field, high heat load applications.

The most practical and available A15 material is Nb_3Sn. In a practical geometry, magnets based on Nb_3Sn technology should be able to exceed 14 – 16 T at 4.2 K. Although this material has been around for 40 years, its use and development has been hampered due to its intrinsic brittleness and strain sensitivity. The challenge for magnet designers lies in incorporating it into a realistic magnet where it is subjected to stresses that could exceed 150 MPa. The future need for higher fields has prompted an increased development effort that has recently resulted in significant progress.

2. US/HEP CONDUCTOR DEVELOPMENT PROGRAM

Funding for a new HEP Conductor Development Program was provided in January, 2000 [1]. This program is focused on industrial development, and is administered by LBNL. The purpose of this work is to develop a new, cost-effective superconductor for use in future accelerator magnets, with the following target specifications:

J_c (non-copper, 12T, 4.2K): 3,000 A/mm^2

$J_{engineering}$(12T): greater than 1,000 A/mm^2

Effective filament size: as small as feasible, while compatible with the J_c and cost-effectiveness requirements

Process unit size: scaleable to greater than 100 kg and average piece lengths greater than 10,000 m in wire diameters of 0.3 mm to 1.0 mm

Wire cost: less than $US1.50/kA-m (12T, 4.2K)

Short heat treatment times: maximum 400 hours; target 50 hours for wind and react magnets

This is envisioned as a multi-year program with two phases that may partially overlap. The first phase (2-3 years) is primarily an R&D program leading to an improved understanding of the factors that influence conductor performance and cost. Using the new knowledge gained from this research as a base, the program will evolve towards a fabrication scale-up phase where the performance and cost-effectiveness can be demonstrated on production-size quantities. This program has been underway for about 3 years, and has achieved considerable technical success. One of the key parameters, critical current density, has been increased from the 2000 A/mm^2 level to over 3000 A/mm^2 at 12 T. A comparison of conductor performance properties is shown in Fig. 1.

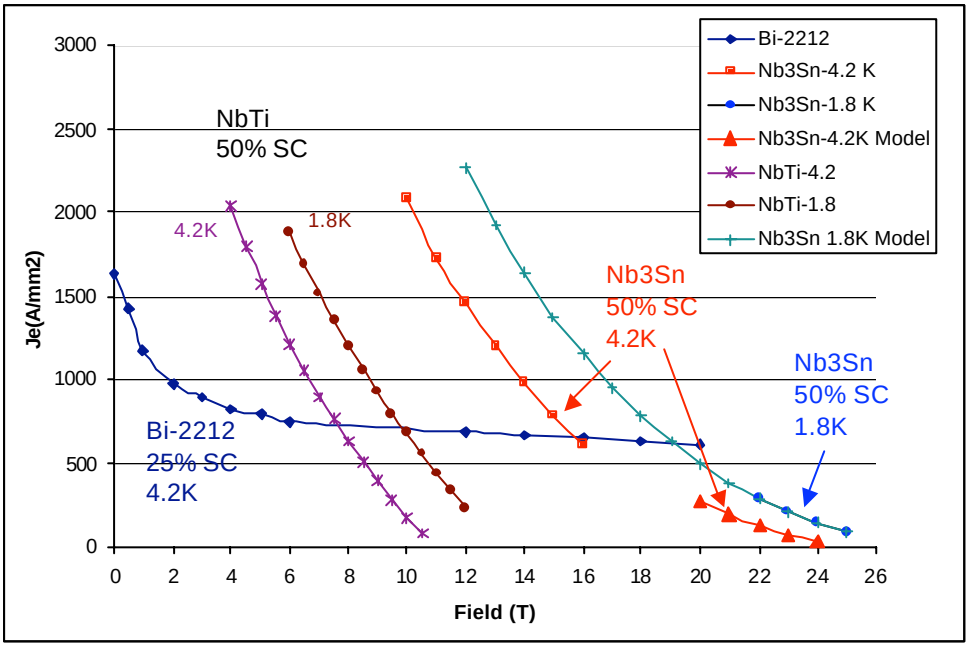

Fig. 1. Conductor Performance Comparison

Nb_3Sn has some excellent properties; high current density at high field and a much higher thermal margin than NbTi. This potential has been demonstrated up to 16 T so far [2]. In achieving this field and associated stress level, many mechanical issues had to be overcome. New designs and fabrication techniques have been developed taking into account the intrinsic properties of the strand and cable both before and after reaction. Nb_3Sn has a higher sensitivity to cabling degradation and the effects resulting from the degradation have significant influence on magnet performance. Developing the superconducting compound is a diffusion process and leads to issues not found in NbTi. Barriers, designed to prevent diffusion of tin into the copper, which can result in a low residual resistance ratio (RRR), are extremely fragile. In addition, barrier breakage can lead to coalescing of the filaments and a large effective filament diameter. These difficulties are enhanced by the desire to make the barriers as thin as possible, particularly in the high performance strands.

Along with excellent performance properties, Nb_3Sn is also known for brittleness and strain sensitivity. The large temperature range (1000 K – 4 K) and high field applications which impose large stresses, calls for careful analysis, appropriate design choices and new fabrication techniques. There are several implications for long magnets that will need to be studied as part of the overall development plan for this technology.

On the positive side, it has been demonstrated in LBNL's HD-1 block magnet [2], that stresses up to 150 MPa do not degrade magnet performance. With the information available at this time it seems prudent to avoid situations of non-uniform compressive stress and to minimize tension as much as possible even though a reacted strand is in axial compression and some current density might be regained by placing the strand in tension. Cables and coils are complex structures and it is not clear if there is any positive effect on overall performance. An example of a design choice is, noting that strain degradation increases with magnetic field, to separate the high field and high stress regions of the magnet. One still needs to be wary of high stress during assembly and cooldown though. One should also be aware that strain sensitivity depends on the strand substructure. Each strand geometry should be evaluated individually. While recent results regarding stress limits are encouraging, more work needs to be done to determine a reasonable working range for magnets.

Field quality is just starting to be addressed. The thicker insulation currently used for coil fabrication and the large thermally-induced movements, make coil size and uniformity control more difficult. Though there is still much to be gained by reducing filament size, it is clear that Nb_3Sn will still suffer from large intrinsic magnetization affects. Fermilab has made progress on both fronts in their cos-theta dipole program [3, 4]. A series of magnets has shown that field quality is more reproducible than originally expected and passive shield has been used to significantly reduce magnetization.

3. FABRICATION METHODS

Nb_3Sn requires heat treatment at 650^0 C for 60 - 100 hours, followed by epoxy impregnation to support the brittle cable and provide insulation. And stress should be limited to between 150 and possibly up to 200 MPa during all stages of fabrication and operation. There are two fabrication methods for Nb_3Sn coils; wind and react and react and wind. These two processes differ up to the point just prior to impregnation.

3.1 Wind and React

Cable considerations

The more extreme case, and unfortunately more favorable for magnet design, is to use a large cable with a small bend radius. As mentioned above, Nb_3Sn strands are more susceptible to degradation and the consequences are more severe. The trade-off between degradation and mechanical stability is the primary consideration in determining the cable dimensions. A large cable with small bending radius requires increasing the winding tension, which in turn requires a more mechanically stable cable, i.e. increased compaction and a greater probability of degradation. An example of such a cable is that used for HD-1 [5]. Parameters and winding conditions for this cable are shown in Table 1.

Table 1. HD-1 Cable parameters and winding conditions

Strand diameter	0.8 mm
Number of strands	36
Cable dimensions	1.36 x 15.7 mm (rectangular)
Winding tension Bend radius	18 kg 10 mm
Insulation	S-2 glass (0.107 mm @ 14 MPa)

The cable was initially rolled to 1.41 mm, annealed and re-rolled to the final thickness of 1.36 mm. The annealing serves two purposes; the cable is more malleable, reducing filament distortion and damage and it also "pre-shrinks" the cable, eliminating a large fraction of the length change during reaction. Figure 2 shows a dilatometry measurement made on a strand and the reduction in length change due to a pre-anneal [6].

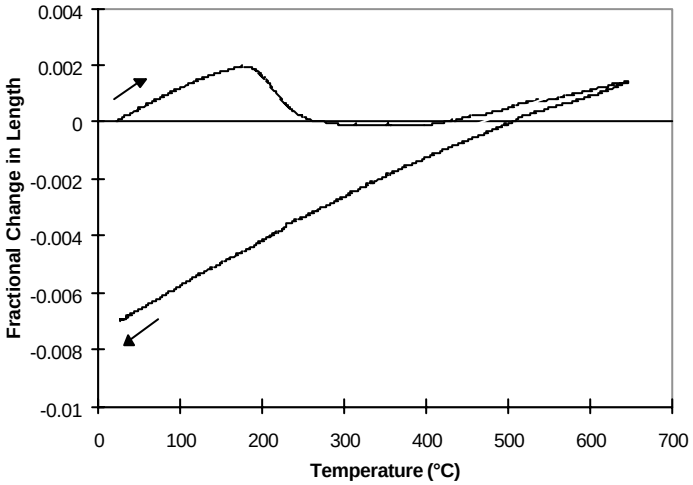

Fig. 2 Length change in Nb_3Sn strand during reaction process

The cable cross section is examined microscopically for barrier cracking and filament distortion which is considered unacceptable. Figure 3 shows an edge of the HD-1 cable.

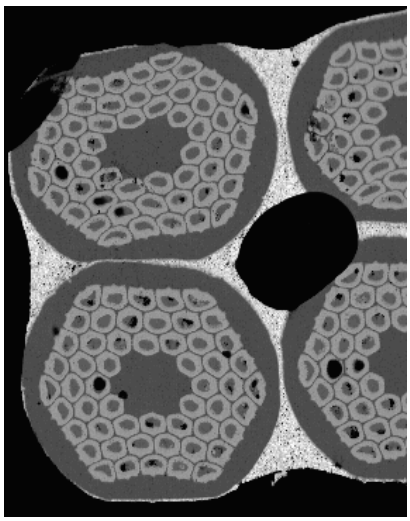

Fig. 3 HD-1 cable cross section

Design and evaluation of Nb_3Sn cables and the relationship to magnet performance is just beginning. Future considerations should include:

Determining the deformation limits of different strands

Cables with a mixture of Cu and superconducting strands

Keystoned and rectangular cables with cores

Cable handling and winding characteristics database

Relate cable parameters to type of strand, width and thickness, core and no core to winding mechanics, i.e. popped strands, winding direction, etc.

With the considerations and minor exceptions stated above, winding the coils is the same as for NbTi. During reaction, the coil is constrained in all dimensions. A pressure of 14 MPa is applied normal to the cable face with moderate compaction in the orthogonal directions. A gap of approximately 1mm/m is used to accommodate coil shrinkage during reaction.

3.2 React and Wind

The react and wind approach is driven by concern over the potential problems in reacting long coils and as the only alternative for winding cols made with HTS, for which wind and react is not an option. The primary limitations are large bending radii, coil sizing (not being able to apply large forces to reacted conductor) and the QC challenge of handling and winding the reacted cable. There are small programs at Brookhaven and Fermilab that have shown some encouraging results [7, 8]. Brookhaven is making "10-turn" coils with Nb_3Sn and HTS and they have plans to fabricate 12 T racetrack coils next year using react and wind. After a couple of fairly successful Nb_3Sn racetrack coils, Fermilab is taking a more fundamental approach by studying the degradation and stability of strands manufactured by different processes. Cable studies look at bending-induced degradation limits, interstrand resistance and cores, and techniques to prevent sintering during reaction. They plan to assess the most promising technologies in small magnets.

4. DESIGN AND ANALYSIS

Each of the coil fabrication techniques results in an epoxy impregnated coil that must be properly constrained without exceeding stresses that could damage the coil during assembly, cooldown and operation. The LBNL design team has developed a design approach that integrates cross section design, generating the coil geometry, CAD and Finite Element Analysis (FEA). Three-dimensional analysis is standard procedure and considered necessary to control and/or limit maximum stress on the conductor. Considerable progress has been made in correlating magnet performance with the FEA models.

5. SUMMARY

Recent work on Nb_3Sn accelerator magnets has given us a point in parameter space that we are comfortable with. Continuing work will tell us how far current constraints and parameters can be expanded. Much more needs to be done to develop the technology for real HEP applications.

ACKNOWLEDGEMENTS

Thanks to Shlomo Caspi, Dan Dietderich, Paolo Ferracin, Hugh Higley, Roy Hannaford, GianLuca Sabbi and Ron Scanlan from LBNL, Arup Ghosh and Ramesh Gupta from BNL and Giorgio Ambrosio from FNAL.

REFERENCES

[1] Scanlan, R.M., Dietderich, D.R., and Zeitlin, B.A., "Development of Cost-effective Nb_3Sn Conductors for the Next Generation Hadron Colliders", Advances in Cryogenic Engineering **48B**, Plenum Press, New York, 2002, pp. 933-940.

[2] Lietzke, A.F., et al., "Test Results of HD-1, a 16 T Block-Dipole Magnet," to be published in the proceedings of the 18th Magnet Technology Conference, Morioka, Japan, October, 2003.

[3] E. Barzi, et al., "Field Quality of the Fermilab Nb_3Sn Cos-theta Dipole Models", proceedings of the 2002 European particle Accelerator Conference, Paris, June 2002, p.2403.

[4] V. V. Kashikhin and A.V. Zlobin, "Correction of the Persistent Current Effect in Nb_3Sn Dipole Magnets," *IEEE Trans. on Applied Superconductivity*, Vol. 11, No. 1, March 2001, pp. 2058-2061.

[5] Hafalia, A.R., et al., "HD-1: 16 T, Nb_3Sn Dipole Magnet Design and Fabrication," to be published in the proceedings of the 18th Magnet Technology Conference, Morioka, Japan, October, 2003.

[6] D. Dietderich, J.R. Litty and R.M. Scanlan, 1997 Cryogenic Engineering Conference and International Cryogenic Materials Conference, July 1997, Portland, OR, pp. 1013 – 1020.

[7] Ambrosio, G., et al., "Design Modifications, Fabrication and Test of HFDB-03 Racetrack Magnet Wound with Pre-Reacted Nb_3Sn Rutherford Cable," to be published in the proceedings of CEC/ICMC, September 2003.

[8] Gupta, R., et al., "Status of High Temperature Superconductor Magnet R&D at BNL," to be published in the proceedings of the 18th Magnet Technology Conference, Morioka, Japan, October, 2003.

SUPERCONDUCTING STRANDS

INVESTIGATION ON TECHNICAL SUPERCONDUCTORS FOR LARGE MAGNET SYSTEMS IN BOCHVAR INSTITUTE

A.K.Shikov, V.I.Pantsyrny, A.E.Vorobieva, G.P.Vedernikov
Bochvar Institute of Inorganic Materials (VNIINM), Moscow, Russia

Abstract
The materials science of technical superconductors in USSR and later in Russia has been concentrated in Bochvar Institute of Inorganic Materials. This paper reviews the main activities of Bochvar Institute in design and development of the NbTi, NbTiTa and Nb_3Sn superconductors. The critical features of design and factors of manufacturing processes determining the superconducting properties of the technical NbTi and Nb_3Sn superconductors are analyzed. The data on tantalum influence on the NbTi wires superconducting properties is given. The examples of NbTi wires designed for large projects such as accelerator (UNK), tokamaks (T-7 and ITER) are presented. The comparison of bronze processed and internal tin Nb_3Sn wires has been done. The properties of the Nb_3Sn wires designed and fabricated for application in toroidal field coil insert and toroidal field coils of ITER magnet system are discussed. The examples of Nb_3Sn wires strengthened by the microcomposite Cu-Nb alloy are presented. The perspectives of the further increase of superconducting properties for both types of Nb_3Sn wires have been estimated.

1. INTRODUCTION

Bochvar Institute of Inorganic Materials (BI) has begun the investigations on the technical superconducting wires in late 1960-s. For shortening the transfer of the designed manufacturing processes from laboratory to the industry, industrial scale equipment was installed in the experimental shop of BI. In this way, full-scale pilot batches of superconducting wires could be produced just after the initial development and testing of designed laboratory samples. The primary objectives were the development of winding wires for the first tokamak in the world with superconducting magnet system (T-7) [1] and for the magnet system of the Serpukhov's accelerator (UNK). Both tasks have been completed successfully [2]. An industrial production of superconducting wires in USSR was then established in 1970-s.

The superconducting wires for many other applications were also designed, including NbTi wires for MRI tomographs, generators, for persistent current switches, for different types of scientific devices – wigglers, gyrotrons etc. [3-6].

Work on Nb_3Sn superconductors was initiated practically at the same time, beginning with the tape conductors produced by liquid phase reaction of the Zr doped Nb with Sn-Cu melt [7]. In the beginning of 1970-s the development of multifilamentary Nb_3Sn superconductors by bronze process and internal tin process was started.

For Tokamak-15 [8], a force-flow cooled conductor (340 m long, 17.4mm by 6.5mm in cross section) consisting of Nb_3Sn-based superconducting transposed wire with 11 individual bronze processed nonstabilized strands (1.5 mm in diameter), two copper tubes (4.0 mm in external diameter, 0.5 mm in

wall thickness), and a 1.2 mm thick electrolytic copper layer incorporating them (Fig.1) was developed [9]. The critical current of such a current-carrying element was larger than 8.5 kA in a field of 8 T. Approximately 90 t of conductor were produced in an industrial way, requesting the production of more than 25 tons of wires. The TF coils were produced by the react and wind method. The positive experience of the use of Nb_3Sn wires in large magnets opened way for further development of even larger Nb_3Sn based magnet systems.

At present, the progress in High Energy Physics and Fusion relies on the successful realization of currently running Projects such as the LHC and ITER. Magnet systems of both facilities consume around 1000 tons of NbTi and Nb_3Sn superconductors each. Therefore the question of cost is one of the important factors altogether with performance parameters. Next generation of accelerators and fusion reactors will require higher magnetic fields (in the range of 12-16 T), which is a challenge for currently existing commercially available superconductors. The possible superconductor candidates for high field (14-16 T) magnetic systems are YBCO, Bi2212, Nb_3Al, Nb_3Sn (Fig.2).

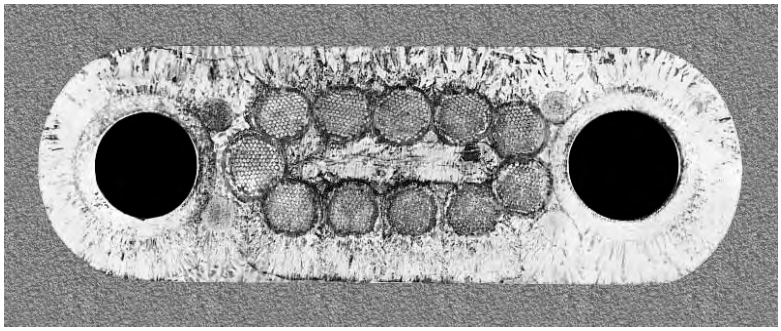

Figure 1. Cross section of force-flow cooled Nb_3Sn conductor for toroidal field coils of T-15

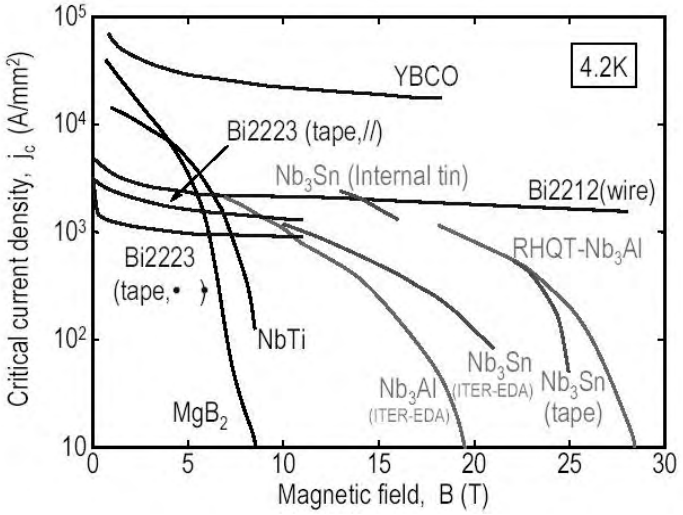

Figure 2. The schematic comparison of current-magnetic field properties for different contemporary superconductors [10,11].

Taking into account the abovementioned cost factor, which practically eliminates the high temperature superconductors, it could be stated that for the nearest future the choice of wires is limited to Nb_3Al and Nb_3Sn, both low temperature superconductors.

2. INVESTIGATION ON NBTI WIRES

The NbTi wires due to excellent mechanical properties and low cost were and still remain the workhorse for the magnetic fields up to 8 T. The main objectives of the initial R&D program were to develop NbTi multifilamentary wires with higher critical current density (Jc), lower losses or finer filaments, longer piece lengths, higher wire uniformity and greater yields. One of the crucial problems was to avoid significant filament sausaging (the variation in filament diameter along the length of the wire). The most important factor influencing on sausaging was the formation of brittle Cu-Nb-Ti intermetallic inclusions at the superconductor-Cu interface. These inclusions do not deform uniformly with the filament during wire drawing, leading to filament sausaging. Introduction of Nb diffusion barrier is now widely used to prevent intermetallic inclusions formation [6].

The nature of deformation of BCC NbTi filaments in FCC Cu matrix by cold drawing also could lead to sausaging through texturing. During the deformation the texture of drawing with direction of z = [011] is developing in NbTi filaments. In BCC NbTi the dislocations slipping system [111](011) is prevailing, therefore (due to the texturing) less than 5 active slipping systems remain. In this case a uniform deformation is substituted by a plane deformation and instead of obtaining cylindrical filaments, the finale shape is ribbon like. To mitigate this effect the local volume fraction of NbTi should be properly chosen through nonuniform arrangement of filaments in the strands cross section [12].

The abovementioned major problems were resolved in the late 70-s and reliable technical NbTi wires with high critical current became commercially available. In 1978 the first tokamak in the world with superconducting magnetic system T-7 has been successfully built and tested. For the Russian accelerator program UNK, 120 tons of NbTi wires with 8910 filaments (6μm in diameter) and critical current density up to 2600 A/mm^2 have been produced. Later on, critical current density up to 3000 A/mm2 (5T, 4.2K) in commercially produced wires has been attained.

Today the limit of accelerator magnets wound from binary NbTi conductors and operated in superfluid helium at 1.9 K lies in the 10-to-10.5T range. It is possible to raise Bc2 of NbTi by addition of Ta. In Bochvar Institute two 4620 filamentary strands were designed and fabricated on the base of ternary NbTiTa alloys with 12 and 20 wt.% Ta (whose layout meets the LHC specifications) [13-17]. The main efforts were focused on the preparation of highly homogeneous alloys and the optimization of heat treatments to achieve high Jc at high fields. At 2K maximum Jc for NbTi-20wt%Ta strand reached 1550 A/mm2 at 10 T and 750 A/mm2 at 12 T. At 1.85K Jc is increased by 20% attaining 450 A/mm2 at 13 T which was about twice higher than that obtained in NbTi strands.

In the framework of the ITER Project the RF Participant Team has manufactured the NbTi Cable, and shipped it to EFDA for further fabrication of poloidal field insert coil (PFCI). The testing of PFCI is planned to be carried out in Japan during 2004. The wire was designed and produced in Bochvar Institute in an amount of 400 kg and cabling was performed at the Cable Institute. The cross section of this wire is presented in Fig.3. The parameters of this wire were as follow: Wire diameter of 0.73 mm; Number of filaments 2346; Filament diameter 9.8 μm; Cu/non Cu Ratio 1.4; Critical current density (by specification) > 2700 A/mm2 (5T, 4.2K); (2800-2900 A/mm2 – measured values). The fabrication of the wire was carried out from composite billets of intermediate size because of the relatively small amount of

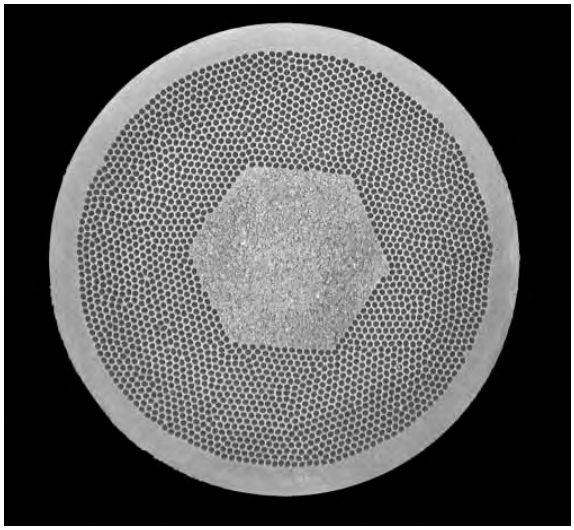

Figure 3. NbTi wire designed and produced for fabrication of ITER experimental poloidal field coil-insert (PFCI);

wire was needed [18]. That is why the critical current density of these wires was specified to be slightly less than it should be in the final wires for the PF coils.

In the course of preparation for the PFCI testing some benchmarking measurements were undertaken. The Bochvar Institute characterized the strands for PFCI in a wide range of temperature and magnetic fields. The same work has been carried out in CEA (France). Comparison of CEA results with those of BI (defined as VNIINM in Fig.4) was done for the five values of B explored.

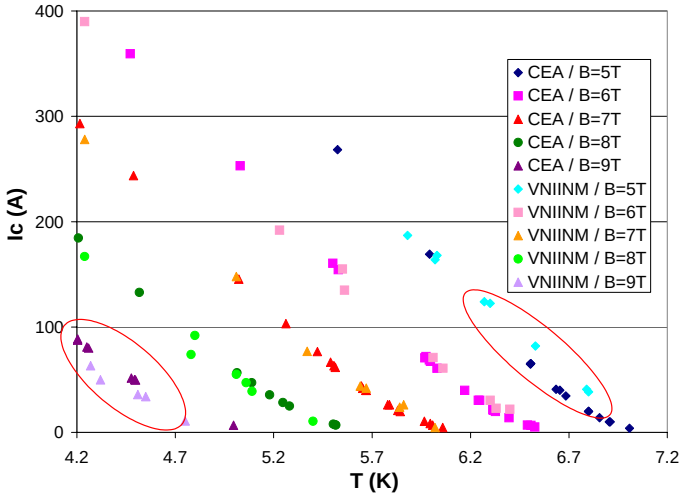

Figure 4. Temperature dependencies of PFCI NbTi strands critical currents for different magnetic fields, measured in BI (VNIINM) and CEA.

For the major part of the data compared a satisfactory consistence between CEA and BI measurements was obtained except for “extreme” magnetic field values (5T and 9T). In those cases, CEA

results are found lower than VNIINM ones at low fields and higher at high field. This is probably hinting at differences in the structure of the tested strands (filaments structure, impurities ratio…).

NbTi wires designed for the ITER PF coils production are presented in Fig.5. In the process of preparation for large scale production of these strands the composite billets were extruded from 250 mm in dia. In accordance with specification Jc should be higher than 2900A/mm^2 with a filament diameter of 6 μm; Cu/SC ratio 1.4 (for the coils PF1 and PF6) [19].

Model fine filament NbTi 0.65 mm wire, intended for operating in fields having sweep rate from 1 up to 4 T/s, has been developed and manufactured in Bochvar Institute (Fig.6) [20]. The wire was fabricated by a single stacking method. Each filament (3.46 μm in dia) was surrounded by a matrix of

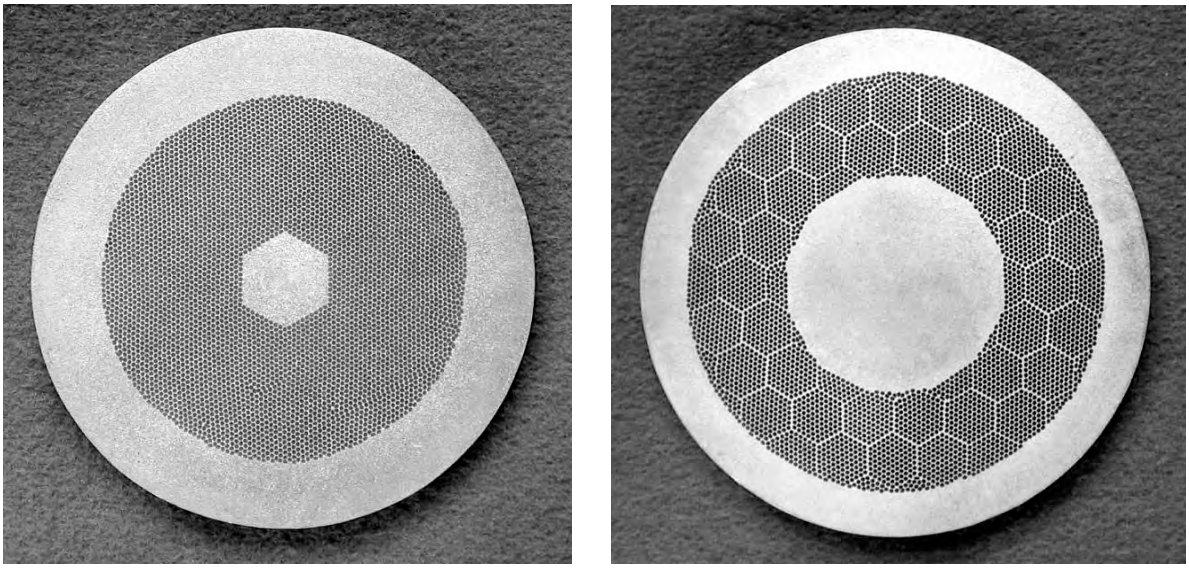

Figure 5. Cross sections of NbTi wires designed for ITER PF1 and PF6 coils.

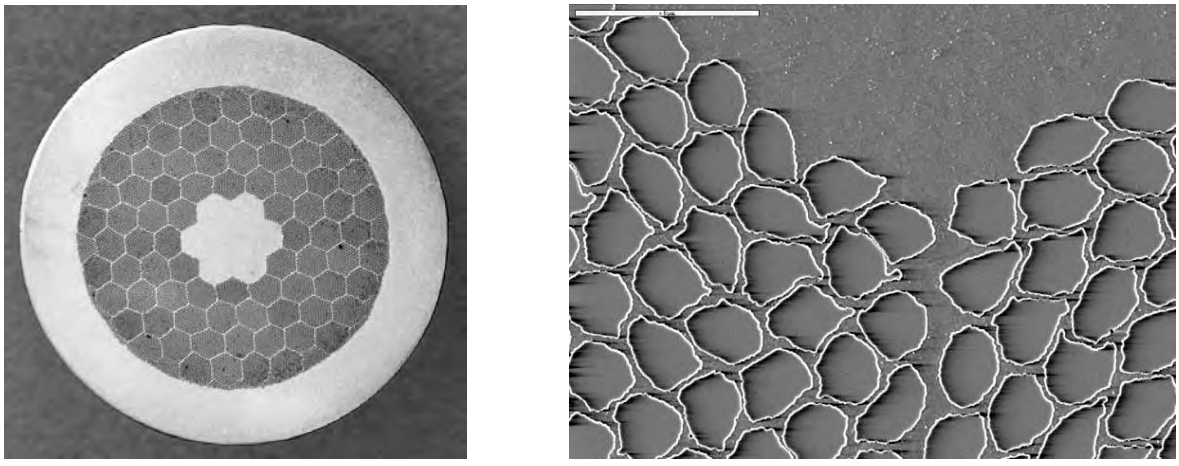

Figure 6. Cross section (a) and fragment of structure (b) of the NbTi wire designed for the application in the magnet systems with fast sweep rate up to 4 T/s.

commercial MN-5 alloy (Cu-5wt.%Ni). The spacing is 0.5 μm. The Cu/non Cu ratio is 1.8. Every 37 NbTi/Nb/CuNi rods were inserted into hexagonal copper tube made from high purity Cu.

The filament zone was arranged in cross section in such a way that the central copper core occupies about 7 % of area. The central copper core, tubes and the external sheath were fabricated from high conductivity copper with (R^{273}/R^{10}) > 250. The critical current density of this strand was higher than 2900 A/mm^2 (5T, 4.2K). A low hysteresis loss values of 51 kJ/m^3 per wire and 144 kJ/m^3 per superconductor volume have been achieved.

3. INVESTIGATION ON NB_3SN WIRES – DESIGN AND PROPERTIES

Two well established viable technologies are generally used for commercial production of Nb_3Sn strands – the so called bronze process and internal tin process. Due to some peculiar differences in these methods the process of optimization could be different, but principal approaches have a lot in common. Critical currents in Nb_3Sn strand depend on the volume fraction of the superconducting phase and the pinning of the magnetic flux vortices on lattice defects, the critical temperature (T_c), and the upper critical field (B_{c2}).

3.1 Bronze processed Nb_3Sn wires

Concerning bronze process two main features should be taken into account:

Disadavantages: Coprocessing of bronze matrix and niobium filaments during all the steps of the manufacture requires numerous intermediate annealing steps due to high rate of deformation hardening and as a consequence limited ductility of the Sn rich bronze.

Advantages: Extrusion of large composite billet is possible at the initial stage of deformation. Good metallurgical bonding of all elements of composite billet is guaranteed.

In bronze processed wires the bronze matrix is prepared by melting Cu and Sn (up to ~ 14-16 %wt of Sn) obtaining an alloy, which is a solid solution on the base of copper. The bronze matrix Cu-16%Sn due to high tin content is a two-phase material with brittle inclusions of intermetallic Cu-Sn phase. The part of Cu-Sn phase diagram is presented in Fig.7a. In the Fig 7b and 7c the microstructures of Cu-16%Sn alloy in cast condition and after homogenization are shown. It is seen that the brittle Cu-Sn eutectoid inclusions are present in the bronze matrix even after the homogenizing heat treatment.

The residual content of tin in the bronze matrix after reaction heat treatment could be less than 0.5 %. Assuming stoichiometric composition of Nb_3Sn phase, the 25-26 % of the area inside the diffusion barrier should be occupied by Nb filaments. Therefore the maximum attainable volume fraction of Nb_3Sn phase is approximately 35% in the area inside the diffusion barrier (Taking into account 37 vol. % increase resulting from complete transformation of Nb into Nb_3Sn).

Taking this into account the requirement of J_{nc} > 800 A/mm^2 (standard 12 T, 4.2 K) assumes the attaining of critical current density in Nb_3Sn phase higher than approximately 2700 A/mm^2 for bronze processed wires, which is not a trivial task.

In the frame of ITER model coils program Bochvar Institute has designed and produced approximately 1 ton of strands for the TF Model Coil Insert conductor, which met the HP-2 specifications [21,22]. The parameters of the designed strand were as follow: Volume fraction of Cu of 60 **%;** Diameter of the strand 0.81 mm; Number of filaments 7225; Diameter of Nb_3Sn filaments of 2.5 μm, Critical current density Jc (12T, 4.2 K, non-Cu) > 550 A/mm^2; Hysteresis losses Qh (non-Cu; ±3 T) < 200 mJ/cm^3. The cross section of the strand is presented in the Fig.8.

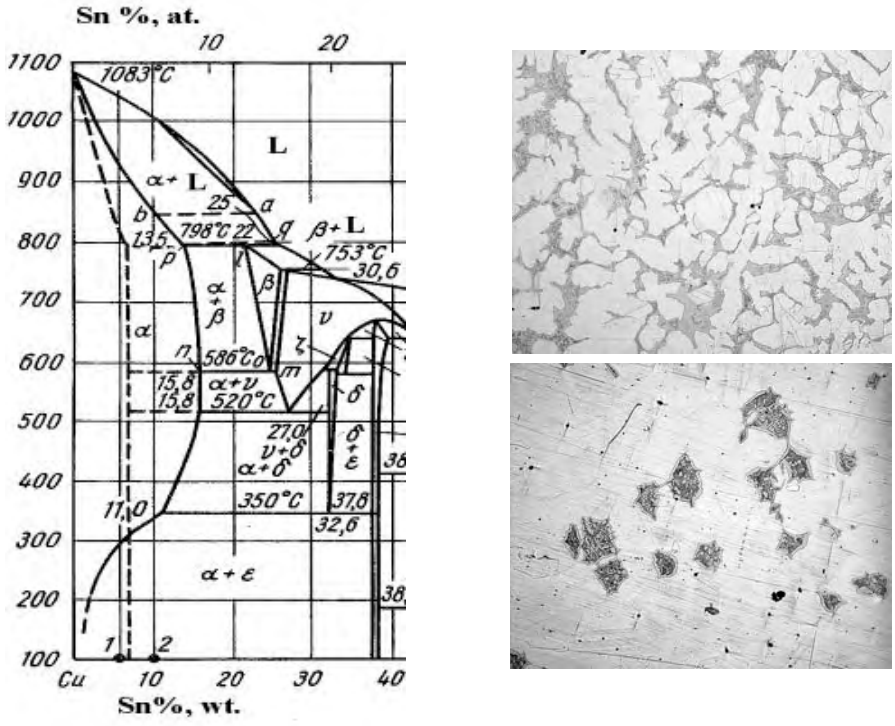

Figure 7. The Cu-rich part of Cu-Sn phase diagram (a) and microstructure of Cu-16%Sn alloy in cast state (b) and after the homogenizing heat treatment (c).

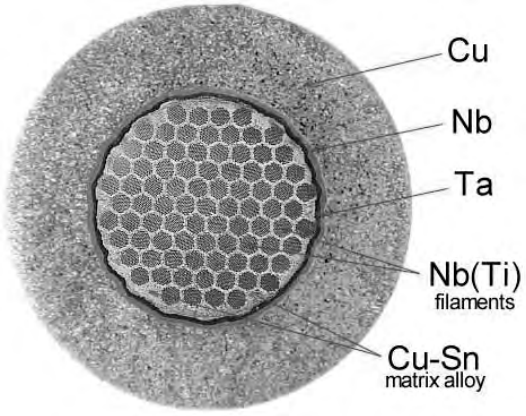

Figure 8. Cross section of the Nb_3Sn strand developed for PFCI in the frame of ITER model coil program.

The cabling and jacketing of the full size conductor were performed by Cable Institute, Coil has been wounded in Efremov Institute in St.Petersburg and successfully tested in JAERI (Japan) [23]. It is important to note that the spread of Jc values on samples heat treated with the TFCI and spreaded along the spiral height was less than 1% (average Jc = 579 A/mm^2) and there was almost no spread in the hysteresis loss values, which were lower than 200 mJ/cm^3[24].

Bronze processed Nb_3Sn wires with enhanced critical current properties have been developed in Bochvar Institute after the completion of the ITER model coil program. The cross section of one of the options is presented in the Fig.9 [25]. Critical current density of newly designed Nb_3Sn wires with 7851

filaments was equal to 774 A/mm2 (12 T, 4.2 K); Hysteresis losses (+/-3T) of 337 mJ/cm3; Cu/(non Cu) ratio of 1.2.

Another option of bronze processed Nb_3Sn wires with enhanced critical current properties is presented in Fig.10 [26]. The enhancement of critical current density has been achieved by the optimization of artificial titanium doping [27]. Each of the 12684 Nb composite filaments contained 4 Nb-Ti alloy rods (Fig.10b). The relationship between the amounts of Nb and Nb-Ti alloy has been chosen to be equal to 2 wt% of Ti in the filament after heat treatment.

The comparison of critical current carrying capabilities of the bronze processed wires designed in the framework of ITER project is given in the Fig.11. It was shown that bronze processed Nb_3Sn wires with low hysteresis losses could be produced with critical current density attaining 800 – 900 A/mm^2.

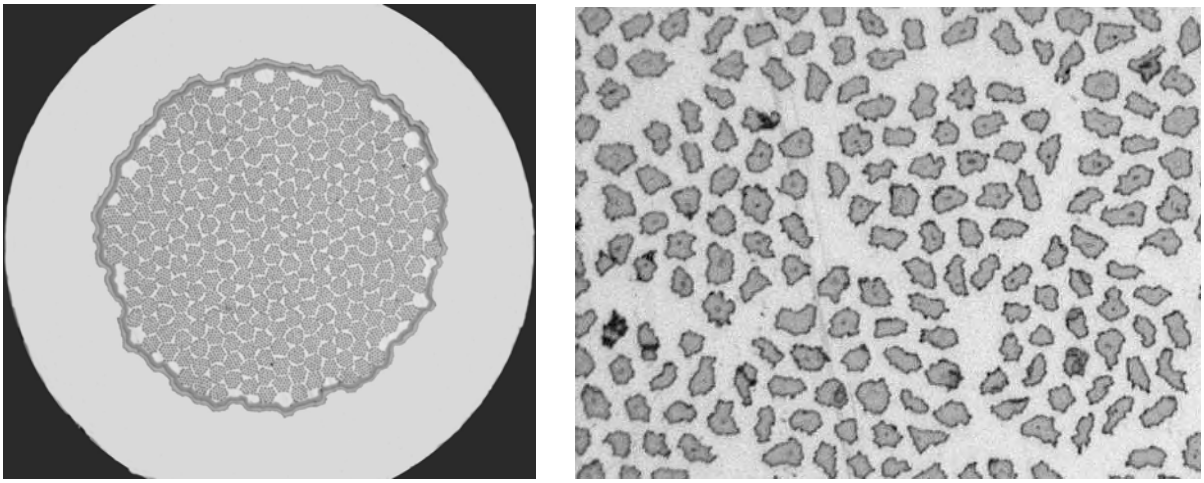

Figure 9. Cross section of the bronze processed Nb_3Sn wire with enhanced critical current density -(a) and the fragment of structure illustrating increased uniformity in the filaments arrangement -(b). ; Number of filaments 7851.

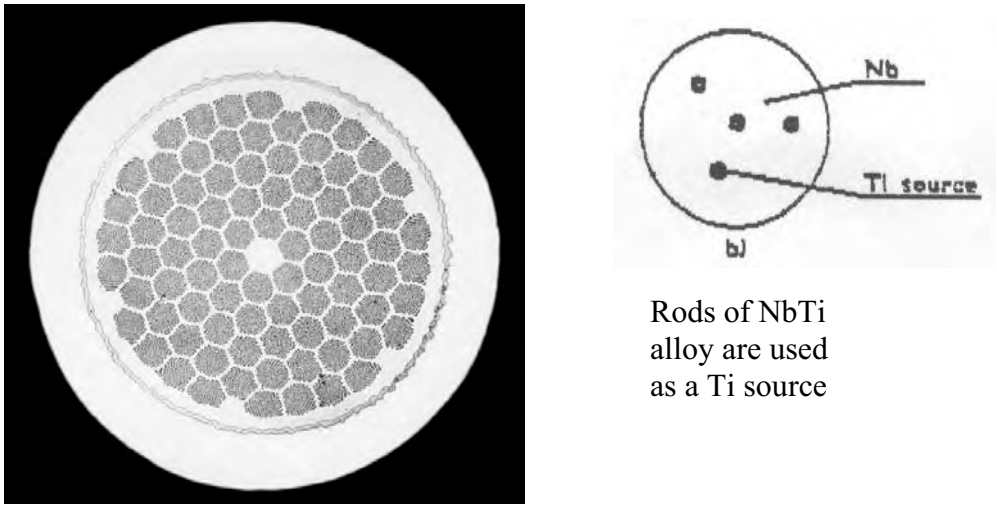

Figure 10. Cross section of the bronze processed Nb_3Sn wire with enhanced critical current density (a) and the fragment of structure illustrating the arrangement of Ti inserts inside the Nb filament (b).

Because the critical current carrying capability of superconducting wires is a structure dependent parameter, the investigations of microstructure including X-ray and electron microscopy methods are constantly under the way in Bochvar Institute as a basis for their development and optimization. Some examples of the Nb_3Sn grains microstructure in bronze processed wires, designed in the frame of ITER project are given in the Fig.12 [28].

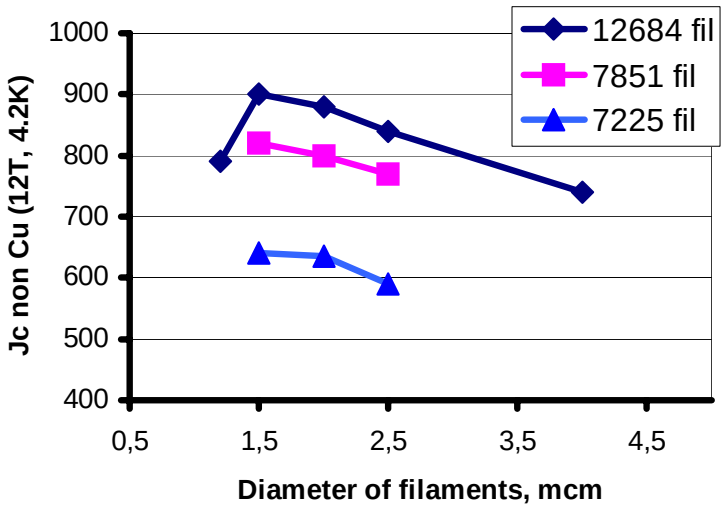

Figure 11. Critical current (non Cu, 12 T, 4.2 K) of bronze process Nb_3Sn wires.

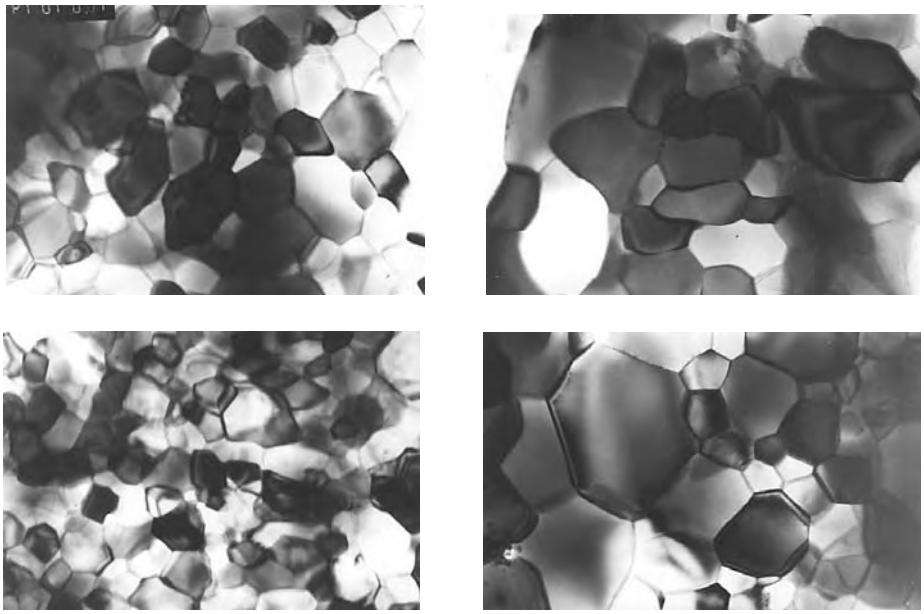

Figure 12. Microstructure of Nb_3Sn phase in bronze processed strands after heat treatment at 575 ^oC 150h + 650 ^oC 200h: a,b – diameter 0.81 mm; c,d – diameter 0.6 mm. (magnification 150 000).

The TEM analysis is local but in general the grain structure consists of the regions with relatively uniform sized small equaxed grains. Some regions could be found with much larger but also almost equal grains. These observations were valid for all investigated samples with slight tendency for diminishing of

the average grain sizes with diminishing of the diameters of Nb_3Sn filaments. A tendency for narrowing of the distribution of grain sizes was also found (Fig.13).

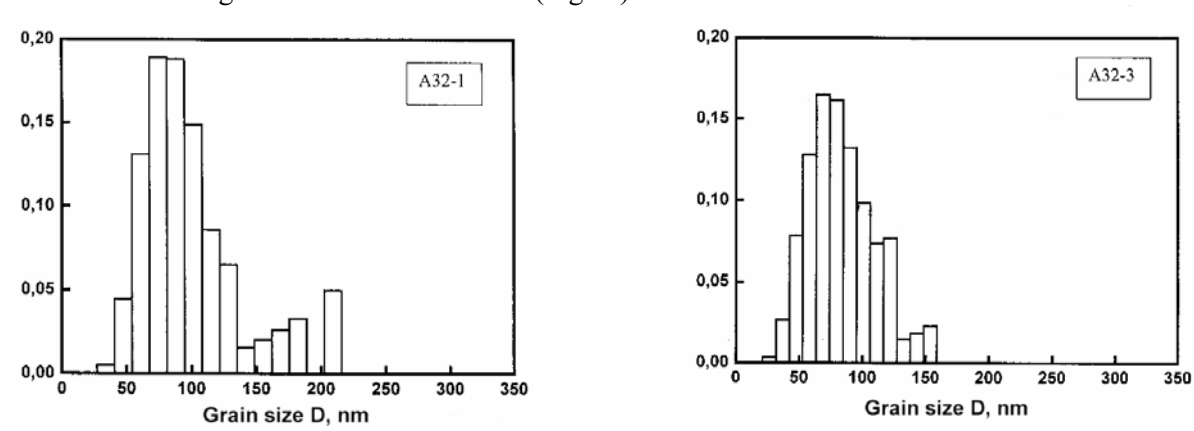

Figure 13. Distribution of the Nb_3Sn grain size in bronze processed strands (a - 0.81 mm in dia and b - 0.6 mm in dia) after heat treatment at 575^0C 150h + 650^0C 200h [28].

Analyzing the data presented in the Fig.13 it could be stated that a further significant enhancement of the current carrying capability of the bronze processed wires could be attained by narrowing the distribution of grain sizes in the Nb_3Sn layers, which corresponds in the plots to shifting the maximum position to the smaller size of grain.

In large magnet systems superconducting wires are usually used in the form of cables having different designs. In some cases (for example CICC) individual wires could be subjected to rather high mechanical loads, which are the combination of the thermal and electromagnetic forces. This is why the mechanical properties of Nb_3Sn wires became to be of primary importance. In BI several Nb_3Sn wires with enhanced mechanical strength have been developed by replacing of the part of stabilizing Cu by high strength high conductivity microcomposite Cu-Nb material [29, 30]. The cross section of a strengthened Nb_3Sn wire is shown in the Fig.14.

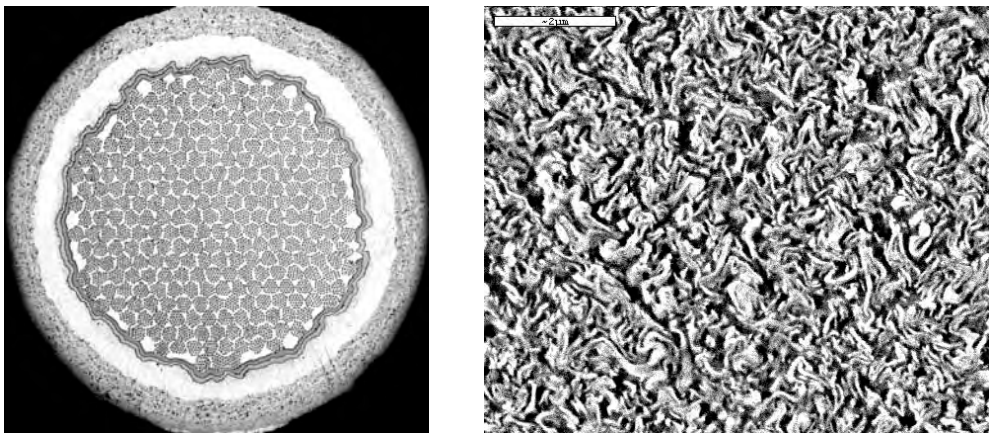

Figure 14. Cross section of strengthened Nb_3Sn wire –(a) and Cu-Nb strengthening material - (b)

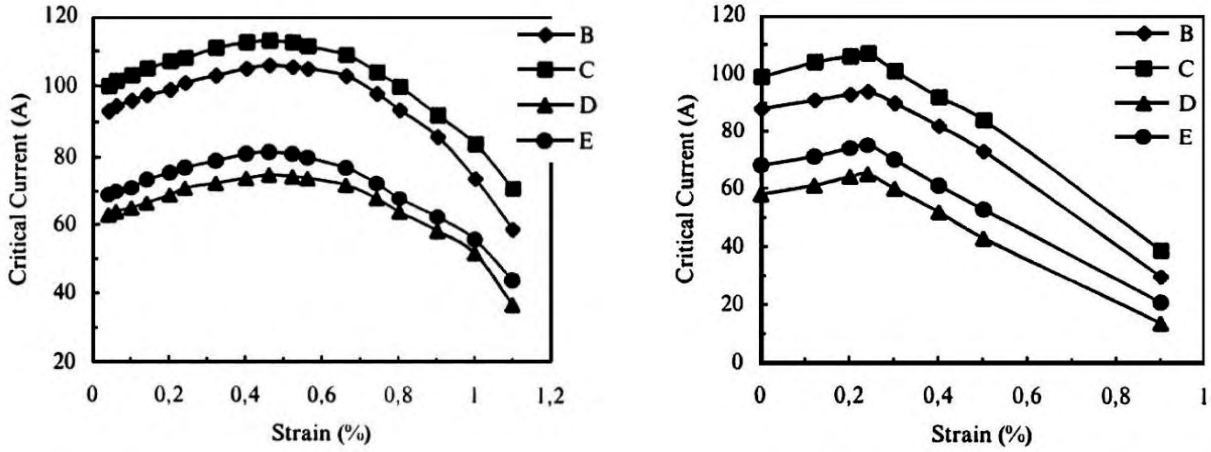

Figure 15. The influence of tensile strain on critical current in 12 T (B,C) and 14 T (D,E) 0.1 μV/cm (B,D) 1 μV/cm (C,E) in strengthened wire – (a) and without strenghening addition – (b).

It was shown that the ultimate tensile strength of the wire could be effectively increased up to 1000MPa in non-reacted state and up to 350 MPa after the reaction heat treatment. Critical current density of reinforced bronze processed wires remains essentially the same. The dependence of critical current density on tensile strain is shown in the Fig.15 [29].

3.2 Nb_3Sn wires – produced by internal tin method

In Nb_3Sn wires produced by internal tin method Nb filaments are embedded into a pure Cu matrix and Sn is provided in a form of separate sources distributed over the strand cross section: pure Sn or alloyed Sn may be used for the Sn sources. The larger Sn inventory available in the matrix of internal Sn strands (>20wt.%) allows a “reaction” of larger amounts of Nb, i.e. the achievement of a larger non-Copper critical current density.

On the other hand, the spacing between the filaments is much smaller, with the risk of frequent superconducting "bridges" during the Nb_3Sn formation, when the volume of the Nb filaments increases to ~ 33% in the area inside the diffusion barrier. These bridges build larger loops for the steady state magnetization currents in the filaments, resulting in large hysteresis losses. It was shown that hysteresis losses increased dramatically when distances between Nb_3Sn filaments decreased to less than 1 μm. Typical internal tin wires designed in BI are presented in Fig. 16.

In ITER type wires the combination of critical current density in the range of 800-1000 A/mm^2 and hysteresis losses lower than 1000 mJ/cm^3 are required. That is why in ITER type internal tin wires the volume fraction of the Nb_3Sn phase was only slightly increased in comparison to bronze processed wires. In high Jc type wires the limitation on the hysteresis losses is not applied, enabling to increase the volume fraction of Nb_3Sn phase significantly.

Nevertheless the design of the strands shown in Fig.16 have been developed in such a way that the amount of Nb_3Sn phase did not differ significantly (in case of ITER type strand the calculated volume fraction of Nb_3Sn phase was only 15% less than in High J_c strand), but the relations of the diameters of Nb filaments and spacings were significantly different. In ITER type strand the ratio d_f/Δ is 2.7 and in High Jc wires this ratio is 4.2. The absolute value of the spacing among filaments chosen was 2.5 μm for ITER type wires and and 1.1 μm for High J_c wires, which results in a high probability of the absence of bridging in ITER type strands and, on the contrary, high level of bridging in High Jc strands. Samples of both

strands were subjected to the standard ITER heat treatment, consisting in the sequence: 575^0C 150h + 650^0C 200h. The superconducting properties are presented in table 1.

The grain structure of the samples investigated was generally similar to the grain structure of bronze processed strands described above. The following difference should however be noticed. The average Nb_3Sn grain size in internal tin strands was slightly larger than in bronze processed ones and the distribution of the grain sizes was generally wider [28]. It should be noted that insignificant differences in microstructures of both investigated internal tin strands could not explain the dramatic difference in their critical current densities (table 1) [31]. It was supposed that strong bridging in High J_c strand was the main reason of high critical current density through better redistribution of superconducting currents between filaments. At the same time strong bridging is negative for stability of the wires.

Due to larger volume fraction of the brittle intermetallic Nb_3Sn phase in internal tin wires the mechanical properties are even more important than for bronze processed wires. It should be also stressed that not only larger amount of brittle phase in the wire could lead to a possible faster degradation of critical current under applied strain, but also the presence of voids in the filaments region of the wire, that are consequence of reaction heat treatment accompanied by liquid phase formation and formation of intermediate Cu-Sn phases with different specific densities, could have a deteriorating effect. This is why the development of internal tin Nb_3Sn wires with enhanced mechanical strength was carried out in Bochvar Institute [32]. Two possible ways of introduction of strengthening microcomposite Cu-Nb elements in the design of final composite billet were tried. In Fig.17 the cross sections of both options are

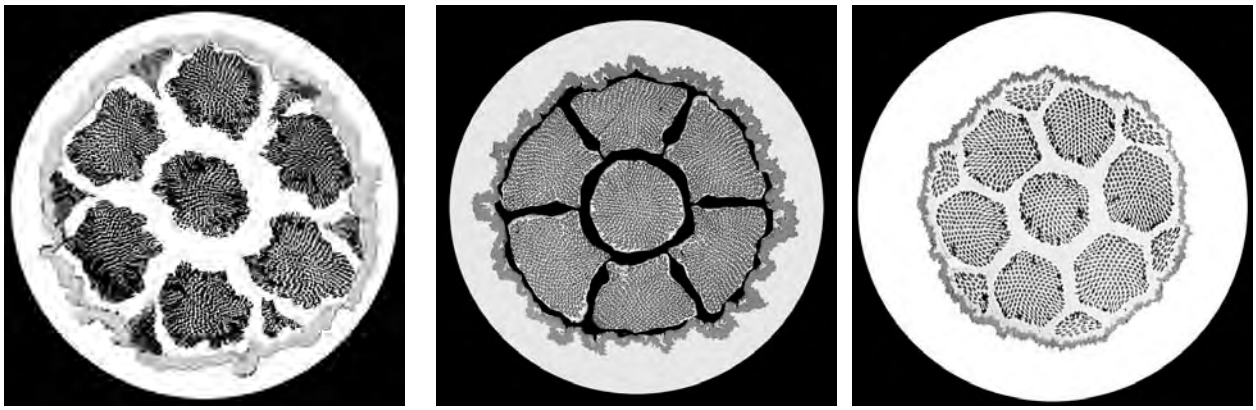

Figure 16. Typical internal tin wires designed in BI. High Jc wires – a),b); ITER type wire – c)

Table 1. Internal Tin Nb_3Sn wires superconducting properties

Definition	ITER type (Sn-P)	High Jc type (S12)
J_{nc}, non-Cu [A/ mm^2] @12 T, 4.2 K, 0.1 μV/cm, no external strain applied	745	2070
n value @12 T, 4.2K, between 0.1 to 1 μV/cm	22	16
B_{c2} (Kramer extrapolation) [T]	29.3	26.4
Tc, [K]	17.5	17.0
W_h, Hysteresis Loss [mJ/cm^3 non-Cu], @± 3T	270	>1000
Calculated Jc_{Nb3Sn} [A/ mm^2] @12 T, 4.2 K	2180	4850

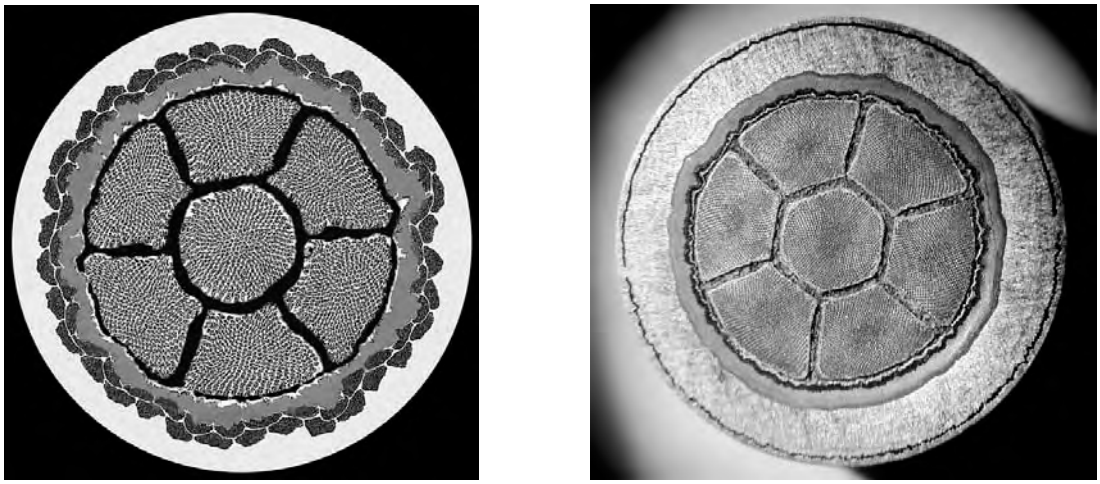

Figure17. Cross sections of internal tin Nb_3Sn wires strengthened by microcomposite Cu-Nb material in the form of rods (a) and tube (b).

shown with the arrangement of Cu-Nb material in the form of rods (fig.17a) and in the form of tube (fig.17b). The critical current density of the strengthened internal tin wire shown in Fig.17(a) was slightly higher than that of a wire with similar design but without reinforcement,, and attained 2376 A/mm^2 (12 T, 4.2 T) for a wire with 0.7 mm diameter.

Comparison of the mechanical properties of the strands with Cu-Nb reinforcing elements and without them before reaction heat treatment and after reaction heat treatment is presented in Fig.18. It was shown that the UTS values of strengthened internal tin Nb_3Sn wires were approximately 30% higher.

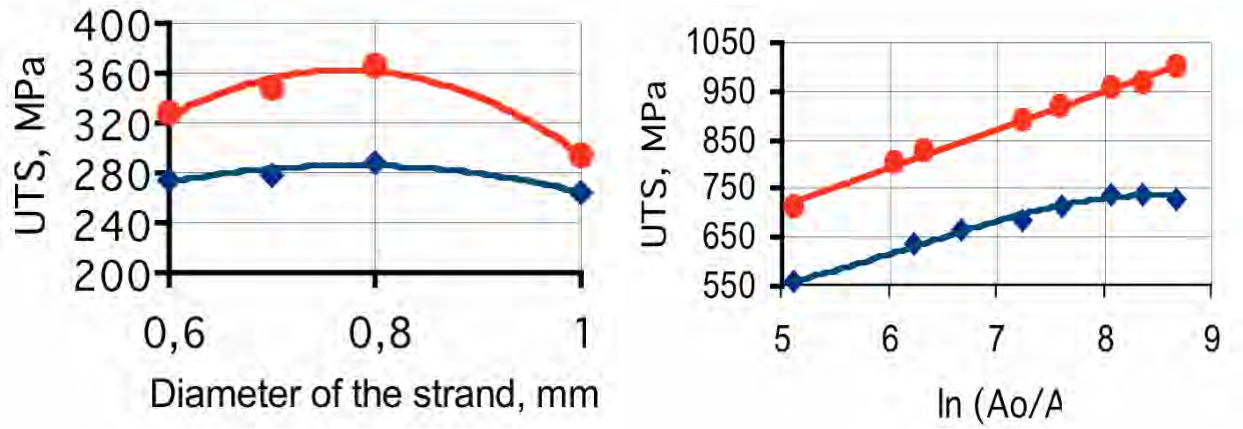

Figure 18. Mechanical properties of the internal tin wires with Cu-Nb reinforcing elements and without them before reaction heat treatment (Fig.18a) and after reaction heat treatment (Fig.18b)

4. SUMMARY

The limit of accelerator magnets wound from binary NbTi conductors and operated at 1.9K is in the range of 10 to 10.5T. We expect that this limit can be shifted to ~12T by the use of ternary alloy NbTiTa.

Nb_3Sn wires seems to be most probable candidate materials for the application in both types of large future devices – fusion reactors and next generation accelerators, with magnet systems reaching 16 T.

Bronze processed Nb_3Sn wires recently have made a good progress in critical current density, attaining 800 A/mm^2 (non-Cu, 12T, 4.2K) in commercially produced wires. In laboratory scaled wires 900 A/mm^2 (non-Cu, 12T, 4.2K) has been attained. Further increase of critical current density up to, potentially, 20% could be expected in bronze processed wires through the optimization of the strands designs and Nb_3Sn layers microstructure.

Internal tin Nb_3Sn wires with critical current density higher than 2000A/mm^2 (non-Cu, 12T, 4.2K) has been designed and fabricated. The question of stability of high Jc internal tin wires has to be investigated due to strong bridging of the filaments.

Mechanical strength of bronze processed and internal tin Nb_3Sn wires could be effectively increased (up to 30-50%) by Cu-Nb microcomposite inserts.

REFERENCES

[1] D.P.Ivanov, V.E.Keilin et al., ”Atomnaya Energia” v.45. (1978) 171. (in Russian)

[2] V.F.Denisov, D.P.Ivanov, A.Ya.Kislov et al. “The results of experiments with plasma on the Tokamak-7 facility with superconducting magnet system” Preprint of Inst.Atomic Energy, IAE-3411/7. Moscow, (1981) (in Russian)

[3] E.V. Nikulenkov, G.K. Zelenskij, L.V. Potanina “Electrophysical and structural properties of multifilamentary superconducting Nb-Ti wire”, Proceedings of ICFA, No.7, (1986) 28.

[4] A.K. Shikov, I.N. Gubkin, G.P. Vedernikov, et al. “NbTi Conductors with Cu-Mn Matrix for D.C. Switches” Proceedings of ICEC17, UK, July 14-17 (1998) 871.

[5] A.Nikulin, B.Yakovlev, E.Plashkin, et al., Trans. Appl. Superconductivity, v.3, (1995) 889.

[6] A.D. Nikulin, G.P. Vedernikov, L.V. Potanina, et al., Proceedings of 15 International Conference on Magnet Technology, October 20-24, Beijing, China, 1998, p.1001

[7] V.Kovaleva, A.Nikulin, V.Pantsyrny, A.Skvorzov, “Metals” No.3, (1980), p.95 (in Russian)

[8] V.Andreev, I.Bondarenko, E.Bondarchuk “2-nd all-union conf. on engineering problems of fusion reactors (Leningrad, 23-25 june 1981) Proceedings – Leningrad, NIIEFA, (1982), v.1, p.6

[9] E.Yu. Klimenko, N.A. Chernopliokov, A.D. Nikulin, et al., “Atomnaya Energia” v.63(4) (1987) 248 (in Russian)

[10] K.Okuno, A.Shikov invited report presented at ICFRM-2003, Kioto, December 2003,

[11] P.Lee, web site: www.cae.wisc.edu/~plee/

[12] G.P. Vedernikov, A.K. Shikov, L.V. Potanina, et al. IEEE Trans. Appl. Superconductivity, v.13, No.2, (2003) 3362.

[13] G.P. Vedernikov, L.V. Potanina, V.Yu. Korpusov, V.A. Drobishev, et al. IEEE Trans. Appl. Superconductivity, v.7, (1997) 1751.

[14] L.Potanina, G.Vedernikov, V. Korpusov, et al. Adv. Cryo. Eng. Materials, v.44, (1998) 881.

[15] L.Potanina, G.Vedernikov, A.Shikov, et al., Adv. Cryo. Eng. Materials, v.46B, (2000) 939.

[16] V.Yu. Korpusov, G.P. Vedernikov, L.V. Potanina, et al., Proceedings of the 18 Int. Cryo. Eng. Conf. (ICEC 18),Narosa Publishing House, (2000) 255.

[17] L.Potanina, G.Vedernikov, A.Shikov et al. Adv. Cryo. Eng. Materials, v.48B, (2002) 891.

[18] G.P. Vedernikov, A.K Shikov, et al. Physica C, №. 354, (2001) 420.

[19] G.P. Vedernikov, A.K. Shikov, M.S. Novikov, et al. IEEE Trans. Appl. Superconductivity, v.12 № 1, (2002) 1098.

[20] G.P. Vedernikov, A.K. Shikov, L.V. Potanina, et al. "Multifilament superconducting wire based on NbTi alloy in a combined copper/copper-nickel matrix"

[21] A. Shikov, A. Nikulin, V.Pantsyrny et al. J. Nucl. Mater. v.283-287, (2000) 968.

[22] A. Shikov, A. Nikulin, A. Silaev, et al. J. Nucl. Mater. v.258-263 (1998) 1929.

[23] N.Cheverev, V.Glukhikh, O.Filatov et al. IEEE Trans. Appl. Superconductivity v.12, No.1, (2002) 548.

[24] I.Abdioukhanov, V.Beliakov, N.Cheverev et al. IEEE Trans. Appl. Superconductivity v.12, No.1, (2002) 1105.

[25] A.Vorobieva, A. Shikov, A. Silaev, et al. IEEE Trans. Appl. Superconductivity, v.11, No.1, (2001) 3588.

[26] A.Shikov, A. Nikulin, E. Nikulenkov et al. IEEE Trans. Appl. Superconductivity. v.9. No.2, (1999) 1441.

[27] A. Nikulin, A.Shikov, A.Vorobieva et al. Adv.Cryog.Eng.Materials, v.42b, (1996) 1337.

[28] V.Pantsyrny, A.Shikov, A.Vorobieva et al. "Investigation on ITER type Nb_3Sn strands and correlation with microstructure" Report presented at workshop … Tsukuba, February 21-23, 2004.

[29] A.Shikov, V.Pantsyrnyi, A.Vorobieva et al. IEEE Trans. Appl. Superconductivity, v.7, No.2, (1997) 1372.

[30] A.Vorobieva, A.Shikov, V.Pantsyrnyi et al. Report 1D-p52 Presented in Magnet Technology conference MT-18, October 21-24, 2003, Morioka, Japan

[31] N.Kozlenkova, A.Shikov, V.Pantsyrnyi and A.Vorobieva. Cryogenics, v.42, (2002) 279.

[32] V.Pantsyrnyi, A.Shikov, A.Vorobieva et al. Report 1D-p53 Presented in Magnet Technology conference MT-18, October 21-24, 2003, Morioka, Japan

THE ACTIVITIES OF ENEA ON SC DEVELOPMENTS

G. Celentano[(1)], A. della Corte[(1)], A. Di Zenobio[(2)], V. Galluzzi[(1)], P. Gislon[(1)], A. Mancini[(1)], L. Muzzi[(1)], A. Rufoloni[(1)], S. Turtù[(1)], A. Vannozzi[(3)]
[(1)] EURATOM-ENEA Association, ENEA C.R. Frascati, Via E. Fermi 45, 00044 Frascati (RM), Italy
[(2)] Edison S.p.A., Foro Buonaparte 31, 20121 Milano, Italy
[(3)] INFM-Physics Department, Univ. of Salerno, 84081 Baronissi (SA), Italy

Abstract
ENEA, as an EURATOM Association, is involved since 1968 in the R&D programs for the development of superconducting strands and conductors for the high field magnets of a Fusion reactor. In this frame, the activities range from strand and sub-cable characterization, to sub-size coil performance testing, from industrial cable and joint manufacturing monitoring to the participation to the international campaigns on full-size conductors and model coil characterizations and to the experiments on current distribution in superconducting cables.
On the high critical temperature superconductors development side, ENEA collaborates since 1987 with Italian Universities and Institutions on YBCO and BiSSCO coated conductors, as well as on MgB_2, making use of a large and functional set of facilities for film deposition and characterization. In this paper, an overview of the research activities which are carried out at the Superconductivity Division of ENEA is presented.

1. INTRODUCTION

Since 1968 ENEA Superconductivity Division operates in the field of applied superconductivity research. Main topics of its scientific activity are the development and characterization of superconductor (SC) devices, strands and cables, the design of conductors and magnets for large scale and high field applications, and the experimental study of the stability and operation limits of prototype coils and conductors. Within this frame, the collaboration with Italian industries contributed during these years to develop the know-how for the manufacturing of SC strands and cable and to acquire the ability of manufacture SC magnets.

In the last 15 years the ENEA activities have been mainly devoted to the research and development programme of the International Thermonuclear Experimental Reactor (ITER) project, culminated in the manufacturing and test of the Toroidal Field and Central Solenoid Model Coils.

The study and development of the high Tc materials has taken, since their discovery in 1987, an increasing space in the group activities, the manufacturing of YBCO tape by means of techniques of thin films deposition and its structural and electrical characterization being the main subject. Also in this field, the collaboration with Italian companies, research agencies and Universities led to significant results.

2. CHARACTERIZATION OF STRAND, SUB-CABLES, FILMS AND BULK SAMPLES

2.1 Structural characterization

2.1.1 X-rays

X-ray diffraction (XRD) analyses allow to control samples structural properties and phase compositions. The lattice parameter determination provides stoichiometric and residual stress information, while texture analyses reveal preferred distribution of crystallographic orientations.

In the development of coated conductors, X-ray diffraction are widely used to extabilish the optimum deposition conditions in order to obtain a good epitaxial growth and stoichiometric phases of superconducting films and buffer layers, and to determine deformation and annealing procedures for the enhancement of cube texture in metallic substrates.

The X-ray θ-2θ scans are performed using a Rigaku Geigerfex diffractometer with Cu-Kα radiation. X-ray diffraction measurements for texture analysis are performed on a Seifert XRD 3003 PTS, equipped with a four circle goniometer, suitable for texture and for residual strain measurements (fig. 1).

Fig. 1: the SEIFERT diffractometer with a four circle goniometer.

2.1.2 Scanning Electron Microscopy

A high resolution scanning electron microscope (SEM) is used for morphological and structural characterizations of superconducting thin films (mainly $Y_1Ba_2Cu_3O_{7-x}$) grown on single-crystal ($SrTiO_3$) or metallic (Ni-alloy) substrates (fig. 2).

A field emission gun SEM LEO1525 is used; its resolution is 1.5nm at 20kV and 2mm working distance or 3.5nm at 1kV and 2 mm working distance, magnification ranging from 20x up to 500kx.

The scanning electron microscope is also equipped with OXFORD INCA Crystal Electron BackScatter Diffraction (EBSD) and Energy Dispersive X-ray Microanalysis (EDX) systems.

The orientation of crystals down to 150nm can be resolved using the EBSD system and quantitative X-ray analysis can be performed by a microanalysis suite.

EBSD is a very important tool for YBCO-based coated conductors analysis, since crystallographic orientations, grain-to-grain misorientations, texture trends and grain boundary types can be characterized and quantified on a sub-micron scale in the SEM. Moreover, EBSD is a surface sensitive technique with data being acquired from a depth of the order of tens of nanometers; using advanced electron optics and in particular FEGSEM, high spatial resolutions are possible. Thus, EBSD is particularly suitable for the characterization of textured thin films.

In the development of coated conductors EDX is widely used to establish stoichiometry and elemental composition of superconducting films and buffer layers and to determine the degree of oxidation of the metallic substrate.

2.2 Electrical characterization

2.2.1 Critical current versus magnetic field in helium bath

The critical current of low-T_c strands and sub-cables can be measured on coiled samples mounted on standard Ti-Va ITER sample holders, or stainless steel sample holders. Sample holders up to 60mm diameter, allowing to test strands, triplets and 3x3 conductors, are immersed in a magnetic field up to 14.5T strength, 0.1% uniformity [1]. A higher magnetic field, 16T, can be achieved restricting the sample holder diameter to a maximum of 35mm. The sample, in the same helium bath of the background solenoidal magnet, can be fed with currents up to 3.5kA.

In the next months a systematic characterisation activity on upgraded Nb_3Sn strands is going to start.

2.2.2 Critical current versus magnetic field and temperature

A variable temperature insert placed in a 12T, 80mm bore superconducting solenoid is used to perform critical current versus magnetic field measurements at temperatures ranging from 4.5K to 100K. Coiled strands, 1m long, about 1mm diameter for measurements with the external field perpendicular to the strand axis, or 3cm long straight pieces of bulk material or film, for measurements with the external field perpendicular to the film plane, can be tested up to 220A sample current.

Superconducting thin films D.C. transport properties in applied magnetic field at temperatures ranging from 4.2K to 300K are measured using an Oxford Instruments helium gas flow cryostat provided with a 12T superconducting magnet with an internal bore diameter of 6cm.

The measurements can be performed varying the angle between the applied magnetic field and the sample surface normal direction. The bias current is limited to 0.5 ÷ 1.0A, depending on the testing temperature.

Both temperature dependence of the electrical resistivity and *I-V* curves measurements are carried out using the four contact technique. The current inversion technique allows to obtain a voltage stability of about 20nV during the measurements.

2.3 Magnetic characterization

A vibrating sample magnetometer is used to measure magnetisation vs. external applied magnetic fields. External field loops up to $\pm$12T are applied, at temperatures ranging from 4.5K to room temperature; samples are small pieces (<10g, some mm^3 volume) of superconducting low-T_c strands, or of high-T_c bulk and films; the apparatus sensitivity is of the order of 10^{-6}emu.

3. SC STRANDS AND COATED CONDUCTORS

3.1 Advanced Nb_3Sn strands

Within the framework of ITER-related projects, new tasks have been recently launched by the European Fusion Development Agreement (EFDA), for the definition and production on industrial scale of an advanced Nb_3Sn strand, to be used in the manufacturing of the ITER high field CS and TF magnets. This is being done with the aim of stimulating the industrial Nb_3Sn strand production capabilities in Europe, as compared to what has been achieved, within the KSTAR project, by USA (IGC) and Japan (Mitsubishi).

An overall critical transport current of at least 200A (at 12T, 4.2K, 0.1 μV/cm) will be required for the upgraded strand, equivalent to a non-Cu J_c of 800A/mm^2, a Cu : non-Cu ratio of about 1 and a strand diameter of 0.81mm.Target value will be 280A, equivalent to a non-Cu J_c of 1100A/mm^2.

Within this framework, ENEA will be involved in the following activities:

- SAMAN: *the preparation and manufacture of conductor samples required for the final optimization of the ITER conductor*. Single strand samples will be jacketed in a SS tube (fig. 2); cabling and jacketing of sub-size samples (9 to about 100 strands) with different jacket diameters, ready to be tested, will be performed; full-size conductor samples will be manufactured, including jacketing and cabling, as well as joint fabrication.

- BARBEN: *the investigation of the bending strain effect on strand*. With the aim of assessing the ratio between the strand twist pitch and the current transfer length of jacketed strands, transport critical currents will be measured at 4.2K, 12T on different samples reacted on barrel sample holders with different diameters.

- ASTEST: *the test of advanced Nb_3Sn strands*. The performances of the advanced Nb_3Sn strands coming from European companies will be tested. Different measurements will be performed: strand layout (diameter, thickness of Cr coating, Cu : non-Cu ratio, twist pitch length and orientation), critical transport current and n-value, RRR, and hysteresis losses by magnetization technique. An extended strand characterization of the critical current dependence on magnetic field, temperature, and strain on a wide range of parameters will be performed by other Associations.

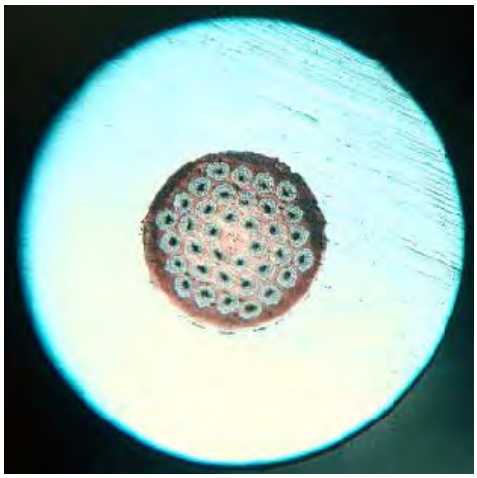

Fig. 2: section of a "jacketed" Nb_3Sn strand inside a stainless steel tube for bending strain testing.

3.2 YBCO Conductors

ENEA is involved in the field of high temperature superconductors (HTS) and a relevant experience in developing high temperature superconducting tapes has been acquired in the last years [2-6].

Due to its good intrinsic transport properties at liquid nitrogen temperature (77K) $YBa_2Cu_3O_{7-\delta}$ (YBCO) was the most studied HTS material, and superconducting tapes were realised using the RABiTS (Rolling Assisted Biaxially Textured Substrate) technique applied on Ni-based substrates. Several binary Ni alloys have been studied such as Ni-Cr, Ni-V, Ni-W [2,3] as well as ternary alloys as Ni-Cr-W, in order to decrease the Ni Curie temperature responsible for magnetic hysteresis losses due to the substrate in AC regimes at 77K, and to improve the Ni mechanical properties. Prior to YBCO deposition, in order to avoid the degradation of transport properties due to Ni diffusion in YBCO film, a buffer layer structure is interposed between the substrate and the superconducting film. Typical structures obtained in the ENEA research framework were NiV-NiO-CeO_2-YBCO (J_C= 0.7MA/cm^2 at 77K and self field), NiV-NiO-CeO_2-YSZ-CeO_2-YBCO (J_C= 0.7MA/cm^2 at 77K self field), NiW-CeO_2-YBCO [4] (J_C=1.2MA/cm^2 at 77K and self field, I_C(77K)=63A, I_C(65K)=130A on 5cm long and 1cm wide samples) (fig. 3).

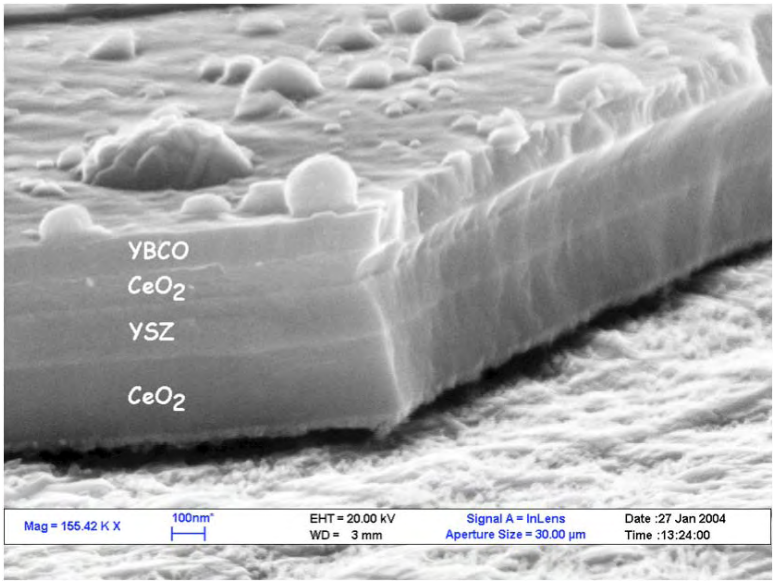

Fig. 3: SEM micrograph of 700 nm thick film cross section. YBCO and different buffer layers can be distinguished.

The whole structures were achieved using the Pulsed Laser deposition technique because of its versatility in the use of different materials and easiness in the transfer of the correct stoichiometry from a starting material (target) to the film, fundamental for obtaining optimal transport properties of YBCO films.

Recently, the effect of Ca doping at the grain boundaries of YBCO films on transport properties has also been studied.

The main goal of the ENEA project is to develop a continuous deposition process for long length YBCO based coated conductors fabrication (fig. 4).

Fig, 4: the ENEA plant for continuous deposition of YBCO-based coated conductors.

3.3 BiSCCO Conductors

Bi-2212 has been successfully synthesized by means of electro-deposition and annealing of its precursors on Ag substrates. Ag is the most widely employed material for BSCCO wires and tapes, because of its chemical inertia with the superconductor as well as with its precursors. In order to improve the physical properties of the substrate, without loosing chemical ones, Ag-buffered Ni based tapes have been studied. In order to inhibit the Ni diffusion towards the Ag films during high temperature Bi-2212 synthesis, which destroys superconductivity, an oxide can be introduced as a buffer layer between Ag and Ni tape. In the past two years a collaboration between ENEA and EDISON led to the development of an oxide buffer layer/Ag architecture on NiCr80/20 tape. Both the buffer layer and the Ag film have been deposited by means of electron beam evaporation, allowing deposition on long lengths. At the moment no BSCCO tape has been yet realised over such a substrate.

4. TEST AND CHARACTERISATION OF SUB-SIZE CONDUCTOR SOLENOIDS

4.1 ENEA Facility

The experience gained in the past years on several NbTi and Nb_3Sn inserts (SAFFO, PUFF and S-Ex experiments) [7-9] and the existing and recently updated facility allowed ENEA to be a candidate for present and future testing of sub-sized magnets in ITER-relevant operating conditions.

Goal of the experiments is to study the stability and the quench propagation in coiled conductors cooled by a forced flow of supercritical helium (CICC), to study the limitation due to the current ramp rate and to the current non-uniformity.

Such a well-instrumented sub-size magnets are also perfect candidates for codes validation.

The available facility is composed by: a refrigerator, recently bought by Linde, with 500W power, able to supply helium at 4.5 and 16K; three background magnets, two made of NbTi (with a maximum field of 3T) and one of Nb_3Sn (with a maximum field of 3T); four DC power supplies, 1kA, 5kA, 6kA, and 16kA respectively, plus several smaller ones; an AC power supply, +100A, +10V; a cryogenic and electric facility suitable for large scale experiments; several data acquisition systems.

By now the ENEA facility (fig. 5) is going to be adapted to host ASTEX, an experiment aimed to study the effect of the current non-uniformity on coil performance, in particular on its stability.

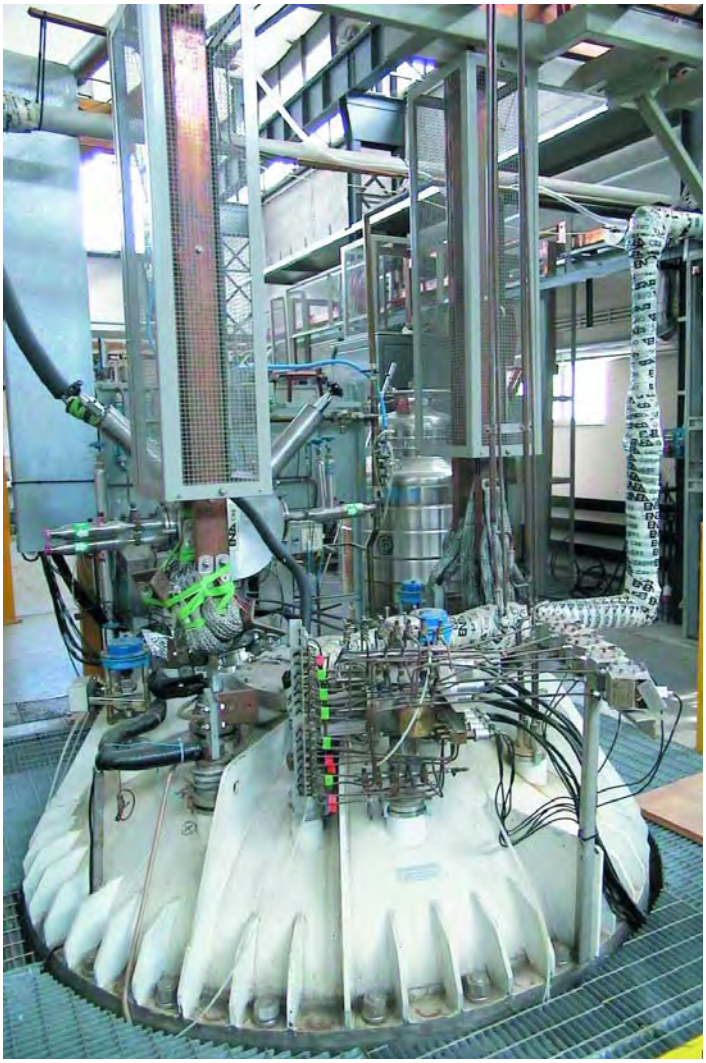

Fig. 5: view of the ENEA facility for testing superconducting solenoid magnets.

4.2 ASTEX (Advanced Stability Experiment)

Inside multifilamentary/multi-stage conductors, current may distribute non-uniformly among different strands or cable sub-elements, both during steady state operation, owing to the different contact resistance of each cable element at the joint, and during current variations, due to the different effective inductance of each sub-element. This has been identified as the main cause leading to premature conductor quench phenomena or to current ramp-rate limitations.

An experiment has been planned by ENEA which is currently in its installation phase, aimed at studying the influence of current distribution on conductor properties, as critical current, AC losses, and stability. To this purpose, a magnet has been coil wound with a sub-size NbTi 36-strands conductor (fig. 6a). The conductor has been opened at both terminations, and subdivided into the four 9-strands last-but-one stages, one of which has been further subdivided into a triplet of strands and the remaining group of 6 strands (fig. 6b). A system of external resistors allows to feed the magnet with a controlled non-uniformly distributed current. The module is fully instrumented, with thermometers, voltage taps, pick-up coils, pressure gauges and helium mass flow meters, in order to characterize its behaviour during both steady state operation and current variations. The module can be fed with a 6kA maximum current, under the effect of a maximum 2.5T background field, for a total maximum peak field of 6T; it will be operated at a temperature of about 5K, with a 10 bar inlet pressure. The hydraulic circuit allows also to reverse the helium flow inside the module with respect to the current supply, in order to study the effect of different initial normal zones on the conductor stability.

Fig. 6: the instrumented ASTEX module and its terminations, at which the cable has been opened and subdivided.

5. PARTICIPATION TO ITER TESTING CAMPAIGNS

ENEA participates with all the other EURATOM associations in the experimental campaigns relevant for the ITER magnet R&D: the Toroidal Field Model Coil (fig. 7), the Central Solenoid Model Coil, the two Central Solenoid Model Coil Inserts in the past and the Poloidal Field Insert in the future.

In collaboration with CEA a NbTi two-legs straight sample has been manufactured and tested in operating conditions relevant for Poloidal Field Magnet, to obtain a complete characterisation of a full-size conductor and a twin box joint [10]. A second sample, PFIS, is going to be tested in the near future.

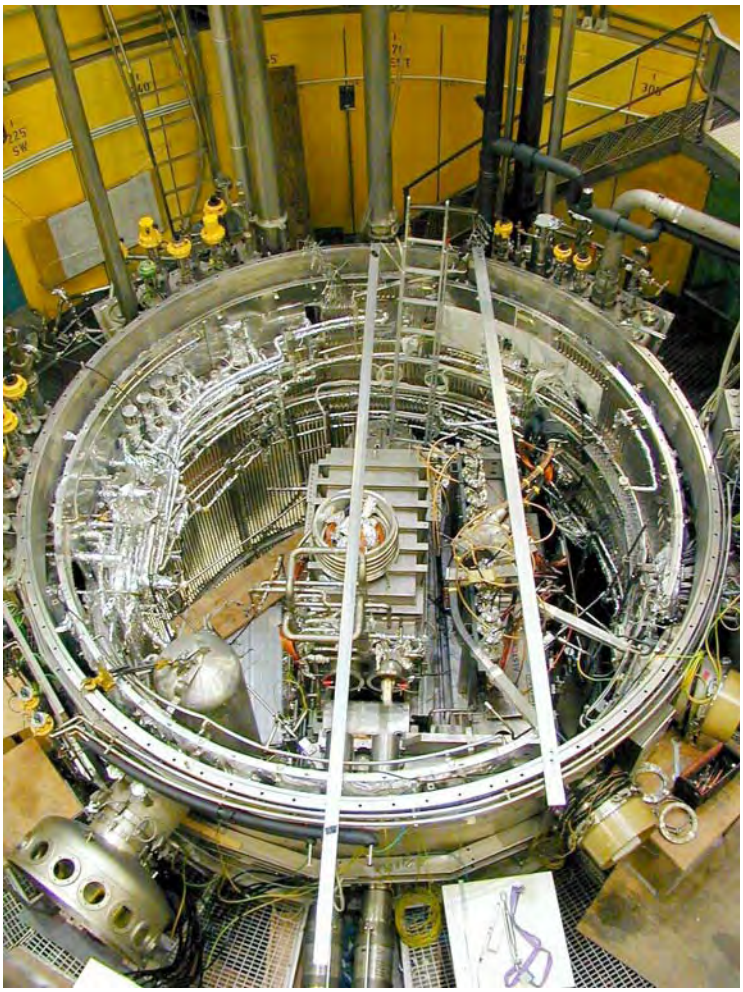

Fig. 7: the TOSKA facility in FzK (Forschung Zentrum Karslruhe), hosting the TFMC and the background LCT coil.

5.1 Measurements on Current Distribution in cables

The knowledge of the actual current distribution in the different operating conditions is a relevant information for the optimization of cable and joint layout of CIC ITER-relevant conductors. Unfortunately, it is not possible to obtain a direct measurement of the current flowing in each petal of the cable; it is therefore necessary to adopt indirect current evaluation by means of magnetic field measurements in regions adjacent to the cable surface. Within this framework, several experiments on full-size magnets and cables have been equipped with Hall sensors' heads, placed around the conductor. ENEA, in collaboration with CREATE, has designed and realized a Data Acquisition System (DAQ) for the Hall Probes Measuring Heads installed at FzK on the TFMC bus-bar during the phase-II test campaign (fig. 8), and has performed the data analysis, with the aim of reconstructing the current distribution in the six petals of the conductor during operation (fig. 9) [11,12]. Future collaborations are foreseen for the current distribution measurements on the HT_c current leads short circuit (Bus-Bar III) at FzK, on the PFIS at CRPP, and on the PFCI conductor at JAERI.

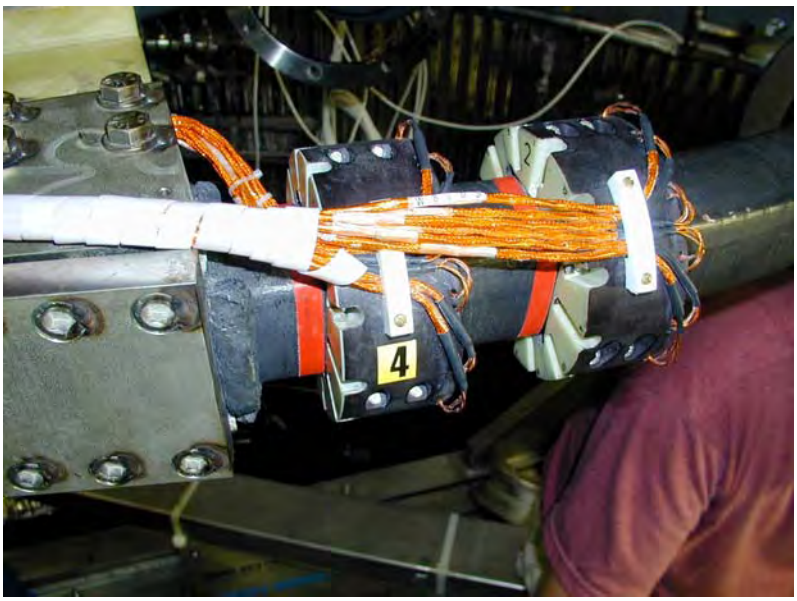

Fig. 8: Hall probes measuring heads installed around the NbTi TFMC BusBar, for the tests performed in the FzK.

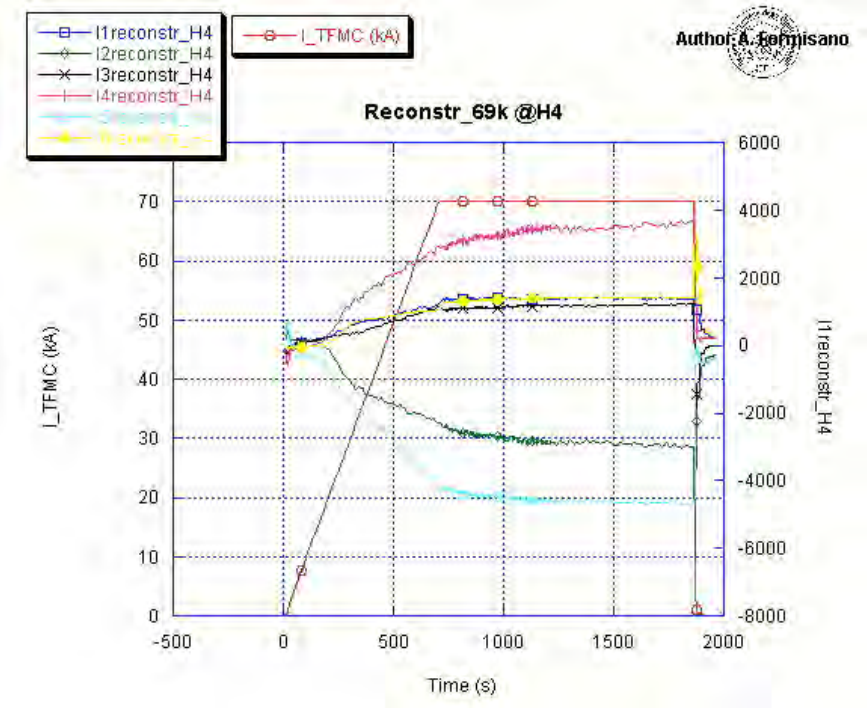

Fig. 9: example of the currents flowing in each of the 6 cable petals, as reconstructed from the Hall Probe signals, during a 69kA test in the TFMC.

6. CODES DEVELOPING AND VALIDATION

ENEA co-ordinates the activities of the group (Bologna, Turin, Udine, and Padova Universities) devoted to the development of a fully-integrated code (thermo-fluid-dynamical + electric + mechanical performances of a magnet realised by jointed superconducting CIC conductors), THELMA. ENEA is now collaborating in the code validation by providing data from different experiments of interest and analysing the results.

7. MONITORING OF INDUSTRIAL ACTIVITIES

Europa Metalli (EM) and Ansaldo Superconduttori (AS) are the two Italian factories which have been more deeply involved with ENEA in the manufacturing of strands, cables and conductors. In fact, under the ENEA monitoring, EM started in 1978 the construction of the NbTi conductor for the first large coil completely designed and wound in Italy by AS in 1980 and installed as one of the background magnets in the SULTAN facility where it reaches 6T in a bore of 1.3m.

The experience gained allowed EM and AS, first of all, to manufacture the conductor and coil for a 12T, Nb_3Sn wind and react magnet, and then to realize at EM the full size conductor for the TFMC that was wound at AS and successfully test at FzK, Karlsruhe (fig. 10) [13].

During year 2003, the collaboration with EM and AS was mainly devoted to the manufacturing of the PF (Poloidal Field) full size conductor samples to be tested in the SULTAN and NAKA facilities.

Fig. 10: picture of a section of the full-size Cable-in-Conduit Conductor adopted for the ITER magnets. External jacket dimensions are about 50 mm x 50 mm.

8. TESTING OF DIODES FOR LHC SUPERCONDUCTING MAGNETS PROTECTION

ENEA superconductivity laboratories host the OCEM activity for cryogenic and electrical testing of the diodes used by CERN to protect the dipole and quadrupole magnets of LHC (fig. 11). The direct and reverse characteristics of the diodes at cryogenic temperatures are checked, together with their ability to withstand current pulses up to 14kA [14].

Fig. 11 : Cryostat insert with four mounted diode stacks ready for testing at ENEA laboratory.

REFERENCES

[1] R. Bruzzese et al., IEEE Trans. on Mag. 27(2) (1991) 2198

[2] E. Varesi et al., Physica C 372-376 (2002) 763

[3] T. Petrisor et al., Physica C, 377 (2002) 135

[4] E. Varesi et al., Supercond. Sci. Technol., 16 (2003) 498

[5] V. Boffa et al., Supercond. Sci. Technol. 13 (2000) 1467

[6] V. Boffa et al., IEEE Trans. on Appl. Supercond. 11 (2001) 3158

[7] E. P. Balsamo et al., IEEE Trans. on Appl. Supercond. 10(1) (2000) 572

[8] E.P. Balsamo et al., IEEE Trans. on Mag. 30(4) (1994) 21

[9] L. Muzzi et al., Cryogenics 43(12) (2003) 699

[10] D. Ciazynski et al., Supercond. Sci. Technol. 17 (2004) S155

[11] T Bonicelli at al.," Proc. 22nd SOFT, Helsinki, 2002

[12] A. Formisano, R. Martone, Proceedings of EUCAS 2003, 15 Sorrento, Italy

[13] H. Fillunger et al., IEEE Trans. On Appl. Supercond.,12(1) (2002) 595

[14] A. della Corte et al., Advances in Cryogenic Engineering, 47A (2002) 131

CRITICAL CURRENT, ELECTRO-MECHANICAL PROPERTIES AND SPECIFIC HEAT OF BRONZE NB_3SN CONDUCTORS

D. Uglietti[°], B. Seeber[°], V. Abächerli[°], Y.X. Wang[*], A. Junod[*], R. Flükiger[°,]*
[°] Groupe Appliqué de Physique (GAP), University of Geneva, - Geneva, Switzerland
[*] Dept. Phys. Mat. Condensée (DPMC), University of Geneva, - Geneva, Switzerland

Abstract
The fabrication process leading to a Nb3Sn wire by using the bronze route with 15.4 wt%. Sn is described. The critical current density, J_c, is studied as a function of the applied magnetic field, B, up to 25T; the uniaxial strain, ε, was measured up to 17. In the second part our device for measuring Ic(ε) is presented. The device is based on the concept of the Walters spring (WASP), which allows to measure long length wires (voltage taps distance up to 50 cm), up to 1'000 A and to obtain an absolute measurement of the strain value. It is thus possible to measure the voltage-current relation of technical superconducting wires and tapes down to 0.01 μV/cm, an important requirement for the characterisation in view of applications like NMR high field magnets which require persistent mode operation with high current densities. Finally specific heat measurements on Nb3Sn wires prepared at GAP have allowed to determine for the first time the overall distribution of Tc in the filaments. The onset of Tc was observed at 17.2 K, the Tc distribution being centred at 15.9 K. This analysis confirms the reduction of Tc due to the Ti addition and the presence of a distribution of Sn in Nb3Sn bronze wires.

1. INTRODUCTION

Currently the main commercial applications of LTS and HTS are magnets, which can be either solenoids, dipoles or multipoles (accelerator magnets). Up to now, Nb_3Sn is the best candidate for high field solenoids operating in persistent mode operation and high field dipoles. In the last years, various attempts have been made to enhance the critical current density, J_c and the upper critical field B_{c2} [1], introducing the additives Ta and Ti to the superconducting phase. There is still room for improvements for Nb_3Sn, mainly by increasing the Sn content and by improving the homogeneity of the A15 layer. In the last years, considerable progress has been achieved on the critical current densities of Nb_3sn wires produced by the Internal Sn Diffusion technique (ISD) [2] and the Powder-In-Tube (PIT) process [3]. The ultimate performances for a certain application can be reached also by better knowledge of the mechanical properties of the wires; in this way the design of the magnet could be adjusted in order to fully exploit the potentiality of the conductor. At GAP the activities are centred on the development of Nb_3Sn bronze wires and the advanced characterisation of the critical current as a function of field and strain. For applications at lower fields (12T-15T), i.e. for accelerator dipoles, bronze wires are actually not yet performing as well as PIT and ISD wires, but at fields exceeding 20T bronze wires constitute the best choice.

In the first part of the paper our activities on the development of bronze wires for high field applications (>21T) are presented. The design has been optimised to reach a higher uniformity in the degree of reaction of the filaments and several wires with different Ti, Ta, content have been manufactured to determine the optimum doping for high field applications [4].

The second part of the paper describes the device for the electro-mechanical characterisation of technical superconducting wires and tapes. In superconducting magnets the compressive and hoop stresses can reach very high values, and knowledge of the behaviour of the critical current as a function of strain and stress becomes an important issue for the optimisation of the magnets and of the conductors. Therefore it is important to have detailed knowledge of this behaviour to obtain strain limited, optimised Nb_3Sn wires for magnets with even higher fields.

In the last part we report about recent specific heat measurements on the Nb_3Sn wires presented in the first part. The specific heat gives information on the distribution of composition inside the whole superconducting sample, and it could be a very powerful tool for the optimisation of the conductors.

2. BRONZE WIRES FOR HIGH FIELD APPLICATIONS

2.1 Fabrication

The Nb_3Sn wires produced at GAP are based on Cu-Sn bronze produced by the Osprey technique. Here we present three wires: two (wire A and B) are quaternary wires and one (wire C) is ternary (see table I). For the fabrication of wire A the filaments consisted of Nb-7.5wt.%Ta rods with NbTi insertions, to form NbTa/NbTi composites [4]. Another way of adding Ti is to use bronze doped with 0.25% Ti and Nb-7.5wt.%Ta rods for the filaments; this method has been used for the fabrication of wire B. We have also manufactured a ternary wire, using Nb-7.5wt.%Ta rods as filaments and the same bronze as for wire A. A typical layout for the three wires is presented in fig. 1.

Table 1

	A	B	C
matrix composition	Cu15.4Sn	Cu15.5Sn0.25Ti	Cu15.4Sn
filament composition	Nb7.5Ta1.0Ti	Nb7.5Ta	Nb7.5Ta
local bronze to filament ratio	2.2	2.2	2.2
global bronze to filament ratio	2.5	2.5	2.5
number of filaments	14'641	14'641	14'641
diameter of filaments	4.5 μm	4.5 μm	4.5 μm
filament spacing	2.1 μm	2.1 μm	2.1 μm
stabilizer material / content	Cu / 20 %	Cu / 20 %	Cu / 20 %
barrier material / content	Nb / 10 %	Nb / 10 %	Nb / 10 %

The deformation process to obtain wires with a final diameter of about 1 mm requires three hot hydrostatic extrusion steps. Before the third extrusion a Nb barrier and a copper stabilisation are added. After the third extrusion step, the rods consisting of 14'641 filaments were drawn into round conductors of 1.25 mm diameter and about one hundred metres length. The local bronze/filament ratio (after the second extrusion step) was chosen to 2.2, while the global ratio was 2.5. The filament diameter was 4.5 μm, the spacing 2.1 μm. Two different reaction treatments (670°C/100h and 600°C/100h-670°C/150h) were performed under a pressure of < 10-5 mbar. Heating and cooling rates were chosen at 30 °C/h.

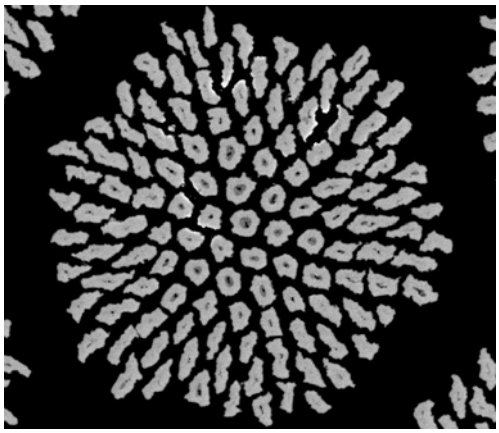

Fig.1. Filament bundle inside a bronze route Nb_3Sn wire (wire A) after reaction.

2.2 Critical currents

The critical current of the three wires has been measured on standard ITER barrels (∅ 40mm) at fields up to 17 T at 4.2K. The wire A was also measured up to 24T at the High Field Magnet Laboratory in Nijmegen; the upper critical field, B_{c2}, has been estimated to be 24T, i.e. markedly lower than the value extrapolated by the Kramer plot based on the data taken between 10 and 17 T. At 17 T, after a heat treatment of 700°C for 150h the critical current of wire B was about 20% higher than for wire A. A two step heat treatment (600°C/100h-670°C/150h) allows to obtain a further increase of 16% respect to the one step heat treatment. At 17T the wire C has almost the same critical current than wire A; at lower fields the I_c increase faster than for the quaternary wires, so we expect lower performances in high field with respect to the Ta,Ti doped wires.

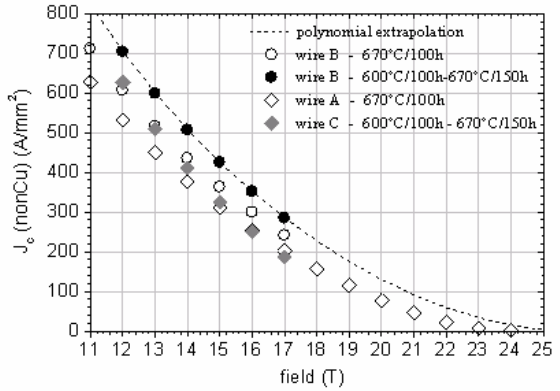

Fig.2. J_c versus B at 4.2K for bronze route Nb_3Sn wires; the J_c criterion is 0.1μV/cm (round wires, ∅ 1.25mm).

The usual method to extrapolate J_c values to higher fields is to fit the J_c data on a Kramer plot with a straight line. In some case this method gives J_c values higher the measured values. We have found that a polynomial fit of the J_c data on a Kramer plot gives values close to the measured ones. The critical current for the wire B has been extrapolated to higher fields fitting the Kramer plot with a polynomial curve (see fig. 2); this method allows more realistic values than the standard linear fit, especially in the 17T - 21T range. In the next section the behaviour of critical current under strain will be presented. Further analysis on the homogeneity of the A15 layers in the wires will be presented in the third section.

3. ELECTRO-MECHANICAL PROPERTIES

Various probes for the measurement of $I_c(\varepsilon)$ have been described in the literature. Ekin et al. [5] developed a sample holder which fits into very high field hybrid magnets. A modified design has been reported by ten Haken et al. [6]. The design of Specking et al. [7] allows higher forces by using a split-pair magnet, but the field strength was limited to 15 T. A common drawback of these methods is the short sample length of a few cm (corresponding to the size of the magnet bore). Voltage taps for the I_c measurement are typically separated by 5 to 10 mm. Due to this short distance, it is difficult to apply the usual 0.1 μV/cm criterion of the standardised critical current measurements [8] and the 1 μV/cm is thus currently used. Another difficulty due to the small high field magnet bores, is the short distance between voltage taps and current contacts (transfer length) [9]. Recently at the University of Twente a new device has been developed, which allows measuring longer samples; the distance between voltage taps is few cm and the current transfer length is of the order of 10 cm.

3.1 Description of the Walters spiral

All the problems due to short length can be overcome by the ingenious design of Walters et al. [10] who wound the wire on a spiral in order to introduce long wire lengths in the reduced high field space. A modified version of the Walters spiral (WASP) has been constructed in Geneva. By keeping one end of the spring in position and by rotating the other end, the wire can be strained either under compression or under tension. Because the spring is made of Ti6Al4V, reversible and linear strains up to 1.4% can be applied at 4.2 K [11]. Due to the sample length of the order of 80 cm, there is no current transfer problem and even the 0.01 μV/cm criterion can be applied. The method of Walters has not been used extensively because of the unreliable soldering process between the superconducting wire and the Ti-alloy forming the WASP. This problem was recently circumvented by using CuBe instead of the Ti-alloy, which however, limits the maximum strain to 0.7% [12]. On the other hand, soldering the total length allowed compressive strains to be applied too. In our implementation of the Walters spring the above mentioned problems have been solved; not only the zero strain on the wire can be determined precisely, but there is also the possibility to solder on the Ti alloy spiral, thus allowing to access to the compressive regime. In addition the effect of the different thermal contractions during the cool-down run can be controlled.

The WASP consists of a Ti alloy; at both ends of the spiral the wire is soldered to copper blocks, which act as current terminals. The wire sits in a grove that has been machined on the spiral; several spirals with different groove size have been built for measuring either rectangular or round wires with different cross sections and also for measuring tapes (up to 4.5 mm in width). The essential part of the modified WASP is shown in fig. 3. The bottom is fixed and the top can be rotated by a d.c. motor located outside of the cryostat. Close above the WASP, but still in the liquid helium bath, a piezoelectric sensor measures the torque. The angular position of the motor can be determined by an optoencoder [13].

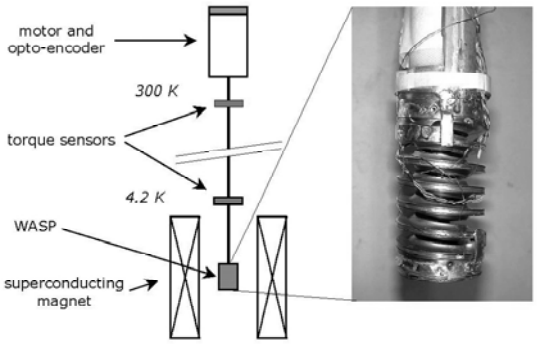

Fig.3 Set-up of Walters spiral (WASP), Geneva design.

3.2 Electro-mechanical properties: $J_c(B,\varepsilon)$

The following wires have been characterised: the wires A, B and C (described in the previous section) and a round binary wire (0.8mm diameter) manufactured by Furukawa for the ITER benchmark test [14].

The variation of the critical current as a function of strain at 17T is shown in Fig. 4a and 4b for the wires A, B and C. Strains ranging from –0.5% to 0.4% has been applied to wire B. The Ekin model has been used to fit the critical current; one of the parameters used in the Ekin model is the critical field, B_{c2}, which can be found by fitting the $I_c(\varepsilon)$ curve. In the case of wire B the transport measurements gave a value of 24T for the critical field. The critical field determined by the Kramer extrapolation of transport measurements in the range 10T-17T is 27T. The critical field obtained by the Ekin model is about 25.5T; this is the B_{c2} at $\varepsilon=\varepsilon_m$. When correcting for the prestrain effect (ε=0.25%) the value of 24.3T is found, which is closer to actual value than the Kramer extrapolated value. We believe that the dependence of the critical current from strain could be used for the determination of the critical field when a direct measurement in high magnetic is not available. This method could be more accurate that the standard Kramer extrapolation.

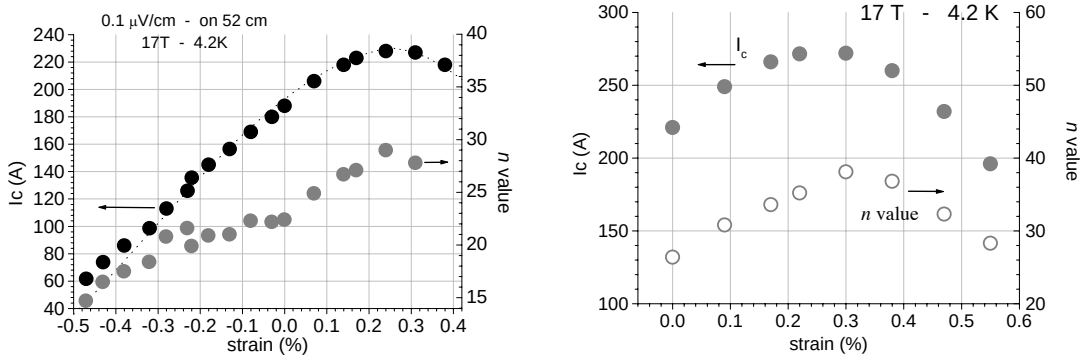

Fig.4a-b Critical current (0.1 μV/cm criterion) and *n* value for the $(Nb,Ti,Ta)_3Sn$ bronze wires (A on the left and B on the right) manufactured at the University of Geneva; both are square wires, 1.37X0.92mm^2, twisted. The dashed line is Ekin's model: p=0.5; q=2; n=1; u=1.7; $a(\varepsilon<\varepsilon_m)$=1250; $(\varepsilon>\varepsilon_m)$=900; B_{c2}=25.5T.

The Furukawa wire was measured following the same procedure as the wire above; in this case the field was 12T. Strain up to 0.9% was applied to the wire and the voltage-current relation was measured over three decades.

3.3 $J_c(B,\varepsilon)$ with a criterion of 0.01 μV/cm: a test for possible wire degradation

On the Furukawa wire it was possible to determine the critical current at 1 μV/cm, 0.1 μV/cm and even at 0.01 μV/cm. The *n* values have been calculated doing a linear fit of the V-I curves in the region between 0.1 μV/cm and 1 μV/cm. All the data have been obtained for both the loading and unloading process, in order to study the effect of the filaments cracking on the V-I curves. In fig.5 the critical current determined with the three criteria are plotted as a function of strain. The ascending branches of the $I_c(\varepsilon)$ curve are very similar, regardless of the criteria. Apparently the maximum value of I_c decreases slightly when increasing the criterion. At the maximum applied strain (0.9%) the I_c depends strongly on the criterion: for instance the 1 μV/cm I_c is reduced of 60%, while the 0.01 μV/cm I_c is reduced of 80%. The large dependence from the criterion is still present when the strain is released back to 0%. The 1 μV/cm critical current suffered a degradation of 5%, while for the 0.1 μV/cm and the 0.01 μV/cm criteria the reduction was respectively 20% and 40%. The high voltage

sensitivity of our device allows to detect the formation of crack, which cause an irreversible behaviour of the critical current.

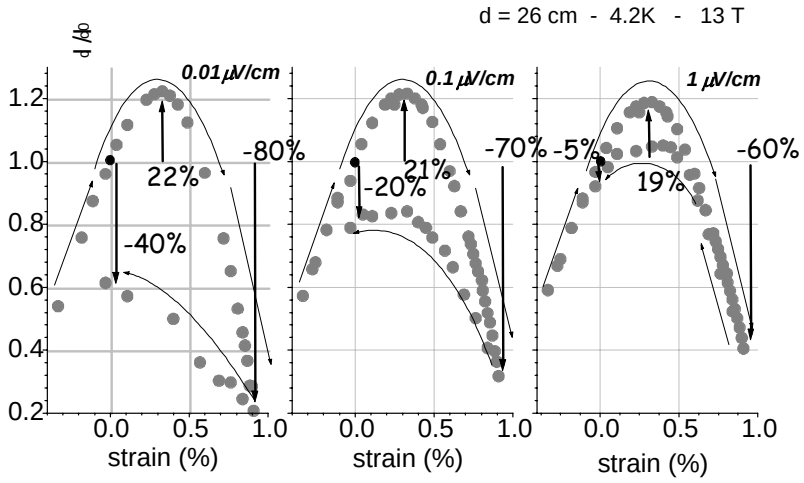

Fig..5 Critical current (0.01 μV/cm, 0.01 μV/cm and 0.01 μV/cm criterion) for the Furukawa ITER wire. The degradation of the critical current at 0.9% and after the strain recovering depends strongly on the voltage criterion: the recovered I_c is 5% lower than the initial value for 1 μV/cm but it is 40% lower for the 0.01 μV/cm.

4. DISTRIBUTION OF T_C BY SPECIFIC HEAT ANALYSIS

The measurement of low temperature specific heat is particularly appropriate to the determination of the critical parameters of superconducting materials, as it indicates the properties of the whole volume, without being influenced by screening effects. In particular it allows to probe multifilamentary wires and to obtain reliable measurements of the distribution of the critical temperature inside the filaments. Specific heat has been measured on a short piece of the wire A and wire C at 0 and 14T, and a distribution of critical temperature has been calculated. The same analysis has been carried out on very homogeneous bulk sample with a composition of 24.8% Sn as determined by the value of residual resistivity and of the ratio c/a of the tetragonal deformation [15]. The results are presented in fig. 6: the T_c distribution of the wires is centred at a lower temperature respect to that of the bulk sample; the reasons for this shift are the lower overall Sn content (this effect is present in both wires) and the presence of Ti which is known to lower T_c [4] (in the case of wire A). In addition the width of the distribution is much larger than for the bulk sample. The reason is the inherent Sn gradient of the A15 layer in bronze route filaments with unreacted Nb cores [16]. The width of the distribution is similar in both wires, so apparently the Ti doping seems to have no influence on the homogeneity of the A15 layer.

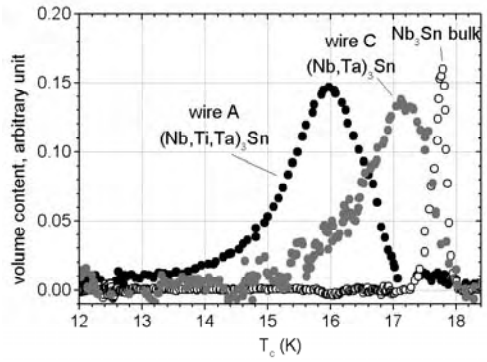

Fig. 6 Critical temperature distribution for the wires A and C, compared to the bulk sample [15].

5. CONCLUSIONS

In the present paper we have described the fabrication process of bronze $(Nb,Ta,Ti)_3Sn$ wires optimised for high field applications. The variation of J_c has been measured as a function of field and uniaxial strain: at 17 T, the non-copper value of J_c reached 285 A/mm^2, the *n* factor being as high as 50. The maximum of J_c vs. strain was determined to $\varepsilon_m = 0.26$ % by means of the modified Walters spiral.

A device to measure the critical current of long length technical superconducting wires and tapes (up to 0.8 meter) carrying up to 1000 A at 4.2 K in fields up to 17 T has been developed. The advantage of this apparatus with respect to the usual linear devices resides in the longer wire length, thus allowing one to use a more stringent criterion for the determination of the critical current (down to 0.01 μV/cm instead of 1 μV/cm). It is also possible to determine the true strain acting on the wire and to apply compressive strain. Another advantage is the high measuring current (up to 1000 A); no problems arise from the current transfer length, the distance between the soldered ends and the voltage taps being ≥ 10 cm; moreover measurements on long lengths are also more representative in the case of twisted wires. The device can be used to better characterise commercial superconducting wires, in particular Nb_3Sn wires for high field NMR applications, and it can be used to study the effect of strain on critical current from the fundamental point of view.

These measurements will be extended to higher fields, a new 21T magnet being recently installed in our laboratory.

Low temperature specific measurements have been carried out to determine the T_c distribution inside the A15 layer of our bronze route Nb_3Sn wires. The same analysis has been done on a homogeneous bulk sample, with a Sn content of 24.8 at. %. The T_c distribution of the wires peaks at a lower T_c value and is considerably wider than that of the bulk sample. The lower T_c onset for the filaments is due to addition of Ti, while the larger width is due to the Sn gradient inside the filaments. Taking into account these results, and knowing the relationship between T_c and the Sn content, it appears that the Sn distribution in the A15 layer of bronze route Nb_3Sn wires can still be optimised, thus letting room for further improvements of J_c.

ACKNOWLEDGEMENT

We would like to thank Okuno Kiyoshi from JAERI for the Furukawa ITER wire.

REFERENCES

[1] H. Krauth, "Conductors for d.c. applications,"in *Handbook of Applied Superconductivity*, B. Seeber Ed. Bristol: Institute of Physics Publishing, 1998, pp. 397-414.

[2] J.A. Parrel, et al., *IEEE Trans. Appl. Supercond.*, vol.13, pp.3470-3, 2003

[3] J. L. H. Lindenhovius, et al. *IEEE Trans. Appl. Supercond.,* vol. 10, pp. 975-978 2000

[4] V. Abacherli, D. Uglietti, B. Seeber, R. Flükiger, "$(Nb,Ta,Ti)_3Sn$ multifilamentary wires using Osprey bronze with high tin content and NbTa/NbTi composite filaments", *Physica-C*, vol. 372-376 pp. 1325-8, 2001

[5] J. W. Ekin, "Strain scaling law for flux pinning in practical superconductors. Part I: basic relationship and application to Nb_3Sn conductors," *Cryogenics*, vol. 20, pp. 611-624, 1980.

[6] B. ten Haken, A. Godeke, and H. H. J. ten Kate, "A new device for measuring the critical current in a tape as a function of the axial and transverse strain, the magnetic field and temperature," *IEEE Trans. Appl. Supercond.*, vol. 3, pp. 1273-1276, 1993.

[7] W. Specking, A. Nyilas, M. Klemm, A. King, and R. Flükiger, "The effect of axial stresses on Ic of subsize NET Nb_3Sn conductors," in *Proceedings of MT-11*, T. Sekiguchi and S. Shimamoto Eds. Tsukuba, 1989, pp. 1009-1014.

[8] International Standard, IEC 61788-2, "Critical current measurement – DC critical current of Nb_3Sn composite superconductors," Geneva: International Electrotechnical Commission, 1999.

[9] J. W. Ekin, "Current transfer in multifilamentary superconductors, I. Theory," *J. Appl. Phys.*, vol. 49, pp. 3406-3409.

[10] C. R. Walters, I. M. Davidson, and G. E. Tuck, "Long sample high sensitivity critical current measurements under strain," *Cryogenics*, vol. 26, pp. 406-412, 1986.

[11] A. Nyilas, private communication.

[12] N. Cheggour, and D. P. Hampshire, "A probe for investigating the effect of temperature, strain, and magnetic field on transport critical currents in superconducting wires and tapes," *Rev. Scient. Instrum.*, vol 71, pp. 4521-4530, 2000.

[13] D. Uglietti, B. Seeber, V. Abächerli, R. Flükiger, "Critical current vs. strain measurements of long length Nb_3Sn wires up to 1000 A and 17 T using a modified Walters spring", proceeding of ASC2002 , Houston, to be published.

[14] H. G. Knoopers, A. Nijhuis, E.J.G. Krooshoop, H.H.J. ten-Kate, P. Bruzzone, P.J. Lee, A.A. Squitieri, "Third round of the ITER strand bench mark test", *in Applied Superconductivity 1997 –Proceedings of EUCAS*, vol.2 pp. 1271-4, 1997.

[15] V. Guritanu, diploma work, University of Geneva, 2003 (unpublished

[16] M. Klemm, E. Seibt and R. Flükiger, *Supercond. Sci. Technol.*, 3 (1990) 249

NB_3SN AND NBTI FOR HIGH FIELD APPLICATIONS WITH EMPHASIS TO FUSION MAGNETS

J.L. Duchateau
Association EURATOM-CEA, CEA/DSM/DRFC CEA-Cadarache
F-13108 Saint Paul Lez Durance Cedex France

Abstract
This paper gives a view of the present situation of the two main materials used for high field superconducting magnets, namely Nb_3Sn and NbTi. Two specific issues are discussed in detail, the strain sensitivity of large Nb_3Sn cables and the potential for a further increase of the maximum field in accelerator magnets through Ta addition in NbTi.

1. INTRODUCTION

Superconducting conductors have to face the request of increasing field for magnets. Several kinds of answers can be brought to this request depending on the application. This trend is illustrated in fusion with the development of Nb_3Sn Cable in Conduit Conductors and the degradation effect linked to bending strain. In Particle Physics there is the idea that Tantalum addition in NbTi could avoid the mutation to the more expensive Nb_3Sn. This idea is examined taking into account in a realistic way the design margins.

2. CABLES IN CONDUIT CONDUCTORS FOR FUSION APPLICATION

In the framework of ITER programs, the ITER partners have carried out an extensive research and development programme for the last 10 years. This program aimed at designing and industrialising the high current (40-70 kA), high field conductors adapted to the superconducting magnet systems of this machine [1]. Europe has been involved in this programme.

The solution retained for the ITER conductor, is the so-called Cabled in Conduit Conductor (CICC), the original concept of which was developed by Hoenig in 1974 [2]. Substantial progress has been made to adapt this concept to the requirements of fusion technology. One major step was the

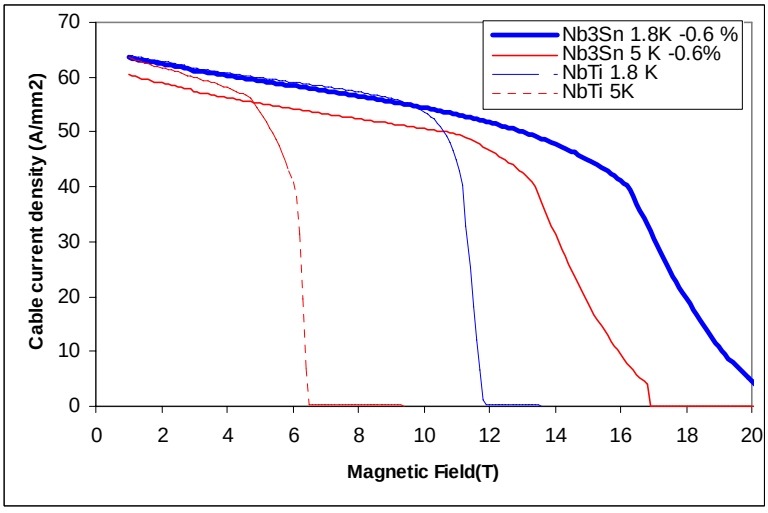

Figure 1: Range of application of NbTi and Nb_3Sn as a function of field and temperature for a typical Cable in Conduit for fusion (15 s fast discharge)

introduction of Nb_3Sn, a more performing superconducting material required by the high level of magnetic field in ITER (12-13 T).

The range of application of NbTi or Nb_3Sn as a function of field and temperature is presented in Figure 1 with the associated current density which is relatively low in comparison with the design current densities in magnets for particle accelerators, and includes the helium with a typical void fraction of 35 %.

In the framework of this program, two model coils were manufactured and tested: the Central Solenoid Model Coil (CSMC) [3, 4, 5, 6] and the Toroidal Field Model Coil (TFMC) [7, 8, 9]. The TFMC program was mainly taken in charge by Europe. Nine hundred meters of TFMC conductor in five pieces were successfully provided for the manufacture of these model coils.

3. AN APPLICATION OF CICC: THE ITER TF MODEL COIL AND ITS CONDUCTOR

3.1 The coil

The winding pack of the TFMC is made by stacking 5 double pancakes (DP1, DP2, DP3, DP4, DP5) with a racetrack shape (Figure 2). Each double pancake is embedded in the spiral grooves machined on both sides of stainless steel plates. The total length of conductor is around 800 meters. The winding pack is enclosed in an 80 mm thick walled stainless steel case.

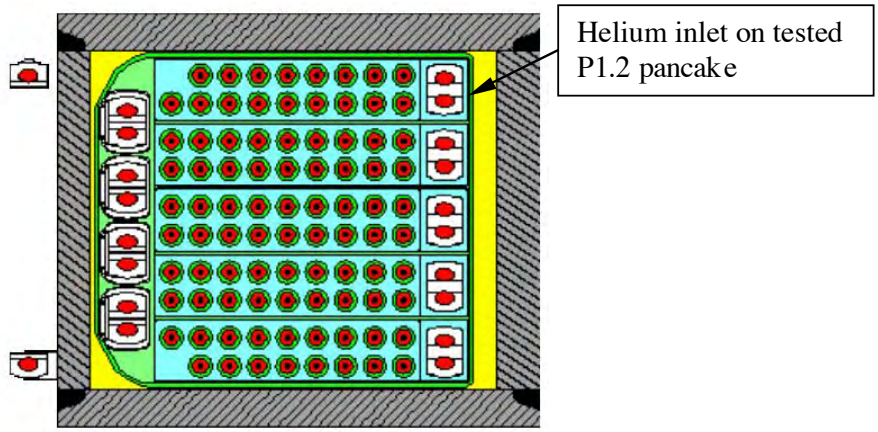

Figure 2: TFMC cross section showing the system of 5 double pancakes embedded in plates and surrounded by a casing.

3.2 The conductor

The cable (see Figure 3) is made of six petals cabled around a central metallic spiral of 10 mm internal diameter and 1 mm thick. The characteristics of the cable are presented in Table 1.

Figure 3: TFMC conductor (Φ=40.7 mm)

Table 1: TFMC conductor characteristics

Cable pattern	3x3x5x4x6
Corresponding twist pitches	25mm/62mm/109 mm/168 mm/425 mm
Number of superconducting strands	720
Number of copper strands	360
Local void fraction in the annulus	36 %
Central hole inner diameter	10 mm
Cable space diameter	37.5 mm
Jacket thickness	1.6 mm

3.3 The strand

Four tons of strands have been produced by Europa Metalli (EM) in Italy. A cross section of the strand is reported in Fig. 4.

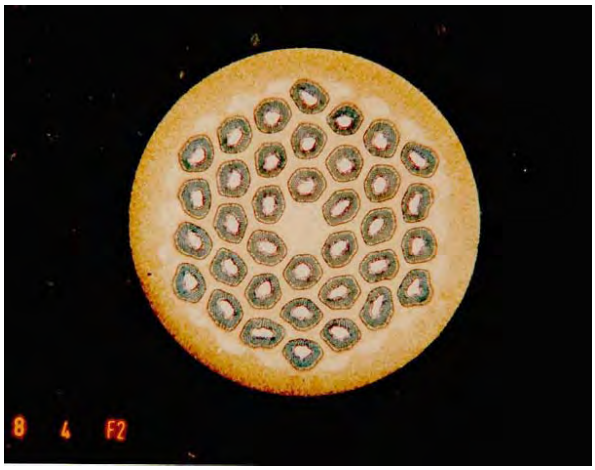

Figure 4: EM-LMI Nb_3Sn strand for TFMC (Φ=0.81 mm)

3.4 Exploration of the limits of the conductor [10]

After current ramping and plateau, the helium entering P1.2 pancake (at the inner joint) was slowly heated. The temperature was simultaneously increased in neighbouring P1.1 pancake to limit the heat exchange between the two pancakes. The voltage drop over the whole pancake was measured using co-wound voltage taps as visible in Figure 5.

The temperature presented in the Figure 5 is the inlet temperature before the inner joint and there is no additional temperature sensor along the conductor. It is known however that the most critical point, where the field is maximum, is situated at about 2 meters from the joint area.

As visible in Figure 5, the voltage increased according to the inlet temperature illustrating the so-called current sharing regime. The conductor is so stable that it is possible to recover after a temperature excursion of 0.5 K above the current sharing temperature.

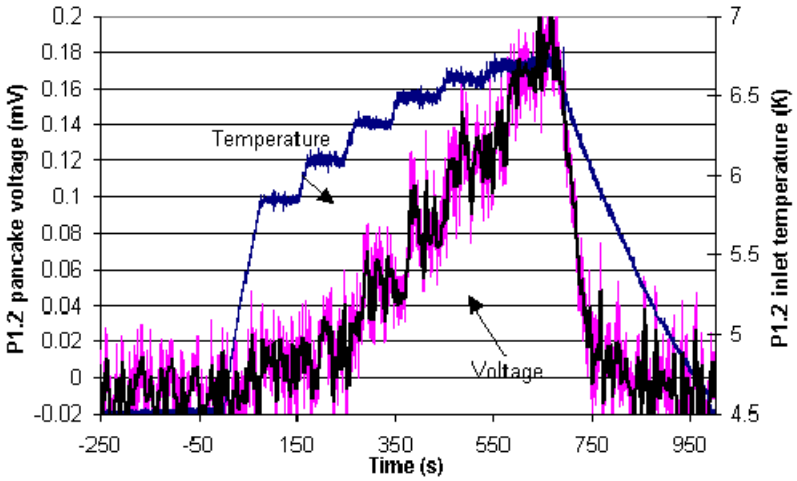

Figure 5: Exploration of the TFMC limits by increasing the P1.2 temperature inlet. Current sharing temperature is reached in the second temperature plateau(Test: 21 November 2002)

4. SENSITIVITY OF NB3SN TO COMPRESSION IN STAINLESS STEEL JACKETED CICC

The sensitivity of Nb3Sn to compressive strain is well known. According to theory the effective strain ($\varepsilon_{effective}$) in a stainless steel conductor is the sum of two terms, namely the thermal compression ε_o due to thermal heat treatment, and the elongation ε_{op} which appears due to the electromagnetic forces in operation.The total strain can be written as follows:

$$\varepsilon_{effective} = \varepsilon_o + \varepsilon_{op} \quad (1)$$

According to theory the maximum value (in absolute) which can be awaited for ε_o is the differential thermal contraction from 923 K to 4 K between steel and Nb3Sn. This parameter is not

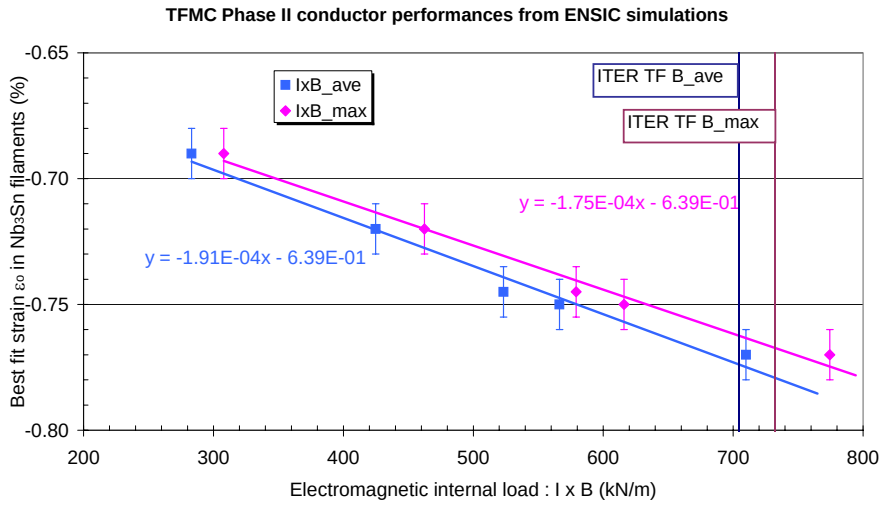

Figure 6. Influence of internal load on ε_0 in TFMC experiment

well characterized, moreover the cable void fraction can attenuate this effect due to imperfect bonding but this phenomenon is not well characterized either. The exploration of the conductor limits, knowing all the others parameters of the Summers model, showed that ε_o is depending on the transverse magnetic load in a way which is not completely understood. This is one of the main results obtained in the TFMC experiment concerning the filament strain $\varepsilon_o$and is reported in Fig. 6. From the TFMC experiment, the following points were highlighted:

1. The Nb3Sn filament strain ε_o is depending on the magnetic load which was not expected by a simple classical model
2. In phase II experiment the TFMC was tested in a magnetic load range relevant to ITER.
3. At ITER TF relevant magnetic load the filament compression ε_o is larger than expected: [0.75, 0.79] instead of 0.6 in ITER design
4. The 'n' value (around 10) is lower than expected (20)

Points 2 through 4 suggest that the simple model of compression during cool down from reaction and stretching during operation is too simple and not effective to account for the experiment. Bending strain, whose effects were initially described by Ekin [11] in 1980 could be an explanation. In the case of CICC's, however, bending strain is not originated as envisaged by Ekin by reacting Nb3Sn strands and winding them on a mandrel. Indeed, according to the model developed by Mitchell [12], the bending strain in a CICC could be induced by the twist of the strands inside the jacket and can appear during thermal compression induced by the cool down from reaction temperature before any loading, or during coil energization due to magnetic load. In this model the strain can vary across the filament section and along the strand with a wavelength of typically 5 to 10 mm. A finite element model has been developed by Mitchell but no quantitative dependency can be given. The following parameters are supposed to play a role :

- the twist pitch of the strand can affect the current redistribution between filaments within a strand and average the effect of strain distribution across the strand section;
- the geometry of the strand and associated effective resistivity of the matrix can also help to average the strain. This can be very different from one company to another;
- the cable void fraction can also play a role to minimize this effect.

4.1 Open issues on strain sensitivity in Nb_3Sn

Based on the discussion above, we can summarise the open issues on strain sensitivity in Nb3Sn in the following list:

- Is the differential thermal contraction applied in the same way in a Cable in Conduit and in a wire soldered on a spring (tests made at Durham and Twente on Walters type spring) ?
- Is applying an axial stress on the wire to strongly compress it, an exact simulation of the effect of the thermal contraction in a CICC ?
- Is the Summers model correctly accounting for behaviour of strands under high compressive strain which are related to stainless steel jackets ? Experiments at Durham and at Twente showed that the decrease in J_{noncu} is more pronounced at high compressions.
- Mechanical properties of Nb3Sn are different according to the vendors : what is the simpler short sample representative of the mechanical properties of the material embedded in a conduit ?

4.2 Experiments to improve understanding of bending strain in representative stainless steel jacketed subsize samples

Experiments have already been performed in the past to improve the understanding of Nb_3Sn under compression on subsize samples (see, as an example, the small cable cross section in Figure 7 and the

corresponding pulling experiment results reported in Figure 8)[13]. These samples did not exhibit a behaviour very different from what was expected from the Summers law.

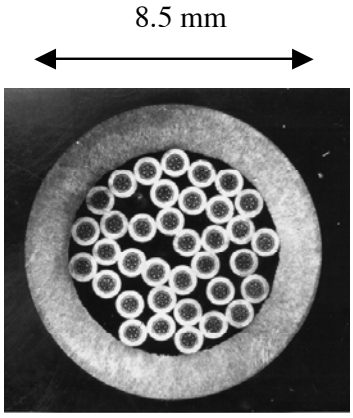

Figure 7: Subsize stainless steel jacketed cable in conduit

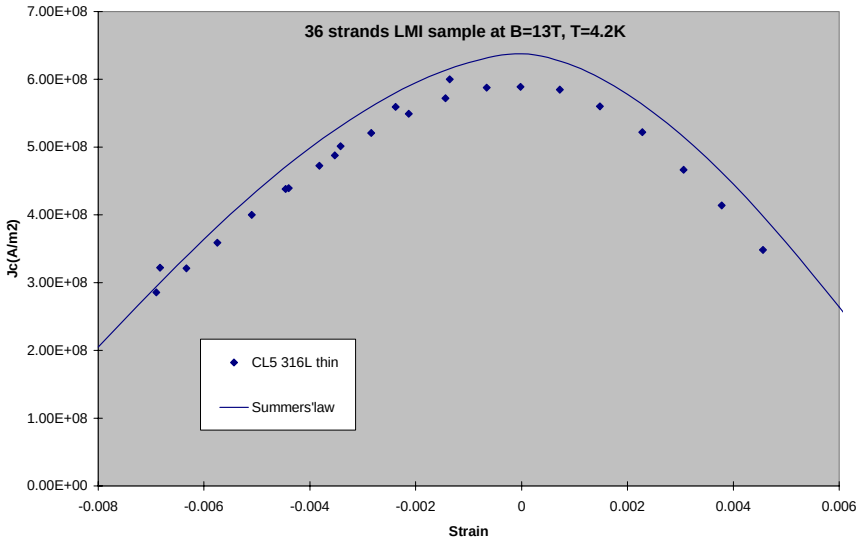

Figure 8: Stretching a subsize (36 strands) Nb_3Sn conductor in the FBI facility

EM strand 12 T 4.2 K (A316 jacket) 1997

A new program has recently been launched in Europe with advanced strands for ITER, to explore the influence of various parameters on bending strain (twist pitch, void fraction, type of strands). The experimental test will be carried out at the FBI test facility at FZK with an improved sensitivity in voltage measurement to gain information about the n value.

Even simpler samples made of one strand such as the one presented in Figure 9, which consists of a single strand jacketed in a stainless steel pipe, can help to explore strain and investigate compression effect on Ic.

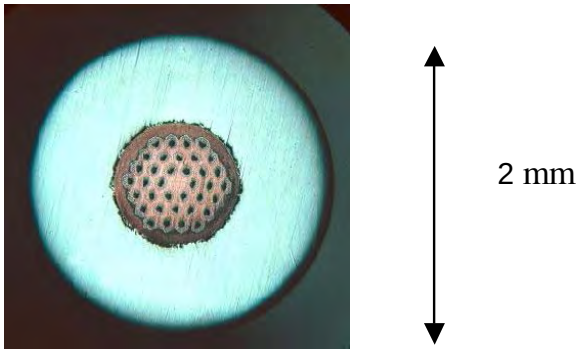

Figure 9: strand manufactured at ENEA to be stretched at FZK on FBI test facility to investigate compression and effect on Ic (courtesy of ENEA)

5. PUSHING NBTI AT ITS LIMITS IN PARTICLE PHYSICS, CAN TANTALUM ADDITION HELP ?

As illustrated in Figure 1, NbTi conductor can perfectly operate at 11 T, at low current density. In practice this possibility was not used extensively. Only the operation of the Large Coil Task coil demonstrated this capacity [14] and this coil was besides used in subcooled mode to provide a background field for the TFMC. A general question is whether tantalum addition can help in Particle Physics to increase the field of dipoles and offer a cheaper solution than the use of Nb_3Sn. This point will be illustrated based on the practical example on LHC dipoles.

5.1 Operation point of LHC dipoles

At 1.9 T and 8.33 T the LHC dipole conductor is far from the critical properties of the conductor. Typically at 8.33 T and 11850 A at constant field, the margin in temperature is 2 K and the margin in critical current is 50 %. This can be presented analytically as well as graphically.

The current density in NbTi at 8.33 T and 11850 A in the cable (nominal conditions) is J=1259 A/mm2. The critical current density in these conditions is:

$$J_c(1.9\ K, 8.33\ T) = 2482\ A/mm^2$$

A simple description of critical current density as a function of field and temperature can be given due to the linear behaviour of the critical current density as a function of field, the parameters of the model are probably not completely exact but the method remains valid:

$$J_c(T,B) = -a[B+B_{c20}((T/T_{c0})^{1.7}-1)] \qquad B_{c20} = 13.87\ T \qquad T_{c0} = 9.2\ K \qquad a = 625$$

The current sharing temperature Tcs of the LHC dipole at this current density is by definition:

$$J = -a[B+B_{c20}((T_{cs}/T_{c0})^{1.7}-1)]$$

$$T_{cs} = T_{c0}[1-J/(a\,B_{c20})-(B/B_{c20})]^{1/1.7} = 4.12\ K$$

These margins can also be illustrated graphically in Figure 10.

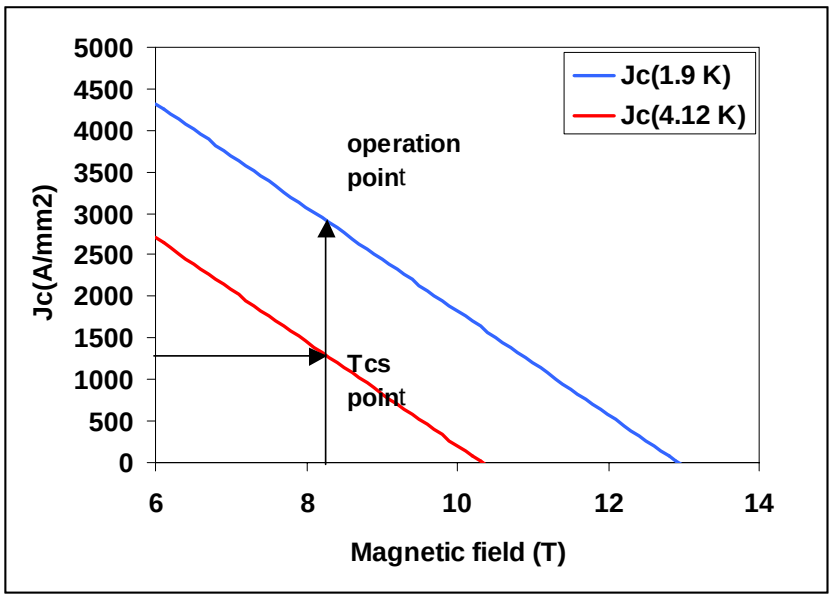

Figure 10 : Tcs in LHC as compared with the (1.9K and 8.33 T) point.

5.2 Consequences of tantalum addition.

From the preceding section it can be seen that the design temperature point of the dipole is not 1.9 K but rather 1.9 K $+\Delta T_{op} + \Delta T_{margin}$, where ΔT_{op} is the temperature increase in operation due to the beam heating, and ΔT_{margin} is the temperature margin to ensure current stability. The sum of these two terms for a LHC dipole, is large due to magnetic instabilities probably associated with the very high mechanical forces.

It is well known that the help of tantalum, whatever the tantalum content in titanium, is effective only if the field is higher that 11 T, in addition the increase in current density vanishes if the design temperature is higher than 1.8 K. It is the case for LHC dipoles at least due to beam heating but also due to additional temperature margin.

6. CONCLUSION

The use of tantalum in LHC dipoles could be envisaged only for a field higher than 11 T. Even in this range of field, the use is questionable due to the design temperature which is substantially higher than 1.8 K.

7. REFERENCES

[1] Duchateau J L, Spadoni M, Salpietro E, Ciazynski D, Ricci M, Libeyre P, della Corte A 2002 Supercon. Sci. Techno. 15 817-829

[2] Hoenig M O et al. 1975 Proc. 5 th Int. Conf. Mag. Tech. (Roma Italy Laboratori Nazionale del CNEN) 519 524

[3] Jayakumar R et al. 1998 Proc. 15 th Int. Conf. Mag. Tech. (Beijing: Science Press) 357 360

[4] Nakajima H et al. 1998 Proc. 15 th Int. Conf. Mag. Tech. (Beijing: Science Press) 361 364

[5] Martovetsky N et al. 2001 IEEE Trans. Appl. Supercon. **11** 2030 2033

[6] Ando T et al. 2002 IEEE Trans. Appl. Supercon. 12 496 499

[7] Salpietro E 2002 IEEE Trans. Appl. Supercon. 12 623 626

[8] Ulbricht A and the ITER L2 project Team 2003 Proc. of the 22 nd SOFT To be published.

[9] Nicollet S et al 2003 Proc. of the 19 th Int. Cryo. Eng. Conf. 161 164

[10] Duchateau J.L et al. 2004 Supercon. Sci. Techno. 17 241-249

[11] Ekin J W 1980 “Filamentary A15 superconductors” editors M. Suenaga and A.F Clark Plenum Press

[12] Mitchell N 2003 Cryogenics 43 255-270.

[13] Specking W, Duchateau J L, Decool P 1998 Proc. 15 th Int Conf. On Magnet Tech. (Beijing: Science Press) 1210 1213

[14] Heller R et al. 1998 Cryogenics 38 519

STATUS AND PERSPECTIVE OF THE NB_3AL DEVELOPMENT IN JAPAN

T. Takeuchi
National Institute for Materials Science, Tsukuba, Japan
K.Tsuchiya
High Energy Accelerator Research Organization, Tsukuba, Japan

Abstract
The RHQT process enables to form a stoichiometric Nb_3Al with fine-grain structures via a bcc supersaturated solid solution and so that a large J_c is achieved over the whole range of magnetic fields without trading off the excellent strain tolerance. A long-length of RHQ processing has been established, and a rectangular but Cu stabilized Nb_3Al strand is about to be commercially available for NMR uses. Another stabilization technique has been developed and likely applicable to accelerator uses. Research activities at the KEK with respect to the low field J_c characterization are also described.

1. INTRODUCTION

Compared to Nb_3Sn that is in the most advanced state of development for future accelerator magnet, Nb_3Al conductor has a better tolerance to strain [1], [2] and a higher critical magnetic field (30 T at 4.2 K) for stoichiometric composition. In Japan, the rapid-heating, quenching and transformation (RHQT) processed Nb_3Al conductor has been mainly developed for a high-resolution nuclear magnetic resonance (NMR) spectroscopy, rather than nuclear fusion and accelerator uses. Accordingly the specification of conductor trial manufactured so far had not been always suitable for the accelerator magnets. That is, an incorporation of stabilizer has been carried out by mechanical cladding of Cu after RHQ operation, and the resultant cross section of strand is rectangular [3]-[7]. This is suitable for NMR magnet, but not for the Rutherford-type cable. Furthermore, optimization of cross-sectional design and transformation heat treatment has been performed to obtain good critical current densities at fields higher than 21 T, which is far away above the target field of accelerator magnet (10-15 T). Thus, even the fundamental critical parameter of J_c at around 10 T has not been always evaluated precisely yet.

However, the High Energy Accelerator Research Organization (KEK) has recently started a research and development (R&D) program of Nb_3Al conductor for future accelerator magnets, and evaluated the J_c precisely at around 10 T for a round and Cu electroplated wire [8], in collaboration with the National Institute for Materials Science (NIMS). Since a making of long-length of conductor [9],[10] and the transformation heat treatment for NMR magnets [11] seem to have a lot in common with that required for accelerator magnets, these results, low field J_c characteristics [8] and a newly developed stabilization technique [12]- [14] will be described in this review article.

2. LONG-LENGTH OF PROCESSING

2.1 Precursor

In the manufacture of Nb_3Al precursor, in contrast to Nb_3Sn, diffusion considerations require that the elemental constituents should be assembled so as to result in Al dimensions of less than 100 nm in the finished wire [5], [17]. As shown in Fig. 1, multifilamentary Nb/Al precursor is prepared by the jelly-Roll (JR) process.

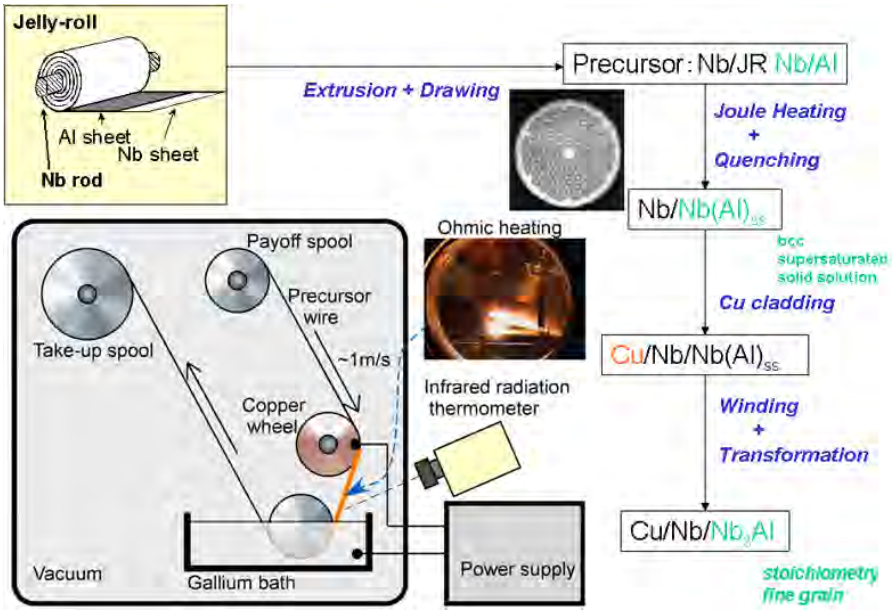

Fig. 1 Schematic illustration of a reel-to-reel joule heating apparatus and the flow chart of the RHQT process

The standard JR precursor is fabricated by rolling a bilayer of Nb and al foils onto a pure Nb rod. Cu cans are necessary for extruding and drawing the monofilament and multifilament, but must be chemically removed off because the Cu would melt during the rapid-heating and quenching (RHQ) treatment. Thus, the standard multifilament has the Nb-matrix structure.

The piece-length of precursor wire 1.35 mm in diameter was so far limited to 300 meters [9], but the NIMS and Hitachi Cable, Ltd., have very recently succeeded in increasing the above mentioned piece-length by a factor of eight (2600 meters), by using a more powerful 4000 ton hydrostatic extrusion machine and enlarging a multifilamentary billet size (about 50 Kg) [15].

2.2 RHQ operation

In addition to making a long-length Nb/Al precursor, a uniform RHQ treatment along the long-length of precursor-wire is of great importance for a scale-up. In a reel-to-reel apparatus for the RHQ operation a JR precursor wire is fed, with a constant speed, from a pay-off spool, around a Cu electrode wheel, into liquid Ga, and onto a take-up spool [2]. During operation a current is passed through the section of wire between a Cu wheel and the Ga in such a way that the maximum joule-heating temperature (T_{max}) is achieved just above the Ga and then the wire gets rapidly quenched. The resultant microstructure and superconducting properties strongly depend on the T_{max}, which might unexpectedly and undesirably vary during a long-length of processing even if the joule-heating current I_{RHQ} could be kept at a constant. This is because a decrease in a liquid Ga level and a warp/vibration of wire would cause the equivalent heating time to increase. There is, however, a plateau region where the wire is quenched from the extended solid solution (1910 to 2060^{o}C) and the resultant T_c and J_c are insensitive to I_{RHQ}. The J_c (21T, 4.2K) is largest in such a plateau region, as shown in Fig. 2. The variation of J_c (21T, 4.2K) with I_{RHQ} in the plateau region is ± 7 %. It is quite difficult to adjust a T_{max} to the destined one with accuracy of a few degrees as is required for Bi oxide superconductors. However, by coordinating a reel-to-reel movement so as to suppress the warp and vibration of wire, the scatter of T_{max} due to factors other than I_{RHQ} could be depressed far less than a half of 150^{o}C that is a temperature width of extended solid solution for the stoichiometric composition. Note the existence of a plateau region that enables the uniform long-length of RHQ processing. The plateau width of the joule heating current is 10.5 A for a 1.35 mm diameter wire, width that is much larger than the controlling accuracy of the constant current supply used.

In order to prevent T_{max} from deviating from the optimum region, the I_{RHQ} for a 300 m length of operation was set in the middle of the plateau region.

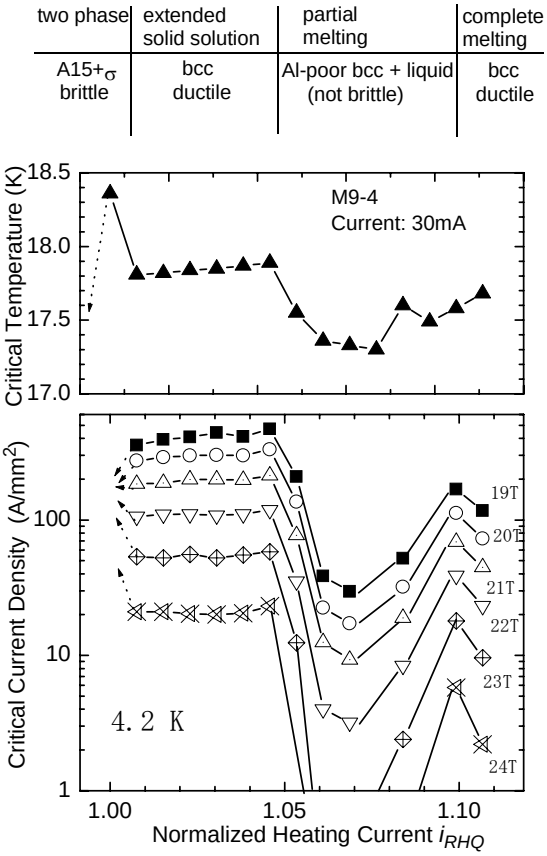

Fig. 2 Variations of T_c and the logarithm of the J_c as a function of joule heating current for the samples that were directly subjected to a transformation annealing at 800°C for 10 h (no deformation). The phases identified with x-ray diffraction and mechanical properties for the as-quenched state, and the speculated high-temperature state from which the wire is quenched are given above the figure.

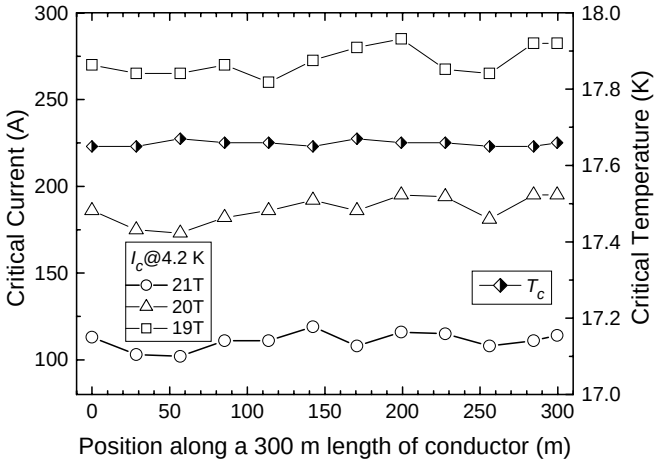

Fig. 3 Distribution of T_c and I_c from point to tail of a 300 m length of RHQ processed wire (1.35 mm diameter) that was subsequently transformation annealed at 800°C for 10 h.

Fig. 4 A newly installed reel-to-reel joule heating apparatus at the NIMS, which is designed to process a long-length of RHQ operation over 2 km for a wire 1.35 mm in diameter.

A 300 m length of RHQ processed wire shows a uniform distribution of T_c and I_c, as shown in Fig. 3. The distribution of T_c and I_c from point to tail of a 300 m length of wire was examined by cutting off, every 30 m, the short section of wire that is subsequently transformation annealed at 800°C for 10 h. The standard deviation of I_c (4.2K) at 21 T along a 300 m wire was about 5 %, which was less than the variation of J_c (4.2K) at 21 T with I_{RHQ} in the plateau region (± 7 %). The section of wire that shows the minimum T_c and I_c (J_c) values (Fig. 3) would determine the superconducting properties of a whole long-length of RHQT JR Nb_3Al conductor. A Cu stabilizer would be subsequently incorporated by a mechanical cladding method and finally transformation annealed.

A new reel-to-reel RHQ apparatus [16] that would be capable of processing a 2 km length of wire is now under installation at the NIMS (Fig. 4). This RHQ apparatus has some improved functions that enable to control the initial acceleration and steady speed of wire along with time, to keep constant the level of molten Ga and hence the spacing of electrodes through RHQ operation, and to prevent an unwanted laxation of wire between electrodes by attaching the pinch rollers in a section between Ga bath and a traverse wheel. I hope that such efforts of enlarging of a multifilament billet (about 50 kg) and RHQ apparatus would allow a long-length of RHQT JR Nb_3Al conductor to be available with a reasonable price.

3. INCORPORATION OF STABILIZER

3.1. External stabilization

One of the important features of the RHQT Nb_3Al conductor is a ductile nature of as-quenched wire at room temperature that enables the conductor to be stranded into Rutherford and cable-in-conduit cables or subjected to the mechanical cladding with Cu. Fig. 5 shows the Cu clad stabilized conductor for NMR uses and compacted-strand-cable consisting three Nb_3Al strands and three Cu wires. In both cases the Cu stabilizer was incorporated after of RHQ operation by utilizing the ductile nature of as-quenched wire. Note that J_c was rather enhanced at the beginning of deformation of the $Nb/Nb(Al)_{ss}$

strand; J_c of the Cu-clad Nb/Nb(Al)$_{ss}$ composite is increased from 150 A/mm^2 to 335 A/mm^2 at 21 T by 42% *RA* as shown in Fig. 5 (c). Such an enhancement in J_c compensates well for the reduction in cross sectional area; I_c at 21 T is increased by 50% for 26% *RA*. The mechanical strains induced at the Cu cladding seems to promote the transformation to the A15 phase, and thereby the desirable transformation from such a disordered bcc phase could occur faster than the ordering of bcc Nb(Al)$_{ss}$. Furthermore, such a transformation seems to cause a fine grain structure because of a high nucleation rate. Thus, J_c increases with increasing *RA* at the beginning of deformation. However, excess deformation at the cladding might also enhance such the order-disorder reaction of the bcc phase, and thus J_c degrades at the large *RA*.

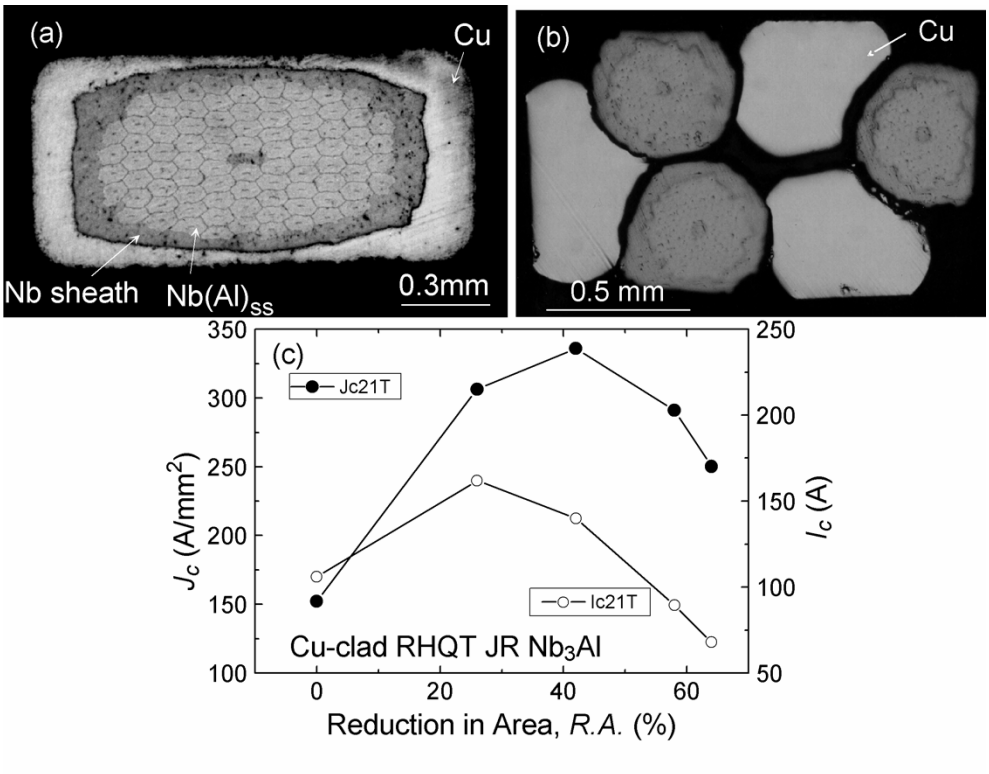

Fig. 5 Cross-sectional views of (a) Cu clad stabilized rectangular Nb_3Al monolithic strand, (b) compacted-strand-cables consisting of 3-Nb_3Al-strands and 3-Cu-wires, and (c) variations of J_c and I_c of Cu clad Nb_3Al as a function of reduction in area at cladding.

3.2. Internal stabilization

The mutual insolubility and non-reactivity of Ag with Nb, even at temperatures higher than1900^{o}C, enables the Ag stabilizer to be initially and internally included as a basic constituent of the strand. Advantages of the internally stabilized RHQT Nb_3Al conductors are as follows,

(1) Less expensive: the Cu cladding process after RHQ operation can be omitted.

(2) Flexibility in decreasing a diameter of precursor wire.

(3) Round cross section of wire: an omission of Cu cladding process relaxes the restrictions of cross sectional shape and wire diameter and the resultant fine wire would enable a high current conductor as required for cabling.

(4) Possible high current conductors such as CICC, Rutherford cables, etc.

(5) No contamination of Ag stabilizer with Ga during transformation annealing: Ag stabilizer is confined in cross section away from the Ga coated surface and thus expected to have high RRR values.

(6) Applicability to newly developed transformation techniques of a transformation-heat-based up-quenching (TRUQ) [18], [19], a double rapid-heating quenching (DRHQ) [20] and Cu-added RHQ process [21].

(7) Freedom of Ag-stabilizer configuration in the cross section: a hexagonal Ag rod that has a jacket of Nb, as a module, could freely replace a JR Nb/Al rod when stacking the subelements. This would result in desirable geometrical-configuration of Ag stabilizer in the cross section and flexibility in volume fraction of stabilizer. In order to increase the r_{Ag}, the Nb center-rod of JR Nb/Al filaments is also replaced with the Ag rod when preparing the starting JR Nb/Al composite. Thus, the r_{Ag} of strand is available in a wide range from 0.06 to 0.345.

Disadvantages over Cu-cladding method are as follows,

(1) Necessity to severely coordinate the reel-to-reel movement: the molten Ag cannot be expected to play a role as a reinforcement material during a reel-to-reel RHQ operation.

(2) Narrow width of J_{RHQ} plateau where as-quenched wires can be drawn without breakage using cassette-roller dies.

(3) Large joule heating current density J_{RHQ}: an electrical resistivity of Ag is much smaller than that of Nb or Nb compounds, and J_{RHQ} gets to be typically one and a half times larger than the conventional one.

(4) Difficulty in increasing a Ag/non-Ag ratio (r_{Ag}) to higher than 1.0 in principle.

(5) Larger magnetoresistance.

(6) Large induced radioactivity in case of nuclear fusion uses.

(7) Slightly reduced n-index in the voltage-current characteristic.

Fig. 6 shows the typical transverse cross-sectional images of internally stabilized RHQT Nb_3Al conductors. Fig. 7 shows the comparison of the critical current I_c and the critical current density J_c between the best performance Cu-clad and internally stabilized RHQT Nb_3Al conductors manufactured so far, of which each J_c was optimized by giving an appropriate deformation after quenching (before transformation). Wire diameters before RHQ operations are 1.35 mm and 1.26 mm, and finished cross-sectional dimensions are 1.81 x 0.8 mm^2 and 0.94 mmϕ in diameter, respectively. The J_c was defined as $(I_c/S_{overall})$ x $(1+r_{Cu(Ag)})$ x $(1 + r_{Nb})$ where S_{overll} and r_{Nb} mean the overall cross-sectional area and Nb/Nb_3Al ratio, respectively. The larger a r_{Ag} is, the smaller the volume fraction of JR Nb/Al filaments of the precursor wire becomes. Thus, the Cu-clad conductor that does not have any Ag stabilizer would include a larger net volume of JR Nb_3Al filaments and thereby could possess higher I_c than the internally stabilized conductor would do, even if at constant diameter of as-quenched wires and the amount of subsequent deformation (reduction in area, *RA*). It is, however, noted that there is no clear difference in the J_c of Nb_3Al filaments between the external and internal stabilization methods, as long as the $Nb(Al)_{ss}$/Nb wire is subjected to deformation.

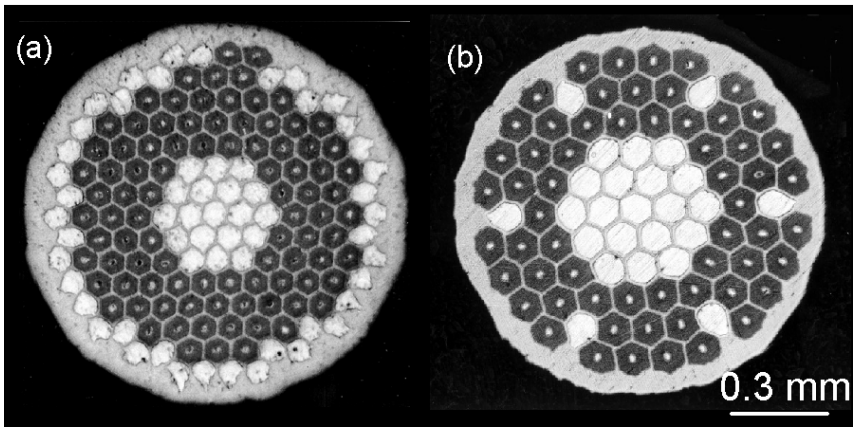

Fig. 6 Transverse cross-sectional images: (a) internally stabilized wire, 1.25 mm in diameter with r_{Ag} of 0.345, (b) internally stabilized wire, 1.27 mm in diameter with r_{Ag} of 0.215.

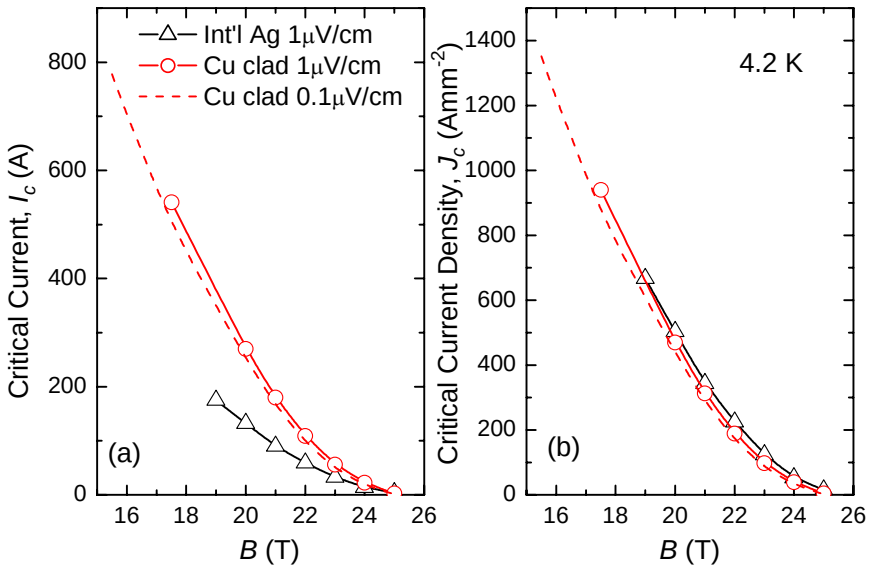

Fig. 7 Comparison of I_c and J_c between externally and internally stabilized RHQT Nb_3Al conductors that have been subjected to 40 %RA after quenching.

Fig. 8 summarizes the effect of deformation on *RRR*, I_c and J_c, as a function of *RA* for Cu clad rectangular conductor (r_{Cu}: 0.4) and internally stabilized wire (r_{Ag}: 0.34), for which the original wire diameters are the same, equal to 1.26 mm before RHQ operations. Note that the deformation after quenching is effective in increasing the J_c in both cases of external and internal stabilization methods. However, the response of *RRR* on *RA* is quite different between external and internal stabilization methods. As mentioned in the previous section, the higher the r_{Ag} value is, the more the *RRR* increases. The *RRR* of internally stabilized conductor runs up to as much as 200 that is about four times larger than the case of Cu-clad conductor. Deformation after quenching decreases the *RRR* of the internally stabilized conductor. Possible reasons for such a *RRR* reduction are (1) the Nb jacket tore during round-to-round deformation and the Ag stabilizer got contaminated with Al during a final heat treatment, or (2) dislocations in the Nb matrix increased with deformation but did not disappear during the final heat treatment and thus the residual resistance of Nb matrix increased. Meanwhile, the contamination with Ga during transformation annealing is inevitable for Cu-clad conductor, and the RRR of Cu-clad conductor is much smaller than the internally stabilized conductor.

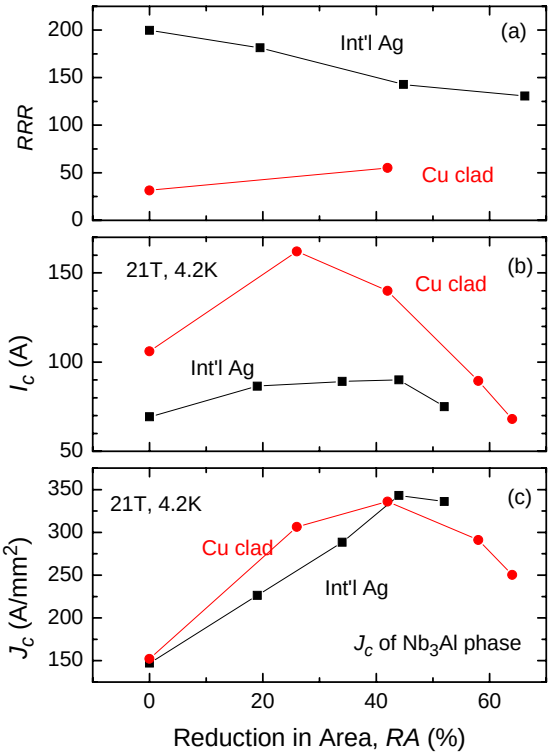

Fig. 8 Effect of RA on (a) RRR, (b) I_c, and (c) J_c.

4. COIL PERFORMANCE

The loading test of coil is the most direct and reliable method to examine the uniformity and performance of a long-length of Cu-clad RHQT JR Nb_3Al conductor. The T_c and J_c of the transformed Nb_3Al conductor strongly depend on the temperature ramp-up rate during transformation annealing, in particular for the conductor that is not subjected to any deformation after RHQ operation as shown in Fig. 9. The transformation to A15 phase started and completed before the temperature reached to 800°C in case of slower ramp-up rates, e.g., 745-760°C for 40%RA and 760-800°C for 0%*RA* samples. Narrower temperature ranges where the transformation proceeds for deformed sample may make such a ramp-up rate insensitive to these critical parameters. It is noted that such temperature ramp-up rate dependencies are consistent with the new transformation technique of TRUQ that utilizes a fast heating to complete the transformation in several tens seconds and improve dramatically critical parameters (T_c: 18.3 K, B_{c2} (4.2 K): 29T). When performing the transformation annealing of a coil that has large thermal capacity, the local temperature and hence the substantial temperature ramp-up rate might differ from place to place in the coil. In order to ensure the uniform distribution of temperature, we must have raised a temperature to 800°C spending more than 10 h but deteriorated significantly the critical parameters, in case of as-quenched and transformed conductors. After all, the deformation processing (Cu-cladding) is very essential and necessary process for the coil heat treatment.

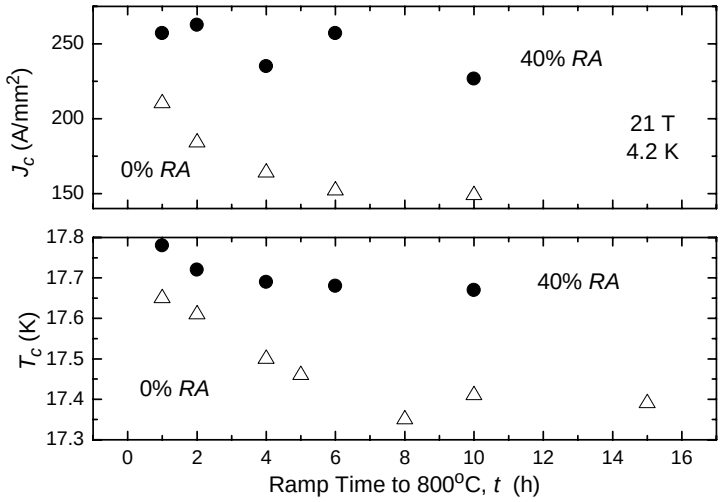

Fig. 9 Effect of the temperature ramp-up rate on critical parameters for RHQT JR Nb_3Al conductors that are subjected to plastic deformation of 0 and 40 % RA before transformation annealing at 800°C for 10 h.

TABLE 1
SPECIFICATIONS OF WIND & REACT NB_3AL SOLENOID COILS

	Previous M11-1	Present ME332	Present ME365
RHQT JR Nb_3Al conductor			
Stabilizer	Cu-clad	Cu-clad	Cu-clad
Piece length (m)	35	370	370
Cross section (mm^2)	1.61x0.71	1.82x0.84	1.81x0.80
Filament diameter	70	74	75.5
Number of filaments	84	132	132
Cu/non-Cu ratio	0.45	0.38	0.39
Insulator	Al_2O_3 fiber	Al_2O_3 fiber	Al_2O_3 fiber
Winding			
Inner diameter (mm)	19.7	90.2	64.6
Outer diameter (mm)	40.8	111.8	99.3
Height (mm)	49.7	200	132.4
Number of turns	311	949	988
Total length of wire	30	300.5	254
Coil			
Impregnation	Beeswax	Beeswax	Beeswax
Transformation	RT→(5h) →800°C→(10h) →800°C→RT		
Coil constant (T/A)	0.00106	0.00562	0.00797

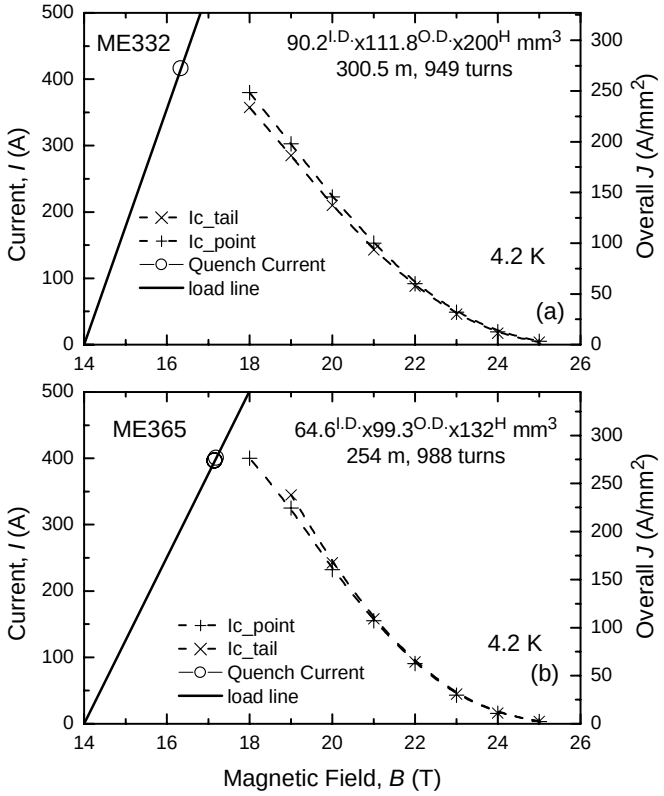

Fig. 10 Load lines of the solenoid coils wound with Cu clad RHQT JR Nb3Al conductors of which lengths are (a) 300.5 m and (b) 254 m, respectively. Overall J is calculated by dividing I with cross section of a bare strand (excluding insulator).

Table 1 shows specifications of two coils examined along with the previous one [7]. The present Cu-clad JR Nb_3Al conductors used for windings are 10 times longer in a piece length and 27-34% larger in cross section of a bare strand than those of previous one. The conductor was insulated with Al_2O_3 fiber, which is mechanically stronger than the glass fiber after heat treatment. Furthermore, a coefficient of expansion of Al_2O_3 is closer to that of a metal. When in the transformation annealing of the coil the temperature was raised to 800°C in 5 h, the temperature-ramp-rate did not cause severe degradation in J_c, at least for the Cu-clad conductors (Fig. 9).

Fig. 10 shows the results of loading test of coils that are wound μ with a long-length of Cu-clad JR Nb_3Al conductor. In the figures, plotted are also the I_c (1V/cm criterion) of short samples that are cut out from point and tail of a long-length of Cu-clad JR Nb_3Al conductor used. The quench currents of these coils are almost the same as the I_c of point and tail short-samples, respectively. This clearly indicates that a long-length of RHQ processing over 300 m and subsequent Cu-cladding was uniformly performed so that a long-length of RHQT JR Nb_3Al conductor gets trustworthy for practical coil applications. The coils denoted by ME332 and ME365, while carrying currents of 416.2 A and 400.3 A at 4.2 K in a bias field of 14 T, generated additional 2.3 and 3.2 T in bores of 90.2 mm and 64.6 mm diameter, respectively. These coils did not show a progressive improvement in performance after repeated quenching, i.e. "training." Quenching currents rather decrease slightly in sequence of 400.3 A, 396.5 A, 396.5 A, 395.7 A, 395.8 A for the ME365 coil. The volume ratio of Cu to $Nb/Nb(Al)_{ss}$ strand of 0.38-0.39 was enough to reduce the risk of a burnout of the conductor for these coils.

5. LOW FIELD J_C CHARACTERISTICS

The I_c and J_c characteristics in field less than 17 T have not been evaluated precisely so far, since the NMR insert coil needs a high current monolithic conductor that has a large cross area and thus the Ic of the Cu clad stabilized Nb_3Al conductor exceeds 500 A below 17 T as show in Fig. 10, making it difficult to determine the Ic without thermal runaway. Tsuchiya et al at the KEK has recently designed and fabricated the I_c measurement probe that can accommodate four solenoid samples 300 mm in length and accept a current up to 1000 A [22], and evaluated the J_c (4.2 K) in field range between 6 T and 17 T for the round Nb_3Al wires 0.8 mm in diameter for accelerator uses [8].

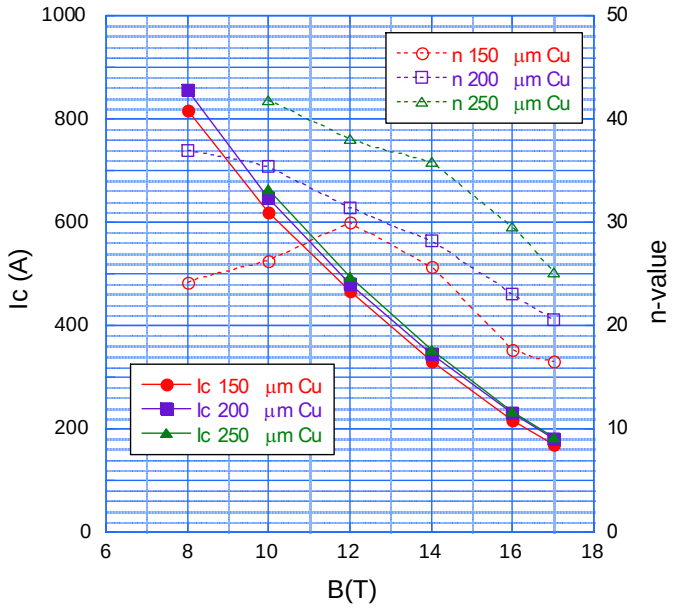

Fig. 11 I_c and n-values of the RHQT Nb_3Al round wire with various Cu stabilizer thickness in fields less than 17 T.

To suppress the thermal runaway during I_c measurement, attention has been paid to incorporate adequate amount of Cu onto a wire. Cu was put onto a wire by electroplating. Fig. 11 shows the I_c and n-value of the RHQT JR Nb_3Al wire 0.76 mm in diameter that is not subjected to any deformation after RHQ operation, transformation annealed at 800°C for 10 h and then electroplated with Cu. The I_c of the samples increases with the thickness of the copper. The differences in the I_c of these samples are larger than the estimated errors, ± 1 %. Roughly speaking, the I_c (200 μm thickness copper) and I_c (250 μm thickness copper) are 5 % and 7 % larger than the I_c (150 μm thickness copper), respectively. The field dependence of this I_c enhancement is not clearly seen in this study. Another point we can find in this figure is that the n-value for thicker copper wire is larger although the n-value of the 150 μm copper sample shows some strange behavior at low field. From these facts, the I_c changes with the thickness of stabilizing copper and the larger I_c sample has larger n-value, we speculated the stress effect as a reason of this behavior and performed the T_c measurement of these samples with and without copper at 0 T, 4.2 K. However we couldn't find a clear difference in the T_c of these samples. They were almost same values, 17.8 ± 0.1 K. Continued study is necessary to understand the copper thickness effect on the I_c. The I_c of the samples with much thinner copper are not shown in Fig. 11. In such case it was hard to measure the critical current, because the wire was easily quenched at over 200-300 A. Thus thereafter we decided to electroplate the copper more than 150 μm thickness.

To obtain the highest J_c in low fields the transformation annealing (Fig. 12) and post RHQ deformation conditions (Fig. 13) were re-optimized. As for the transformation annealing, the best I_c was obtained in the heat treatment of 15 h at 775 °C and the next was the heat treatment of 10 h at 800 °C, which has been adopted for the high field NMR conductor. Roughly speaking, if we take higher temperature, the optimum duration becomes shorter. However, it is found that 725 °C is too low for the second heat treatment and 825 °C is too high to obtain a good characteristic at 10 T. Also, it is interesting to note that the I_c becomes sensitive to the change of the annealing condition with decreasing the field.

A number of observations can be made with regard to the effect of the area reduction. After the area reduction, the J_c is easily increased, however, the increase ratio changes depending upon the samples. The optimum reduction in area to obtain a high J_c at low field (below 17 T) is about 20 %. This value is slightly smaller than the value, 40 %, which has been reported for the high field NMR conductors. Therefore, we can speculate that the optimum reduction in are for enhancing the J_c would increase with a field-intensity.

The optimum conditions of the transformation annealing and the reduction in area to obtain high J_c values in fields less than 17 T are slightly different from the values optimized for high-field (21T at 4.2 K or 23.5 T at 1.8 K) NMR conductors. The highest non-Cu J_c at 10 T and 4.2 K was 1734 A/mm^2 for the RHQT JR Nb_3Al wire 0.69 mm in diameter, of which Nb/Nb_3Al ratio and reduced filament size was 1.04 and 47 μm.

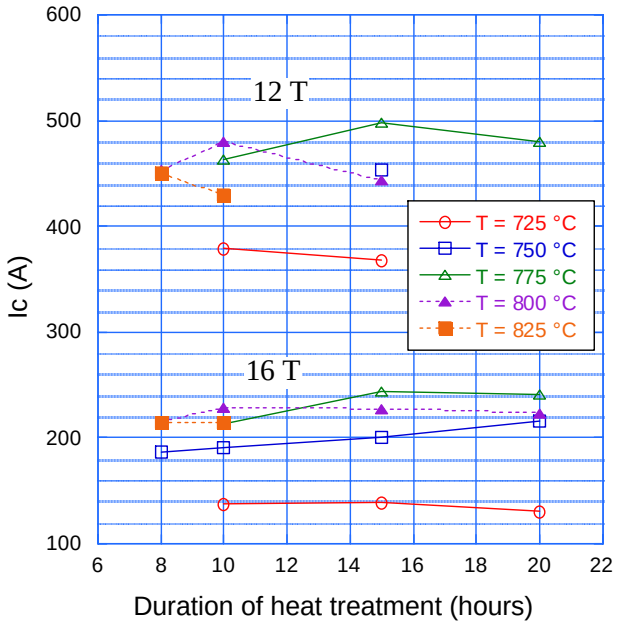

Fig. 12 Effect of the transformation annealing on the I_c for the quenched wire that is not subjected to any deformation after RHQ operation.

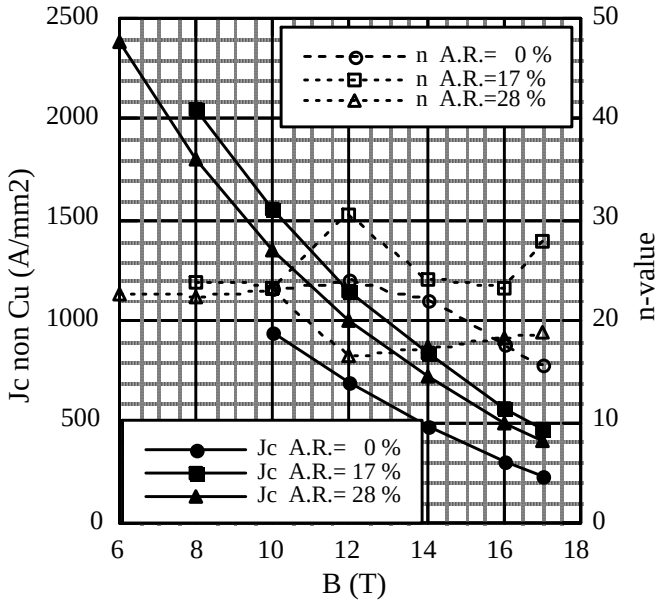

Fig. 13 Effect of the reduction in area subjected after RHQ operation on the non-Cu J_c and n-value.

6. SUMMARY

Current status of the RHQT JR Nb_3Al conductor developed in Japan has been described. Although the Cu stabilizer is incorporated by mechanical cladding and the resultant strand cross-section is rectangular, a 300 meter length of conductor is about to be commercially available for NMR uses. Further attempts have been made to increase the piece-length of conductor up to more than 2000 meters by enlarging the multifilament billet size up to 50 kg and the RHQ apparatus. For accelerator uses, the internal stabilization technique would be useful because the strand has a round shape.

ACKNOWLEDGEMENTS

A part of this study was financially supported by the Budget for Nuclear Research of the Ministry of Education, Culture, Sports, Science and Technology (MEXT), based on the screening and counselling by the Atomic Energy Commission, and by Research Promotion Bureau of MEXT under the contract No.(15-213 and) 15-332.

REFERENCES

[1] T. Takeuchi, Y. Iijima, K. Inoue, H. Wada, B. ten Haken, H. H. J. ten Kate, K. Fukuda, G. Iwaki, S. Sakai and H. Moriai, "Strain Effects in Nb_3Al Multifilamentary Conductors Prepared by Phase Transformation from bcc Supersaturated-solid-Solution," *Appl. Phys. Lett*. 71 (1997) 122-124.

[2] T. Fukuzaki, T. Takeuchi, N. Banno, N. Tatsumi, H. Ogiwara, and H. Wada, "Stress and strain effects of Nb_3Al conductors subjected to different heat treatments," *IEEE Trans. Appl. Supercondivity*, 12 (2002) 1025-1028.

[3] M. Kosuge, T. Takeuchi, K. Tagawa, N. Banno, M. Yuyama, H. Wada, K. Nakagawa, T. Yamanaka, and H. Moriai, "Incorporation of stabilizer to rapid-quenched and transformed Nb_3Al multifilamentary superconductors," *IEEE Trans. Appl. Superconductivity* 10 (2000) 1034-1037.

[4] T. Takeuchi, "Nb_3Al conductors - rapid-heating, quenching and transformation process -," *IEEE Trans. Appl. Superconductivity* 10 (2000) 1016-1021.

[5] T. Takeuchi, "Nb_3Al conductors for high field applications," *Supercond. Sci. Technol*. 13 (2000) R101-R119.

[6] T. Takeuchi, "Nb_3Al superconductors," *IEEE Trans. Appl. Superconductivity* 12 (2002) 1088-1093.

[7] T. Takeuchi, N. Banno, T. Fukuzaki, T. Kiyoshi, S. Matsumoto, H. Wada, K. Aihara, Y. Wadayama, M. Okada, K. Tagawa, and K. Nakagawa, "Stabilization and coil performance of RHQT-processed Nb_3Al conductors," *IEEE Trans. Appl. Supercond.* 11 (2001) 3972-3975.

[8] T. Kobayashi, K. Tsuchiya, T. Shintomi, N. Banno, T. Takeuchi, S. Nimori, "Development of Nb_3Al Superconducting Wire for Accelerator Magnets,"IEEE Trans. Appl. Superconductivity (in press).

[9] T. Fukuzaki, T. Takeuchi, N. Banno, K. Tagawa, N. Tatsumi, H. Ogiwara, and H. Wada, "Effect of rapid heating, quenching and transformation conditions on the superconducting properties and microstructure of Jelly-Roll processed Nb_3Al superconductors," Supercond. Sci. Technol. 15 (2002) 1404-1409.

[10] T. Takeuchi, K. Tagawa, T. Fukuzaki, N. Banno, K. Aihara, K. Fukushima, M. Kosuge, M. Yuyama, F. Matsumoto, T. Kiyoshi, N. Tatsumi, S. Matsumoto and H. Wada, "Transport properties of long-lengths of RHQT processed Nb_3Al conductor," IEEE Trans. Appl. Superconductivity 13 (2003) 3454-3457.

[11] T. Takeuchi, N. Banno, K. Tagawa, T. Kobayashi, K. Tsuchiya, N. Tatsumi, T. Fukuzaki, M. Kosuge, H. Wada, Y. Iijima, A. Kikuchi and K. Inoue, "Microstructure and *n*-Value of RHQT Processed Nb_3Al Superconductors for NMR Uses", IEEE Trans. Appl. Superconductivity (in press).

[12] K. Tagawa, T. Takeuchi, T. Kiyoshi, K. Itoh, H. Wada and K. Nakagawa, "Trial to incorporate Cu stabilizer in rapid-quenching processed Nb_3Al wires," Adv. Cryogenic Engin. Edited by U. Balu Balachandran et al., Plenum Press, New York, 46 (2000) 975-980.

[13] T. Takeuchi, K. Tagawa, N. Banno, M. Kosuge, M. Yuyama, H. Wada, A. Kikuchi, Y. Iijima, and K. Inoue, "Development of Internally Stabilized RHQT Nb_3Al Superconductors", Supercond. Sci. Technol. 16 (2003) 1173-1181.

[14] T. Takeuchi, N. Banno, A. Kikuchi, Y. Iijima, K. Inoue, H. Kitaguchi, H. Wada, K. Tagawa, and K. Fukushima, "External and internal stabilization methods of RHQT Nb_3Al superconductors," ICMC

[15] K. Tagawa, T. Takeuchi, H. Kitaguchi, et al., unpublished

[16] T. Takeuchi, unpublished

[17] Y. Iijima, M. Kosuge, T. Takeuchi and K. Inoue, "Nb_3Al Multifilamentary Wires Continuously Fabricated by Rapid-Quenching," Adv. Cryogenic Engin. Edited by R. P. Reed, F. R. Fickett, L. T. Summers and M. Stieg, Plenum Press, New York, 40 (1994) 899-905.

[18] T. Takeuchi, N. Banno, T. Fukuzaki, and H. Wada, "Large improvement in high-field critical current densities of Nb_3Al conductors by transformation-heat-based up-quenching method," Supercond. Sci. Technol. 13 (2000) L11-L14.

[19] N. Banno, T. Takeuchi, T. Fukuzaki, and H. Wada, "Optimization of the TRUQ (Transformation-heat-based up-quenching) method for Nb_3Al superconductors," Supercond. Sci. Technol. 15 (2002) 519-525.

[20] A. Kikuchi, Y. Iijima, N. Banno, T. Takeuchi, K. Inoue, S. Nimori, M. Kosuge and M. Yuyama, "Microstructure and J_c-B performance of DRHQ processed Nb_3Al wires," IEEE Trans. Appl. Superconductivity (in press).

[21] Y. Iijima, A. Kikuchi, N. Banno, T. Takeuchi, K. Inoue, "Direct Formation of A15 Phase through RHQ Treatment in RIT-Processed Nb/Al-Cu Precursor Wire," IEEE Trans. Appl. Superconductivity 13 (2003) 3410-3413.

[22] K. Tsuchiya, T. Kobayashi, T. Shintomi, N. Banno, K. Itoh, S. Nimori, T. Takeuchi, "Measurement of V-I characteristics of commercial multifilamentary NbTi wires," Physica C 401 (2004) 265-269.

DEVELOPMENT OF LTS AND HTS SUPERCONDUCTORS FOR ACCELERATOR MAGNETS AT EAS AND EHTS

Helmut Krauth
European Advanced Superconductors (EAS) and European High Temperature Superconductors (EHTS), Hanau, Germany

Abstract
The actual development of the two affiliated companies EAS and EHTS in the field of Technical Superconductors for Accelerator Magnets is described. EAS is active in the development of multifilamentary conductors by mechanical hot and cold working, based on NbTi and Nb_3Sn ("LTS") as well as BiSrCaCuOxide (Bi-2223) HTS tapes produced by the powder-in-tube (PiT) route. Nb_3Sn conductors are produced by the Bronze route and also by a PiT process. The latter is performed in a co-operation with SMI/Netherlands. EHTS is developing thin film HTS tapes based on YBaCuOxide (Y-123).

1. INTRODUCTION

Accelerator magnets for high energy and nuclear physics have always been an important application for Technical Superconductors. EAS (until June 2003 a division of Vacuumschmelze GmbH & Co. KG, Hanau/VAC) has participated since the beginning in the development and production of conductors for both accelerators and detector magnets. Some milestones are given in Fig. 1.

1970	Big European Bubble Chamber (BEBC),CERN
1971	PLUTO Detector, DESY
1979	ISR Quadrupoles,CERN
1986	ALEPH Detector, CERN
1987	HERA Quadrupoles, DESY
1990	CLEO Detector, Cornell
1991	H1 Detector, DESY
1992	CLAS Torus, CEBAF
1997	ATLAS Detector, CERN
1998	LHC Dipoles and Quadrupoles MQM/MQY, CERN

Fig 1 Major Accelerator and Detector Magnet Projects with EAS Conductors

In many of these projects the specifications were very demanding and required significant development effort. As such accelerator applications have frequently acted as a technology driver for superconductor industry.

The progress in understanding technical superconductors and their production technology is visible in Fig. 2 and Fig. 3. Fig. 2 shows the conductor of the Big European Bubble Chamber (BEBC) at CERN using then advanced technologies such as continuous electron beam welding, but with on the other hand thick untwisted filaments and "strands" without transposition. Figure 3 shows the modern equivalent, the conductor for the ATLAS detector, with a fully transposed Rutherford cable of low Cu-ratio fine filament strands, co-extruded with ultra-pure aluminium for stabilization.

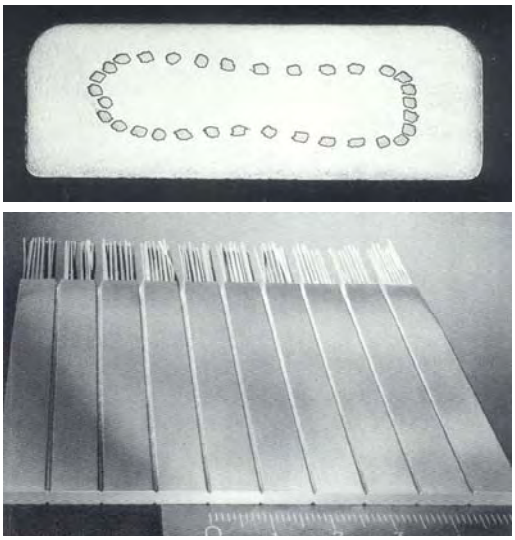

Multifilamentary Strand
8,8 x 3 mm²
32 Filaments, untwisted
Cu Ratio 25

Composite Conductor
10 Strands in parallel
e-beam welded
90 x 3 mm²
$I_c \approx 8000A$ @ 4.2 K, 5 T

Fig. 2 BEBC Conductor 1970

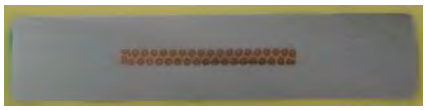

Conductor

Dimension	57 x 12 mm²
Unit length	1730 m
Total length	56 km
Critical Current	> 58 kA @ 4.2 K; 5 T
Operating Current	20.5 kA @ ~ 4.8 K; 3.8 T
RRR (ALU)	> 1000

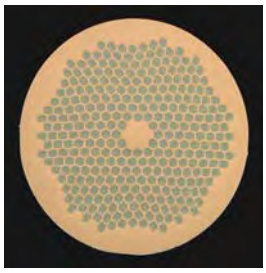

Cable

No. Of strands	38
Dimension	26 x 2.3 mm²

Strand

Diameter	1.3 mm
Cu : NbTi	1.2
Critical Current	> 1700 A

Fig. 3 ATLAS Conductor 2000

So far virtually all accelerator and detector magnet projects have been realized with NbTi conductors. It is expected that this will change in future and that Nb_3Sn technology will play a significant role. Also, on a longer term, HTS conductors may become important. In the following the LTS development activities going on at EAS will be described [1, 2]:

- Conductors for pulsed accelerator magnets (NbTi, Nb_3Sn) [3]
- Conductors for high field (>10 T) accelerator magnets (Nb_3Sn) [4]

As concerns HTS, application specifications are as yet only vaguely defined, so conductor development is of a more general nature. The present status and on-going activity will be presented for

- Bi-2223 multifilamentary tapes with a silver (-alloy) matrix (EAS) [5]
- Y-123 thin film tapes ("coated conductors") on a stainless steel substrate (EHTS) [6]

European High Temperature Superconductors (EHTS) is a sister company to EAS founded in March 2004. EHTS is producing and developing Y-123 based on the IBAD/PLD technology pioneered by ZFW Göttingen.

2. DEVELOPMENT OF METALLIC SUPERCONDUCTORS FOR ACCELERATORS

The present state of the art of NbTi conductors is best represented by the conductor family of keystoned Rutherford cables presently produced in large scale for LHC. Depending on coil type the cables consist of 22 to 36 strands, coated with a thin Sn-Ag layer to control the adjacent and transverse resistance between the strands in the cable. Examples of strand cross sections are shown in Fig. 4.

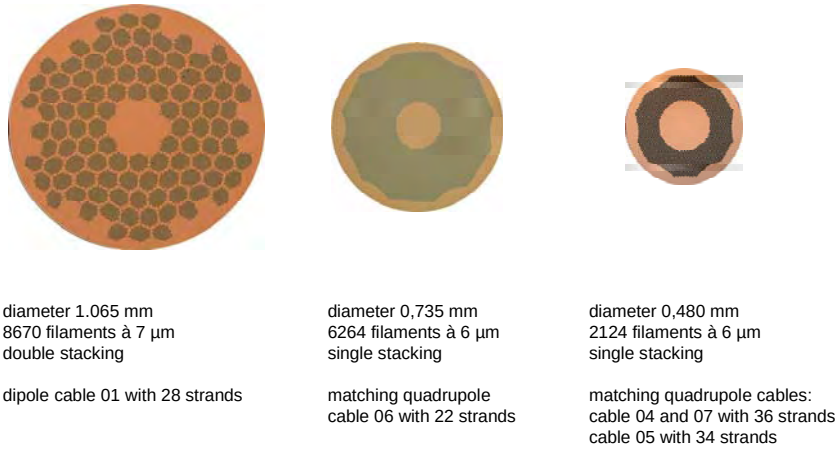

Fig. 4 LHC strands from EAS

Typical strand characteristics are:

- 2000 to 9000 filaments with 6 to 7 µm diameter in a pure Cu matrix
- Each filament protected by a Nb barrier against formation of Cu-Ti intermetallics
- Single stacking or double stacking design

The development of further advanced conductors for new projects is directed towards:

- Pulsed magnets for fast cycling accelerators (mainly NbTi)
- High field magnets for accelerator up-grades (such as LHC)
  or the next generation of circular hadron colliders (such as VLHC) making necessary Nb_3Sn (or related) technology.

3.1 Conductors for fast ramped magnets

In existing superconductor magnets for accelerators, such as LHC, the conductor design is based on field quality considerations at injection field. In fast cycling accelerators pulse field loss considerations are becoming essential [3].

An example is the planned FAIR project (Facility for Antiproton and Ion Research) at GSI/Darmstadt (Gesellschaft für SchwerIonenforschung). Two synchrotrons are foreseen:

- SIS 100 with B_{max} = 2 T and dB/dt = 4 T/s
- SIS 300 with B_{max} = 6 T and dB/dt = 1 T/s

It is obvious that pulse losses have to be reduced as much as possible to operate such a machine most economically. The consequences for the conductor design are as follows

- Further reduction of filament diameter to 3.5 µm (or below)
- Tight twist pitch

- Resistive barriers in the cable (strand coating, central high resistivity tape in the cable core e.g. of stainless steel)

Based on the LHC experience 3.5 µm strand designs were developed, tested and optimized with respect to

- Avoiding filament shape distortions and related excess magnetization
- Avoiding proximity enhanced magnetization at injection conditions (see Fig. 5 for magnetization measurements of the strand and the bare filament bundle by etching the matrix)

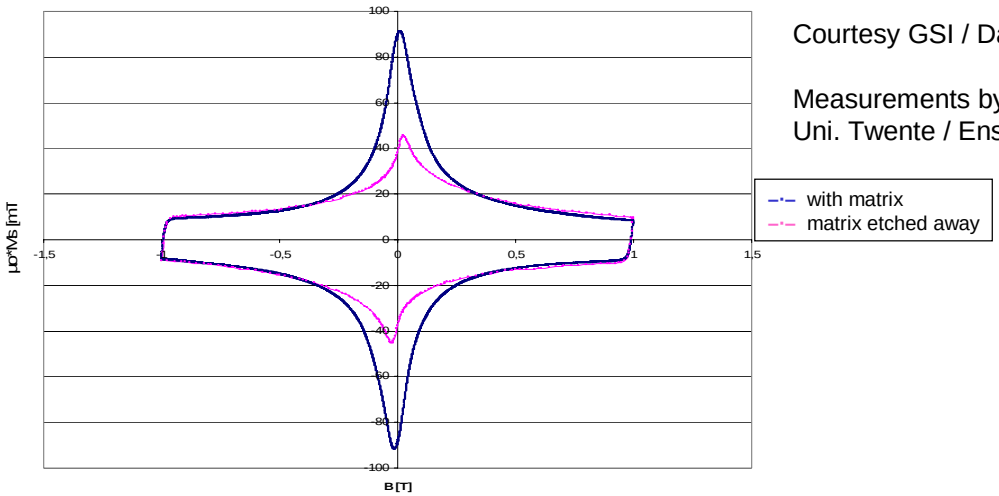

Courtesy GSI / Darmstadt

Measurements by
Uni. Twente / Enschede

Magnetization of 3.5 µm NbTi filaments
with Cu-matrix present
with Cu-matrix etched away

⇒ Proximity coupling sets in below 0.3 T

Fig. 5 NbTi/Cu: proximity coupling

As an intermediate result, a strand with 12300 filaments and a current density of well above the specified 2750 A/mm² @ 5 T, 4.2 K, 0.1 µV/cm was successfully developed and produced.

It is important to mention that Bronze Route Nb_3Sn conductors are best suited for pulsed magnets at higher fields. Low loss Nb_3Sn strands were developed and produced as part of the ITER project for nuclear fusion. Due to the relatively large amount of bronze within a Bronze Route Nb_3Sn strand it is possible to avoid filament bridging and intergrowth during reaction treatment and the related volume growth. Fig 6 shows examples with and without filament bridging by properly choosing the local Bronze to Nb ratio [1, 2].

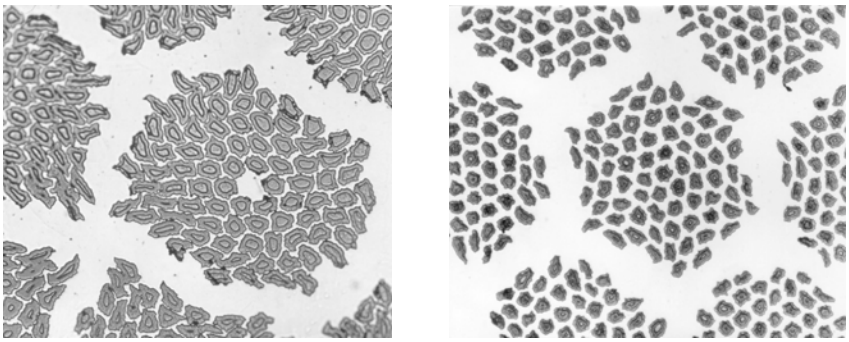

Filament bridging due to low local bronze ratio

→ n-value highest
→ effective filament diameter ≈ bundle diameter

Avoidance of filament bridging due to high local bronze ratio

→ reduced n-value
→ low d_{eff}, low losses

Fig. 6 Nb_3Sn : Avoidance of filament bridging in reacted Bronze Route Nb_3Sn Conductors

3.1 Nb3Sn conductor development for high field Accelerator Magnets

At magnetic fields well above the present LHC field level the capabilities of NbTi are exhausted, even with sub-cooling to 1.8 K. High field Accelerator Magnets with a field of 12 T or 15 T have therefore to be built with Nb_3Sn (or related materials) [4]. Unfortunately the presently almost exclusively used Bronze Route Nb_3Sn conductors exhibit too low a current density for Accelerator Magnets. High current density routes have to be applied instead, such as Internal Tin (IT) and Powder-in-Tube (PiT). Of these two routes the PiT approach seems to exhibit the best prospects for accelerator and other high current density applications.

EAS has therefore launched a joint development programme together with SMI/Enschede in the Netherlands to develop conductors with parameters suited also for Accelerator Magnets [2]

An example of conductor design and typical parameters of PiT Nb_3Sn strands is given in Fig. 7. Figure 8 summarizes some major achievements with PiT conductors made by SMI.

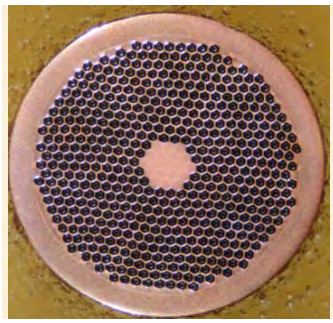

504 filament PiT
at intermediate diameter

Mono filament
- Nb or NbTa tubes
- $NbSn_2$ based powder

Multifilamentary wire
- 36 to 504 filaments in a Cu matrix
- Typical wire diameter 0.5 to 1.3 mm
- Filament diameter 20 to 60 µm
- Short heat treatment
- Well defined geometry

Fig. 7 Nb_3Sn PiT Design

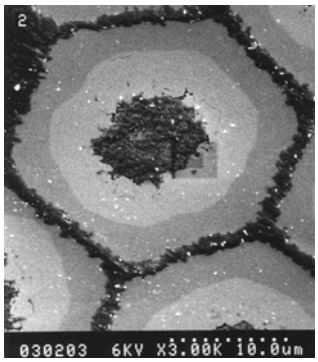

Cross section of a PiT filament
after heat treatment
(typ. 64 h / 675 °C)

From outside:

- Cu matrix
- Unreacted Nb layer
- Nb_3Sn layer
- Residual powder core

Non Cu jc up to 2400 A/mm² @ 12 T, 4.2 K, 0.1 µV/cm
1300 A/mm² @ 15 T, 4.2 K, 0.1 µV/cm

Fig. 8 Nb_3Sn PiT performance

Intensive additional development is needed to further enhance the performance of the conductors and especially to scale-up the production technology. But the envisaged specifications

- 1500 A/mm² @ 15 T or 3000 A/mm² @ 12 T (4.2 K, 0.1 µV/cm)
- Effective filament diameter $d_{eff} \cong$ 40-50 µm
- Wire diameter up to 1.25 mm

would seem to be well within reach of PiT Nb_3Sn.

4. CERAMIC HIGH TEMPERATURE SUPERCONDUCTORS (HTS) DEVELOPMENT

The ceramic HTS materials discovered in the late 1980s were opening up new application prospects of superconductors, especially because of their high critical temperature but also because of their extraordinary high field properties, at least at low temperature. Thus, both, operation at elevated temperature near liquid nitrogen (77 K) and high fields well above 20 T at liquid helium temperature became possible.

The most promising candidates for technical superconductors turned out to be the BiSrCaCuOxides $Bi_2Sr_2Ca_2Cu_3O_x$ (Bi-2223, $T_c \cong$ 110 K) and $Bi_2Sr_2CaCu_2O_x$ (Bi-2212, T_c = 85 K) and $YBa_2Cu_3O_x$ (Y-123, $T_c \cong$ 90 K). Except for Bi-2212 the conductor geometry has to be that of a thin flat tape in order to texture the ceramic materials such that the grains are well connected for superconducting current flow. Bi-2212 round wires with high critical current density at low temperatures around 4.2 K and at high fields were already demonstrated by EAS (VAC at that time) in 1989. This development is presently suspended at EAS because of the inferior properties of Bi-2212 as compared with Bi-2223 for most applications.

At present EAS and EHTS concentrate on the tape development for Bi-2223 and Y-123, respectively. In the course of the material research and conductor development it has been found that a mono-axial (out-of-plane) texture is sufficient to allow high currents to flow in polycrystalline Bi-2223. It is therefore possible to produce high current density Bi-tapes by a PiT route with appropriate precursor powders, cold working and final thermo-mechanical treatment. On the other hand, Y-123 has to be bi-axially textured, which is, so far, only possible via thin film processes by depositing the YBCO-layer on an appropriately textured flexible template.

4.1 Bi-2223 PiT tapes [5]

Bi-2223 tapes are produced by starting with inserting precursor powder of optimized phase composition in a silver tube. After cold working a certain number of these monofilaments are bundled in an outer silver tube and than extruded/drawn to final diameter and than flattened by rolling. After

that the Bi-2223 phase is formed and textured by a sequence of heat treatment and rolling steps (Thermo mechanical treatment). The resulting typical tape geometry is shown in Fig.9.

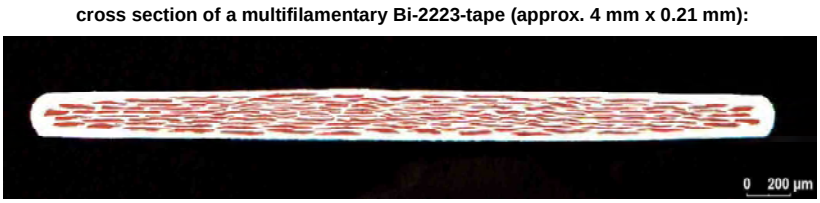

width:	approx. 4 mm
thickness:	approx. 0.21 mm
number of filaments:	121
filling factor:	approx. 30 %
material of matrix:	Ag
material of sheath:	AgMg
I_c long lengths (up to 1000 m)	≈ 100 A @ 77 K, self field

Fig. 9 Bi-2223/Ag Tape geometry and performance

In order to intrinsically strengthen an AgMg alloy is used for part of the matrix of the conductor. Depending on the application, geometry and design can be varied. Some options are given in Fig. 10.

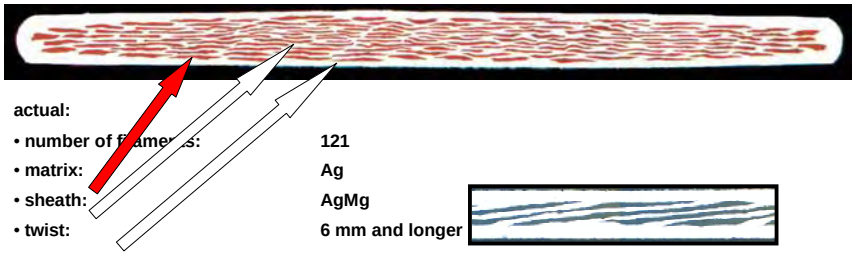

actual:	
• number of filaments:	**121**
• matrix:	**Ag**
• sheath:	**AgMg**
• twist:	**6 mm and longer**
options:	
• number of filaments:	**37, 55, 85, 121, 253 or more**
• filling factor:	**(26-33) %**
• matrix:	**AgAu (up to 8at.-% Au)**
usual unit lengths:	**500 m or more/ less (depends on order, up to 1300 m)**
usual production lengths:	**>1300 m**

Fig. 10 Bi-tape design options

Ag-Au alloy is used for current leads of LTS magnet systems for example, because of the low thermal conductivity of this alloy in the relevant temperature range. Presently EAS is delivering such tapes for the leads of the magnet systems of LHC.

The current carrying capability of Ag/AgMg tapes at “standard HTS-conditions” i.e. 77 K, self field is presently about 100 A, corresponding to 120 A/mm². The temperature dependence is given in Fig. 11.

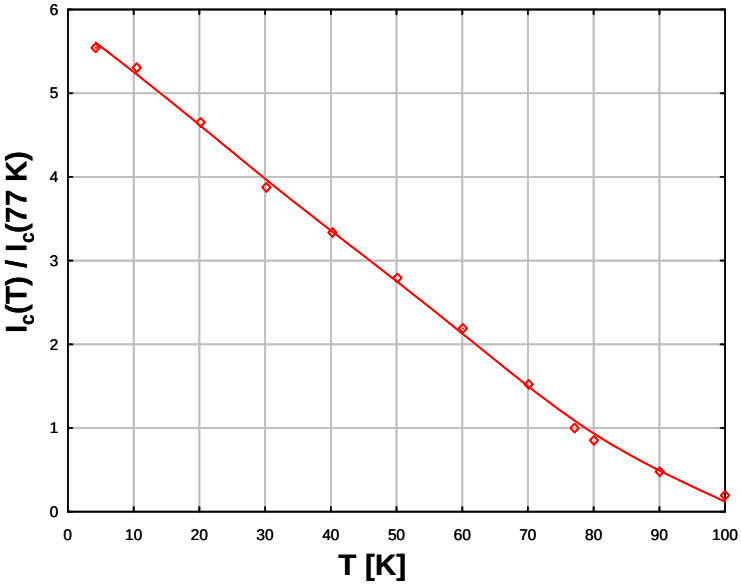

Fig. 11 Temperature dependence of critical current in self field

Unfortunately the field dependence at 77 K is very steep and strongly dependent on field direction, as can be seen in Fig. 12.

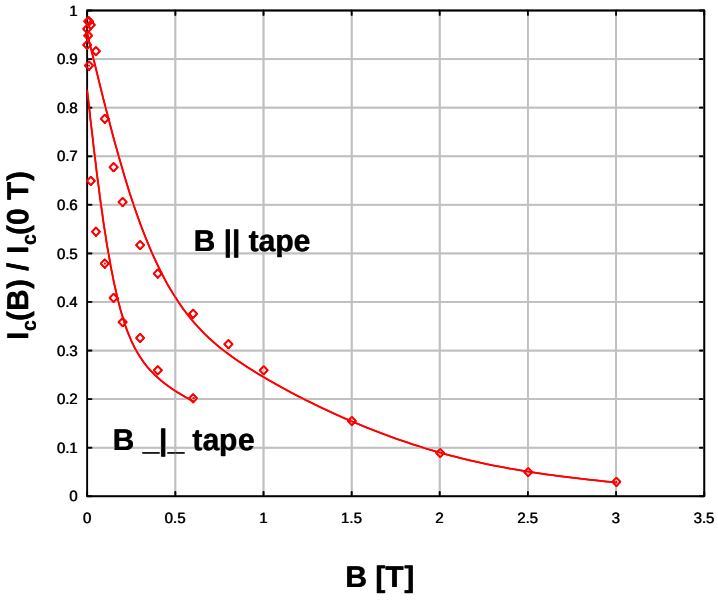

Fig. 12 Field dependence of critical current at 77 K

The Bi-based tapes are therefore limited to low field applications at 77 K. This situation improves significantly however at lower temperatures: this is already appreciable at 65 K, and below 20 K high field magnets become possible. Figures 12 and 13 show the field dependence at 20 K and 4.2 K, respectively.

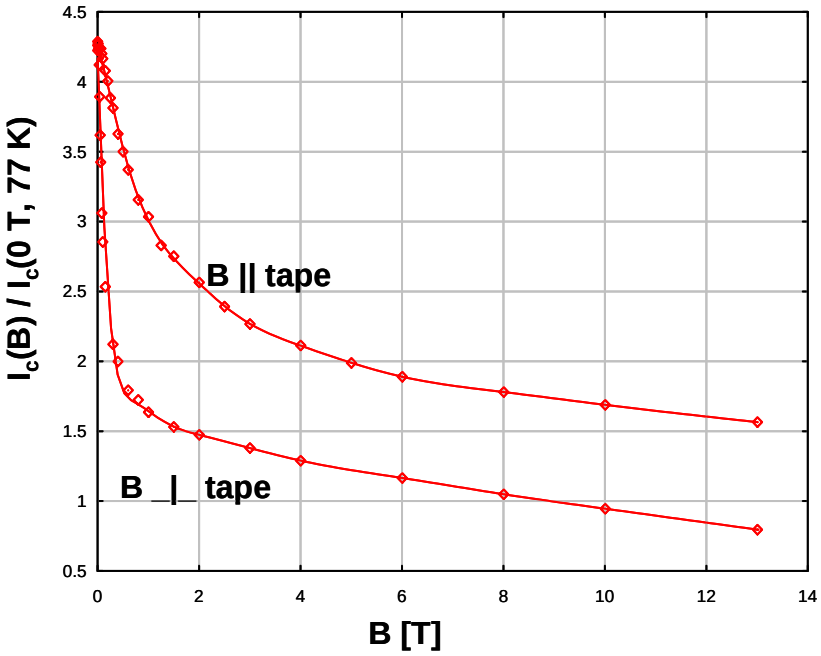

Fig. 13 Field dependence of critical current at 20 K

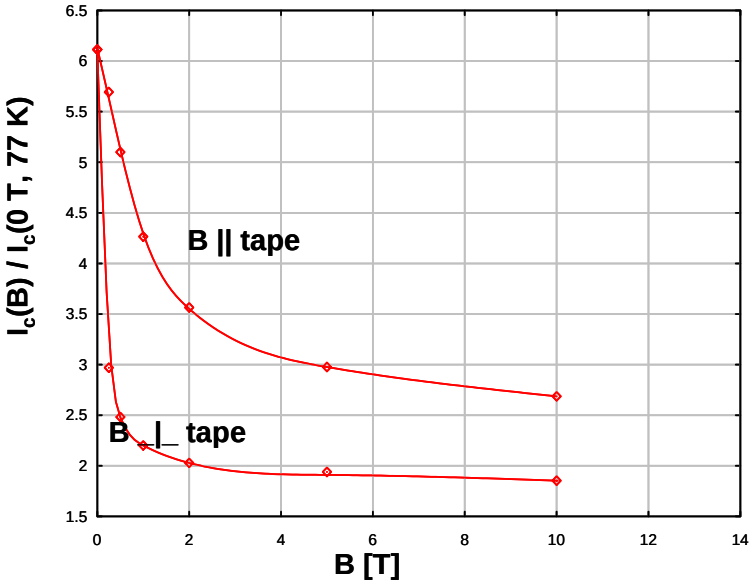

Fig. 14 Field dependence of critical current at 4 K

The multifilamentary nature of Bi-tapes allows twisting of the wire (prior to flattening) similar to metallic superconductors, and thereby the reduction of ac losses (at least for the field components parallel to the tape).

An important aspect of ceramic superconductors is their mechanical properties. For handling at room temperature the critical limits of the AgMg strengthened tape for tensile loading are 100 MPa, and for bending 60 mm diameter. At low temperature the critical tensile stress increases to 150 MPa.

The production of Bi-2223/AgMg tapes with above parameters is very advanced and unit lengths of 1000 m and more are produced and delivered routinely.

In addition high current conductors can be produced as fully transposed cables by the Roebel technique, as shown in Fig. 15.

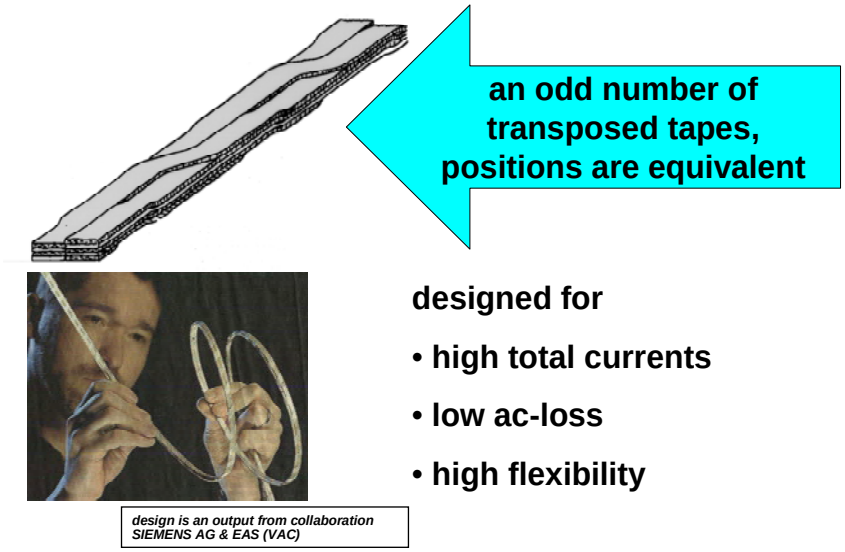

Fig. 15 Bi-2223 tape Roebel conductors with high critical current suitable for ac applications

4.2 Y-123 Thin Film tapes [6]

Due to the even more pronounced grain connectivity problem Y-123 tapes have to be produced by thin film techniques in order to achieve the bi-axially textured structure needed. The basic architecture is as follows: flexible metallic tape, ceramic buffer layer to isolate substrate and superconductor from each other and providing/transferring the texture for the superconductor layer, and environmental protection layer. There is a relatively large diversity of methods to produce such tapes. The route followed presently by EHTS is based on:

- Stainless steel tape (50-100 µm
- Ion Beam Assisted Deposition (IBAD) of Yttrium Stabilized Zirconia (YSZ) buffer and, optionally, texture improving CeO_2-layer deposition (1 to several µm)
- Pulsed Laser Deposition (PLD) of Y-123 layer (1-3 µm)
- Sputtered Au or Ag layer (< 1 µm)

Fig. 16 gives an impression of the architecture (not to scale)

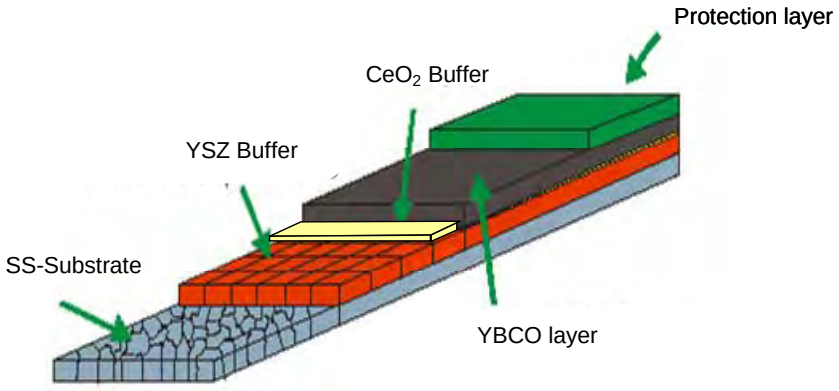

Fig. 16 Y-123 tape architecture

The chosen route was based on the excellent results of ZFW Göttingen achieved with this process. Figure 17 gives a survey of worldwide achieved performance in terms of I_c per tape width (A/cm) and tape length (m).

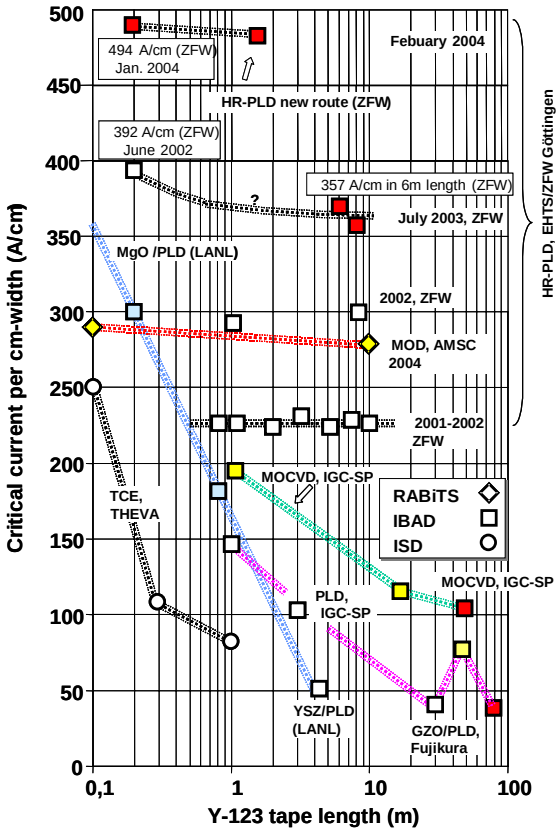

Textured Template:

RABiTS:	Buffer on textured metal substrate
IBAD:	Buffer texturing by assisting ion beam
ISD:	Buffer texturing by selecting optimum deposition angle

Y-123 Deposition:

PLD:	Pulsed Laser Deposition
TCE:	Thermal Co-Evaporation
MOD:	Metal-Organic solution Deposition
MOCVD:	Metal-Organic Chemical Vapor Deposition

Fig. 17 Worldwide achieved performance of Y-123 tape conductors in terms of critical current per width vs. length (10 cm to 100 m) as of May 2004

Presently EHTS is engaged in scaling up the developed ZFW technology, with the following

- Production of long lengths (10 m → 100 m → » 100 m)
- Continuous process and product control

- Addition of electrical stabilizer and protection material
- Application related characterization and development

4.3 Status and Prospects of HTS Conductor Application

The discovery of the Cu-oxide based HTS technical superconductors gave rise to great expectations concerning their application. Now more 15 years later, more realistic assessments can and must be made.

Genuine large scale applications have yet to become reality. Only in a niche application, current leads of LTS magnet systems, are Bi-tapes routinely used. In other fields Bi-tapes were very successfully used in demonstration models and prototypes e.g. power-cables, motors, transformers and magnets. Bi-tapes can be produced in length ≥ 1000 m and having good homogeneity, sufficient for most envisaged applications, but there are still hurdles to be overcome, both technical and economical. The brittleness of the ceramic material, and the associated cryogenics add complexity. In addition, the cost of the superconductor and the cryogenic system are still prohibitive for large scale applications if economic considerations are predominant, at least where more conventional solutions are feasible.

As regards the superconductor, the figure of merit is the cost per kAm, i.e. the production cost per length (incl. materials) versus performance as determined by the critical current at HTS standard conditions (77 K, self field). For Bi-conductors the cost per kAm are at 150-200 €/kAm and can still be reduced by increasing performance and by streamlining production. One penalty of Bi-tapes is of course the price of silver, setting an expected lower limit of tape cost at 20-30 €/kAm.

Compared to Bi-tapes, Y-123 tapes are manufactured starting with much cheaper materials (except for some chemical routes) such that Y-123 tape costs are dominated by the processing costs. At present processing and related costs per kAm are much higher than 1000 €/kAm but it can be estimated that, by process scaling-up and for very large quantities, costs of Y-123 tapes may be very much be reduced, possibly below Bi-2223 tape cost.

Another incentive to develop Y-123 tapes in addition to optimizing Bi-2223 tapes is the fact that at elevated temperature the critical current density in Y-123 is less field dependent than in Bi-2223. At a given temperature Y-123 therefore allows to generate a higher field than Bi-2223. A synopsis of the status and the prospects of applications of Y-123 in comparison to Bi-2223 are given in Fig. 18.

	Bi-2223 multifilamentary			Y-123 thin film		
	77 K	20 K	4 K	77 K	20 K	4 K
Current Leads	+++	→	+++	0	→	0
Power Cables / Bus Bars	++	÷	÷	+	÷	÷
FCL	0	÷	÷	+	÷	÷
Transformer	++	÷	÷	0	÷	÷
Motor / Generator	0	++	÷	(+)	(+)	÷
Magnets	÷	++*)	++*)	(+)*)	(+)*)	(+)*)

+++	Product
++	Tested successfully in demonstrators
+	Tested in laboratory scale
(+)	Promising
0	Questionable
÷	Not interesting and/or not possible

*) strongly dependent on magnetic field

Fig. 18 Synopsis of status and prospects of Bi-2223 and Y-123 tape application

5. CONCLUSION

NbTi-based technical superconductors and superconducting magnet technology for particle accelerators, and high energy and nuclear physics have been pushed forward in a symbiotic manner over more than 35 years now. It is expected that this development will continue by virtue of a number of ongoing projects. Besides that, the use of Nb_3Sn also in accelerator magnets will become more important, e.g. for upgrades or even more for a future large circular hadron collider. As high current density Nb_3Sn composites are mechanically much more sensitive than NbTi composites, magnet designs have to become more conductor friendly, in addition to conductor manufacturers' endeavour to reduce the consequences of this sensitivity. This requires also in future a very tight cooperation between all parties involved.

The situation is even more complex concerning applications of HTS conductors. Whereas for Nb_3Sn both, the wind-and-react and the react-and-wind technique, may be applied, for HTS the brittle ceramic conductor has to be handled during the complete magnet fabrication process. It is nevertheless expected that HTS will find its place also in accelerator and detector magnets beyond its already established use in current leads of LTS systems, because HTS offer new opportunities ranging from special magnets operating at elevated temperature to very high field magnets at low temperature.

REFERENCES

[1] H. Krauth, Fabrication and Application of NbTi and Nb_3Sn Superconductors, in: Niobium, Science and Technology, Niobium 2001 Limited and TMS, 2001-2002, pp 207-220

[2] H. Krauth et al.: Some Remarks on the Development of Commercial NbTi and Nb_3Sn Superconductors, International Workshop on progress of Nb-based Superconductors, Tsukuba, Japan, Feb. 2-3, 2004

[3] G. Moritz, Fast pulsed Superconducting Magnets, EPAC 2004, Luzern, Switzerland, July 5-9, 2004

[4] A. Devred, High-Field Accelerator Magnets beyond LHC, Proc. PAC, 2003, pp 146-150

[5] T.J. Arndt et al., Progress in the Preparation of Technical HTS tapes of type Bi-2223/Ag-alloy of Industrial Lengths, ASC04, Jacksonville, USA, October 3-9, 2004 see also EAS Website www.advancedsupercon.com

[6] A. Usoskin et al., Long Length YBCO Coated Stainless Steel Tapes with high Critical Currents, ASC04, Jacksonville, USA, October 3-9, 2004

NEXANS ACTIVITIES AND PLANS ON HTS MATERIALS. HIGH-PERFORMANCE BI2212 TAPE AND BULK CONDUCTORS FOR MAGNET TECHNOLOGY.

J. Bock, F. Breuer, C.-E. Bruzek, N. Lallouet*, M.O. Rikel and H. Walter*
Nexans SuperConductors GmbH (Hürth, Germany), * Nexans (Jeumont, France)

Abstract
Nexans activities on HTS materials are briefly reviewed with the emphasis on materials for magnet technology–Bi2212 bulk conductors for current leads, the first commercial application of HTS materials in electrical engineering; and long-length Ag-sheathed Bi2212 tape conductors for high magnetic field applications at low temperatures, the material that only recently has proven to be technologically competitive to other high-field superconductors. Recent advances of Nexans: fabrication of kilometre lengths of reinforced multifilamentary Bi2212 tapes with excellent engineering critical current densities of Je(4.2 K, sf) = 1200 A/mm2; Je(4.2 K, 20T) = 510 A/mm2 (parallel field) and 380 A/mm2 (perpendicular field) and Je(20 K, 5 T) = 300 A/mm2 (parallel field) and 170 A/mm2 (perpendicular field).

1. INTRODUCTION

Commercialisation of high-temperature superconductors (HTS) is on agenda since end of 1990s [1]. Though the price-to-performance goals formulated at that time are not fully met, the progress in materials development [2], an increased number of running projects on prototype demonstrator devices with continuously growing participation of industry [3] clearly shows that real commercialisation is not a very far future.

As one of the world biggest cable manufacturers, Nexans (former Cable and Components sector of Alcatel separated in 2001) has a clear strategy on utilization of HTS materials in the energy sector. The main focus is on the development of superconducting cables for transmission and distribution. Nexans is the major manufacturer of a 660-m long superconducting cable to be installed at the Long-Island Power Authority in early 2006 (the DOE funded LIPA project headed by AmSC, a supplier of Bi2223 tape conductors [4, 5]). Nexans coordinates an EU-funded project Super3C that aimed at development and fabrication of a 30-m long 1-phase cable completely based on the YBCO coated conductors [6]. These activities are carried out at Nexans cable plant at Hannover in close collaboration with Nexans competence centres in Almaden (Norway) and Kale (France).

Development of conductors for cables is another activity of Nexans. First-generation BSCCO wires are manufactured at Nexans cable plant in Jeumont (France) using precursor materials produced by Nexans SuperConductors (Hürth, Germany) [7, 8]. Assembled Bi2212 tape conductors is Nexans contribution to a 800 kJ SMES project [9] funded by Délégation Générale pour l'Armement. Nexans also develops all-chemical route for second-generation ReBCO coated conductors [10].

Continuing production of raw HTS materials, Nexans SuperConductors more and more focuses on development of components that can be easily integrated in the real systems. Nexans YBCO monodomain bulk materials are widely used in levitation devices [11]. Nexans is currently involved as a supplier of complete superconducting bearing for a 4 MVA superconductor motor project headed by Siemens [12].

this example, is an absorber held at a higher temperature than the coil to minimize the refrigeration cost. Clearly, this will be a very difficult magnet, with regard to achieving field strength as well as field quality. The gap height is a key parameter: the smaller the gap the more straightforward it is to achieve field strength and field quality, but the higher the energy deposition in the coil from the forward-going collision debris. The required height of the gap must take into account the width of the forward cone of collision debris, the divergence of the beam, and alignment and orbit errors. It may be advantageous to include some sort of low-mass "bridge" between the upper and lower coils, which could reduced deflections under the magnetic forces, but not initiate full hadronic showers.

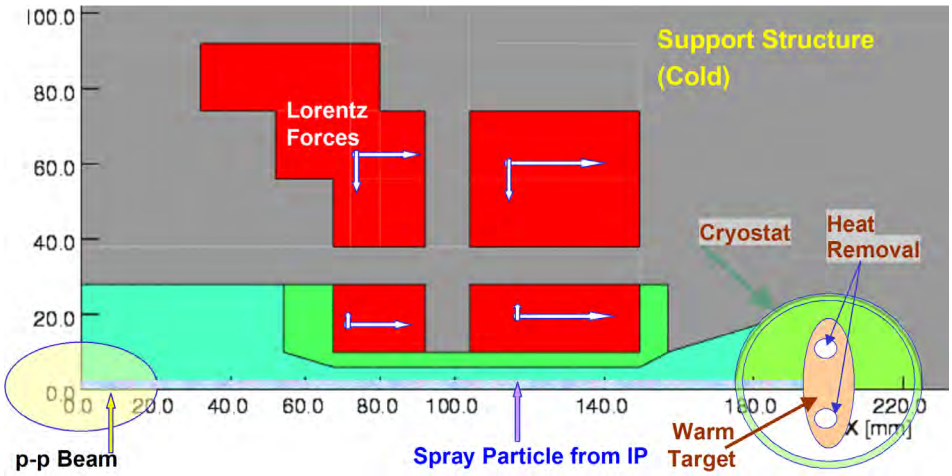

Fig. 6 Design concept for a 15 T dipole with block-type coils and an open mid-plane..

While Nb_3Sn offers a clear and promising path to the magnet parameters required for a luminosity upgrade of the LHC, this is far from a mature technology. Thus technology development will be a crucial aspect of the US LARP magnet R&D program. Among the issues that must be addressed are the superconductor itself, where achieving high J_c with small effective filament size and good strain tolerance remains a challenge, cabling, coil winding and reaction procedures, conductor-friendly coil and support structure designs, and radiation hard materials for coil impregnation and support structures. An important tool for technology development is the so-called "sub-scale" model program[8], which utilizes small racetrack coils, about 15 cm long, assembled in pairs in a "common coil" geometry as shown in Fig. 7. These allow relatively inexpensive and quick tests of various superconductor, fabrication, material, and instrumentation issues.

Over the next one to two years the top priorities of the US LARP magnet R&D program are to do coordinated magnet conceptual design and accelerator physics studies, to determine the most likely IR upgrade options and the boundary conditions on them, to develop the superconducting cable and other technologies for the new magnets, and to build and test a simplified model quadrupoles and, if possible, dipole. The first model will be a quadrupole, which will be made from two layers of an eventual four-layer magnet, which will most likely be assembled using the "bladder and key" method[9], as shown in Fig. 8. When resources permit, a simplified open mid-plane dipole will be constructed possibly using coils from the HD-1 dipole (see below). Figure 8 shows a cross-section of concept for this magnet[10].

3. US BASE PROGRAM IN HIGH FIELD MAGNET R&D

The US LARP magnet R&D builds on a base program at BNL, FNAL and LBNL in the development of high-field accelerator magnets for future hadron colliders. Indeed, the ambitious goal of US LARP, to develop magnet designs to a production ready state using the difficult Nb_3Sn superconductor, have a good chance to success only because the LARP is supported by the base program.

The Nexans melt-cast centrifugal forming process for bulk Bi2212 is widely used for development and production of current leads, bifilar coils for fault-current limiting devices currently successfully integrated in a 10 kV distribution power grid at Siegen (Germany) [13]. Appreciation of the fact that any superconducting cable should be in future protected by an FCL device enhances the Nexans efforts to develop FCL technology for high-voltage transmission lines. As a supplier of melt-cast tubes Nexans participates in a Matrix FCL project for a 138 kV transmission level (the DOE-funded project headed by IGC Superpower [14]).

In this contribution to WAMS workshop, we present current advances at Nexans on HTS materials for magnet technology: Bi2212 bulk conductors for current leads and long-length Ag-sheathed Bi2212 tape conductors.

2. BULK 2212 FOR CURRENT LEADS

Current leads are the first commercial application of HTS materials in electrical engineering. Nexans focuses on development of Bi2212 bulk current leads using Nexans-patented melt-cast process (MCP) [15]. In this process, Bi2212 with admixture of Sr sulphate is molten in Pt crucibles and then cast either in moulds to produce rod-shaped conductors or centrifugally cast in rotating preheated moulds to produce bulk tubes. In both cases Ag contacts are incorporated during casting. Subsequent heat treatment converts the quenched products in Bi2212 phase (see [15] for details). The process is well established and thanks to the bulk nature of conductivity is characterized by high reproducibility.

Various shapes (rods or tubes) and sizes (up to 60 cm length) are available (Fig. 1a) covering current levels from 0.2 to 20 kA. The corresponding (77 to 4 K) heat leak varies from 10 mW to 2.2 W (Fig. 1b). Note that the large heat leak in case of tube conductors of 200 mm outer diameter is mostly due to their short length (≤100 mm); using three longer (300 mm) tube conductors of 70 mm diameter, it is possible to transfer the same current with three time smaller heat leak.

The basic material properties are summarized in Table 1. The critical current density as function of magnetic field and temperature is shown in detail in Fig. 2.

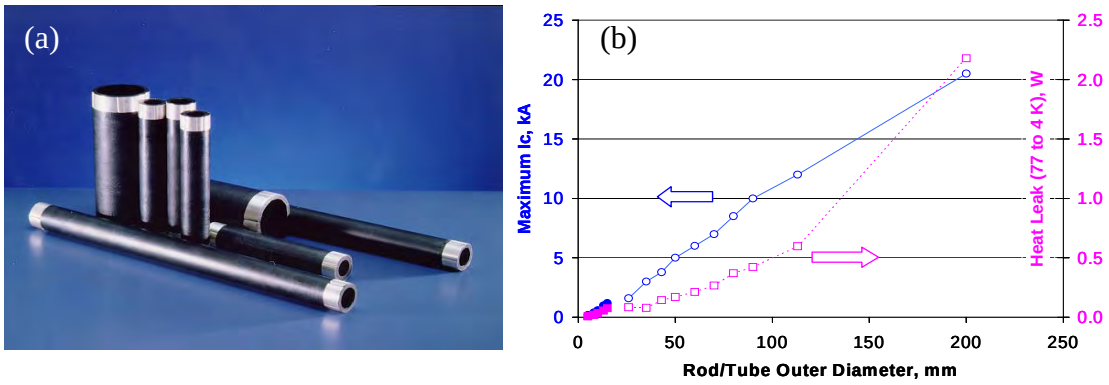

Fig 1. (a) Tubular current leads and (b) maximum I_c (circles) and heat leak (squares) as function of tube (open symbols) or rod (closed symbols) outer diameter. The tube wall thickness can be varied from 3 to 8 mm.

Table 1

Basic properties of MCP Bi2212 current leads

Tc(R=0) K	Jc (sf), kA/cm^2 (a)		Heat conductance @77K	Specific heat @77 K (b)	Contact resistance μΩ·cm²		Thermal expansion K^{-1}	Failure point (c), N	
	77 K	4.2K			77 K	4.2K		5 mm	8 mm
90–92	0.6–2.0	> 10	**< 1 W/m·K**	~120Ws/Kg·K	~2	<0.05	$3.5 \cdot 10^{-6}$	~70	~250

(a) mainly limited by self-filed effects; (b) changes with admixture; (c) results of four-point bending tests on rods

Because of almost an order of magnitude higher thermal conductivity at 77K (~70 W/m·K [16]), similar heat leak properties in alloy (AgAu) sheathed Bi2223 tapes are only available in ~100 times longer lengths. This makes Bi2212 bulk current leads much less expensive and at the same time reliable solution for a number of applications. Successful use of Nexans current leads is reported by Oxford Instruments–Research Instruments (Abingdon, UK), ACCEL (Bergisch Gladbach),Intermagnetics (Lathan, NY), Mitsubishi Electric Corp. (Kobe, Japan). Bulk current leads are considered the material of choice for 4.2 K-to-1.8 K current transfer [17].

Note that further optimisation of bulk Bi2212 materials, mainly with respect to their irreversibility field at 77 K is in progress for both current lead and FCL applications.

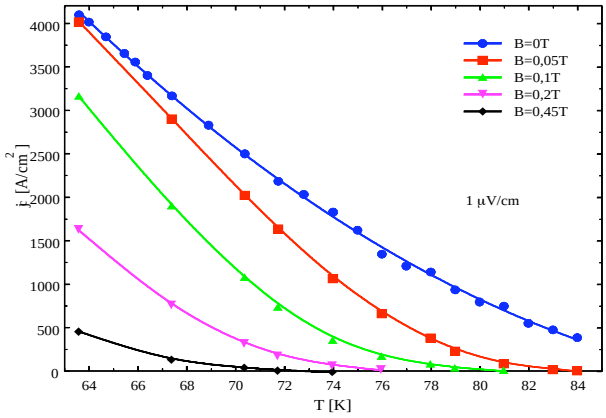

Fig. 2. Temperature dependence of critical current density in 5-mm diameter MCP Bi2212 rods as function of magnetic field.

3. BI2212 TAPE CONDUCTORS

Although BSCCO-based conductors (both 2223 and 2212) did not meet price-to-performance ratio that makes them attractive for a widespread use in transmission cables [2], the low-temperature performance makes them materials of choice for magnet applications at intermediate temperatures and for high magnetic field applications at low temperatures [18]. For magnet applications below 20 K, melt-processed Ag-sheathed Bi2212 tapes and wires appear to be more promising than Bi2223 conductors because of the better performance and the ability to apply Wind & React technology [19-21].

(a)

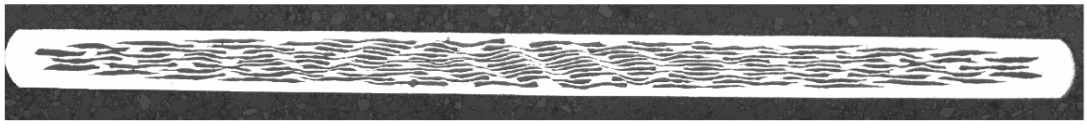

(b)

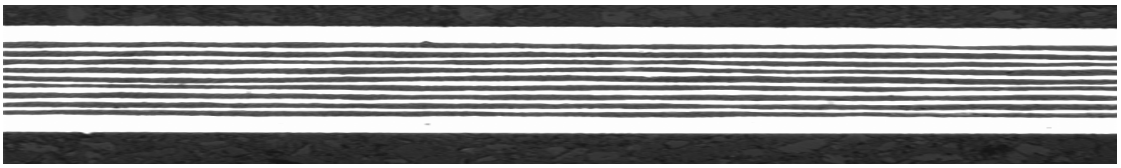

Fig. 3 (a) Transverse and (b) longitudinal cross sections of the as rolled tapes (0.25 x 4.2 mm) with fill factor of 32% AgMg alloy is used as an outer sheath.

Bi2212 conductors at Nexans are developed within a 800kJ SMES demonstrator project. Within this project [9], Nexans has to deliver about 40 km React & Wind multifilamentary tapes with the requirement on the operating current of 100A at 20K in a 5.6 T field parallel and 2.0 T field perpendicular to the tape surface. The first problem addressed was the problem of precursor material. Based on the melt-cast process, we developed precursor specially designed for melt processing OPIT Bi2212 conductors in terms of sharpening melting event and minimizing final phase separation during the melting step. Highly robust and reproducible technology was developed that resulted in conductors with almost twice better performance achieved both at Nexans [7] and Oxford Superconductor Technology (OST) [20]. At OST, Nexans precursor contributed to the successful production of Bi2212 pancake coils for a 5-T insert that reached 25.1 T central field [20].

The 85-filament conductors are prepared via standard OPIT method using pressed Bi2212 precursor rods. Figure 3 shows the geometry of as rolled tape.

In September 2003, we reported our results on optimising tape thickness and heat treatment (maximum processing temperature) in short (10 cm long) and medium (10 m long) samples with the fill factor of 32% [7]. In tapes reinforced with oxidized AgMg alloy that can withstand tensile stresses at 77 K up to 150 MPa and strains up to 0.15% before current degradation, we reproducibly obtained engineering current densities Je (4.2 K, sf) = 940 ± 20 A/mm2, Je (4.2 K, 20 T) = 430 A/mm2 (parallel field), Je (20 K, sf) = 540 A/mm2, Je (20 K, 5T) = 330 and 190 A/mm2 (parallel and perpendicular fields, respectively). We have also shown that 80% short-sample performance can be attained when samples are uniformly distributed over the load of a dummy 1.5-km long tape.

The main advances since then are processing of kilometre tape lengths, further improving conductor performance by increasing the fill factor to 38%, and assembling melt-processed tapes in stranded four-ply conductors reinforced with stainless steel tape to facilitate coil manufacturing.

Using principally the same heat treatment in 100%O2 as reported earlier [7], we melt processed 1.5 km long tape load without any visual bubbling in the piece lengths up to 950 m. Adjusting Tc of the tape to 85–87 K by post annealing, we were able to improve Ic(77 K, sf) of the tape above 10 A and show its 15%.

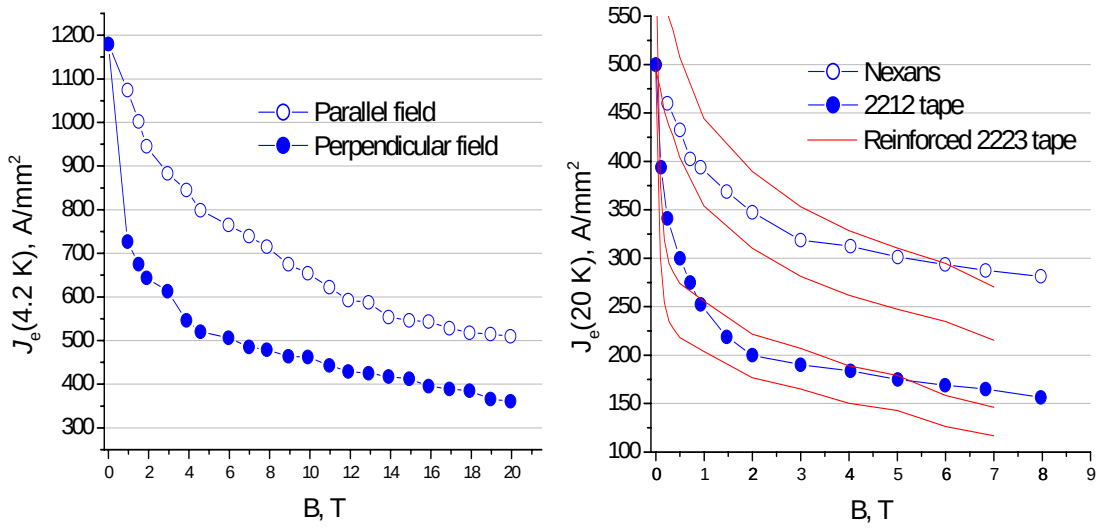

Fig. 4. Field dependence of J_e at (a) 4.2 K and (b) 20 K in magnetic fields parallel and perpendicular to the tape surface. The upper and lower curves for 2223 tape conductors in (b) are calculated from J_e(20K,B)/J_e(77K,sf) data using the J_e(77K,sf) = 113 and 90 A/mm^2 characteristic of reinforced tape made by American Superconductor Corp. [22].

uniformity by continuous Ic measurements. The uniformity of Ic(4.2 K, sf) was found to be better than 3% by measurements on 10 cm-long samples uniformly distributed within the same load.

Increasing the fill factor to 38%, we obtained high-performance tape conductors with average Je (4.2 K, sf) of 1040 A/mm2 (averaging over about 50 samples uniformly distributed over 1.5 km length). The highest Je (4.2 K, sf) = 1230 A/mm2. The self-field performance attained in the kilometre length is about 85% of the world record values [20, 21]. Figure 4 shows the field dependence of Je (4.2 K) for the short (10 cm long) sample. At 20 T, Je (4.2 K) in the perpendicular field is above 77% performance of the one of the best round wire [20]. The n-values are of an order of 15 as in [20].

Performance of Nexans best 2212 tape at 4.2 K is approximately 50% better than that of 2223 conductors available on the market and, as is shown in Fig. 4b, almost coincides with that of the reinforced 2223 tapes at 20 K [22].

4. SUMMARY AND OUTLOOK

In this contribution, we briefly reviewed the Nexans activities on HTS materials and presented in more detail our results on two materials for magnet technology–the melt cast processed Bi2212 bulk current leads that are in our production list since 1995 and melt processed B2212 tapes conductors that are only at the development stage, but already show very high potential to become soon a commercial product.

Production and development of variety of HTS materials requires resources, but gives a real synergy. The advances in 2212 precursor and conductors reported in this paper are a good example of such synergy. Based on the technology of melt cast processing developed for bulk Bi2212 [15] and understanding the difference in requirements on BSCCO precursors for melt processing Bi2212 and Bi2223 conductors [7, 8], we developed a new Bi2212 precursor that has shown excellent performance in OPIT conductors produced at both Nexans and OST. This development has a clear feedback to the melt cast processing of bulk Bi2212 materials. We are currently optimising heat treatment of bulk MCP Bi2212 in order to improve its c-axis conductivity; we anticipate significant improvement in performance of conductors for current leads and components for FCL devices.

Fabrication of high-performance Bi2212 OPIT tape conductors in kilometre lengths reported in this paper clearly shows that they can be considered as real conductors for magnet applications at 4.2–20 K. Note that as in [7], the recent conductors were optimised with respect to their geometry (tape thickness) and maximum processing temperature. It is known that conductor performance strongly depends on solidification conditions; optimisation of these conditions may give further significant improvement [23]. However, even with the achieved performance, 2212 conductors are highly competitive with best 2223 conductors at 4.2–20 K. Note that, in general, Bi2212 OPIT conductors were studied essentially less than their 2223 counterparts. We believe that, having much more transparent than 2223 melt-processing heat treatment, 2212 conductors can be further significantly improved. In addition to optimising the heat treatment parameters discussed above, the most important directions of further studies are :

- choice of proper cation composition in order to improve performance and expand the window for processing temperatures [7, 19];
- introduction of nanoparticles as pinning centres that may improve the irreversibility field [24] and shift the possible working temperature to the 40–50 K range;
- improving homogeneity of final conductors in order to improve n-values.

Correlation of critical current with microstructural properties [25] suggests that 50% better performance of 2212 conductors should be considered as a very realistic anticipation.

For magnetic applications in a persistent mode, it is worth noting that completely superconducting joints between bulk and OPIT 2212 conductors are easily achievable.

ACKNOWLEDGEMENTS

We would like to acknowledge fruitful discussions with Dr. S. Pavard, J. Ehrenberg, S. Arsac, J.-M. Saugrain (Nexans), and Dr. Ken Marken (OST, USA). This work was supported in part by Délégation Générale pour l'Armement.

REFERENCES

[1] P.M. Grant and T.P. Sheahen, Cost projections for high temperature superconductors, Preprint to ASC'98 (see http://arxiv.org/ftp/cond-mat/papers/0202/0202386.pdf).

[2] A.P. Malozemoff, D.T. Verebelyi, S. Fleshler, D. Aized and D. Yu, HTS Wire: status and prospects, Physica C 386 (2003) pp. 424-430.

[3] Peer Review 2004: http://www.energetics.com/supercon04.html.

[4] J.F. Maguire, F. Schmidt, F. Hamber, T.E. Welsh, Development and demonstration of a long length HTS cable to operate in the Long Island Power Authority transmission grid, Paper 1LT01 submitted to Proc. ASC2004.

[5] F. Schmidt and A. Allais, Superconducting cables for power transmission application– Review, Paper submitted to Proc. of this workshop.

[6] Nexans press release
(see http://www.nexans.com/internet/Content.nx?f=se&contentId=2176).

[7] C.-E. Bruzek, N. Lallouet, E. Flahaut, D. Bourgault, J.-M. Saugrain, A. Allais., S. Arsac, J. Bock, J. Ehrenberg., D.E. Wesolowski and M.O. Rikel, High-performance Bi2212/Ag tape produced at NEXANS, Paper submitted to Proc. EUCAS2003.

[8] M.O. Rikel, A.Wolf, S. Arsac, M. Zimmer, and J. Bock, Effect of precursor phase composition on 2223 phase formation in Ag-sheathed tapes, Paper submitted to Proc. ASC2004.

[9] P. Tixador, B. Bellin,; M. Deleglise, J.C. Vallier, C.E. Bruzek, S. Pavard, J.-M. Saugrain, Design of a 800 kJ HTS SMES, Paper 1LH01 submitted to Proc ASC2004.

[10] D. Isfort, O. Castano, D. Cavaillon-Pinod, B. Hoppe, J. Ehrenberg, M. Klein, S. Arsac, A. Wolf, S. Donet, J. Bock, Up-scaling of buffer and YBCO deposition for coated conductors, Paper 1MR04 submitted to Proc. ASC2004.

[11] H. Walter, S. Arsac, J. Bock, S. O. Siems, W.-R. Canders, A. Leenders, H.C. Freyhardt, H. Fieseler, M. Kesten, Liquid hydrogen tank with cylindrical superconducting bearing for automotive application, IEEE Trans. on Appl. Supercond. 13 (2003) 2150; S.O. Siems, W.-R. Canders, H. Walter, J. Bock, Superconducting magnetic bearing for a 2 MW / 10 kWh class flywheel energy storage system, Proc. EUCAS 2003 (to be published by IOP).

[12] Siemens press release A&DLD200203231d / CT 200204007d (2002).

[13] .J. Bock, F. Breuer, H. Walter, M. Noe, R Kreutz, M Kleimaier, K-H Weck and S. Elschner, Development and Successful Testing of a MCP BSCCO-2212 Components for a 10MVA Resistive Superconducting Fault Current Limiter, Supercond. Sci. Techn., 17, pp. S122–S126.

[14] X. Yuan, K. Tekletsadik, L. Kovalsky, J. Bock, F. Breuer, S. Elschner, Superconducting fault current limiter for transmission-level applications, paper 2LC03 submitted to Proc. ASC2004.

[15] .J. Bock, H. Bestgen, S. Elschner, and E. Preisler, Large shapes parts of melt cast BSCCO for applications in electrical engineering, IEEE Trans. Appl. Supercond., Vol.3 (1993) 1659-1653.

[16] T.J. Arndt, A. Aubele, H. Krauth, M. Munz, B. Sailer, Progress in the preparation of technical HTS-tapes of type Bi-2223/Ag-alloy of industrial lengths, Paper 1MT02 submitted to Proc ASC2004.

[17] J. Pfotenhauer 2002, private communication.

[18] Mazur L J, Kellers J, Pegrum C M and Cardwell D A 2003, Handbook of Superconducting Materials vol. 1 (Bristol: IOP) p. 27.

[19] G. Duperray and P.F. Herrmann, Handbook of Superconducting Materials vol. 1 (2003) Bristol: IOP, p. 449.

[20] H. Miao, K.R. Marken, M. Meinesz, B. Czabaj and S. Hong, Development of Bi-2212 conductors for magnet applications, submitted to Proc. ICMC2003.

[21] T. Hasegawa, N. Ohtani, T. Koizumi, Y. Aoki, S. Nagaya, N. Hirano, L. Motowidlo, R.S. Sokolowski, R.M. Scanlan, D.R. Dietderich, and S. Hanai, Improvement of superconducting properties of Bi-2212 round wire and primary test results of large capacity Rutherford cable, , IEEE Trans. Appl. Supercond., 11 (2002) 3034-3037.

[22] Web site of Amercian Superconductor Corporation: http://www.amsuper.com/products/htsWire/.

[23] M.O. Rikel, D. Wesolowski, A.A. Polyanskii, X.Y. Cai, K. Marken, H. Miao, and E.E. Hellstrom, Effect of solidification conditions on microstructure and electromagnetic properties of melt processed Bi2212/Ag tapes, Physica C, 372–376 (2002) 1839-1842.

[24] B. Ni, M. Kiuchi, and E.S. Otabe, Enhancement of critical current density and flux pinning in Bi2212 thick films due to MgO addition, IEEE Trans. Appl. Superocnd., 13 (2003) 3695-3698.

[25] M.O.Rikel, S. Pavard, and C-E. Bruzek, unpublished result.

PRESENT STATUS AND FUTURE PERSPECTIVES FOR NI-SHEATHED MGB_2 SUPERCONDUCTING TAPES

G. Grasso, A. Malagoli*, A. Tumino*, C. Fanciulli*, D. Nardelli*, C. Bernini*, M. Vignolo*, V. Braccini*, C. Ferdeghini*, A.S. Siri*, M. Modica**, R. Marabotto***
*INFM-LAMIA & Columbus Superconductors srl, Corso Perrone 24, 16152 Genova, Italy
** Ansaldo Superconduttori SpA, Corso Perrone 73r, 16152 Genova, Italy

Abstract
The present status of ex-situ Nickel-sheathed MgB_2 superconducting tape development is described. Typical critical current data of short conductors are presented as a function of the temperature and of the magnetic field. The results achieved so far on longer lengths are also reported and related to the short sample data. The lower critical currents observed in the longer tapes have been related to the damage of the superconducting core due to winding and to a residual fluctuation of the superconducting cross section observed along the tape length. Multifilamentary conductors, manufactured so far in short lengths, should represent the solution to solve the long length degradation.

1. INTRODUCTION

The recent discovery of superconductivity in MgB_2 at a temperature of 40 K [1] has immediately attracted the interest of the researchers searching for a new material to be implemented in various industrial applications. In spite of several years of continuous development, indeed, YBCO and Bi-2223 conductors still require substantial improvements, and it is not clear yet which material will reach a more desirable performance-to-cost ratio that will finally enable large scale applications in a liquid nitrogen environment. On the other hand, the recent progresses in cryogen-free cooling technology have opened new perspectives for the efficient use of superconductors cooled in the 20-30 K temperature range. High temperature cuprate superconductors have already gained a clear benefit from the possibility to lower their working temperature, and in very recent times several examples of fully functional devices have appeared, most of which based on Ag-sheathed Bi-2223 multifilamentary tapes. In the next future, these devices are expected to reach the market, especially that of AC applications, basically in the field of improving the power quality [2].

On the other hand, the potential current carrying capability of the MgB_2 phase has been also studied over the same temperature domain, soon after its discovery. First critical current measurements performed on polycrystalline samples by Bugoslavski et al. [3] have shown that grain boundaries are virtually transparent for the intergrain critical current flow. At 20K, irreversibility fields in the range 3-5 Tesla have been reported on polycrystalline samples, and relevant inductive critical currents for magnetic fields up to 1-2 Tesla have been measured [3]. These preliminary critical current values are roughly comparable to those of the present state Ag-sheathed Bi-2223 and Bi-2212 superconducting tapes for similar temperature-field conditions. Following this observation, the search for a suitable procedure for the fabrication of polycrystalline MgB_2 wires has been immediately started.

The idea of implementing the well-known Powder-In-Tube method to the fabrication of MgB_2 conductors has been successfully accomplished short time after the first experiments [4-6]. While different solutions to manufacture MgB_2 wires and tapes have been also studied [7], indeed, the Powder-In-Tube method has been widely preferred thanks to the peculiar properties of the compound. The rather small MgB_2 grain size, the relatively long coherence length, and the almost complete absence of granular behaviour are all positive aspects in favor of the use of the PIT method.

Relatively high critical current values were first reported on monofilamentary tapes, prepared by filling reacted MgB_2 powders inside metallic tubes, and by carrying out the typical mechanical deformation by wire swaging, drawing and rolling to thin wires or tapes without applying any heat treatment to sinter the grains [8,9]. These conductors however presented fairly reduced T_c values (about 30 K) compared to the expected one (about 38 K), due to a poor grain connectivity and a high lattice strain induced by cold working, and accordingly their high temperature behaviour has been negatively affected.

Following these early understandings, both in-situ and ex-situ processing routes for the manufacturing of MgB_2 conductors have been proposed: in both cases the conductor undergoes a final heat treatment at high temperature after the mechanical deformation, that can be either a simple sintering or a complete phase formation process. These approaches have definitely narrowed the many options for the choice of the sheath material that are theoretically possible, because a chemical compatibility with the MgB_2 compound is now required. Results have been reported with most of the workable pure elements and alloys, but the most promising results have been reported so far with Iron, Nickel, and Copper sheaths. Best transport properties at temperatures around 20 K are achieved on conductors that undergo a heat treatment at temperatures of the order of 900°C, and only Iron or Nickel can sustain such a high temperature without completely poisoning the MgB_2 phase.

Our choice has been particularly focused on MgB_2 conductors manufactured with high purity Nickel sheath, mainly because of electrical stability reasons. Furthermore, Nickel can be easily turn into a non magnetic material by appropriate alloying with Chromium or Vanadium. The ex-situ route has been preferred for the scaling up of the manufacturing process, because it is believed, on a first stage, to be probably more reproducible over long length than the in-situ process. It is indeed very difficult to achieve a correct mixture of very fine Mg and B grains to be homogeneously reacted inside the sheath, especially for multifilamentary conductors where filaments can be very thin.

2. EXPERIMENTAL

Monofilamentary and multifilamentary Nickel-sheathed MgB_2 tapes have been prepared by means of the PIT method following the ex-situ route, that differentiates from the in-situ one by the filling of already reacted MgB_2 powders into the metallic tube of typical size 12.7 mm x 6.0 mm (outer diameter x inner diameter) and up to 2 meters in length.

MgB_2 powders were either commercial ones, manufactured by HCStarck, or as a result of the reaction from amorphous Boron and Magnesium mixtures. In both cases, similar results in terms of final tape properties have been achieved. After packing the reacted powders inside the Nickel tube with an initial density of about 1.5 g/cm^3, they are cold worked by swaging, groove rolling and finally by drawing in many steps without intermediate annealing to round wires of about 1.5-2.0 mm in diameter. Then the wires are cold rolled to flat tapes of about 4 mm in width and 0.35 mm in thickness, with a superconducting filling factor of about 17%, i.e. an average transverse superconducting cross section of 0.24 mm^2.

Multifilamentary tapes are fabricated by a similar process, in which seven pieces of hexagonal monocore wires are stacked inside a second Nickel tube, that undergoes again the entire mechanical deformation process. In the unreacted state, MgB_2 tapes carry an appreciable critical current at 4.2K, of the order of 10^5 A/cm^2, as a consequence of the high powder packing density that is achieved by the cold working procedure; on the other hand, the transport properties at higher temperatures or in an applied magnetic field are strongly limited by the reduced T_c value (about 30 K), which is a consequence of the large MgB_2 lattice strain induced by the prolonged cold working procedure. A final heat treatment at about 900°C in Argon atmosphere is therefore required, mainly to recover the original T_c value by partially healing the accumulated lattice strain, and to improve the grain connectivity.

The manufactured MgB_2 conductors have been characterized by means of transport critical current measurements at 4.2 K. Self field critical currents have been measured as a function of the temperature, while the magnetic field dependence of the critical current of short samples have been

measured both at the INFN-Genoa laboratories in a field up to 2 Tesla, and at the Grenoble High Magnetic Field Laboratory (GHMFL), in applied fields up to 20 Tesla oriented both parallel and perpendicular to the superconducting tape surface. The pancake samples have been measured at the INFM-Genoa laboratory with an applied backup field up to 5 Tesla.

3. RESULTS

The self field as well as the magnetic field dependence of the critical current of short portions of monocore MgB_2 tapes cut from 200 meter long conductors are reported in fig. 1. The self field critical current values are very high and in excess of 100 A at all the temperatures we have measured. The magnetic field strongly depresses I_c though, especially at high temperatures. Only at 20 K, a field of 2 Tesla does not reduce I_c much below the desired 100 A level. Measurements have been performed for different orientations of the magnetic field with respect to the tape, but the anisotropy of the critical current is not significant at temperatures of 20 K and above, at least for fields up to 2 Tesla.

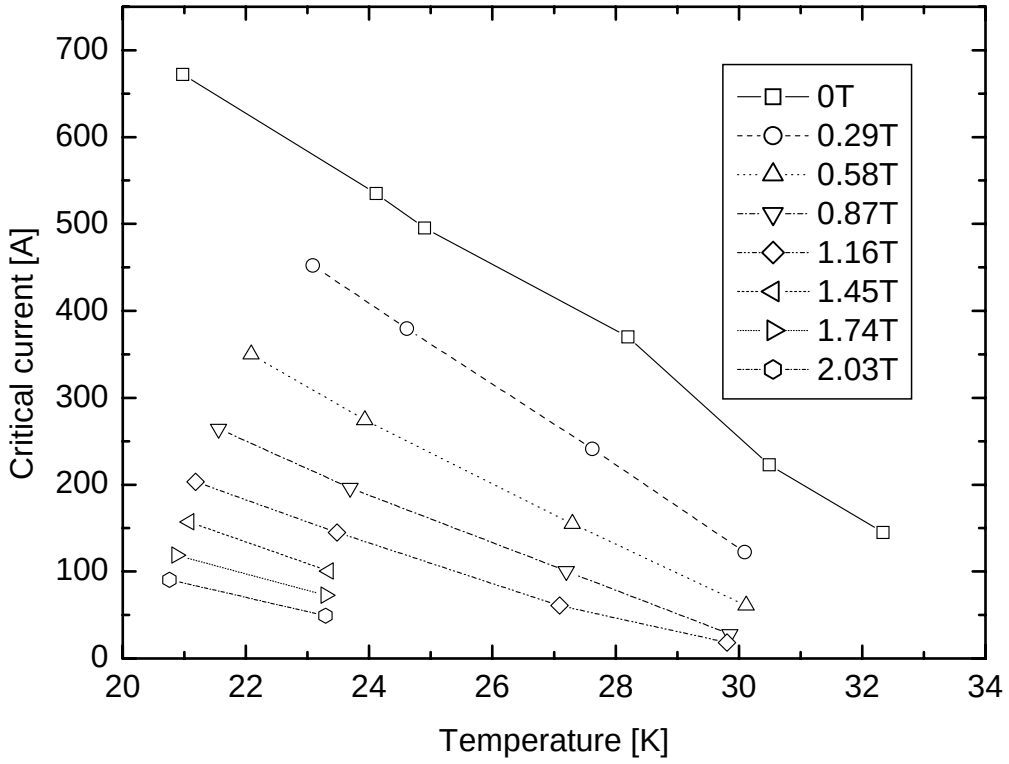

Fig. 1: Critical current as a function of the magnetic field and of the temperature between 20K and 33 K.

The situation is quite different at 4.2K, as shown in fig. 2, where the anisotropy of the critical current is reported for the same conductor, and is evident above 4 Tesla. In this case, the 100 A critical current level is reached for a magnetic field of 5 Tesla applied parallel to the tape widest surface. The critical current is not measurable for fields below 1 Tesla because it is well in excess of 1000 A. Self field critical current density at 4.2 K extrapolates to a value of about 10^6 A/cm^2, while irreversibility fields are of the order of 8 T and 12 T with the field oriented perpendicular and parallel to the tape, respectively. These values are typical for polycrystalline MgB_2 materials and are in between the values commonly reported for single crystals, which are especially low [10], and for the thin films, which can be instead much higher, in some cases in excess of 50 Tesla [11].

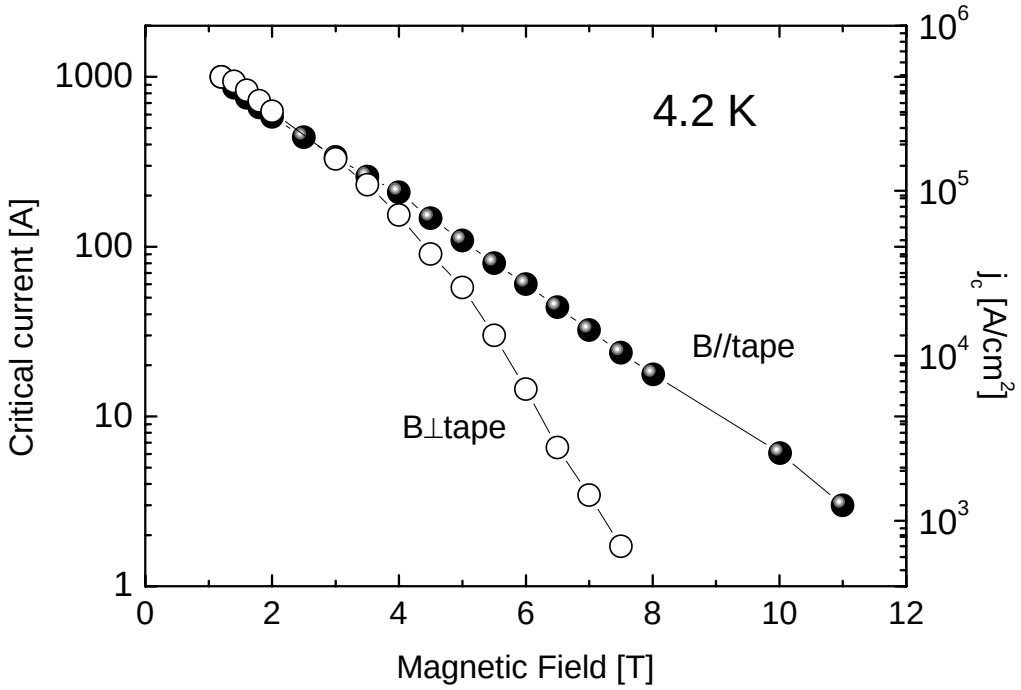

Fig. 2: Anisotropy of the critical current at 4.2 K measured for a monocore tape up to a field of 11 Tesla.

The manufactured conductors have been initially used to realize a series of pancakes, both with the react and wind (R&W) as well as with the wind and react (W&R) process. About 10 meters of monofilamentary tape have been used for each pancake. The critical current of the pancakes have been measured at 4.2 K in liquid helium bath. An additional magnetic field up to 5 Tesla has been superimposed to the field generated by the pancake. The critical currents of the R&W and W&R pancakes have been reported as a function of the magnetic field in fig. 3, together with the short sample critical current reported in fig. 2. The W&R pancake presents a critical current value that is much nearer to the short sample critical current than the R&W pancake. The latter presents a critical current that is only about 60% the short sample critical current.

The drop in critical current between the W&R and the R&W pancakes can be directly attributed to the mechanical damage induced on the tape by the handling and winding procedure. As the inner diameter of the pancakes is 50 mm., and the superconducting core of the tape has an average thickness of about 80 μm, it results that the bending strain applied with the winding reaches about 0.16%, i.e. of the same order of magnitude of the critical strain value of our monocore MgB_2 tapes.

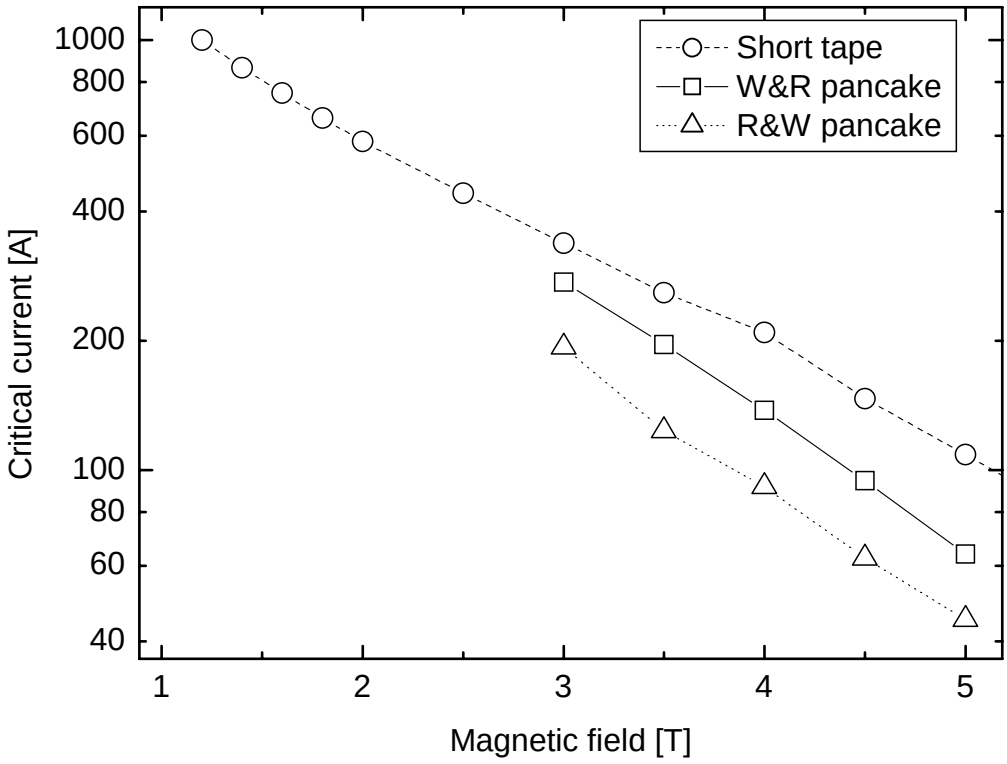

Fig. 3: Critical currents at 4.2 K as a function of field for a W&R pancake, a R&W pancake, and a short tape for comparison.

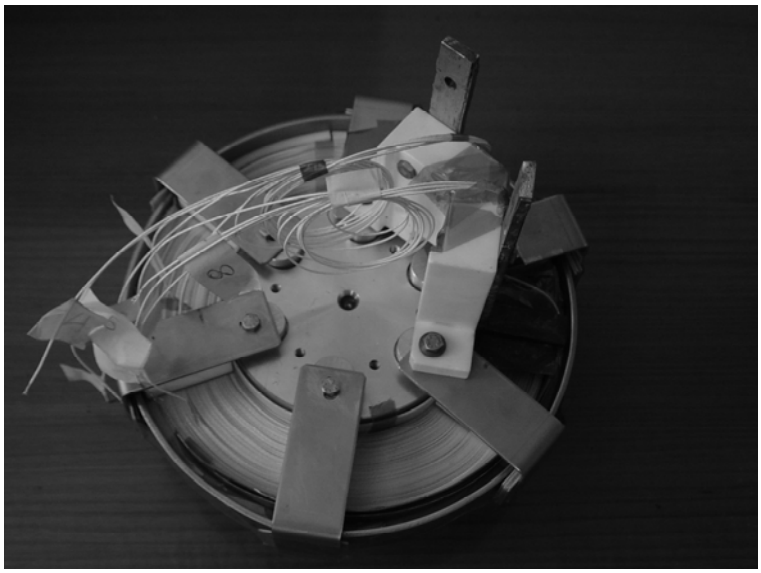

Fig. 4: Picture of an MgB_2 pancake realized with 100 meters of monocore tape.

To reduce the effect of the bending strain and to study longer portions of conductor, R&W pancakes have been realized with larger inner diameter of 120 mm and with up to 100 meters of tape. A picture of one of these pancakes manufacture by Ansaldo Superconduttori SpA is presented in fig. 4. Ansaldo Superconduttori has built setups for the large pancake measurement both in liquid helium, as well as in a cryogen free environment. Preliminary critical current measurements of these pancakes have been performed at 4.2K in self field. The best pancakes typically quenched at a critical current of about 350 A, that corresponds to a maximum magnetic field on the conductor of about 0.8 Tesla. Again, a reduced critical current level is observed with respect to the short sample results.

A possible explanation for the reduced critical currents observed over the long lengths has been attributed to fluctuations of the transverse superconducting cross section. To investigate this hypothesis, sections of the pancakes have been cut and analyzed with the optical microscope in order to determine the superconducting cross sections at different positions along the conductor. An entire section of a pancake is shown in fig. 5 as an example. Preliminary analysis has revealed that the cross section of the superconducting core fluctuates by a factor of the order of ±30%. It is therefore possible that most of the critical current reduction over long lengths is caused by this effect.

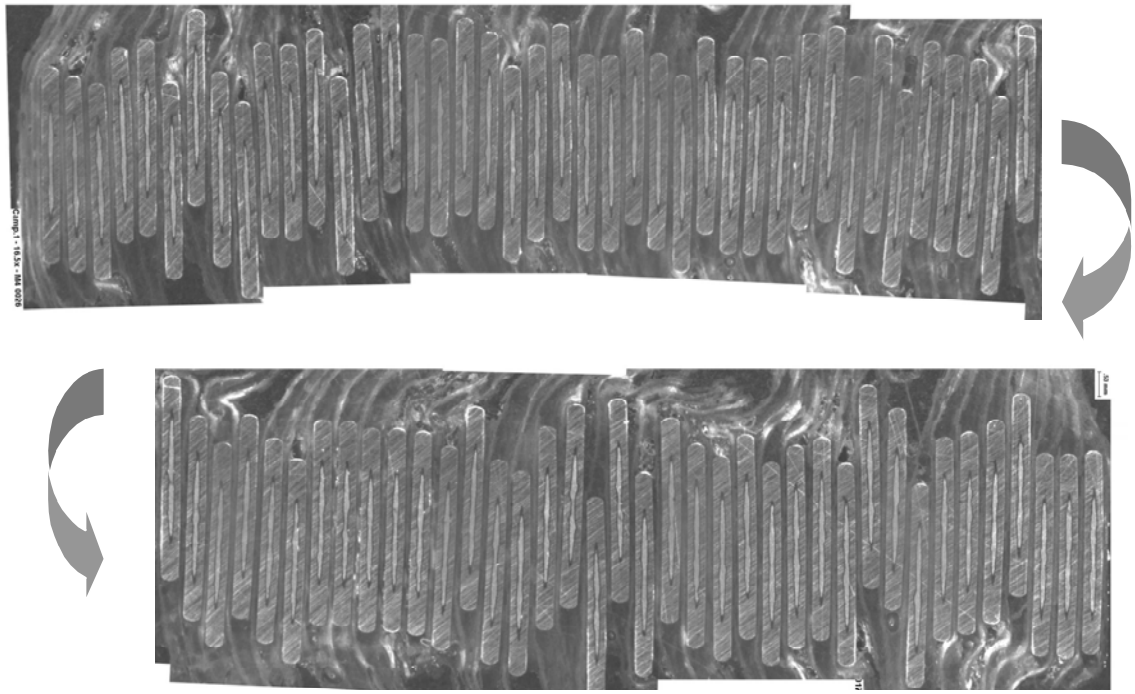

Fig. 5: Cross sectional cut of a pancake realized to study the local fluctuations of the monocore tape transverse cross section along the length.

In order to reduce fluctuation of the superconducting cross section along the tape length, and to improve the tape mechanical properties, multifilamentary conductors are required. Multifilamentary tapes have been therefore prepared as described in the previous paragraph. As Nickel reacts with MgB_2, a very thin Niobium barrier has been introduced between the superconducting core and the matrix material to avoid a strong poisoning of the superconducting core. A typical transverse cross section of a 7-filament tape is reported in fig. 6. The best short samples realized with such a process have reached self field critical current densities very near to that of the monocore tapes, i.e. 10^5 A/cm^2 and 10^6 A/cm^2 at 30K and 4.2K, respectively. Preliminary testing of the mechanical properties of the multifilamentary tapes have shown that the critical bending strain can be increased to 0.3% without any change in the sheath material. Once developed in long lengths, the multifilamentary conductors will be therefore able to better withstand the conductor handling and winding during the pancake manufacturing by the R&W technique.

Fig. 6: Transverse cross section of a multifilamentary tape with similar critical current than the monocore ones. A diffusion barrier in Niobium is present around each filament.

4. CONCLUSIONS

In this paper the present state of Nickel sheathed MgB_2 superconducting tapes has been presented. Monofilamentary tapes have been already manufactured in pieces up to 100 meters in length, and used to wind pancakes. High critical currents have been measured at temperatures up to 20 K in moderate applied magnetic fields. The characterization of the short and long lengths has shown that monocore tapes are not the ideal configuration to be employed for the realization of windings. Fluctuations of the superconducting filament cross section, and its brittleness make R&W pancakes hardly feasible with a similar critical current level of the short lengths. Recent advances in the cold working procedure has allowed to realize multifilamentary tapes that show similar critical currents than the monocore ones, but capable of sustaining a larger bending strain and hopefully with a lower fluctuation of the superconducting cross section. If the development of these multifilamentary conductors will be successfully extended to lengths exceeding 1000 meters, it is expected that this conductor will become very attractive both for DC and AC applications operated in the temperature range between 20 and 30 K.

5. ACKNOWLEDGEMENT

The authors acknowledge the financial support of the European Network Human Potential Programme contract n. HPRI-1999-CT-00030 for the experiments performed at GHMFL.

6. REFERENCES

[1] J. Nagamatsu, N. Nakagawa, T. Muranaka, Y. Zenitani and J. Akimitsu, Nature 410 (2001) 63.
[2] Y. Huang et al., presented at MRS Fall Meeting 2003, Boston(USA), 1-5 Dec 2003, to be published in Proceedings.
[3] Y. Bugoslavsky, G. K. Perkins, X. Qi, L. F. Cohen, and A. D. Caplin, Nature 410 (2001) 563.
[4] S. Jin, H. Mavoori and R. B. van Dover, Nature 411 (2001) 563.
[5] S. Soltanian, X.L. Wang, I. Kusevic, E. Babic, A.H. Li, M.J. Qin, J. Horvat, H.K. Liu, E.W. Collings, E. Lee, M.D. Sumption and S.X. Dou, Physica C 361 (2001) 84.
[6] H. L. Suo, C. Beneduce, X. D. Su and R. Flükiger, Supercond. Sci. Technol. 15 (2002) 1058.
[7] P. C. Canfield, D. K. Finnemore, S. L. Bud'ko, J. E. Ostenson, G. Lapertot, C. E. Cunningham and C. Petrovic, Phys. Rev. Lett. 86 (2001) 2423.
[8] G. Grasso, A. Malagoli, C. Ferdeghini, S. Roncallo, V. Braccini, M. R. Cimberle, and S. Siri, Appl. Phys. Lett. 79 (2001) 730.
[9] H. Kitaguchi, H. Kumakura, and K. Togano, Physica C 363 (2001) 198.
[10] A. D. Caplin, Y. Bugoslavsky, L. F. Cohen, L. Cowey, J. Driscoll, J. Moore and G. K. Perkins, Supercond. Sci. Technol. 16 (2003) 176.
[11] V. Ferrando, P. Manfrinetti, D. Marré, M. Putti, I. Sheikin, C. Tarantini, and C. Ferdeghini, Physical Review B, 68 (2003) 94517.

STATUS AND PERSPECTIVES FOR TECHNICAL USE OF MgB_2 WIRES

Sonja I. Schlachter, Wilfried Goldacker
Forschungszentrum Karlsruhe, Institut für Technische Physik, P.O. Box 3640, 76021 Karlsruhe, Germany

Abstract
Since the announcement of the discovery of superconductivity in MgB_2 in 2001 a lot of work has been done worldwide to develop wires and tapes for technical applications. The comparatively high T_c of 39 K and the absence of weak link behavior in MgB_2 raise hope to use MgB_2 as a cheap conductor at elevated temperatures around 20 K, replacing or complementing NbTi wires or HTS tapes. Although first applications of MgB_2 wires are currently arising, many obstacles have still to be overcome before MgB_2 can be used as a technical conductor. The main efforts worldwide concentrate on the improvement of current carrying capability, enhancement of irreversibility and upper critical field and on the improvement of thermal and mechanical stabilization of the conductors.
In this paper we illustrate the current status of MgB_2 wire and tape development and present a first technical application. As an outlook we highlight the perspectives for technical MgB_2 wires and for using these conductors in magnets, current leads, etc.

1. INTRODUCTION

The discovery of superconductivity in the binary compound MgB_2 by Akimitsu et al. 2001 [1] initiated a worldwide intensive investigation of this material as thin film, bulk and from the beginning also already as a wire or tape composite. The critical temperature of 39 K, the highest among many superconducting borides and borocarbides so far [2], motivated the R&D activities due to the chance having a new superconductor in between the LTS and HTS materials which can be cooled cryogen free with GM- or pulse-tube coolers to an operation temperature of about 20 K. The hope to raise the critical temperature by substitutional alloying was not successful yet and will be limited to negligible effects regarding the state of the art knowledge about the properties of MgB_2. Although MgB_2 has an anisotropic layered hexagonal crystal structure (P6/mmm) with alternating Mg and B layers (see Fig. 1)

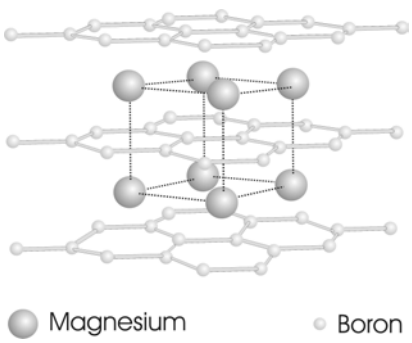

Fig. 1: AlB_2-type crystal structure of MgB_2 with alternating Mg and B layers

and anisotropic properties with respect to thermal expansion, compressibility, resistivity, critical current, irreversibility field and upper critical field, granularity as in the HTS perovskite $YBa_2Cu_3O_x$ was not found. The explanation for this positive feature is a sufficient large coherence length of $\xi_{ab} = 10$ nm (in plane) and $\xi_c = 5$ nm (out of plane parallel *c*-axis) [3]. Therefore already quite early high transport currents were realised in wire and tape composites made by the powder in tube (PIT) technique applying different sheaths of Fe, Nb, Ta, Ni, Monel, Cu, steel, etc. and precursors from commercial MgB_2 (ex-situ method) and Mg+B powder mixtures (in-situ methods). The magnetically measured current densities in self field exceeded 10^6 Acm^{-2} at 4.2 K, which is comparable to the technical and commercial low T_c superconductor NbTi. For MgB_2 conductors a heat treatment of the final wire at $T = 600$-$900°C$ is applied to sinter the MgB_2 grains to a compact filament (ex-situ route) or to react the phase from the elements regarding the in-situ route.

Thin films, commonly *c*-axis textured, gave the first indication for quite high upper critical fields of 40 T ($H \parallel a,b$) [4] and more in this material. The irreversibility field in thin films, wires and tapes is usually 5-10% lower than H_{c2}. Recent theoretical considerations on the paramagnetic limit expect possible upper critical fields up to 70 T [5]. In a specific thin film sample the critical current density of 200 $kAcm^{-2}$ (self field) showed a surprising low field dependence up to high fields of 10-12 T at 4.2 K, indicating that effective flux pinning is a key to improved conductors and a sufficient thermal stabilisation necessary at low fields to avoid thermal driven transitions. The results in thin films however still scatter in a large range, since the applied different preparation methods are not trivial and not reproducible due to the difficulties in processing the quite volatile element Mg in a vacuum deposition process.

In the first wires and tapes upper critical fields were only in the range of 15 – 17 T [6]. The quite recent progress of the preparation methods towards small sized MgB_2 grains led to significantly improved upper critical fields and irreversibility fields.

For technical conductors, additional properties as mechanical strength and thermal stabilization are important. The mechanical properties depend strongly on the composite structure, the choice of the sheath materials and the heat treatment temperature. The critical currents show a slight reversible degradation under the compressive prestress originating from the sheath [7]. A moderate steel reinforcement can enhance the mechanical properties of the wires significantly, higher steel contents lead to irreversible degradations of the critical current density [8]. An effective or sufficient thermal stabilization of MgB_2 wires is presently not given and would require a multifilamentary structure with very thin filaments of a few micrometer in diameter and a low resistance sheath which can carry the normal current above I_c. These properties are not realized yet, for high transport currents in low fields most conductors quench well below the critical current and burn through in the high current regime (low temperature and field).

2. PREPARATION METHODS FOR MgB_2 CONDUCTORS

MgB_2 conductors are prepared by means of the powder in tube technique (PIT), with the choice of two different precursor routes, either with pre-reacted MgB_2 powder (ex situ method) or with powder mixtures of Mg and B (in situ method). The powder is filled into a metal tube and deformed to a wire or tape. Ex-situ or in-situ refers to the phase formation before manufacturing the PIT conductor or forming the phase in the final conductor from the elements applying a heat treatment, respectively. For some improved preparation routes Mg alloys [9] or boron compounds [10] are used as precursors or the precursors are mixed with fine powders of a secondary minority phase [11].

The ex-situ method has the advantage that the MgB_2 particle size can be adjusted by grinding processes, leading to small grains in the filament for enhanced flux pinning [12]. With this route cold worked ex-situ conductors can be produced, which are not only suitable for a cheap industrial production process but also allow the use of a wide selection of sheath materials [13]. However, cold worked PIT conductors have a limited filament densification, much lower currents and poorer

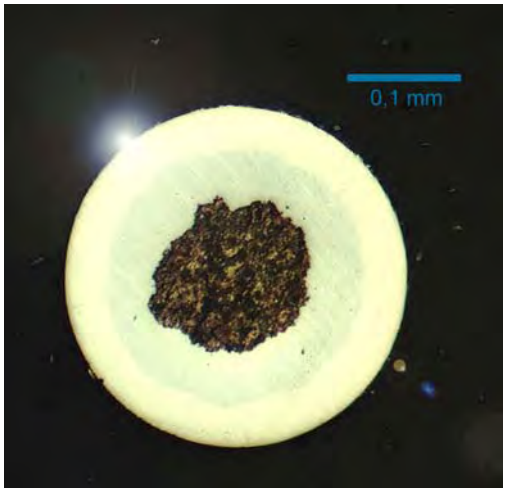

Fig. 2: Optical micrograph of a MgB_2/Fe/SS current lead wire cross section (Ø = 310 µm)

mechanical properties. Therefore the application of a heat treatment is commonly preferred since it provides well connected grains [14] and better mechanical properties of the conductor [15]. The ex-situ route has the disadvantage that favourably a heat treatment has to be applied at quite high temperatures of 900-950°C to sinter the MgB_2 grains dense via a decomposition-reformation process. However, since MgB_2 has no defined melting point and decomposes at T > 900°C the sinter effect is limited and the danger of thick chemical reactions with the sheath is favoured, as commonly observed.

The in-situ phase formation takes place at much lower temperatures of 600-650°C and has the advantage that the in-situ MgB_2 formation leads automatically to very well connected grains. A disadvantage of this route is that the final MgB_2 grain size in the filament depends on nucleation and grain growth and the mixture and grain size of the Mg and B powders. Actually the in-situ method is more and more preferred since the chemical reaction with the sheath is reduced for the low-temperature processing methods and a good grain connection is achieved [16].

Both fundamental conductor geometries, round wires and flat tapes are developed by the different

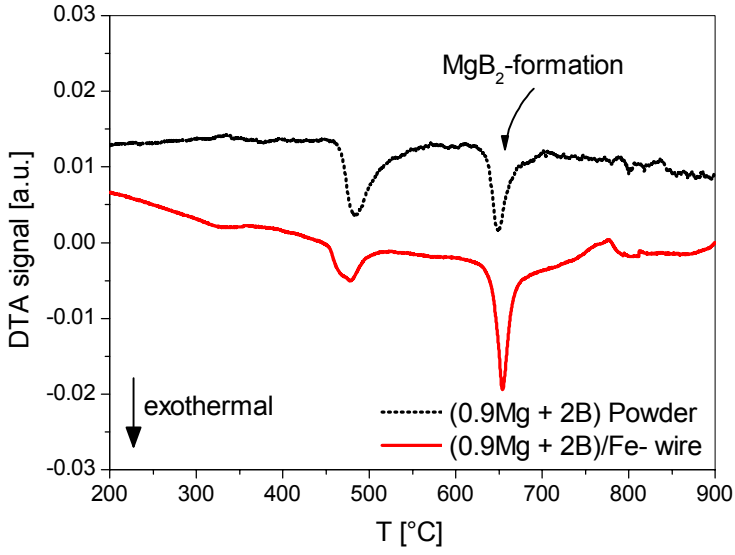

Fig. 3: DTA characterisation of a MgB_2/Fe wire and the corresponding Mg + B precursor powder mixture

Fig. 4: SEM image of MgB_2 phase in the filament of a MgB_2 /Fe wire

groups worldwide. Tapes give the chance to take advantage of the anisotropy of the superconductor via a textured MgB_2 phase [17]. Although indeed a current anisotropy was reported in tapes, especially in higher fields, the advantage for the critical currents is limited, since the mechanism achieving the texture is a mechanical orientation of grains close to the filament sheath interface and the texture effect is limited to this part of the filament. However for future much thinner filaments this option has to be considered again. Another advantage of tapes is the high densification of the filament material due to the high rolling pressure during deformation which improves the density of MgB_2 [18]. Therefore tapes often show higher current densities compared to wires. Round wires are the preferred conductor geometry for layered windings in coils and much better suited for low AC loss conductors, especially for applying a filament twist.

As sheath materials Fe, Cu, Nb, Ta, Steel, Ni and different alloys are used, which allows or requires different annealing temperatures. Fe has the overall best properties and Cu a stronger chemical reaction with the filament during heat treatments, Nb and Ta negligible chemical reaction but an unfavourable thermal expansion coefficient and Steel and Ni in contact to the filament react strongly during the heat treatment and are used for cold processed conductors only.

Multifilamentary conductors were rarely presented so far since the current densities are commonly smaller compared to monocores due to filament inhomogeneities and irregularities of the geometry from sausaging effects.

3. METHODS TO OPTIMISE THE CRITICAL CURRENT DENSITIES

As in the classical LTS superconductor Nb_3Sn, flux pinning in MgB_2 occurs at the grain boundaries or defect structures and scales with the grain size or defect density. Different methods can be applied to improve flux pinning. Successful examples are:

- Controlled phase formation: a control of the nucleation and growth process of MgB_2 in in-situ processed wires from commercial powders was achieved by applying a heat treatment with partial phase reaction during the deformation and a final heat treatment at quite low temperatures of 640°C, the low temperature onset of the phase formation regime, which favours nucleation and limits the grain growth. For round wires with commercial Mg and B precursors the highest current densities were achieved comparable to the best tapes.

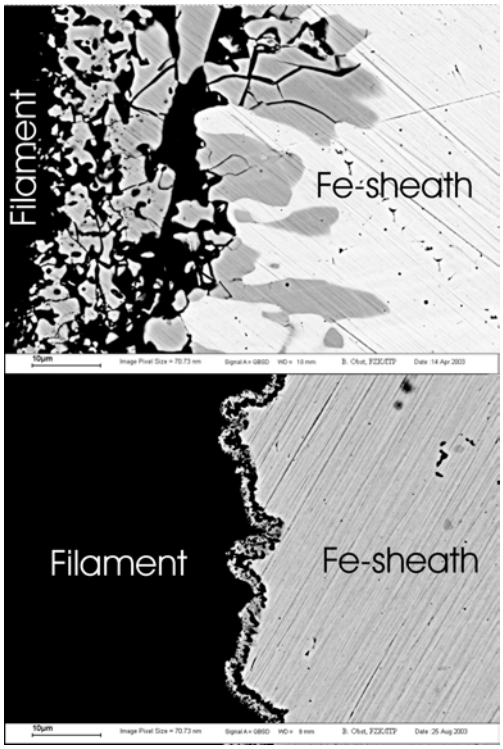

Fig. 5: Reaction layer at the filament sheath interface of MgB_2 /Fe wires heat treated at 905°C (top) and at 640°C (bottom)

- Neutron irradiation of such wires created an additional defect structure in the scale of several nanometers and led to significantly further improved current densities, irreversibility fields and upper critical fields, indicating that the density of flux pinning centers was not at an optimum in the unirradiated wires [19, 20].
- Mechanically alloyed precursors (intensive milling of powders from the elements) led to a mixture of the elements in the nanometer scale and a beginning phase formation. DTA measurement showed that the reaction temperature was significantly reduced to about 500°C [21].
- SiC secondary phase particles in the nanometer scale added to the filament in a fraction of 5-20% is presently the most effective method to create homogeneously distributed pinning sites and enhances the current densities by nearly one order of magnitude at higher fields [11, 22].
- Improved Mg precursor powders processed by plasma spraying with a grain size of 300 nm, induced also small MgB_2 grains and improved the current densities and the critical field values H_{irr} and H_{c2} [22].

For some examples and routes also a decrease of the phase formation temperature was observed. An example is the tape from mechanically alloyed powder [21].

There are additional more or less effective combinations of MgB_2 with secondary phase particles which proof that particle additions in the nanometer scale, which do not react with MgB_2 during the heat treatment, are a practical way to limit the grain size of the MgB_2 phase and to enhance the density of pinning sites in the filament.

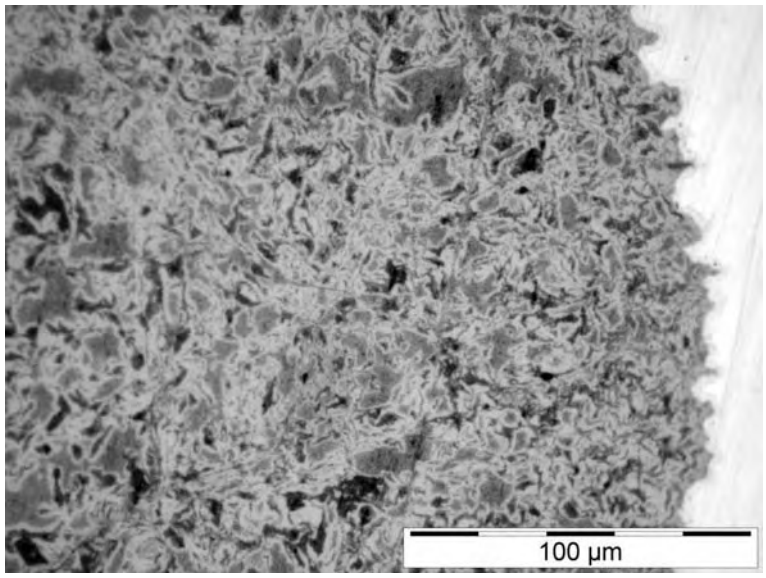

Fig. 6: Optical micrograph of the filament section of a MgB_2/Fe wire heat treated at 640°C showing the meander like layered MgB_2 phase (light colour) and the Boron rich secondary phase (dark grey colour)

4. EXAMPLE OF A MECHANICALLY REINFORCED IN-SITU MgB_2 WIRE WITH THIN FILAMENTS FOR SPACE APPLICATION

In this section we present some characteristics and limitations of MgB_2 conductors taking as an example a very thin stainless steel reinforced MgB_2 wire, developed for a satellite application. In this case a mechanical reinforcement and a wire thickness as small as possible to keep the thermal conductance low and an operation current of 2 Amps DC below 17 K was demanded.

4.1 In-situ preparation applying a low-temperature heat treatment

Thoroughly mixed commercial Mg powder and amorphous Boron powder (both -325 mesh) with an atomic Mg/B ratio of 0.9/2 were filled in Fe tubes of 99.5% purity (10 mm outer diameter, 1.5 mm wall thickness) and swaged down to 1.8 mm with two intermediate heat treatments at 600-620°C to release stresses in the Fe sheath. During these heat treatments a partial reaction of the MgB_2 phase takes place. In a next step the wires were inserted into precision stainless steel (SS) tubes (AISI 316) of 2.5 mm outer diameter and 0.3 mm wall thickness and drawn to a final diameter of 310 µm (see Fig. 2 with a further intermediate heat treatment to release stresses in the sheath. The final low temperature annealing was performed at 640°C for 1h with subsequent furnace cooling. To limit the reaction kinetics, the annealing temperature was set at the low temperature onset of the exothermal phase formation dip in the DTA curve which has its minimum at 650°C, corresponding to the melting point of Mg, as shown in Fig. 3. The final wire cross section is composed of approximately 20% MgB_2, 40% Fe, 40% SS, the filament diameter is approximately 140 µm. During deformation samples were extracted from the batch at some thicker wire diameters and annealed to investigate the influence of the filament thickness on the current carrying capacity. SEM pictures of the filament microstructure showed MgB_2 grains in the scale of 10-20 microns, an indication of an effective nucleation (Fig. 4). The reaction with the Fe sheath was strongly reduced to a layer of only 1-2 µm thickness (20-30 µm for annealing at 900°C) as shown in Fig. 5. The resulting microstructure of MgB_2 looks layered like a pastry, obviously forming an effective percolation path for the supercurrents (Fig. 6).

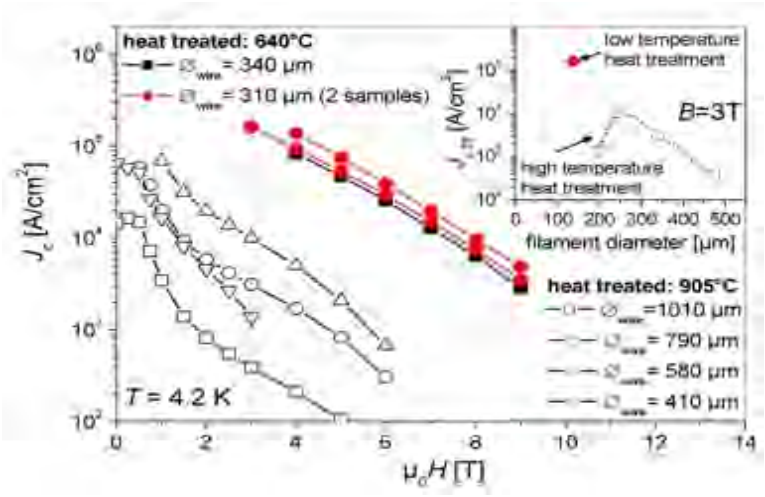

Fig. 7: Transport critical current density $J_c(B)$ of current lead wires, old batch = high temperature heat treatment at 905°C (3 samples having thicker filaments for comparison) and new batch = low temperature heat treatment at 640°C. The insert shows the correlation of the critical current density with filament diameter at B=3 T

4.2 Enhanced transport critical currents, irreversibility fields and upper critical fields

In Fig. 7 the transport critical current densities of in-situ wires with small filaments (∅ = 310 µm and 340 µm) and low temperature heat treatment and the former batch (high temperature annealing) from ref. [16] are shown together. In the insert the dependence of the current densities on filament thickness is given. For the former batch the critical current density increases with decreasing diameter down to 200-250 µm, but further reduction of the filament diameter leads to a decrease of J_c. An

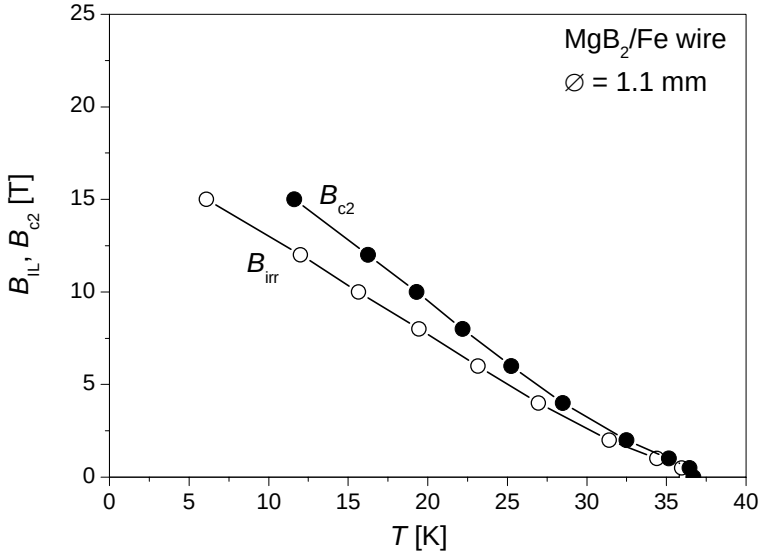

Fig. 8: Irreversibility field B_{irr} and upper critical field B_{c2} with temperature obtained from electrical resistivity transitions for a MgB_2/Fe wire. The values were determined as described in the text

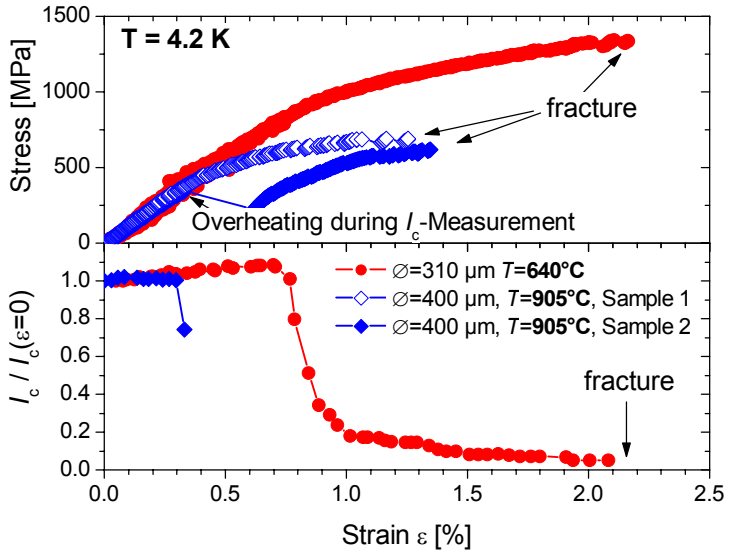

Fig. 9: Critical current and tensile stress vs. axial strain for an MgB_2 current lead annealed at low temperatures (T = 640°C). Equivalent data for 2 samples annealed at high temperatures from ref. [16] are added for comparison

critical current densities were 150 kAcm^{-2} at 4T, 40 kAcm^{-2} at 6 T and 10 kAcm^{-2} at 8 T (4.2 K) for the 310 µm thick wire. However below 3-4 T the wires are not sufficiently stabilized for high transport currents and burn through exceeding a definite current level.

The field dependent resistive T_c transitions $R(T,B)$ of the wires with 650-750 µm thick filaments (wire diameter 1.1 mm) were measured with small constant DC currents of I = 30 mA. For each magnetic field the temperature for the upper critical field $T(B_{c2})$ was determined from $R(T)$ as the temperature where $R = 0.9 \cdot R_{normal}$ and the temperature for the irreversibility field $T(B_{irr})$ was determined as the temperature, at which the electric field between the voltage tabs is 1 µV/cm. In Fig. 8 these data are plotted as $B_{c2}(T)$ and $B_{irr}(T)$. A linear extrapolation of $B_{c2}(T)$ and $B_{irr}(T)$ to T = 0 K gave values of 18 T and 22 T respectively, which are remarkable high for non doped MgB_2 round wires made from commercial non modified powders.

4.3 Mechanical properties

The critical current as a function of axially applied strain given in Fig. 9 was measured at 4.2 K in small background fields of 0.5 or 1 T (to reduce the currents and to avoid overheating). Measurements of two wires from the former batch with different steel contents (40 % and 30 %) are also shown. The former samples showed already a degradation of the critical current at 0.27 % and 0.3 % strain since the steel clad was softened through the high annealing temperature. With the first strain induced crack in the filament one sample burned through immediately and the second became hot in the crack section, which caused plastic deformation in the sheath and a related drop in the load display. The second wire with already broken filament could be strained further until final fracture at 1.5 % strain. The tolerable stresses were 320 MPa and 350 MPa, respectively, and the yield strength (0.2 % strain) was 220 MPa.

Contrary the wire with low temperature treatment showed a strongly improved mechanical performance. Tolerable strains of 0.7 % without current degradation were observed, corresponding to stresses of about 800 MPa. The main reason for this improvement is attributed to the low annealing temperature of 640°C, which is low enough to avoid softening of the stainless steel clad. The crack

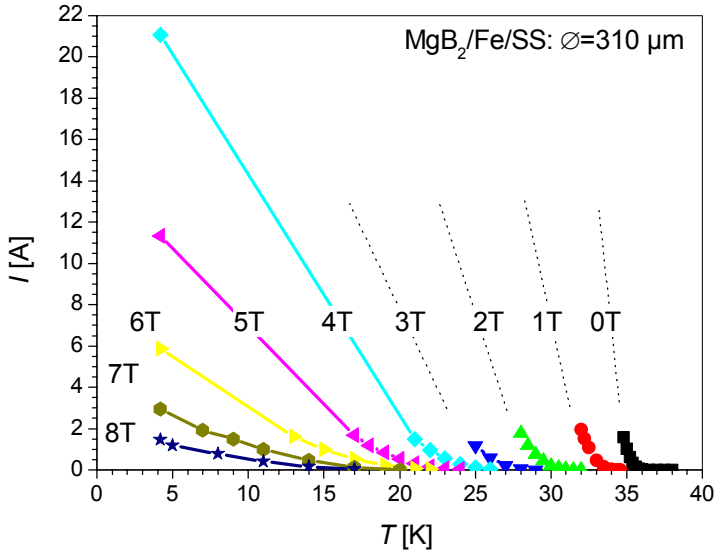

Fig. 10: Transport critical currents of MgB_2/Fe/SS current lead wires with field and temperatures. At $T > 4.2$ K the currents were measured with a Quantum Design PPMS device (I limited to I_{max}=2A)

formation in the filament occurs steadily and not as abrupt as it is the case in the former wires, obviously favoured by an effective transverse compressive stress component in the filament which keeps the filament material compact.

The recovery of the critical current density upon strain can also be understood. It was shown that T_c is reduced under pressure in particular under non hydrostatic stress conditions. [24,25]. If the precompression of the thermal stress of the matrix is compensated by applied external tensile stress, improved superconducting properties are the consequence. This behavior is very similar to Nb_3Sn wires or Chevrel phase wires and very favourable for technical use.

4.4 Thermal stability

A detailed investigation of the whole $E(I)$ transition in MgB_2 conductors gave some information about the onset and contribution of thermal effects. Such effects were found at all current levels and background fields and depend on the transport current density level [26]. At high transport currents, thermal effects can significantly increase the slope of $E(I)$. As a consequence the calculated n-values become larger and may be overestimated. A contribution of such a successive energy dissipation to the shape of the $E(I)$ transition is very difficult to detect especially for small E-values, the observed heat fluctuations however indicate their presence. The comparison of different MgB_2 monofilamentary wires showed that both a homogeneous microstructure and a high current carrying percolation path have a significant influence on the intra-filamentary thermal stabilisation, the occurrence of hot spots and the dissipation of the energy approaching I_c. The distribution of the local critical currents and current density, a consequence of the microstructure, especially inclusions of secondary phases, plays an important role for the ignition of the complete quench at high transport currents. For the low temperature heat treatment surprising low n-values of only 15 not depending on background field were observed in one sample batch. An explanation might be the presence of an effective percolation path and an intra-filamentary current sharing at I_c [26].

For the presented thin MgB_2 wire, transport critical currents at higher temperatures and in fields are given in Fig. 10 and n-values determined from the I-V curves are shown in Fig. 11. Plotting the n-values versus transport currents indicates the presence of thermal effects by the deviation from a linear behaviour (left side of Fig. 11). The large reserve for the demanded transport currents of 2 Amps at 17 K and below (seeFig. 10), allows the use of these wires in the satellite application.

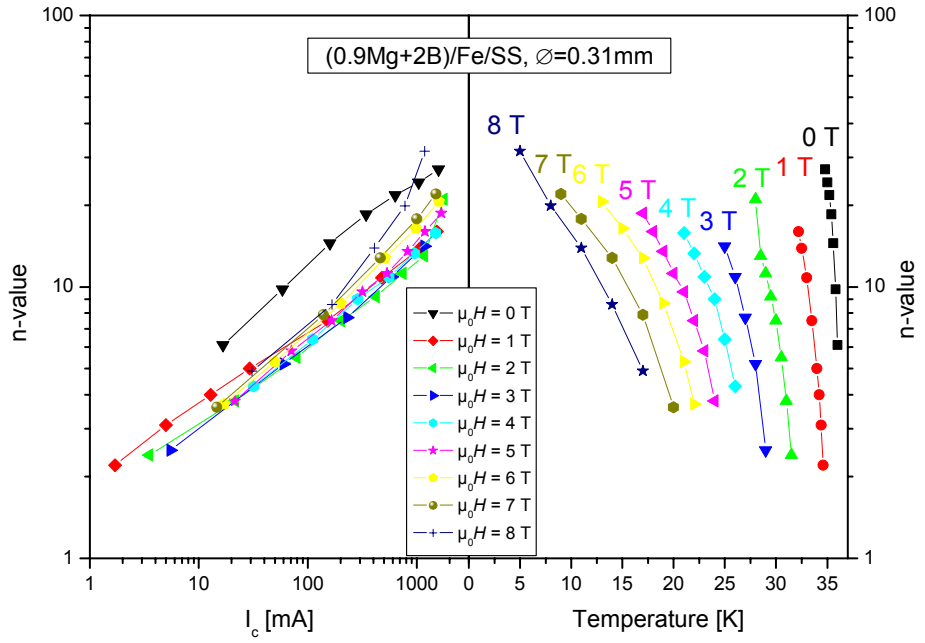

Fig. 11: *N*-values calculated from *E(I)* transitions in the range 0.5-5 μV/cm for the critical current data of Fig.10, plotted versus transport critical current (left side) and temperature (right side)

For a final statement about the true intrinsic *n*-values of MgB_2 filaments and for the development of a stabilised technical conductor, a multifilamentary structure with thin filaments, homogeneous microstructure, regular filament geometry and a sufficient external thermal stabilisation is absolutely necessary to eliminate the contribution of heat generation to the I_c transition in the filaments.

5. COMPARISON WITH THE MOSTLY ADVANCED FABRICATION METHODS

As already mentioned above, different methods were successful to enhance the critical current density in MgB_2 wires and tapes. Already an optimisation of the precursors using smaller particles [22, 12] or applying low temperature heat treatments [16] leads to smaller grains in MgB_2 and an enhancement of the critical current densities and the critical fields, irreversibility field and upper critical field. Neutron irradiation induced in addition a defect structure in the scale of a few nanometer, which led to a further enhancement of the critical current density and shows that the flux pinning site density was still too low. More effective is doping of MgB_2, in particular with SiC particles of nanometer size. Comparing the critical current densities of the advanced MgB_2 conductors in Fig. 12 illustrates the effect of improved pinning, the slope of the *I*(*B*) curve becomes smaller which correlates with higher current densities at higher fields and improved H_{c2}. However, all advanced conductors have a common disadvantage, the onset of the critical temperature is shifted to lower values by up to a few Kelvins. This effect has negative influence on the critical currents and upper critical fields at 20 K. Table 1 gives some characteristic data for the advanced conductors.

Table 1: Comparison of the critical current densities $J_c(B)$ of MgB_2 /Fe wires and tapes with different precursors at 4.2 K and 20 K.

Method	J_c [kA/cm^2] at 4.2 K, 7T	J_c [kA/cm^2] at 4.2 K, 9T	J_c [kA/cm^2] at 20 K, 3T	Reference
Commercial Mg, commercial B	20.6	5.8		This Work
Mechanical alloying	39.7	11.6	9.4	Fischer *et al*. [21]
10 % SiC-doping	58.5	16.2	60	Dou *et al.* [11]
Nano-Mg Commercial B	48.9	27.6		Yamada *et al.* [22]
Nano-Mg + 10 % SiC-doping		40		Yamada *et al.* [22]

6. OUTLOOK TOWARDS TECHNICAL WIRES AND APPLICATIONS

With the example of a thin reinforced MgB_2 wire for a satellite application, the possibly first application of MgB_2 was achieved. The mechanical data were excellent meeting all technical requirements so far. In this special application a large reserve of the transport current was given, which allows the risk to use a non thermal stabilized conductor.

One of the main challenges to approach technical MgB_2 conductors which possess all necessary features is an improved preparation technique for a multifilamentary composite structure with small filaments and regular filament and conductor cross section geometry. Sausaging of the filaments, a typical hint of the PIT route, and secondary phase inclusions have to be avoided since both serve as a source for hot spots and thermal instability. So far multifilamentary conductors are limited to 7 or 19 filaments and show a degradation of the critical currents compared to the monocores. In addition a low resistive sheath, preferably Cu, is required in contact with the filament to enhance the thermal stabilization. Reaction layers between filament and sheath have to be eliminated to support the current sharing and energy transfer at the I_c transition. As a consequence improved low temperature preparation routes are required to restrict or avoid the chemical reaction. Modified precursors already showed some progress in this sense and provide an optimistic outlook for improved conductor preparation routes in the near future. Advanced precursors are also asked for an improvement of the MgB_2 microstructure and the incorporation of pinning sites in the nano scale. Further increased values for H_{irr} and H_{c2} in wires approaching the dirty limit and the values already measured in thin films, are crucial for a breakthrough of this material in competition to LTC conductors.

Since the improvement of the current density and critical fields through small MgB_2 grains or doping correlates with a decrease of the critical temperature by a few degrees the application at higher temperatures as 20 K cannot take full advantage of the improvement of the transport current and critical fields. Transport currents and critical fields scale almost linear with temperature between 4.2 K and T_c. From this situation one can estimate that actually an application at 20 K is limited to background fields of about 5 Tesla if the best conductor performance is available in long lengths.

Due to the absence of granularity in MgB_2 the realisation of persistent mode contacts connecting conductor ends seems possible. This is the motivation for the interest in one of the most promising future applications, persistent mode low field MRI coils for 20 K operation. The demonstration of a small MgB_2 coil, which created a field of 1 T at 4.2 K was presented recently [27].Another promising application in energy technique might be the fault current limiter, also operated at temperatures around 20 K. MgB_2 wires are quite suitable for this purpose since the resistivity of the sheath can be selected and adjusted via the choice and combination of the material. If thermally stabilised wires are available the application in motors, generators, transformers and short cables will surely also be

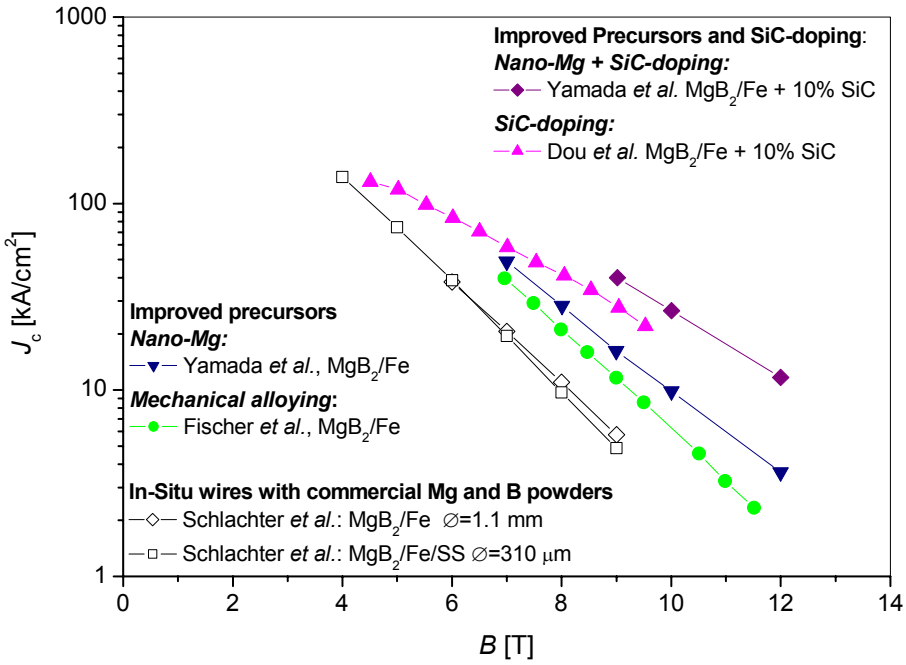

Fig. 12: $J_c(B)$ of a MgB_2/Fe wire (Ø = 1.1 mm) and a MgB_2/Fe/SS wire (Ø = 310 µm) made from commercial Mg and Boron powders without doping (this work) in comparison to $J_c(B)$ of MgB_2/Fe wires with improved precursors. The improvement of precursors and resulting increase of J_c especially in high magnetic fields was achieved by mechanical alloying (Fischer *et al.* [21]), use of Mg powder with nano grain size (Yamada *et al.* [22]), and SiC-doping (Dou *et al.* [11] and Yamada *et al.* [22]).

considered. Nevertheless if the bottlenecks of the PIT-route are overcome and reliable techniques for the industrial production of technical multifilamentary MgB_2 wires are achieved with a performance of the actual best results for the current densities and critical fields, MgB_2 conductors might come into economical competition with NbTi for use at 4.2 K or even for operation close to 20 K. The most successful preparation route actually, MgB_2 doped with 10% nanosize SiC, is already in work for the long length industrial process [27].

REFERENCES

[1] J. Akimitsu; 2001 Symp. on Transition Metal Oxides, 10 January 2001 (Sendai); J. Nagamatsu, N. Nakagawa, T. Muranaka, Y. Zenitani and J. Akimitsu; *Nature* **410** (2001) 63

[2] C. Buzea and T. Yamashita; *Supercond. Sci. Technol.* **14** (2001) R115–R146

[3] A. D. Caplin, Y. Bugoslavsky, L. F. Cohen, L. Cowey, J. Driscoll, J. Moore,G. K. Perkins; *Supercond. Sci. and Technol*. **16** (2003) 176–182.

[4] S. Patnaik, L. D. Cooley, A. Gurevich, A. A. Polyanskii, J. Jiang, X. Y. Cai, A. A. Squitieri, M. T. Naus, M. K. Lee, J. H. Choi, L. Belenky, S. D. Bu, J. Letteri, X. Song, D. G. Schlom, S. E. Babcock, C. B. Eom, E. E. Hellstrom, D. C. Larbalestier; *Supercond. Sci. and Technol*. **14** (2001) 315

[5] A. Gurevich; *Phys. Rev. B 67* (2003) 184515

[6] S. L. Bud'ko, C. Petrovic, G. Lapertot, C. E. Cunningham, P. C. Canfield, M-H. Jung, A. H. Lacerda; *Phys. Rev. B* **63** (2001) 220503(R)

[7] W. Goldacker, S. I. Schlachter, J. Reiner, S. Zimmer, A. Nyilas, H. Kiesel; *IEEE Transactions on Applied Superconductivity* **13** (2003) 3261.

[8] W. Goldacker, S.I. Schlachter; *Physica C* **378–381** (2002) 889.

[9] A Matsumoto, H Kumakura, H Kitaguchi and R Hatakeyama; to be published in *Supercond. Sci. and Technol.* (proceedings of the EUCAS 2003 conference, September 14-18, 2003, Sorrento, Italy).

[10] L.D. Cooley, Kyongha Kang, R. Klie, Q. Li, A. Moodenbaugh, R. Sabatini; http://xxx.lanl.gov/abs/cond-mat/0403130.

[11] S. X. Dou, S. Soltanian, J. Horvat, X. L. Wang, S. H. Zhou, M. Ionescu, H. K. Liu, P. Munroe, M. Tomsic, *Applied Physics Letters* **81** (2002) 3419

[12] P. Lezza, V. Abächerli, N. Clayton, C. Senatore, D. Uglietti, H.L. Suo, R. Flükiger; *Physica C* **401** (2004) 305.

[13] G. Grasso, A. Malagoli, M. Modica, A. Tumino, C. Ferdeghini, A.S. Siri, C. Vignola, L. Martini, V. Previtali, G. Volpini; *Superc. Sci. Technol.* **16** (2003) 271.

[14] A Polyanskii, V Beilin, I Felner, M I Tsindlekht, E Yashchin, E Dul'kin, E Galstyan, M Roth, B Senkowicz and E Hellstrom; Supercond. Sci. and Technol. **17** (2004) 363.

[15] Sonja I. Schlachter, Wilfried Goldacker, Johann Reiner, Silke Zimmer, Bing Liu, and Bernhard Obst; *IEEE Transactions of Applied Superconductivity* **13** (2003) 3203.

[16] Goldacker W, Schlachter S I, Obst B, Liu B, Reiner J, Zimmer S; to be published in Supercond. Sci. and Technol. (proceedings of the EUCAS 2003 conference, September 14-18, 2003, Sorrento, Italy).

[17] H. Kumakura, A, Matsumoto, H. Fujii, H Kitaguchi, K, Togano, *Physica C* **382** (2002) 93.

[18] R. Nast, S.I. Schlachter, W. Goldacker, S. Zimmer, J. Reiner, *Physica C*, **372-376** (2002) 1241

[19] M. Eisterer, B. A. Glowacki, H. W. Weber, L. R. Greenwood, M. Majoros; *Supercond. Sci. and Technol.* **15** (2002) 1088.

[20] S.I. Schlachter, W. Goldacker, B. Obst, M. Eisterer, H.W. Weber; to be published

[21] C. Fischer, W. Häßler, C. Rodig, O. Perner, G. Behr, M. Schubert, K. Nenkov, J. Eckert, B.Holzapfel, L. Schultz; accepted for publication in *Physica C*

[22] H. Yamada and M. Hirakawa, H. Kumakura, A. Matsumoto, H. Kitaguchi; *Applied Physics Letters* **84** (2004) 1728.

[23] W. Goldacker, S.I. Schlachter, B. Obst, M. Eisterer, submitted to Supercond. Sci. and Technol., Feb. 2004.

[24] S. I. Schlachter, W. H. Fietz, K. Grube, W. Goldacker; *Advances in Cryogenic Engineering* **48** (2002) 809.

[25] S. Deemyad, T. Tomita, J.J. Hamlin, B.R. Beckett, J.S. Schilling, D.G. Hinks, J.D. Jorgensen, S. Lee, S. Tajima; *Physica C* **385** (2003) 105.

[26] W. Goldacker, S. I. Schlachter, B. Liu, B. Obst, E. Klimenko, *Physica C* **401** (2004) 80.

[27] M.D. Sumption, M. Tomsic, M. Bhatia, Y. Hascieck, S.X. Dou, E. W. Collings; Presented at the ICMC Topical Conference February 10-13, 2004, Wollongong, Australia

EDISON ACTIVITIES ON HTS AND MgB_2

S. Zannella and G. Giunchi
EDISON S.p.A., Via Ugo Bassi 2, I-20159 Milano, Italy

Abstract
This paper summarizes the main results obtained by Edison in the frame of its R&D activities in the field of High Temperature Superconductors (HTS) and the recently discovered MgB_2. Several processes are under development for their fabrication and the market penetration will be determined essentially by their cost and the exhibited electrical performances. Our efforts are focused on the continuous deposition of HTS layers on metallic substrates, by electrochemical and vacuum based technologies, and on the fabrication of MgB_2 manufacts, bulk and filaments, by liquid Mg infiltration.

1. Y-123 COATED CONDUCTORS

$YBa_2Cu_3O_{7-\delta}$ Coated Conductors (CC) have gained a great deal of attention thanks to their high critical current density, above 1 MA/cm^2 at 77 K, weakly dependent on magnetic fields. High current densities CC's have been demonstrated by many groups using Rolling Assisted Biaxially Textured Substrates (RABiTS) [1, 2] made of Ni and Ni-alloys. The intermediate deposition of a buffer layer is required to enable a textured growth of the YBCO layer and to prevent interdiffusion of metallic and spurious nickel oxide particles into the superconducting YBCO layer. Among the in-situ vacuum techniques, we selected the thermal co-evaporation process for its relatively low cost associated with its inherent capability to prepare high quality YBCO films uniformly over large areas [3] at relatively low temperatures below 700 °C.

Biaxially textured pure Ni and Ni-5at.%W alloy tapes have been employed as flexible metallic substrates. The tape fabrication and properties are described in detail elsewhere [4]. The 80 μm thick metallic tapes are characterized by a surface roughness better than 15 nm. To enable a continuous deposition, the vacuum chamber has been equipped with a reel-to-reel system (see figure 1) and with vibrating conveyors. The latter enable to refill in-situ the evaporation sources containing the different precursors. YBCO/CeO_2 layers have been grown as described in detail elsewhere [5, 6]. The continuous process consists of the following sequential steps: i) tape recrystallization and surface treatment, ii) 100 nm thick CeO_2 film deposition and iii) 0.5-2 μm

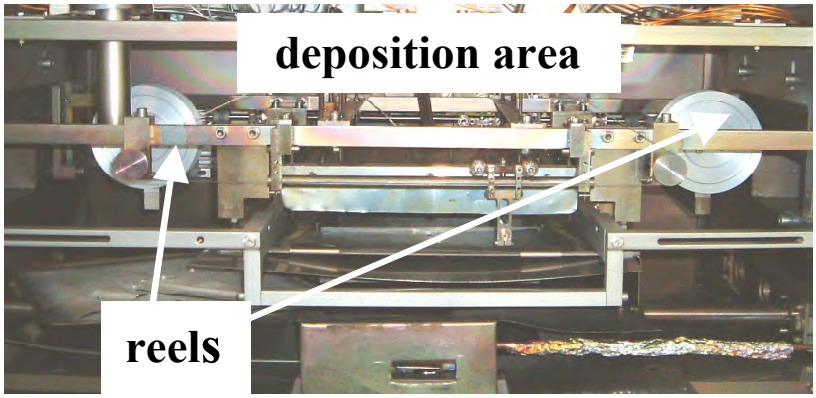

Fig 1. Reel-to-reel system for the continuous deposition of long length YBCO CC.

thick YBCO layer deposition. At the end of the process the chamber is backfilled with 500 mbar of oxygen and the samples cooled down to room temperature.

After recrystallization Ni tapes have been found to be full cubic {001}<100> biaxially textured with in-plane and out-of-plane full width half maximum (FWHM) values ≤ 8°. The degree of biaxial texture for both CeO_2 and YBCO layers have been studied. In figure 2(a) and 2(b) are reported the (111) CeO_2 and (113) YBCO layers pole figures, respectively. Typical in-plane and out-of-plane FWHM values are ≤ 6° for both CeO_2 and YBCO layers.

The morphological analysis are carried out by means of scanning electron microscopy (SEM). In figure 3(a) is shown typical smooth and crack free YBCO layer surface, which accounts for the excellent superconducting performances of the YBCO film. Cross section SEM image, depicted in figure 3(b), shows a very uniform and dense 1 μm thick YBCO layer

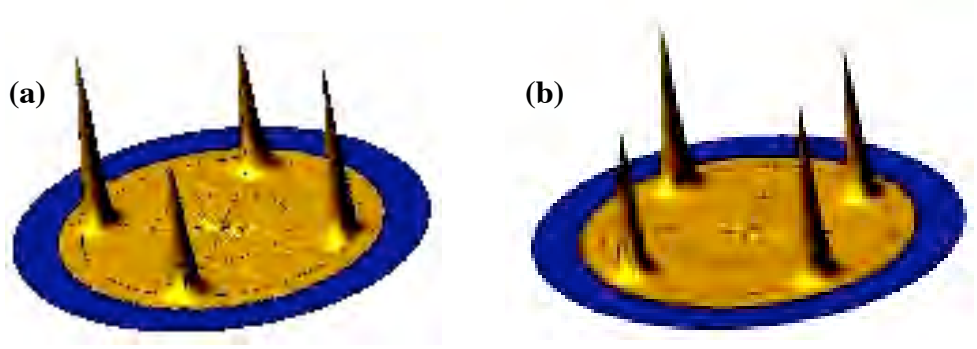

Fig. 2. (a) (111) CeO_2 peak and (b) (113) YBCO peak pole figures.

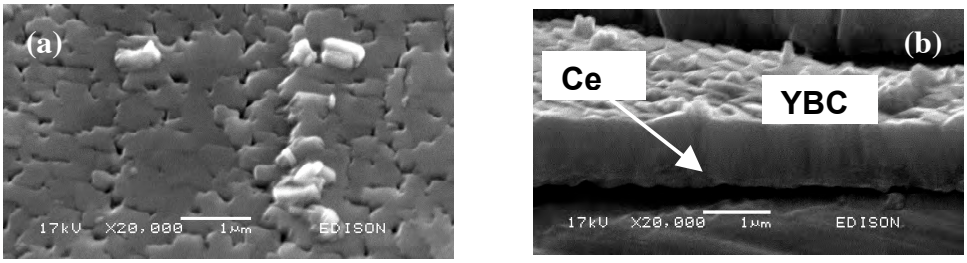

Fig. 3. (a) SEM picture of YBCO surface; (b) cross section of 1 μm thick YBCO film onto CeO_2 / Ni tape.

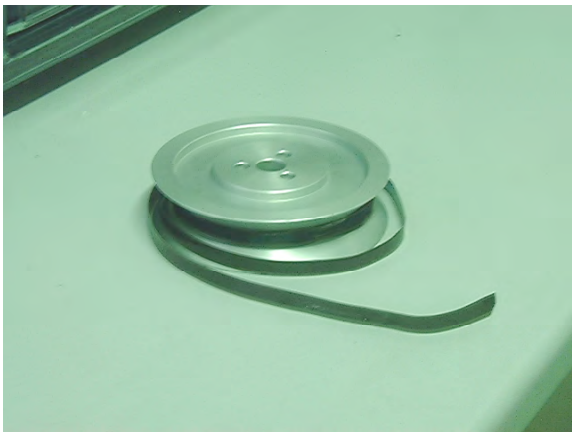

Fig. 4. 1 meter long YBCO coaterd conductor.

Remarkable critical current densities at 77 K, in the range 1-3 MA/cm^2 , have been obtained on 20 cm long YBCO CC by static and continuous deposition, suggesting that this route is scalable to an industrial process for the production of long coated conductors. Recently we succeeded to fabricate 1 meter long YBCO CC's (see Fig. 4). End-to-end critical current densities J_C of 0.6 μm thick YBCO, in the 1÷2 MA/cm^2 range, at 77 K self field, have been measured by transport measurements.

2. ELECTRODEPOSITED BI-2212

In the framework of the HTS coated tape activity EDISON is also studying a continuous process for the electrochemical deposition of Bi-2212 film on several meter long silver tapes. The process is based on sequential elemental depositions and alternate thermal treatments[7], see Figure 5.

The pilot plant to perform the BSCCO-2212 deposits on both sides of Ag tapes is built up through three main units, see Figure 6:

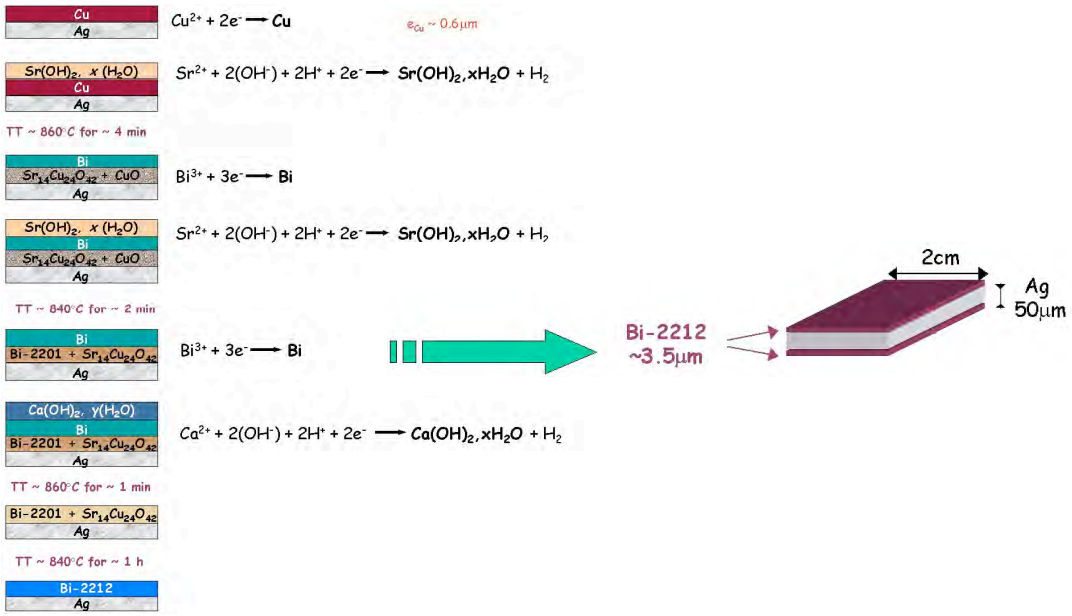

Fig. 5. The electrochemical process for Bi-2212 tapes.

a) the electrowinning copper section (Fig. 6a), in which the Ag tape (20mm wide and 50 μm thick) moves through a washing section, a coppering section and a final washing and drying section. (typical tape's speed of this section is 1m/minute);b) the modular Bi, Sr, Ca electrodeposition sections (Fig. 6b),that is followed by two washing section and a winding-on reel (typical tape's speed of this section is 30 cm/minute);

c) the heat treatments furnace (Fig. 6c), in which all the intermediate thermal treatments are performed passing the tape through a 5-stages tubular vertical oven with cooled heads (typical tape's speed of this section is 30 cm/minute).

The longer final heat treatment, of the order of 1 hour is made at the moment batch wise.

Fig. 6. Pilot plant for Bi-2212 : a) copper electrowinning ; b) Bi, Sr, Ca electrodeposition cells, c) furnace.

Starting from a 15 m long Ag tape we have produced several superconducting Bi-2212 tapes of good quality (some tens of cm long and 1 cm wide), see Figure 7. The Bi-2212 phase in small scale laboratory sample is very pure, in the pilot plant sample at the moment presents dark grains, due to the secondary phase, $(Sr,Ca)_{14}Cu_{24}O_{41}$, as detected by microanalysis. In Figure 8 the morphology of the deposited Bi-2212 film are displayed. In Figure 9 it is shown the electric field versus current density curve for a 20 cm long sample. The transport measurement is at 77 K in self-field.

Fig. 7. A strip of the Bi-2212 coated tape , with voltage taps for transport V(I) measurement

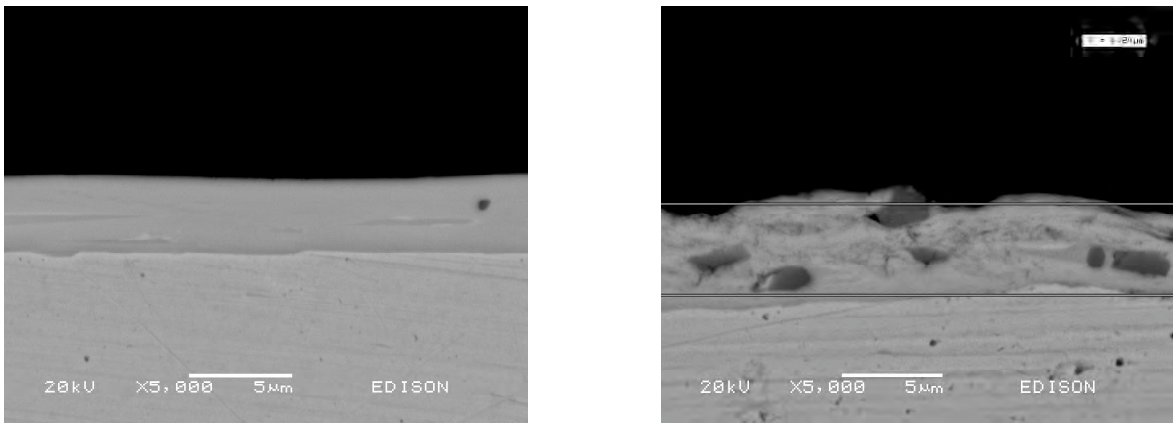

Fig. 8. SEM images (BSE mode) of cross section of the Bi-2212 deposit on the Ag tape : (left) good quality laboratory tape; (right) pilot plant tape.

The critical current density is larger than 20,000 Acm^2 and the n value of the interpolating power law is equals to 8.7. The critical current density value must be compared with the best values of 47,000 A/cm^2 obtained in the past by us at the laboratory scale with the same techniques, for very short samples, few cm long [8]. The key process variables to be controlled are: a) the uniform deposition of the elements on the tape, avoiding border effects; b) fine tuning of the annealing temperatures in a open vertical oven; c) assure constant electrolytic bath concentration during the time.

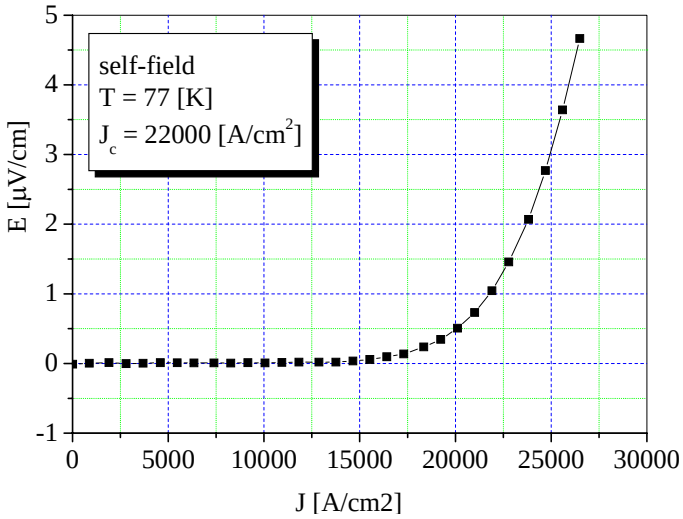

Fig. 9. Transport E(J) measurement on Bi--2212 electrodeposited tape.

3. MgB_2

Among the "in situ" techniques to produce MgB_2 manufacts, in EDISON we have developed a new technology, which we call the Reactive Liquid Infiltration (RLI) to describe the relevant aspects of process[9]. Indeed the liquid Mg infiltration in a powdery crystalline Boron preform, inside a closed container, is self driven by the pressure originated by the Mg volume increase at the melting point and is further aided by the Mg and crystalline B interface affinity, so that no external pressure is needed to reach very high homogeneity and high density, also when the permeation is several cm deep. This aspect represents the main advantage of the RLI technique that, in principle, can be applied either to bulk or to wire manufacts [10,11] without the need of hot pressing apparatus. A selection of the typical bulk manufacts prepared in our lab is reported in Figure 10.

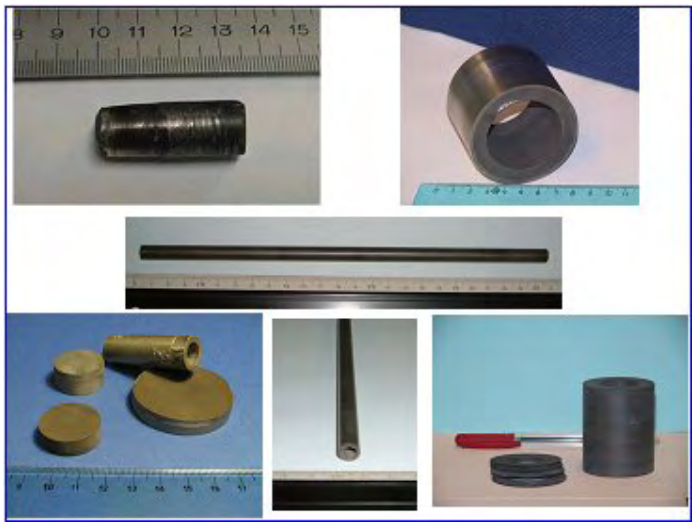

Fig. 10. MgB_2 bulk manufacts obtained by the RLI technology.

The peculiar microscopic morphology of the resulting material, illustrated in Figure 11, is characterized by large grains embedded in a matrix constituted by finer grains. This granularity does not prevent the flowing of the supercurrents through the grain boundaries, as was revealed by Magneto-Optical imaging [12].

does not prevent the flowing of the supercurrents through the grain boundaries, as was revealed by Magneto-Optical imaging [12].

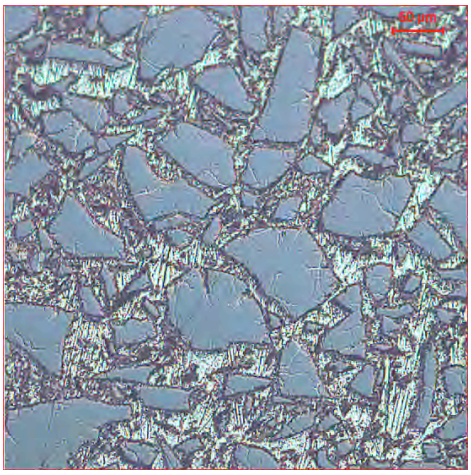

Fig. 11. Optical microscope image of a polished section of a typical bulk MgB_2 obtained by RLI

The superconducting characteristic of the RLI manufacts are similar to the best reported up to now, for samples obtained with more sophisticated preparative technologies [13,14]. As far as bulk samples are concerned the critical current densities at different temperatures and applied magnetic fields, measured in magnetization cycles, are displayed in Figure 12. The effect of doping, mainly C or SiC, in the increase of the flux pinning has been recently verified by several authors [15,16]. Experiments are underway if the same effects can be detected in the framework of the RLI techniques. Other outstanding characteristics of the bulk MgB_2 obtained by RLI are connected to the high values of the n exponent of the power law $V(I) \sim I^n$. The following simple exponential relation interprets the experimental values deriving from transport measurements of the V(I) [17] :

$$n(B,T)= n_o \exp(-\alpha B/(1-T/T_c)^{\beta}) \qquad (1)$$

where n_o, α, β are scaling parameters. The scaling parameters found from a fit based on T_c=39 K are reported in Table 1.

Table 1. Best fit parameters for the n (B,T) formula (1)

MgB_2 Samples	n_o	$\alpha(1/T)$	β
Bulk	103	0.30	1.33
Monofilament wire	130	0.38	1.00
7-filaments wire	37	0.145	1.33

As a practical benefit of the high n values of the bulk we have checked the possibility of having a persistent current in MgB_2 rings. In particular it has been verified that in rings of dimensions (ϕext/int=47/25mm; h=1 mm), immersed in liq. He, a remnant magnetic field of 0.51 T remains for more than 20 hours, after switching off an external field of about 1.5 T. The effective persistent current on the ring correspond to a density current of 1.250 A/mm^2 [18].

The present quality of the superconductive characteristics of the RLI bulk MgB_2 open the ways to applications at intermediate temperatures between 10 and 30 K and at intermediate magnetic fields , up to 2-3 T. The most appealing system should be the current leads, the permanent magnets for motors and shielding apparatus and also as variable inductor for Fault Current Limiters.

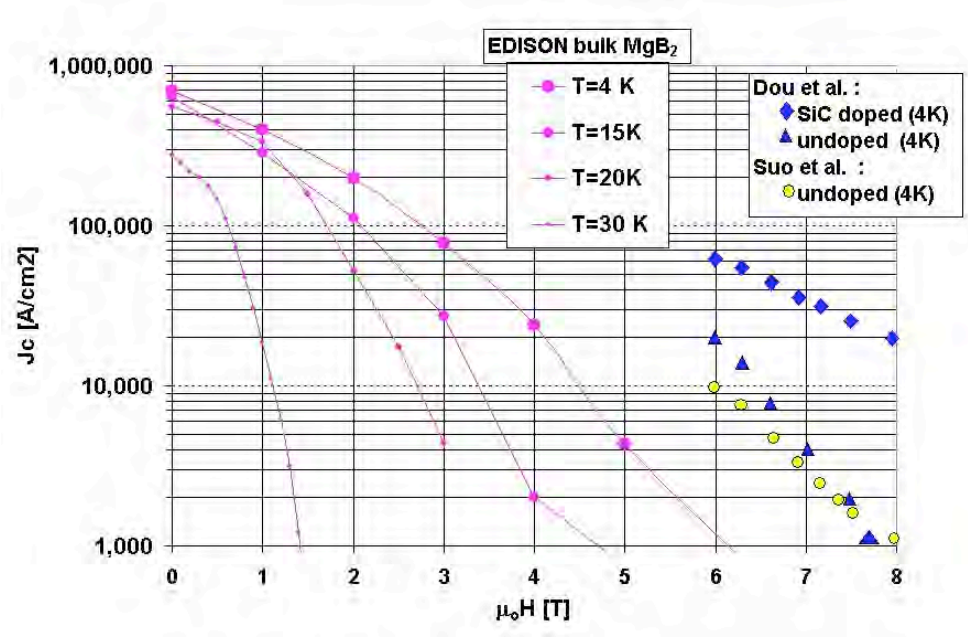

Fig. 12. Critical current densities of a bulk MgB_2 obtained by RLI, as compared with some outstanding samples (Dou et al. [13], Suo et al.[14])

ACKNOWLEDGEMENTS

We acknowledge the partial support of CNR and MIUR to the research on Y-123 coated conductors (L.95/95) and Bi-22121 electrodeposited tapes (L. 488/92) respectively and the CNR-IENI Institute in Lecco for its support in the MgB_2 preparation. The work on Y-123 coated conductors is performed together EMS and CNR-IMEM Institute in Parma, and the textured Ni, Ni alloys, are supplied by IFW in Dresden.

REFERENCES

[1] D.P. Norton et al., Science 274, 775 (1996).

[2] De Boer B., Reger N., Fernandez L., Eickemeyer J., Berberich P. and Prusseit W., IEEE Trans. Appl. Supercond. 11, 3477 (2001).

[3] Kinder H., Berberich P., Prusseit W., Rieder-Zecha S., Semerad R. and Utz B., Physica C, 282-287, 107 (1997).

[4] J. Eickemeyer, D. Selbmann, R. Opitz, B. de Boer, B. Holzapfel, L. Schultz and U. Miller, Supercond. Sci. Technol., 14, 152 (2001).

[5] M. Bindi, A. Botarelli, A. Gauzzi, L. Gianni, S. Ginocchio, B. Holzapfel, A. Baldini, S. Zannella, Supercond. Sci. Technol., 17 (2004), pp. 512-516.

[6] L. Gianni, A. Baldini, M. Bindi, A. Botarelli, A. Gauzzi, S. Zannella, Supercond. Sci. Technol. Proc. of the EUCAS 2003 Conf., in press (2004).

[7] F. Legendre et al., Eur. Phys. J. A 1 (1998) 191-196.

[8] G. Villard et al., IEEE Trans. on Appl. Supercond. 11 (2001), 3038-3041.

[9] G. Giunchi, Int. J. Mod. Phys. B17, 453-460 (2003)

[10] G. Giunchi, S. Ceresara, G. Ripamonti, S.Chiarelli, M.Spadoni, IEEE Trans. on Applied Superconductivity 13(2) , 3060-3063 (2003)

[11] G. Giunchi, S. Ceresara, G. Ripamonti, A. Di Zenobio, S.Rossi, S. Chiarelli , M. Spadoni, R.Wesche, P.L. Bruzzone, Supercond. Sci. Technol. 16, 285-291 (2003)

[12] L. Gozzelino, F. Laviano, D. Botta, A. Chiodoni, R. Gerbaldo, G. Ghigo, E. Mezzetti, G. Giunchi, S. Ceresara, G. Ripamonti, M. Pojer, Phil. Mag. B82, 1-11 (2002)

[13] S.X.Dou, S. Soltanian, J.Horvat, XL Wang, S.H. Zhou, M Ionescu, HK Liu, P Munroe, M. Tomsic, Appl. Phys. Lett. , 81(18), 3419-3421(2002)

[14] H.L. Suo, C. Beneduce, M. Dhalle, N. Musolino, JY Genoud, R Flukiger, Appl. Phys. Lett. 79(19), 3116-3118 (2001)

[15] R.H.T. Wilke et al. Cond-Mat #0312235 (15/12/2003)

[16] S.X. Dou, AV. Pan, S. Zhou, M. Ionescu, X.L. Wang, J. Horvat, H.K. Liu, P.R. Munroe, Journal of Appl. Physics ,94(3), 1850-1856 (2003)

[17] G.Giunchi, S.Raineri, R.Wesche, P.L.Bruzzone, Physica C,401(1-4), 310-315 (2004)

[18] G.Giunchi, S.Raineri, G.Ripamonti, A. Matrone, G.Masullo, R.Quarantiello, EUCAS 2003, Sorrento (Italy), to be published.

THE INFN RESEARCH PROGRAM ON MGB_2 APPLICATION OF MAGNESIUM DIBORIDE TO PARTICLE PHYSICS

Riccardo Musenich
Istituto Nazionale di Fisica Nucleare, Via Dodecaneso 33, 16146 Genova, ITALY

Abstract

As soon as the discovery of the superconducting properties of magnesium diboride (MgB2) has been known, several research activities started in the italian universities, research centers and industries. The INFN project, Ma-Bo, aims to understand if magnesium diboride could be used for particle physics applications: magnets, thin films for accelerating cavities, thin films for detectors and other devices. Some of the results obtained in the first two years are given in the paper.

1 INTRODUCTION

The discovery of the superconducting properties of magnesium diboride (MgB_2) [1], an already known binary compound, has renewed the interest of many researchers towards applied superconductivity. This interest is based on the material characteristics that appear favourable to technological applications: high critical temperature (39 K), upper critical field higher than 18 T, lack of weak links, low anisotropy and high critical current density (several GA/m^2 at 20 K and 0 T). Last but not least, the cost of the material is low.

Although the discovery was recent, the techniques developed to fabricate HTS conductors were promptly applied to the new material and, at present, MgB_2 wires and tapes are available in several hundreds meters lengths. The conductor manufacturing process is rather simple and consequently, the conductor cost is comparable with that of low T_c superconducting wires. Two routes can be followed to fabricate MgB_2 conductors using the powder-in-tube (PIT) technique: the in-situ (the tube is filled with the precursor powders) and the ex-situ (the tube is filled with MgB_2 powders) methods.

The main drawback of magnesium diboride is the low irreversibility field that can limit the application of the material to low field magnets. However, there are many signals of a possible enhancement of the irreversibility line by acting on the structure and on the morphology of the material [2].

To nowadays knowledge, the use of magnesium diboride can be imagined in large scale applications as material for conductors either to wind superconducting devices generating field lower than 4 T and operating at about 20 K or to fabricate energy transport lines.

As regards particle physics devices, the possible applications of magnesium diboride are magnets, rf cavities and particle detectors.

2 MGB_2 RESEARCH PROGRAMS IN ITALY

As soon as the discovery of the superconducting properties of MgB_2 has been known, several research activities (mainly fundamental) started in Italy by research institutions (CNR, INFM, universities) with ordinary funds. Few months later, the

Italian industries operating in the manufacture of superconductor devices (Ansaldo Superconduttori, Columbus Superconductors, Edison, Europa Metalli, Pirelli) started R&D activities. It is of particular interest the birth of Columbus Superconductors, a new company devoted to the development and fabrication of diboride conductors.
Finalized projects are funded by INFN (Ma-Bo project, 2002-2004) and by MIUR, the Ministry of Research (2004-2006).

Ma-Bo, the INFN program on magnesium diboride applications to nuclear and particle physics, started at the beginning 2002. Six INFN sections and laboratories, with 30 people involved (about 10 FTE), have joined this project: Genova, Frascati National Laboratories, Legnaro National Laboratories, Milano, Napoli, Torino. Ma-Bo is in collaboration with ENEA, INFM (LAMIA laboratory in Genova), Ansaldo Superconduttori and Columbus Superconductors.

3 THE INFN RESEARCH PROGRAM ON MgB_2

The research project Ma-Bo aims to understand if magnesium diboride could be used for particle physics applications. The research activities are related to: magnets, thin films for cavities, thin films for detectors and other devices.

3.3 Accelerating cavities

The application of superconducting materials to accelerating cavities requires low rf dissipations that means not only good characteristics of the superconductor itself (high T_c, low normal state resistivity, large gap, absence of weak links) but also a homogeneous, clean and pure surface. Several techniques can be used to deposit MgB_2: laser ablation, evaporation, sputtering. In order to obtain films suitable for accelerating cavities only magnetron sputtering in several conditions has been used.

Although good quality films were obtained onto small substrates, several problems in using MgB_2 for rf resonant cavities have been found:

- MgB_2 is a double gap superconductor: the lower gap (Δ_π=2.8 meV) limits the behavior of the material exposed to the rf field. The value of $2\Delta/kT_c$=1.7 is close to the Nb_3Sn one.
- A homogeneous, pure (i.e. single phase) film must be deposited onto large area substrates but the presence of magnesium and boron oxides cannot be completely avoided.
- The material is chemically instable if exposed to atmospheric humidity.

The above-mentioned problems leaded us to abandon the study of the application of MgB_2 to rf cavities.

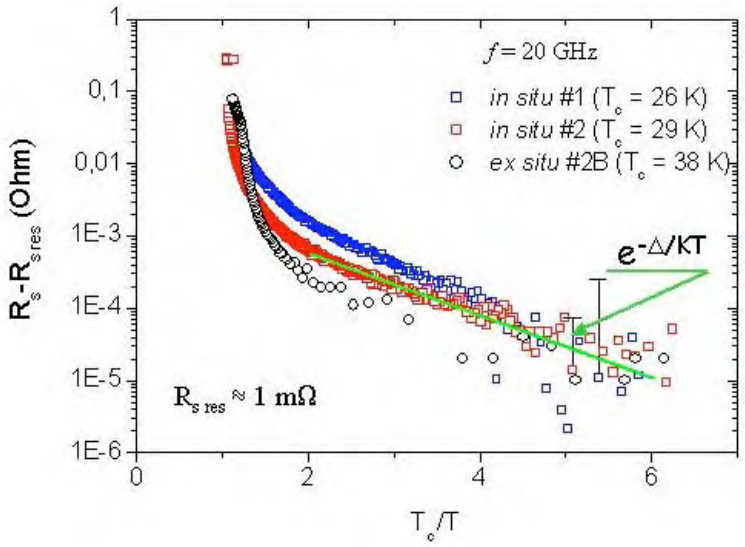

Fig.1. Rf resistance of a MgB_2 sample (R.Vaglio, University of Napoli and INFN)

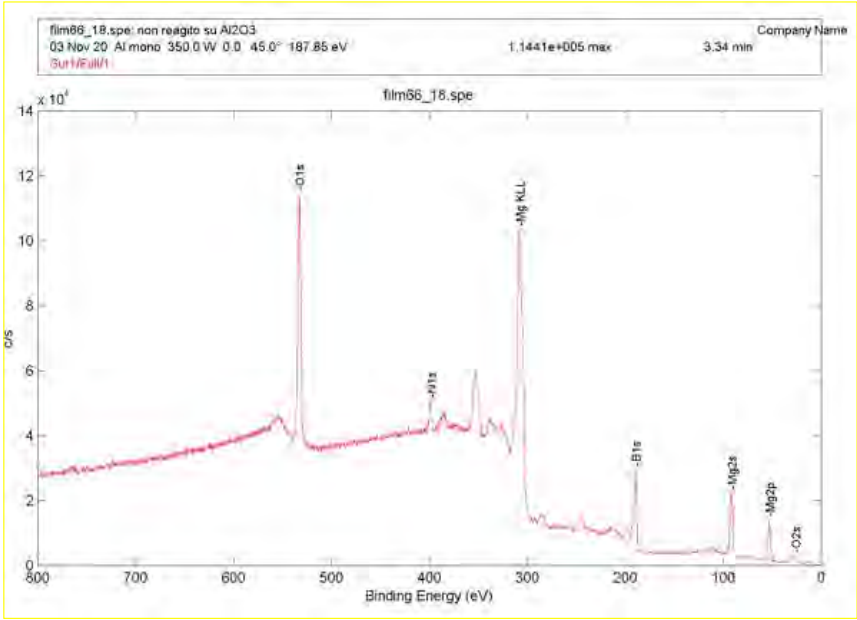

Fig.2. The XPS spectra of MgB_2 films show the presence of MgO, B_2O_3 and BN.

3.4. Detectors

Some MgB_2 properties make it a possible material for radiation:

- Low activation energy;
- Good radiation hardness;
- High thermal conductivity;
- Short recovery time.

Recently, the use of MgB_2 films as neutron detector has been proposed [4]: the energy released by the neutron reaction with ^{10}B partially destroys the superconductivity of a MgB_2 film.

Part of the INFN activity is devoted to the study of microstrip detectors based on magnesium diboride.

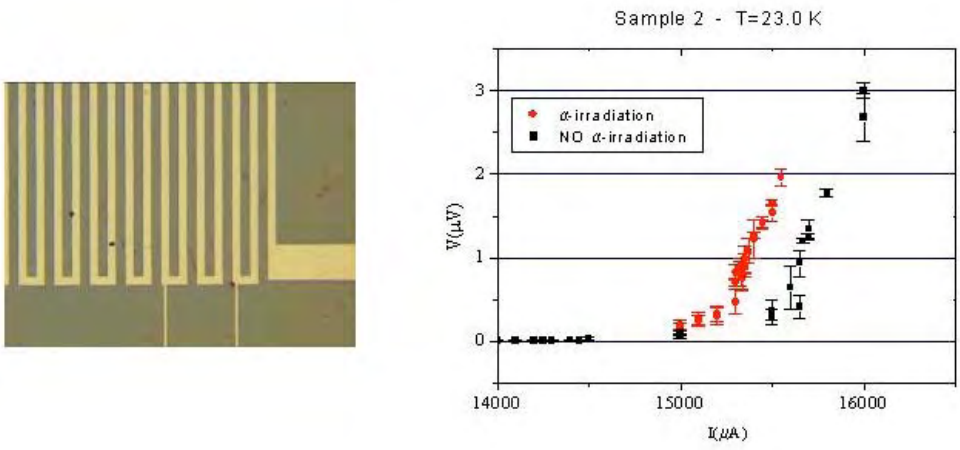

Fig.3. Effect of α irradiation on a 20 μm MgB_2 microstrip
(E.Monticone, IEN Torino, and M.Truccato, University of Torino and INFN).

3.5 Magnets

The most promising application of MgB_2 is the fabrication of conductors. The interest of INFN in this field has joined the one of other research groups and industries in Italy leading to a common program devoted to the development of magnet. One of the goals of the research program was to demonstrate the feasibility of react & wind MgB_2 coils.

Magnesium diboride-based conductors are prepared by INFM-LAMIA laboratory and by Columbus Superconductors using the powder-in-tube (PIT) method and following the ex-situ route [3]. Pure nickel tubes are filled with commercial MgB_2 powders (the powder density inside the tube is 1.3 g/cm^3) and cold worked in several steps without intermediate annealing. Both monocore and multifilamentary tapes are obtained using the described method. The conductor has a critical current in the order of 10^9 A/m^2 at 4.2 K and zero applied field. Fig.4 shows a monocore tape whose typical dimensions are 4 mm × 0.35 mm, with a metal/superconductor ratio about 5, i.e. a superconductor cross section area of 0.24 mm^2. As a final step, the tape is heat treated at about 900°C in argon atmosphere, using an in-line oven, in order to enhance its transport properties. The critical current of the tape, after the heat treatment, is shown in fig.5. The critical current density at 4.2 K, measured in liquid helium bath, between 3.5 and 12 T is shown in fig.6.

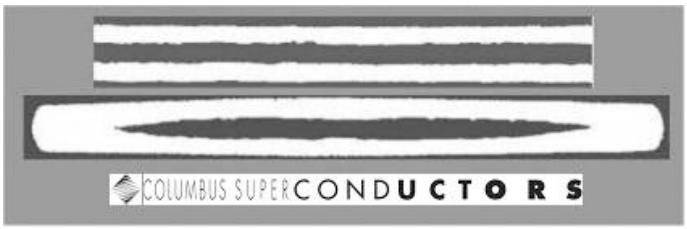

Fig.4. Cross and longitudinal section of a monocore tape produced by Columbus Superconductors

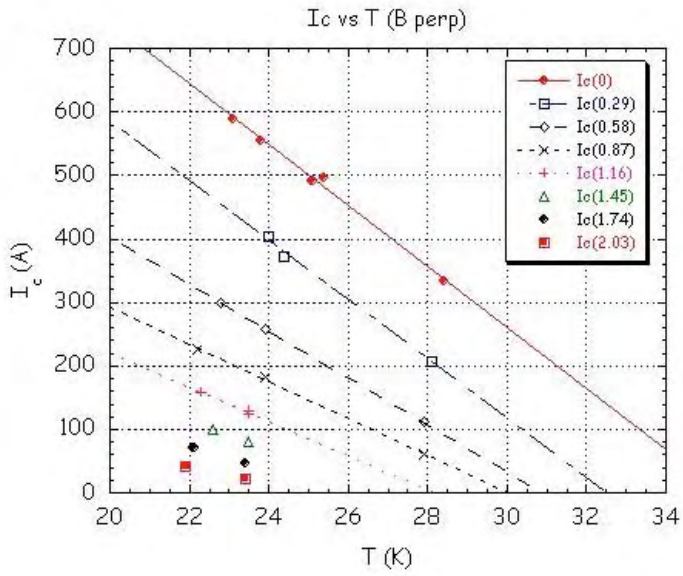

Fig.5. Critical current of the monocore tape between 0 and 2T (INFN-Genova)

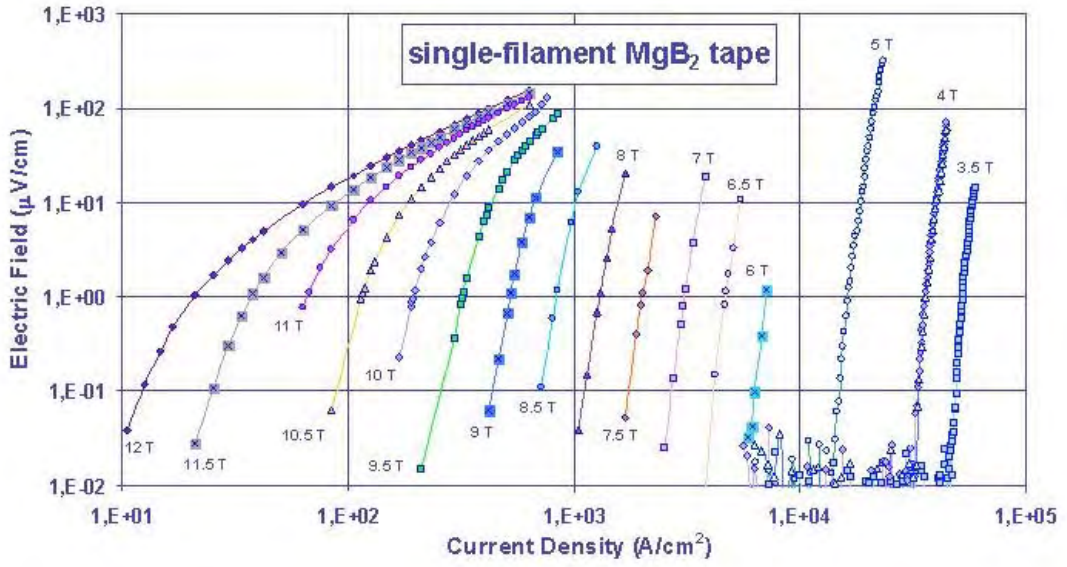

Fig.6. Critical current density at T = 4.2 K (INFN-LASA, Milano)

The tapes are used to wind solenoids and pancake coils using the react & wind technique (the tapes already undergo the heat treatment). A 6 layers solenoid, 15 cm diameter, was wound with 80 m of MgB_2 tape. The pancake coils were wound with 40 m tape (the external diameter is 20 cm).

The solenoid was tested in liquid helium: despite local dissipation at one of the exits, it reached 53 A before quenching [5]. It is worth noting that no resistance was detected at the layer transitions.

Fig.7. Solenoid and pancake coil (Ansaldo Superconduttori, Genova)

The pancake coils gave better results: the maximum quench current reached by a pancake coil in liquid helium was 343 A corresponding to a field of 0.76 T at the conductor, and 0.21 T at the coil center.

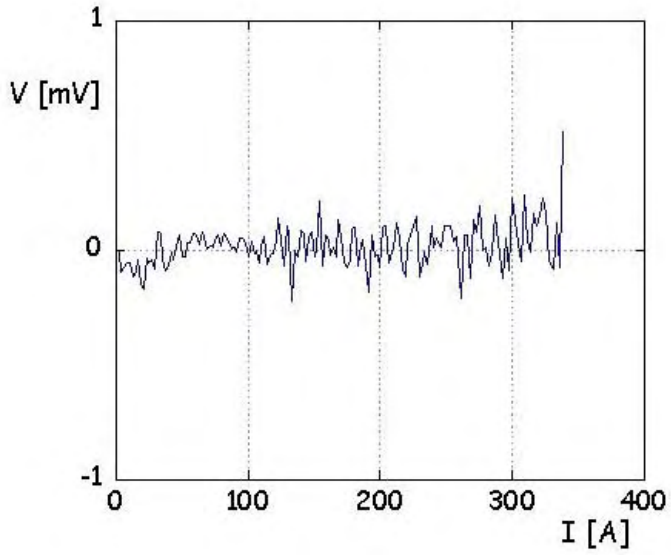

Fig.8. V-I curve of the pancake #8 tested in liquid helium bath

MgB_2 pancake coils were also tested at variable temperature between 15 K and 38 K. The coils are connected to a cryocooler and supplied via a couple of cryogen free current leads with HTCS bars. The result of the tests of the Ansaldo Superconduttori coil #10 is shown in fig.9.

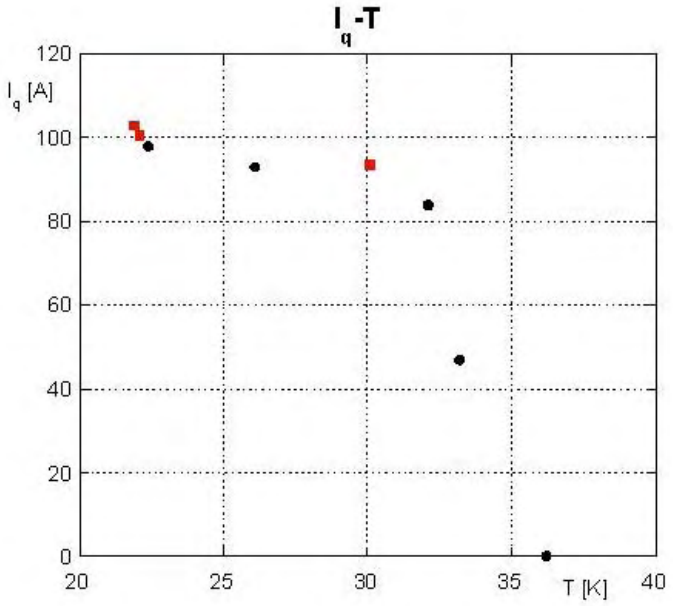

Fig.9. Quench current of the pancake coil #10 (Red squares: values obtained increasing the temperature at constant current. Black circles: values obtained increasing the current at constant temperature.)

4 CONCLUSIONS

Magnesium diboride is a low cost material with high critical current density and without weak link problems. Moreover cable and tapes can be easily produced using techniques already developed.

Looking at the applications of MgB_2 to nuclear and subnuclear physics, the perspective can be schematized as follows:

- Till now, neither MgB_2 nor other superconducting materials can compete with niobium for application in accelerating cavities.
- Magnesium diboride seems a possible candidate as material for radiation microstrip detectors.
- The feasibility of magnets has been clearly demonstrated. Magnesium diboride can be considered a promising material for the construction of magnets for accelerators (dipoles for syncrotrons or beam lines, cyclotrons) and detectors. Low field (less than 3 T) magnets will be probably the first step but there are several indications about the possibility of a field improvement.

Due to the excellent results, particularly as regards magnets, a new research program concerning the application of MgB_2 will be presented to INFN.

ACKNOWLEDGEMENTS

The Ma-Bo collaboration owes to Fondazione TERA for its contribution that made possible the construction of the cryogen free apparatus for the coil tests.

REFERENCES

[1] J. Nagamatsu et al., *Nature*, 410 63, 2001.
[2] D. Larbalestrier, presented at *EUCAS 2003*, Sorrento (Italy) 2003.
[3] G. Grasso et al., *Appl. Phys. Lett.*, Vol.79, 2001, pp. 230–232.
[4] K.Takahashi et al., *Physica C*, Vol.392-396, 2003, pp.1501-1503
[5] R.Musenich et al., presented at MT-19, Morioka (Japan) 2003. To be published on *IEEE Trans. on Appl. Supercond.*

SUPERCONDUCTING CABLES

CABLE DESIGN FOR FAST RAMPED SUPERCONDUCTING MAGNETS (*Cos-θ* DESIGN)

A.K. Ghosh
Brookhaven National Laboratory, Upton, New York, USA

Abstract
The new heavy ion synchrotron facility proposed by GSI will have two superconducting magnet rings in the same tunnel, with rigidities of 300 T-m and 100 T-m. Fast ramp times are needed, which can cause significant problems for the magnets, particularly in the areas of ac loss and magnetic field distortion. The development of the low loss Rutherford cable that can be used is described, together with a novel insulation scheme designed to promote efficient cooling. Measurements of contact resistance in the cable are presented and the results of these measurements are used to predict the ac losses, in the magnets during fast ramp operation. For the high energy ring, a 1m model dipole magnet was built, based on the RHIC dipole design. This magnet was tested under boiling liquid helium in a vertical cryostat. The quench current showed very little dependence on ramp rate. The ac losses, measured by an electrical method, were fitted to straight line plots of loss/cycle versus ramp rate, thereby separating the eddy current and hysteresis components. These results were compared with calculated values, using parameters which had previously been measured on short samples of cable. Reasonably good agreement between theory and experiment was found, although the measured hysteresis loss is higher than expected in ramps to the highest field levels.

1. INTRODUCTION

GSI is planning a new heavy ion accelerator consisting of two superconducting synchrotron rings placed one above the other in the same tunnel [1], and ramping with a rise time of a few seconds. The lower ring, having a magnetic rigidity of 100 T-m, will use magnets based on the Nuclotron design [2]. The upper ring was originally planned to be 200 T-m and use magnets based on the RHIC design [3], but this ring has recently been increased to 300 T-m. As a prototype for the original 200 T-m ring, a 1m long model dipole was built, based on the RHIC single layer *cos-θ* design, but with various modifications to enable high ramp rates. The model was successfully tested for quench behaviour and ac losses at ramp rates up to 4T/s:

To date, superconducting accelerators with high field magnets have all worked at relatively slow ramp rates and have been able to use Rutherford cable without incurring too much ac loss. At high ramp rates ~ 1T/s however, coupling between the strands of a conventional Rutherford cable would produce high ac losses and unacceptable field distortion. Coupling may be reduced by increasing the resistance between strands in the cable (by coating the strands with a highly resistive coating), but there are reasons to believe that this can impede current sharing and thereby make the magnet more susceptible to quenching at high ramp rates. Because coupling in Rutherford cables is very anisotropic, it may be reduced greatly by increasing the crossover resistance via a resistive core foil, while still leaving a low resistance in the other direction. Cables with Kapton-core foils were first tried more than 20 years ago [4] and have been the subject of ongoing research. We show that cores reduce the coupling losses without affecting the quench performance of magnets.

In this paper we describe the development of a low loss Rutherford cable suitable for use in fast ramping magnets, using the RHIC strand and cable as the starting point. The losses arising from the strand and cable are examined and a suitable selection of the cable is made which is fabricated and wound into single layer coils. Following that, the quench behavior and the losses of a prototype magnet is described. Most of what is presented here can be found in earlier publications, Ref. [5-9]

The parameters of the RHIC strand and cable are in Table 1, and the wire cross-section is shown in Fig. 1.

Table 1:
Parameters of the RHIC Cable

Wire diameter (mm)	d_w	0.648
Filament diameter (mm)	d_f	6.0
Cu/Sc ratio	m	2.25
Wire twist pitch (mm)	L_w	13
Wire coating		None, (bare copper)
No. of strands in cable	N	30
Cable width (mm)	$2c$	9.73
Cable mid-thickness (mm)	$2b$	1.166
Cable Keystone angle (deg)		1.2
Cable lay pitch (mm)	p	74

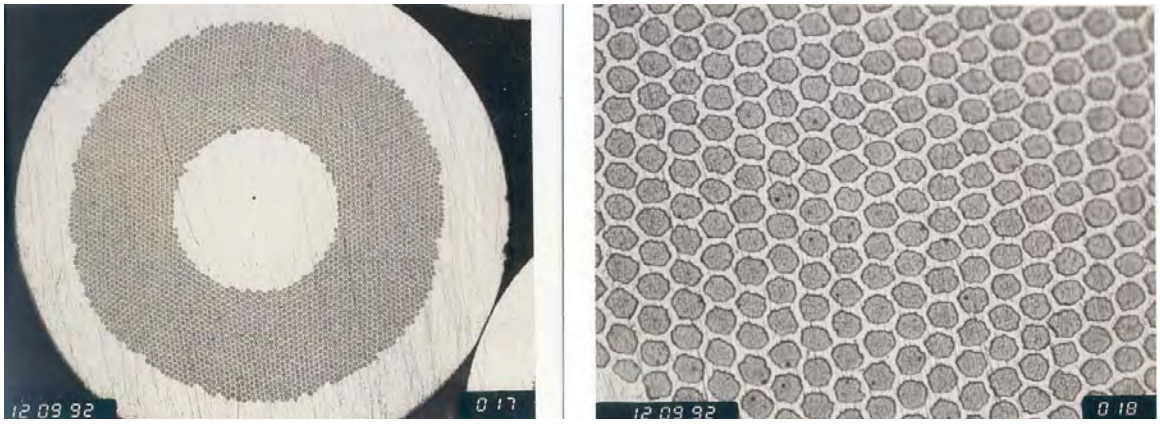

Fig. 1 RHIC strand cross-section

2. CABLE DESIGN

2.1 Strand losses.

At the strand level, the eddy current magnetization (and losses) due to a changing B-field transverse to the wide face of a cable, $\dot{B}$ is controlled by the wire twist pitch and the inter-filament matrix resistivity and is given by

$$M_e = \frac{2\dot{B}\tau_f}{\mu_o} \qquad (1)$$

where τ_f is the inter-filament coupling time constant

$$\tau_f = \frac{\mu_o}{2\rho_{et}} \left\{ \frac{L_w}{2\pi} \right\}^2 \qquad (2)$$

and ρ_{et} is the effective transverse resistivity across the wire, depending on the copper matrix, the interface resistance between NbTi and copper, and the geometry. In the case of the RHIC strand which has copper as the interfilament matrix, $\rho_{et} \sim 1.0 \times 10^{-10} \Omega$.m. This was calculated from magnetization measurements made at CERN [10] on annealed strand. To reduce this loss component, the twist pitch was reduced from 13mm to 3mm. However for the very tight twist pitch the critical current density, J_c, of the wire degrades as shown in Fig. 2.

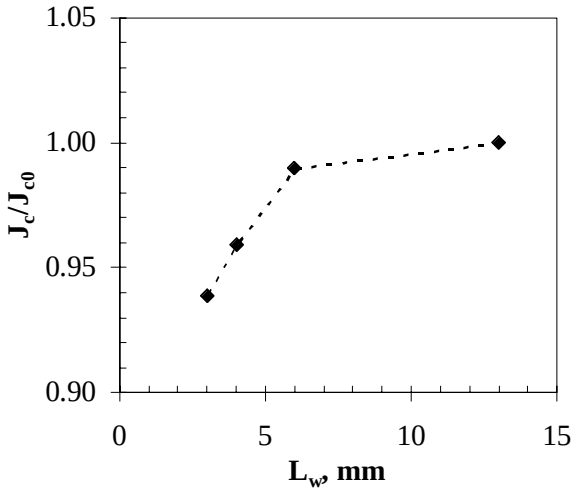

Fig. 2 Jc/Jc0 as a function of twist pitch for the RHIC strand

Hence for the prototype magnet the strand was chosen with a twist pitch of 4mm, which reduces the filament-coupling by an order of magnitude, without a significant loss of J_c. In the future increasing the matrix resistivity by using Cu-0.5%Mn alloy might be a better option to further reduce this component of eddy-current loss [11].

2.2 Cable Losses

In Rutherford cables, the dominant source of loss in changing transverse field is due to the inter-strand coupling magnetization, that are determined by the strand *crossover resistance* R_c and the strand *adjacent resistance* R_a as shown in Fig 3. (Reproduced from Ref. [6])

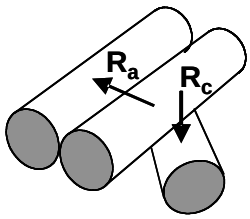

Fig. 3 Crossover and adjacent resistances between strands in a cable (note that R_a is defined to be over the same length of wire that R_c occupies).

The eddy currents flowing between the strands can be suppressed by increasing these inter-strand resistances, however very high R_a and R_c could lead to quench current degradation in magnets at high

ramp rates due to a lack of current sharing between the strands. In the absence of a definite theory, we have therefore decided to make the contact resistance high enough to control the losses, but no higher than necessary. To quantify how high, we need to look at the three types of inter-strand coupling in Rutherford cable.

a) Cable coupling via R_c in transverse field

$$M_{tc} = \frac{1}{120}\frac{\dot{B}_t}{R_c}\frac{c}{b}\,p\,N(N-1) \tag{4}$$

where M_{tc} is the magnetization per unit volume of cable, p is the cable twist pitch, $\dot{B}_t$ is the rate of change of field transverse to the broad face of the cable, N is the number of strands, c is the half width of the cable and b is its half thickness.

b) Cable coupling via R_a in transverse field

$$M_{ta} = \frac{1}{6}\frac{\dot{B}_t}{R_a}\,p\frac{c}{b} \tag{5}$$

where M_{ta} is the coupling magnetization due to R_a in transverse magnetic field.

c) Cable coupling via R_a in parallel field

$$M_{pa} = \frac{1}{8}\frac{\dot{B}p}{R_a}\,p\frac{b}{c} \tag{6}$$

where $\dot{B}_p$ is the rate of change of field parallel to the broad face of the cable. Because c is always much greater than b, it may be seen immediately that the loss in transverse field is much greater than in parallel field. From (4) and (5) we see that the ratio is:

$$\frac{M_{tc}}{M_{ta}} = \frac{R_a}{R_c}\left\{\frac{N}{20}(N-1)\right\} \tag{7}$$

A typical value for the factor in brackets is ~50, which means that a given crossover resistance causes 50 times more loss than the same adjacent resistance. It follows that we can make $R_a \sim R_c\,/50$ without increasing the loss too much. It is this inherent anisotropy in the loss mechanism that is the reason for choosing cored cables. For the SIS200 prototype magnet designed to operate to 4T at 1T/s, a target value of 50 μΩ for R_a and 5 mΩ for R_c was set.

2.2.1 Cored-cable development

The RHIC cable was chosen for this development as strands were readily available and since the prototype magnet was based on the RHIC design. For bare copper strands it is known that the inter-strand resistance is very variable due to the oxide that develops on the surface of the bare wire. R_a and R_c can vary significantly from cable to cable and with the coil-curing heat-pressure cycle that is utilized in coil fabrication. Following LHC where *Sn-4%Ag* solder coated strands are used to control cable Rc in the magnets, it was decided to coat the RHIC strands with ~ 1 μm of *Sn-4%Ag* to control R_a. Additionally the wire diameter was reduced to 0.638mm in order to accommodate a 25 mm thick resistive core without over compacting the RHIC cable.

During the development of cored-cables, several different foils have been tried, namely:

a. 25 μm thick stainless steel 304, annealed
b. 25 μm thick stainless steel 316, annealed
c. 25 μm thick anodized titanium
d. 25 μm thick Cu-30wt%Ni (CDA 715), half-hard and annealed

e. 50 μm thick Brass
f. 75 mm thick Kapton

Tapes were all 8mm wide which is the maximum size than can be used without problems at the edges. Fig. 3 and 4 shows a cross-section of the cored cable.

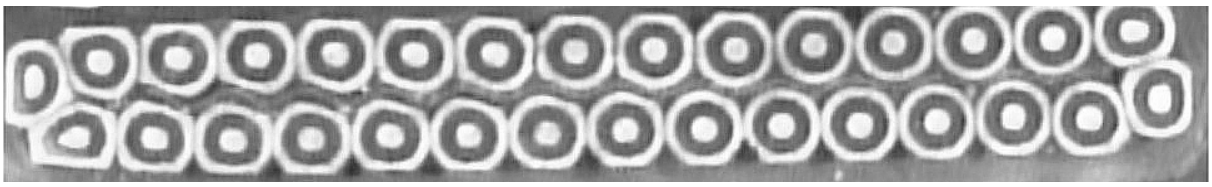

Fig. 3 Cross section of a cored cable

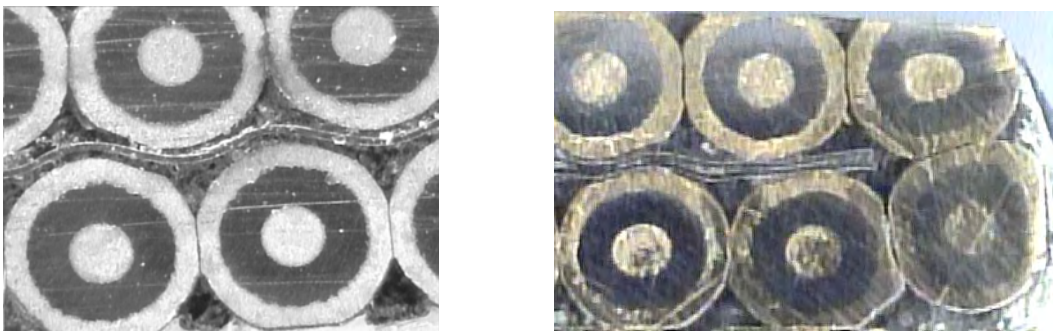

Fig. 4 Local region showing the stainless steel core foil in the middle and at the edge.

The initial cables were made at New England Wire Technology (NEWT) using a hollow mandrel, such that the foil was fed through the central hole of the hollow shaft of the cabling machine. Most of our experience is with stainless steel tapes. One of the problems encountered was the incidence of foil bunching in the cable, which was due to variation in the back-tension of the tape. Stainless steel tape needs to have very tight packages so that a high tension can be applied to prevent core-bunching. To eliminate post cleaning of the cable we used Wakefield 4BR vanishing lubricant that was dripped onto the mandrel which is the usual practice for cabling. Following an initial cabling run where cable lengths of ~ 100m where made with SS and Ti-tapes, a longer cable of 600m using SS was fabricated with nominal RHIC dimensions. An examination of the core revealed another flaw; that of perforations of the foil at the strand cross-over region. Such perforations have been observed earlier in 12 μm SS-foils used in experimental LHC cables. The Ti-foil showed very significant perforations of the foil, whereas the SS-foil showed incidence of perforations only at the minor edge. Fig. 5 shows the nature of the perforation, which seems to be due to shear stress being applied to the foil after it has been compressed at the cross-over region.

From successive experimental cabling runs, we found that the incidence of perforation in SS-foil is greatly reduced by annealing the strands at 200C for several hours. The initial cables were made with fully cold-worked strands with RRR ~ 40. Increasing the cable thickness by 15 μm also reduced the perforations by a factor of two. However, using the machine at NEWT, perforation free cables could not be fabricated using a single layer of SS-foil. Even using a lubricant like Mobil 1 along with 4BR was not very effective in solving this problem. Some of the other drawbacks of the hollow mandrel is making spice joints of the tape and excessive wear of the mandrel.This type of cabling needs additional work.

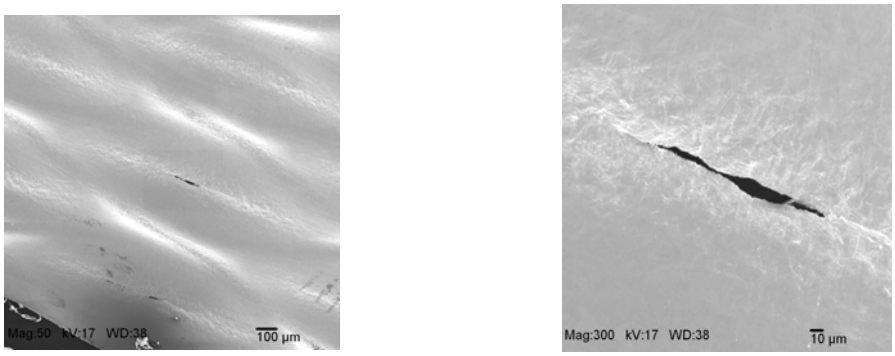

Fig. 5 SEM photograph of a perforation in the SS-foil

To fabricate perforation free cored cable, we resorted to using two layers of 25 μm thick SS-tape, and increasing the cable thickness to accommodate the extra layer. This was the type of cable that was finally used in the prototype magnet. We were also successful in making "good" cable with 50 μm Brass (95-5) tape with mid-thickness 10 μm over the nominal value of 1.166 mm. This foil by far is the easiest to use as a core. This might be due to the fact that Brass has an elastic modulas that matches the SC (superconducting)-wire and has good elongation property. Brass has an order of magnitude lower resistivity (3-6 μΩ-cm) than SS which is typically ~ 70 μΩ-cm. However the resistivity of the foil is not significant in determining R_C (see next section). An interesting candidate is Cu-30wt%Ni which has a resistivity of 38 μΩ-cm and a modulas that is slightly higher than the SC wire. An experimental cable has been fabricated by Lawrence Berkley Lab (LBL) which shows no foil perforation, and is being evaluated for inter-strand resistance.

Experimental cables were also fabricated at LBL where they use a slotted mandrel (cabler has a solid shaft that is the most common situation) with the tape being fed close to the Turkshead. The "vanishing" lubricant 4BR was used. In this case perforation-free cored cable using a single layer of 25 μm thick SS-foil has been made. Periodic wrinkling of the foil is observed which will always be present due to the greater difference in the modulas of SS and the SC-wire. This cabling method is probably better than the hollow mandrel option as it would appear that single layer foils can be successfully used in the cable.

2.3 Interstrand Contact Resistances R_A and R_C of Cored Cables

A complete description of the electrical method to measure the interstrand contact resistances (ICR) is given in Ref. [12]. Most of what is described here can be found in Ref. [7] and Ref. [13].

Samples described here are from cable fabricated during two separate cabling runs (run GSI-003 and GSI-004) at New England Wire Technology (NEWT) and then insulated at BNL. The cable has standard RHIC insulation: two wraps of Kapton®, each 25 μm thick, with 50% overlap of each wrap, and a polyimide-based heat-set adhesive on the outside of the inner wrap and on both sides of the outer wrap. that bonds the different layers of the cable together after it has been cured. The samples are prepared as ten-stacks: 10 pieces of cable that are stacked on top of each other (with alternating keystones) and then cured. We use four spacer cables above and below the actual sample pieces; only the middle two cable pieces are tested. The 10 cable pieces are stacked into a fixture and cured. The curing cycle is the one used for the RHIC dipole magnets. It is shown in Fig. 6.

Much work has been done at CERN to optimize the coating of the strands in the superconducting dipoles for the Large Hadron Collider (LHC) [14-15]. As the LHC conductor is also coated with *Sn-4%Ag solder*, many of the mechanisms of oxide formation on the strands as described in the LHC references above are likely also at work in the cable described here. It is necessary to point out that, apart from the core, another fundamental difference between the LHC cable and the cable described here is the cable curing method: LHC curing is done with the curing pressure applied throughout. In the RHIC curing cycle, the pressure is completely released as the cable is heated from

135 °C to 225 °C (at which point a rather modest pressure of 7 MPa is applied to aid in the polyimide bonding). The pressure is also completely released as the cable is cooled from 225 °C to 135 °C. Thus oxidation is more likely to occur during this time for the RHIC procedure than for the LHC procedure as oxygen has easier access to the uncompressed wire surfaces than to compressed wire surfaces. Pre-annealing of the cable in air for durations of 2-8 hours was also evaluated.

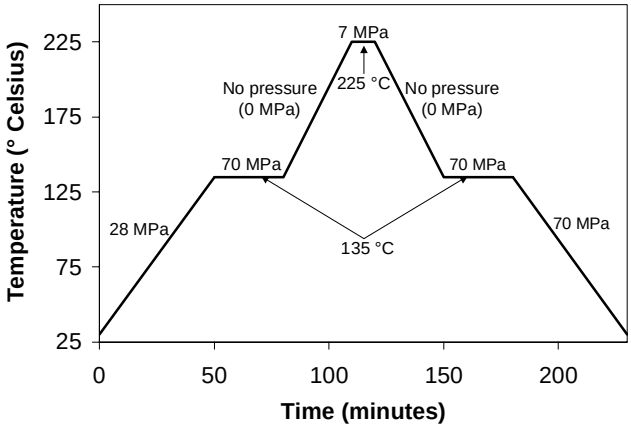

Fig. 6 RHIC Coil curing cycle

2.3.1 Results of the ICR Measurements

Each ten-stack contains two test samples; the results presented here are averages of the measured samples. In cases where the two samples in a ten-stack differed significantly, we prepared additional samples to clarify the results.

During the cabling run, GSI-003 six different cables were formed: Cables A and B both have a thinner *Sn-4%Ag* coating than the other cables and use annealed strands, cables A through D have a single 25 µm SS- foil, while cable E has two layers of the 25 µm SS-foil, and cable F has 1 layer of a 50 µm brass foil. For run GSI-004, segment A and B are made using 2 layers of SS-foil. Segment-B was used to fabricate the coils of the prototype magnet. The results are given in Table 2. The nominal mid-thickness for the RHIC cables is 1.166 ± 0.006 mm.

Table 2

R_A and R_C Results

	Sn-Ag Coating, µm	Cable Thickness, mm	Foil	R_a (µΩ) After Cabling	R_a (µΩ) 6 months later	R_c (mΩ)
GSI-003-A	0.66	1.138	25 µm SS	**100**	**139**	
GSI-003-B	0.66	1.180	25 µm SS	**72**	**147**	**14**
GSI-003-C	1.04	1.187	25 µm SS	**28**	**80**	
GSI-003-D	1.04	1.202	25 µm SS	**18**		**12.5**
GSI-003-E	1.04	1.173	2·25 µm SS	**21.5**	**25**	**62.5**
GSI-003-F	1.04	1.175	50 µm Brass	**8.5**	**45**	**0.66**
GSI-004-A	1.00	1.164	2·25 µm SS	**55**		
GSI-004-B	1.00	1.174	2·25 µm SS	**74**		

All the cored cables show an R_C significantly higher than R_A In core-less cables, one typically finds R_A~R_C. The cables with the thinner $Sn_{95\%wt}Ag_{5\%wt}$ coating (A and B) display a higher R_A which is likely caused by more oxidation due to the thinner coating. Furthermore, we also see that the thinner cables within a given coating thickness (A vs. B and C vs. D) show a higher R_A than the thicker cables.

We believe that the reason for this is increased compaction leads to better contact between the strands across the width of the cable. Also the data suggest that there is some aging effect on R_A. Experiments were also done which clearly show that R_A is significantly lower at the cable edge than it is along the flat area [7]. It is also interesting to note that for these same cables, R_A measured between 2.5-10 μΩ when the samples were cured without releasing the pressure at the intermediate steps. Pre-annealing the cable increased R_A significantly higher than the target value of 50-100 μΩ

R_C for the cored cables is not significantly determined by the resistivity of the metal foil. It is mostly dominated by the surface contact between the strand and the foil. I speculate that the main effect comes from a mismatch of the mechanical properties of the foil and the strand. During cable formation at the Turkshead, the strand and the foil is stretched. After exiting the Turkshead the cable and the foil contracts with a relative difference. This shows up as periodic wrinkling of the SS-foil, which also implies that the strand-foil nesting is disturbed from the location at the point of cable formation. Brass seems to provide a lower surface contact resistance as its modulas matches that of the superconductor so that there is little differential shrinkage after the Turkshead.. Cables made with Cu-30wt%Ni are being evaluated. Loss measurements on 40cm long samples were also made at the University of Twente. The correlation with the resistance measurements was quite good. Details are in Ref. [6]

3. PROTOTYPE MAGNET PERFORMANCE

This section reports the successful initial test of a 1m fast-ramped superconducting model dipole built as part of the magnet R&D program for GSI. The magnet was designed to meet specifications for the SIS200 accelerator: 4 T central field, 1 T/sec ramp rate. Because the RHIC arc dipoles can operate at 4 T, GSI and BNL worked together on a model magnet program based on the RHIC design. Use of the RHIC cross-section enabled the work to take advantage of much of the RHIC design and tooling and some of the RHIC magnet components, thereby getting the effort off to a fast start. However, it has been necessary to make significant modifications to the magnet design, especially the superconductor (described in previous sections), to build a magnet that can ramp 20 times faster than RHIC and have much lower eddy current energy losses.

3.1 Magnet Construction

The cable used for coil fabrication was GSI-004-B, with the standard RHIC insulation. This insulation provides substantial impedance to the flow of helium between the interior of the cable and the reservoir just outside the coil. To allow more rapid heat exchange, a laser was used to cut away about 25% of the insulation on the thin edge of the insulated cable (Fig. 7). The holes in the insulation were precisely made so that the coils could be wound and cured without developing turn-to-turn shorts. Turn-to-turn standoff voltages of 1.1 kV were observed for both the straight section and end regions of a test coil that was cut in half and collared. This is less than the nominal test condition, > 2 kV, for RHIC coils but sufficient for the SIS200 application.

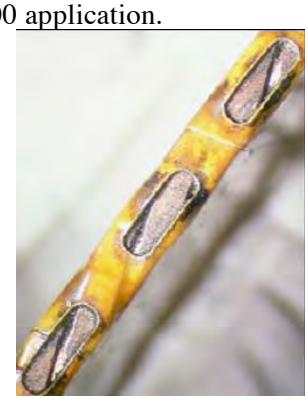

Fig. 7 Cable inner edge

Where feasible, magnet components were made from insulators rather than metals. In the GSI magnet (Fig. 2), the three wedges used in the coil to control field quality were G11 rather than Cu. The cable is ~ 25 μm thicker than the RHIC cable, resulting in a cured coil (32 turns) that is oversize by 0.9 mm. The G10 end pole spacers and Ultem® coil end saddles were modified to take account of the oversize cable. The shims placed between the coil and the pole were made of G11 and reduced in thickness to compensate for the oversized coil.

The coils were collared with Kawasaki high-Mn stainless steel collars. (The collars were designed for the LHC D2/D4 IR dipoles, also made using a variation of the RHIC arc dipole design .) As a handling aid, collars are assembled into 15 cm-long packs before being placed on the coils. G10 tubes were used to assemble these packs. It was possible to replace the brass keys used to lock the collars around the coils with G11 everywhere except for 2 cm at the non-lead end, where brass was used. At the lead end of the magnet, the collars have a larger inner diameter because of the radial space needed to bring the lead at the pole of the coil beyond the end of the coil. For the GSI magnet, the brass pieces used to fill this volume were halved in thickness and doubled in quantity, and the pieces of brass were insulated from one another.

The yoke laminations were 0.5 mm thick and punched from low coercivity 3.3% Si-steel (H_c = 31 A/m). The laminations were coated with B-stage epoxy and glued into blocks 254 mm long. Five blocks make up a half yoke. Each half yoke is supported against axial motion by three stainless steel rods that run through holes in the yoke and restrain the yoke with stainless steel nuts insulated from the yoke by G10 washers. G10 tubes are placed around the stainless steel rods to insulate the rods from the yoke. The two yoke halves are aligned with respect to one another with G10 alignment keys at the yoke mid-plane. The yoke is held together by welding a stainless steel shell around it. There is a welding backup strip at the mid-plane but the strip is not welded to the yoke.

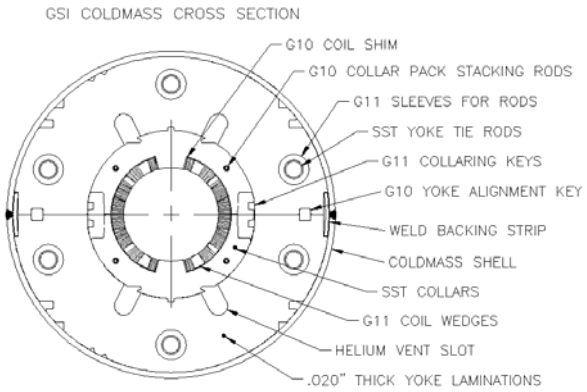

Fig 8. Cross section of the cold mass

In RHIC magnets, quenches at high ramp rate are likely to originate in the "ramp" section of the cable, at the end of the pole turn of the coil, where the cable is filled with solder to keep it rigid as it is moved by G10 fixtures to a larger radius so that it can be brought past the end of the coil and spliced to the cable from the other coil. The splice between the two coils halves is itself a possible source of quenching. However, the high value of R_C in the cored cable was judged to be sufficient to prevent such quenching in this magnet, so this region of magnet construction was the same as for RHIC dipoles. The magnet has no beam tube in it. Standard RHIC construction is used to restrain the axial motion of the coil.

3.2 QUENCH TEST RESULTS

The magnet was tested in pool boiling helium (4.5 K nominal). It was initially operated at the RHIC ramp rate, 0.053 T/s (Fig. 3). The sixth and last quench at this ramp rate was at 7.76 kA (4.38 T central field), approximately equal to the short-sample limit of the cable and ~ 10% above the 4 T

design. A different power supply was used for quenching at high ramp rate. It was found that both the magnet and this supply could ramp at 2 T/s, twice the design. Quench testing was carried out at this ramp rate. Further power supply improvements enabled the magnet to be ramped continuously to 4T and 4T/s without any quenches.

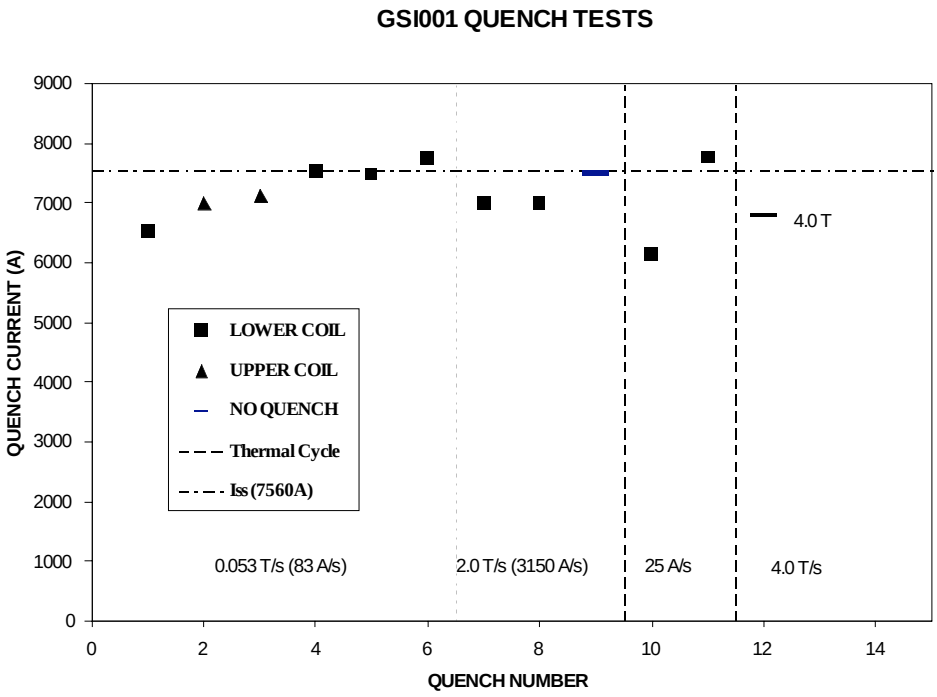

Fig. 9 Quench history, showing six quenches at 0.05 T/s, followed by two at 2 T/s, then stable operation at 7.5 kA. The horizontal line indicates the estimated short-sample limit of the magnet.

3.3 Loss Measurements

The energy loss was measured by recording the average voltage and current of the magnet over periods of 1/60 s. The cycle for a typical measurement is shown in Fig. 10

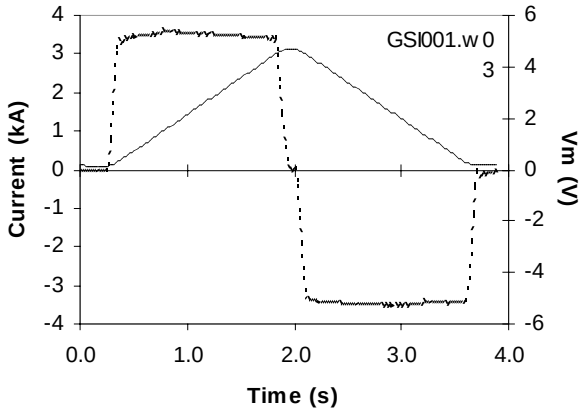

Fig. 10 Vm (dashed line) and I (solid line) for a typical energy loss measurement.

For each period, the energy was calculated as the VI product times the time between points. The magnet's voltage was measured by a precise voltmeter (HP3458A). The voltage taps on the magnet were placed on the superconducting leads, close to the coil (i.e., between the coil and the

splice that joins the magnet's leads and the power supply's leads). The current was measured by a voltmeter of the same model, which recorded the output of a DCCT (Holec).

A typical energy loss for this magnet is ~ 0.2% of the magnetic field energy, so considerable effort was invested in checking for and minimizing errors. The power supply control system was modified to minimize differences between the up ramp and the down ramp. The feedback circuit was adjusted to essentially eliminate overshoot. The control software generated smooth transitions between constant current and ramping. Each such transition accounted for typically 5% of the total ramp time. Dwell times at the minimum and maximum currents (typically 0.4 s and 0.2 s respectively) were minimized.

Two checks for offsets in the voltage were made with the power supply connected to the magnet but with the supply's reference input shorted. The first check was for DC offsets. There was no DC offset in the output voltage. Second, the effect of voltage errors was checked by programming the reference voltage to generate a fake, perfect current signal and measuring an apparent energy loss. For a 2 T/s ramp to 5 kA, an apparent loss of 1 J was measured, much smaller than the magnet's measured loss under these same conditions, ~80 J. The current offset is small, 0.2 A, and does not affect the measured energy loss.

Several other items should be mentioned. The measurement was not affected by the material used for the cryostat liner. We checked that the resistance of the splice between the two coil halves did not contribute measurably to the energy loss. Initially, measurements were made at constant dI/dt. At the highest ramp rates, we implemented an algorithm to correct for the ~ 8% drop in transfer function due to saturation at 4T so that the ramp would be at constant dB/dt. No significant difference was found between these measurements. The ramp rate quoted covers the entire time spent while ramping (including the smooth onset and roll-off of the ramp) but not the dwell times at high or low current. The AGS Booster Synchrotron, a possible source of perturbations of the 60 Hz AC signal, did not operate while these measurements were underway.

Details of the loss calculation in the magnet can be found in Ref. [9]. Fig. 11 shows the experimental measurements at select fields which are fitted to straight lines.

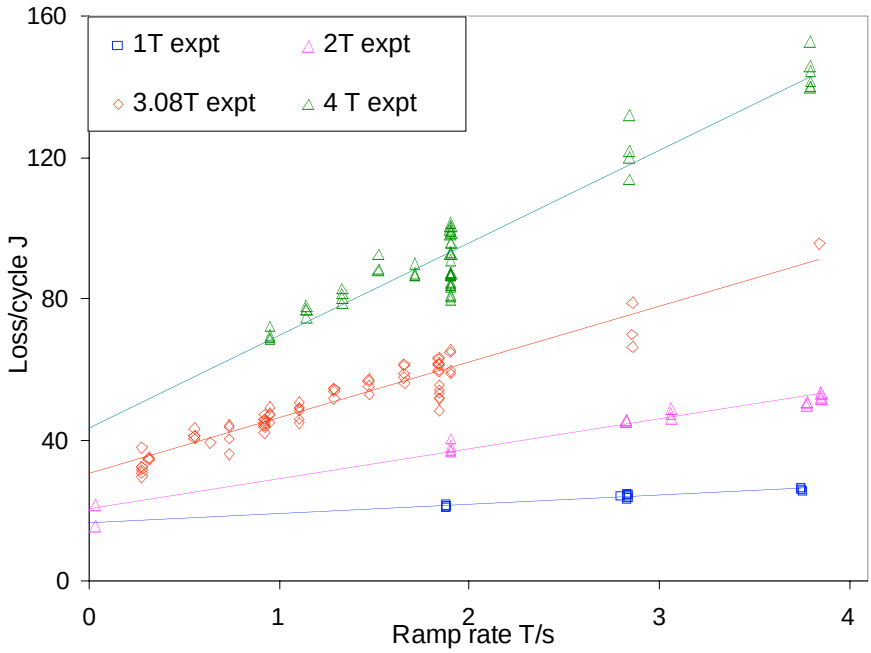

Fig 11. Experimental data of loss per cycle versus dB/dt for various values of maximum field

In order to compare the calculation with experimental data, the data points are fit to straight lines and the gradients (that due to eddy current loss) and intercepts (hysteresis loss) are compared with calculations. First we examine the rate dependent term which is assumed to be a sum of the strand loss and the cable loss. Fig. 12 shows the gradient plot. The eddy current losses are dominated by the inter-filament strand loss. The solid line is the inter-filament strand loss. The two dashed lines are for different assumptions about the cable coupling loss via R_A in transverse field. As noted in [6], this loss can be increased by up to a factor 3 if the R_A contact is predominantly at the edge of the cable and, as noted in [7], we have seen clear indication that R_A is lower at the edge than in the centre. The calculation uses the following measured quantities: R_C=60 mΩ, R_A=64 μΩ, and matrix resistivity ρ_{et} =1.1 $x10^{-10}$ Ω-m. Also shown is a quadratic fit to the data (dot-dash line). From Fig. 12, it would appear that the edge concentration gets stronger at high fields, perhaps an effect of the increasing forces.

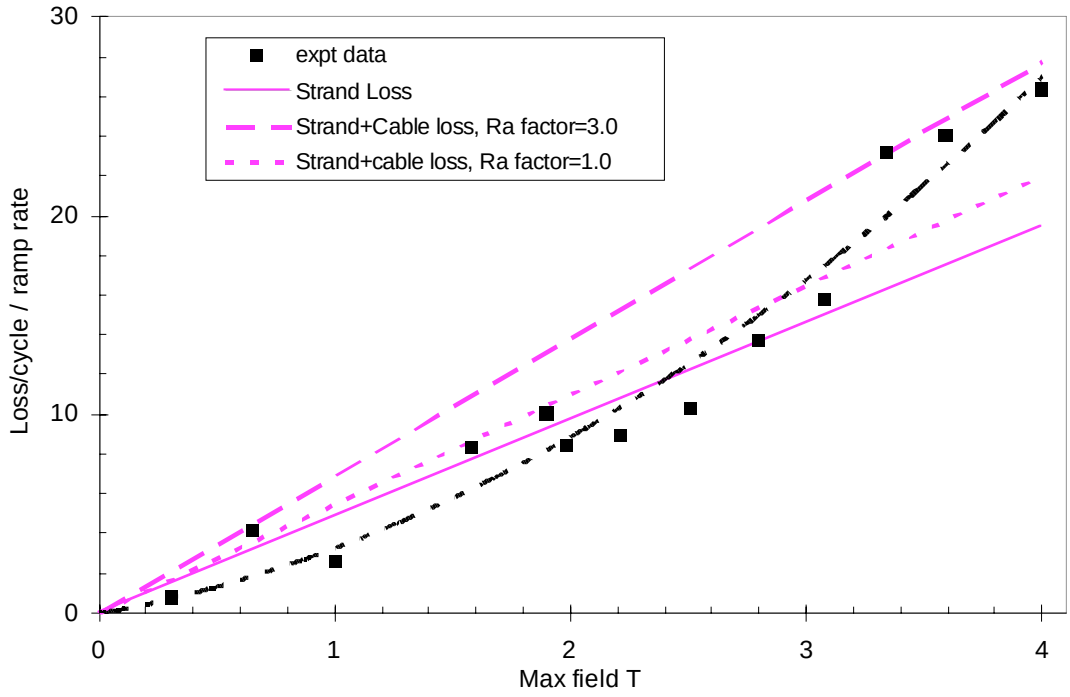

Fig 12 Experimental and calculated gradient of (loss per cycle vs. ramp rate) vs. maximum field.

Secondly the intercept of the plots in Fig. 11 at zero ramp-rate, which is the hysteresis loss per cycle, is plotted. Theoretically, this loss comprises three terms: the superconductor hysteresis loss, the enhancement caused by transport current and the iron loss. Fig 13 shows each of the calculated terms. It may be seen that the transport current correction has not made much difference. The iron hysteresis makes an increasing contribution at high fields, but does not fully explain the upward curvature of the experimental data. Nevertheless, the general level of agreement is reasonably good.

4. CONCLUSIONS

Even in the fastest sweeps of 4T/s to 4T, the 4T-model dipole has shown no effect of ramp rate on quench current. AC losses show the expected behaviour of a hysteresis component plus a component comprising coupling and eddy currents, which increases linearly with ramp rate. Using a set of parameters derived from measurements on short samples of wire and cable, we have calculated hysteresis and rate dependent components of loss which are in very reasonable agreement with the measured losses. The rate dependent losses seem to confirm that our conductor has an adjacent

resistance R_A which is lower at the edge of the cable than in the centre and that, perhaps, this effect gets stronger at high fields, i.e. at high stresses. Hysteresis loss is generally as predicted, but the experimental plots show a somewhat stronger upward curvature at high fields; we have no explanation for this.

Overall, the lack of an effect of ramp rate on quench current and the rather low and predictable ac losses show that this method of coil construction is very suitable for fast ramping accelerator magnets.

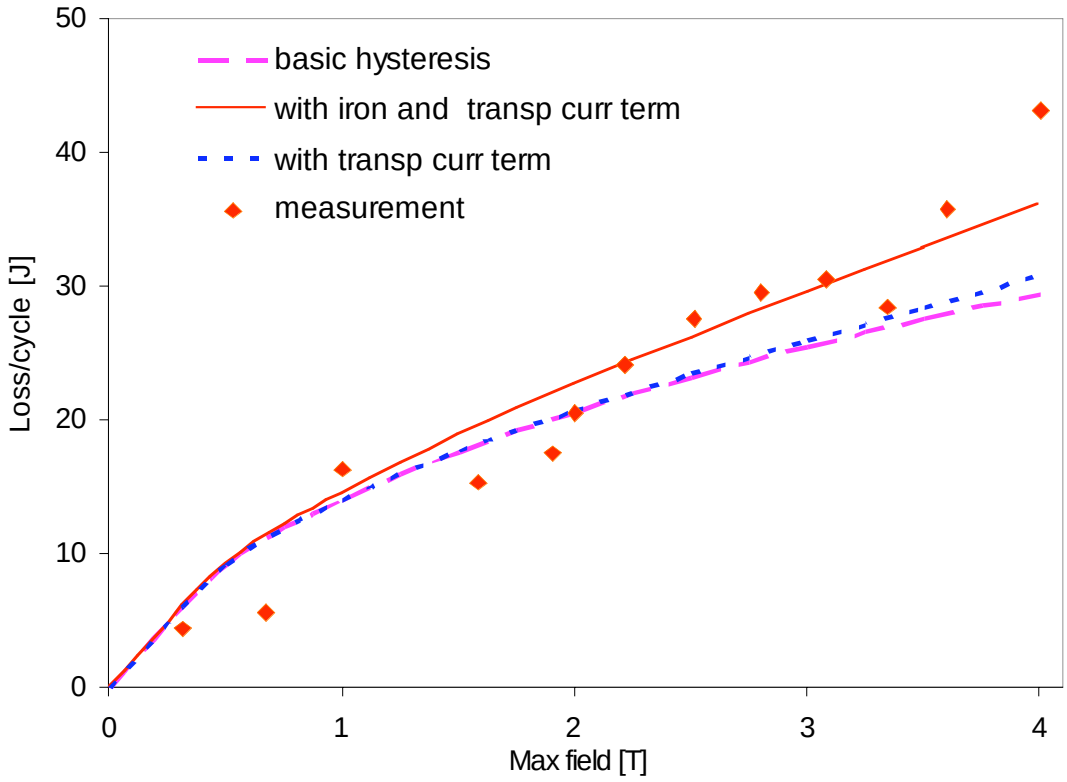

Fig. 13 Calculated and experimental data of hysteresis loss per cycle (intercept of loss vs. dB/dt plots.

ACKNOWLEDGEMENTS

I would like to acknowledge the work of all the collaborators on the GSI prototype magnet development. They are the following: from BNL, M. Anerella, G. Ganetis, P. Joshi, A. Marone, J. Muratore, J. Schmalzle, R. Soika, R. Thomas, P. Wanderer, from GSI, C. Muehle, J. Kaugerts, G. Moritz, and Consultants to GSI, M. N. Wilson, W.V. Hassenzahl.

REFERENCES

[1] G. Moritz et al, “Towards Fast-Pulsed Superconducting Synchrotron Magnets,” Proc. 2001 Particle Accelerator Conf. (2001) 211.

[2] A.D. Kovalenko et al, “Superferric Model Dipole Magnet with the Iron Yoke at 80K for the GSI Future Fast Cycling Synchrotron”, IEEE Trans Appl Superconductivity, Vol 13 (2003) 1335.

[3] M. Anerella et al, "The RHIC Magnet System," Nucl. Inst. Meth. A, Vol 499,(2003) 280.

[4] D. Wake, D. Gross, R. Yamada and B Blatchley, IEEE Trans MAG-15, No 1,(1979) 141.

[5] M.N. Wilson et al, "Design Studies on Superconducting $Cos\theta$ Magnets for a Fast Pulsed Synchrotron", Proc MT-17, IEEE Trans. Appl. Superconductivity Vol 12, (2002) 313.

[6] R. Soika et al, "Inter-strand Resistance Measurements in Cored Rutherford Cables", IEEE Trans Appl Superconductivity, Vol 13 (2003) 2380.

[7] M.N. Wilson, A.K. Ghosh, B. ten Haken, W.V. Hassenzahl, J. Kaugerts, G. Moritz, C. Muehle, A. den Ouden, R. Soika, P. Wanderer, W. A. J. Wessel, "Cored Rutherford Cables for the GSI Fast Ramping Synchrotron", IEEE Trans Appl Superconductivity, Vol 13, (2003) 704.

[8] P.Wanderer et al, "Initial test of a fast-ramped superconducting model dipole for GSI's proposed SIS200 accelerator", Proc. 2003 Particle Accelerator Conference, Portland OR USA, May 12- 16, 2003,

[9] M. Wilson et al, "Measured and calculated losses in a model dipole for GSI's Heavy Ion synchrotron", MT-18 Morioka, Japan, Oct 20-24, 2003.

[10] S. Le Naour, "Test Report on Magnetization measurements made on RHIC wires with CERN test station", CERN Tech. Note 2003-03, (2003)

[11] A. K. Ghosh, W. B. Sampson, E. Gregory, S. Kreilick, and J. Wong, "The effect of magnetic impurities and barriers on the magnetization and critical current of fine filament NbTi composities", IEEE. Trans. on Magnetics, vol. 24, (1988) 1145.

[12] A. P. Verweij, Electrodynamics of Superconducting Cables in Accelerator Magnets, Ph.D. Thesis, University of Twente, Enschede, The Netherlands, (1995).

[13] R. Soika and A.K. Ghosh, "Interstrand resistances in cored Rutherford-type superconducting cables", submitted to Cryogenics (2004).

[14] D. Richter, J. D. Adam, J.-M. Depond, D. Leroy, and L. R. Oberli, "DC Measurement of Electrical Contacts between Strands in Superconducting Cables for the LHC Main Magnets", IEEE Trans. Appl. Superconductivity, vol. 7, (1997) 786.

[15] D. Richter, J. D. Adam, D. Leroy, and L. R. Oberli, "Strand Coating for the Superconducting Cables of the LHC Main Magnets", IEEE Trans. Appl. Superconductivity., vol. 9 (1997) 735.

CABLE DESIGN AND RELATED ISSUES IN A FAST-CYCLING SUPERCONDUCTING MAGNETS

A.D.Kovalenko
JINR, Dubna, Russia

Abstract
Hollow superconducting cables for a fast-cycling synchrotrons are discussed. The essential features of the cable designed for the Nuclotron at JINR are presented. New versions of a hollow NbTi superconducting cable are described. The first test results with a cable that has been designed for an operating current of 12 kA at B = 2 T, dB/dt = 4 T/s and pulse repetition rate f = 1 Hz are presented. Further possibilities of using hollow cables both for dipoles with bore field of 4-6 T operating at repetition rate of 0.5 Hz and low field (B=1-1.5T) magnets operating at f = 10-20 Hz are discussed.

1. INTRODUCTION

The Laboratory of High Energies (LHE) of JINR has a long-term experience in design and construction of fast cycling (f = 1 Hz) synchrotron magnets. The first model 2T dipoles based on a cold window-frame yoke and superconducting coil made of hollow composite NbTi cable were constructed and tested at the Laboratory early in the 80's [1]. The R&D work was carried out in accordance with the program of construction the new heavy ion 6A GeV synchrotron, named Nuclotron [2]. The accelerator was built in five years (1987-1992) and put into operation in 1993 [3]. The operating magnetic field of the Nuclotron dipoles is 2T at a ramp rate up to 4T/s and pulse repetition rate f = 1 Hz. The key problem, namely the design of adequate superconducting cable, has been solved at the Laboratory by A. Smirnov with co-authors [4]. The technology for the cable production was well developed. Stable reproducibility of the cable performances has been achieved. The existing equipment at the LHE allows fabrication of about 150 meters of cable per day.

The JINR/GSI collaborative R&D work for the design of new cable options started three years ago. The work is connected with the proposal of construction of a "International Facility for Beams of Ions and Antiprotons at GSI" [5]. The facility consists of several new accelerator rings based on fast ramped superconducting magnets. In particular, 2T dipoles operating at repetition rate up to 1 Hz will be used for the synchrotron SIS100, and 6T dipoles with field ramp not less than 1 T/s should be designed in accordance with the project goal of SIS300. The idea of an SPS upgrade at CERN requires a design of a magnet with at least 4T and field ramp of 4 T/s. In addition, there is a general interest in the design of fast-cycling superconducting synchrotrons operating at f = 10-20 Hz. The concept of a hollow superconducting cable is very promising for all of the cases mentioned above.

2. THE NUCLOTRON CABLE

A general view of the original Nuclotron hollow superconducting cable (HSC) is shown in Fig.1. The main parameters are listed in Table 1. The standard industrial SC wire design of the Bochvar Research Institute [6] was used.

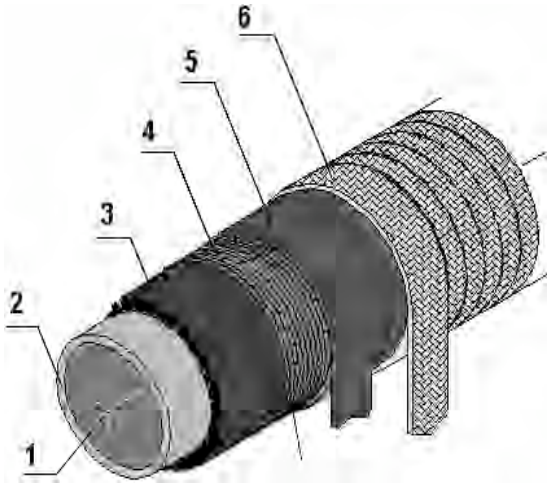

Figure 1. General view of the Nuclotron HSC: 1- two-phase helium, 2-copper-nickel tube, 3- superconducting wire, 4- nichrome wire, 5-kapton tape, 6-glassfiber tape.

Before the final design of the Nuclotron cable, more than 30 different short samples were fabricated and tested. The technology of the Nuclotron cable production and the test results were described earlier [7]. It is important to emphasize two essential features of the design: first, the AC eddy current loss in the cable is very close to the measured one in the SC wire and second, the weak ramp rate limitation (RRL). The dependence of the relative quench current degradation (RRL) on the external magnetic field ramp rate is shown in Fig.2.

Table 1
Main parameters of the Nuclotron cable

Cable diameter with insulation	7 mm
Cooling channel diameter	4 mm
Tube outere diameter	5 mm
SC wire diameter	0.5 mm
Number of the wires	31
Lay pitch of the wires	47 mm
Cu/NbTi ratio	1.38
Number of filaments	1045
Filament diameter	10 μm
Twist pitch of the filaments	5 mm
Minimum I_c per strand at 5 T and 4.2 K	165 A

The optimization of all other parameters was made to obtain the following operating performances at f = 1 Hz pulse repetition rate: quench current higher than 7500 A at B = 2 T and field ramp rate dB/dt = 4 T/s, AC power losses per NbTi volume q = 68 mJ/cm^3 per cycle.

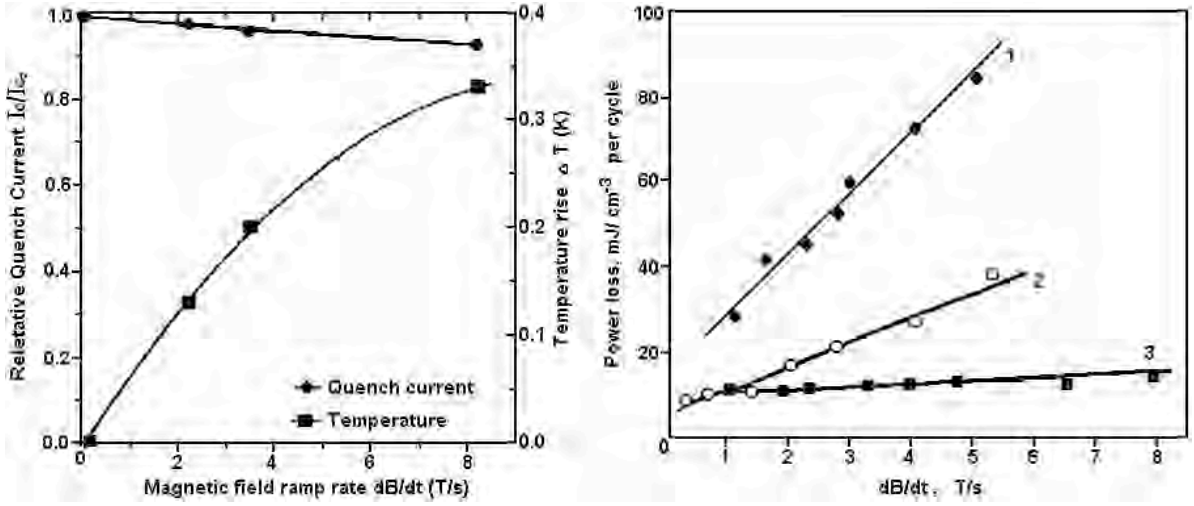

Figure 2. Nuclotron cable (short sample measurements): left diagram – quench current degradation and the superconductor temperature rise versus external magnetic field ramp rate. (I_{co} – critical current at dB/dt=0.1 T/s. The experimental data refer to a short sample): right diagram – the eddy current power loss for different cable samples (Nuclotron cable corresponds to curve - 3).

We emphasize that for a given SC cable and a fixed coolant temperature neither the relative quench current nor the superconductor temperature increase with magnetic field ramp rate depend on the field amplitude. Up to now there are no other SC cables with similar properties. The measured degradation for HSC is only 4.8 %. The stronger ramp rate limitation of the Rutherford cable is caused by higher AC losses and higher thermal resistance between the superconductor and the helium. The comparison of the Nuclotron hollow cable and the proposed several new versions of the "cable-in-conduit", aimed at operating in fast-cycling synchrotron magnets, is presented in [9].

3. NEW OPTIONS OF HOLLOW SC CABLE

As a follow-up of the development described above, it was proposed to use wires of special cross-section (keystoned or trapezoidal) instead of round wires[10]. The main design goal is to increase both the engineering current density as well as the operating current, without loosing the dynamic properties of the cable. A view of the cable cross-section is shown in Fig. 3.

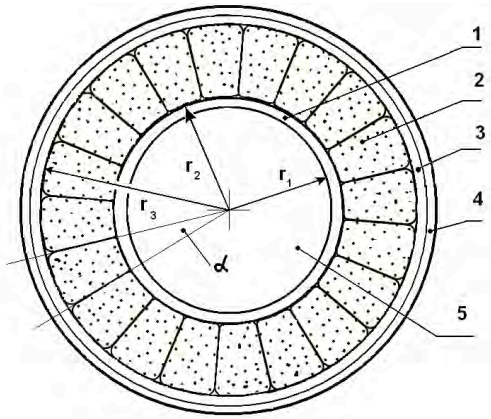

Figure 3. Hollow superconducting cable based on keystoned wires: 1 – copper-nickel tube, 2 – profiled superconducting wire, 3 – nichrome wire, 4 – electric insulation layers, 5 –channel for coolant, α - the wire angular size.

The dimensions of the cable cross-section, number of the wires and the sizes of their cross-sections, cooling channel diameter are optimized for the specified operating conditions. We are planning to carry out R&D works in the following directions:

- design and test the cable (option HSC-K1) for an operating current of 12 kA at B = 2 T, dB/dt = 4 T/s and pulse repetition rate f = 1 Hz;
- investigate the possibility to reach an operating current of 30 kA at B = 6 T, dB/dt =2…4 T/s and pulse repetition rate f = 0.25 …0.5 Hz. (option HSC-K2)

A draft layout of the both cable options, HSC-K1 and HSC-K2 was made. Their main design parameters are listed in Table 2 [11].

Table 2
Main Characteristics of designed HSC-K

	HSC-K1	HSC-K2
Operating parameters:		
- magnetic field, T	2	6
- current, kA	12	30.0
- helium temperature, K	4.6	4.6
- ramp rate, T/s	4	4
AC losses:		
- per NbTi volume, mW/cm^3	45.2	30.1
- per 1 m coil length, W/m	3.8	20.4
Helium channel diameter, mm	4	4.6
Copper-nickel tube diameter, mm	5	5.6
Number of strands	15	12
Strand cross-section, mm^2	0.789	3.62
Cu/NbTi ratio	1.38	1.38
Nb50-Ti50 filament diameter, μm	6	4
Twist pitch of filaments, mm	5	5
Bending nichrome wire diameter, mm	0.2	0.3
Cable diameter with insulation, mm	7.16	10.52
Structural current density, A/mm^2	234	248

The HSC-K1 option is suitable for manufacturing a single-layer winding of the Nuclotron style dipole, whereas the HSC-K2 can be considered as a possible alternative for a fast ramped 6T dipole. The first optimization of HSC-K type cable aimed at the design of a 4T cosine theta style dipole was also done. The results are presented in the next section. Note that both HSC-K1 and HSC-K2 are high current cables, in the range of 12 kA. Nevertheless, SC magnets with an operating current of 12 kA have been designed for the LHC. Much higher operating currents are used in the SC magnet design for ITER research. Other equipment like high current leads, power supplies, etc. have been developed and are available at different laboratories.

3.1 HSC-K1 cable version test results

3.1.1 Manufacturing

Test samples of the cable version were manufactured and tested. For adjustment of tools and mechanics a prototype sample of such HSC was manufactured at the LHE. Fig. 4 presents the photograph of the sample cross-section. The trapezoidal cross-section was prepared by rolling a round 1.05 mm SC wire to the sizes of trapezium 0.73 mm high x 1.21/0.94 mm at the bottom and top sides respectively. The copper-nickel tube was coated with epoxy compound and wrapped

with fifteen profiled wires. Winding 0.15-mm diameter synthetic thread under tension in a spiral around the strands provided fixation of the wires and a suitable pre-stress.

The first fabrication experience with the new cable showed that the general idea is feasible, nevertheless, the production technology has to be improved further. The next step was manufacturing of the profiled wire at production stage. The first developed batch was fabricated at the Bochvar Research Institute. A single stacking multifilament composite wire manufacturing process was used. The billet was 130 mm in diameter. The NbTi rods were muffled with 1.5 mm thick Nb barrier and inserted in tubes of Cu–5%Ni-alloy. 127 cylindrical trimetal components were mounted in one hexahedral copper tube. Then 78 copper tubes with NbTi filaments were mounted in a copper shell. The total amount of superconducting filaments in the composite is 10644. The copper non copper ratio in the composite is 1.8. The 1-mm diameter wire was manufactured with 5 intermediate heat treatments at the temperature of 648 K for 24 hours each. The wire was twisted with a pitch of 8 mm. At the final stage of drawing the round wire was keystoned. A view of the resulting cross-section is shown in Fig.5 [12].

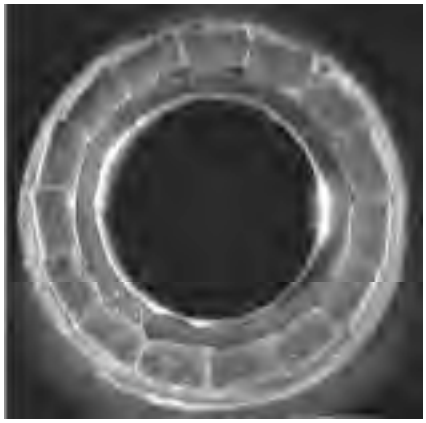

Figure 4. Photo of the HSC-K1 prototype cable (outer diameter is 7.16 mm).

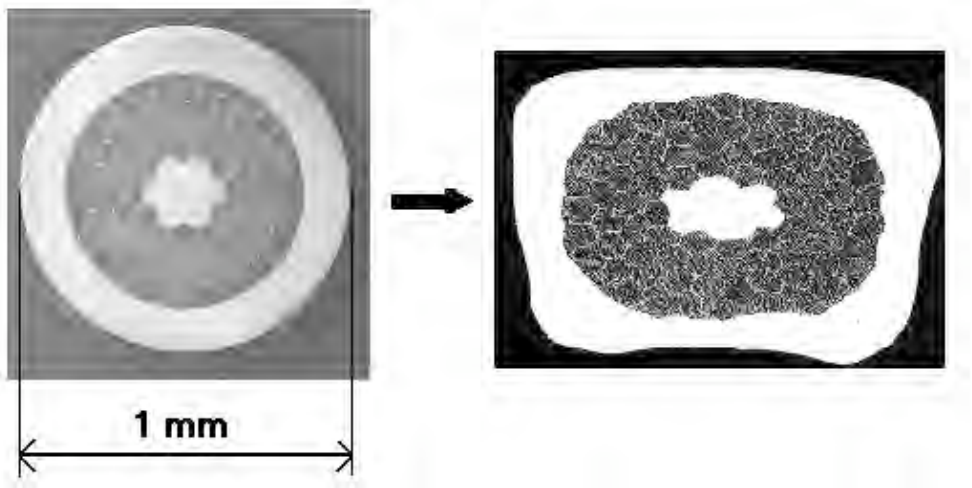

Figure 5. Photos of the HSC-K1 first industrial prototype.

3.1.2 The wire tests

The critical current and AC loss measurements of the wire were performed at the LHE. The dependence of the wire's critical current on external magnetic field is shown in Fig. 6.

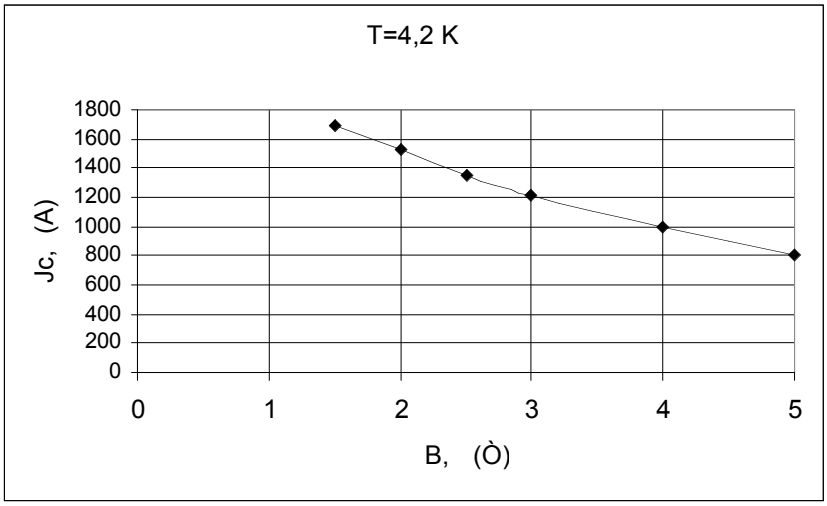

Figure 6. Critical current of keystoned wire versus external magnetic field B at T = 4.2 K.

The measured value is 1400 A at cable operation conditions B = 2 T and T = 4.46 K. Thus the expected critical current of the new cable, consisting of 15 wires, amounts to 21 kA. The AC loss in the wire was measured by calorimetric method. For B = 1.05 T and dB/dt = 2.1 T/s the measured value is about 22.4 mW per cm**3 of the wire. A pilot amount of the new cable was manufactured.

3.1.3 The cable sample test

Actual current leads and the power supply of our test facility are limited to an operating current of 9kA. So we can not excite the new cable directly to 20kA. Thus, it was proposed to test the critical current of the new cable using a closed current loop made of the tested cable itself. The current in the loop is excited by the pulsed magnetic flux in the aperture of the Nuclotron dipole, installed at the existing SC magnet test facility.

The sample tests were performed in October 2003. The magnet was ramped at dB/dt=4 T/s up to B = 2.2 T with pulse repetition rate f = 1 Hz. The current in the magnet winding was measured by a Rogowsky coil, placed at the current lead outside from the cryostat. Both measuring coils were calibrated before the measurements. A 13 kA current, with a 26 kA/s rise time was induced in the sample at the same repetition frequency. No quenches occurred in the sample. During test we could not reach the quench current due to insufficient mutual inductance between the magnet and the tested cable loop. We are planning to repeat the measurements after rearrangement of the test conditions.

4. FAST RAMPED 4T DIPOLE

The concept of hollow superconducting cable can be applied to the design and construction of a fast-ramped 4...6 T dipoles of the future synchrotrons with pulse repetition rate of 0.25...0.5 Hz. It is clear that a "cosine theta" cable arrangement (dipoles and quadrupoles) should be used in this case. A preliminary design of a dipole has been performed.

4.1. Concept of the magnet

A general description of our approach to a fast cycling 4T-magnet was presented in [13]. The magnet has a circular aperture of 100-110 mm. The coil is made with hollow superconducting NbTi cable. It was supposed that a single layer coil will be used. The number of turns in the coil is 12-14; i.e. 6-7 turns per half winding. A larger number of turns is not efficient and limited by available space. The dependence of the magnetic field on the operating current of the magnet is shown in Fig.7. Thus, the cable operating current value should reach of 30 kA. It is possible to reduce the operating current or increase the peak magnetic field with a double-layer coil. The calculations (2D) of the main dipole field were made for different numbers of turns. The angular positions of the turns was chosen to minimize the higher field harmonics.

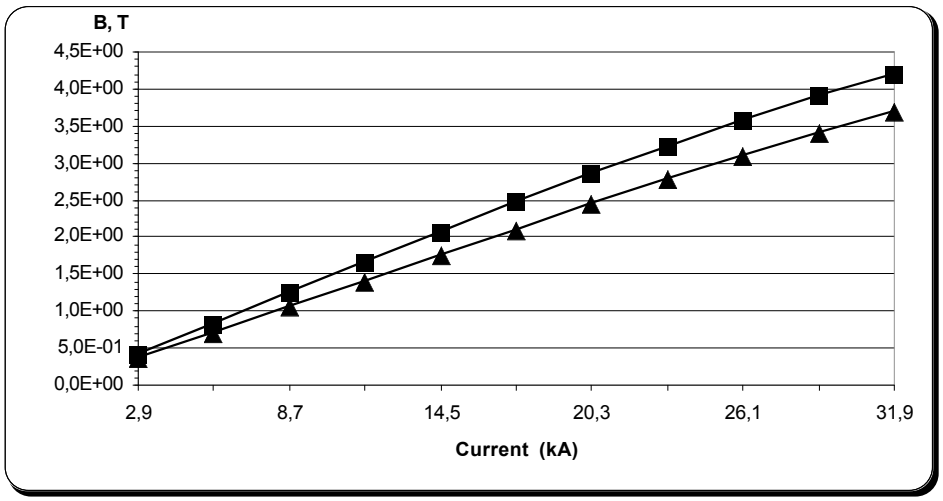

Figure 7. Ddependence of the dipole main field on operating current (for 6 & 7 turn windings).

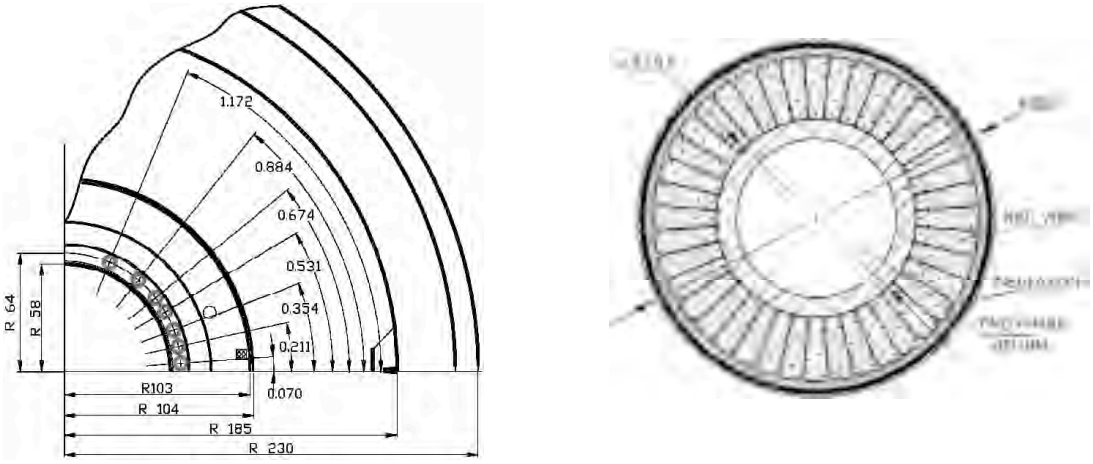

Figure 8. Optimized geometry of the coil for a fast-ramped 4T superconducting dipole magnet and cable cross-section.

4.1.1 Minimization of the cold mass

The magnet cold mass (T = 4.4 K) is limited to the coil and collar only. Cooling of the collar is provided through thermal contacts with the coil. The yoke (iron shield) temperature could stay at the level of T = 50…80 K. A small vacuum gap of 0.5-1.0 mm between them is sufficient. Experimental data on the SIS100 model 2T dipoles tests have shown a number of advantages of such a design concept and practical feasibility [14]. The mechanical characteristics, the strength

and the rigidity that are required in the coil and the collars at the force level corresponding to 4 T are well known and feasible.

4.1.2 AC loss, cable & cooling

The main part of the heat load in the magnet comes from the AC loss in the superconducting cable. The static heat flow from the 50 K yoke to the magnet cold mass will not exceed about 1W per meter magnet length. The heat inflow through the yoke support post and suspension parts is negligible as well. The AC power loss caused by the eddy currents in the beam pipe walls is estimated to be about 0.5W/m. We considered the pipe made as a stainless steel tube, 0.5 mm in thickness, for dB/dt =2 … 4 T/s. A new hollow high current cable is under design and test. The first step, namely a new cable operating at 13 kA and B=2.2 T have been made. The critical current of the wire short sample was about 950 A at T = 4.36 K and B = 4 T (see Fig.6.). Thus, taking the number of wires in the cable equal to 40 it will be possible to provide operating a current of 30 kA with about 30 % safety margin. The preliminary cross section of such cable is shown in Fig. 8. The external diameter of the cable is about 8.92 mm including electrical insulation. The calculated AC power loss in the cable is about 1 J/m per cycle at B = 4 T and dB/dt = 4T/s. Note that the averaged value of dB/dt across the cable is about twice less (in the case of a single layer coil). To remove the heat from the coil two phase helium mass flow rate of m = 1.9 g/s should be provided. The helium pressure at the coil inlet depends on the magnet length. For the magnet length of 2.6 m the pressure of p = 1.25 bar is sufficient. Of course, collars with suppressed eddy current power loss are supposed to be used.

4.1.3 The further R&D

A reasonable plan for the future R&D should address the following points:

- reduce the AC power loss in the cable using SC filaments of smaller diameter;
- study possibility of using Nb3Sn instead of NbTi wires;
- test new versions of the cables based on keystoned wires;
- design of a 6 T magnets based on a hollow cable.

5. SUPERFERRIC MAGNET AT REPETITION RATE OF 10-20 HZ.

Our first estimate on the possibility to construct superconducting Nuclotron-type dipole and a cryomagnetic system of a rapid cycling synchrotron (up to 10 Hz) was presented at MT-15 [15]. The extrapolation was based on experimental data obtained for the Nuclotron dipole with a cold iron yoke. Nevertheless, window-frame cold yoke is not optimal design concept for a very fast cycling (f >> 1 Hz) superconducting magnet. Moreover, the results of the recent R&D on SC hollow cables have demonstrated the possibility to produce a cable with much higher operating current and engineering current density compared to that was used for the Nuclotron. A version of superferric dipole magnet with the yoke at T = 50-80 K was also tested successfully. Thus, we can consider superferric H-type magnet with superconducting coils made from a hollow superconducting cable and the yoke at temperature of 50-80K. The cable operating current is chosen in the range of 12…25 kA. Thus, it is possible to obtain a magnetic field of 1.2-1.5 T in a magnet aperture of 55mm x 110 mm (v x h), taking 4 or 2 turns per pole. The external magnetic field in the cable will reach about one half of the field in the magnet gap, i.e. B = 0.6 - 0.75 T. The field ramp in the coils would be respectively dB/dt = 12…15 T/s at f= 10 Hz and dB/dt = 24….30 T/s at f = 20 Hz,. The Nuclotron cable have been tested at B= 2 T and dB/dt up to 8 T/s. We are planning to test the existing cable as well as the new versions at operating conditions suitable for 10-20 Hz superferric magnets.

ACKNOWLEDGEMENTS

The author wish to thank H.Khodzhibagiyan and A.Smirnov for discussion on the subject of the paper as well as E.Fischer and G.Moritz for fruitfull collaborative work. The R&D work on the new cables design is supported by the JINR/BMBF project.

REFERENCES

[1] N.N.Agapov et al., Cryogenics, June 1980, pp. 345-348.

[2] A.M. Baldin et al., IEEE Trans. Nucl.Sci. NS-30 (1983) 3247-3251.

[3] A.D. Kovalenko, Proc. EPAC-94, London, 1995, Vol.1, pp.161-164.

[4] A.A. Smirnov et al., J. de Physique, colloque C1, suppl. An N1, 45 (1984) 279-282.

[5] "An international accelerator facility for beam of ions and antiprotons. Conceptual design report". Available:http://www.gsi.de/GSI-Future/cdr/

[6] G.P. Vedernikov et al., Proc. 17 Int. Conf. on Magnet Technology, Geneva, Sept.2001

[7] F. Chovanec et al., Cryogenics, 21 (1981) 559-562.

[8] A.M. Baldin et al., Adv. Cryogen. Eng. 39 (1994) 501-508.

[9] H. Khodzhibagiyan et al., Proc. MT-18, Morioka, October 2003 (in press)

[10] N.N.Agapov et al., Proc. ASC 2000,

[11] H.Khodzhibagiyan et al., ASC 2002, Houston, August 2002.

[12] H. Khodzhibagiyan et al., Proc. EUCAS 2003, Sorrento, September 2003 (in press).

[13] A.D. Kovalenko et al., *EUCAS'2001,* Copenhagen, August, 2001. Elsevier Science B.V. Physica C 372-376 (2002), 1394-1397.

[14] A.D. Kovalenko et al., Proc. ASC 2002, Houston, August 2002.

[15] N.N.Agapov et al., Proc. MT-15, Beijing, October 1997.

CABLE DESIGN AND R&D FOR NED

D. Leroy
CERN, Accelerator Technology Department, Geneva - Switzerland

Abstract
This paper presents the work package on conductor development as a part of the Next European Dipole (NED) program supported by EU. The results of a dipole preliminary magnetic design to reach 15 T in the bore are summarised From this preliminary design, a strand and cable specification has been derived to place orders in European industries. The various steps foreseen for the strand development are indicated.

1. INTRODUCTION

The NED project is one of the Joint Research Activities (JRA) accepted by EU in view of developing in Europe high field accelerator magnets [1].

Six institutes have agreed to collaborate to the NED JRA:

- CCLRC-RAL (United Kingdom)
- CEA/DSM/DAPNIA (France)
- CERN/AT (International)
- INFN – Milano/LASA and – Genova (Italy)
- University of Twente (The Netherlands)
- University of Wroclaw (Poland).

The Phase I of NED, which is supported by EU is articulated around three main work packages: (1) Thermal Studies and Quench Protection (TSQP), (2) Conductor Development (CD) and (3) Insulation Development and Implementation (IDI).

The CD work package is coordinated by CERN. The core of the CD work package will be devoted to Nb_3Sn strand and cable development. It includes the preliminary designs of a large-aperture and high-field (up to 15 T) Nb_3Sn dipole magnet in order to derive the Nb_3Sn meaningful strand and cable specifications suitable for large field magnet applications. A technical specification will be written and an order will be placed according to the CERN procedures. The high critical current density of 3000A/mm^2 at 12 T, 4.2K, represents a new technical challenge for the European superconductor industry, which will also invest in this ambitious program. Within the limited funding, it was then decided to concentrate the Nb_3Sn strand fabrication on two routes: the Powder In Tube (PIT) and the Internal Tin Diffusion (ITD).

CERN will make the follow-up of the contract. The characterization measurements will be performed in the associated laboratories:

- Strand critical current measurements (following a standardized protocol) at CEA/Saclay, INFN-Milano/LASA, University of Twente.
- Strand magnetization measurements at INFN-Genova.
- Cable critical current measurements at University of Twente.

2. RESULTS OF THE PRELIMINARY MAGNETIC STUDIES

A preliminary design of a large-aperture (up to 88 mm), high-field (up to 15 T), Nb_3Sn dipole magnet has been made to derive conductor specifications. The design is based on a two layer cable distribution.

2.1 Magnet Overall Structure

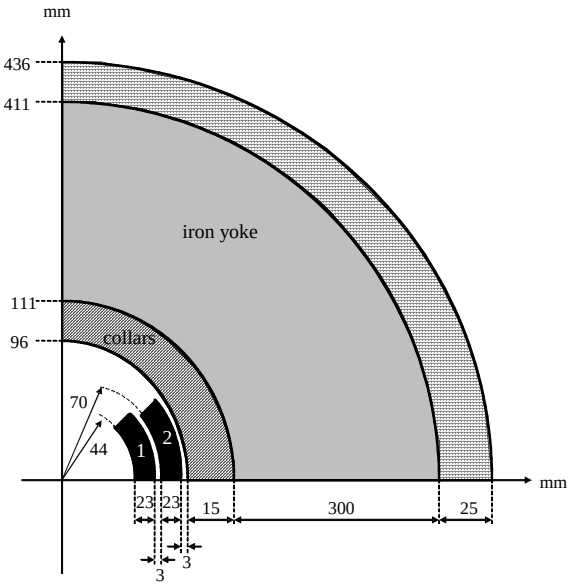

Fig.1.Magnet overall lay-out

Fig.1 shows a schematic magnet overall layout. The coil aperture is 44 mm; there is 3 mm space between the two layers. The iron yoke is separated from the coils by an intermediate spacer (collars) of 25 mm thickness and is surrounded by a 28 mm thick stainless steel shrinking cylinder. The inner layer consists of 4 blocks of conductors while the outer is made of 3. The adjacent blocks are separated by a distance of at least 2 mm. The iron yoke is 350 mm thick.

2.2 Results of an impact study

An impact study of a few variables on the conductor has confirmed that the main parameter influencing the bore field is the overall current density in the coil. The latter is dominated by the critical current density in the non-copper and the insulation thickness. Both have not been considered as a free parameter because they depend so much on the technology, which will be developed in the frame of the NED program. The insulation thickness of 0.2 mm on each side of the cable represents 17% of the total conductor surface.

With a critical current density in the strand non-copper area of 1500 A/mm^2 at 15 T, 4.2 K, the bore field as calculated is 14.4 T at 4.2 K for a maximum quenching field on the conductor of 15 T taking into account a cable degradation of 10 %. To reach 15 T in the aperture, the magnet has to be operated at 1.9.K as shown on the load lines represented in fig.2. The pressure on the broad face of the cable, only due to the magnetic forces amounts to 150MPa.

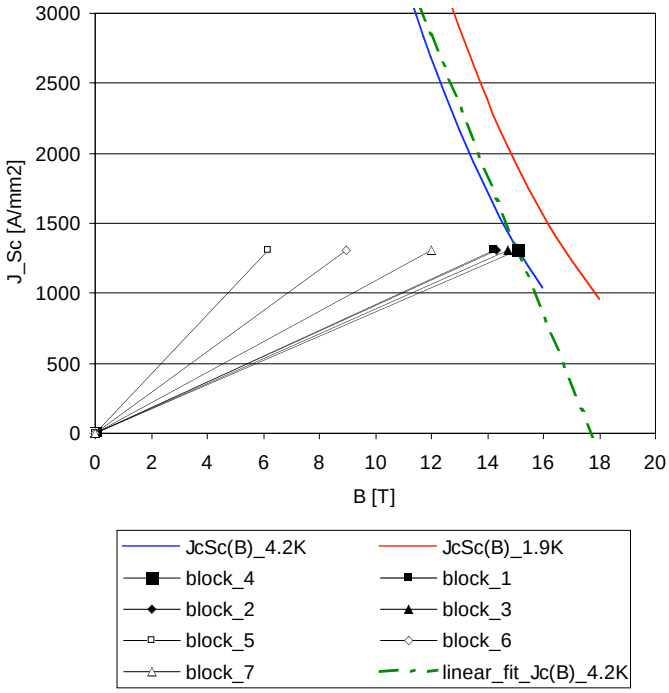

Fig.2.Load Lines

2.3 Overall characteristics of a 88 mm, two layer magnet design

The number of conductors is 19 for the inner layer and 26 for the outer layer. The 2 layers of coil winding use the same cable of 40 strands having a diameter of 1.25 mm

2.3.1 Strand and Cable Characteristics

Table 1 Strand and Cable characteristics

strand diam.	strand number	Cu/ non_Cu	height	width inner	width outer	insulation	Jc_str at 15T, 4.2K	Jc_cab at 15T, 4.2K
[mm]			[mm]	[mm]	[mm]	[mm]	[A/mm^2]	[A/mm^2]
1.25	40	1.25	26	2.175	2.375	0.2	666.67	417.1

2.3.2 Magnet Characteristics

Table 2 Magnet Characteristics

Field [T] / Current [A]	L [mH/m]	Wm [kJ/m]	Max pressure [MPa]	Fx, result. [MN/m]	Overall diameter [mm]
14.42 / 28660	4.4	1810	148	15.8	1004

Calculations with a cable degradation of 10%.

3. STRAND CHARACTERISTICS

Figures 3 and 4 show cross-sections of the strands based on the two foreseen technologies. NED will not make use of a collective barrier in the ITD process.

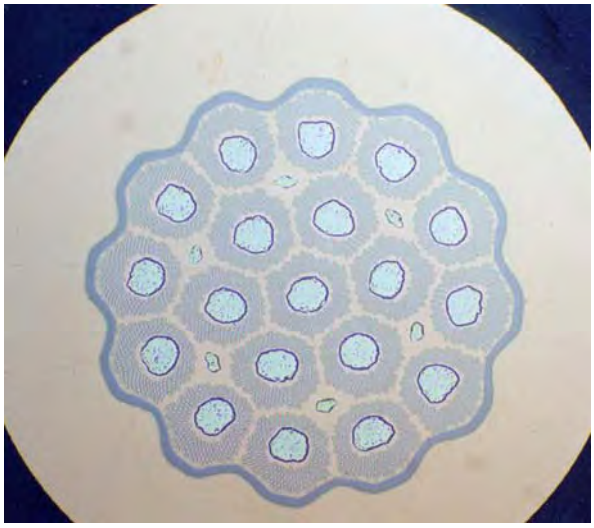

Fig. 3 I T D (ALSTOM)

Fig. 4 P I T (SMI)

3.1 Strand Characteristics for NED

The strand specification for NED will be based on a critical current density of 1500 A/mm^2 at 15 T, 4.2 K and 3000 A/mm^2 at 12 T, 4.2 K The effective filament size is smaller or equal to 50 μm. The strand diameter is determined by the maximum cabling capacity of 40 strands.

Table 3.Strand Characteristics

Strand diameter	1.25 mm
Effective Filament diameter according to billet design	< 50.0 μm
Copper to non-copper volume ratio	1.25 ± 0.10
Filament twist pitch after cabling	30 mm
Filament twist direction	right-handed screw
Minimum critical current at 4.222 K	1636 A at 12 T
	818 A at 15 T
RRR (after full reaction)	> 200
n-value @ 15 T and 4.2 K	> 30

4. CABLE CHARACTERISTICS(PRELIMINARY)

Table 4 indicates the characteristics of the cable. The dimensions are preliminary and will be decided after cabling tests and measurements of the current degradation.

Table 4. Cable Characteristics

Cable width	26 mm
Cable mid-thickness at 50 MPa	2.275mm
Keystone angle	0.22 degrees
Cable thin edge thickness	2.175 mm
Cable thick edge thickness	2.375 mm
Cable transposition pitch	~180 mm
Number of superconducting strands	40
Critical current at 4.222 K, with field normal to broad face	29440 A at 15 T 58880 A at 12 T
Minimum critical current at 4.222 K of extracted strand	736 A at 15 T 1472 A at 12 T
n-value @ 15 T and 4.222 K	> 20
Residual resistance ratio before reaction after reaction	≥ 70 ≥ 120
Cable transposition direction	left-handed screw thread
Minimum unit length	145 m

5. PROGRAM FOR NED CONDUCTOR

To obtain high a critical current density of 3000 A/mm^2 in a strand of 1.25 mm is very difficult. The firms having a contract have to optimize the raw materials, the Sn and Nb content.
The fabrication process must be suitable for large production. Billets of circa 70 kgs have to be produced and reach piece lengths of strands larger than 1000 m. Many metallurgical tests have to be performed on the strands.

A working group under the leadership of A. den Ouden will make the standardization of the electrical characterization. The follow-up of the contract will foresee several milestones related to payments. The indicative program of development is summarized in Table 5.
The programme requests to make cabling tests with the strands under development to measure the effect of the billet design on cable degradation, if any.

Table 5 .Indicative program of development, fabrication and milestones.

Steps	Date	Description	Milestones
	December 2004		Progress report
1	June 2005	Qualification of initial strand designs	Fabrication/tests of at least 10 kg of strand and relevant cabling tests Progress report
2	December 2005	Qualification of final strand design	Fabrication/tests of at least 10 kg of strand and relevant cabling tests. Progress report
3	June 2006	Total strand production	Fabrication/tests of total strand quantity and cabling tests. Progress report
4	December 2006	Total cable fabrication	Total cable quantity delivery Final report

6. CONCLUSION

The paper gives the general characteristics of the strand and the cable to be developed for the Next European Dipole (NED).The main characteristics are coming from a preliminary magnet design. The main features of the strand are a diameter of 1.25 mm and a current density in the non copper of 3000A/mm^2 at 15 T, 4.2 K. This current density is very ambitious The strand fabrication will be based on Nb_3Sn material following the two routes of Internal Tin and Powder in Tube. Orders will be placed in the European superconductor industries to develop the strand and cable within the next 3 years.

ACKNOWLEDGEMENTS

The author wishes to thank O.Vincent-Viry for the magnetic calculations of the preliminary magnet design and all the participants of the NED Collaboration lead by A. Devred

REFERENCES

[1] A. Devred, D.E. Baynham, L. Bottura, M. Chorowski, P. Fabbricatore, D. Leroy, A. den Ouden, J.M. Rifflet, L. Rossi, O. Vincent-Viry and G. Volpini High Field Accelerator Magnet R&D in Europe" Proceedings of the MT18 Conference, 20-24 October 2003, Morioka, Japan

HIGH FIELD CABLE DEVELOPMENT FOR ITER

P. Bruzzone
EPFL-CRPP, 5232 Villigen-PSI, Switzerland

Abstract
The milestones of over one decade conductor development for the high field magnets of ITER are reviewed, keeping an eye at the actual feed-back from the R&D results into the design. The review includes the fields of ac loss, stability, quench, n-index and joints. Finally, the issues of the transverse load degradation in Nb_3Sn CICC and the thermo-siphon effect in the dual channel CICC are discussed.

1. INTRODUCTION

In modern science, since Newton and Galileo, the idea (theory) always comes before the praxis (experiment). The progress is stimulated by models, hypothesis and abstractions. The experiments are not themselves the source of the progress, but the (mandatory) certification of an achieved advance. Atomic physics, relativity, quantum mechanics, standard model have been described decades before the related, crucial experiments.

In the field of technology, the roles are reversed. The practical achievements (inventions) are in use long before an organized understanding is established. Those who built (and partly still build) bicycles, medicines, generators and bombs are not necessarily aware of the "science" behind it. Our daily culture also privileges the practical know-how rather than the conscious understanding.

In the field of big science, it is not unusual to mix the traditional identity of science and technology, mostly due to the fact that the actors tend to be the same persons. It may happen to hear a young scientist claiming that the experiments are the source of the knowledge ("you must keep making experiments till you find something"). On the other hand, the progress in technology, outside the marketplace, is sometime slow down by dogmatic conservatism (fidelity to models) and reluctance to deviate from the beaten path.

Reading the following review of over one decade of R&D activity for the ITER conductor, the thought may arise that we are not dealing with fast developing, advanced technology items like cell phones, genetic engineering products, personal computers, power lasers, etc. The author actually shares such thought.

2. THE BASIC CONSTRAINTS FOR THE LAYOUT OF THE ITER CONDUCTOR

What makes different the superconducting magnets for "next step" fusion device in comparison to most superconducting coils is the large stored energy. Most constraints on the design choices for winding and conductor follow directly from the combination of large size and high field.

The electromagnetic loads for the ITER coils can be roughly represented by the product $B{\cdot}J{\cdot}R$, where B is magnetic field up to 12-13 T, J is the current density and R is the radius of the winding, up to 15 m. To withstand the huge loads, a large fraction of the winding cross section consists of structural material, typically austenitic stainless steel, resulting in smeared operating current density much lower compared, for example, to accelerator magnets. A bath-cooled option is forbidden for ITER magnets: the mechanical loads do not allow a helium transparent winding because of the poor smeared modulus and mechanical stability of such windings. The largest ever bath-cooled magnet is the large helical device (LHD), with 930 MJ stored energy [1]. The rigidity requirement for the big ITER coils, with stored energy in the range of 10 GJ, together with the need of removing the

dissipated heat at high rate, imply monolithic, potted coils with direct cooling. The forced flow cooling option is mandatory.

The peak magnetic field for the toroidal field coils and central solenoid of ITER is in the range of 12-13 T. In principle, many superconducting materials can operate at the ITER field with adequate current density. However, considering that the need of superconducting, high field material is in the range of 500 t on a time scale of few years, the practical choice is restricted to Nb_3Sn because of the cost and the reliability of the industrial procurement. Alternative candidate materials, to be watched for the "over-next" step, could be Nb_3Al and doped MgB_2, providing that the market stimulates an adequate industrial development.

The size of the conductor, i.e. the range of operating current, is also indirectly dictated by the large stored energy. In case of quench, the stored energy is too large to be adsorbed in the winding without irreversible damage. An effective extraction of the energy requires a relatively short dump of the current (few seconds). To quickly dump the energy at reasonable voltage (≤ 14 kV), the self-inductance, i.e. number of turns must be small and the current must be large. All ITER conductors are at $I_{op} > 45$ kA.

The large size of the ITER conductors is actually the key issue for R&D investigations. In the past decades, large operating experience has been accumulated in the range of 10 – 20 kA conductors, but the engineering problems of very large conductors (up to 68 kA for the ITER toroidal field conductor) are still a virgin ground.

3. SELECTED OPTIONS FOR THE ITER CONDUCTOR

More practical constraints for the conductor design are given by the winding layout. The initial design of ITER coils was by layers, with substantial optimization of conductor size and cost by grading. Presently, all the ITER magnets are wound by double or multiple pancakes, which is a friendly approach for large magnet manufacture, but brings a penalty on the conductor cost (no grading). In other words, each coil is wound only from one conductor type [2].

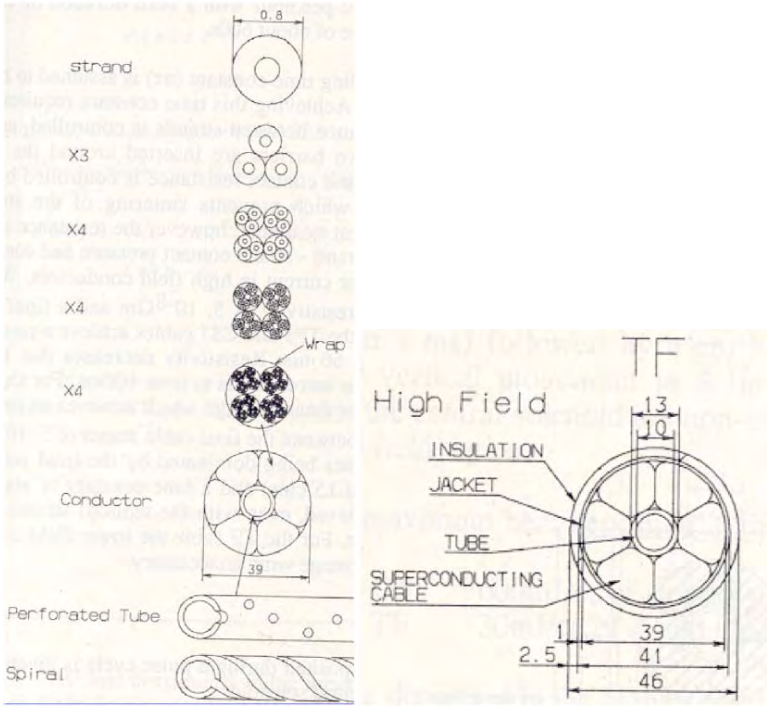

Fig. 1 ITER TF conductor layout according to 1993 design

Among the different design options for forced flow conductors, ITER adopted since the beginning the cable-in-conduit design for all the conductors, following an approach started in US over twenty five years ago [3] and also retained in the NET project [4]. A monolithic option design has been not considered in the ITER R&D. The current range for monolithic conductors is limited to about 20 kA [5]. At the size of ITER conductor, a traditional monolith would be very problematic because of the huge ac loss.

However, the large length of the conductor sections (over 500 m) and the heat removal requirement (high mass flow rate) do not allow a plain CICC design because of the large pressure drop. A parallel channel had to be added to decrease pressure drop, giving raise to the dual channel CICC, where the multistage cable is stranded around a helium transparent spiral, which defines the central channel.

4. DEVELOPMENT MILESTONES FOR THE ITER CONDUCTOR

The first sketches of the ITER conductor were drafted in 1992 and circulated at the MT-13 Conference in 1993, see Fig. 1. Comparing those early sketches with the latest conductor design [2], one could draw the conclusion that twelve years of intensive and expensive R&D activities have not substantially modified the conductor design. Indeed, the amount of feed-back has been intentionally very limited.

During the EDA (Engineering Design Activity, 1992-2001), as well as CTA (Coordinated Technical Activity, 2001-2002) and ITA (ITER Transitional Activity, 2003 and following years), an International Team planned, coordinated and monitored the R&D tasks carried out at the National Teams in Europe, Japan, Russia and US. In the field of superconductivity, the major partners of the collaboration have been JAERI (Japan), MIT and LLNL (US), NIIEFA, VNIINM and VNIIKP (Russia), CEA, CRPP, ENEA, FzK, UT (Europe, under the management of EFDA-CSU, Garching).

Both laboratories and industries carried out development activities for ITER conductors. The performance of the Nb_3Sn strand has been in the focus of the industrial activity in the years between 92 and 97, i.e. the procurement time for the Model Coil conductors, see for example [6-7]. The improvement of the Nb_3Sn performance continued in the scope of the KSTAR conductor manufacture [8] and later. Strand coating involved several companies worldwide [9]. The cabling development was carried out at the manufacturers, i.e. Showa, New England Electric, EM-LMI and VNIIKP. The jacketing by pull-through method was carried out at three companies, Ansaldo, EM-LMI and VNIIKP [10].

4.1 Coupling currents loss

The interstrand coupling loss in large CICC's is an issue for fusion conductors. The available data base was not very solid fifteen years ago. It was generally accepted that the Cr plating on the strand surface cuts the interstrand current loops [11]. However, this statement went through plenty of corrections in the last decade.

Investigations on the role of the Cr plating were carried out with respect to the coating thickness and coating type. A surprising large variation of coupling loss was found comparing cable made by identical strands coated by different vendors [9], see Fig. 2.

Other parametric studies on ac loss in CICC of Nb_3Sn strands revealed a strong influence of the void fraction [12], the electromagnetic load [13], the bending load [14] and the number of load cycles [15]. In summary, the interstrand contact resistance is of frictional nature in CICC and it is found to evolve in time. The interstrand coupling loss is initially high and drops quickly, after few load cycles, to the level of the interfilament loss.

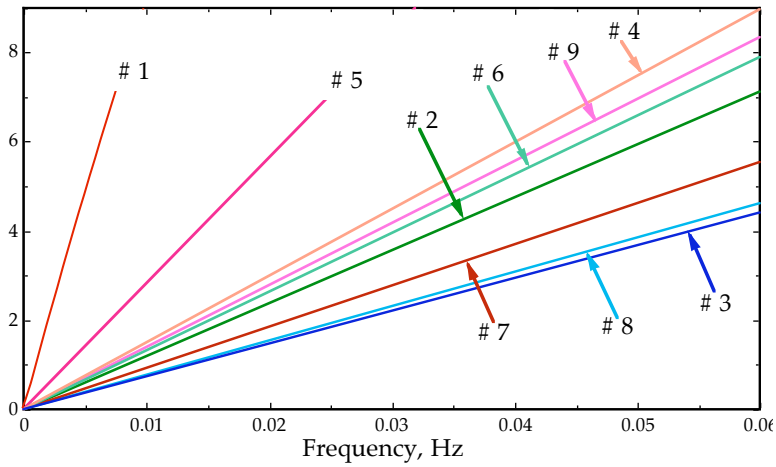

Fig.2 Coupling current loss vs. frequency of the ac field, normalized as mJ/cc of strand, for cables made from the same strand, but coated by nine different Cr vendors [9]. For comparison, #1 is made of non-coated strands. The lowest loss (#3) is about five time smaller than the largest loss (#5)

A number of large current loops with very long decay time constant seem to survive the cyclic load, see Fig. 3. The loss curve after cyclic load shows strong non-linearity at very low frequency, due to the overlapping effect of several loops with different time constant and affecting different volumes. The ac loss for fast field changes ($t < 1$ s) is negligibly low. For slow field changes ($t > 100$ s) the loss constant is larger, but the actual power loss is not an issue.

As the time constant is a function of the history and of the time scale of the field change, reliable ac loss calculations are not realistic. However, the largest incertitude in the loss estimate is in the less critical operation range (slow magnet charge). Generally, the ac loss is not seen as a major problem for Cr plated Nb_3Sn CICC. The criteria for ac loss presently retained in the ITER conductor design are conservative.

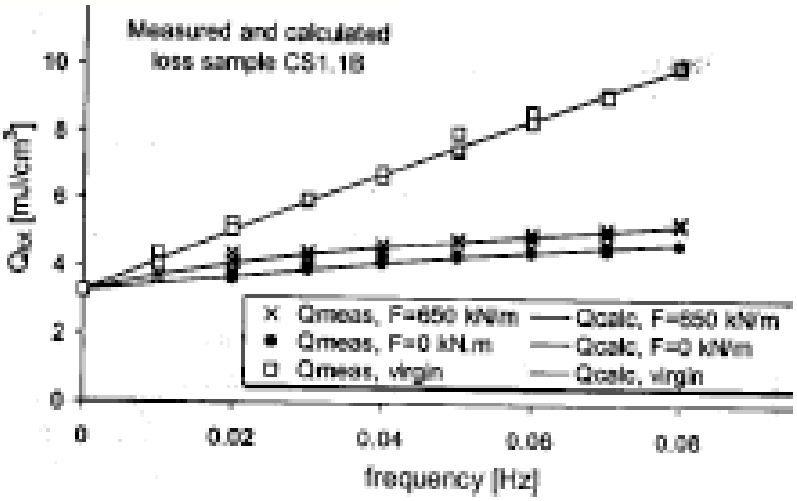

Fig.3 Coupling current loss vs. frequency of the ac field, for a full size Nb_3Sn CICC (Model Coil conductor) before any load (virgin), and after 38 load cycle (at 0 load and full load) [15]

4.2 Transient stability

The issue of transient stability has drawn lot of attention in the ITER conductor design, leading, in the initial phase, to a very conservative attitude, e.g. retaining a temperature margin of 2 K on top of the

maximum predicted operating temperature, because of the unknown behaviour at plasma disruption and imposing a large copper fraction in the Nb_3Sn composite strand.

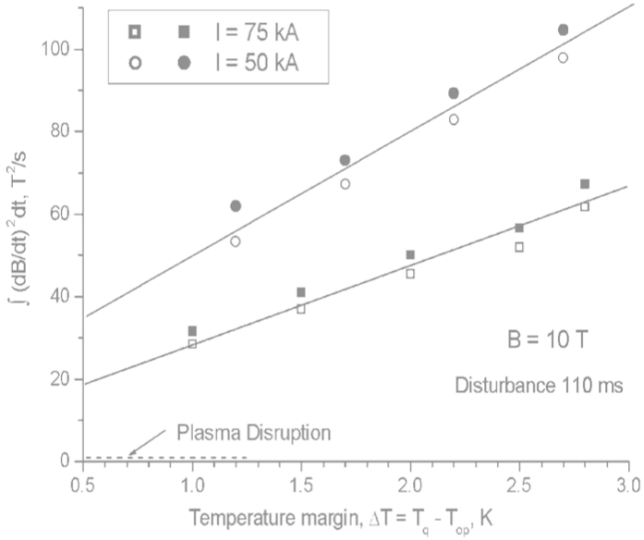

Fig.4 Transient field stability results on a Nb_3Sn CS model coil conductor at two levels of operating current. Open dots indicates recovery, full dots are for quench

During the test in SULTAN of a CS model coil conductor large field transients perpendicular to the conductor axis, well above the plasma disruption events, have been applied under relevant operating conditions. A convenient way to qualify a field transient of any shape is by the time integral of the square of the field change, $\int \dot{B}^2 \, dt$, in units of T^2/s. The field transient caused by a plasma disruption in ITER is smaller than 1 T^2/s at the high field section of the ITER coils. The test results on the Nb_3Sn full size conductor, see Fig 4 proved that a very marginal temperature margin is necessary to withstand a field transient like the plasma disruption [16].

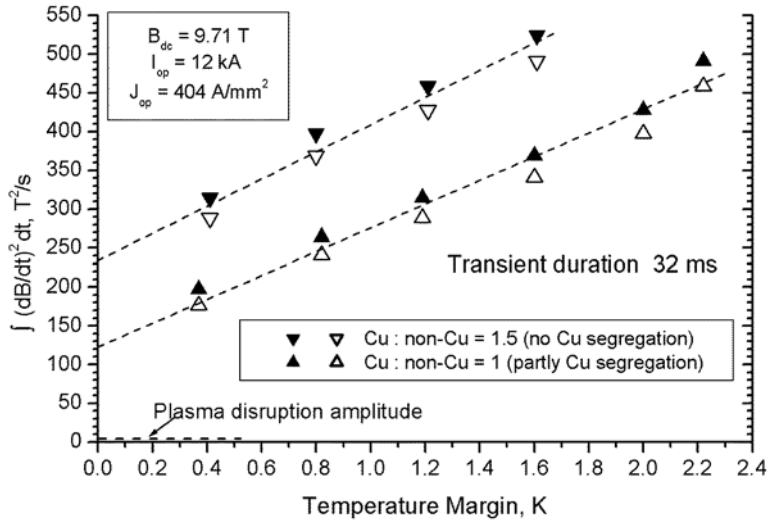

Fig. 5 Transient field stability results for two Nb_3Sn sub-size conductors identical except the location of the stabilizer, either fully included in the strand cross section or partly segregated

Encouraged by this result, another transient field experiment has been carried out, where two Cr plated Nb_3Sn cable-in-conduit conductors (CICC) are series connected and exposed to the same pulsed field. The only difference between the two sub-size CICCs is the location of the stabilizer, either homogeneously distributed in the composite with Cu:non-Cu = 1.5, or partly segregated , with

Cu:non-Cu = 1 in the composite and other Cu wires bundled in the cable. The transient field stability result, see Fig. 5, proved that, although the segregated copper marginally contributes to transient stability, the Cu:non-Cu = 1 is largely sufficient for the ITER stability requirement [17]. Other transient stability experiments, e.g. [18] on the effect of the void fraction, confirmed the very high stability of Nb_3Sn CICC.

The results on transient stability and copper segregation had a feed back on the conductor design: dropping the Cu:non-Cu ratio from 1.5 to 1 and giving up the large temperature margin, could have dramatically reduced the amount of strand to be procured. However, see section 5, the layout did not change substantially because the large engineering margin, originally retained for transient stability, was later re-allocated to balance the transverse load degradation.

4.3 Joint development

The joint development for ITER conductors was carried out independently, in parallel, by four participants of the project. The proposed joint layouts [19-20] are different in geometry (e.g. lap joint and butt joint) and use also different technologies (explosive bonding, vacuum brazing, soldering, etc.).

The test of the CS and TF model coils provided the opportunity to test a large number of joints, manufactured by the industry according to different layouts, under realistic operating conditions. The test results [21-22], showed that, whatever the joint design, the average resistance of over 50 joints falls into the same range, 1.2 – 2 nΩ, which is satisfactory for the ITER requirement.

As far as ac loss and resistance distribution, not all the joint perform in the same way. However, the importance of these issues for the ITER coils is not yet clarified.

4.4 Critical current vs. mechanical load

The test of Nb_3Sn strand under mechanical load has been a continuous activity for the ITER R&D. In the last two years, more effort has been done, mostly in Europe (Univ. of Twente and Univ. of Durham).

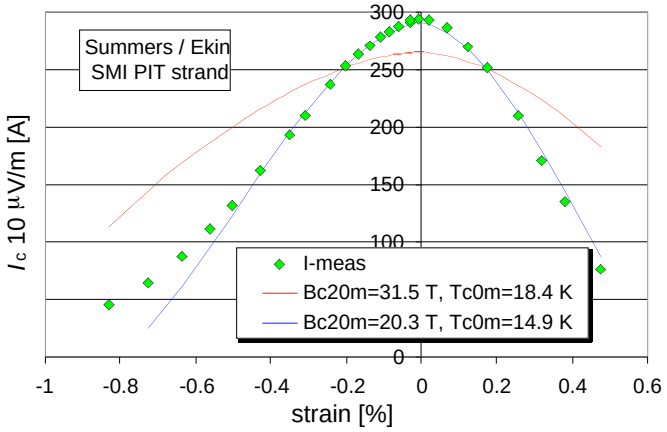

Fig. 6 The I_c vs. axial strain of Nb_3Sn strand is not properly fit by the Summers law [23]

The validity of the traditional scaling laws (Summers law) has been questioned by recent investigations in the range of high, axial compressive load. As an example, Fig. 6 [23] shows a curve of I_c versus axial strain. If the Summers law is applied using realistic, physical parameters for B_{c2} and T_c, red curve in Fig. 6, the fit is very poor. To improve the match, the critical parameters must be pushed into a non-realistic range. Yet, a satisfactory fit can be achieved only over a limited range of strain. Alternative scaling (deviatoric strain, interpolating fit) formulae are under discussion in the ITER community [23-24].

Other I_c experiments [25-26] focused on the sensitivity of Nb_3Sn strand to bending load, providing possibly a key to understand the transverse load degradation in CICC.

Plenty of I_c test vs. axial load have been carried out at the FBI facility at FzK on subsize CICC with different jacket material. Full size conductors are tested under electromagnetic transverse load in the SULTAN test facility.

The ITER conductor design criteria have been updated several times to update the improved strand performance as well as the degradation due to the transverse load. However, as the two effects somehow balance, no real feed back is observed on the conductor layout.

5. TWO OPEN ISSUES FOR DEVELOPMENT

5.1 Effect of transverse load on large Nb_3Sn CICC

Results obtained on ITER Model Coils and test conductors in SULTAN Test Facility revealed that Nb_3Sn strand properties are permanently reduced in the cable after operation. The results suggest that transverse loading during operation is causing a drop in J_c and *n*-value due to bending effects and/or enhanced local pressure at cable crossings [27]. A particular disturbing phenomenon is the a priori reduced index of resistive transition *n* of the cable compared to the value of the constituent strands.

A crucial experiment [28] has been set up to assess the actual amount of degradation which affects a Nb_3Sn CICC compared to a monolithic conductor where the strands are supported against local, enhanced transverse load. A section of a full size ITER CICC has been solder filled (except the central channel) after heat treatment.

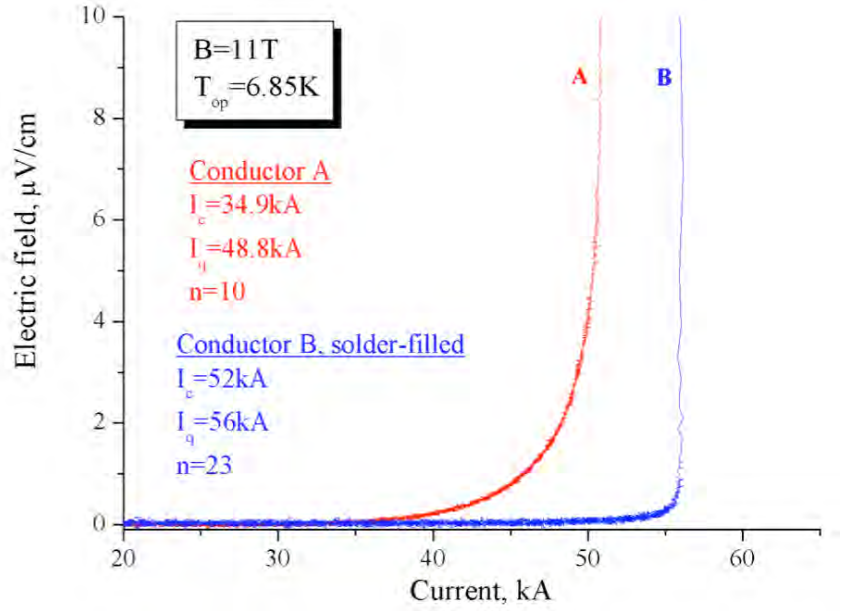

Fig. 7 Comparison of DC performance for a Nb_3Sn CICC and an equivalent monolith conductor [28]

The dc performance of the two conductors, identical except the solder filling, is shown in Fig. 7. Conductor A develops early voltage and a thermal runaway before any voltage can be observed on conductor B (the solder filled). A direct comparison between conductors A and B revealed a higher performance of conductor B in spite of a higher residual strain of the Nb_3Sn filaments in the solder-filled conductor B. The amount of degradation is of the order of 30-40% (although the background field was identical for the test in Fig. 7, conductor B has a higher peak field due to the higher current/self-field). The power-law index of conductor A drops from 15-20 for strands to n_A=10 in the cable, while in conductor B no such reduction of n is observed, n_B=23.

The sensitivity to mechanical loads, both axial compressive strain and transverse load, is the main open issue for Nb_3Sn CICC. In the medium-long term, the issue must be solved to exploit in full the potential of the newly developed Nb_3Sn strands. This may require a substantial design review and a deviation from the present CICC layout (not likely to happen within the ITER project)

5.2 Thermo-siphon effect on dual channel CICC

During an ac loss test in SULTAN of an ITER prototype conductor [29], it has been observed that the moderate heat generated by ac loss in the bundle region is poorly removed as the flow tends to stagnate in the bundle and the heat exchange with the helium flowing in the central channel is not effective. As a consequence the temperature slowly increases in the bundle, eating up the temperature margin of the conductor till, eventually, the conductor quenches.

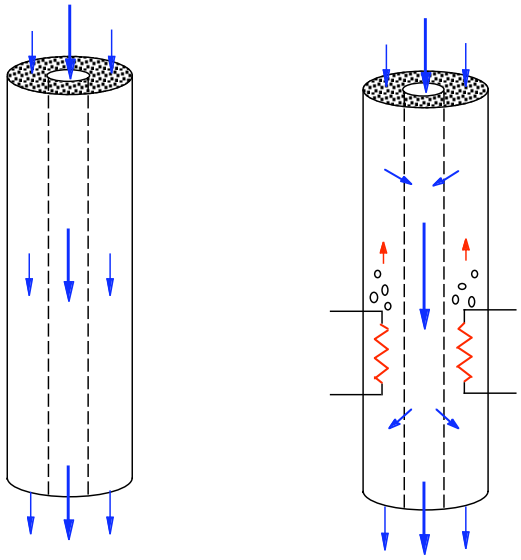

Fig. 8 Schematic view of a dual channel CICC vertically oriented, with flow from top to bottom

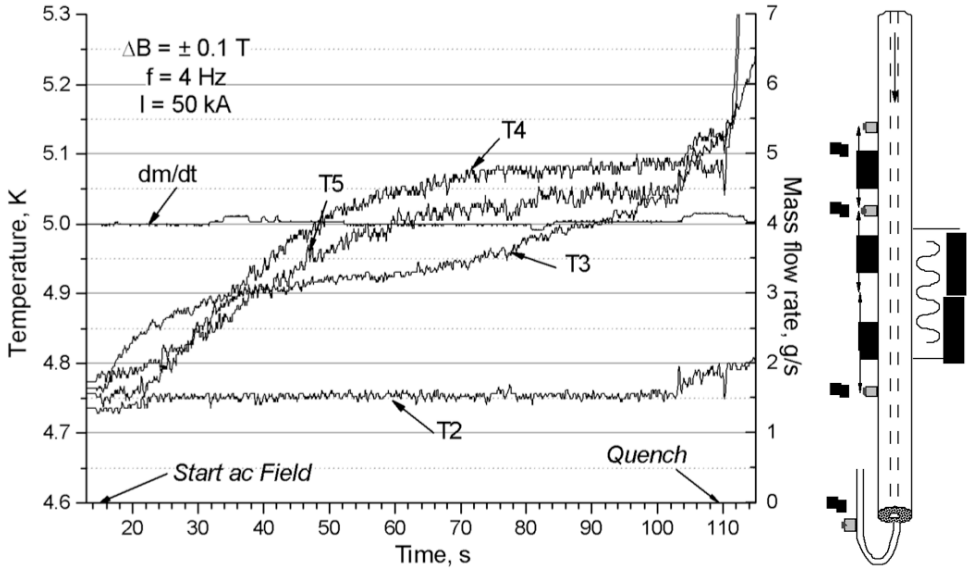

Fig. 9 Summary plot for the ac loss experiment showing how the thermo-siphon effect leads to a quench [29]

A schematic of the sample, vertically oriented with coolant flow from top to bottom, is shown in Figure 8. In the actual experiment, the "heater" is the ac loss generated in the strand bundle by ac field. The plot of the results in shown in Fig. 9. The ac loss power input, separately measured at

another run, is in the range of 4 W, which, at an overall mass flow rate (bundle + central channel) of 4 g/s, corresponds to a temperature increase of ≈ 0.25 K (see also T5 behavior). During a run with long ac field sweep, it is observed that the overall mass flow rate is constant, but the temperature sensor T3, upstream of the ac field, increases, what brings evidence of flow stagnation/reversal in the bundle region. This effect, analytically investigated in [30], can be explained with the buoyancy of the lighter, heated helium in the bundle, which opposes the top-to-bottom flow. In the central channel the flow increases to maintain the overall flow constant. At the operating conditions in Figure 3 (6 T, 50 kA, 4.7 K), the temperature margin of the conductor is 1.2 K (separately measured) and no quench is expected for the moderate heat input of 4 W (+0.25 K). However, because of the poor heat removal due to the thermo-siphon effect, the actual local temperature keeps increasing (see T3 and T4 in the plot of Figure 9) till a quench occurs.

The above result is a serious warning for the straight leg of the toroidal field coils of ITER, where a similar situation (heat deposition in the strand bundle by nuclear radiation and ac loss) may lead to a dangerous reduction of the retained temperature margin in operation and eventually to a quench.

6. CONCLUSION

The R&D for high field ITER conductor, carried out in the last twelve years under an international collaboration, was intended rather as a validation than as an input for the design. Despite the efforts of the ITER team, the R&D activities suffered of lack of coordination, with un-necessary duplication and dispersion of resources.

The results of R&D experiments did not confirm in full the assumptions of the design criteria, which were in some area over-conservative (ac loss, stability) and in other area optimistic (mechanical load degradation). In technology area (e.g. joints and Nb_3Sn strand layout) where no detailed layout specification existed, it has been proved that several options lead to the same performance result.

The feed back of R&D in the design has been intentionally very limited. The initial, generous engineering margin has been largely (ab)used to balance the unexpected, negative results. For example, the extra margin resulting from unexpected high transient stability and from the strand performance, now largely exceeding the original specification, has been re-cycled to cope with the dramatic degradation due to transverse load (BxI) in the CICC.

The interest of the industry in the ITER conductor remains modest and insufficient to trigger internal activities in R&D and logistic (except Russia). The impressive progress in strand performance of the last three years has not been triggered by the ITER project.

There is good confidence that the ITER high field conductors will fulfill their duty. On the other end, the experience and the results accumulated in the last twelve years of R&D activity could allow a different design approach, should we start again from scratch in a new fusion project…

REFERENCES

[1] S. Imagawa et al., Proc. Symp. Cryogenic Systems for Large Scale Superconducting Applications, Toki, NIFS-PROC- 28, 112, 1996.

[2] ITER FEAT, Design Description Document, IAEA Vienna 2003.

[3] C.J. Heyne, D.T. Hackworth, S.K. Singh, J.L. Young, P.A. Sanger, Proc. of 8th Symp. on Engin. Probl. Of Fusion Research, 1148 San Francisco 1979H.

[4] NET pre-design report, Fusion Engineering and Design 21, February 1993.

[5] P. Bruzzone, Forced Flow Conductor Manufacture, Wiley Encyclopedia of Electrical and Electronic Engineering, Suppl. 1, 643-665, Wiley&Sons 2000.

[6] P. Bruzzone, N. Mitchell, M. Steeves, M. Spadoni, Y. Takahashi, V. Sytnikov, IEEE Mag 32, 2300 (1996)

[7] N. Mitchell et al., Proceeding of MT-15, 347, Beijing Oct 1997, Science Press 1998

[8] M. Kim, K. Kim, Y. Chang, B. Lim, S. Kim, C. Yoon C, Physica C 354, 406-409 (2001)

[9] P. Bruzzone, A. Nijhuis, H.H.J. ten Kate, Proc. of ICMC 96, Kitakyushu, 1243 May 96

[10] V. Sytnikov et al., Proc. of ICMC 96, Kitakyushu, 799 May 96

[11] T.M. Mower, Y. Iwasa, Cryogenics 26, 281, (1986)

[12] A. Nijhuis, H.H.J. ten Kate, P. Bruzzone, L.Bottura, IEEE Trans. Magn. 32, 2743 (1996)

[13] A. Nijhuis, H.H.J. ten Kate, P. Bruzzone, IEEE Trans. Appl. Supercond. 7, 262 (1997)

[14] P. Bruzzone, A. Nijhuis, H.H.J. ten Kate, Proc. of MT-15, 1295, Beijing Oct 1997, Science Press 1998

[15] A. Nijhuis, N. H. W. Noordman, H.H.J. ten Kate, N. Mitchell, P. Bruzzone, IEEE ASC 9, 1069 (1999)

[16] P. Bruzzone, IEEE Appl Supercon 10, 1062 (2000)

[17] P. Bruzzone, et al. IEEE Appl Supercon 11, 2018 (2001)

[18] A. Terasawa et al. Proc. of ICMC 96, Kitakyushu, 1265 May 96

[19] P. Bruzzone et al., IEEE ASC 7, 461 (1997)

[20] P. Bruzzone, Adv. Cryog. Eng., 45, 737- 744 (2000)

[21] N. Martovetsky et al., IEEE ASC 11, 2032 (2001)

[22] D. Ciazynski et al., IEEE ASC 12, 543 (2002)

[23] A. Nijhuis, Communication at the EFDA magnet expert meeting, February 2004

[24] D. Hampshire, Communication at the EFDA magnet expert meeting, February 2004

[25] A. Nijhuis et al., Communication at MT-18 Conference, Morioka, October 2003

[26] H. Nunoya et al, Communication at MT-18 Conference, Morioka, October 2003

[27] J. Minervini, Communication at CEC-ICMC Conference, Anchorage, September 2003

[28] G. Pasztor, P. Bruzzone, A. Anghel, B. Stepanov, Communication at MT-18 Conference, Morioka, October 2003

[29] P. Bruzzone, Communication at Piers Conference, Pisa, March 2004

[30] R. Zanino et al., Communication at CEC-ICMC Conference, Anchorage, September 2003

SUPERCONDUCTING CABLES FOR POWER TRANSMISSION APPLICATIONS – A REVIEW

F. Schmidt, A. Allais
Nexans – Superconducting Cable System (Hanover – Germany)

Abstract
Superconducting power transmission cables have taken a step towards industrial transfer. The use of high temperature superconductor tapes enables cable operation with a liquid nitrogen cooling system. The interest for such components in an electrical network is undeniable, especially to mitigate the consequences of fault events. The integration of a high voltage cable in a network is always a particular case, and in the field of superconducting cables several designs are already available to fulfill the technical and environmental requirements. The development issues for the project of a high voltage underground cable of 600 m at 138 kV in New York are presented. Previous and ongoing projects of superconducting cables for similar applications are also reviewed.

1. INTRODUCTION

Since the discovery of ceramic-based high temperature superconductors in the late 1980´s, the interest in superconducting cables for power transmission and distribution purposes has been renewed., The development of High Temperature Superconducting (HTS) Cables for high capacity power transmission has been started over the last decade to take advantage of the efficiency and operational benefits due to the use of liquid nitrogen for cooling, which represents a cheap and environmental friendly medium. Several prototypes were developed mostly for testing in laboratory setups.

2. CABLE DESIGNS

Different cable concepts have been developed. Presently there are in principle two main types of superconducting power cables, distinguished by the type of dielectric used. The so called ‘warm dielectric design’ is based on a flexible support with stranded HTS tapes in one or several layers forming the cable conductor. This conductor, cooled by the flow of liquid nitrogen, is surrounded by a cryogenic envelope employing two concentric flexible stainless steel corrugated tubes with vacuum and superinsulation in between. A schematic view is shown in Figure 1. The outer dielectric insulation, the cable screen and the outer cable sheath are at room temperature. Compared to conventional cables, this design offers a high power density using the least amount of HTS-wire for a given level of power transfer.

The second type of HTS cable design is the ‘cold dielectric’ (see Figure 2). Using the same phase conductor as the warm dielectric, the high voltage insulation now is formed by a tape layered arrangement impregnated with liquid nitrogen. (LN2). Thus LN2 is used also as a part of the dielectric system in the cold dielectric cable design. The insulation is surrounded by a screen layer formed with superconducting wires in order to fully shield the cable and to prevent stray electromagnetic field generation. Three of these cable phases can now either be put into individual or, alternatively, into a single cryogenic envelope.

Fig. 1 - Warm dielectric superconducting cable. The dielectric is outside the flexible cryostat tube

Fig. 2 - Cold dielectric superconducting cable. This is a coaxial cable where the dielectric between core and shield is maintained at cryogenic temperature.

Fig. 3 Triaxial cold dielectric cable design.

A special type of cold dielectric cables is represented by the 'triaxial design', shown in Figure 3. In such a design the three phase conductors are concentrically arranged on a single support element divided by wrapped dielectric, which has therefore to withstand the phase-to-phase voltage.

The differences in superconducting power cable designs have significant implications in terms of efficiency, stray electromagnetic field generation and reactive power characteristics. In the warm dielectric cable design no superconducting shield is present, thus no magnetic shielding effect can be expected during operation. As a consequence, higher electrical losses and higher cable inductance are significant drawbacks relative to the other superconducting cable designs. Additional spacing of the phases is necessary in warm dielectric configuration due to electrical losses influenced by the surrounding magnetic field. No such requirements exist for cold dielectric cables, for which Table 1, reproduced from [1], shows a calculation example compared to conventional cables and overhead lines. On the other hand, the warm dielectric configuration seems easier to achieve as many components and manufacturing processes are well-known from conventional cables. The cold dielectric cable is more ambitious as it involves new developments in the field of dielectric materials and also needs more complicated cable accessories, such as terminations or joints.

A Comparison of Power Transmission Technologies				
Technology	Resistance (Ω/km)	Inductance (mH/km)	Capacitance (nF/km)	(MVAR/km)
Cold Dielectric HTS	0.0001	**0.06**	200	1.08
Conventional XLPE	0.03	0.36	257	1.4
Overhead Line	0.08	1.26	8.8	0.05

Table 1 Electrical characteristics example of 120 kV class cables

3. DESIGN ISSUES OF A COLD DIELECTRIC TRIPHASE SUPERCONDUCTING CABLE

The following considerations are based on the experience acquired during the first steps of the development of a 600m High Voltage superconducting underground cable in the US electrical network in Long Island – New York (LIPA project). We have pointed out the relations between the system requirements and the cable design.

The main system requirements are the rated current, the voltage, the length, the pipe size and the fault conditions, i.e. fault current and duration. Note that a superconducting cable has very low impedance compared to the other cables in the network, so in case of a fault the current would be naturally driven to it. The pipe size is also of economical interest for retrofitting applications of superconducting cable in existing pipes.

First of all, the number of superconducting tapes to be used depends upon their critical current and the rated current of the cable. The security margin must take into account any possible degradation during manufacturing and handling, as well as the influence of the cable self magnetic field. The judicious choice of the lengths of the conductive layers ensures an adequate current sharing between the different conductor layers.

The dielectric is composed of a wrapped layer of dielectric material impregnated with liquid nitrogen. The thickness of this layer depends on the voltage level.

Any boiling of the liquid nitrogen is prohibited in order to maintain dielectric strength. The consequence in term of mechanical damage due to pressure increase and dielectric breakdown would

be fatal to the cable. In that respect, the requirements are very challenging for the cooling system which has to evacuate the losses along a very long length, insuring that the nitrogen remains in the liquid state at every point. Three parameters g the cooling system design: the hydraulic diameter, the cable length and the losses. The hydraulic channel is indeed the gap between the cable and the inner diameter of the cryostat. The outer diameter of the cryostat is imposed by the pipe size and the installation conditions. In the case the LIPA project, three phases have to be installed by pulling through the installation pipe. The vacuum between the two corrugated steel tubes of the cryostat has to be sufficiently large to have low losses (less than 2W/m), so the spacing is fixed early in the design. The inner diameter of the cryostat is a function of the pipe size. The outer diameter of the cable depends upon the thickness of the copper stabilization layers, which have to withstand the fault conditions, and of the high voltage dielectric. Indeed the HTS tapes have little influence on the size of the coaxial cable, however their AC losses, added to the cryostat losses, impose the minimum mass flow of liquid nitrogen needed to achieve an overall temperature gradient in the cable of about 12 K (physical limit of the liquid nitrogen state : 65 K to 77 K). The mass flow, the hydraulic diameter and the length induce a pressure drop. To ensure liquid nitrogen stability the minimum pressure is to be selected according to the dielectric requirements at 77K. The pressure drop therefore is a limiting aspect. The working ranges of pressure and temperature are fixed and impose a compromise between the different cable design parameters (Figure 4).

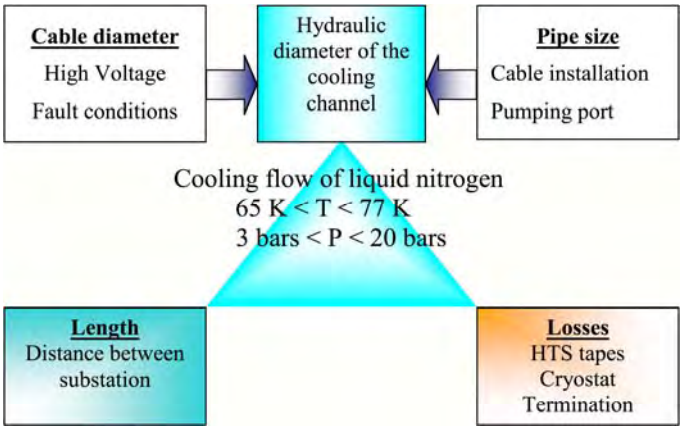

Figure 4 - Cooling system requirements and relevant cable design parameters

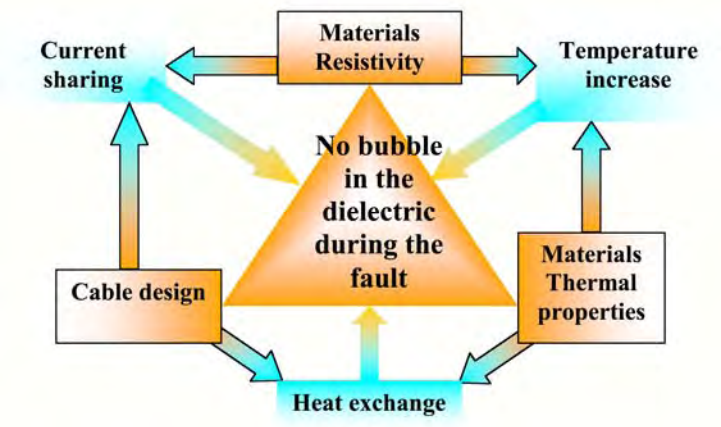

Figure 5 - Fault condition requirements and relevant cable design parameters

The overall goal of the cable design must be to find the appropriate values in the space of design possibilities that fulfill all specifications during normal operation and fault conditions. The fault current specified for such a cable can be huge. In the LIPA project it goes up to 30 times the rated current during a dozen of periods at 60 Hz, i.e. a few hundred milliseconds, which is the time needed to clear the fault by the conventional network security measures. The aim is to avoid the boiling of nitrogen during this time. Three phases can be identified during a fault, i.e. the current sharing, the corresponding Joule effect and the temperature increase in each layer. The current sharing is a consequence of the cable design, i.e. the mutual inductances, and the layers electrical resistances. The heat generation depends on the layers resistance. The temperature increase and the transient heat exchange are driven by the thermal properties of the layered structure of the cable. These coupled effects are summarized in Figure 5.

4. SUPERCONDUCTING CABLE PROJECTS OVERVIEW

Various superconducting cable projects have been started in the past. An overview of the different projects is given in Table 2. Although this table gives a good general view, it does not represent goals and specificities of each individual project. However, it can be seen that the majority of projects make use of the cold dielectric cable configuration, which clearly emerges as the most beneficial. It can also be stated that for the North American and the Japanese markets, retrofitting and cable installation in ducts are respectively the main foreseen applications.

A closer look at some of the projects shows that, among the ongoing ones, the LIPA project will result in a cable at both the highest voltage level and the highest power rating. Compared to e.g. the Sumitomo/TEPCO project, this cable will also have more than twice the power density. Moreover, LIPA is the only project where a fault current is explicitly specified and, at the same time, it will be the longest superconducting cable ever built.

Location	Main partners	Utilities	Cable			Use	Status
			Dielectric type	Number of phases	Characterictics		
U. S. A.	Pirelli / ASC		Warm	1	50 m / 115 kV / 2 kA	Demonstrator	Complete
Berlin	Pirelli (ex-Siemens) [1]		Cold	1	50 m / 110 kV / 2.1 kA	Demonstrator	Stopped
Italy	Pirelli / ASC	ENEL / Edison	Cold	1	30 m / 132 kV / 3 kA	Demonstrator	?
Detroit	Pirelli / ASC	Detroit Edison	Warm	3	120 m / 24 kV / 2.4 kA	Network	Failure
Paris	Pirelli / ASC	EDF	Cold	1	50 m / 225 kV / 2.6 kA	Demonstrator	Complete
Tokyo	SEI	TEPCO	Cold		30 m / 66 kV / 1 kA	Demonstrator	Complete
Tokyo	SEI	TEPCO	Cold	3	100 m / 66 kV / 1 kA	Demonstrator	Complete
Albany (NY)	SEI / IGC	Niagara Mohawk	Cold	3	350 m / 34.5 kV / 0.8 kA	Network	Ongoing
Japan	Furukawa		Cold	1	500 m / 77 kV / 1 kA	Demonstrator	Ongoing
Carrollton (Ga)	Southwire / IGC	Southern California Edison	Cold	3 (rigid)	30 m / 12.5 kV / 1.25 kA	Plant supply	Complete
Copenhagen	NKT / NST [1]	Elkraft	Warm	3	30 m / 36 kV / 2 kA	Network	Complete
Columbus (Ohio)	Southwire	American Electric Power	Cold	3	300 m / 12.5 kV / 2.5 kA	Network	Ongoing
Kunming (China)	Innopower / Innova [2]	Yunnan Electric Power	Warm	3	30 m / 35 kV / 2 kA	Network	Ongoing
Long Island (NY)	ASC / Nexans	Long Island Power Authority	Cold	3	610 m / 138 kV / 2.4 kA	Network	Ongoing

[1] Cryogenic envelope supplied by Nexans. [2] Cryogenic envelope and dielectric supplied by Nexans.

Table 2 Superconducting power cable projects overview

5. CONCLUSIONS

The development of High Temperature Superconducting power cables has been going on for about ten years and it has resulted in a variety of projects on warm and cold dielectric designs. The first move from laboratory demonstrations to field applications is currently done and represents a necessary step towards the commercialization of this new product. Superconducting cables have significant benefits for power transmission and distribution applications that provide new aspects and possibilities in network planning and operation, and will therefore help to place this technology in the future market.

REFERENCES

[1] J. Howe et al., Very low impedance (VLI) superconductor cables: Concepts, operation implications and financial benefits, white paper, Nov. 2003

[2] S. Honojo et al., Verification test of a 66 kV High-TC superconducting cable system for practical use, CIGRE 2002, 21-202

SURVEY OF EXPERIMENTAL FACILITIES IN EU LABORATORIES RELEVANT TO CONDUCTOR R&D FOR FUTURE ACCELERATOR MAGNETS

Andries den Ouden
University of Twente, Faculty of Science and Technology, Low Temperature Division,
P.O. Box 217, 7500 AE Enschede, The Netherlands

Abstract
A critical evaluation for possible application in future accelerator magnets of existing and newly developed superconductors requires knowledge of their properties by experimental verification under representative operational conditions. A first attempt is made to define the experimental requirements to enable such an elaborate evaluation and to survey the availability and the capabilities of existing measuring facilities in Europe..

1. CANDIDATE CONDUCTORS FOR FUTURE ACCELERATOR MAGNETS

1.1 NbTi

With the development of the LHC at CERN the ultimate performance limits of NbTi conductors operating at 1.9 K with maximum fields of about 9 T have been fully exploited, both for the main regular lattice dipole and quadrupole magnets and for the magnets in the IR regions close to the experiments. Without considering an even larger circumference of the present tunnel only limited upgrades of existing LHC components can be expected employing NbTi conductors.

1.2 Coated YBaCuO.

Despite their challenging (Jc,B,T)-properties and the rapid improvement of performance and long length production of coated YBCO conductors [2] possible large scale applications competing NbTi or Nb3Sn should not be expected within the coming 10-15 years. Besides, a comprehensive and generously supported research program hardly exists in Europe.

1.3 Nb3Al.

Despite its superior strain properties compared to Nb3Sn the difficulties in controlling and improving Jc(B.T), manufacturability, cryogenic stability, filament size and phase stability impedes (large scale) application of this very challenging superconductor in accelerator magnets within 15 years. In contrast to Japan and the United States no serious R&D programs on Nb3Al exist in Europe.

1.4 BiSrCaCuCo.

The research on BSCCO conductors during the last decade has been mainly focused on 50-60 Hz AC, low field power applications of BSCCO-2223 tape conductors. A well concerted effort on basic material research and demonstrator development for a wide range of possible applications has been significantly supported by both the European commission within the 3rd, 4th and 5th EU Framework Programs and by national research programs. Despite the establishment of a well organized, lively and highly competent R&D community the European Commission has not approved a single BSCCO proposal within the present 6th framework program.

Applicability of the present generation of BSSCO conductors in accelerator magnets is not attractive regarding the awkward tape geometry, the relative large filament size, the lower engineering current density Je if compared to Nb3Sn, the Jc-strain sensitivity and the conductor costs. Regarding the

above discussed funding situation also application of BSCCO conductors in accelerator magnets cannot be expected within 10-15 years.

1.5 MgB2.

The critical properties of the most recently discovered superconductor MgB2 appear to be very challenging as a possible competitor of NbTi at relatively low fields at elevated temperatures (~20 K) and possibly also as a very high field LTS conductor. The present R&D is organized mainly in national programs in many European countries. Only 1 EU-fp6 program at present has been awarded: "HIPERMAG" is a 2.5 M€ funded, 3 years program involving 13 partners from 9 EU-countries and focuses mainly on optimization of material properties and control of the manufacturability of multi-filamentary conductors. Considering more specifically application in high Jc high field accelerator magnets, at present no specific benefits in performance, mid-term availability and price compared to NbTi are expected.

1.6 Nb3Sn.

European R&D of Nb3Sn conductors has been driven mainly by the EFDA/ITER program for application in fusion reactors. A significant concerted effort by industry and research centers has resulted in a quality controlled, large scale production of large CICC's containing Nb3Sn wires exhibiting a moderate Jc (800-1200 A/mm2 @ 12 T) and low losses by controlling both the filament size (~5-10 μm) and the wire contact resistance. Investigations in this program on the Ic –strain sensitivity focus mainly on the longitudinal strain though also other strain components (bending strain, pressed wire to wire contacts) contribute significantly to the local strain state under Lorentz forces in CICC's.

It is remarkable that in contrast to laboratories in Japan and the United States, despite several interesting R&D programs in Europe confronted with performance limitations of Nb3Sn conductors, only the University of Geneva and the Bochvar Institute in Russia have reported on more fundamental aspects of these limitations. These aspects comprise for instance grain growth during the heat treatment, the specific influence of ternary or quarternary additions to the Nb3Sn, Sn gradients in the Nb3Sn layer and the corresponding critical properties of Sn deficient, of-stochiometric parts of such layers.

Despite the complexity of Nb3Sn coil manufacturing several well performing model dipole magnets have been realized since 1990 illustrating the potential of Nb3Sn conductors in this field. The enormous improvement in Jc, mainly the result of a well organized DOE funded program in the US, has further opened challenging prospects of application of Nb3Sn conductors for accelerator magnets and coil manufacturing technology.

To summarize above, only Nb3Sn conductors show the potential for application in a next generation of high-field, large bore, field quality accelerator magnets in a timeframe of 5-10 years. Therefore this survey on measuring facilities focuses mainly on issues related to Nb3Sn superconductors.

2. NB3SN ACCELERATOR MAGNET PROGRAMS IN EUROPE

After the successful performance of the 11 T dipole magnet MSUT in 1995, developed by the University of Twente, it lasted till 1998 till two mainly technology oriented, moderately funded European programs were established aiming at the realization of model accelerator type Nb3Sn magnets. A CERN-University of Twente program focuses on an 88 mm bore, 10 T, high field quality model dipole magnet. CEA/Saclay develops a model of a Nb3Sn version of the existing LHC lattice quadrupole magnet, which will be possibly used as a final focusing magnet inside the TESLA detector.

In January 2004 the EU-fp6 research program NED, part of the Integrated Activity Care, has started its activities towards a 90 mm bore, 15 T model dipole magnet which can be used as an upgrade of the 10 T limited conductor test facility FRESCA at CERN. Due to limited funding in Phase 1, this program focuses mainly on Nb3Sn conductor development at European industry aiming at a conductors exhibiting a non-copper Jc of 1500 A/mm2 @15 T, 4.3 K, a Cu:Sc ratio of 1-1.2 and a filament size smaller then 50 µm. The conductors should be capable to withstand transverse pressures of up to 160-180 MPa. In phase II, which has not yet been approved for funding, the manufacturing of the magnet system should be realized.

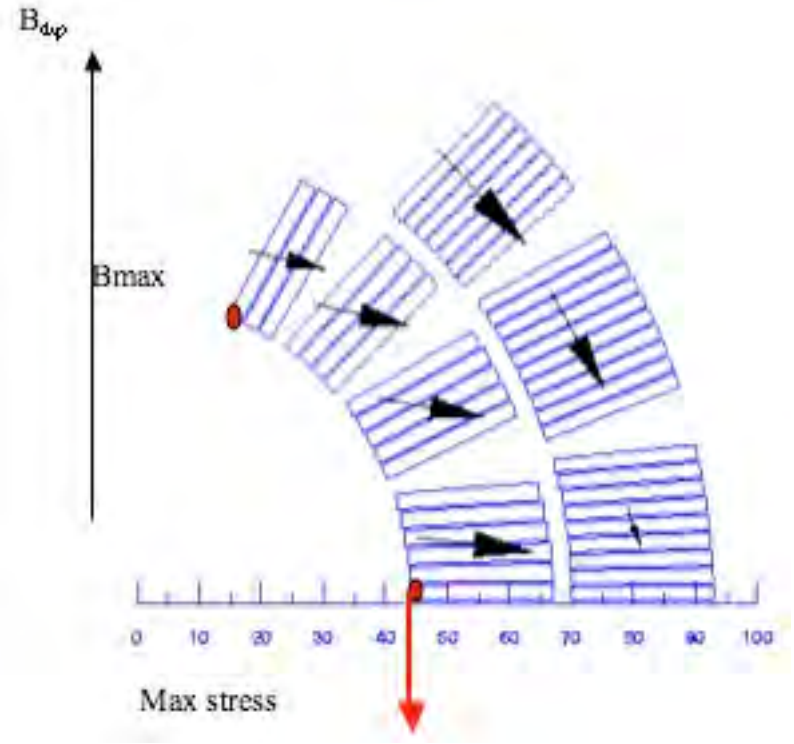

Figure 1. Possible conductor arrangement for the 90 mm bore, 15 T NED dipole**.**

Though the NED program includes a limited effort on magnet design Figure 1 shows a proposed cross section of the coils. The Rutherford cables in this design contain 30-32 strands of 1.25 mm diameter and a stainless steel core to limit the Rc to about 40 100 µΩ. For the moment only the wind-and-react method for coil manufacturing is considered.

3. FACILITIES TO MEASURE CRITICAL CONDUCTOR PROPERTIES

3.1 Wire requirements

To obtain magnets with required field amplitude and field quality, operating reliably for many years, conductor properties and coil manufacturing should reach a high level of control, reproducibility and reliability. Especially quality control of the conductor properties and performance is a prerequisite for successful magnet operation.

The flow diagram in Figure 2 shows qualitatively the relation between the properties of the wires developed and delivered by the manufacturers on magnet performance. The red/bold marked properties require critical experimental verification.

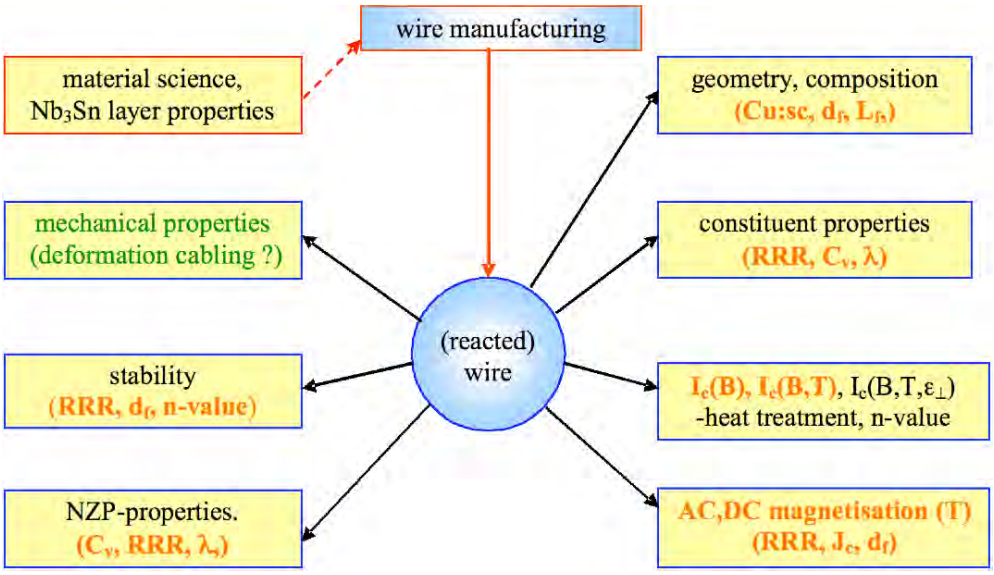

Fig. 2. Schematic presentation of the relation between the conductor properties which should be known by measurement (in red/bold) and their impact on magnet performance.

3.1.1 Measuring facilities for $C_v(T)$ and $\lambda(T)$.

The determination of the matrix RRR, the Cu:Sc ratio, the filament pitch L_p and the geometrical filament size d_f is rather straightforward and is routinely carried out at both by manufacturers and by users.

Facilities to measure $C_v(T)$ and $\lambda(T)$ at cryogenic temperatures of the wire constituents or of the composite itself are summarized in Table I.

Table I. $C_v(T)$ and $\lambda(T)$ Measuring facilities in Europe

	$C_v(T)$	$\lambda(T)$	remarks
University of Geneva (home built facility)	X		small samples
University of Southampton (PPMS)	X		
Johannes Keppler Institue (PMMS)	X		
CEA Saclay		X	insulated cable stack (1.8K)
University of Twente		X	idem (4.3 K)
INFN-LASA		X	idem (4.3 K)

Though many but mostly contradictory data from different sources are widely available it is highly recommended to establish a world-wide data base on material propeties which contains indisputable data of relevant material properties at cryogenic temperatures.

3.1.2 $I_c(B)$ or $I_c(B,T)$ measuring facilities on wires

Especially the sample preparation and the measurement of $I_c(B)$ or preferably $I_c(B,T)$ of very high current density Nb_3Sn wires is rather demanding. Because of the strain sensitivity of I_c the mounting history and the materials choice is determinative for the measured I_c at a certain field. However, so far no alternative procedures other than the standard ITER procedures exist for sample handling during the heat treatment at about 650 ^{0}C and the mounting of the reacted wire on the sample holder for

critical current measurements of very high current density wires. As an example, Figure 3 shows the expected critical current at 4.2 K of the proposed Nb_3Sn wires for NED.

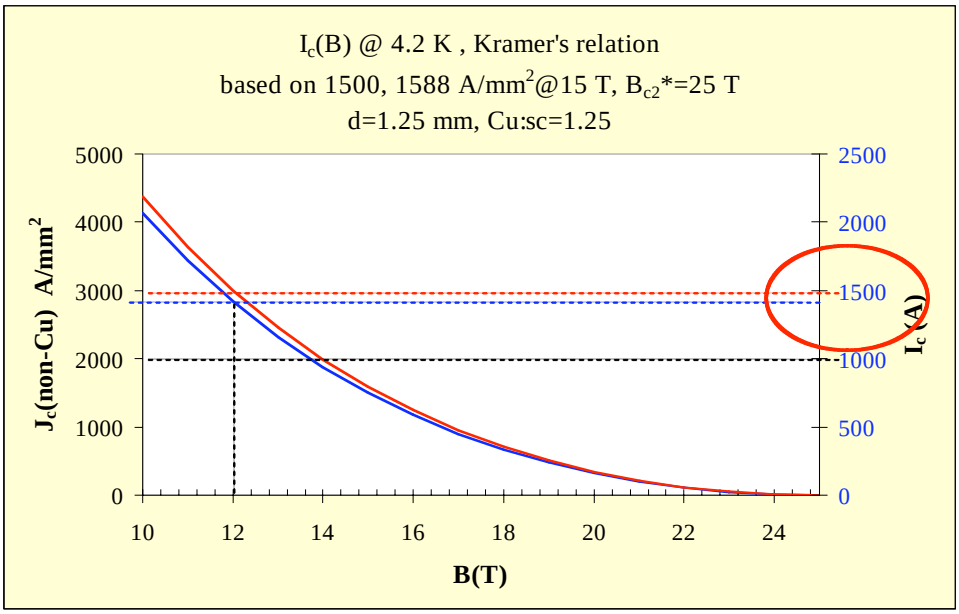

Fig. 3 Expected $I_c(B)$ at 4.2 K of a 1.25 mm Nb_3Sn wire in the NED program with a non-Cu J_c of respectively 1500 and 1588 A/mm^2 @ 15 T.

Compared to e.g. ITER Nb_3Sn wires with a typical I_c of 500 A @ 12 T the rather high critical currents at relatively high fields of the next generation of Nb_3Sn conductors put severe demands on the existing measuring capabilities in Europe. Only a few institutes in Europe have reported experience on such high current/high field measurements at low electric field levels (< 1 μV/m), but the results may still vary by about 10 %, which is rather poor if I_c serves as a quality parameter.

3.1.3 Wire magnetisation measuring facilities

Filament magnetization resulting from persistent currents have a direct impact on the field quality of accelerator magnets at low fields during particle injection in the accelerator. A more indirect effect occurs during particle injection when the current through the coils is kept constant but the filament magnetization and therefore all field components nevertheless show a time-dependent decay. During the first few mT of the field ramp after particle injection the field components snap-back to the value at the beginning of the particle injection. Decay and snap-back result from a rather subtle interplay between the filament magnetization and the slow redistribution in the coils of so-called Boundary Induced Coupling Currents (BICCs).

Though the misleading concept of an effective filament diameter is widely used, it is the magnetization M ~(J_cxd_f) which is determinative for above static and time-dependent field errors. Since the present generation of of high-current density Nb_3Sn wires still exhibit a rather large magnetization below 2 T, knowledge of M is imperative and can only be obtained by direct magnetization measurements. Also for fast cycling magnets with a dB/dt in the range of several T/s experimental determination of M and matrix coupling current losses are strongly required.

Several laboratories in Europe are capable to measure the filament magnetization M by the Vibrating Sample Magnetisation technique, SQUID Magnetisation or the standard pick-up coil technique at relevant field strengths (up to 4T) and temperatures (1.8-4.3 K). Only the pick-up coil technique enables AC-loss measurements at field sweep rates of 0.1-1 T/s. Despite the resembling techniques differences in the range of 20 % between different laboratories are no exception.

3.2 Rutherford cable requirements

Since for accelerator magnets only the usage of high current Rutherford cables is considered figure 4 shows similar to figure 2 the relation between the cable properties and their impact on magnet performance. It should be noted that the cable insulation is included in these considerations.

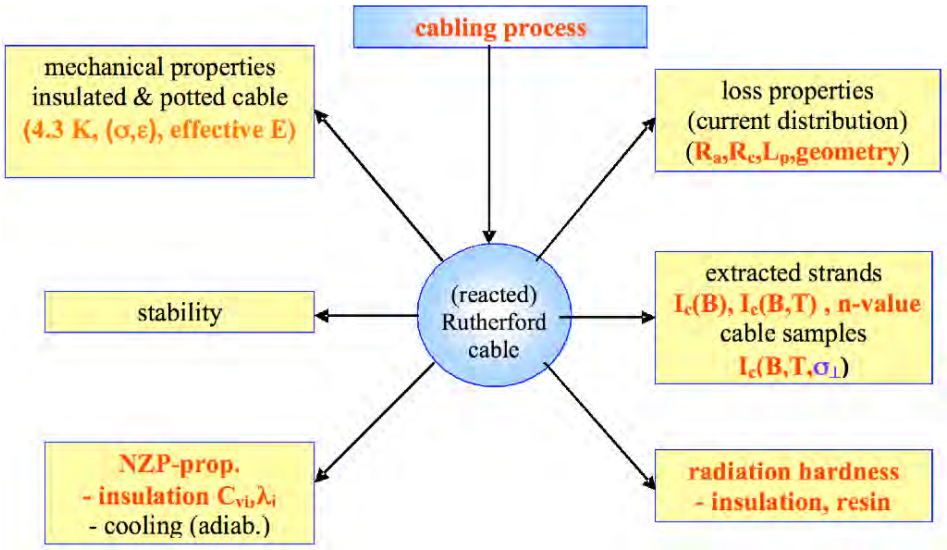

Fig. 4 Schematic presentation of the relation between the cable properties which should be known by measurement (in red/bold) and their impact on magnet performance.

3.2.1 Cabling facilities

Due to the large differences in hardness, Young's modulus and yielding properties of the materials inside non-reacted NbSn wires (Cu, Nb, eventually Ta barriers, Sn or highly densified powder) the cabling process into highly compacted Rutherford type of cables often results in damage of the internal wire structure. This is reflected by a current degradation compared to virgin strands larger than 10 % and tin contamination of the copper matrix during the heat treatment. This immediately implies that a good performing wire not necessarily results in a good performing cable. Since the relation between internal strand lay-out, the deformation history of the strands and the type of strand on one hand and the cable dimensions on the other hand are not well understood yet, the result of cabling of NbSn wires at present is rather a process of trial and error. It is characterized by an iterative learning process exploring the parameter space (cable width, thickness, pitch, keystone angle, core tension, wire tension) followed by microscopic inspection of the cross section or I_c measurements of heat treated extracted strands. To obtain a satisfying result (i.e. I_c degradation < 8-10 %, mechanical stability of the cable, good core position, acceptable residual twist) many of such iterations may be necessary. Even a complete adaptation of the strand lay-out may be required after this iterative process.

At present such an experimental cabling facility with skilled, experienced people does not exist in Europe.

3.2.2 $I_c(B)$, $I_c(B,\sigma_\perp)$, NZP, current distribution and stability measuring facilities for cables

The well known I_c dependency of Nb_3Sn conductors on axial strain manifest itself in a different way in Nb_3Sn accelerator magnets. In this case however the perpendicular stress component determines the occurrence of I_c reduction or permanent I_c degradation of the cables. Presently a stress limit of

150 MPa is used in high-field magnet design and the performance of all Nb_3Sn model magnets tested have shown that this is an appropriate limit. Typical I_c behaviour of different Nb_3Sn Rutherford cables under transverse pressure is shown in figure 4 resulting from experiments at the University of Twente.

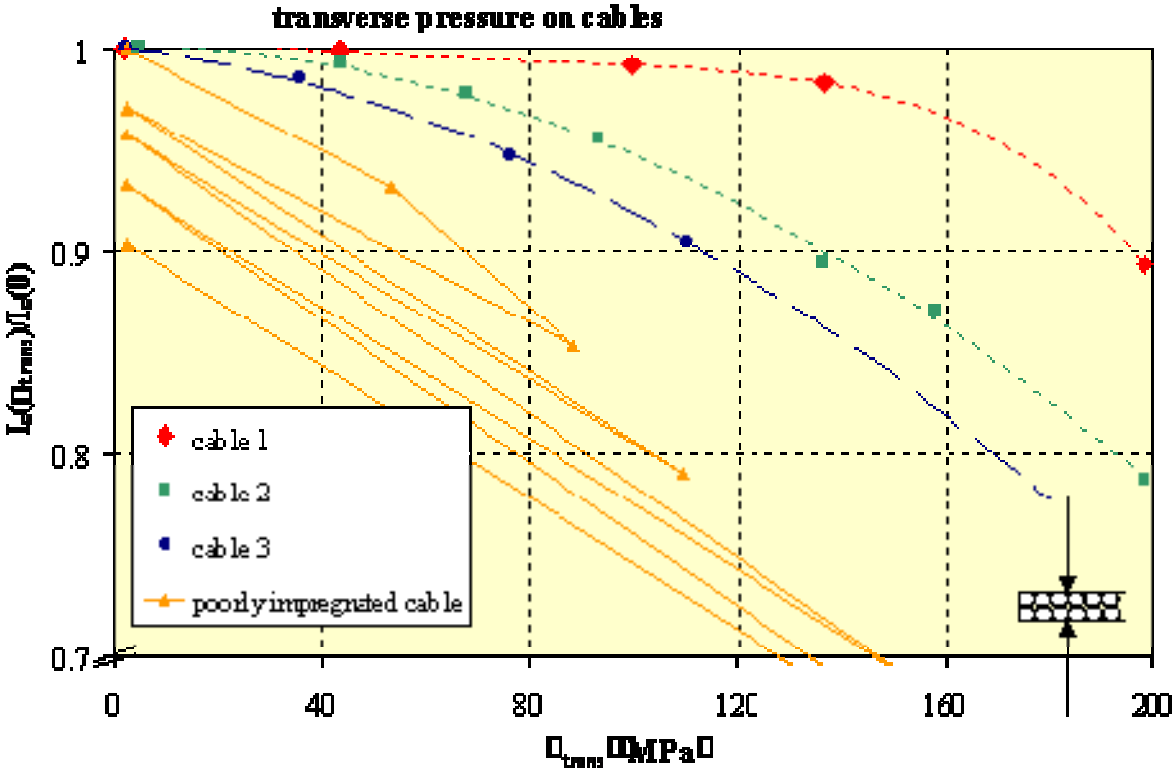

Fig. 5 Typical reduction of the normalized critical current of 3 different Nb_3Sn cables under transverse pressure @ 11 T, 4.2 K. At pressures above 160 MPa permanent I_c degradation occurs for most cables. Also shown is the behaviour of a cable which lacks of compete resin penetration inside the cable.

The I_c sensitivity to transverse pressure is not well understood yet in terms of cable and strand properties and should be measured for each specific strand-cable-insulation-core combination.

$I_c(B)$ measurements of cables are preferred above I_c measurements on extracted strands. The subsequent handling steps of strand extraction, heat treatment and final mounting on a sample holder demand utter caution and are rather prone to introduce additional damage to the filaments. Like for regular I_c measurements on virgin wires hardly any reported experience exists on such high current density wires extracted from Rutherford cables.

Also NZP, AC loss and stability measurements on cables are to be preferred above indirect measurements of related wire c.q. cable properties. In table II the capabilities of existing facilities for cable measurements are summarized.

Table II. Exisiting facilities for cable measurements

	CRPP SULTAN	Cern FRESCA	UT		FZK FPI
current supply	cold transformer	RT-PS or cold transformer	cold transformer		RT-PS
sample current (kA)	100	40	45		10
max. field (T)	11 solenoidal	10 dipole	15 soldenoidal		14 split pair
operating temperature (K)	> 4.3 forced flow He	1.8 or 4.3	4.3		4.3
max. field region/ sample length (m)	0.4	2 x 0.7	0.04 (U-shape)	0.6 (helical)	0.4
$\sigma_{\perp}$ (MPa)	RT prestress possible	RT prestress < 100	< 250	-	axial tensile stress only
NZP/stability meas.	yes	yes	no	no	possibly
experience/capability current distribution measurements	yes/yes	yes/yes	yes/no	yes/no	no/no
additional features	- AC field 0.4 T 0.01-6 Hz - 3 T pulse field	- Hall sensors curr. distr. meas.	-	-	-
sample preparation/ sample mounting	demanding/ demanding	demanding/ easy	demanding/ easy	demanding/ easy	demanding/ demanding

Both the SULTAN and FRESCA facility offer a wide range of relevant cable measurements. FRESCA is a very flexible, dedicated facility to investigate Rutherford cables whereas SULTAN is more suited for long lasting measurements on large CICC's. However, considering the expected I_c(B, 4.3K)-values for the proposed NED cables, shown in figure 5, only the SULTAN facility is presently suited to perform most of the required measurements on Rutherford cables. With the upgrade in 2004 of the magnet facility at the University of Twente dedicated (B, $\sigma_{\perp}$) measurements on short samples of 0.04 m have also become feasible.

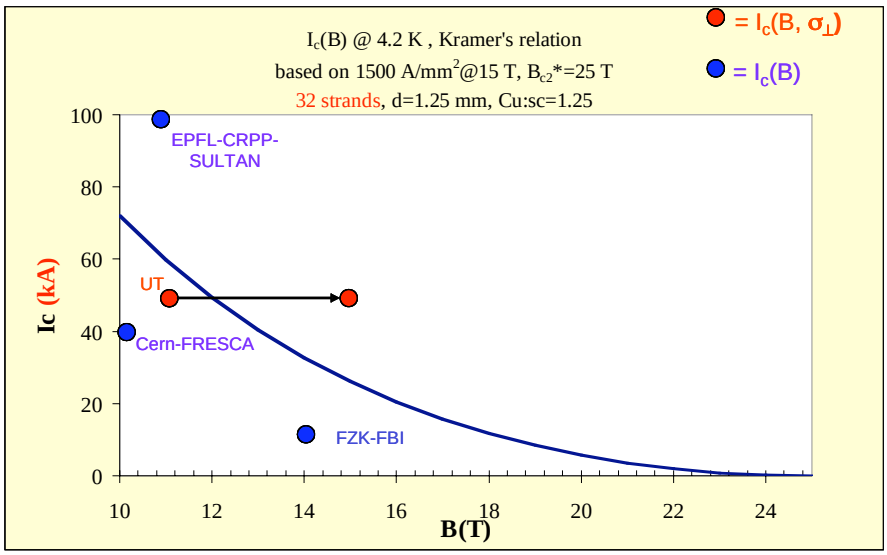

Fig. 6. Expected I_c(B) values for the proposed NED cable. Also shown are the measuring capabilities of existing facilities in Europe for cable measurements.

With the development of the 15 T NED dipole an upgrade of the very flexible FRESCA facility, dedicated for Rutherford cable research, becomes feasible and could offer unique services to the accelerator community.

Regarding its unique features for testing many relevant properties on a wide range of superconducting cables the SULTAN facility offers presently indispensable services to Europe.

3.2.3 Measuring facilities for Rc and Ra.

Though many parameters determine the amplitude and time constants of the different types of coupling currents, the dynamic field quality (including decay and snap-back) and the heat dissipation by the associated losses in accelerator magnets is mainly controlled by the resistance Rc between crossing strands in the Rutherford cables. For fast cycling magnets the preferred Rc value should lie in the 1-100 mΩ range, while for slowly ramped magnets Rc may range from 20 to about 200 μΩ. In both cases the resistance Ra between adjacent strands should be controlled accordingly.

Rc can be obtained by the V-I method proposed by Verweij, which principle is depicted in figure 7.

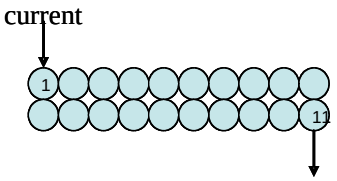

Fig. 7. Principle of the V-I method for R_c measurement.

Current is supplied to strand 1 and extracted at strand (Ns-1) on a cable piece of with a length of an integer cable twist pitches. By measuring the voltage between strand 1 and all other strands at the same longitudinal position at 4.2 K and under a representative transverse pressure, Rc can be derived. Though the method is rather inaccurate when Rc and Ra differ more than an order of magnitude this relatively simple method offers a good indication of the Rc range. Besides, it offers a convenient method to trace the evolution of Rc under cyclic loading of a cable stack, which is possible at the University of Twente, FZK and CEA-Saclay.

Rc can be obtained indirectly by measuring electrically or calorimetrically the losses of a cable stack of a few twist pitches long at 4.2 K under representative transverse pressure, exposed to an AC magnetic field oriented both parallel and perpendicular to the wide side of the cable. An additional feature of this method is that the total loss including strand coupling loss and hysteris loss is obtained. At present such measurements are carried out at the University of Twente and CCRP-Villigen.

4. SUMMARY.

For the last decade Nb3Sn conductor research in Europe has been mainly driven by the EDDA/ITER program accompanied by the development of dedicated measuring facilities for moderate-current density wires or large CICC's. Much experience has been gained to investigate experimentally the most relevant properties of Nb3Sn strands. The existing facilities are also adequate to investigate a new generation of high-current density Nb3Sn conductors.

However, for Ic(B) measurements or more dedicated NZP/stability measurements , both required on a routinely basis during the development of a new generation of very high current Nb3Sn Rutherford cables, the existing facilities are inadequate because of their lack of flexibility during sample interchange (costs, time) or because of their insufficient I(B) capabilities.

Regarding the complexity of cabling of high-current density Nb3Sn strands and the complete lack of experience in Europe on this issue it is highly recommended to set-up a European experimental cabling facility.

ANNEX - PRESENTATIONS

23 Mars 2004

ALSTOM plan and activities on LTS materials

Ch VERWAERDE

ALSTOM

WAMS 2004

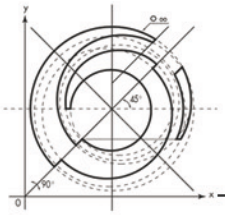

Outline

- ALSTOM situation
- LHC wires and cables
- Nb3Sn wires
  - Bronze route
  - Internal tin route

250

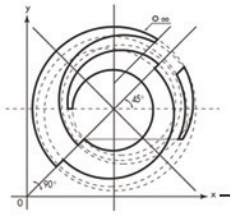

ALSTOM

ALSTOM SITUATION

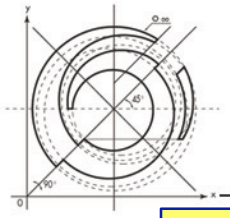

Superconductivity at ALSTOM

ALSTOM

ALSTOM Magnets and Superconductors, SA (MSA)

250+ employes – Turnover 30M€+

MSA - WIRE

Superconducting wires

(NbTi, Nb3Sn, AC wires)

Superconducting cables

(Triplet, 6+1…, Rutherford, Wire in Channel, CICC, Aluminium cladded cables, …)

MSA - MAGNETS

Magnets for High Energy Physics (LHC, …)

Magnets for Fusion Research (ITER, …)

Other Magnets (including resistive)

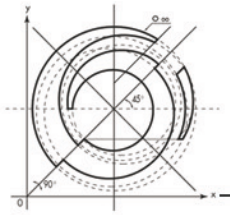

ALSTOM

MSA LHC Cables for main dipoles
Up to date

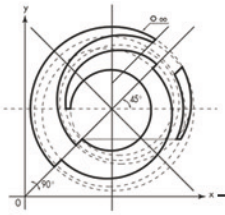

Cable unit length delivery (shipped)

ALSTOM

From the beginning of project to Jan 2004 :

72.4% of the total UL1 number (target 62.5%)
35.0% of the total UL2 number (target 33.3%)
46.6% of the total UL3 number (target 33.3%)

have been delivered by MSA*

* From CERN dashboard 01-31-04

254

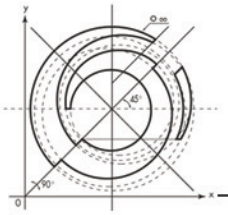

IMPROVEMENTS

ALSTOM

Copper can cracking

Acid cleaning

Monofilament billet decohesion

Training workers

Multifilament breaks

Monofilament billet break germination

Strand magnetization

strand coating

And more……

Main problems are behind us
(we hope so !)

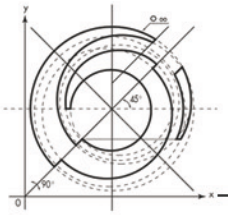

BUSINESS ACTIVITY

OUTPUT: outer wire

number of breaks per billet since start of project mobile average on 20 billets (in black)

number of actual useful unit lengths produced per billet since start of project (in red)

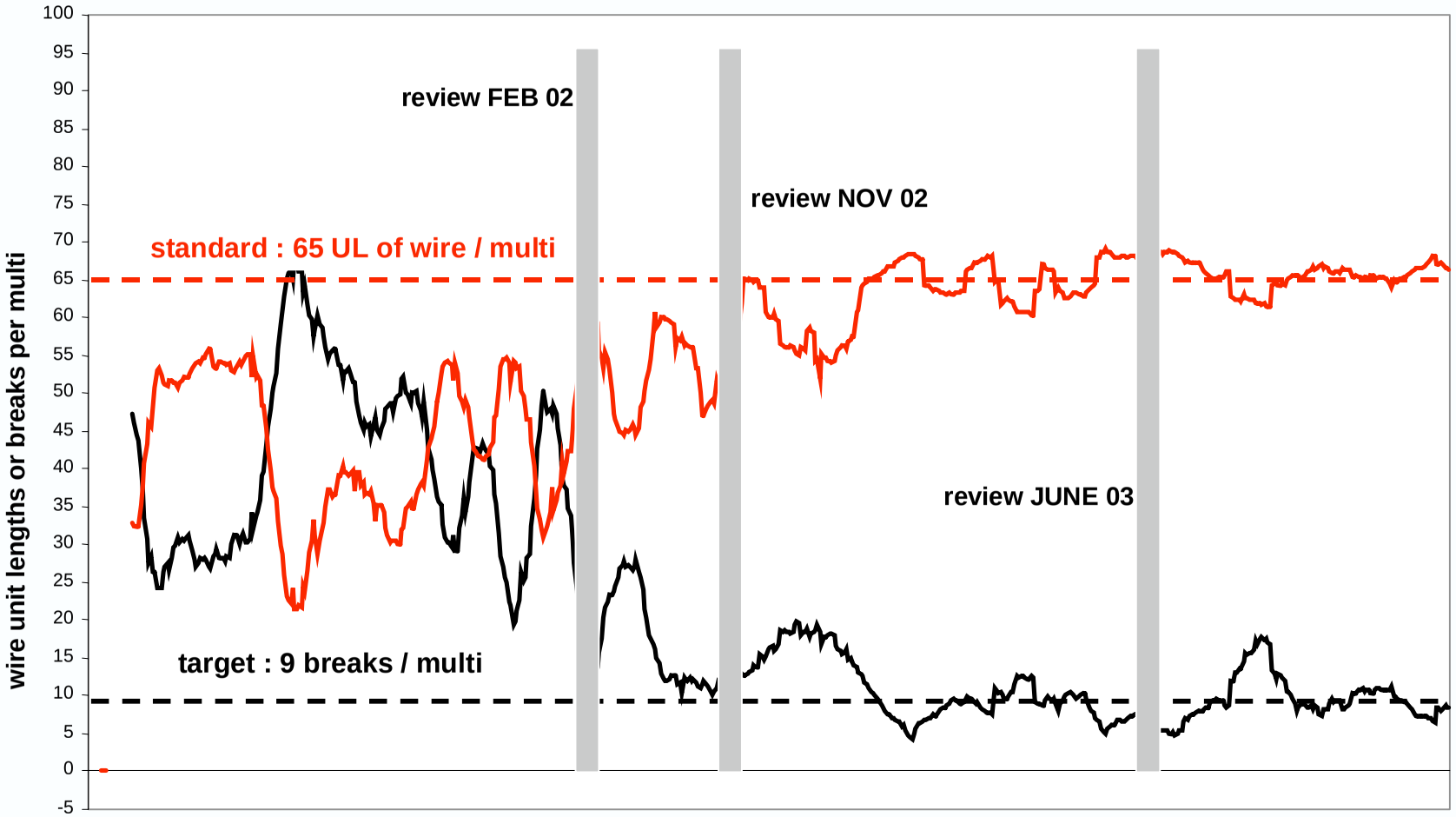

OUTPUT: inner wire

number of breaks per billet since start of project mobile average on 20 billets (in black)

number of actual usable unit lengths produced per billet since start of project (in red)

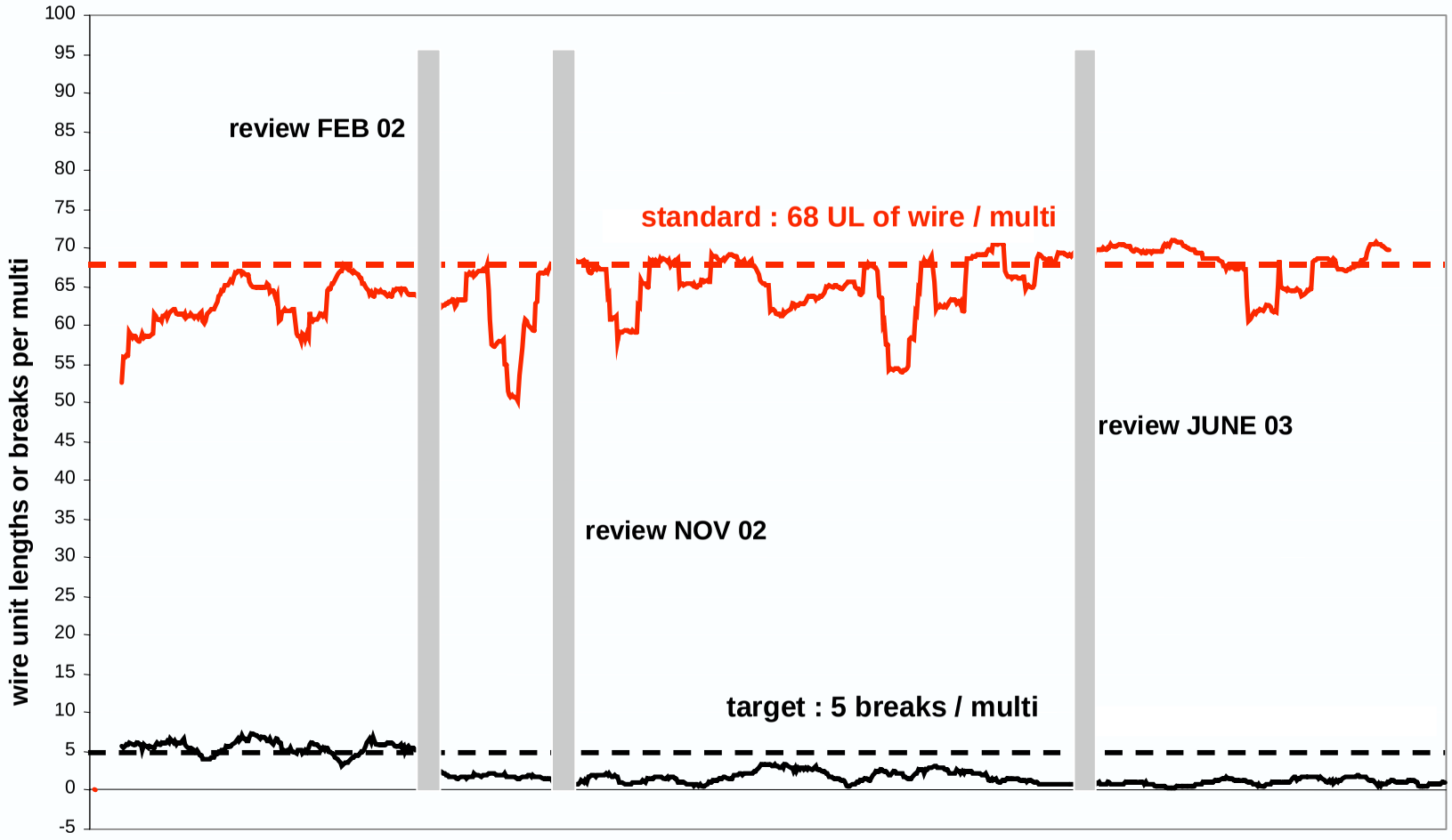

IMPROVEMENTS (2)

production yield continue to increase :

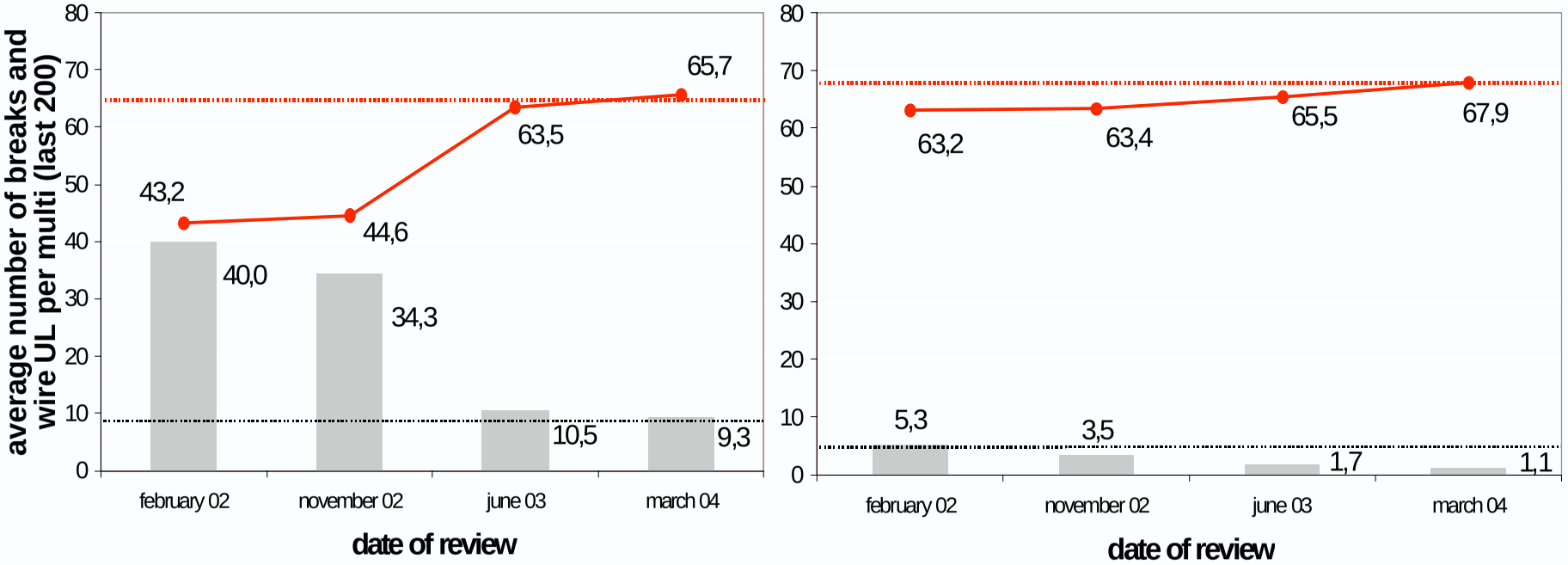

Targets of breaks and yields are definitively achieved on last 400 multi-filament billets

IMPROVEMENTS (3)

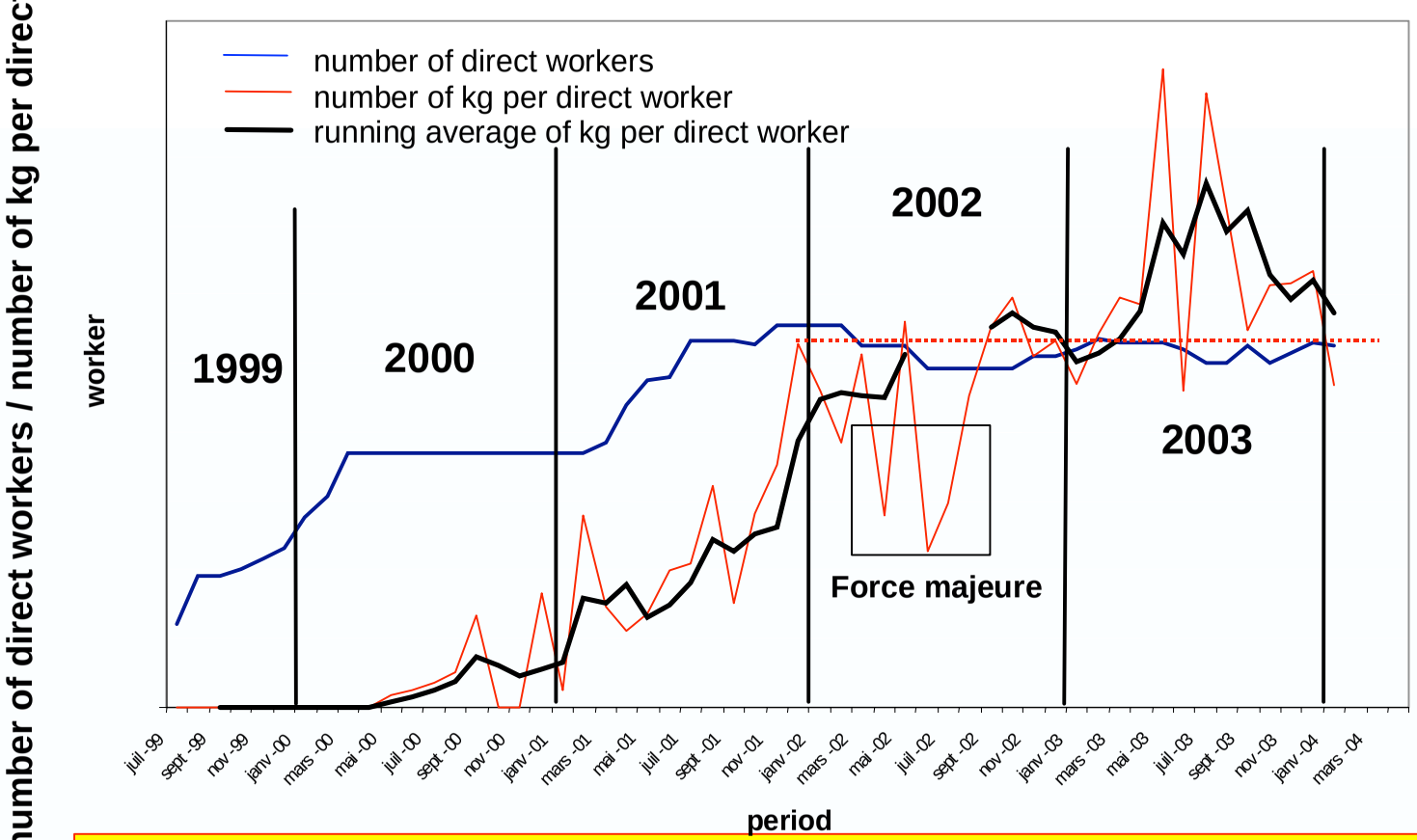

The “plateau production” reached in early 2003 has been achieved on a long period of more than one year : it is really a plateau

cable unit length delivery (shipped) : up to date (2)

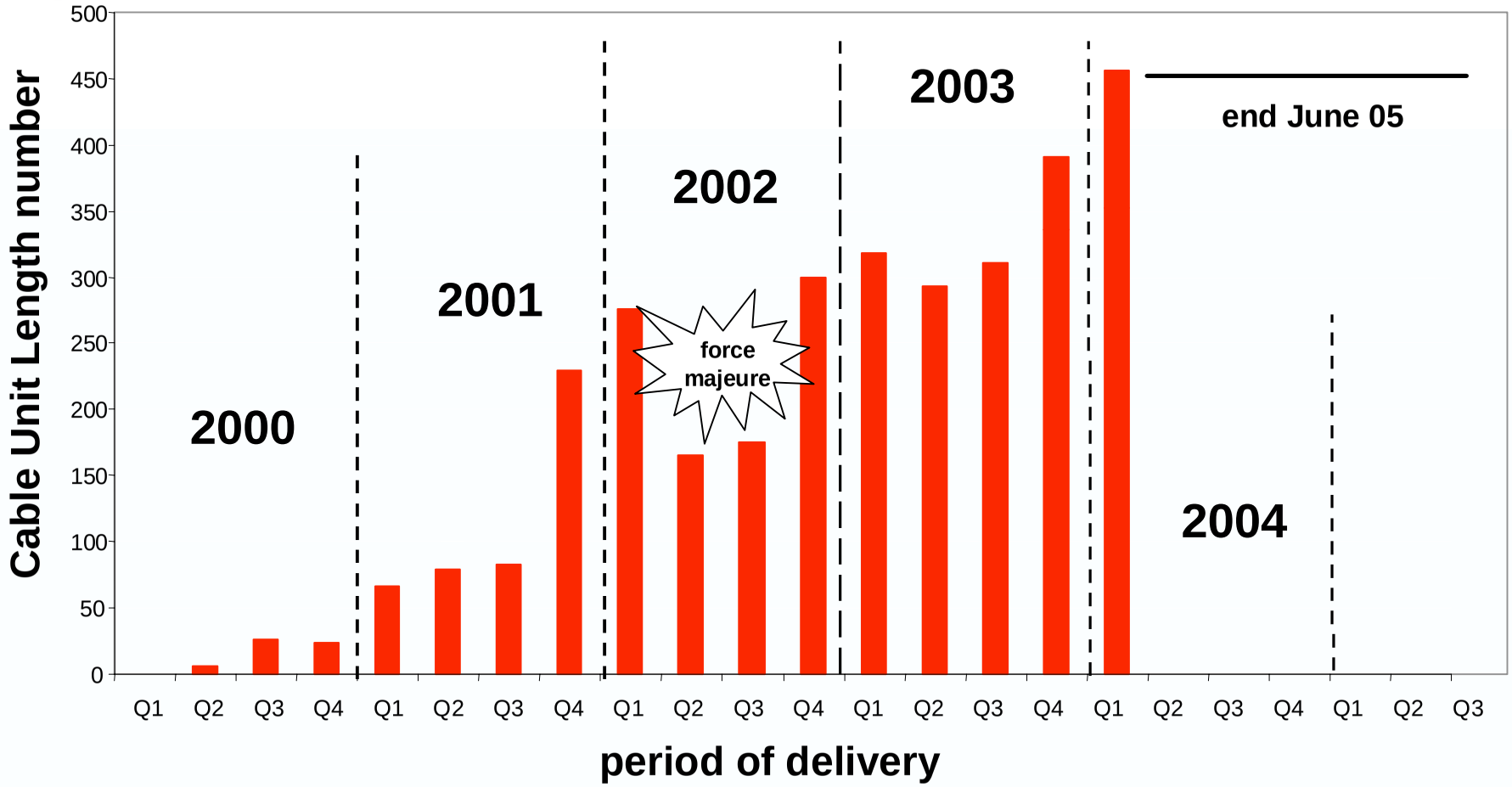

MSA forecast end of cable delivery in June 2005

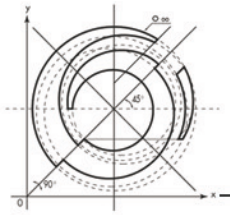

Nb3Sn Wires

- Bronze route
- Internal tin route
  - CEA Quadrupole
  - ITER
  - High energy physics

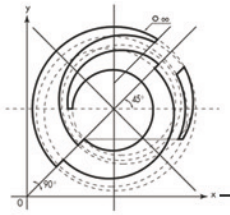

Nb3Sn Wires

- Bronze route
- Internal tin route
  - CEA Quadrupole
  - ITER
  - High energy physics

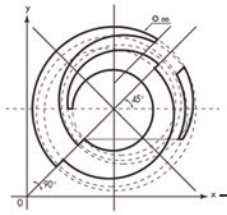

Typical wires for RMN application

ALSTOM

1. Diameter = 1mm
2. Cu/NonCu ratio= 0.2 à 0.5
3. Filament diameter = 2 à 4 µm
4. Type of wire : bronze route
5. Electrical properties:
   a. N-value @ 14 T ~ 40
   b. Ic @ 14 T ~ 170 A

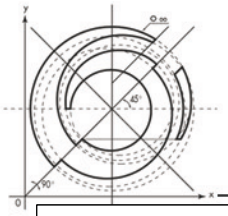

MSA wire for RMN application

ALSTOM

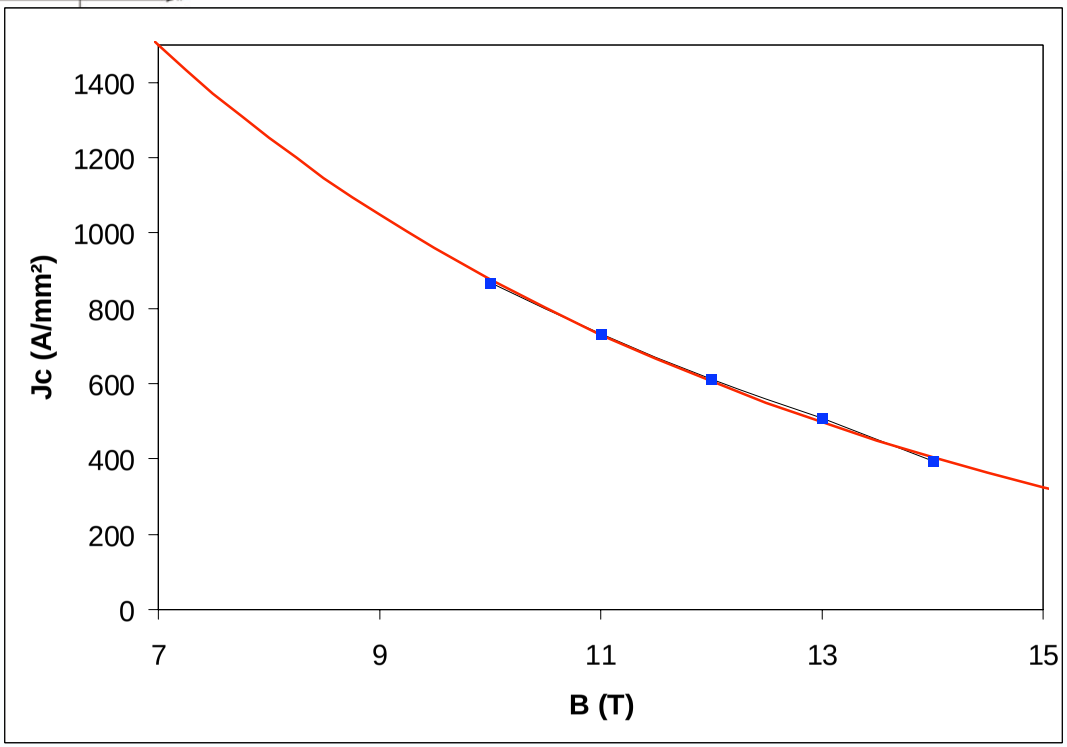

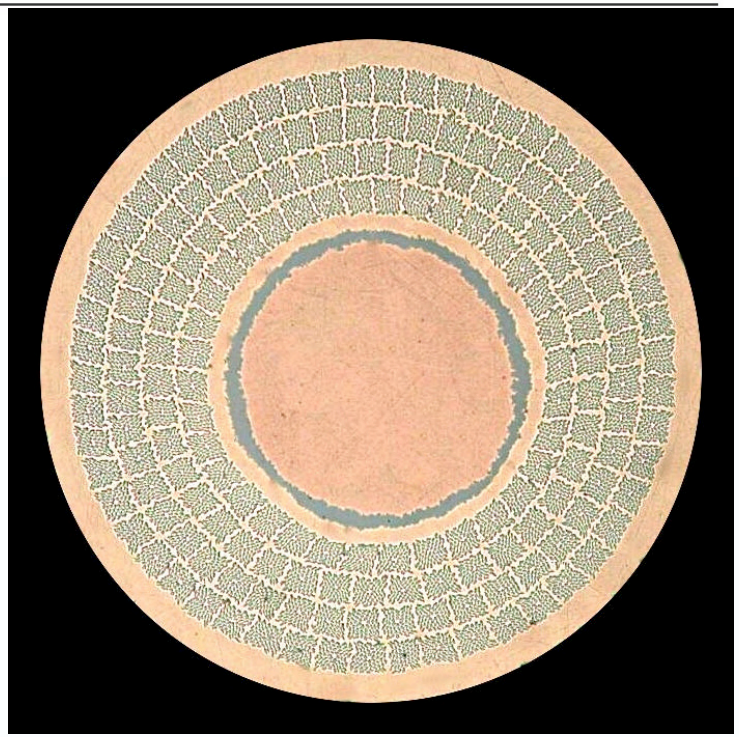

9800 filaments

Cu/NonCu=0.2

Φ_{wire}=0.800 mm

T = 4.2K

N-Value $_{12T}$ = 55

B(T)	10	11	12	13	14
Ic (A)	365	308	258	214	166
Jc $_{Non\ Cu}$ (A/mm²)	868	732	613	509	395

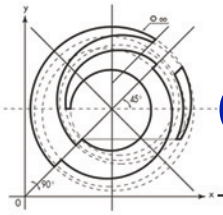

Optimisation of the wire

ALSTOM

microstructure optimisation

Optimisation HT

+

No change of the layout

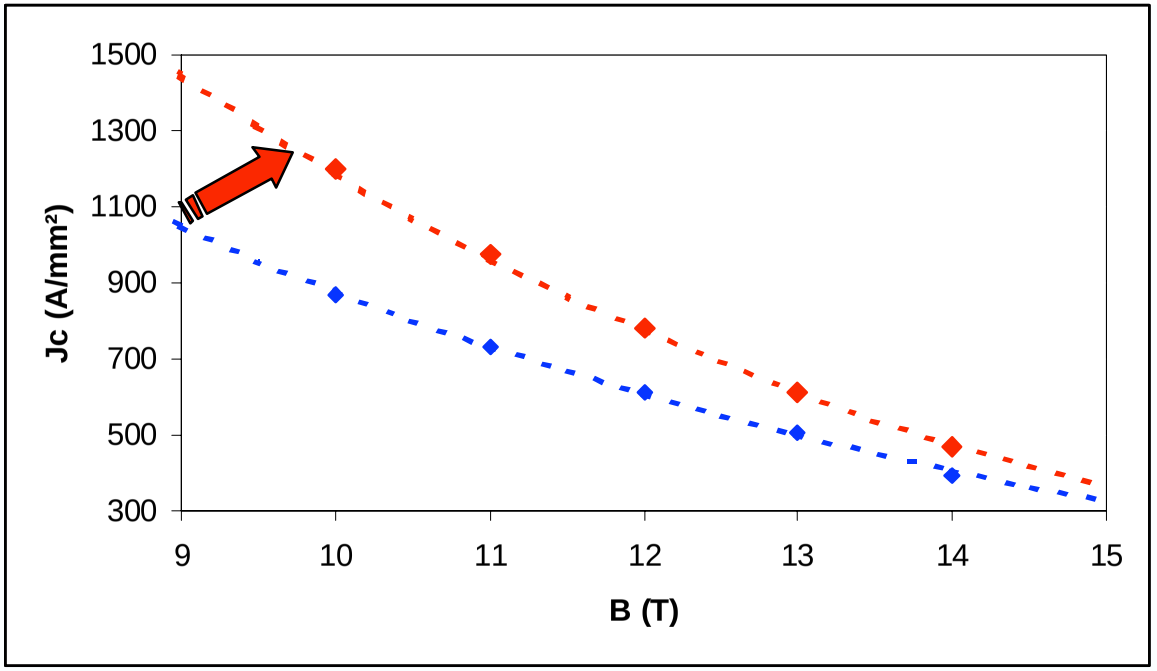

B(T)	10	11	12	13	14
Jc $_{\text{Non Cu}}$ (A/mm²)	868	732	613	509	395
Jc $_{\text{Non Cu}}$ (A/mm²) optimised	1197	974	**781**	614	468

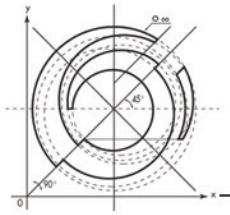

Nb3Sn Wires

- Bronze route
- Internal tin route
  - CEA Quadrupole
  - ITER
  - High energy physics

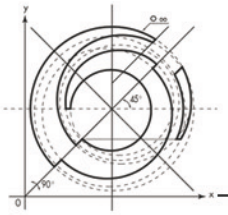

ALSTOM

Quadrupole using LHC design

- Wire specification

  1. $I_c \geq 405$ A à 7 T

  (↔ $J_c \approx$ **700 A/mm²** à12T& Copper/NonCopper ratio=1.4)

  2. $W_h \leq 450$ mJ/cm^3 non Copper)

- Rutherford cable

  1. With inox insert
  2. Dimensions similar to the LHC cable)

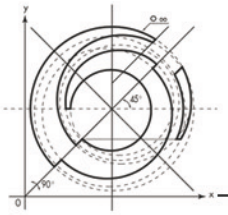

CEA Quadrupole

ALSTOM

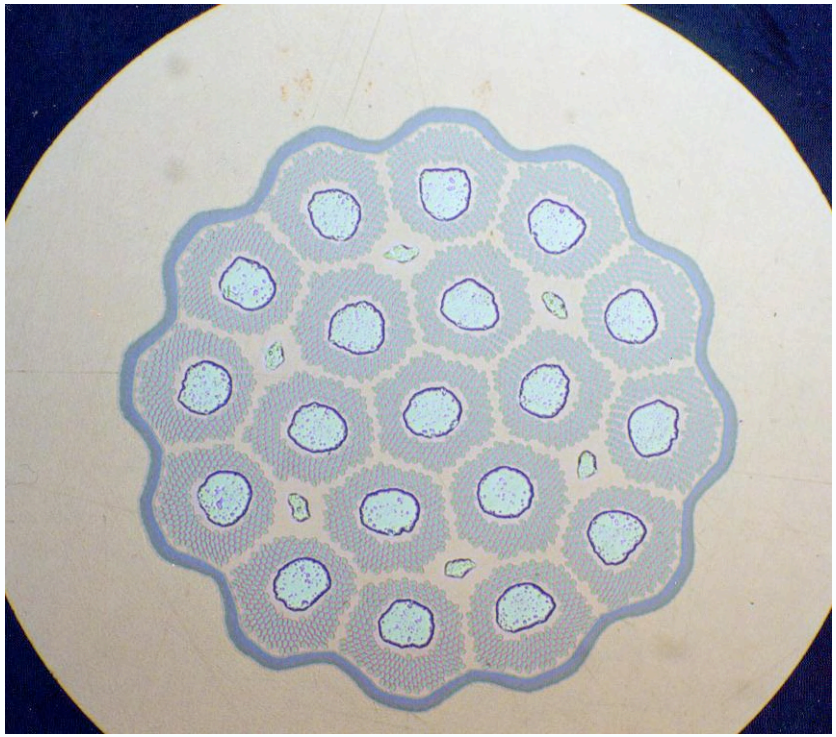

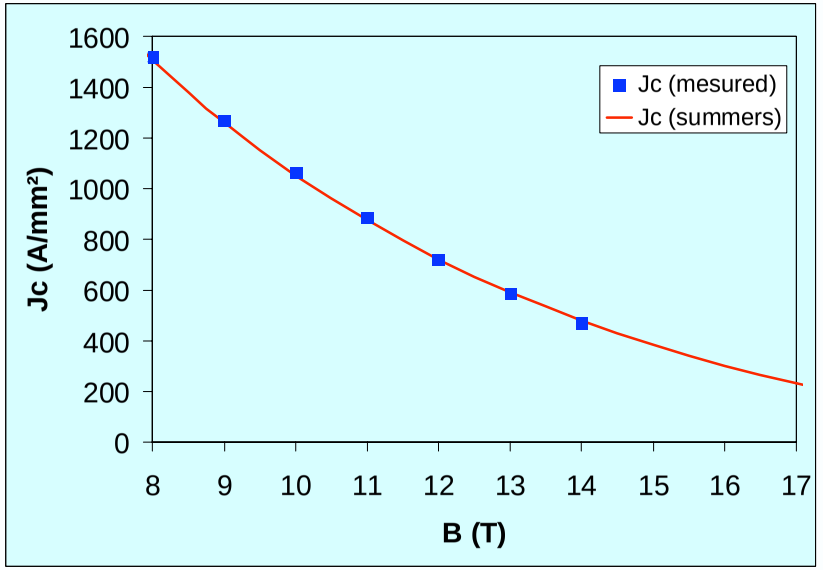

+

Non copper losses = 530 mJ/cm^3

Cross section of the designed billet

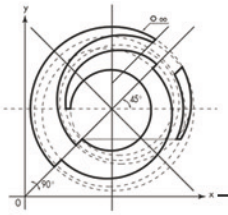

CEA Quadrupole

ALSTOM

State of the art in year 2000 :
(P.J. Lee)

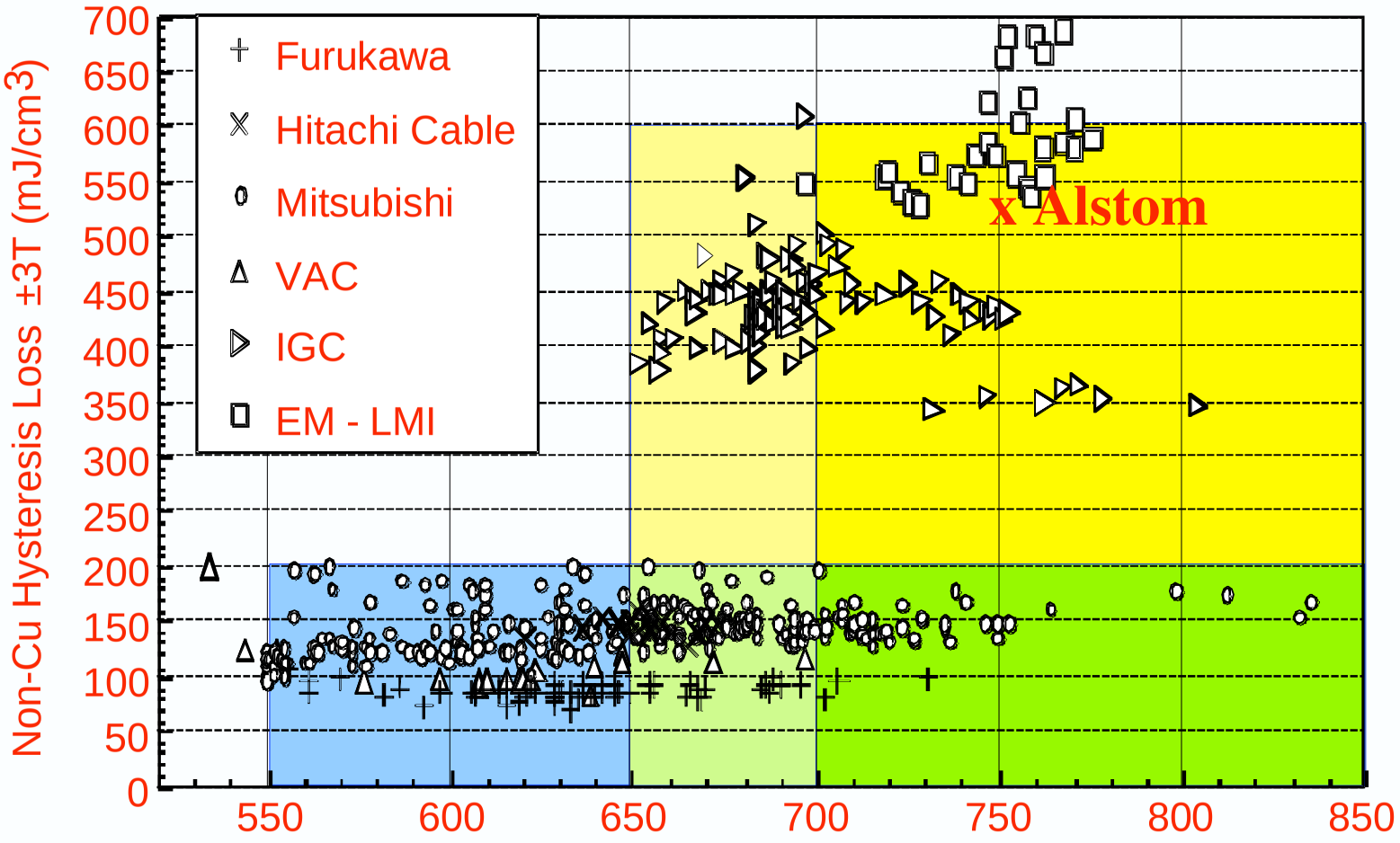

269

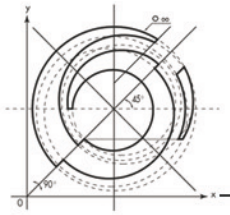

Improvement

ALSTOM

Unit length

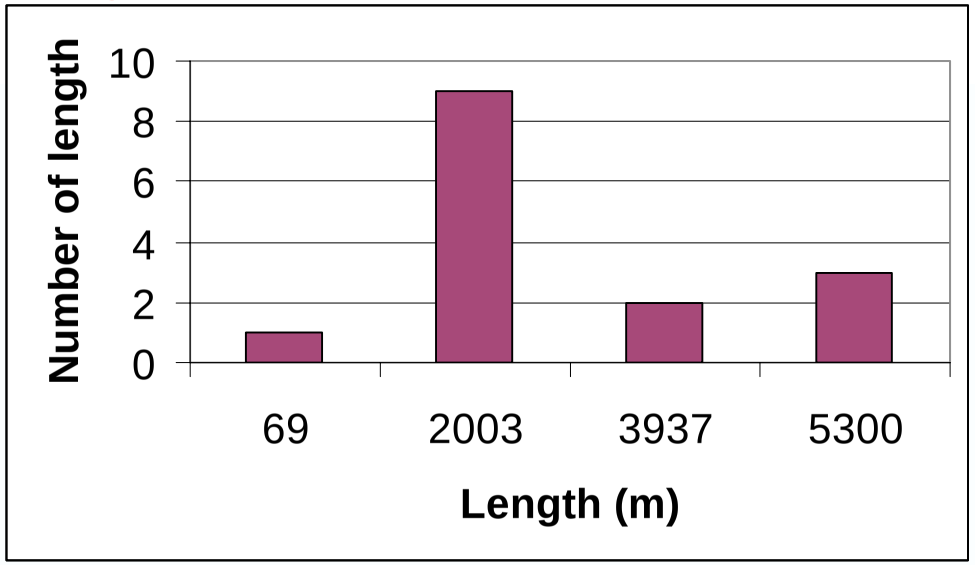

Technology improvements

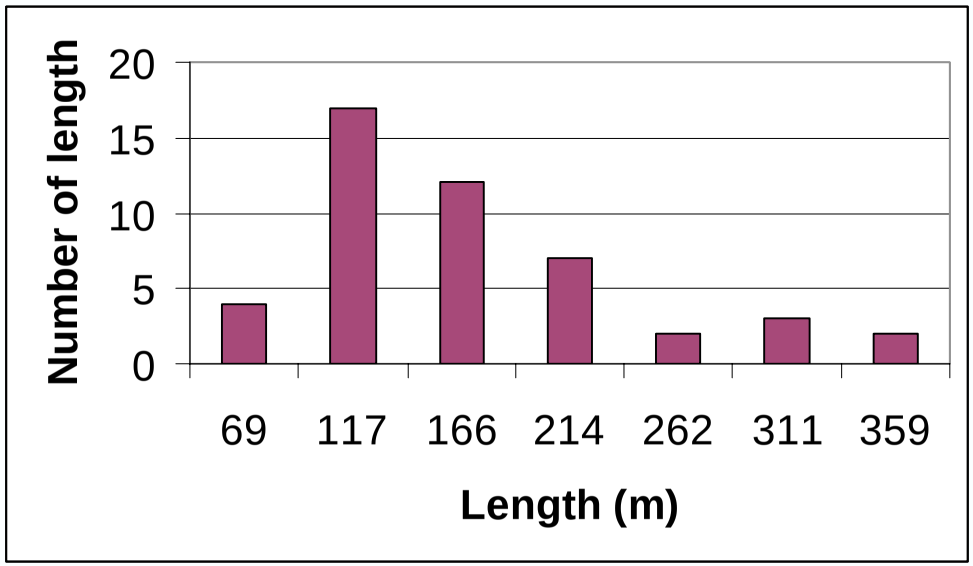

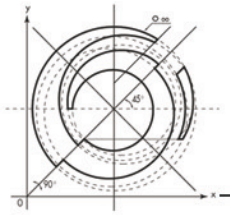

Nb3Sn Wires

- Bronze route
- Internal tin route
  - CEA Quadripole
  - ITER
  - High energy physics

271

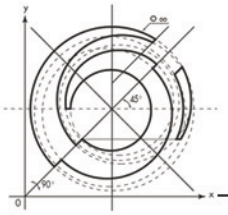

EFDA technical specification

Parameter	
Diameter (mm)	0.81 mm ± 3 µm
Chrome coating	2 µm +0,5/-0,0 µm
Cu / Non Cu ratio	0.90 - 1.5
Twisting (mm)	≤ 20 mm
Ic (4.22K;12T;0.1µV/cm)	>200 A 800A/mm² & Cu/NonCu=1 (Target : 1100A/mm² & Cu/NonCu=1)
N-value @12T & 4,2K	>20
RRR	>100
Losses (± 3T)	< 1000 mJ/cm³
Unit length	>1500 m

272

old results (1997)

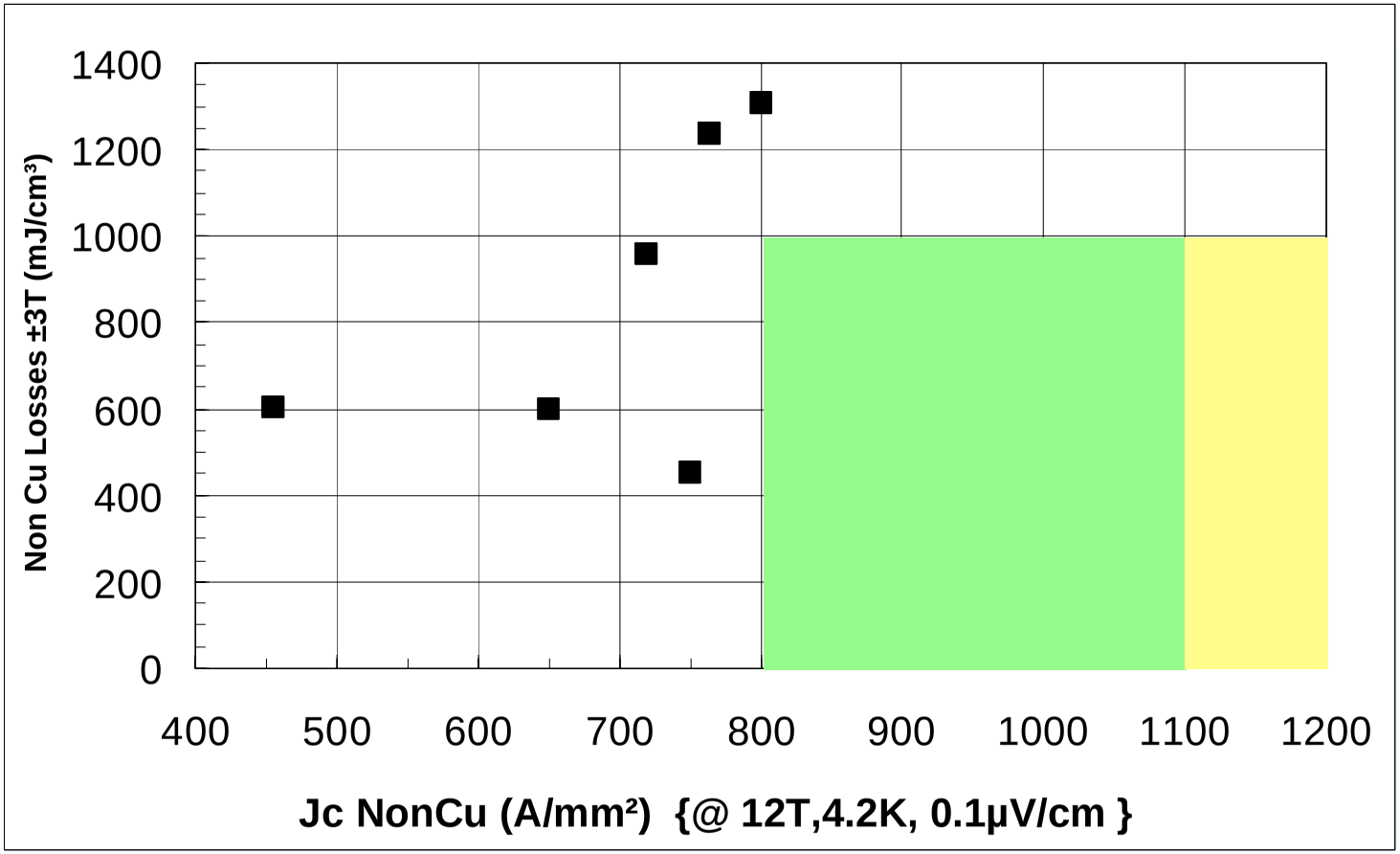

Presently, manufacturing of new Nb3Sn billets for EFDA contract

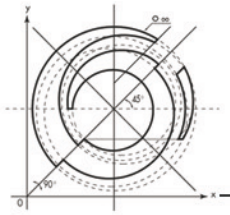

ALSTOM

Nb3Sn Wires

274

- Bronze route
- Internal tin route
  - CEA Quadripole
  - ITER
  - High energy physics

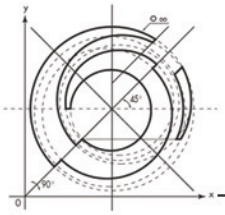

High energy physics needs

ALSTOM

1. Quadrupole magnet for TESLA (CEA Collaboration)

- Nb_3Sn conductors :
  - non-Cu J_C up to 2000 A/mm^2 @12 T and 4.2 K
  - Losses : effective diameter < 50 µm
- Cable :
  - To manufacture a Rutherford cable

2. Care

- Nb3Sn conductors :
  - non-Cu JC up to 1500 A/mm2 @15 T and 4.2 K
  - Losses : effective diameter < 50 µm

275

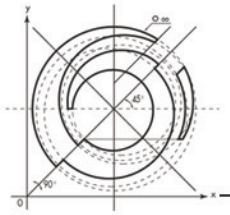

R&D program

ALSTOM

Work program : Taguchi method

		State 1	State 2
1	Type of diffusion barrier	A	B
2	Diffusion barrier material	A	B
3	Filament diameter	A	B
4	Spacing between filament	A	B
5	Sn/Nb ratio	A	B
6	Number of sub elements	A	B
7	Cu/Non Cu ratio	A	B

276


ALSTOM
www.alstom.com

ShapeMetal Innovation B.V.

The producer of Nb_3Sn PIT conductors

SMI
SHAPEMETAL INNOVATION B.V.

- Het Lentfert 31
  7547 SN Enschede
  The Netherlands

- Tel. +31 (0)53 434 07 04
  Fax. +31 (0)53 435 86 42
  Email: jlsmi@worldonline.nl

SMI activities

and

plans on PIT Nb_3Sn

J.H. Lindenhovius SMI, Enschede

H. Krauth EAS, Hanau

Outline

- 1974 - 1990 ECN (history)
- 1992 - 2004 SMI (activities)
- 2004 - SMI - EAS (plans)

1974 – 1990

Development at Energy Research Foundation

ECN in Petten (NL)

- With pilot productions for Fusion and Accelerators

European Fusion Program

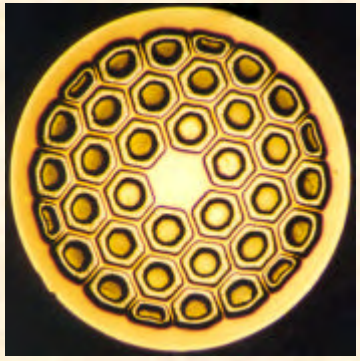

Cables for 12T coils of SULTAN-2 facility

(Coils are now part of ENEA test facility)

'85 –'86 **PIT strand with 36 filaments** (12,2T; 4.2K)						
Dia (mm)	Cu (%)	OD Nb (µm)	Ic (A)	N-value	Jc non-Cu (A/mm^2)	Weight (kg)
1.0	58	108	350		1060	167

Magnet development program of CERN

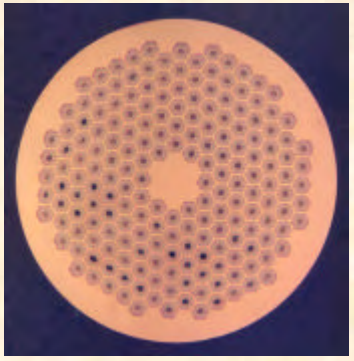

1 m Nb_3Sn model magnet ('87)
(ELIN made single pole)

'87 PIT strand with 192 filaments for B-cable (12T; 4.2K)						
Dia (mm)	Cu (%)	OD Nb (µm)	Ic (A)	N-value	Jc non-Cu (A/mm^2)	Weight (kg)
0.9	55	44	544	55	1898	47

'87 B-cable (Keystoned Rutherford) (12T; 4.2K)				
Dimensions (mm)	# strands	Ic (kA)	Jc non-Cu (A/mm^2)	Length (m)
1.45/1.77 x 16.4	36	18,8	1520	240

Magnet development program of CERN in co-operation with UT

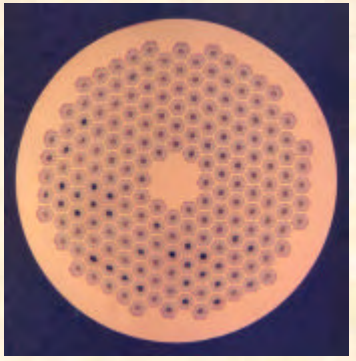

11,5T Nb_3Sn 1 m model magnet ('90)

(Keystoned Rutherford Cables made by LBL Berkeley)

'90

PIT strand with 192 filaments for A-cable

(12T; 4.2K)

Dia (mm)	Cu (%)	OD Nb (µm)	Ic (A)	N-value	Jc non-Cu (A/mm^2)	Weight (kg)
1,25	53	62	657	40	1139	53

'88-'89

PIT strand with 192 filaments for B-cable

(12T; 4.2K)

Dia (mm)	Cu (%)	OD Nb (um)	Ic (A)	N-value	Jc non-Cu (A/mm^2)	Weight (kg)
1.0	53	49	541	40	1465	57

1992 – 2004

Activities of ShapeMetal Innovation SMI in Enschede (NL)

- 1992 – 1995

  Main activity:

  Development and Production of SMA applications

- 1995 – 2004

  Development of PIT conductors

  With small production for Fusion, Accelerators and Laboratory Magnets

Development projects on PIT

(1995 – 2004)

- Fine filament conductor
- High field conductor
- Stress – strain behaviour
- Cabling
- Extrusion

Fine filament conductor

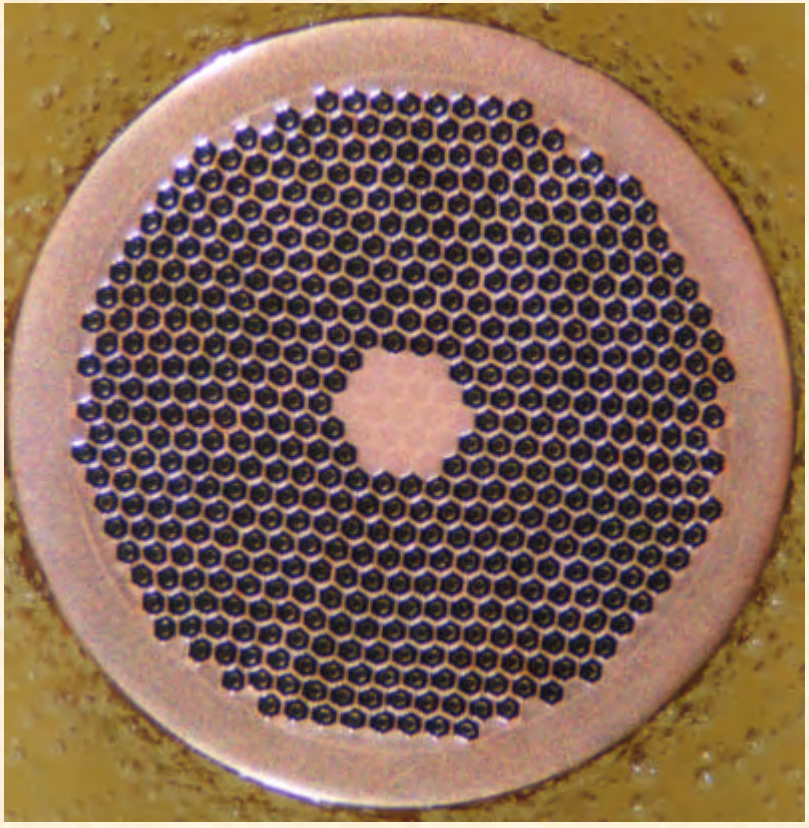

Binary conductor

- 504 filaments
- Matrix OFHC copper ca. 52%
- Diameter 0.9 mm; OD Nb 27,5 µm
- RRR value > 100
- Jc non-Cu: 1350 A/mm² at 12T
- N-value ca. 40 at 12T

In production for UT dipole magnet

Advanced Iter conductor ???

High field conductor

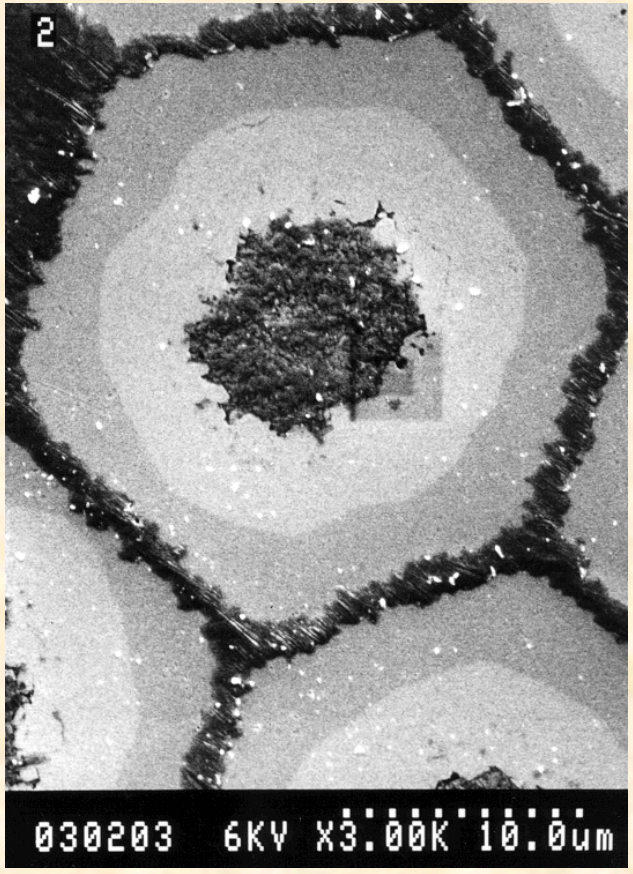

Tertiary conductor

- 192 filaments
- Matrix OFHC copper 45 - 53%
- Diameter 1.0 mm; OD Nb 50 µm
- RRR value : >100
- Jc non-Cu : max. 2450 at 12T
  max. 700 at 18T
- N-values : > 40 at 12 Tesla

In regular production for accelerators

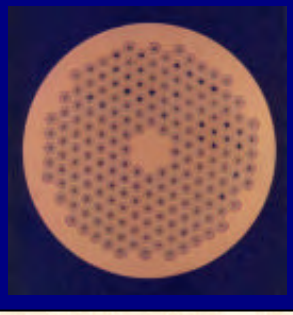

Powder in Tube conductors

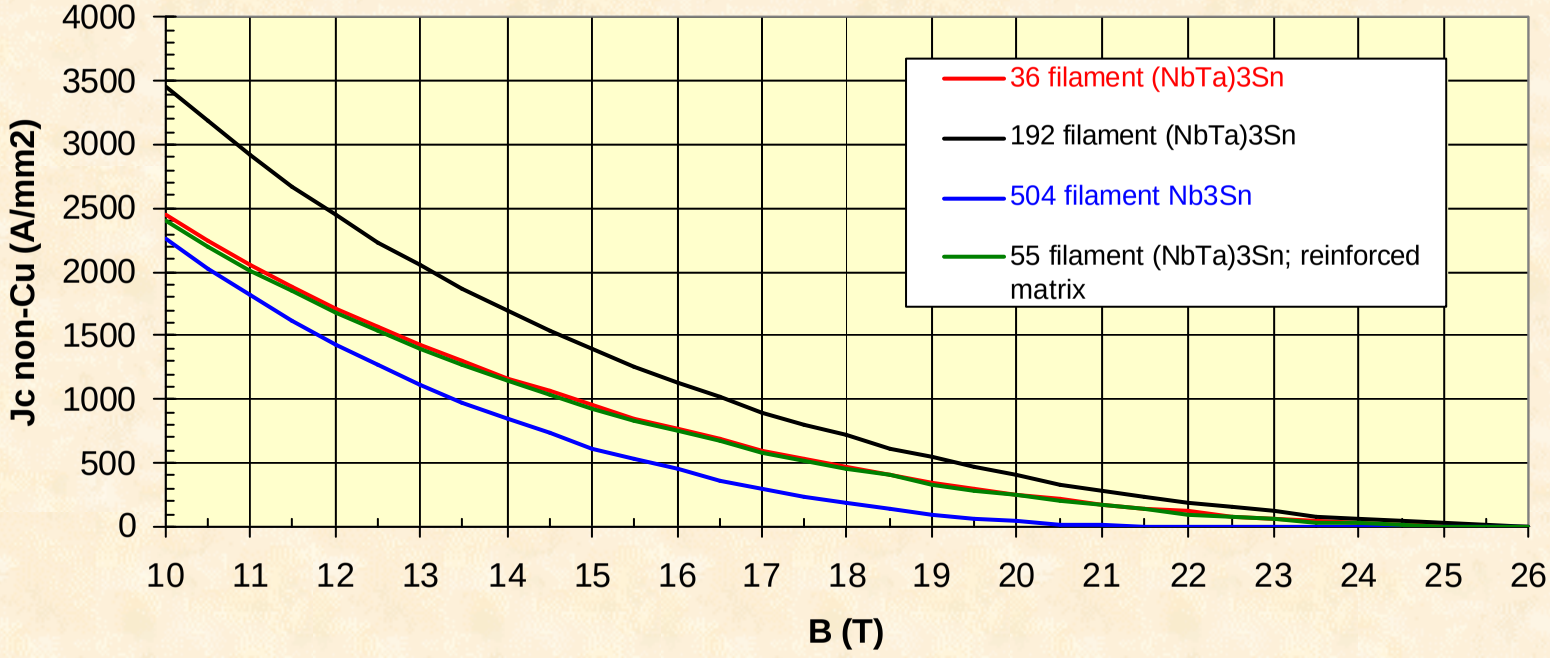

Stress – strain behaviour

UNIVERSITÉ DE GENÈVE

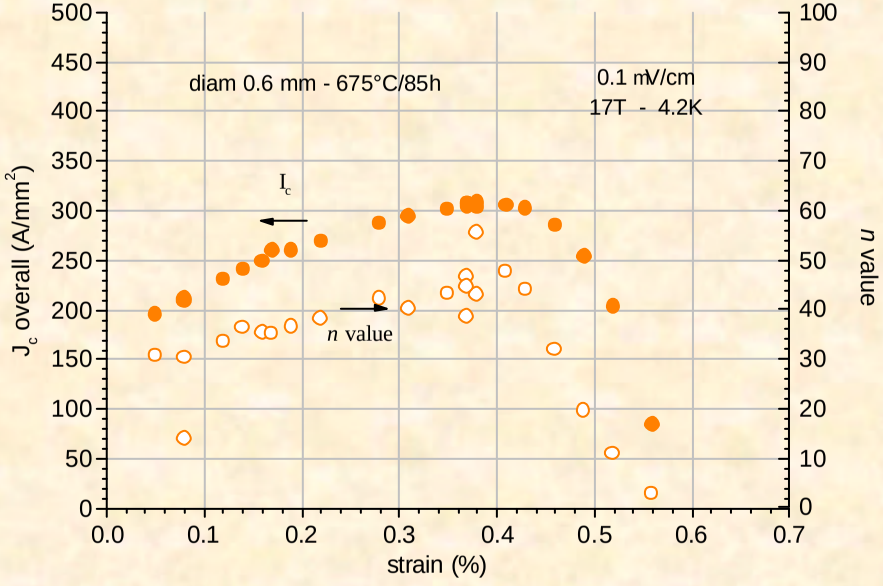

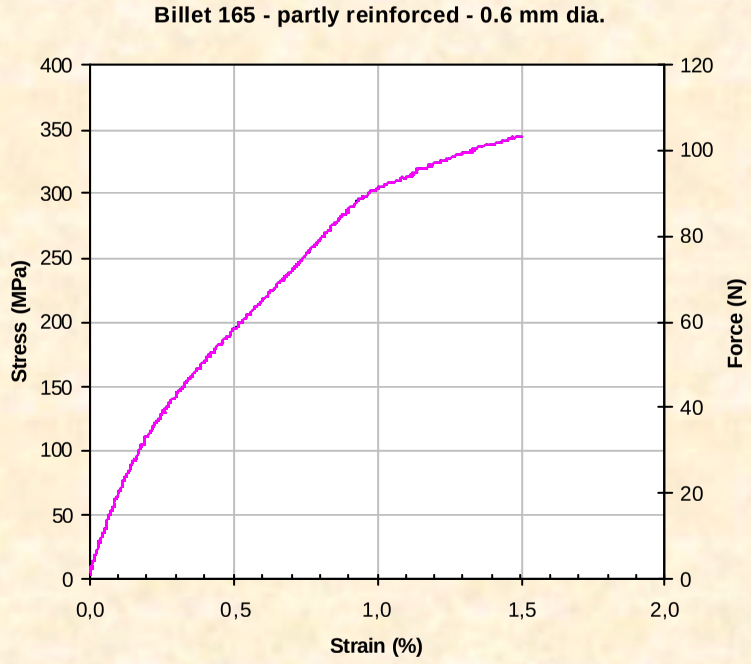

Experimental Procedure

Longitudinal Cross-Section

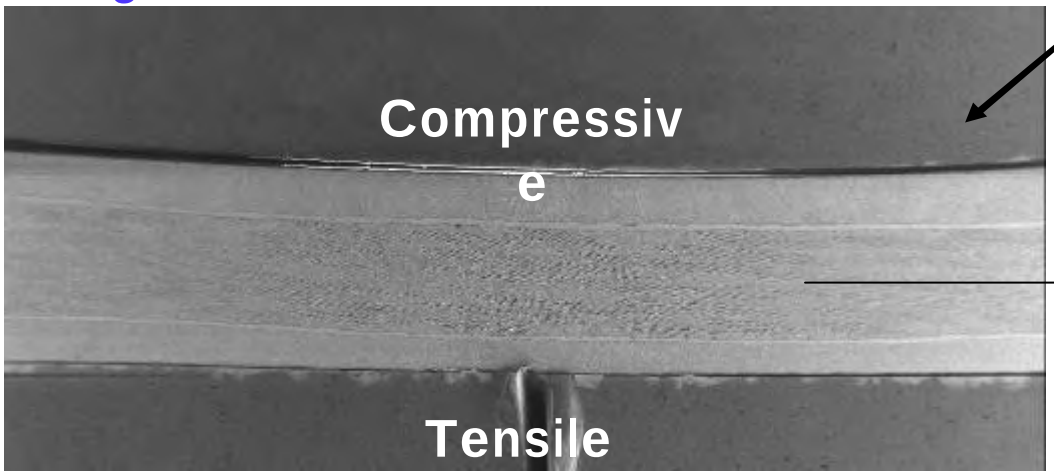

Stainless steel clamp, bent to 0.5% of wire radius

Neutral Axis

- 1 cm-long samples were mounted in stainless steel clamps with a radius of 200x the radius of the wire.
- Longitudinal face hot-mounted, ground, and polished to 0.05 mm
- Samples etched in 37% HNO_3, 13% HF for ~10 sec. to reveal crack location
- Images acquired on field-emission scanning electron microscope and optical microscope
- All wires received manufacturer recommended heat treatment

Mitsubishi wire in clamp

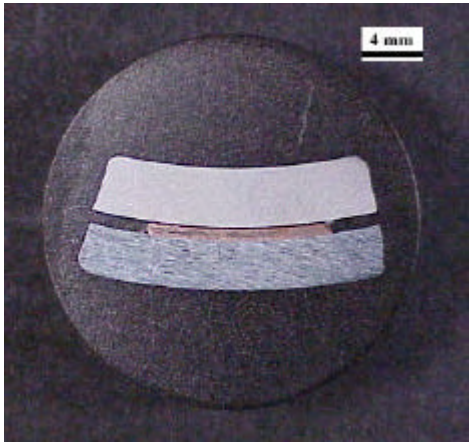

SMI Powder-in-tube Billet 34(Ta)

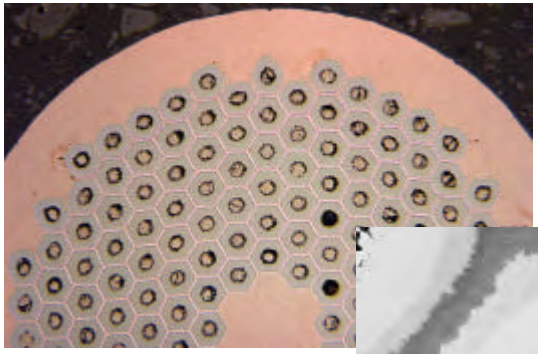

Transverse Cross-section

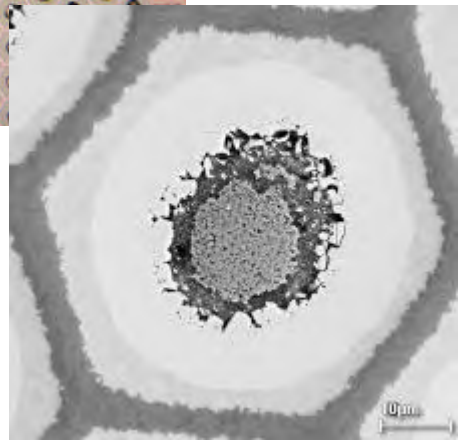

0.5% strain

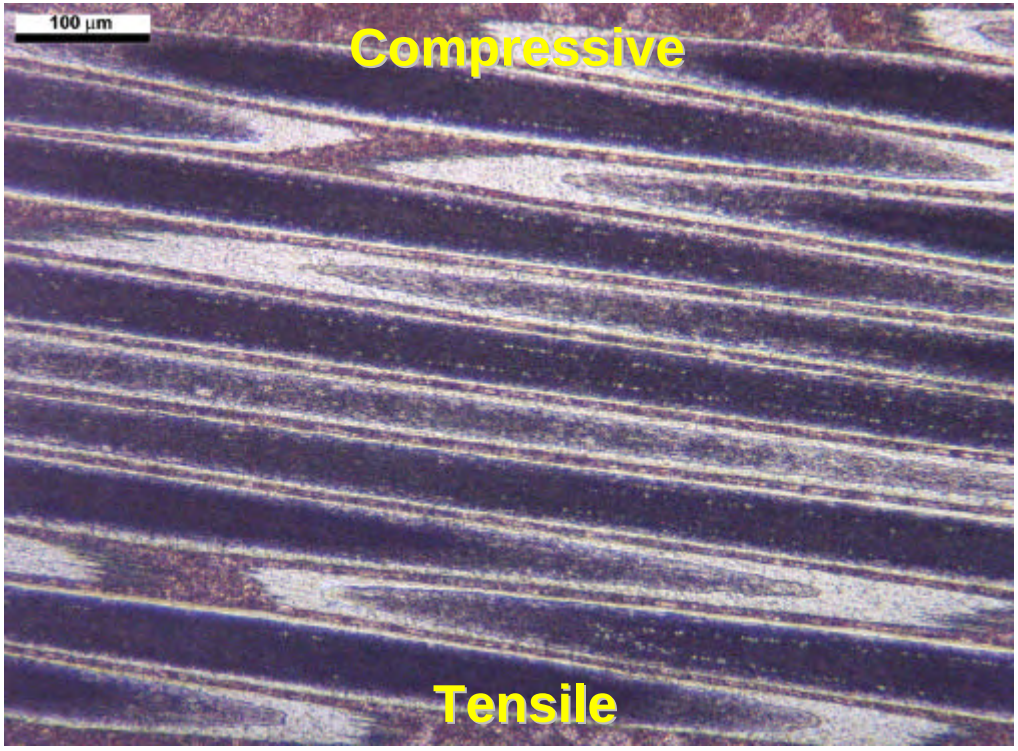

•No cracking seen at 0.5% strain

SMI Powder-in-tube Billet 34(Ta)

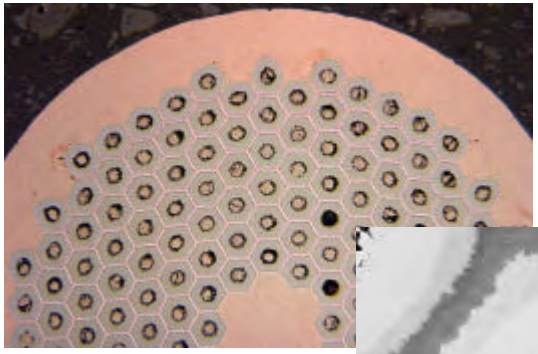

Transverse Cross-section

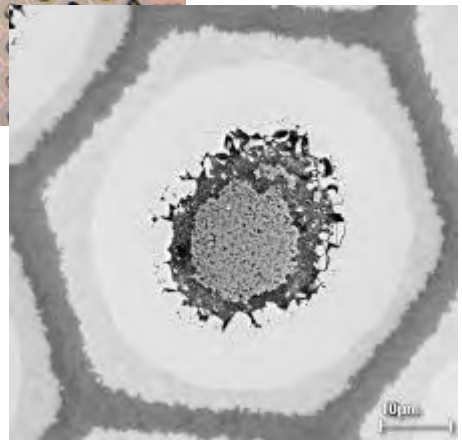

0.625% strain

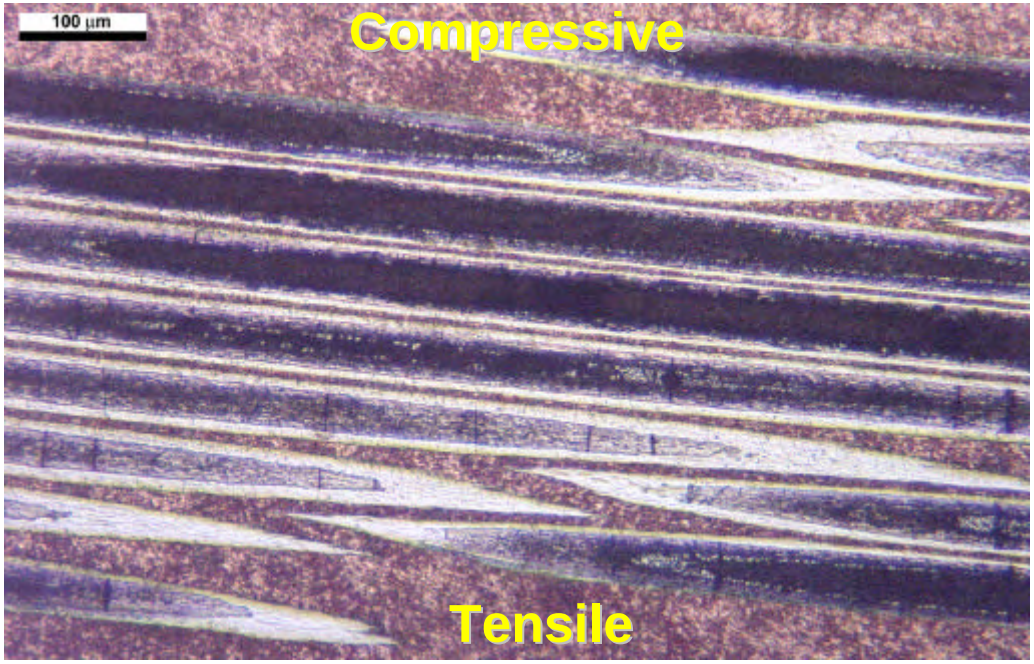

- Trans-filamentary cracking present at 0.625%
- Ductile Nb arrests crack propagation

Cabling

Keystoned Rutherford cable (LBL Berkeley)

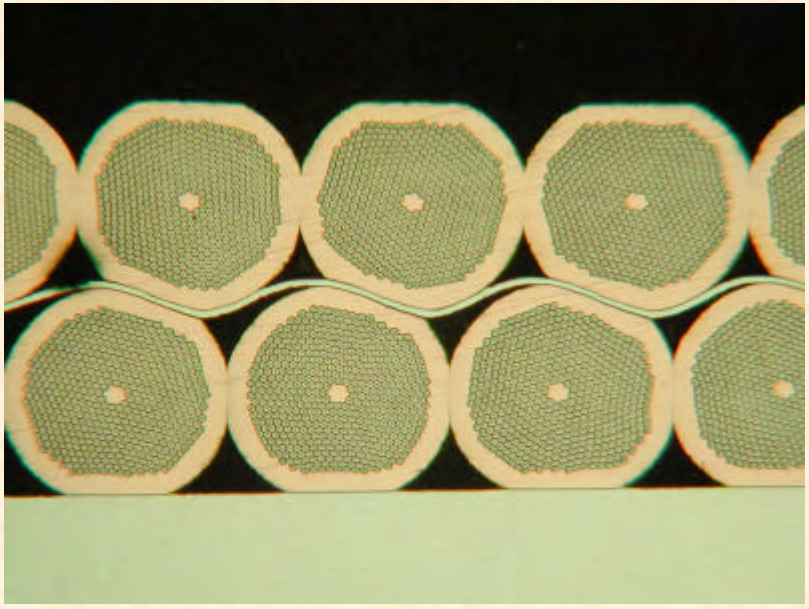

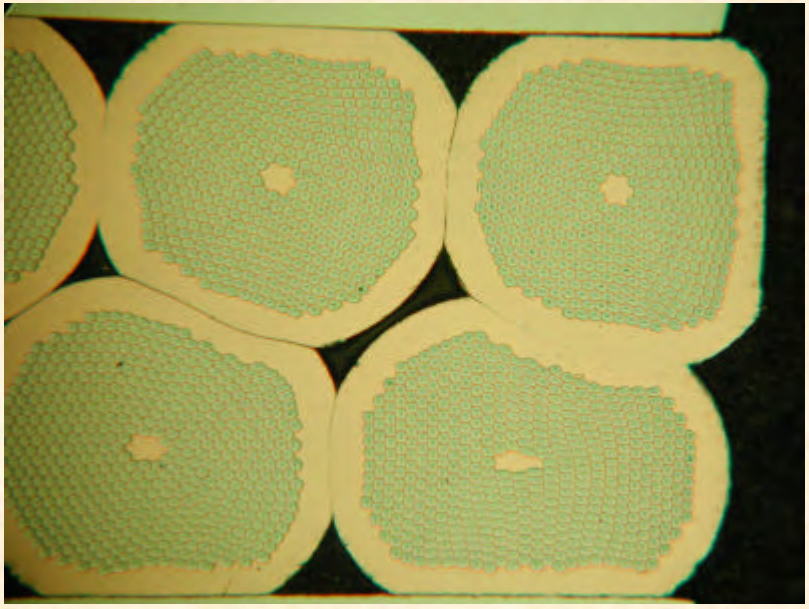

Extrusion

- Extrusion succesful of
  - Small billets (since longer times)
  - Middle sized billets (recently)
- Extrusion of large billets expected soon

SMI's activities

today

- Fermilab

  small quantities; 1.0 mm dia
  tertiary conductor (192 fil)
  Ic > 700A @ 12T; 4.2K
  filament dia < 50 µm

- CERN – UT (Nb_3Sn dipool)

  last small part (< ¼); 0.9 mm dia
  binary conductor (504 fil)
  Cu 45 - 60%
  Ic ³ 460 A @ 10,8T; 4.2K
  N-value ³ 40 at 10,8T; 4.2K

- Iter qualification

  100 kg; 0.81 mm dia.
  binary conductor (1st test billet)
  Ic < 280A @ 12T;4.2K
  hysterese loss £ 500 kJm^3 (± 3T)

- Laboratory and other magnets

  small quantities; 0.5 – 1.2 mm dia
  binary/tertiary conductors (36–192 fil)
  reinforced matrix on request
  with high Ic values

SMI's plans on PIT Nb_3Sn

- Make co-operation with EAS succesful
- Qualify for:
  - Fusion (ITER)
  - Accelerator projects (e.g. CARE/NED)
  - NMR
- Start large scale production

Next European Dipole (NED)

Strand specification (Nb_3Sn)

– diameter	1,25 mm
– Cu	55 % (Cu : SC = 1,25 : 1)
– Jc non-Cu	1500 A/mm^2 @ 15T; 4.2K
– filament diameter	< 50 microns
– piece length min.	1 km (pref. 3 km)
– tot. length	16 km (1 + 5 + 10 km)

Cable specification

– type	Keystoned Rutherford
– number of strands	40 (max.)

Development for NED

With regard to following topics

- Powder composition
- Cross section
  (in relation with cabling properties)
- Heat treatment
- Barrier
- Extrusion

What are the Limits in Present High J_c Nb_3Sn Wire Designs?

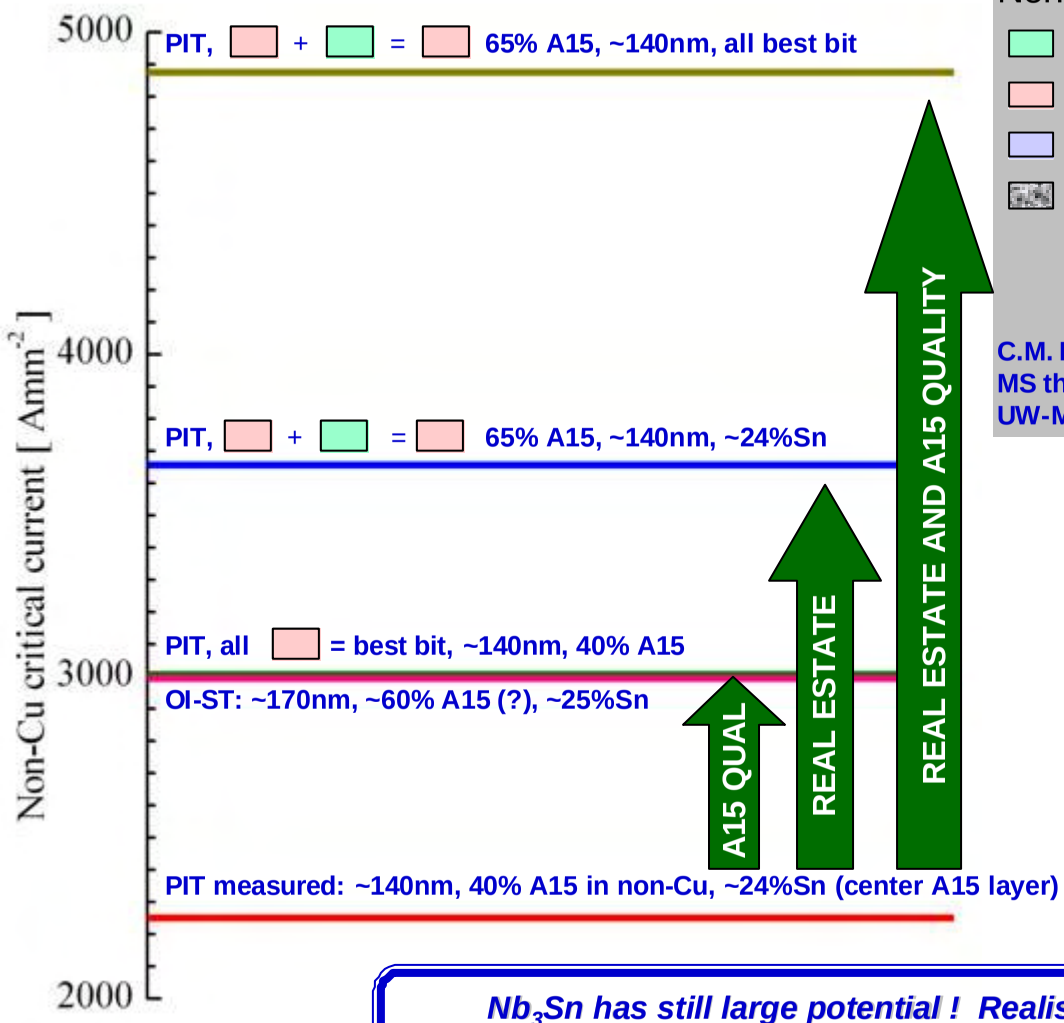

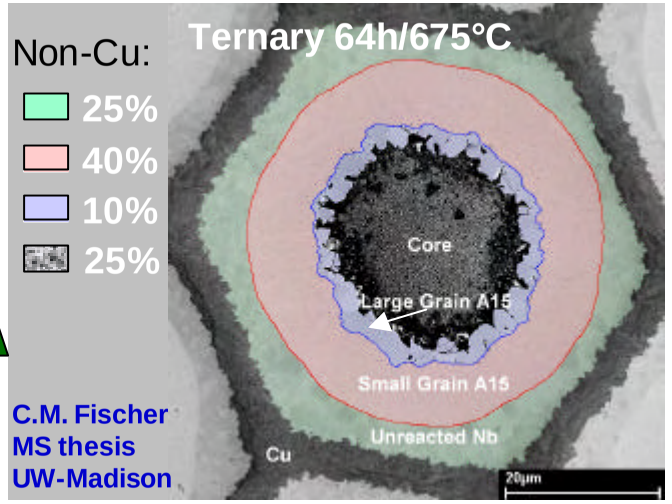

Pinning wise:

- SMI-PIT $Nb(Ta)_3Sn$
  - Grains ~140nm
- OI-ST $Nb(Ta)_3Sn$ 2900 A
  - Grains ~170nm
- At 12T => vortices
  - Spacing ~14nm
- More possible?

Nb_3Sn has still large potential ! Realistic ?
~5000 Amm^{-2} physical limit with present wire designs?
Getting the Sn up and homogeneous is important!

Complete HEP program includes complementary SBIR/STTR work

- FY 2001

  *Nb_3Al--$1,200K

  *PIT Nb_3Sn--$1,100K

  *MJR/Int. Sn Nb_3Sn--$400K (+$500K direct HEP)

- FY2002

  *PIT Nb_3Sn--$1,500K

  *MJR/Int. Sn Nb_3Sn--$700K(+$440K direct HEP)

  MJR Nb_3Al--$60K direct HEP

  *SC Processing--$1,000K

Outokumpu Activities and Plans on LTS and HTS Materials

Rauno Liikamaa 23.03.2004

Contents

- **The Superconductors Buissness Line in Outokumpu**
- **Nb_3Sn Projects**
- **HTS Activities**

Organization

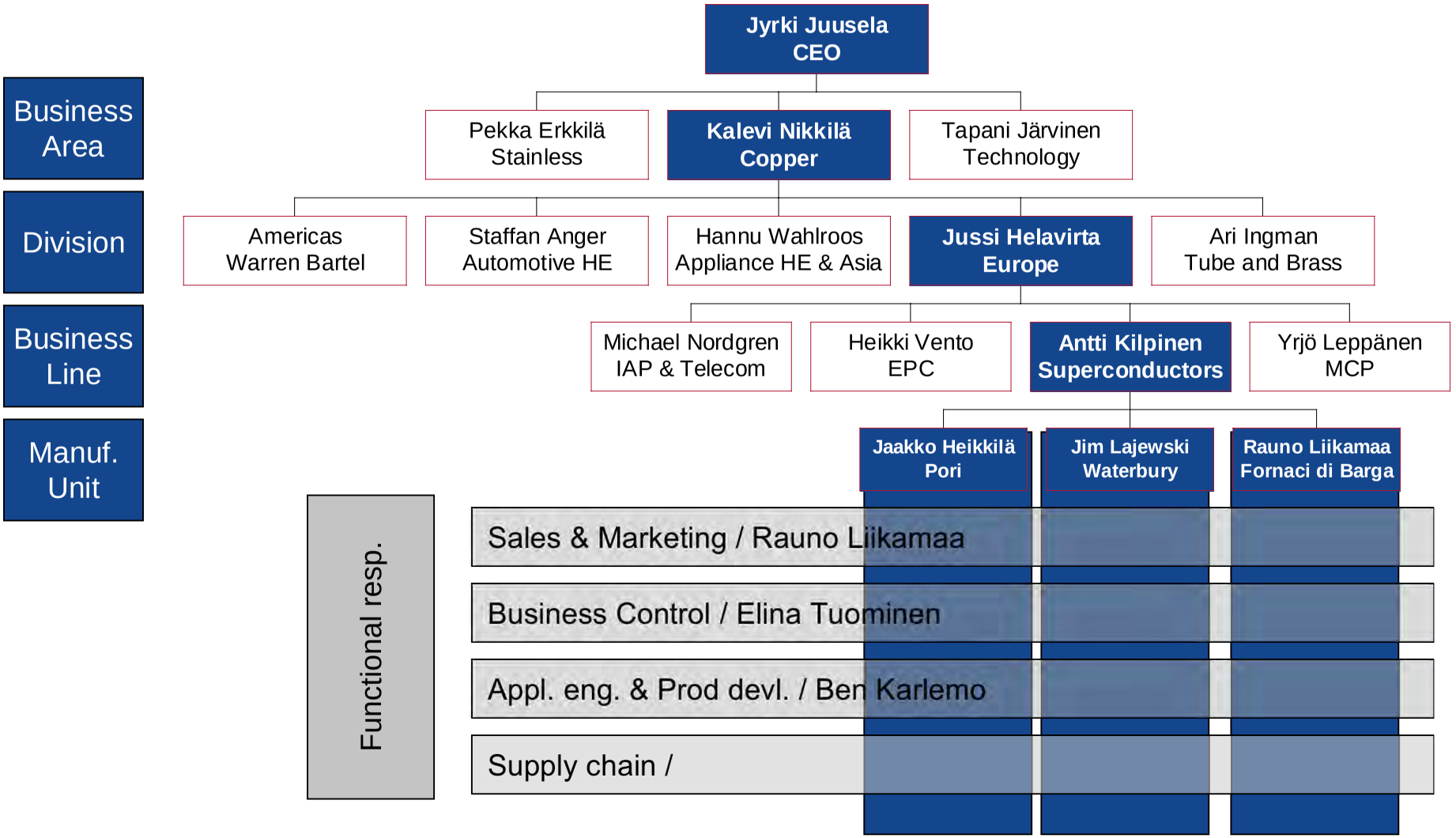

Superconductor Business: Products and Applications

- **NbTi**
  - Monolithic wires
  - Wire in Channel
  - Cables
- **Nb_3Sn**
  - Internal Tin
  - Bronze
- **Applications**
  - MRI
  - NMR
  - Specials
  - Projects
    - LHC
    - CMS
    - ATLAS
    - Wendelstein 7-X
    - Kstar
    - Others

Superconductor Business: Essential Assets

- In House High Purity Oxygen Free Copper
  - Billets, cakes, Rods
- Complete set of Machinery for Copper Cold and Hot Working
  - Several Hot Extruders
  - Hydrostatic Extruder
  - Rodex (Continuous Extrusion, Cu and Al)
  - Drawing (e.g. Europe's Longest Bench)
  - Profile Manufacturing
- Availability of Outokumpu Intellectual Property

Nb_3Sn Projects

Fabrication Process of Internal-Tin Nb_3Sn CICC

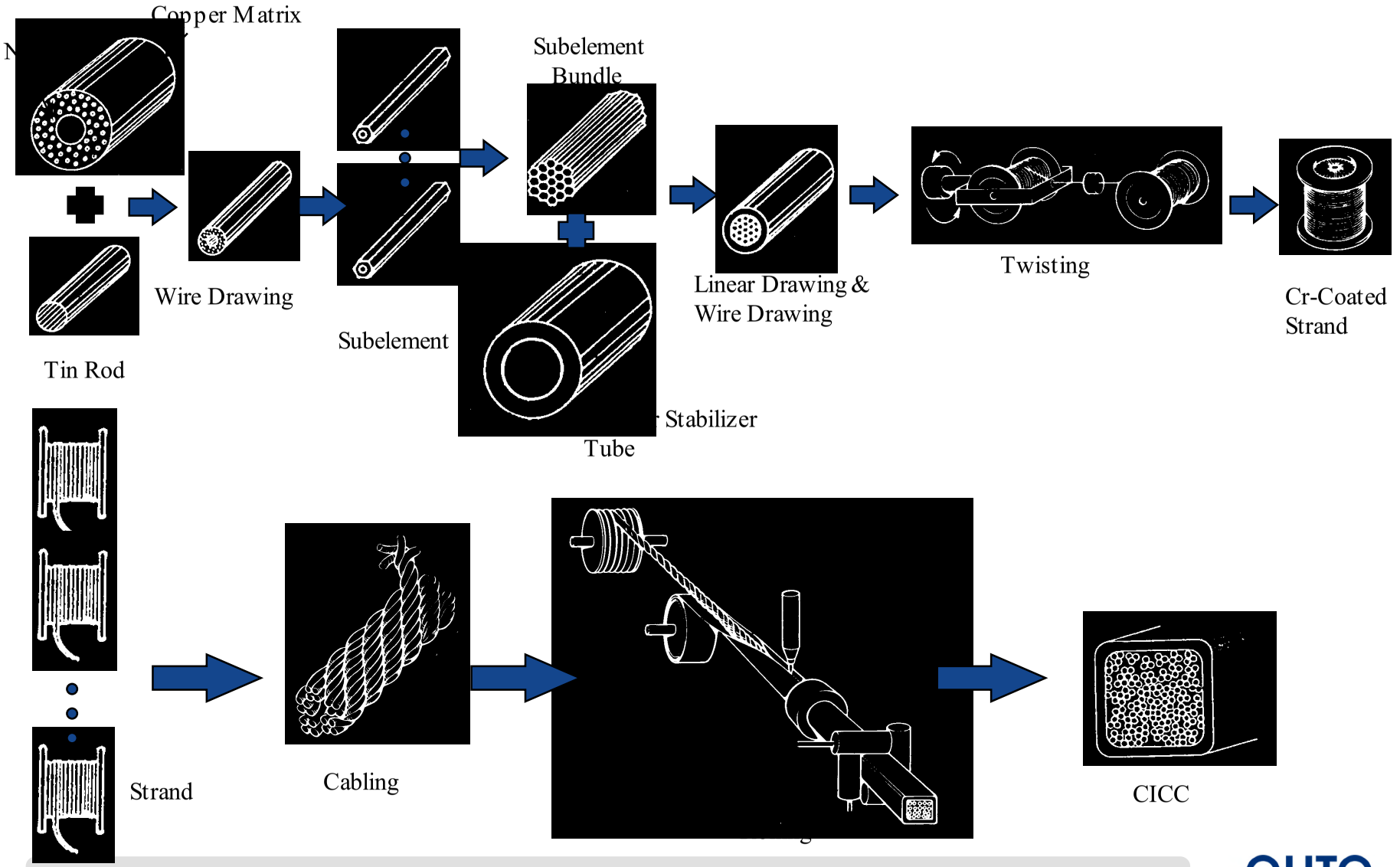

OUTOKUMPU

Nb_3Sn for the TF Model Coil

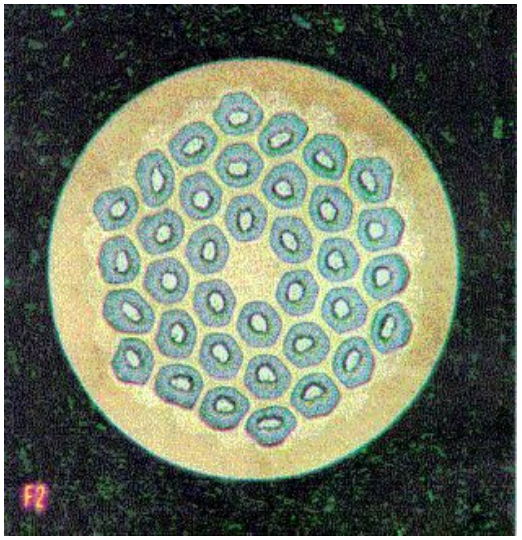

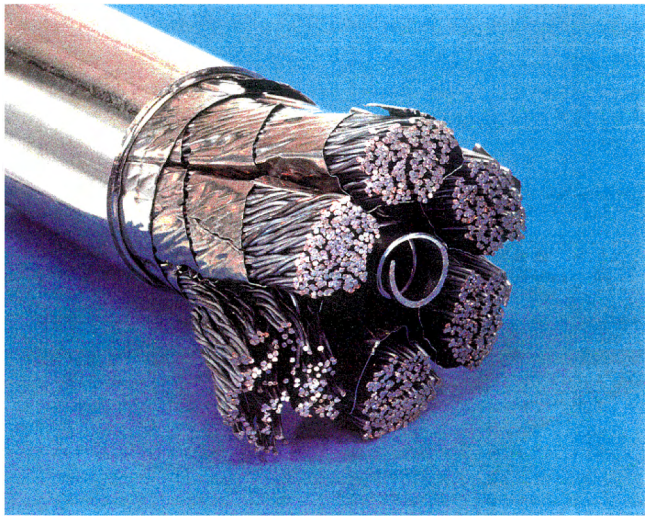

- Fornaci di Barga

Diameter (mm)	0.810 ± 0.003
Twist pitch (mm)	≤10
Twist direction	RHH
Cross-section (mm^2)	0.5153
Cu/nonCu ratio 1.50 ± 0.05	
NonCu cross-section (mm^2) 0.2061	
Cr thickness (µm)	2.0 +0.5/-0

- About 4 tonnes of strand manufactured mid 90's
- About 1 km of conductor manufactured
- Successfully tested at FZK (80 kA)

Projects in High Energy Physics Area:

- Conductor Development Program for High Energy Physics, Since 2002
  - Supported by U.S. Department of Energy Subcontract through Lawrence Berkeley National Laboratory
  - Highly focused on Nb3Sn (internal-tin).
- SBIR Subcontracts from small companies and national labs

<u>In other areas</u>:

- NHMFL (National High Magnetic Field Laboratory), Since 2002
  - 450 km of internal-tin strand for 45T-Hybrid magnet.
  - Delivery to be completed by the end of March.
- High Field DC laboratory magnets
  - High current, high strength Nb3Sn has been supplied to small magnet manufacturers.

Projects in the Fusion area

- CS Model Coil, 1993 –1997
  - Supplied 4.5 metric tons of HP-1 type internal-tin Nb3Sn strand with Cr-plating.

- LDX-F (Levitated Dipole Experiment), 1998 - 1999
  - A joint Columbia University & MIT Project.
  - 1.3 MA, 0.8 m diameter, 5 T Floating Coil Experiment for High-Temperature Plasma Experiments and Fusion Science Research.
  - Solely supplied 2 metric tons of highly customized internal-tin Nb3Sn Cable-In-Channel.
  - React & wind approach was adopted.

311

Projects in the Fusion area

- KSTAR (Korea Superconducting Tokamak Advanced Research), Since 1998
  - Requires high performance internal-tin Nb3Sn (HP-3 type).
  - Conductor supplied:
    - 6 metric tons of internal-tin Nb3Sn strand for TF and CS coils.
    - (12 metric tons of NbTi strand for PF coil (sole supplier).)
- ITER-EFDA, 2004
  - Pre procurement order of advanced TF Coil Nb3Sn strand.
- ITER-US
  - Pre procurement order of advanced CS Coil Nb3Sn strand under preparation by the US party.

OKAS-Nb_3Sn for High Energy Physics

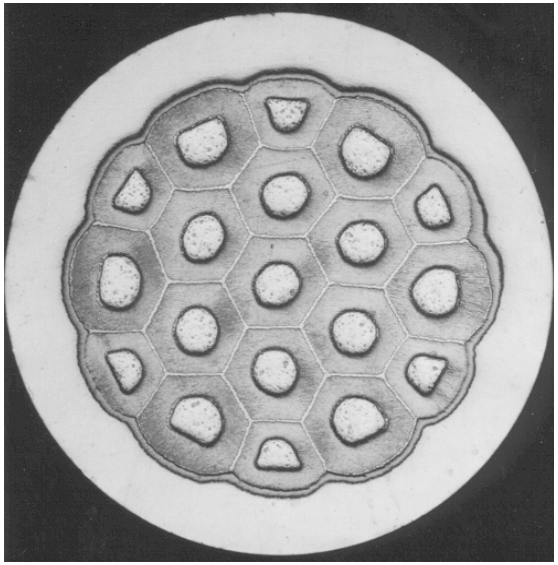

Conductor Characteristics	
Bare Dia. (mm)	0.60
Cu/non-Cu Ratio	0.6
No. of Filaments	26000
Filament Dia. (μm)	2.0
Non-Cu Q_h (kJ/m^3)	6210
D_{eff} (μm)	

Measurement Criteria
I_c: 0.1μV/cm,
n-value: 0.1~1.0μV/cm

B (T)	11.0	12.0	13.0	14.0	15.0	16.0
I_c (A)	517	431	348	287	224	166
n-value						
N-Cu J_c (A/mm^2)	2952	2460	1985	1640	1277	949

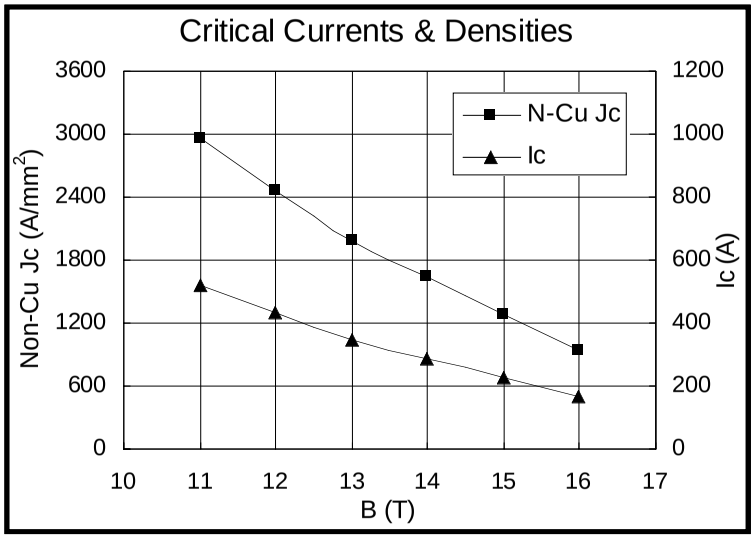

Current Density & Hysteresis Loss

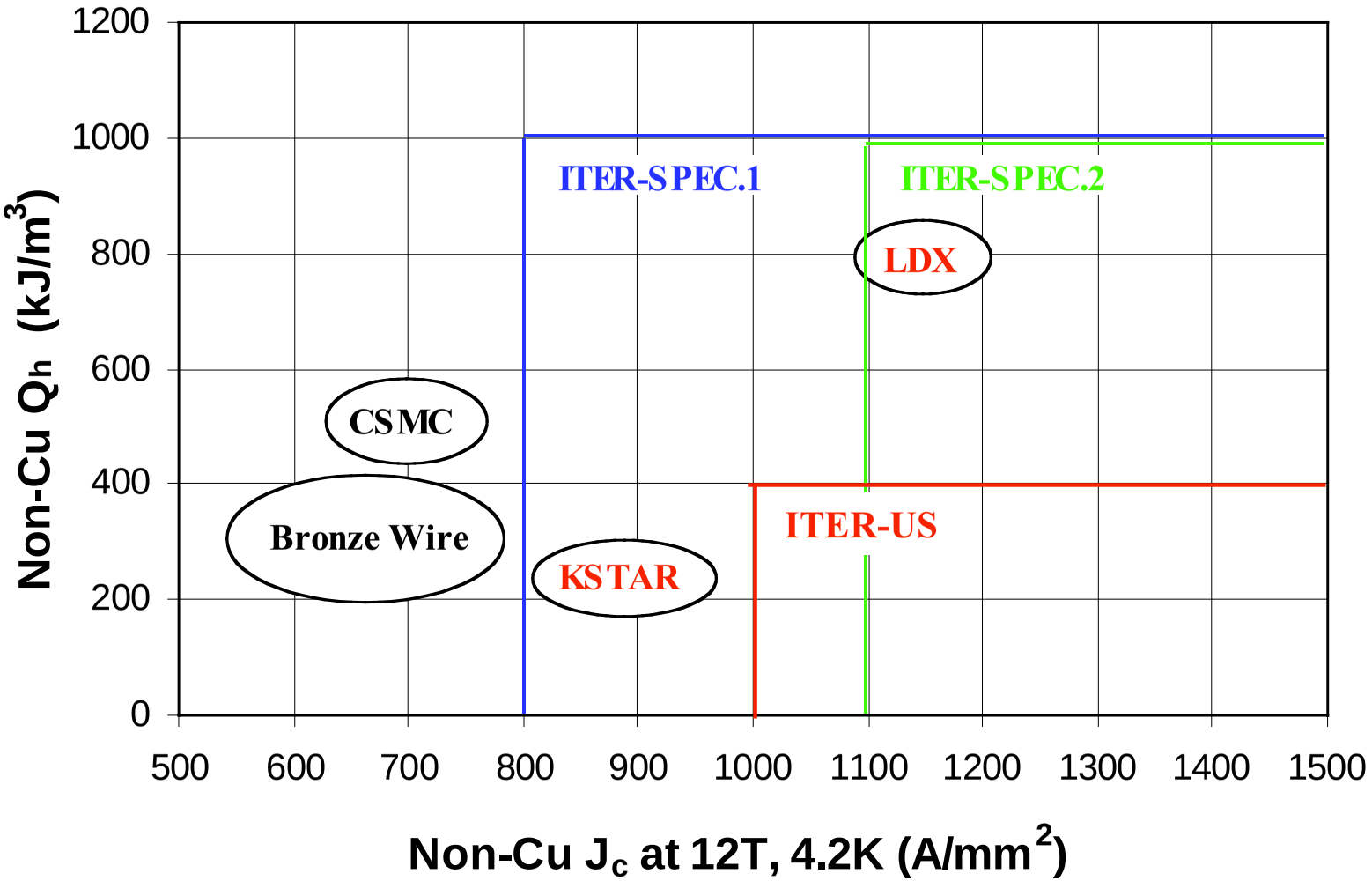

Summary

- Need for the Further Nb_3Sn development
  - Both non-Cu Jc and AC loss have been improved.
  - Further improvement is required to secure higher margin.
  - More aggressive (higher temp.) heat treatment for reaction is necessary to optimize Jc.
  - Scale-up of both sub-element billet and restack unit is in progress.

HTS Activities

- Joint project with CNR-IMEM and Edison to develope coated conductors
- 16:30 Today Dr. Zannella will give a presentation about this subject.

Siemens Activities in Superconductivity

PART I :

- **Large Scale HTS-Applications**
- **System Aspects, Design & Integration**

PART II :

- **Technical HTS-conductors and HTS-windings**
- **Is HTS Technology mature for Large Scale High Field Magnets ?**

J. Rieger
Siemens Corporate Technology
Erlangen, Germany

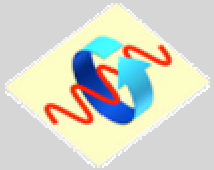

Large Scale HTS-Applications MRI Magnets

LTS Technology

- With first laboratory scale magnets in early 1980´s Siemens co-developed a multi-million dollar business
- Siemens Medical Solutions and Oxford Magnetic Technologies manufacture app. 1200 MRI-Magnets/yr.
- LTS MRI Magnet Systems from 0.5 T up to 3.0 T
- World market for MRI has a volume of ≈ 3 Mrd $/yr.

HTS Technology

- OMT OR10 - The world´s first MRI-magnet with HTS-magnet coils
- Cryofree conduction cooling with a GM-type refrigerator for T_{op}≈20K
- DC-pancake windings for a low field open MRI-system
- C/P ratio is essential to beat conventional electromagnets or permanent magnets

Large Scale HTS-Applications
HTS-Transformer

Railway traction or distribution isle grid

- Weight = 50% - Volume = 50% - Efficiency = 92 → 99%
- Oil-free = environmental benefit, no fire hazard

Technical Characteristics

- P = 1 MVA, f = 50 Hz, U = 25 kV, single-phase
- I_{US} = 360 A, I_{OS} = 40 A , B_{HTS} < 500 mT, ≈ 7 km Bi-Tape
- Forced flow subcooled LN_2 (dielectric reasons) T_{op}=67K

Operational experience

- short circuit, no load experiments, frequency variation, load variations, asymmetric operation
- design-tools and loss-models predict measurement results
- Successful testing of operation with a converter (harmonics)
- Transformer executed a load characteristic experiment with a 1 hour drive cycle „Wunstorf-Lehrte“
- Proven ability to drive ONE hour without cryocooler

Development challenges

- low AC-loss conductor – twisted filaments, high j_e
- reliable compact cryogenic system – n*100W
- FRP Cryostat with long vacuum stability for a warm iron core

Power & Sensor Systems
Power Components & Superconductivity

Large Scale HTS-Applications
HTS-Motor / -Generator

First HTS-Industrial Motor (400kW) in Europe (2001) (BMBF funding)

- 3 yrs. continuous testing in a rough factory environment
- test with power converter passed in 4/02
- 4-pole, n = 1500 rpm, f = 50 Hz, x
- "invisible" cooling system
- Test-Bed for scale-up of s components

still in operation !!!

♦ compactness ♦ efficiency ♦ stability

4 MVA HTS-Generator (2002-2005) (BMBF funding)

- Development for application on-board of ships
- Rotor with HTS-windings and brushless excitation
- Stator with Air-core winding from Cu-Litz
- U = 6,6 kV, 2-poles, f = 60 Hz, n = 3600
- Full-Load Testing with a converter and in the public grid in the new Siemens Systemprüfhaus, Nürnberg
- Testing with a gasturbine in discussion

entering Phase III - within schedule !

System Aspects, Design & Integration
Key Technologies for HTS-applications

- **HTS conductors**
  - physical application know-how : T_{op}, I_{op}, B_{op}
- **Winding Know-How** - Design & Manufacturing
  - mechanical, chemical & thermal tolerances
  - handling, contact & joining technology
  - qualitiy control
- **Electrotechnical system integration**
  - design and construction rules & tools
  - operation : converter-machine model
  - protection concept
- **Cryo and vacuum technology (rotating)**
  - closed cycle cooling system
  - possibility to exchange primary cooler
  - heat transfer by self-controlled thermosiphon

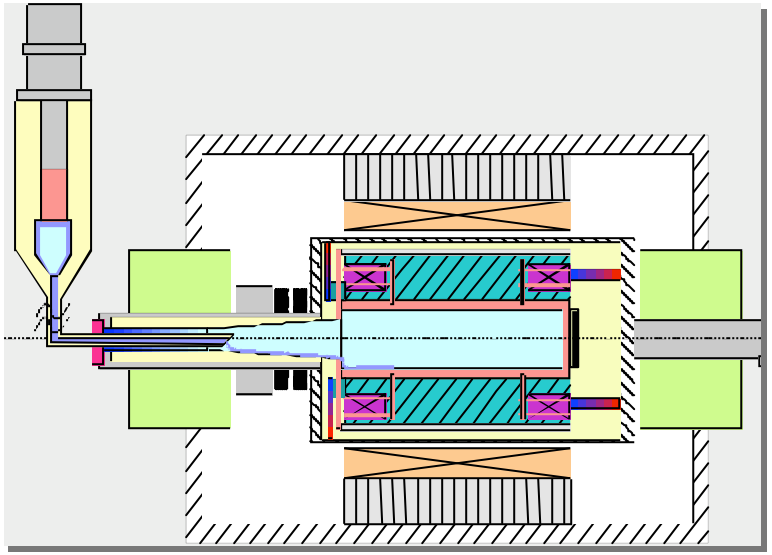

Power & Sensor Systems
Power Components & Superconductivity

System Aspects, Design & Integration Development Process

Material, Cryog	Production of powe engineering equipme	System integration
Development of HTS-Material and Cryo-Equipment in cooperation with external partners	Design, systemengineering, and construction of components and power engineering equipment	Integration in systems, test of systems and development of a market entry with business units

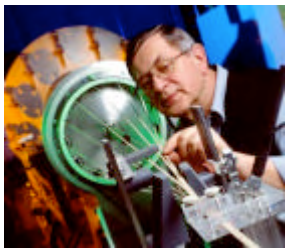

Technical Conductors

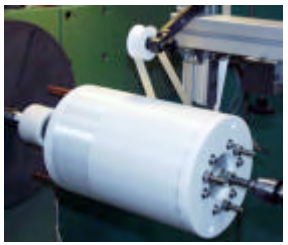

Design of windings

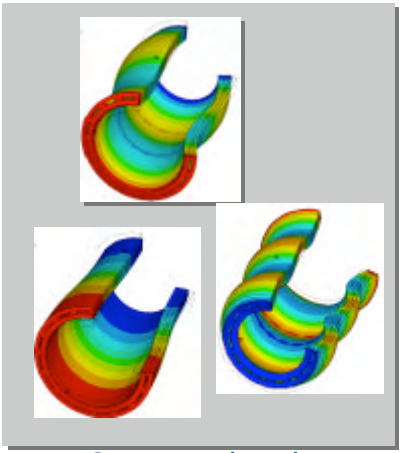

Systemengineering
Multiphysics-Simulation

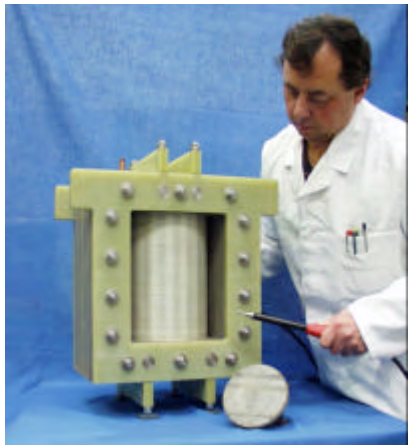

HTS-Choke Coil

HTS-MRI-Magnet

Power & Sensor Systems
Power Components & Superconductivity

System Aspects, Design & Integration
Multiphysics Analysis

Electrodynamics
Shielding of Higher harmonics from the HTS windings with a damping shield

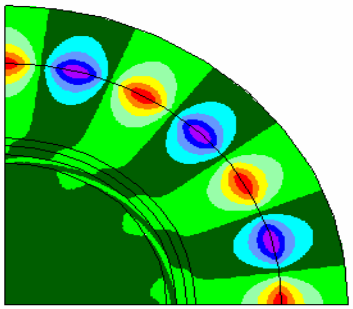

Cooling
Thermal Heat-Transfer between Coldhead and Rotor

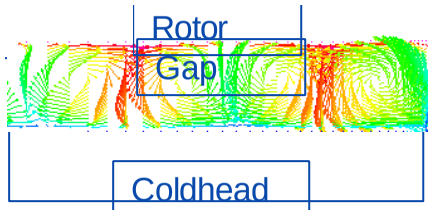

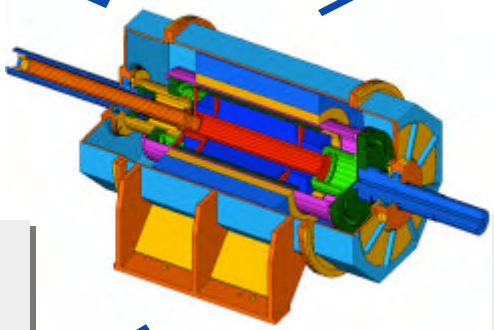

Magnetostatic Winding
Calculte magnetic fields for critical current, forces and moments in the conductors

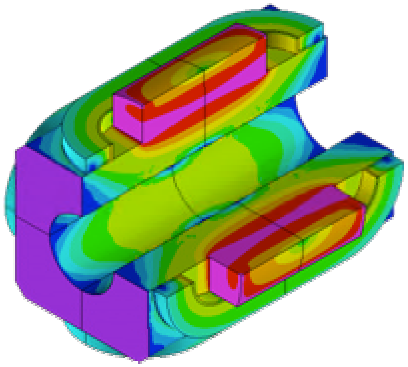

Structural Mechanics
Dislocations, tensions induced by centrifugal and magnetic forces

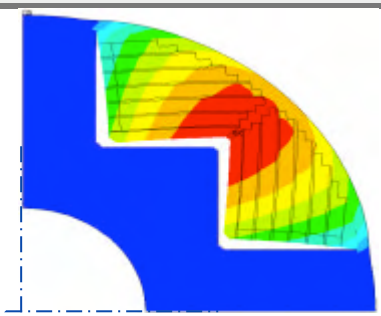

Power & Sensor Systems
Power Components & Superconductivity

System Aspects, Design & Integration
Cryogenics

Thermosiphons comprise ...

... closed-cycle cooling system

... Self-Control

... high thermal heat transfer capacity

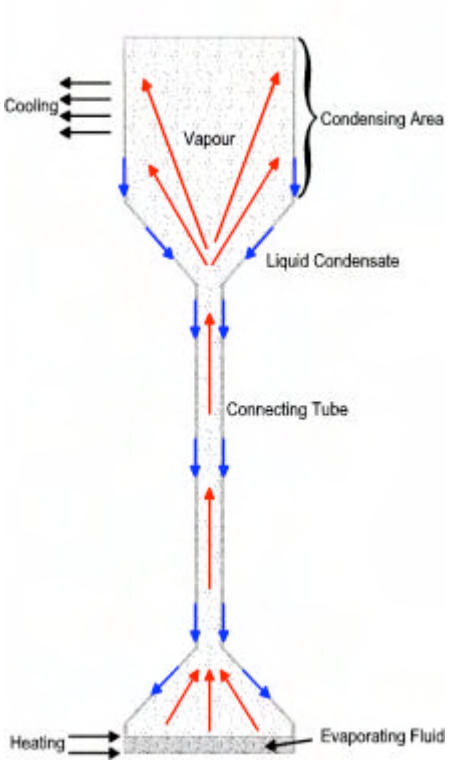

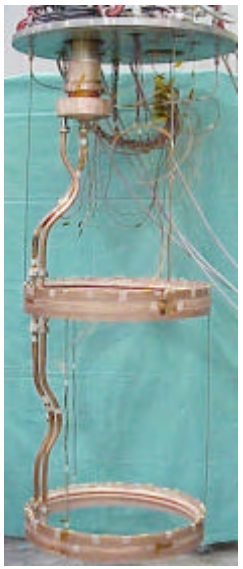

25-30K (Neon):
HTS MRI Magnet
(cooling testbed)

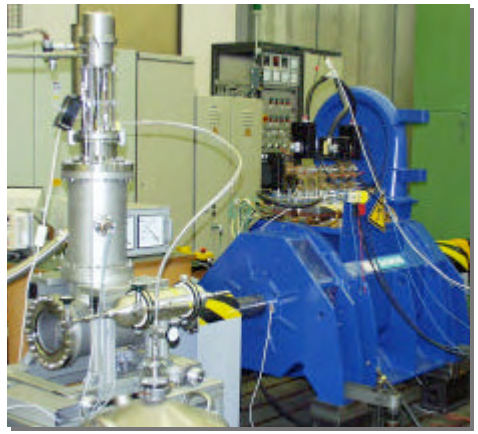

25-30K (Neon):
HTS Motor

4.2K (Helium):
Superc. Switch

4.2K (Helium):
MRI magnets

Power & Sensor Systems
Power Components & Superconductivity

Technical HTS-Conductors & HTS-Windings Requirements

Requirements for flexible HTS Conductor

- **availability in km-batches**
- **mechanical properties**
  - mechanically reinforced
- **high current capacity 0.1 – 5 kA**
  - large superconductor content
- **low Cost 10$/kAm (DoE)**
  - high engineering current density j_e
  - high critical current density j_c
- **low AC-losses (<0.45mW/Am /77K)**
  - short twist
  - thin filaments
  - High transverse resistivity

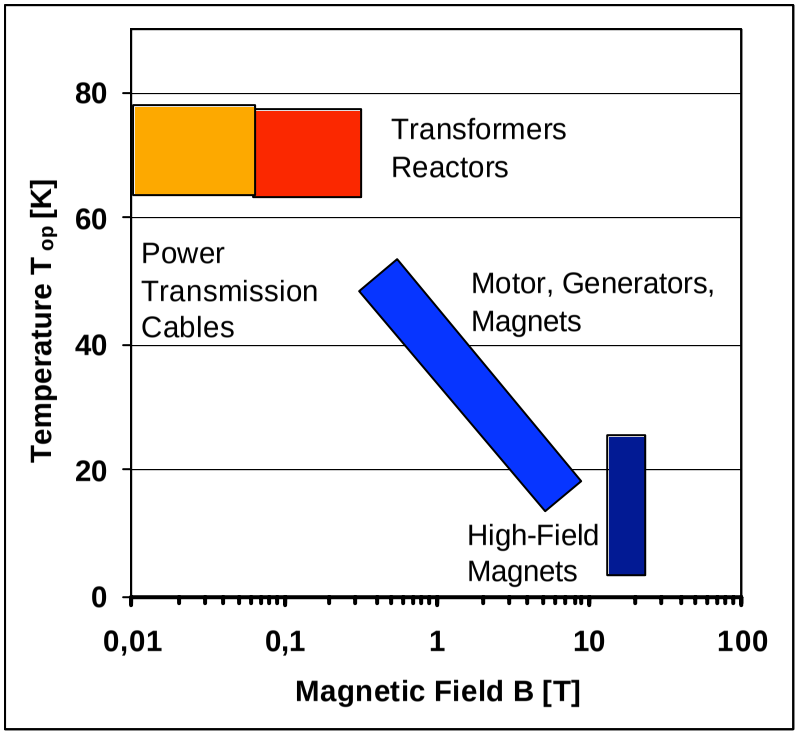

Operational parameters for Power engineering equipment

Power & Sensor Systems
Power Components & Superconductivity

Technical HTS-Conductors & HTS-Windings Application Ranges - Material Selection

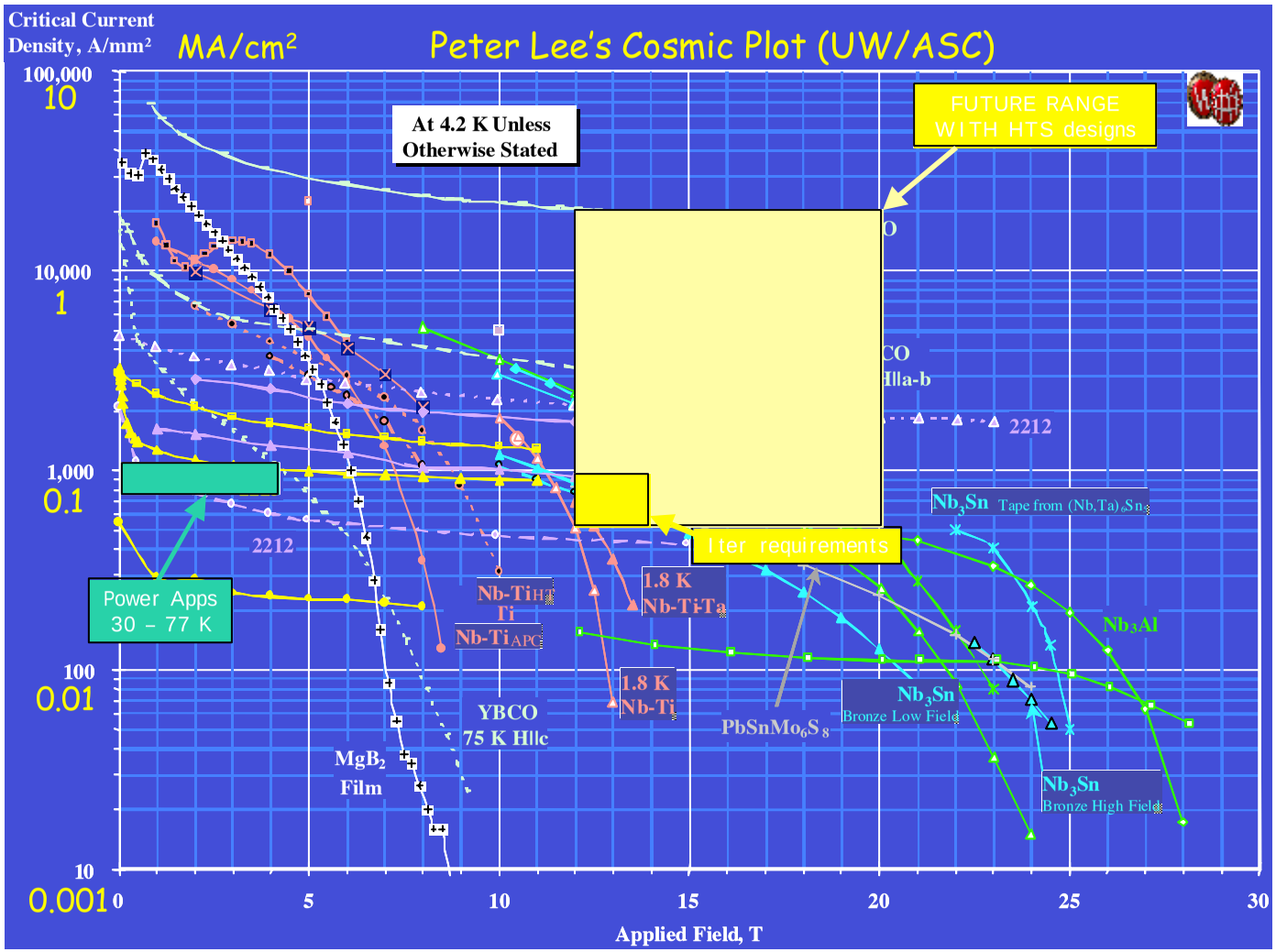

Power & Sensor Systems
Power Components & Superconductivity

Technical HTS-Conductors & HTS-Windings
HTS-Tape Conductor Properties

Parameter	Bi-2223/Ag-Tape	YBCO-CC-Tape	YBCO-CC-Tape outlook
Type	AgMg / Ag	IBAD / PLD	CSD
Available length	500-1500 m	10 m	>100 m
Width x thickness [mm^2] (typ.)	4 x 0.25	4 x 0.1	10 x 0.15
SC fill factor λ	25-35%	1-3 %	1-3 %
Critical current I_c(77K,0T)	80…140 A	120 A	+
Current Density j_e (77,sf)	100 A/mm^2	300 A/mm^2	125 A/mm^2
Current Density j_e (25,4T perp)	100 A/mm^2	340 A/mm^2	220 A/mm^2
Stabilized, insulated Current per width	200 A/cm	> 200 A/cm	+
I_c(66K)/ I_c(77K)	1.7	2.1	
$I_c(0.1T_{\|\|})$ / I_c(0T)	0.80	0.55	
$I_c(0.1_{\perp})/I_c$(0T)	0.31	0.47	
AC-loss $0.1T_{\|\|}$, 50Hz	0.3-1.0 mW/Am	<0.003 mW/Am	< 0.003 mW/Am
AC-loss $0.1T_{\perp}$, 50Hz	15 mW/Am	15 mW/Am	45 mW/Am
Critical bending radius	50 mm	< 15 mm	< 25 mm
Critical Tension (axial)	100…150 MPa	400 MPa	150
Handling	Robust	Sensitive	+
Insulation	wrapped, extruded	Not available	+
Stability, Normal resistance	High, < 10 mΩ/m	Low, > 1 Ω/m	+

Power & Sensor Systems
Power Components & Superconductivity

Technical HTS-Conductors & HTS-Windings
Which critical current to use ?

Which critical current to use ?

- **High critical current I_c** keeps winding effort low (=cost) and keeps inductance low
- **High engineering current densities j_e** for compact windings (power density) in motors, generators, transformers, magnets, …
- **High current per width I_c/w** is required esp. in transmission lines (power cables)

From the I_c of the tape to the attainable current density J_w in a winding (M.Oomen)

- Critical current (density) at 77K in self field $I_{c,sf}$
- Critical current density at the operating point (Temperature, cooling technology , magnetic field) $j_e(T_{op},B_{op})$
- Critical current density of a stabilised tape (device depend requirements)
- Critical current density of an insulated tape (varnish, extruded, wrapped, process temperature ?)
- attainable current density in a winding (fill factor, cooling design, winding type) J_w

Final Results :	**Bi2223**	**YBCO (PLD)**	**YBCO (MOD/CSD)**	
j_e 77K, sf	100 A/mm^2	300 A/mm^2	125 A/mm^2	bare tape
J_w 77 K, 0.1 $T_{\|}$	35 A/mm^2	42A/mm^2	25 A/mm^2	winding
J_w 25 K, 4 $T_{\perp}$	60 A/mm^2	204 A/mm^2	130 A/mm^2	winding

YBCO-tapes are comparable/better than Bi-2223-tapes for high power density windings

Power & Sensor Systems
Power Components & Superconductivity

Technical HTS-Conductors & HTS-Windings AC-Current and High-current Applications

HTS Tapes for AC-applications - Twisted Tapes

Magnetisation Loss : $P_{mag}/I_c = p_{co} B^3 / (B_{co}^3 + B_{co} B^2) f / 50Hz + q_{co} (B / B_{co})^2 (f / 50Hz)^2$

- parallel field loss can be decreased by increasing w/l_p
- perpendicular field loss is independent of w/l_p – tape width determines AC-loss
- minimum parallel field loss (0.3 mW/Am) = hysteresis loss of filaments
- width / Twist- ratio > 0.3 causes degradation
- twist length typical : 8…14 mm
- engineering critical current density j_e = 50-65 A/mm^2
- Resistive matrix Ag-Pd possible – Barrier concept technical not mature

High-current conductors - Roebel bar conductor

- Critical current assembled conductors : $I_{c,design} = \Sigma I_{c,tape}$ = 673 A, $I_{c,cable}$ = 400 A (77K)
- Self-field induced I_c reduction to 60…70% of nominal $I_{c,design}$
- Self-field model for I_c reduction : increasing # of tapes and increasing critical current $I_{c,tape}$
- BUT : cabled conductors are designed for high field windings – self field is uncritical
- NO affection of tape properties (n-value, I_c) by cabling process
- AC-loss behaves as for a monoblock
- scaling of transport AC-losses for different conductors with Norris Ellipse model

Power & Sensor Systems
Power Components & Superconductivity

Technical HTS-Conductors & HTS-Windings
High Current Assemble

Roebel bar conductor

- modular concept for high-current conductors
- transposed strands for low ac-loss
- insulated strands - thin coated plastics
- flexibility for coil winding
- long-lengths production - semiautomatic
- developed for HTS transformers
- presently not applicable for YBCO

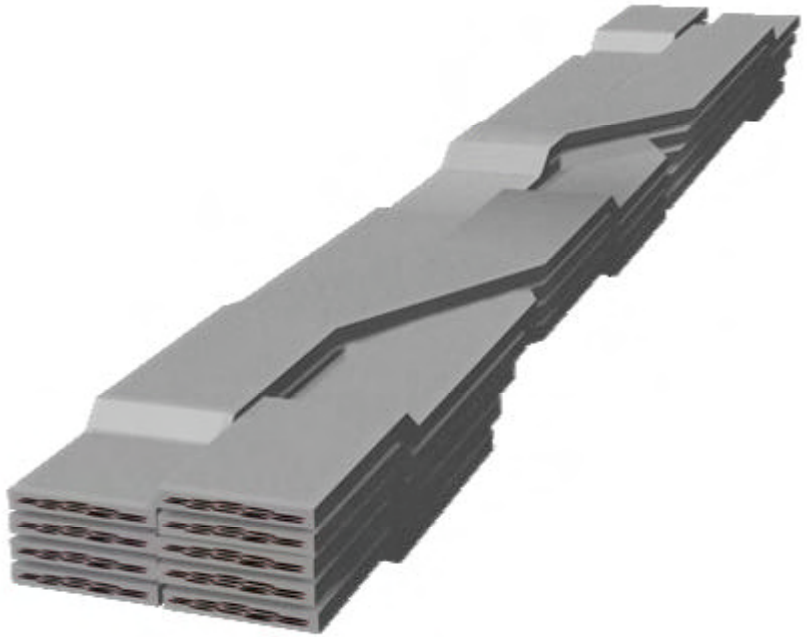

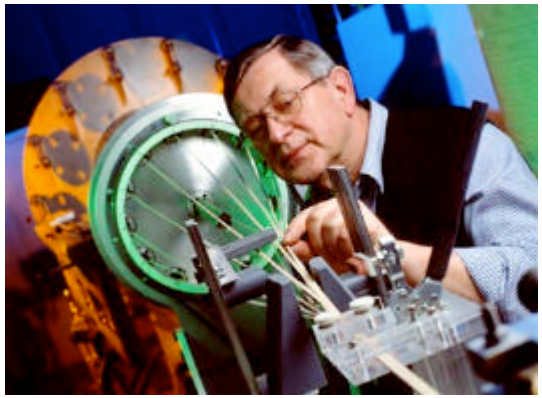

Laboratory Cabling Facility LARA

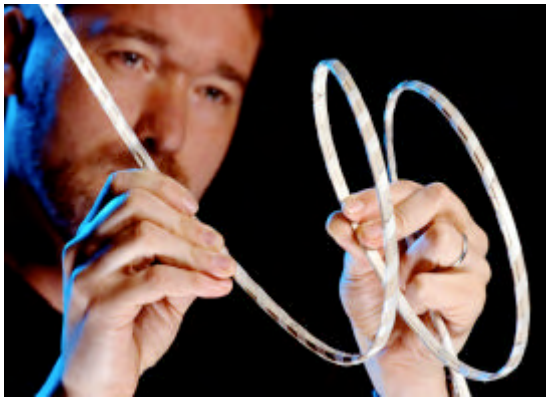

Flexible conductor

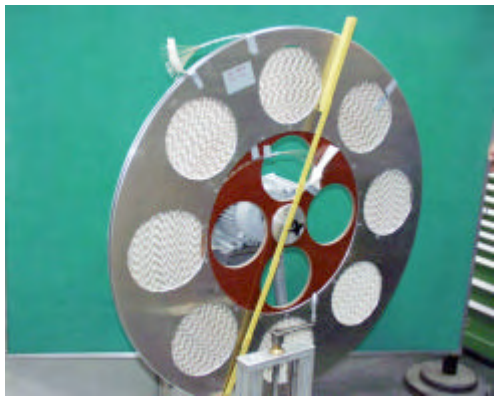

13-strand conductor, length=160m

Power & Sensor Systems
Power Components & Superconductivity

Technical HTS-Conductors & HTS-Windings
Solenoid Layer Windings – Traction transformer

Primary windings

- High voltage solenoid windings
- Bi2223/Ag-conductor, high-strength sheath
- thermoplastic coated insulation
- 9 Discs of solenoid layer windings with inter-coil connection
- 19 layer per disc, 2016 turns in total
- I_N = 40 A
- AC-operation, T_{op} = 67 K

Secondary windings

- Low voltage windings with high amperage
- 13-strand Bi2223/Ag-Roebel conductor
- thermoplastic coated insulation
- Internal or external (!) FRP-mandrel
- 1 layer with 56 turns
- I_N = 360 A
- AC-operation, T_{op} = 67 K

Power & Sensor Systems
Power Components & Superconductivity

Technical HTS-Conductors & HTS-Windings
Roebel windings – HTS-Choke coil

High amperage windings

for power engineering equipment with current 100...1000 A require assembled conductors

HTS-Choke coil

- Cable 13-strand fully-transposed, 105 m length, 13 x 0.9mm^2
- $I_{c,sf,T_{op}=66K)}$ = 443 A, $I_{c,sf,77K}$ = 247A
- Elementary conductor 1362 m high-strength Bi-2223 tape
- winding with 6 layers and 192 turns
- Internal cooling channels for LN_2 bath cooling
- Dry winding and vacuum resin impregnation
- P = 208 kW (reactive) L = 5.5 mH, f = 50 Hz,
- Axial Field at $I_c(T_{op})$/50Hz = 585mT

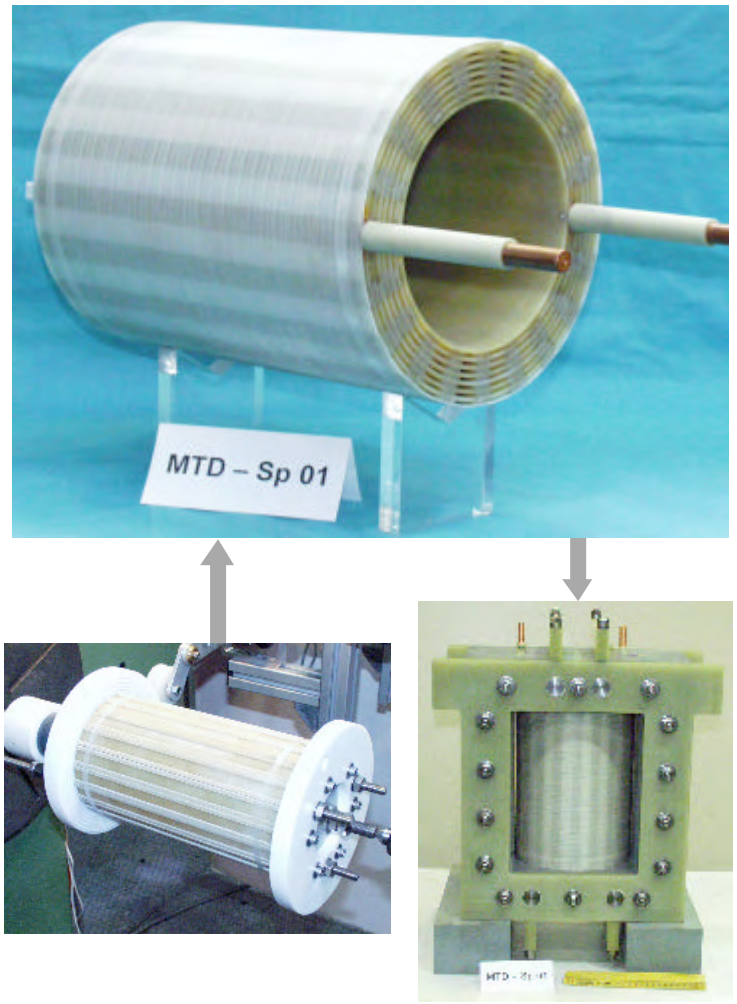

Power & Sensor Systems
Power Components & Superconductivity

Technical HTS-Conductors & HTS-Windings
Racetrack Windings – Motor, Generator

HTS-Racetrack winding

- Bi2223/Ag-conductor, single-strand,
- thermoplastic coated insulation, Cu-mandrel
- Wet-winding with expoxy resin
- ≈ 100 windings
- conduction cooling, T_{op} = 20...30K
- DC-current operation with I = 40 A

Pole windings of 400kW HTS-Motor

HTS-Experimental windings

- commercial winding machine adjusted for winding of HTS tapes
- measurement and control of winding tension
- flexible adjustment for any kind of coil
- HTS tape handling, guidance, co-winding
- dry-winding, wet winding and vacuum impregnation

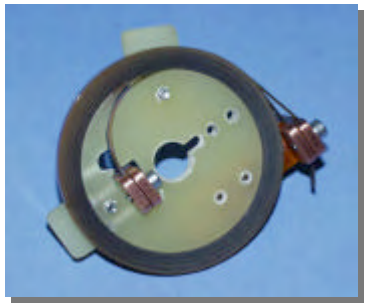

1st pancake winding from 10m YBCO CC

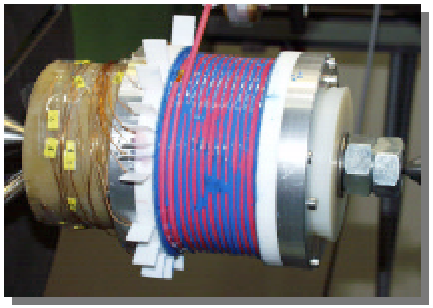

Multi-layer solenoid from Bi2223-tape

Power & Sensor Systems
Power Components & Superconductivity

Technical HTS-Conductors & HTS-Windings Present Status

From the viewpoint of a magnet or power equipment manufacturer

HTS-Winding Technology (for Bi-tapes) is developed and proofed :

- applications in 4 K, 20...30 K, 60...80K temperature ranges
- winding adapted to flat tapes : 3...5 mm x 0.1...0.3 mm and assembled conductors (2n+1)-strand with typ. 7...10 mm x 1...4 mm
- wet winding or dry winding with vacuum resin impregnation (all React & Wind)
- low post-processing temperatures (insulation & tape)
- splicing and joining technology for elementary tapes (Bi - not CC)
- bath cooling or conduction cooling via eg. Mandrel
- intrinsic stabilization in Bi/Ag-tapes or co-winding with metal-tape

Further developments should preferrably allow a FORM-Fit replacement of the conductor by YBCO CC with a high engineering current density j_e

Whishes for the future :

no anisotropy, round wires, long batches, low C/P, tiny filaments , ...

Is HTS Technology mature for Large Scale High Field (LSHF) Magnets ? - Design-Process

Replacement Approach

Substitute 1:1 LTS-Technology

- LTS : CICC, Compaction of jacket onto cable , W&R, LHe-coolant, T_{op} = 4.2K, $B_{op} \geq$ 13T
- Performance as good as LTS
- Competitive C/P ratio drives replacement
- Improve performance and reduce process cost of HTS
- new mechanical concepts

Enabling Approach

Exploit advantages of HTS-conductor by Re-Design of Magnets

- performance under high fields B>20T
- enhanced T_{op} = 20...30 K enables cryo-free cooling and lowers cost of operation
- higher temperature margin ΔT - enhanced stability
- new mechanical concepts

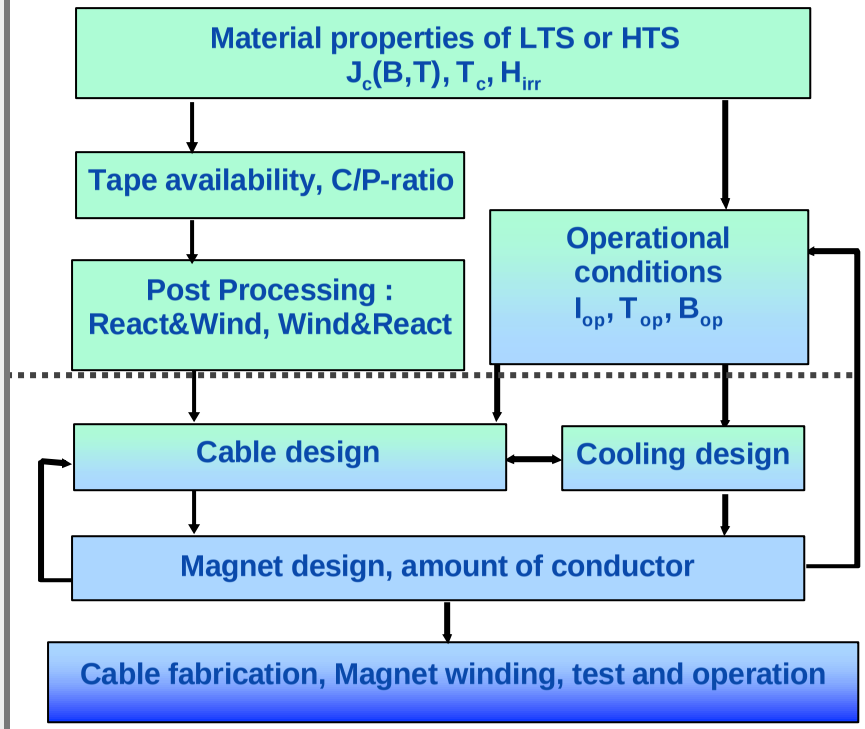

Power & Sensor Systems
Power Components & Superconductivity

Is HTS Technology mature for Large Scale High Field (LSHF) Magnets ?

Parameter	LTS Magnet	HTS Magnet
Conductor	Nb3Sn CCIC	Assembled Conductors of Bi/Ag-Tapes or YBCO CC
Current density j_e	Reference	Multiple - no strain dependence below ε_c
C/P ratio	Reference	Lower (YBCO-CSD)
Insulation	External wound prepregs	Bi : available YBCO-CC : tbd
Magnet construction	Self-supporting	Supporting plate/mandrel
Magnet fabrication	Wind & React (high risk)	React & Wind (minized risk)
Stability	Low Stability Internal Cu and Cryogenic stabilization	Intrinsic (Ag), Impregnation (Pb) or Add-on conductor (Cu) Bi : high stability YBCO : low stability
Stability margin ΔT	mK Range	10 K Range = reduced quench risk
Cooling	Direct internal He-Cooling	Indirect via separate (He-)channel, conduction cooling
Operation	Pulsed mode possible	Small field change rates dB/dt
Magnetic field B	Limited B	Very small dj_c/dB for B>>13T
Investment	High	Medium (2^{nd} Gen CC)
Cost of operation	High (4K)	Medium (20K)
R&D needs	Small	Concept for 20K Magnets, C/P-improvement, low cost process (CSD)
Status	**Close to Saturation**	**Development with potential**

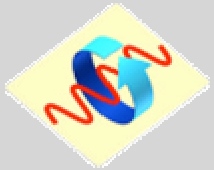

Is HTS Technology mature for Large Scale High Field (LSHF) Magnets ? - Roadmap Matching ?

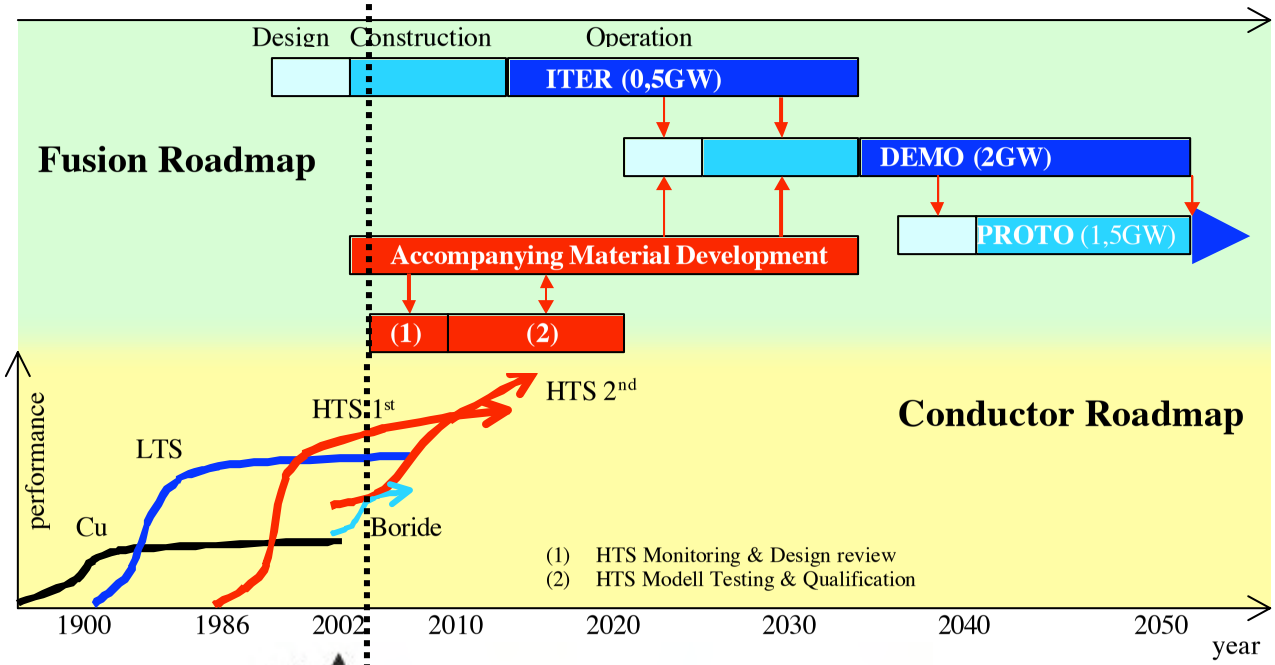

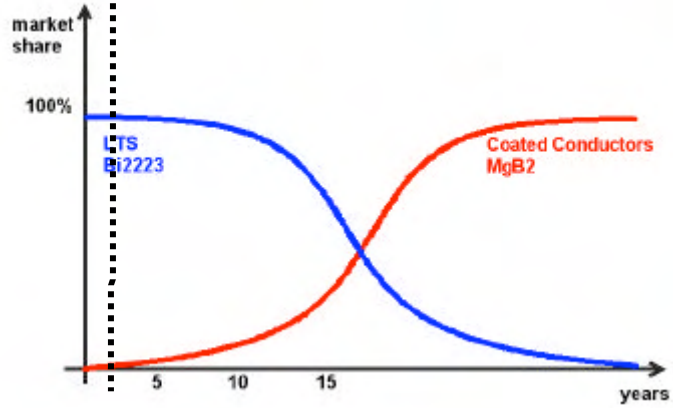

Status : 5/2002

Accelerator Magnets should accelerate the Development speed for HTS-Conductors !

Summary

Status

- HTS is economically not competitive at the moment to substitute (1:1) Nb_3Sn in LSHF-magnets
- HTS wire meet most j_e and mechanical requirements, AC-loss dependent on field ramp rate requirements
- **A Redesign of the magnets (T≈20..30K, high B-field) will fully exploit the advantages of HTS**
- Winding technology for Bi/Ag-Tapes is well developed and 1st transfers for form-fit YBCO CC are successful
- Modelling tools for the design of HTS-windings regard the specific field and temperature $j_c(B,T)$, n(B,T) etc.

Outlook

- **Develop new Magnet concepts for the use of HTS in LSHF applications**
  including concepts for mechanical forces, cooling, thermal and electrical stabilization.

- Monitor and drive further progress in the **development of secondary key components**
  (Cryocoolers, Cryostats, sealings, bearings etc.)

- **Monitor and drive the HTS-material development constantly**

Bi2212	low cost production process, fine filamentary high current wires
Bi2223	lower process cost by production ramp up, performance increase j_e, low AC-loss
YBCO	long length production with low cost process, stabilization, joining, insulation
MgB_2	(4.2K application ?) current density, preparation progress, multifilamentary wires

Power & Sensor Systems
Power Components & Superconductivity

CONCLUSIONS

Conclusions

Lucio Rossi
CERN

The Workshop on Accelerator Magnet Superconductors has gathered 102 registered participants of various areas:

- Material science and engineering
- Magnet design and magnet technology for particle accelerators and detectors
- Accelerator physics
- Fusion magnet technology
- Low Tc and High Tc superconductors and cables

Most of attendants were from research laboratories, with a considerable presence from universities and industries; eight European companies, active in superconducting material and cables, were present which is a considerable success, and all discussed their plan for Superconductor R&D in near-mid term.

The 33 speakers gave very high quality talks (see http//:amt.web.cern.ch/amt) a broad view of the progress and expectation in the different areas, providing the necessary link to the final scopes: superconducting magnets for the next generation particle accelerators.

The main conclusions can be summarized as follows:

1. Type of magnets

After a generation of accelerators based on NbTi conductor wound magnets powered in a static (or slowly ramped) mode, a need for new designs is appearing at the horizon:

a. High field magnets necessitating a non-copper critical current density around 1500-3000 A/mm^2 in the field range 10-15 T. This scope is addressed by the 7 institutes of the network HHH that are participating to the **NED (Next European Dipole)** Joint Research Activity, in which a 13-15 T dipole is under study and development.
b. Pulsed magnets with the peak field in the range 2-6 T and to be cycled at 1-10 Hz. This scope is today mainly addressed by the FAIR project at GSI.

Despite the fact that the two types of magnets are very different and in particular pulsed magnets that rely on NbTi while high field magnets need Nb_3Sn conductor, there is an important area of common interest (in addition to obvious synergies in cabling, testing, computing, etc): the necessity of heat removal from coils at a sustained level, of the order of 10 W/m – 50 W/m.

These characteristics call for a revision of the cable design and coil technology (in particular insulation). Furthermore, the most likely applications: FAIR project, LHC upgrade of the intersection region, LHC upgrade of the injector chain, RIA (USA project for radioactive isotope) as well as other applications that might be envisaged

in farther future, all necessitate use of radiation resistant materials. A program of development and testing in real condition of new insulating materials is deemed very necessary.

2. Financial support for conductor R&D

New materials need a long time of development to be used in practical conductor with certain characteristics:

a. Uniformity of J_c and other properties along length and among different assemblies
b. Appropriate (small) filament size, limited coupling
c. Possibility to control the stabilizer amount
d. Workability in long length
e. Adaptability to cabling with high packing factors (85-90%) with moderate degradation
f. Compatibility with insulation and practical winding techniques

To reach these goals and to provide the necessary quantity of conductors needed to exercise the new magnet technologies and designs, our community needs a continuous R&D financial support to industries and laboratories to allow multi-year program, like the one established by the DOE (US Dept. of Energy- High Energy Physics Office) since a few years. With the restriction of basic R&D in all laboratories, financial support from EU is certainly a key issue for a progress in the high J_c-high field superconductor.

3. Status of Low T_c superconductors

a. **Nb_3Sn**: today is the ONLY viable practical material for fields in the 10-20 T region, *thus confirming the early choice of NED*. Europe has companies active in all processes (bronze, ITD and PIT). But there is a strong feeling that NED, which has total EU funds of 600 k€ for Nb_3Sn development, must be complemented as soon as possible with an additional program otherwise its effort will not have the necessary continuity. NED is mainly aiming to conductor with controlled filament size, *an early choice that today has proved to be necessary to avoid the instability effect.*
b. **NbTiTa** characteristics have been reviewed and the conclusion is that a moderate effort, both financial and technical, would be needed here to bring the material in the game. The investigation should aim on how to "transform" the higher critical field into critical current. Ideas have been put forward: improved homogeneity, forged ingots for grain size reduction. The size of the effort, estimated to be of the order of 300 k€, might also fit the possibility of National Institutes.
c. **Nb_3Al**: the progress of the rapid quenching technique are noticeable, although somehow frustrated by continuous increase of existing on-the-market Nb_3Sn in the 10-20 T region. The key issue, in addition to the real production cost that is maybe too early to be assessed, is the difficulty of addition of stabilizing metal. However, its superior mechanical properties that might be compatible with the R&W technique makes this material a possible choice for the long-term project, like LHC upgrade in energy.

d. **MgB_2**: given the characteristics, once developed in practical conductor, for accelerators, it can be a candidate for stand-alone magnets, especially where liquid helium is not easily available. In addition, it can be a good candidate for ancillary equipments like current leads and current bus bars. Of course its intrinsic low cost plays an important part in the interest: however the difficulty of avoiding magnetic materials like iron as sheath might impede large applications.

4. Status of High T_c superconductors

a. Today the engineering current density is nominally better than Nb_3Sn at the edge of high field (beyond 16 T). Round **Bi-2212** wires are really tempting for very high field magnets: however use in highly packed (85-90%) 20 kA cables is to be proved in a real production and mechanical properties are still not at the level of Nb_3Sn. However, the gap is shrinking and here one can profit from development done for other applications (1 GHz NMR). A specific R&D aimed to particular points of accelerator magnets (large currents with good compaction, stabilizer minimization, insulation thickness, etc.) is needed before making possible its use in state-of-the-art prototypes.

b. **Bi-2223** is not the best material for accelerators since in the area where it is competitive, above 30 K, the current density performance is limited by drop in the irreversibility critical field. In addition, it is only available in tapes – which implies change in cable technology or winding – and its cost is not likely to become comparable to the one of Nb3Sn (which is already 4-5 times the one of NbTi!), mainly due to considerable silver: of course this obstacle is common to Bi-2212.

c. Coated conductor, **YBCO 123**, has shown tremendous progress and now excellent current density of more than 10,000 A/mm^2 @ self field, 77 K has been demonstrated in relatively long length (range 10-100 m). The engineering current density is also progressing: more than 100 A/mm^2 and very likely to reach 300 very soon. One can state that this is the material offering more hope for magnets in the liquid nitrogen range (T > 65 K). Even for low temperature applications, it is a serious competitor to Bi2212 with I_c (4.2K, 15T)= 10 I_c (77K, 0T). Despite these very good characteristics, and differently from Bi-2212, many critical points have not yet been addressed: filament size and twisting, round wire (to make easier flat compacted cables), control of stabilizer among others. However the possible lower cost of coated conductors with respect to Bi-based conductors and the strong push from material and electro-technical industries, together with larger margin of improvement, make this material one of the most promising, at least in the author's opinion, to compete with Nb_3Sn in the high field domain.

In conclusion, material development is always an area of great excitement, with many new happenings. It is clear that the workshop has pointed out that new materials, which are an essential ingredient for progress in magnet and accelerator technology, require:

- **Suitable magnet design**
- **Suitable cable design**
- **Suitable insulation**
- **Suitable finance support, with a reasonable continuity**

This workshop will be followed by a complementary workshop more dedicated to winding and magnet construction technology in 2006.